

J

# PRECIPITATION MEASUREMENTS FROM SPACE

## WORKSHOP REPORT

(NASA-TM-85329) PRECIPITATION MEASUREMENTS  
FROM SPACE: WORKSHOP REPORT. AN ELEMENT OF  
THE CLIMATE OBSERVING SYSTEM STUDY (NASA)  
446 p HC A19/MF A01 CSCI C4F

N83-25269  
TRFO  
N83-25316  
Unclas  
19611  
G3/47

**DAVID ATLAS and OTTO W. THIELE**  
EDITORS

BEST AVAILABLE COPY

**OCTOBER 1981**

**LIBRARY COPY**

FEB 9 1982

LANGLEY RESEARCH CENTER  
LIBRARY NASA  
HAMPTON, VIRGINIA



National Aeronautics and  
Space Administration

**Goddard Space Flight Center**  
Greenbelt, Maryland 20771

**PRECIPITATION MEASUREMENTS FROM SPACE**

**WORKSHOP REPORT**

**April 28 – May 1, 1981**

**Editors**

**David Atlas and Otto W. Thiele**

**AN ELEMENT OF THE CLIMATE OBSERVING SYSTEM STUDY**

**GODDARD LABORATORY FOR ATMOSPHERIC SCIENCES  
GODDARD SPACE FLIGHT CENTER  
GREENBELT, MARYLAND**

## PREFACE

The need for describing precipitation on a multitude of time and space scales is fundamental to advancing the state-of-the-art in weather and climate predictability. Precipitation is both a cause and an effect of atmospheric behavior since it involves thermodynamic changes of state that influence the energy available to atmospheric circulation at virtually all scales of motion.

Scientific planning for the U.S. National Climate Program, and for its international counterpart, the World Climate Research Program, has recognized precipitation as a critical climate parameter for diagnostic and processes studies and as a basic indicator of the state of climate itself. Our ability to observe and characterize precipitation is complicated by the irregular manner in which it occurs in time and space, thus supporting the requirements for global scale measurements from space.

The Workshop on Precipitation Measurements from Space, supported by both the NASA Global Weather and Climate Research Programs, is an attempt to examine the broad scientific needs for precipitation measurements from space and address the techniques already available or proposed for meeting these requirements. Accordingly it is expected that the workshop conclusions and recommendations will play a major role in helping to shape the future NASA Space Observations Program.

Robert A. Schiffer, Manager, NASA Climate Program  
John S. Theon, Manager, NASA Global Weather Program

## CONTENTS

	<u>Page</u>
EXECUTIVE SUMMARY .....	vi
1. INTRODUCTION .....	1-0
2. REQUIREMENTS .....	2-0
2.1 Summary of Requirements and Recommendations .....	2-1
2.1.1 Summary of Requirements .....	2-1
2.1.2 Summary of Recommendations .....	2-2
2.2 Discipline-Oriented Requirements – General .....	2-2
2.2.1 Operations .....	2-2
2.2.2 Research .....	2-3
2.3 Specific Discipline Considerations .....	2-3
2.3.1 Global Climate .....	2-3
2.3.2 Agricultural Uses for Precipitation Information .....	2-4
2.3.3 Hydrological Uses for Precipitation .....	2-5
2.3.4 Severe Thunderstorms and Local Weather .....	2-6
2.3.5 Global Weather .....	2-7
2.4 Requirements Analysis .....	2-9
3. SAMPLING PROBLEMS .....	3-0
3.1 Introduction .....	3-1
3.2 Rainfall Estimation .....	3-1
3.3 Satellite Systems .....	3-2
3.4 Sampling Strategy .....	3-2
3.5 Recommendations .....	3-3
4. GROUND-TRUTH MEASUREMENT SYSTEMS .....	4-0
4.1 Introduction .....	4-1
4.2 Scope .....	4-1
4.2.1 Coverage .....	4-1
4.2.2 Resolution .....	4-1
4.2.3 Global Extent .....	4-1
4.2.4 Measurement of Rainfall .....	4-2
4.3 Ground-Truth Measurement Parameters and Techniques .....	4-2
4.3.1 Measurement Parameters .....	4-2
4.3.2 Measurement Techniques .....	4-2
4.3.3 Platform or Geographical Locations .....	4-3

CONTENTS (Continued)

	<u>Page</u>
4.4 Recommendations . . . . .	4-3
5. VISIBLE (VIS) AND INFRARED (IR) TECHNIQUES . . . . .	5-0
5.1 Summary of Conclusions and Recommendations . . . . .	5-1
5.2 Satellite Data Sources . . . . .	5-1
5.3 Summary of Techniques . . . . .	5-2
5.3.1 Time-Independent Indexing Schemes . . . . .	5-2
5.3.2 Time-Dependent Life-History Techniques . . . . .	5-4
5.4 Applications . . . . .	5-6
5.5 Assessment of Techniques . . . . .	5-7
5.6 Improvements . . . . .	5-7
5.7 Recommendations . . . . .	5-8
6. MICROWAVE RADIOMETRY AND HYBRID PRECIPITATION MEASUREMENTS . . . . .	6-0
6.1 INTRODUCTION . . . . .	6-1
6.2 BACKGROUND . . . . .	6-1
6.2.1 Theory . . . . .	6-1
6.2.2 Previous Microwave Work . . . . .	6-2
6.3 Microwave Measurement Problems . . . . .	6-6
6.3.1 Beam Filling . . . . .	6-6
6.3.2 Effective Rain-Layer Height . . . . .	6-7
6.3.3 Cloud Liquid Water . . . . .	6-7
6.3.4 Rain Over Land . . . . .	6-8
6.4 Recommended Measurement System . . . . .	6-8
6.5 Recommendations . . . . .	6-9
7. SPACEBORNE RADAR . . . . .	7-0
7.1 Introduction . . . . .	7-1
7.2 Combined Measurements . . . . .	7-1
7.3 Candidate Systems Concepts . . . . .	7-1
7.3.1 Generic Systems . . . . .	7-1
7.3.2 Orbit Considerations . . . . .	7-2
7.4 Candidate Spaceborne Radar System . . . . .	7-2
7.4.1 Shared Systems . . . . .	7-3
7.4.2 Dedicated Systems . . . . .	7-4

CONTENTS (Continued)

	<u>Page</u>
7.5 Required Research and Development Steps . . . . .	7-5
7.5.1 Initial System Studies . . . . .	7-5
7.5.2 Modeling and Simulation . . . . .	7-6
7.5.3 Experimental Program . . . . .	7-6
7.5.4 Algorithm Development . . . . .	7-7
7.6 Recommendations . . . . .	7-7
APPENDIX A – PROGRAM AGENDA . . . . .	A-1
APPENDIX B – WORKSHOP PARTICIPANTS . . . . .	B-1
APPENDIX C – TABLE OF ACRONYMS . . . . .	C-1
APPENDIX D – CONTRIBUTED PAPERS . . . . .	D-1

ILLUSTRATIONS

<u>Figure</u>	<u>Page</u>
1 The Role of Moisture and Liquid Water in a Synoptic System . . . . .	2-8
2 Typical Viewing Geometry for Microwave Remote-Sensing of Ocean Surface and Atmosphere . . . . .	6-2
3 Scattering and Extinction (Absorption plus Scattering) by Rain at 18.35 GHz (the solid and dashed lines represent temperatures of 20° and 0°C, respectively) . . . . .	6-3
4 Brightness Temperature at 19.35 GHz as a Function of Rainfall Rate Over the Ocean . . . . .	6-4
5 Computed Horizontally and Vertically Polarized Brightness Temperature at 37.0 GHz as a Function of Rain Rate . . . . .	6-4

TABLES

<u>Table</u>	<u>Page</u>
1 Precipitation Requirements . . . . .	2-10

OMIT TO  
P 2-0

## WORKSHOP ON PRECIPITATION MEASUREMENTS FROM SPACE

### EXECUTIVE SUMMARY

#### INTRODUCTION

Precipitation is important in a myriad of practical and scientific ways throughout a multiplicity of disciplines. These include weather, climate, hydrology, and oceanography in which precipitation is a key factor for analysis, diagnosis, prediction, and verification. Practical applications arise in many other fields including agriculture; forestry; water resources; commerce which involves specialized uses for precipitation information in communications, transportation and industry; and a broad spectrum of other societal needs. More recently, the crucial role of precipitation as a key element in the weather and climate system, both as a forcing function and a response variable, has been re-emphasized. Precipitation must therefore be observed globally. Moreover, as one of the two fundamental descriptors of climate, global observations of precipitation are, like temperature, essential as a means of correctly initializing global circulation models (GCM) for extended range weather prediction.

These are but a few examples of many needs for global spaceborne measurements of precipitation. Obviously, not all applications require global observations nor can all of the requirements (e.g., flood warning) be met with a given spaceborne observing system. However, the needs are numerous and so important that they should no longer be neglected.

This Workshop focused on identifying the needs for precipitation measurements from space and then resolving the various ways of meeting those needs. An attempt was made to specify observations in terms of accuracy, resolution, etc. according to the application. Although a broad consensus usually exists in a particular user community, it is not possible to specify the observational requirements alone because they are as diverse as the disciplines and applications previously mentioned would indicate.

Nevertheless, some focus on precipitation requirements emerged, particularly relating to global climate, in which space observations can and must play a crucial role. A survey revealed that monthly averages of global precipitation with an accuracy of 25 percent over  $(100 \text{ km})^2$  areas and daily totals of continental precipitation with an accuracy of 10 percent over  $(25 \text{ km})^2$  areas will satisfy in some way about 80 percent of reported requirements involving both research and applications. A review of the state of the art indicates that these accuracies and resolutions could be obtained through space technology supplemented by conventional methods.

At present, the most critical gap in global precipitation observations is over the oceans. Here it seems obvious that measurement from space is the only logical approach, and we should proceed to fill this gap without delay.

#### VISIBLE AND IR METHODS

A variety of visible (VIS) and infrared (IR) methods have been developed for observing cloud properties and using them as proxies for ground-level precipitation. These are by far the most simple and, indeed, the only space techniques for which substantial prior records exist. They are also the only ones that can and have been used with existing satellites. Although none of the VIS/IR methods appear to be applicable to all precipitation types and climatic regimes, even relatively simple schemes provide climatologically useful precipitation amounts for convective storms up to subtropical latitudes for sufficiently large areas,  $(100 \text{ km})^2$  and time periods of days to weeks. However, there is concern about the variability of any VIS/IR estimation scheme for particular precipitation types (e.g., stratiform) and comparative evaluation of a variety of techniques is needed.

The application of VIS/IR methods for geosynchronous satellites to precipitation estimates in individual storms is risky even though some success has been evidenced. We recommend that these methods be used with caution until further evaluated and then only to specify broad classes of rain rates or amounts. This approach appears to be useful for flash-flood warnings because it indicates amounts above hazardous thresholds. Nevertheless, calibrated radars are highly preferred for this purpose wherever they are available.

All VIS/IR methods would be improved through complementary measurements using spaceborne passive microwave radiometers over the ocean and suitable radar systems over land or ocean. However, the latter can now be flown only on low Earth orbiters (LEO's) which provide only two observations per day. Thus, in the near future, geosynchronous VIS/IR cloud proxy measurements will have to be relied upon to measure at least the diurnal variability of precipitation.

Recommendations for VIS/IR methods are as follows:

1. Continue the use of simple cloud-indexing schemes to produce climatologically useful rainfall estimates over land and the oceans.
2. Continue efforts to verify and automate the present National Earth Satellite Service (NESS) technique of estimating rainfall in support of flash-flood forecasting with due regard for the cautionary remarks above.
3. Because island stations have generally been used to calibrate the latter methods, assess the representativeness of the island data by calibrated radar (see ground truth). If improved shipborne rain gages or quantitative shipborne radar can be developed, also use these.
4. Evaluate and compare current and proposed VIS/IR and other methods within a carefully designed "experiment" in which ground rain-gage networks and/or well-calibrated radars are available (see ground truth).
5. Because hybrid methods involving VIS/IR and complementary systems appear to offer the greatest promise for most purposes, make them the focus of a development and test effort.
6. Make the following improvements in current practices and future systems: (a) increase coverage of LEO's to at least four observations per day; (b) maintain accurate absolute calibrations on all VIS/IR sensors; (c) increase visible brightness resolution to 8 bits; and (d) improve GOES IR resolution to 1 km.
7. Broaden the program for establishing a global cloud climatology (International Satellite Cloud Climatology Project (ISCCP)) to include oceanic rainfall.
8. Continue to support efforts for developing and testing improved techniques in support of agricultural interests (e.g., AgRISTARS\*).

## MICROWAVE RADIOMETRY

Microwave radiometry (MR) offers greater promise than VIS/IR because of the more direct physical relationship between the radiation and the precipitation. However, it is limited to oceanic regions in which background brightness temperatures are nearly constant. MR also suffers from errors caused by unfilled instantaneous fields of views (IFOVs), variable effective height of the rainfall, unknown cloud-water content, and variations in hydrometeor types, shapes, and phase in intense convective storms. The optimum wavelengths also have restricted dynamic range. However, simulations indicate that the most serious error can be overcome by using smaller IFOVs. MR appears to be especially useful as a supplement to VIS/IR methods for measuring stratiform oceanic precipitation.

In the millimeter wavelength (~3-mm) band, MR appears to be sensitive mainly to the depth and intensity of snow aloft and is useful as an adjunct to other methods in mapping the areas (but not the intensity) of precipitation over either ocean or land backgrounds. Because such wavelengths do not require inordinately large antennas, they currently provide the only real hope of mapping oceanic precipitation from geostationary satellites. (See the section on "soil moisture.")

---

\*Agriculture and resource inventory surveys through aerospace remote sensing



Recommendations for MR are as follows:

1. It is likely that future oceanic and polar missions will require improved high-resolution microwave radiometers such as the large-aperture multichannel microwave radiometer (LAMMR) for measuring sea-surface temperature, surface winds, and sea ice. Because such measurements require corrections for precipitation, a future LAMMR should also be optimized for measuring oceanic precipitation.
2. Over the oceans, a hybrid radar/microwave radiometer in the 1- to 2-cm band appears to be a viable option that should be explored in simulations and aircraft flights.

## SPACEBORNE RADAR

A variety of schemes for measuring precipitation from space were first proposed in a 1974 workshop on active microwaves (NASA, 1975). Some of these schemes still deserve consideration. Because prior thinking has often led to excessively sophisticated and costly systems, the present workshop has focused mainly on relatively simple concepts.

The most elementary system approach is to modify the Seasat-type (2.2-cm) radar altimeter by adding a precipitation mode. A slightly more complex approach is a dual-wavelength radar radiometer in the 1- to 3-cm band such as that developed in Japan for aircraft trials. This method combines the capacity of the radar to measure reflectivity near the top of the rainfall where attenuation is negligible and deeper into the rain by using the radiometers to correct for attenuation (over the oceans only).

The surface target attenuation radar (STAR) exploits the excellent relation between the attenuation coefficient and rainrate in the 1- to 2-cm band. The method uses surface echo cross sections measured in rain-free regions adjacent to storms or, in the case of land, values recorded previously in the absence of rain. Attenuation and rainfall are then deduced from the differences between actual and expected surface signal strengths. Two wavelengths are required for providing sufficient dynamic range in rain rate.

Another variant is the frequency agile rain radar (FARR), which uses the sensitive frequency-dependence of rainfall reflectivity relative to the very weak frequency dependence on the surface targets to distinguish rain from ground.

Finally, an adaptive pointing radar, which scans selectively and automatically only within the regions of clouds and probable rain that have been identified on images of a forward-viewing IR radiometer, solves the long-standing conflicts between the needs for high resolution, wide-swath width, and adequate signal-sampling time. Such an adaptive pointer may be applied to any of the radar schemes. At the expense of a sophisticated onboard computer, it overcomes the need for such brute force schemes as pushbroom antennas.

Recommendations for spaceborne radar are as follows:

1. A Seasat-type radar altimeter in the 2-cm band will be one of the key instruments on the next ocean topography and circulation mission. A simple modification would permit its use for precipitation measurements at nadir. Although the sampling would be poor, such data would serve as calibrations for either passive VIS/IR or MR schemes. We strongly recommend that a precipitation mode be included in any future radar altimeter.
2. A dual-wavelength STAR system should be subjected to a thorough feasibility study, developed, and aircraft flight tested. The method can also be used as a precipitation estimator near the melting level either with or without surface echoes as a reference.
3. The frequency agile rain radar (FARR) should be subjected to a thorough feasibility study, developed, and aircraft flight tested.
4. See recommendation 2 under "Microwave Radiometry."
5. An adaptive pointing radar system that selectively samples probable precipitation areas as indicated by a forward-viewing passive IR imager deserves serious consideration. Adapting such a method to the STAR or

FARR appears to offer the greatest hope for a global spaceborne precipitation measurement system. We strongly recommend simulations and aircraft flight trials.

6. Over the continental United States the bistatic radar method of Nathanson (this report) with a single transmitter in geosynchronous orbit and a multiplicity of ground-based scanning receivers warrants a thorough feasibility study and preliminary test.

## SOIL MOISTURE

For many agricultural and climatological purposes, soil moisture is the ultimate goal of precipitation measurements. Passive microwave radiometry in the 20- to 50-cm bands and active systems in the 5- to 8-cm band hold promise for useful estimates of soil moisture in the future. In the near term, various features of the time sequence of IR surface temperatures from geosynchronous satellites appear to be well-related to soil moisture. Variants of this method may also be used with IR observations from intercalibrated LEOs. Soil moisture is well correlated with the antecedent precipitation index (API). Also, with soil moisture, precipitation may be estimated through the moisture balance equation.

Recommendations for inferring soil moisture:

1. Precipitation and soil moisture should be considered in tandem.
2. On-going efforts for estimating soil moisture from geosynchronous IR observations and variants of this method should be intensified.
3. If microwave radiometric and radar methods result in useful estimation of soil moisture, they should also be evaluated for estimating antecedent precipitation.

## GROUND TRUTH

The lack of accurate area-wide ground-truth precipitation calibration facilities (PCFs) has impeded the full development and operation of a spaceborne precipitation measurement capability. The GARP<sup>1</sup> Atlantic Tropical Experiment (GATE) radar rainfall data appear to be the first useful data set available on oceanic precipitation. At present, rainfall data from ships and island stations are highly variable and are believed to contain large biases.

The development of retrieval algorithms by any space method, as well as the evaluation and comparison of competitive techniques, requires faithful and accurate depiction of the four-dimensional distribution of precipitation by ground-truth systems. The accuracy and precision of long-term measurements that involve either multiple instruments or a sequence of satellites and probable changes in methodology require a precise and accurate ground-based PCF that will continue in operation over the long term.

Recent developments in measuring rainfall by differential polarization radar/reflectivity methods (ZDR) and other dual-parameter techniques have demonstrated potential for greatly improved accuracy over standard radar techniques. This capability is especially important because coastal and island radars are required for ground truth over the sea. The NASA 10-cm SPANDAR<sup>2</sup> radar at Wallops Island, Virginia, is ideally located and is well-suited for these purposes. Any such ground-truth facility must also use rain-gage networks, disdrometers, and remote sensors such as microwave and optical attenuation links to ensure the best possible accuracy. A transportable transfer standard radar is also required for calibrations in a variety of climactic regimes.

Finally, considerable improvement and modernization is possible and is required in rain-gage technology (especially for shipboard use) and in data collection and management.

---

<sup>1</sup>Global Atmospheric Research Program

<sup>2</sup>Space Range Radar

Recommendations for ground truth measurements are as follows:

1. We strongly recommend the establishment of a PCF consisting of a sensitive high-resolution 10-cm radar with differential polarization, substantial surface rain-gage networks, and microwave and optical links. The primary PCF should be at a convenient coastal station that experiences a variety of precipitation types. The NASA Wallops Island SPANDAR radar is a prime candidate for such a PCF. The NOAA National Severe Storms Laboratory (NSSL) radar facility is similarly useful for such a PCF in the midwest.
2. A similar but more modest PCF is needed for the long term in the tropical Pacific, perhaps at Johnston Island, where land effects should be minimal. A transportable transfer standard radar is also proposed for shorter duration ground-truth experiments in various climatic regimes. The ground-based NEXRAD radars now under development should be similarly equipped and ultimately become secondary precipitation standards within the United States.
3. At the earliest opportunity, we should conduct an extended ocean expedition to obtain accurate radar rainfall data similar to but better than those gathered during GATE. Various land-based meteorological experiments involving well-calibrated radars and rain-gage networks that have been proposed for the future should be exploited as targets of opportunity for ground-truth evaluation of candidate spaceborne methods.
4. Promising new techniques for ground truth should be developed. Some candidate techniques are: path-integrated microwave and optical extinction, electro-optical disdrometers (especially on ships), and low-cost vertically pointing Doppler radar. Simple, reliable, rugged, and easily deployable data collection platforms communicating through satellites should also be developed.

### Sampling

The precise measurement of precipitation from space is fraught with numerous problems including those relating to sampling. Sampling problems, can however, be lessened through concurrent development of the observing strategy design with the precipitation measurement system design. In this regard, the general principles of proper experimentation (e.g., clear specification of the objectives, measurement system, estimators, and data management) must be given careful attention.

Five categories of statistical problems that derive from the requirement that precipitation be properly sampled are:

- An agreed upon definition of precipitation requirements in terms of resolutions and accuracies
- The determination of the stochastic and historical characteristics of precipitation on space scales up to an orbital swath width of 1000 km to 1500 km and time scales ranging from hours to months to be used for (a) selecting sensor scanning patterns, revisit times, and orbital characteristics; and (b) determining the transfer function between the "true" precipitation and that observed by a remote sensor
- The development and modification of statistical theory to handle the multivariate nature of the precipitation process
- The selection of appropriate statistics for intercomparison with alternative systems for determining precipitation and for comparison with accurate "ground truth"
- The special problems of diurnal variability and the possible use of periodic measurements from low Earth orbiters supplemented by sequences of near-continuous IR proxy measurements from geosynchronous earth orbiters.

Problems in all of these categories need to be addressed for numerous precipitation types and climatic regimes. The establishment of precipitation models and their statistical properties is one of the primary motivations behind the earlier ground truth recommendations. Furthermore, we believe that the time has come for a field comparison of alternative satellite precipitation estimation systems to provide information and direction to future designers.

It must be emphasized that the success of remote sensing techniques will depend greatly upon the integration of applicable sampling theory and the establishment of a firm foundation of statistical properties of area-wide

precipitation. This is particularly true for an adaptive or selective scanning radar approach. (See spaceborne radar.) The data required to develop such a foundation can be obtained from an adequate area-wide ground-truth system (see ground truth) such as will be provided by the proposed NEXRAD network. Useful data sets based on special experiments such as GATE can be exploited to conduct the necessary simulations of sampling strategies and the expected accuracies.

Recommendations for sampling are as follows:

1. Conduct a field evaluation of satellite techniques that are available now for estimating precipitation with adequate ground-truth.
2. Improve or further develop sampling theory and estimation methods for univariate and multivariate stochastic processes to support estimation of ground level precipitation.
3. Pursue the characterization of precipitation over a wide range of weather and climate regimes and geographical locations.
4. Further develop understanding of sampling requirements based on analysis of existing data and results from the field evaluation experiment to provide the design criteria for the sampling strategy of a future global precipitation experiment.
5. Improve the "adjustment schemes" for handling subscale precipitation processes.
6. Develop physical and stochastic models for simulating precipitation processes associated with d. and e. above.

#### Conclusion

The measurement of precipitation from space on a global scale is a formidable problem because as yet there are no guaranteed methods which can be relied upon to perform under all circumstances around the world. Nevertheless, we already have some VIS and IR techniques that provide climatologically useful data in the subtropical belt. Also, over the oceans we are quite confident that these methods can be extended to extratropical regions by means of improved microwave radiometers. The use of combinations of measurement systems should be most valuable in filling the great gaps in our knowledge of oceanic precipitation, and it would serve a broad spectrum of users both in climate research and global weather prediction.

Furthermore, for the first time, we now have a set of conceptual methods including spaceborne radar, either by itself or as part of a hybrid system, which show promise of operating over both land and ocean. At the very least, these approaches deserve serious feasibility studies and field trials. In short, the needs have been well articulated and the technology is within reach. Therefore, it is time to proceed with a strong and well-ordered program of study and development as summarized here and as detailed in this report.

9  
Y

## 1. INTRODUCTION

## 1. INTRODUCTION

The workshop on "Precipitation Measurements from Space" was organized by the NASA/Goddard Laboratory for Atmospheric Sciences with the joint participation of the National Oceanic and Atmospheric Administration's (NOAA's) National Earth Satellite Service and the National Climate Program Office (NCPO). This workshop was a follow-on activity associated with the Climate Observing System Study (COSS) initiated by NASA in 1980.

At the first COSS workshop (1980), it became clear that precipitation, one of the fundamental descriptors of climate, was not being adequately measured on a global basis. Precipitation data over the oceans are particularly sparse. Furthermore, such global data requirements are not being addressed under other planned earth and environmental observational programs. Subsequently, the importance of and need for space measurements of global precipitation were reiterated and more strongly emphasized at the joint ICSU/COSPAR Commission A Study Conference (1980) concerning space observations for climate research. Thus, the next logical step was to explore, as a high-priority item, ways to obtain more complete information on this key parameter.

There is a broad spectrum of needs for precipitation measurements, both for research and for applications. Experimental satellite techniques for rainfall measurements have been tested but often with ambiguous results, particularly over land areas. Now, with the emergence of the National and World Climate Programs, precipitation measurement has taken on added dimensions. Precipitation is not only a key climatic index with a host of practical implications, but it is a major component of both the global energy and water budgets. For these reasons, precipitation must be observed accurately and with reasonable uniformity over the globe, presumably by satellite methods.

This does not imply that the sole driving force for improved precipitation measurements are the needs of the climate program, or that satellites alone are likely to be able to do the job. To the extent possible, the observing system should be capable of meeting the full range of needs, from local flood warnings on up. Also, where necessary and possible, the observing system may be a composite of two or more techniques (e.g., satellites and ground radar or gages).

With these ideas and views in mind, the precipitation workshop was planned with the following primary goals:

- To critically assess the various existing and proposed methods for measuring precipitation from space
- To establish research and development guidelines for realizing near-, intermediate-, and long-term objectives.

In connection with these goals, the following six key topics and related questions were identified for particular attention at the workshop:

### ● REQUIREMENTS FOR PRECIPITATION MEASUREMENTS

It was not the intention at this workshop to redevelop specific measurement requirements but rather to survey and synthesize documented user needs for precipitation data, including the disciplines of climate, agriculture, hydrology, severe storms, and global weather. For climate, requirements have been well documented by the Global Atmospheric Research Program (GARP) (1975), the NASA Climate Program (1977), the National Climate Program 5-year Plan (1980), and the NOAA Climate Program Plan (1981). Other precipitation requirements are identified in the more specialized plans of various agencies, by the World Meteorological Organization (WMO) in a number of program plans (e.g., WMO, 1980) and by various research disciplines and commercial interests. To obtain better insight on current thinking in all areas, however, a wide-ranging survey was conducted before the workshop. A summary of these results is included in the body of this report under "Requirements."

### ● SAMPLING PROBLEMS

Precipitation is intermittent in space and time, and its statistical characteristics may depend upon precipitation type, geographical location, season, and time of day. Thus, one session of the workshop was devoted to evaluating the impact of the statistical nature of precipitation on the choice of sampling strategies for both space and "ground-truth" measurements. Also, the determination of spatial and temporal sampling characteristics required by observational systems for meeting measurement requirements was an important workshop objective.

- GROUND-TRUTH MEASUREMENT SYSTEMS

Ground-truth measurements are a fundamental requirement for both designing the observing system and for validating space precipitation measurements, therefore, the specific needs for various ground-based techniques and combinations require careful study. There are important questions concerning the adequacy of rain-gages, density of gage networks, use of radar as the ultimate tool, and the need for upward-looking microwave radiometers. The selection of representative geographical locations for ground-truth measurements and/or benchmark sites is of obvious importance.

- VISIBLE (VIS) AND INFRARED (IR) TECHNIQUES

The purpose here is to address the basic VIS and IR Satellite methods for estimating rainfall, and the accuracies achieved in various time/space domains. Significant limitations in terms of type of rain (convective/stratiform), transportability of the method from one geographical region to another, satellite viewing conditions, diurnal effects, types of orbit, etc. are key questions that must be answered.

- MICROWAVE RADIOMETRY AND HYBRID TECHNIQUES

The basic theory and performance of microwave radiometry for making precipitation measurements must be reassessed for two purposes: (1) to see how the results of previous experiments (ESMR-5\* and SMMR) may be better understood and improved, and (2) to provide insights for optimizing future instruments. Furthermore, every opportunity should be taken to compare microwave data against other ground-based information such as those gathered during the GARP Atlantic Tropical Experiment (GATE). Also important is the comparison of microwave radiometry precipitation measurement techniques with VIS and IR methods and exploring ways in which they can be used in combination to provide improved data.

- SPACEBORNE RADAR

The potential of spaceborne radar as the ultimate tool for making direct precipitation measurements over the entire globe must be seriously considered. A number of approaches can be taken that involve conventional pulsed radar, coherent Doppler, dual wavelength, and/or polarization, etc. All these possibilities must be subjected to detailed feasibility studies. An important consideration is the possible combination of active and passive microwave techniques and hybrid schemes involving VIS and IR channels. The goal is to exploit advances in technology that promise to overcome the long-standing obstacles to the effective use of spaceborne meteorological radar.

The findings of the working groups for these topics are reported in the next six sections. Additional details are contained in the reprints (Appendix D) of the papers presented at the workshop.

## REFERENCES

- Global Atmospheric Research Programme, 1975: The Physical Basis of Climate and Climate Modeling, WMO-ICSU Joint Organizing Committee, GARP Publication Series, No. 16. Geneva, Switzerland.
- ICSU/COSPAR, 1980: Space-Based Observations in the 1980's and 1990's for Climate Research: A Planning Strategy. Commission A report to the Joint Scientific Committee for the WMO/ICSU World Climate Research Program.
- National Aeronautics and Space Administration, 1975: Active Microwave Workshop Report. NASA Report SP-376, 270-367. Washington, D. C.
- National Aeronautics and Space Administration, 1977: Proposed NASA Contribution to the Climate Program. Washington, D. C.

\*Nimbus 5 electrically scanning microwave radiometer

National Aeronautics and Space Administration, 1980: Climate Observing System Studies: An Element of the NASA Climate Research Program. Goddard Space Flight Center Workshop Report. Greenbelt, Maryland.

National Oceanic and Atmospheric Administration, 1980: National Climate Program – Five-Year Plan. NOAA S/T 79-153. Washington, D. C.

National Oceanic and Atmospheric Administration, 1981: The NOAA Climate Program Plan. Washington, D. C.

World Meteorological Organization, 1980: The role of satellites in WMO programmes in the 1980's. WMO Planning Report 36, WMO-No. 494, Geneva, Switzerland.



N83 25270

21

## 2. REQUIREMENTS WORKING GROUP

### PARTICIPANTS

Dudley G. McConnell, Chairman  
Paul H. Hwang, CoChairman  
Otto W. Thiele  
Eugene M. Rasmusson  
Yale Mintz

Norton D. Strommen  
Robert F. Dale  
Richard K. Farnsworth  
Robert F. Adler  
John H. E. Clark

2. REQUIREMENTS

2.1 SUMMARY OF REQUIREMENTS AND RECOMMENDATIONS

2.1.1 Summary of Requirements

Although as much of the full spectrum of precipitation measurement requirements as can be identified is considered in the proceedings of this workshop, the focus here is on climate. It was recognized at the outset that, in proceeding toward a global climate observing system, much (if not most) global climate information would result from operational systems (both satellite and conventional), and, conversely, any space system or technique that might be proposed for climate measurements must meet as many operational weather and real-time applications requirements as possible. It is already apparent that some precipitation requirements, in both operations and research, have such stringent coverage, resolution, temporal, and accuracy constraints that they obviously cannot be completely met through remote sensing from space within the foreseeable future. It is equally obvious that current ground-based facilities (rain gages and radar) are also inadequate and would have to be augmented. Nevertheless, a large number of climate applications, assessment, diagnostics, predictability and research problems can and must be addressed with space data where conventional methods are clearly impractical.

The major gaps in the availability of useful global precipitation information are as follows:

- a. Over the Oceans
- b. Over Land, where rain gages and ground radar systems are few or nonexistent. Few continental areas of the world other than North America and Europe even approach adequate ground-based measurement systems.
- c. Detection and measurement (or estimation) of cyclonic (stratiform) precipitation by using space observations. (The several visible (VIS) and infrared (IR) satellite techniques that are now in use and that have potential global capability are almost entirely restricted to convective precipitation detection.)

From a relatively detailed survey of precipitation requirements and through insights gained from the workshop participants, it is apparent that about 20 percent of the requirements (i.e., spatial resolutions below 10 km with correspondingly high temporal and accuracy requirements) are over land and will have to be met with ground-based systems in the foreseeable future. On the other hand, it is also apparent that about 80 percent of reported precipitation requirements for a wide range of purposes can be met in some way through space technology supplemented by conventional methods. The climate research and applications requirements falling into this 80 percent category can be summarized as follows:

	Spatial Resolution	Temporal Resolution	Accuracy
Global	100 by 100 km	Monthly averages	25% 10%
Continental	25 by 25 km	Daily totals*	

\*With sufficient sampling to detect diurnal component.

Table 1, which appears later, contains more detail about requirements for specific applications.

On the basis of current capabilities reported in other sessions of the proceedings, it is particularly encouraging to note that a large share of this comprehensive requirement could probably be met now by using existing satellite techniques and conventional measurements. Section 4 describes VIS and IR satellite methods. The "Requirements" working group specifically recognized that data are now available for:

- providing useful information to climate-oriented users
- enabling the systematic evaluation of the data and identification of specific needs for further improvements, and

- promoting user familiarization and the development of user methodologies including satellite-derived data.

For long-term global climate research needs, and even for certain applications problems, the primary goal is to obtain precipitation information over land and oceans in a representative way for unambiguous comparative analysis. The measurements must also have long-term stability and reliability for effective analysis of monthly, seasonal, and interannual fluctuations. Absolute accuracy is a secondary requirement.

### 2.1.2 Summary of Recommendations

The following recommendations are based on the recognition that "requirements," though well-documented, are so variable and dependent on so many factors that further refinements would not be realistic at this time. Accordingly, we should (1) continue to develop useful precipitation information from available sources and (2) plan for new techniques where appropriate; specifically, we should:

- Develop stable records of indices of precipitation (even rain/no rain discriminators) until quantitative techniques have been proven. All such records should be easily accessible by specific geographical location.
- Process the operational data to provide statistical distributions (within 2½-by-2½ grid square or 1-by-1 degree if possible) of cloud IR temperatures as a useful index of precipitation for diagnostic studies of the tropics and continental summers. The data thus compacted would be in a form suitable for further time-averaging for climate purposes.
- In view of the paucity of global oceanic rainfall information, develop a record of base-period means for the period (4 years) of ESMR-5 microwave data. This would involve the use of microwave data for middle latitudes and use of the IR data supplemented by the highly reflective cloud (HRC) (Kilonsky and Ramage, 1976) data over the tropical Pacific to tune the microwave data for extension to the tropical Atlantic.
- Establish a precipitation climatology project, develop refined precipitation data products from the FGGE data set as a starting point, and expand the data sets both forward and backward in time as available data and verified new techniques permit.
- Because the proposed International Satellite Cloud Climatology Project (ISCCP) promises to compile and archive extremely valuable global cloud information, the project should be aware of and include the needs for precipitation in the design of the archive.
- Develop satellite precipitation estimation techniques in conjunction with improvements in terrestrial techniques to enhance the validity of both approaches and to facilitate user acceptance. With user feed backs, proceed with the development of long-term reliable precipitation records and tailored data sets that have been specified and justified.
- Develop a space-based capability for ocean precipitation measurements. In the meantime, expand oceanic precipitation data collection through improved techniques on ships of opportunity.

## 2.2 DISCIPLINE-ORIENTED REQUIREMENTS – GENERAL

The research and operational communities have different points of view. Researchers must appreciate the limitations and constraints on the data, but, to do so, they must receive adequate documentation regarding the measurement and data-base development. As techniques improve, researchers will want to be able to reprocess the original data on certain occasions. On the other hand, because operational users need a readily usable product, reliability and timely communications are key factors. The following paragraphs describe significant operations and research considerations.

### 2.2.1 Operations

- Reliability. Operational users must be assured of a continuous flow of data that match or surpass the reliability of existing systems. Thus, system design should avoid single points of failure (e.g., at a downlink site) that threaten the entire system.

- **Cost.** In the severe budget environment and the likelihood of spreading user charges, the space-acquired data must be cost-competitive with existing data sources. The system might be designed to meet requirements at modest cost and stringent requirements (high spatial and temporal resolution) at higher cost.
- **Timeliness.** Most operational users provide their output at specific times. Therefore, the input data must be available at specific intervals. This often becomes a communications problem for instance to communicate rainfall rates to hydrologists who make flash-flood forecasts.
- **Compatibility with User Applications Techniques.** The space-acquired information must be furnished in usable amounts and in the proper form for insertion into user systems. Thus, the data-handling system must convert satellite-sensed data (radiances) to geophysical data appropriately averaged and formatted.
- **Operational climate users require a stable record.** Therefore, if changes in the instrumentation or data-handling process disturb the continuity of the record, climatological users must be able to adjust.
- **In general, satellite techniques must show advantages over existing methods if they are to be adopted.**

### 2.2.2 Research

Many of the operational considerations also apply to researchers, but, in addition, researchers specifically want: (a) access to the raw data, (b) detailed calibration and registration information, and (c) documentation on algorithms, programming, etc.

## 2.3 SPECIFIC DISCIPLINE CONSIDERATIONS

### 2.3.1 Global Climate

2.3.1.1 **Operations and Services.** Climate diagnostics consists of the study of climate fluctuations whose time scales are longer than the lifetime of typical weather systems but shorter than the time scales of climate normals. Some examples are blocking episodes, pronounced seasonal anomalies, global-scale atmospheric teleconnections, and interannual-scale ocean-atmosphere oscillations (e.g., the Southern Oscillation). Diagnostic precipitation data are required for evaluating surface hydrological parameters (e.g., precipitation, runoff, and soil moisture, the large-scale atmospheric hydrologic cycle, and the latent heat contribution to the atmospheric heat balance).

Although the specific precipitation data requirements depend largely on the particular application, they tend to cluster on the following scales:

- **Spatial scale** – Large regional to global
- **Spatial resolution** – 200 to 500 km
- **Time scale** – Few weeks to few years
- **Time resolution** – Week to month

Note that accurate averages for diagnostic time/space scales require a much finer time/space network of basic precipitation measurements. In this regard, the basic data requirements may not be very different from applications with more stringent time/space averaging requirements. The accuracy requirements are even more difficult to define. In areas of low precipitation, the absolute accuracy requirements may be quite high, whereas, in regions of high precipitation, the requirements are usually less stringent. In general, the accuracy should be adequate for defining significant year-to-year variations.

Although highly accurate precipitation estimates on the time/space scales specified would be desirable, a great deal of information can be obtained from simple but stable indices of precipitation or even a few levels of discrimination of precipitation amount. The requirement for precipitation estimates over much of the Earth's surface, coupled with the requirement for a relatively coarse time/space resolution, points to the use of a statistical rather than a detailed life-cycle approach for generating the long and stable time series required for diagnostic applications.

Future research and developments in sensor systems will undoubtedly lead to improvement in the accuracy of precipitation estimates from remote sensors. However, convincing evidence indicates that current operational IR and VIS data, if properly processed, are adequate for estimating precipitation on diagnostic time/space scales over the areas of the Earth, including the tropics and the midlatitude continents during the warm season, where precipitation is primarily convective in nature. The key requirements for broadscale use of these data for operational and research purposes is that the statistical summarization required for reducing the raw pixel values to a more manageable data set of frequency distributions of equivalent blackbody temperatures be incorporated into the basic processing operation.

**2.3.1.2 Model Development and Research.** The combined use of precipitation measurements and numerical general circulation models can greatly advance our understanding of the dynamics of climate and help in making short-period (i.e., monthly and seasonal) climate predictions with such models (Mintz, 1981).

The interaction between the condensation heating field and the motion field is especially strong in the tropics. However, we now have neither adequate information about the distribution of the condensation heating in space and time nor about the motion field, which, within the tropics, cannot be adequately approximated from the pressure field. We must know much more about at least one or the other of these two strongly coupled fields. Insofar as the condensation heating is concerned, we must know the corresponding average daily precipitation, averaged for areas of the order of  $(100 \text{ km})^2$ , with an accuracy in this time and space average of about 0.5 mm/day.

Although the precipitation itself is not a physical-state variable, precipitation over the continents can be used to initialize one of the most important physical-state variables of a climate model (namely, the soil moisture). This can be done by soil moisture budget calculations from daily (or weekly) amounts of precipitation at the resolutions and accuracy previously indicated.

### 2.3.2 Agricultural Uses for Precipitation Information

Precipitation data required for meeting the needs of agriculture have very different time and spatial resolution requirements. The major categories are strategic and tactical planning for on-farm decision-making, monitoring, and real-time assessment for large-crop regions and research. Timeliness and cost of data acquisition are critical in the first two categories, but accuracy needs are not as stringent ( $\pm 20$  percent). The last category, research, has very high accuracy requirements, but it is generally not as tightly constrained by time and cost considerations.

Although data needs are limited primarily to the crop-growing season and regions, in cases where irrigation is widely used, monitoring of data from outside water-sources regions is important. This would include current precipitation and snowpack build up during the winter season to evaluate potential water supplies for meeting the next season's irrigation needs. Precipitation data may or may not be converted to an index, (i.e., soil moisture, etc. for aiding users in decision-making). Agricultural users would not need precipitation information over the ocean. Most agricultural users consider the satellite data as a potential source to incrementally add to the information obtained from ground observations. In summary, precipitation is used in agriculture for:

- a. Strategic (climate) planning and tactical (weather) operations on the basic production unit – the farm
- b. Precipitation impact assessment on agricultural production on a state, regional, national, and international basis for planning
- c. Research in support of a and b
- d. Daily average precipitation for daily soil-moisture budgets for small areas (experimental plots) for irrigation planning and management decisions.
- e. Daily end-of-day (weekly, monthly) average precipitation over "county" for crop-reporting of district-size areas  $(20 \text{ to } 100 \text{ km})^2$
- f. Spectrum of hourly rates over small areas for soil erosion, nutrient, and runoff losses to larger areas

Key points related to agricultural requirements and applications are:

- a. The most rapid payoff comes from immediate applications to daily problem-solving and decision-making.
- b. The use of climate models would not provide an immediate payoff. These would be used in longer range planning.
- c. The state of the art of precipitation measurements from space is not as good as the existing surface network for measuring precipitation in the United States and Europe, but, for requirement a, these measurements may improve surface-derived means for other areas of the world, especially for verifying areas that receive no precipitation.
- d. Obtaining mean precipitation for county-size areas (40 by 40 km) would go a long way toward fulfilling both requirements a and b.

### 2.3.3 Hydrological Uses for Precipitation Information

Precipitation is one of the most important processes in the hydrologic cycle. It can be viewed as the "driving force" in many hydrologic models. Proper location of rainfall accumulations in time and space influences predictions on which flood warning, reservoir management, and water-supply decisions must be made.

2.3.3.1 Data Exchange. A key concern is supporting better exchange of existing water-related data before requesting support for new methods of acquiring the same kinds of data. The community of water resource data users should attempt to support individual data procedures in making their products available to all interested parties in an ADP usable form. For example, the precipitation and soil-moisture information routinely generated by the River Forecast Centers of the National Weather Service (NWS) is of significant interest to agricultural and climatological data users.

2.3.3.2 Data-Error Considerations. It is particularly important to determine the maximum allowable error for data in hydrology and other related fields and to assess the temporal and spatial resolutions associated with these maximum allowable errors. Data specifications submitted by users of rainfall data are often for the optimum resolutions. This is not surprising because, when asked for only one set of numbers, users request the best. Often specifications developed in this manner require more detail than can be used operationally although they may be appropriate for research studies. These specifications may impose requirements beyond the current state of the art and, lacking near-term benefits, discourage investment in any remote-sensing methods. Publishing the least-stringent beneficial requirements would show greater opportunity for success and encourage the investment of time and capital into acquiring practical data.

2.3.3.3 Data Requirements for Forecasting. Data required for hydrologic forecasts can best be discussed by dividing the forecasts into three classes:

- Flash flooding
- River stage
- Water-supply forecasts

Flash-flood advisories are issued primarily to save lives. They alert the public, who must then determine where danger threatens and make an immediate response. The detail in a forecast depends on the spatial and temporal resolution available to the reporting system and the delay time from measurement of data to the dissemination of the warning. Although optimal temporal resolution would be about 10 minutes with spatial resolutions of a few kilometers, temporal resolutions of 1 to 6 hours with spatial resolutions as coarse as 10 to 40 km would give beneficial information. This is especially true in areas that do not have weather radars in which the rain-gage density is very low.

River-stage forecasts are issued to aid in reducing property damage, as well as in preserving lives. These forecasts are issued to alert the public to the extent of flooding and, in some cases, the times that a river is expected to rise to critical points, such as flood stage. A flood forecast must be issued to give the public sectors that are prone to flood damage the maximum possible response time to protect life and property. Because the expense involved in protecting

or moving property may be large, it is important that the forecast neither underestimate the flood, thus permitting excessive flood damage, nor overestimate inundation, resulting in unnecessary expenses in responding to the flood warning. The degree of accuracy required for this forecast is relatively high for the data to be input to the forecast model. Models used by the National Weather Service are generally run on areas at least as large as headwater basins that are about  $(500 \text{ km})^2$ . Although models are being adapted to run on an hourly basis, they are now usually run on a 6-hour basis. On the basis of these requirements, a satisfactory temporal resolution would be 1 to 6 hours with a spatial resolution of about 20 km. However, beneficial use can be made of data with a 24-hour temporal resolution and spatial resolutions nearing 1 degree of latitude or longitude.

Water-supply forecasts are used to estimate water supplies for urban and agricultural uses from days to a few months into the future. A water-supply-forecast model generally estimates the rainfall or snowmelt that is expected to flow into a reservoir or other collecting point from precipitation observed up to the time that the forecast is produced and from precipitation that can reasonably be expected to occur between the time the forecast is issued and the projected time of the forecast flow. Desired spatial resolution for input data to this forecast model would vary depending on the catchment, but could be about 20 to 200 km. Although temporal resolutions as large as 1 month would be useful, the shorter the interval between issuance of the forecast and the expected occurrence of the forecast flows, and the more frequently the forecasts are to be issued, the smaller the temporal resolution would need to be.

**2.3.3.4 New Techniques.** The economics and logistics of new techniques should be discussed when the technique is first publicly described. Published discussions of new techniques and systems for data acquisition should consider the economical and logistical requirements for operational use, as well as the technical details of the measurement. Developers of rainfall estimation systems should be aware of the most likely uses of their data, the expected initial unit price of the data, and how it fits in with any existing systems. By considering the operational systems for which remotely sensed data could be used, the researcher can do much to prevent data-processing problems from delaying or preventing their method from going into operational use. By understanding the achievable accuracies with existing versus proposed data systems and the corresponding unit data costs, the developer can compare the costs and the advantages to be obtained by a new method with those of any current systems and thereby be better able to direct his research efforts and to portray his or her method in the best possible light.

#### 2.3.4 Severe Thunderstorms and Local Weather

Because of the rapidly changing nature of intense mesoscale phenomena, the time and space resolutions of the necessary observations probably have the most stringent requirements of any time/space scale. The spectrum of uses and potential uses for rainfall information in the severe storm area ranges from the direct use of rain-fall-rate information in flash-flood detection and study, to tropical-cyclone rain-fall and its relation to storm energetics and intensification, and to model initialization and verification with rainfall data.

The observational requirements vary from application to application. Although some of the requirements could be met with low-orbit satellite observations, the high time frequency (down to tens of minutes) of some of the requirements dictates geosynchronous observations. This high altitude negates most ideas of a "direct" observation of rain rate with microwave techniques, but does not preclude a hybrid technique with a microwave rain/no rain sensor to give coarse rain boundaries and magnitude to be estimated from cloud-top information derived from VIS and IR channels.

For flash-flood detection, high time and space resolution information is needed for rainfall rate, especially at higher rain rates. Although this information is usually obtained from radar data, recent attempts have been made to obtain useful data on the necessary time and space scales from geosynchronous satellite VIS and IR (window) data (Scofield and Oliver, 1977; Griffith et al., 1978). These techniques depend on empirical relations between satellite observation of cloud parameters and radar or rain-gage estimates of rainfall. Although clouds are correlated with rainfall, the lack of a strong physical basis for the empirical relations make the techniques susceptible to errors when applied to various geographical, seasonal, or synoptic situations.

Observations of tropical-cyclone rainfall over water are important for: (a) studying and monitoring storm latent-heat release and rainfall patterns in relation to storm energetics, (b) estimating rainfall potential and land fall, and (c) model initialization of tropical-cyclone models. Using rainfall-rate information deduced from the EMSR-5, Adler and Rodgers (1977) and Rodgers and Adler (1981) have shown that the data are useful in determining the

rainfall characteristics of these storms and that the data appear to be potentially useful in monitoring and making short-term prediction of their intensity. In addition, knowledge of total storm rainfall and rainfall distribution in the storm just before land fall may be helpful in forecasting coastal flooding.

Regional-scale and mesoscale numerical models are important in forecasting and understanding precipitation events. However, precipitation information should also be important in initializing and verifying such models. Numerical models of this type are typically initialized with temperature, pressure, moisture, and wind information at synoptic scales. Information at smaller scales can be added through low-orbiter sounding data, geosynchronous sounding (VAS), and some "cloud-track" winds. However, rain-rate data would provide indirect evidence of divergence and the ageostrophic component of the flow on subsynoptic scales. Tarbell et al., (1981) used this approach to indicate a forecast improvement when using observed (rain-gage) rainfall against no rainfall information. Rainfall-rate information may also be useful in initializing tropical-cyclone models.

Rainfall information is also important in verifying regional models because it is one of the most important forecast variables on this scale and it is the only variable routinely observed at the mesoscale, even with rain gages.

### 2.3.5 Global Weather

Meteorologists appreciate the fact that moisture can play an important, if not dominant role, in supplying energy to tropical and extratropical weather systems. In the tropics, where the air is almost saturated, only the slightest amount of uplift is required to initiate the release of vast amounts of latent heat to fuel systems as diverse as convective cloud clusters and hurricanes. The role of latent heating on extratropical systems is much more subtle. Although the primary energy source from synoptic-scale systems is often the release of gravitational potential energy through the sinking of cold air and the rising of warm, the latent heat that is eventually realized through slow uplift of large masses of air appears to significantly modify the evolution of the system.

Midlatitude mesoscale systems are also fueled by latent-heat release but in a different manner. The dominant mode of uplift is convective, such as that associated with convective cells in a squall line. In many cases, after the systems are initiated, they are driven mainly by the convective heat release, and larger scale baroclinic energy conversions play only a minor role.

Through the use of conceptual models, such as convective instability of the second kind (CISK), dynamicists have understood the consequences of latent-heat release on tropical systems, despite the paucity of rainfall and moisture data. The more subtle effects of latent heating on extratropical systems will require much more extensive observational coverage of moisture and precipitation for understanding its consequences. The flow chart in Figure 1 will help in understanding some of the effects of water on a synoptic-scale system. Horizontal and vertical motions both affect the distributions of liquid water and water vapor. When vapor condenses the resulting latent heating can in turn create horizontal temperature gradients and vertical motions result to maintain a state of geostrophic and hydrostatic balance. Thus, a complicated nonlinear interaction occurs between the moisture and liquid-water distributions on one hand and the motion field on the other through the agency of latent heating. An indication of how much condensation, and thus latent heating, is occurring is provided by the field of precipitation.

The conclusion is that precipitation measurements alone will not enable us to unravel the effects of latent heating on synoptic-scale systems or the general circulation of the atmosphere. Satellites, in conjunction with conventional observations, must provide simultaneous distributions of water vapor, liquid water, and precipitation if the complex interactions between the motion fields and the moisture fields are to be understood.

There are simple methods of discerning the immediate effects of latent heating on vertical motion fields, derived by solving the thermodynamic equation of the quasi-geostrophic omega equation, but it is impossible to check the accuracy of these techniques without the ground truth provided by reliable moisture, liquid-water, and precipitation measurements.

A frequent problem in analyzing precipitation data is that they tend to be very spotty. Local values of rainfall rates are strongly influenced by orography, and thus a single station may not be representative of regional rainfall rates. Furthermore, if convective precipitation is occurring in a system, the proximity of a station to a cell can completely influence the rainfall rate and mean rates over an area are difficult to evaluate. Thus, it is often essential to measure precipitation with a very dense network.



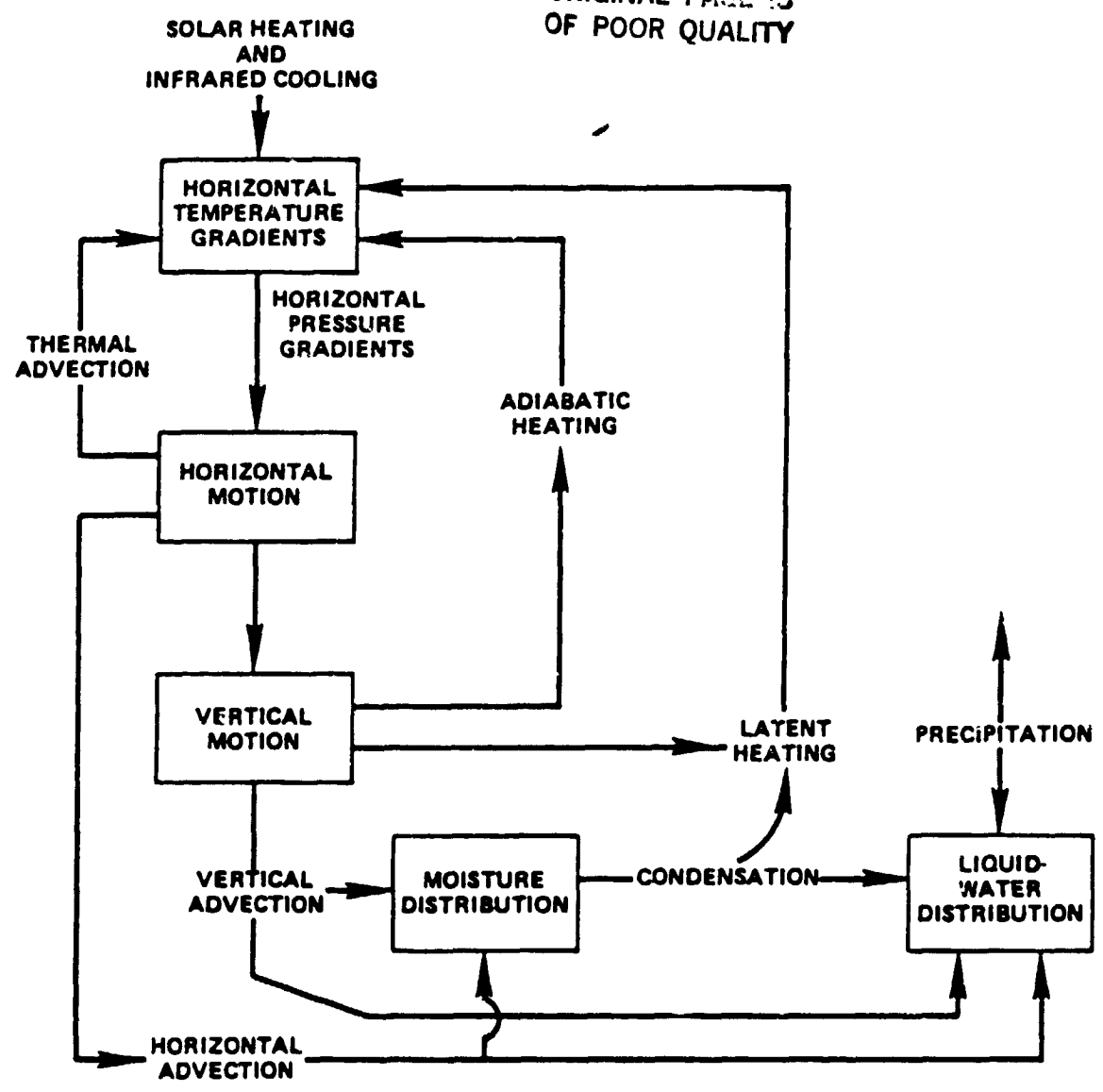


Figure 1. The Role of Moisture and Liquid Water in a Synoptic System

To develop a thorough understanding of moisture as it affects not only the general circulation but the synoptic and mesoscale systems, we must be able to sense precipitation over a fairly dense network of stations and simultaneously sense vapor and liquid-water distributions. Unfortunately, precipitation measurements are lacking for oceanic regions where satellite microwave measurements of total liquid-water content of the atmosphere are apparently straightforward. Making microwave measurements of liquid water over land is difficult because of the rapidly varying brightness temperature of the ground, but precipitation measurements are possible.

Global requirements for precipitation measurements are 3-hourly measurements with an average separation between stations of no more than 100 km, at least initially. The present network of stations over North America could probably be extended to satisfy this requirement. However, coarser scale measurements of vapor and liquid water must also be available. The conventional radiosonde network could provide the vapor data, but technology does not exist for providing the liquid-water data unless the NOAA radar network could be used for this purpose.

## 2.4 REQUIREMENTS ANALYSIS

In an attempt to develop a meaningful precipitation measurement specification for this workshop, a rather exhaustive inquiry of "requirements" was made. The intent was to form a realistic basis for climate observational system design considerations and for developing techniques and processing strategies for obtaining useful climatic data from existing sources. Although the emphasis was on climate, precipitation requirements for all identifiable disciplines and applications were reviewed.

Although a better recognition and description of certain requirements, including some refinements resulting from the workshop deliberations, broad requirements as outlined in various source documents (such as the Global Atmospheric Research Programme Publication 16 (1975), The Proposed NASA Contribution to the Climate Program (1977), the Role of Satellites in WMO Programmes in the 1980's (1980), and the Climate Data Management Workshop Report (1979), remain essentially valid. For a number of operational and special research applications, however, more detailed requirements, usually in terms of higher resolution and accuracy, are indicated, and some of these have been reflected in the foregoing subsections. Both the detailed and the broader needs for precipitation measurements indicate that the spectrum of "requirements" is almost limitless. This became especially apparent when a survey was conducted in preparation for this workshop. The survey was wide-ranging to obtain as comprehensive a view of precipitation information needs as possible. Although climate was the primary interest, it was necessary for practical reasons to assess the extent to which other measurement requirements could be met. The broad spectrum of the user community from which information was sought included state climatologists, the academic research community, and government and private organizations concerned with operations, research, and applications in the fields of climate, weather, agriculture, hydrology, forestry, energy, and water resources. From such a diverse group and variety of interests (over 100 responses) one would expect unique and highly specialized requirements for precipitation information. Measurement frequencies ranged from continuous to one per week, spatial resolutions from a few meters to zonal, temporal averages; from 5 minutes to 1 year, and accuracies from 0.5-mm/hr to rain/no rain events. With this wide range, however, a pattern did emerge which indicates that many of the requirements, at least at the useful level, could be met with space techniques directly or in combination with conventional measurements. The resulting general specification was outlined earlier in the "Requirements" summary section. Somewhat more detail relative to specific applications is included in Table 1.

The more stringent measurement requirements (i.e., less than 10 km), with correspondingly high temporal and accuracy requirements, must obviously be met with currently available or improved conventional systems or perhaps with specialized observational systems tailored to the particular need.

Some of the significant comments contributed in the requirements survey (which are not inconsistent with the general conclusions reached at the workshop in connection with specifying requirements) are:

- Widely differing tolerances may be acceptable, depending on applications of the data. One should relate: (a) intended data uses, (b) areal coverage needed, (c) resolutions and accuracies, and (d) tolerable costs associated with each requirement.
- There is a wide variation in requirements between research and operations.
- Many requirements are dependent on the time of year.

Table 1  
Precipitation Data Requirements

Application	Accuracy	Resolution	
		Horizontal (km)	Temporal
1. Global climate			
Global	10-25%	200-500	1 week-1 month
Continent	10	25	1 day
2. Global weather	10	100	1 day
3. Synoptic weather forecast	10	100	6-12 hr
4. GCM	0.5-2 mm/day	100	1 day
5. Tropical cyclone (over water)	10-30%	2-20	0.5-6 hr
6. Thunderstorm/flash flood	10-30%	1-10	10-30 min.
7. Mesoscale modeling	10-25%	25-100	15-60 min.
8. Crop-yield modeling	10-30%	50	1 day
9. Soil-moisture evaluation	20%	20-100	1 day
10. Water-supply forecast	10%	10	1 day
11. Hydrological structure design	50%	10	1 week

(For the details of hydrological requirements, see Hudlow, et al. "Hydrological Forecasting Requirements for Precipitation Data from Space Measurement," (Workshop Preprint). For practical reasons, requirements of hydrological and agricultural applications for underdeveloped countries are substantially relaxed.)

- The unique characteristics of different regions dictate a variety of resolutions, accuracies, and sampling frequencies e.g., coastal regions (sea and land-breeze precipitation), arctic/antarctic regions (few measurements are necessary because average accumulation is only 3 to 5 cm/yr), oceans (more detail are needed over tropical oceans than over temperate oceans), island data (small island precipitation should be distinguishable from surrounding ocean rain).
- Precipitation data and information should be accessible according to geographical sectors.
- To have confidence in satellite measurements or estimates, they must be correlated with ground-based measurements, but there is also strong concern about large errors in rain-gage measurements.
- Long homogeneous series of internally consistent precipitation data are required.
- Although absolute calibration is not particularly important, reliability is essential. Considerable accuracy could be traded for it.
- For real-time applications (i.e., flash floods, hurricanes), communications are more important than high accuracy.
- Precipitation events should be distinguishable according to convective or stratiform origin.

- To be most useful, the spatial scale of space precipitation measurements should be better than that derived by isohyets based on existing ground observations.
- A space measurement system should be able to distinguish between rain and snow.
- Correlative data for clouds, sea-surface temperature, and winds are needed with comparable accuracies.
- Negative departures of precipitation are more critical than positive departures.
- Ocean precipitation data, especially more finely gridded data between 20°S and 20°N, are a major requirement for global heat-balance studies.
- For energy flux over oceans, the accuracy needed is about the same as that for ocean evaporation [ $\approx 1$  cm/month over a  $(500\text{-km})^2$  grid].
- The difference between ocean evaporation and precipitation is proportional to heat and salt flux at the surface (buoyancy flux), which are needed for ocean circulation modeling. It is especially important to have rain rate in heavy rain over short periods for the vertical mixing parameter.
- Ocean precipitation must be measured reasonably well because it can affect the determination of ocean-wind stress.
- Two-week averages over a  $(250\text{-km})^2$  grid are useful for calculating soil moisture with models.
- Compatibility of space precipitation measurements with NWS station data is desirable.
- Strong interest was expressed in whether passive or active satellite rainfall estimates can be used to verify daily rainfall reports made by thousands of cooperative observers throughout the United States, (and soon throughout the world) for AgRISTARS.
- Accumulated daily rainfall over land is now more important than intensity.
- For climate analysis, diagnostics, and empirical prediction, mean precipitation is needed over the entire Earth (i.e., over land, weekly averages over  $(100\text{-km})^2$  areas; over oceans, monthly averages over  $(200$  to  $500\text{-km})^2$  areas).
- GCM modeling requires global precipitation data on a suitable grid  $(100$  to  $250\text{ km})^2$  for model comparison and general circulation diagnostics.
- For synoptic and mesoscale model initialization, precipitation rates are most important. In heavy rain, accuracies are less important; even 20 percent is useful.

The results of the requirements investigation involving all known sources rather conclusively supports the position that space measurements can and indeed must be used to provide a large share of precipitation information. This is particularly true for global climate in connection with ocean areas and sparsely populated regions.

#### REFERENCES

- Adler, R. E., and E. G. Rodgers, 1977: Satellite observed latent heat release in a tropical cyclone. Mon. Wea. Rev., 105, pp. 956-963.
- Griffith, C. G., W. L. Woodley, P. G. Grube, D. W. Martin, J. Stout, and D. N. Sikdar, 1978: Rain estimation from geosynchronous satellite imagery – visible and infrared studies. Mon. Wea. Rev., 106, pp. 1152-1171.
- Kilnosky, B. J., and C. S. Ramage, 1976: A technique for estimating tropical open ocean rainfall from satellite observations. J. Appl. Meteor., 15, pp. 972-975.
- Mintz, Y., 1981: Precipitation measurement requirements for general circulation climate model development and applications (see Appendix D).
- Rodgers, E. B., and R. F. Adler, 1981: Tropical cyclone rainfall characteristics as determined from satellite passive microwave radiometer. To appear in Mon. Wea. Rev., March 1981.
- Scofield, R. A., and V. J. Oliver, 1977: A scheme for estimating convective rainfall from satellite imagery. NOAA Technical Memorandum NESS 86, 47 pp.

- Tarbell, T. C., T. T. Warner, and R. A. Anthes, 1981: An example of the initialization of the divergent wind component in a mesoscale numerical weather prediction model. To appear in Mon. Wea. Rev.
- Global Atmospheric Research Programme, 1975: The Physical Basis of Climate and Climate Modeling, WMO-ICSU Joint Organization Committee.
- National Aeronautics and Space Administration, 1977: Proposed NASA Contribution to the Climate Program.
- National Oceanic and Atmospheric Administration, National Climate Program Office, 1971: Report of the Climate Data Management Workshop. Washington, D. C.
- World Meteorological Organization, 1980: The Role of Satellites in WMO Programmes in the 1980's, Annex II; Geneva, Switzerland.

LN83 25271

D2

### 3. SAMPLING PROBLEMS WORKING GROUP

#### PARTICIPANTS

John A. Flueck, Chairman  
Robert F. Crane, CoChairman  
Charles R. Laughlin, CoChairman  
Thomas L. Bell  
Jose G. Meiten

Eberhard Ruprecht  
David A. Short  
John S. Theon  
John L. Vogel

### 3. SAMPLING PROBLEMS

#### 3.1 INTRODUCTION

Precipitation estimates from satellites are subject to a number of uncertainties involving design characteristics, satellite positioning, natural variability of precipitation, and the noncontinuous acquisition of data. The sources and sizes of these uncertainties are in need of proper evaluation and estimation. The present sampling and estimation theory seems to be adequate for some measurement problems (e.g., determining precipitation at a point), while others require further theoretical work (e.g., determining the time history of precipitation over large areas).

#### 3.2 RAINFALL ESTIMATION

The measurement of precipitation presents us with sampling and estimation problems on many spatial and temporal scales. Even the adequacy of rain gages to measure "point" rainfall merits consideration (e.g., Gertzman and Atlas, 1977). See Section 4, on "Ground Truth Measurement Systems."

Theory and observations indicate that the temporal rate of change of area-averaged rain rate depends upon the size of the averaging area (Crane, 1981; Flueck, 1981; Laughlin, 1981). Statistical analysis of small scale features in the precipitation field (cells) shows an average lifetime of the order of 15 minutes and an average areal extent of 5 km<sup>2</sup> (Crane, 1981). The larger cell clusters of interest in flash-flood warnings have an average lifetime of the order of 1 hour and an areal extent of the order of 100 km<sup>2</sup> (Crane, 1981; Raschke and Ruprecht, 1981). GARP Atlantic tropical experiment (GATE) radar data have been analyzed by numerous researchers (e.g., Arkin, 1978; Austin, 1978; Laughlin, 1981; Lovejoy and Austin, 1980) to determine the statistical characteristics of meteorological phenomena over the tropical Atlantic. The correlation time for rain rate averaged over a region of (280 km)<sup>2</sup> was of the order of 7 hours (Laughlin, 1981).

Conversely, spatial variability of rain accumulation depends on the accumulation interval (Vogel, 1981). Mignogno et al. (1980) found significant variability of daily rainfall over distances smaller than 10 km.

A diurnal component in rainfall rate has been identified over many areas. For example, Wallace (1975) described the component for rain gage stations over the continental United States. In some areas average rainfall was observed to vary by more than a factor of 2 during the day. Potential biases in rainfall estimates due to causes such as diurnal variation in rainfall need to be investigated and considered when formulating sampling strategies. (See Section 3.4.)

Satellite observations have been used to obtain information about the larger scale characteristics of precipitation, from macroscale to global, and for time scales that range from months to years. For example, Rao et al. (1976) using Nimbus-ESMR-5 data, show that global precipitation over the oceans is concentrated in the tropics, and at approximately 45°N. More regionally, Kilonsky et al. (1976) have examined precipitation patterns in the tropical Pacific using satellite visible (VIS) and infrared (IR) radiometry data. Their analysis indicates substantial interannual variability in rainfall: the average rainfall between latitudes 8° and 20°N increased significantly from May 1971 - April 1972 to May 1972 - April 1973. In addition, satellite data are used in investigations of smaller time and space scales as more information about rainfall characteristics is learned from the various estimation techniques (Section 5) that use high resolution satellite VIS and IR radiometry data.

It is evident from even a cursory review of observational data and analyses that precipitation is a very complex phenomenon. Further meteorological and statistical research is needed to gain a better understanding of global precipitation characteristics on all time and space scales, including vertical structure, if suitable sampling strategies for useful precipitation estimation are to be designed. Although substantial amounts of precipitation data are available over the United States from gage networks and radar, and some data are available over the ocean (e.g., GATE), observations are needed in other areas of the world for the various precipitation types and for all seasons. Additional data sets from climatic regions identified by Crane (1981) might be used to make initial site selection for further evaluation. Radar observations should be obtained over dense rain gage networks. The rain gage data can be used to obtain temporal statistics for long records and to evaluate the use of radar as a secondary standard for the evaluation of precipitation estimated from space observations. The radar, in turn, can be used to obtain more detailed and accurate area statistics.

The possibility of using satellite measurements (such as GOES IR data) to provide proxy space-time correlation functions and information about possible diurnal variability, where ground-based observations may be unavailable, should be investigated.

In addition, multivariate statistical data analysis techniques should be used for further examination of the detailed structure of precipitation. These techniques (e.g., Mosteller and Tukey, 1978) have already proved to be useful in analyzing precipitation data (Flueck, 1981). Rodgers et al. (1979) found discriminant analysis useful for delineating rainfall areas over land conditional on surface temperature. Other multivariate techniques such as principal components, multivariate estimation, and canonical correlation should also be useful in examining the statistical characteristics of precipitation. The end products of such research are plausible statistical models of precipitation in time and space with realistic stochastic components (Flueck, 1981). With these models in hand, more satisfactory sampling and estimation schemes can be developed.

### 3.3 SATELLITE SYSTEMS

The satellite systems that are currently used to estimate precipitation were not designed for that purpose. They are limited by their spatial and temporal resolution and by the portions of the electromagnetic spectrum that they can detect. Most satellite instruments have fields of view (FOV's) ranging from 1 km to 50 km in diameter that provide spatial average estimates for regions significantly larger than the small-scale features of the precipitation field. Furthermore, these averages are for "proxy" variables (e.g., cloud-top temperature) which are not always easily related to the variable of interest (e.g., rainfall rate).

When the transfer function relating rain rate to the proxy variable is linear, estimates of peak rain rates require information about the spatial distribution of rain activity within the FOV (the "beam filling" problem), but estimates of average rain rate do not require this additional information. On the other hand, when the transfer function is non-linear, errors in the estimation of precipitation rate within the FOV depend (at least) on the number, intensity, vertical extent, phase (ice/water), and spatial organization of the unresolved subscale features. These features are not directly observable by current or planned satellite sensor systems. The size of the probable error in precipitation estimates due to missing information about subscale features can be inferred using statistical models based on ground-based data sources. A statistical bias can be corrected for, but an inherent uncertainty in the estimates will remain. This uncertainty will place limits on our ability to distinguish the changes in area-averaged rain rate from changes due to the effects of sampling.

Estimation of precipitation rate by a spaceborne sensor may be improved and uncertainty reduced by including information from other instruments such as microwave radiometers and VIS and IR sensors. Data at different wavelengths or spatial resolutions, measurements from satellites with different orbital characteristics, soil-moisture estimates from satellites, and, when available, data from surface sensors may be combined in a multivariate adjustment scheme to provide the best possible estimates. Improvement is possible when the various sensors depend differently on the subscale features, so that each sensor provides additional information for use in the inversion process required for precipitation estimation.

To better understand the advantages and limitations of the current techniques used to estimate rainfall rate and the proposed improvements of those techniques, a comparative field experiment should be conducted that is designed to yield unambiguous answers (Flueck, 1981).

### 3.4 SAMPLING STRATEGY

Each attempt at precipitation sampling and estimation should follow the dictates of proper experimentation (Flueck, 1981b). In particular, careful attention should be given to the matching of the observing strategy (i.e., the sample and measurement design) and the resolution and accuracy of the precipitation measurement desired.

Given the objectives, the precipitation variables, and the desired precision, the sampling design usually focuses on the following: (1) how best to select the observations (usually by minimizing mean square error); (2) how frequently to sample; and (3) what estimator to use for the precipitation characteristic (parameter) of interest (Flueck, 1981). Each of these components contain inherent problems that must be properly considered.



Satellite sensors usually take "snapshots" of the FOV. The sampling problems associated with determining the instantaneous precipitation rate within the FOV of the sensor were described earlier. In selecting a satisfactory sampling strategy for a satellite system designed to estimate integrated quantities (e.g., accumulated rainfall for flood warning, or mean precipitation rates for climate research) sampling problems of a different sort must be considered. The sampling strategy chosen depends on the type of data required of the system. For instance, to determine daily accumulated rainfall accurate to 10 percent may require hourly sampling times. Monthly average rainfall over an area 280 km in diameter determined with similar accuracy requires only twice-a-day sampling (Laughlin, 1981). Sampling theory provides an analytical tool for answering quantitatively the question of how accurate a given sampling strategy will be, when the underlying statistics of the measured quantity are known. Laughlin (1981) gives an example of such a procedure applied to rainfall measurement in the GATE area. In general, as one relaxes the demand for high-spatial resolution, sampling frequency can be substantially reduced. Precipitation statistics in other areas and seasons should be obtained and a similar analysis repeated for them.

Although sampling twice daily may prove to be sufficient in many areas, the possibility of bias due to a diurnal cycle in average rainfall must be considered. Unless such a bias can be convincingly accounted for on a statistical basis, methods for inferring the amplitude and phase of the suspected cycle from auxiliary observations may have to be developed. Possibilities include the following: (1) use of cloud data from geosynchronous satellites as proxy evidence for diurnal variations; (2) for climatic purposes (e.g., 1-month averages), design of an inclined orbit so as to obtain a different local sampling time each day; or, (3) least economical, use of multiple satellites with sun synchronous orbits sampling sufficiently frequently to measure the diurnal cycle directly. All of these approaches require further research and more data on diurnal variability to establish how much additional sampling is needed to monitor a diurnal effect.

Maximum use of the two-dimensional spatial correlation of rainfall should be made to determine optimal spatial sampling patterns. Where correlation lengths are large, lower spatial density of observations is required. In the case of adaptive sensing schemes, such as proposed by Atlas (1981) where the sensor samples only at a selected number of points, it is especially critical that the spatial autocorrelation pattern be estimated and used to design a sampling strategy which trades off observing time and accuracies.

Although there are a number of estimators in the sampling literature that use auxiliary information (e.g., ratio and regression type estimators), it is likely that either improved versions of these estimators or new estimators will be needed for the satellite-based estimation of precipitation. In fact, it appears that satellite estimation of precipitation could have a major impact on the development of multivariate sampling theory. Finally, where analytical solutions are not readily forthcoming, computer simulation should be encouraged (Flueck, 1981).

### 3.5 RECOMMENDATIONS

We have attempted to highlight the statistical sampling and estimation problems associated with designing a satellite system for measuring precipitation. Some of the statistical tools and precipitation data needed for designing an effective system are already available, but further work is required in a number of areas. Our recommendations are as follows:

- Conduct a field evaluation of the satellite techniques that are presently available for estimating precipitation with adequate ground truth.
- Improve or further develop sampling theory and estimation methods for univariate and multivariate stochastic processes to support estimation of ground-level precipitation.
- Pursue the characterization of precipitation over a wide range of weather and climate regimes and geographical locations.
- Further develop understanding of sampling requirements, based on analysis of existing data and results from the field evaluation experiment, to provide the design criteria for the sampling strategy of a future global precipitation experiment.
- Improve the "adjustment schemes" for handling subscale precipitation processes.
- Develop physical and stochastic models for simulating precipitation processes to be used in studies of sampling effects and in improving adjustment schemes.

## REFERENCES

- Atlas, D., 1981: Adaptively pointing spaceborne radar for precipitation measurements. (See Appendix D).
- Austin, P. N. and S. G. Geotis, 1978: Evaluation of the quality of precipitation data from a satellite borne radiometer. Report under NASA grant NSG 5024; Department of Meteorology, Massachusetts Institute of Technology, Cambridge, Massachusetts.
- Crane, R. F., 1981: Sampling problems-overview. (See Appendix D).
- Flueck, J. A., 1981: Some statistical problems inherent in measuring precipitation. (See Appendix D).
- Flueck, J. A., 1981b: Comparative experimentation: Some principles and prescriptions. Conference on Teaching of Statistics and Statistical Consulting. J. Rustagi and D. Wolfe (eds.), Academic Press, New York, New York.
- Kilonsky, B. J. and C. S. Ramage, 1976: A technique for estimating tropical open-ocean rainfall from satellite observations. J. Appl. Meteor., 15, pp. 972-975.
- Laughlin, C. R., 1981: On the effect of temporal sampling on the observation of mean rainfall. (See Appendix D).
- Lovejoy, S. and G. L. Austin, 1981: The estimation of rain from satellite borne microwave radiometers. Quart. J. R. Meteorol. Soc., 106, pp. 255-276.
- Mignogno, M. J., C. E. Duchon, A. G. Eddy, and A. D. Nicks, 1980: An investigation of the dependence of meso-scale rainfall parameters on pixel size. Research Report under USDA 58-7B30-9-69 and NASA 913-177-55-43-02. School of Meteorology, The University of Oklahoma, Norman, Oklahoma.
- Mosteller, F. and Tukey, J. W. (1977): Data analysis and regression: A second course in statistics, Reading, Massachusetts. Addison-Wesley Publishing Company.
- Rao, M. S. V., W. V. Abbott III, and J. S. Theon. 1976: Satellite-derived global oceanic rainfall atlas (1973 and 1974). NASA SP-410, Washington, D. C.
- Raschke, E. and E. Ruprecht, 1981: Microwave radiometry sampling problems demonstrated with Nimbus 5 rain rates versus GATE data. (See Appendix D).
- Richards, F. and P. Arkin, 1981: On the relationship between satellite observed cloud cover and precipitation. Mon. Wea. Rev., 109, No. 5.
- Rodgers, E. B., H. Siddalingaiah, A. T. C. Chang, and T. Wilheit. 1979: A statistical technique for determining rainfall over land employing Nimbus-6 ESMR measurements. J. Appl. Meteor., 18, pp. 978-991.
- Vogel, J. L., 1981: Rain gage network sampling statistics. (See Appendix D).
- Wallace, J. M., 1975: Diurnal variations in precipitation and thunderstorm frequency over the conterminous United States. Mon. Wea. Rev., 103, pp. 406-419.

N83 25272

D3

#### 4. GROUND-TRUTH WORKING GROUP

##### PARTICIPANTS

Robert Serafin, Chairman  
Thomas A. Seliga, CoChairman  
Roger M. Lhermitte, CoChairman  
Jeffrey A. Nystuen

Steve Cherry  
V N Brngi  
Roy Blackmer  
Gerald M Heymsfield

## 4. GROUND-TRUTH MEASUREMENT SYSTEMS

### 4.1 INTRODUCTION

Ground-truth measurements of precipitation and related weather events are an essential component of any satellite system designed for monitoring rainfall from space. Such measurements are required for testing, evaluation, and operations; they provide detailed information on the actual weather events, which can then be compared with satellite observations intended to provide both quantitative and qualitative information about them. Also, very comprehensive ground-truth observations should lead to a better understanding of precipitation fields and their relationships to satellite data. This process serves two very important functions: (a) aiding in the development and interpretation of schemes of analyzing satellite data, and (b) providing a continuing method for verifying satellite measurements.

### 4.2 SCOPE

#### 4.2.1 Coverage

Several schemes are available for measuring rainfall ground truth. They range from single-site point measurements with rain gages of all types, to networks of gages, to radars operating alone or in combination with gages. Watershed responses to rainfall may also be useful for this purpose. Although a number of rain-gage networks and radars are available, most existing systems are inadequate for most ground-truth needs. This is particularly true over the oceans, where point measurements are often inaccurate, unavailable or inaccessible.

Also, although important and extremely useful, the operation of sufficiently dense rain-gage networks on the continents is often sporadic and designed for other purposes. These assessments lead to two major conclusions regarding the ground-truth system:

- Oceanic coverage must be available.
- A permanent continuously operating facility is required.

#### 4.2.2 Resolution

The adequacy of any ground-truth system normally depends on the needs and applications envisioned for the satellite observations. However, because of attendant problems in the satellite systems used for rainfall measurements and the need to improve our understanding of how satellite observations relate to precipitation, a specialized ground-truth facility is required. This implies that:

- The permanent facility must be capable of spatial and temporal resolutions that are better by a factor of 10 than are possible or contemplated with satellites.
- Observations must include detailed information on related meteorological phenomena, and these must be available in three dimensions.

#### 4.2.3 Global Extent

Geographical and seasonal differences in meteorology and climate response add another requirement to ground-truth observations. Thus, consideration must be given to occasional deployment of a ground-truth system in different selected regions of the world. Also, existing high-resolution rainfall monitoring systems should be used when possible for ground-truth data. This implies that:

- A portable ground-truth observational system should be available for deployment at selected site locations throughout the world.
- Existing ground-truth facilities should be identical and should be used when feasible.
- Data accumulated during national or international observational field programs, such as in GATE, should be employed for ground-truth purposes.

#### 4.2.4 Measurement of Rainfall

The usual method of measuring rainfall is the collecting rain gages. The utility of arrays of such gages is well known and traditionally has provided the standard for comparison with other methods, such as radar. Other devices for point measurements are available, however, and may offer advantages over the standard rain gages. For example, the disdrometer gives fast-response rainfall rate estimates, as well as the measure of drop size distribution. Of all the available remote sensing methodologies, radar is the most useful and highly developed technique. Its advantages include large spatial coverage, real-time, data processing, continuous monitoring, the possibility of oceanic coverage, and three-dimensional observations. Furthermore, the dual-polarization and dual-wavelength measurement schemes for measuring rainfall should lead to significant improvement in radar-derived estimates of rainfall rate compared with conventional Z-R relationship methods. This means that for the immediate future:

- Rain gage networks must be used as the standard method for ground-truth observations of rainfall.
- The advantages and potential of radar in monitoring the extent and amount of rainfall are of great value to any ground-truth system and must be incorporated.

### 4.3 GROUND-TRUTH MEASUREMENT PARAMETERS AND TECHNIQUES

#### 4.3.1 Measurement Parameters

At the Earth's surface, the most important parameter to be measured is the rain (or snow) intensity and its associated particle-size distribution. The interpretation of satellite microwave (and IR) observations in terms of the radiative transfer equations requires that the ground-based truth measurements be extended to vertical profiles of air temperature and of liquid-water content, which could be derived from radiosonde data. Over the ocean, measurements of sea-surface temperature, sea state (including foam coverage) and wind speed at the sea surface are needed in addition to the requirements previously mentioned.

#### 4.3.2 Measurement Techniques

A rain gage is the traditional instrument for measuring rain intensity and is normally included in the prototype standard meteorological station required both here and elsewhere. This standard station would include wind speed and direction, temperature, humidity, and pressure measurements and would provide data in a standard and convenient form.

Doviak (1981) examined several methods for estimating rainfall with radar. Among these are differential reflectivity, dual-wavelength measurement of reflectivity only, measurement of reflectivity augmented with surface gages, and microwave absorption. Doviak concluded that no "perfect" method exists for measuring high-resolution rainfall rate but that dual-parameter methods appear to be most promising.

Seliga (1981) presented results of the differential reflectivity technique whereby the reflectivity factor is measured for horizontal and vertical polarizations. This dual-parameter measurement technique permits unambiguous measurement of rainfall if the drop size distribution is exponential (an assumption that is generally accepted) and if other influences such as canting and oscillation of raindrops are negligible. The results are quite persuasive. This technique is particularly attractive because, if implemented properly, the statistical uncertainty in instantaneous measurement is effectively eliminated.

A conventional meteorological radar with a maximum range that exceeds 100 km should therefore be part of a network of stations or even be used alone for precipitation intensity measurements. The processing of the radar data should go beyond the conventional use of the Z-R relationship and include dual-wavelength, dual-polarization, three-dimensional data analysis, etc. New methodologies based on the availability of a Doppler radar used in a variable-azimuth-display (VAD) mode also offer promising ways to evaluate mean precipitation intensity over (100 to 500 km)<sup>2</sup>. However, this technique is only applicable to widespread precipitation systems.

Two new instrument techniques were proposed for ground-based precipitation measurements, and their feasibility should be investigated. The first instrument is a low-power inexpensive CW Doppler radar used in a vertically pointing

mode, essentially observing vertical velocity distribution of the particles, which can be related unambiguously to the drop size distribution and precipitation intensity. The second instrument, which measures rainfall over the water, senses the underwater noise and noise spectrum produced by the rain falling on the water surface. Nystuen (1981) suggests that it is possible to measure rainfall rate on the surface of the ocean by "listening" to the audio noise with a hydrophone below the surface. Both the noise power and the spectral power density appear to be proportional to rain intensity, which indicates that the instrument can easily accommodate a wide range of precipitation intensity. The results are promising, indicating that a significant rain signal-to-background noise margin exists in wind speeds as great as 14 knots and that rainfall rates as small as 0.5 mm/hr can be detected. Nystuen suggests that simple tethered buoys could be used to place hydrophones well below the surface, thereby obtaining a large catchment area. Measurements of the audio noise spectrum would be used to deduce the drop size distribution and rainfall rate. Although this technique is not proved and is in its early research stages, the urgent need for good surface measurements over the ocean dictates that the method be pursued further.

Land-based vertically pointing microwave radiometers should also be implemented at selected "ground-truth" sites that operate on the same satellite frequency channels to provide climatological insight on data similar to those collected by the satellite.

#### 4.3.3 Platform or Geographical Locations

It is highly desirable to assemble a land-based sophisticated measuring system, including an up-to-date high-sensitivity radar with Doppler dual-wavelength, dual-polarization capabilities, and assisted by a network of well-instrumented stations. This would provide for a thorough analysis of the satellite observations through their comparison with this sophisticated ground-truth system. It must be remembered, however, that the satellite will observe rain intensity over various parts of the globe, and geographical biases of weather or precipitation conditions should therefore be considered.

These considerations are particularly crucial for satellite observations over the oceans, and it is recommended that full advantage be taken of any existing network or platforms for installing or deploying a measuring system specifically designed as a ground truth for satellite data. This includes commercial, research or naval vessels, instrumented buoys, oil drilling rigs, commercial and military aircraft, etc. This concept may call for the design of a standard meteorological station that would include standard recording capability and that could either be installed temporarily aboard a moving platform or be part of a fixed network. The ground-truth data provided by this station, in association with other existing instruments, would be used for comparison with and interpretation of satellite data collected at a location selected for its meteorological interest or representativeness.

#### 4.4 RECOMMENDATIONS

The recommendations of the Ground-Truth Working Group are based upon perceptions of the current deficiencies inherent in measurement of precipitation from space and represent the results of discussions within the group. The approach is comprehensive. However, the number of recommendations has been kept to a minimum to focus on the most important needs:

- The NEXRAD system, associated with the NWS network of surface measurements, offers an unprecedented opportunity for obtaining superb ground-truth measurements over virtually the entire land mass of the United States and its offshore region, extending perhaps 200 km beyond the coast. It is recommended that dual-parameter measurements be made a part of each NEXRAD radar. Adding differential reflectivity measurements to NEXRAD should not result in a large incremental cost, but should provide substantial benefits in improved precipitation measurements.
- Those engaged in evaluating and using satellite measurements of precipitation must plan to make better use of the comprehensive high resolution arrays of instruments that will be deployed in a variety of mesoscale field research programs to be conducted in the coming decade. CCOPE, SESAME, SCPP, CDMP, a national winter cyclone study, TRIP, and others offer unique opportunities for complete three-dimensional atmospheric and surface measurements. The users of satellite data should concentrate much of their effort on analyzing data collected during these field experiments and should include their objectives within the

framework of the program planning documents. This will ensure that the observational networks are designed to meet the ground-truth needs for satellite observations.

- The equivalent of a national standards laboratory for evaluating precipitation estimation techniques is needed. Such a laboratory would make use of the best in situ and remote-sensing instruments available and would provide accurate three-dimensional measurements of precipitation and clouds during all seasons, over land and water, with resolution at least one order of magnitude better than that expected from spaceborne measurements. It is recommended that Wallops Island be considered for this laboratory because of its location and its sophisticated radar facilities capable of very high resolution observations.
- The development of promising new techniques for ground-truth measurements should be encouraged and supported. Microwave attenuation and simple vertically pointing CW Doppler radar should be considered as alternatives to conventional gages. Doppler radar measurements that penetrate only tens of meters above the surface would be uncontaminated by vertical air motion and would permit complete description of the drop size distribution. Because single-pulsed Doppler radar techniques can provide accurate measurements of precipitation in stratiform rain and in snow, they should be considered as well.
- Ground-truth surface "benchmark" measurements over the ocean, where a substantial fraction of the global rainfall occurs, are essential. The feasibility of hydrophone monitoring of ocean rainfall, as proposed by Nystuen (1981), should be investigated. Ships of opportunity with improved rain gages and possibly periodic recordings (approximately 15-minute intervals) of ship-surface radar returns should be used.
- Despite the many opportunities that exist for evaluation and testing in the United States, many important typical weather systems occur in other parts of the world. It is therefore recommended that a transportable "transfer standard" precipitation measurement system be developed. This system would consist of a radar, other remote sensors, instrumented buoys, and surface stations. Most, if not all, of these sensors would be capable of communicating by satellites to a U.S. or field-based ground station. Data-collection platforms — simple, reliable, rugged, and inexpensive — that can be moved and deployed around the globe, on land, or on ships should be developed. An instrumented aircraft with upward, downward, and side-view windows should be considered as part of this network to permit comprehensive atmospheric truth for evaluation of satellite techniques in locations around the globe.

The foregoing recommendations encourage the essential ingredients needed for ground truth. Their implementation will fill the serious gaps that now exist in accurate and reliable atmospheric truth data sets and will ensure that satellite data collected in the future will be used more effectively for precipitation and weather and climate monitoring.

#### REFERENCES

- Doviak, R. J., 1981: A survey of rain measurement techniques. (See Appendix D.)
- Nystuen, J. A., 1981: Using underwater ambient noise levels to measure rainfall rate: A review. (See Appendix D.)
- Seliga, T. A., and V. N. Bringi, 1981: The differential reflectivity dual polarization method of rainfall measurements. (See Appendix D.)

D4

N83 25273

5. VISIBLE AND INFRARED TECHNIQUES WORKING GROUP

PARTICIPANTS

David W. Martin, Chairman  
Roderick A. Scofield, CoChairman  
Robert F. Adler  
Eric C. Barrett  
Cecilia G. Griffith

Earl S. Merritt  
Andrew J. Negri  
Colin S. Ramage  
Donald P. Wylie



## 5. VISIBLE (VIS) AND INFRARED (IR) TECHNIQUES

9  
Y

### 5.1 SUMMARY OF CONCLUSIONS AND RECOMMENDATIONS

A number of techniques for inferring precipitation information from satellite VIS and/or IR cloud data have been developed during the past 10 years. The methods divide into two general classes. Indexing techniques, which are not time-dependent, attempt to identify rain clouds and count their occurrence or measure the area of rain. Life history methods measure rate of change parameters of individual convective clouds or clusters of convective clouds in addition to other characteristics. Both techniques calculate rainfall by means of statistical coefficients based on earlier cloud/rain comparisons.

On the scale of climate (250 km and larger, one month and longer), simple indexing schemes (e.g., Hawaii method) give useful results over tropical oceans. Except where diurnal cycles may be large in predominantly convective rainfall, the more complicated life history techniques are not needed for this application. Over remote or unsettled land areas, indexing schemes have demonstrated skill in estimating rainfall if they are carefully tuned to local conditions. Serious problems arise when techniques (including life history) are transferred from one climatological regime to another and from one storm type to another. No technique has demonstrated skill over midlatitude oceans and polar regions.

On the scale of weather (hours to days, tens to hundreds of kilometers) gages and radars may not be adequate even in settled land areas. There bispectral techniques (e.g., Montreal method) can provide a useful depiction of rain area. Indexing techniques are used almost daily for assessing crop conditions. Although life-history techniques now apply only to convective rains, they have demonstrated skill both in locating rain in stronger storms and in indicating at least major categories of intensity. This capability has led to the use of the National Earth Satellite Service (NESS) technique in flash-flood forecasting.

The initial objective in attempting to meet even the most basic set of requirements for global rainfall climate statistics with a current and near-historical satellite data base should be to produce estimates of monthly mean rainfall over the oceans and remote lands. Therefore, we recommend that existing indexing techniques be applied as they have been over the tropical oceans; that new indexing techniques be developed, tested, and applied over the midlatitude oceans; and that present indexing techniques be extended to remaining remote lands.

The long-term objective in attempting to meet needs for rainfall climate statistics should be to produce uniform estimates of global monthly rainfall. To accomplish this, we recommend support for efforts to devise a global technique. This could be a pure VIS/IR indexing technique or (more likely), one that includes active or passive satellite microwave observations to calibrate the cloud statistics available (usually more frequently) from VIS/IR data. For the benefit of all techniques, we recommend support for research aimed at a better understanding of the relationship of precipitation processes to cloud brightness and temperature and changes of these in time; that experiments for systematically comparing competing techniques be conducted; and that adequate gage and calibrated radar ground-truth systems be established for one or two tropical and midlatitude ocean areas.

### 5.2 SATELLITE DATA SOURCES

For climatic studies, the best record of satellite data is the series of ESSA/NOAA mercator and polar stereographic mosaics. Except for a 9-month period in 1978, these continue back to 1971 and are available from Environmental Data and Information Service (EDIS), NOAA. A few collections (e.g., that of the Space Science and Engineering Center, University of Wisconsin-Madison) extend (in VIS imagery only) back to 1966.

A second noteworthy series from low-orbiting satellites is the EDIS archive of digital VIS/IR data. Except for the 1978 hiatus, this record extends back to 1972.

Of much potential value are the three-dimensional nephanalyses produced by the U. S. Air Force (USAF) Global Weather Central automated cloud-analysis model. These cloud analyses have been archived on magnetic tape since 1971 for the Northern Hemisphere (since 1974 for the globe) by the USAF Environmental Technical Applications Center (ETAC) and are available from the World Data Center-A, Asheville, North Carolina.

ORIGINAL PAGE IS  
OF POOR QUALITY

Several agencies maintain archives of digital data from geostationary satellites. The Japan Meteorological Agency Meteorological Satellite Center has a 2-year archive of data from the Geostationary Meteorological Satellite (Himawari), which was launched in 1977. Digital data for the period November 30, 1978, through November 30, 1979, also are archived at the University of Wisconsin. Meteosat data for the period between satellite launch in November 1977 and failure 2 years later are archived by the European Space Agency's Space Operations Centre although the Centre is not presently providing data services. Archives for the Geostationary Operational Environmental Satellite (GOES) series are maintained by EDIS, NASA/Goddard Space Flight Center (GSFC), Colorado State University, and the University of Wisconsin-Madison. The archive at Wisconsin includes both East and West satellites, beginning in February 1978 (with some breaks before November 1978) and November 1979, respectively. The Indian Ocean GOES is archived at Wisconsin for 1 year, beginning in November 1978. Of special interest are the archives of data from Synchronous Meteorological Satellite-1 (SMS-1) covering the 1974 Global Atmospheric Research Program Atlantic Tropical Experiment, which are maintained as complete archives at both GSFC and at Wisconsin and as a compacted archive at World Data Center-A, Asheville, North Carolina.

### 5.3 SUMMARY OF TECHNIQUES

This section summarizes in concise, functional form the major schemes that use VIS/IR satellite data to derive estimates of rainfall. The schemes generally are of the form:

$$R = a_0 + f(I, \Delta I, \sigma_I^2, A(I_0), \Delta A/\Delta t, \dots)$$

where

- R = rainfall
- I = intensity parameter (temperature, brightness)
- A = area
- $\sigma^2$  = variance

They can often be expressed as some form of the relation:

$$R = a_0 + g \sum_{i=1}^N a_i f_i$$

where  $g$  is derived from other sources,  $a_i$  are constant coefficients, and  $f_i$  are independent variables.

#### 5.3.1 Time-Independent Indexing Schemes

5.3.1.1 Montreal/McGill (Bellon et al., 1980) - To serve the objective of precipitation forecasting, this method extends statistical relations between VIS/IR data and radar echo area over  $10^5 \text{ km}^2$  to larger regions.

The functional form is:

$$R_v = a_1 A$$

where

- $R_v$  = volumetric rainrate
- $a_1$  = climatological rainrate
- A = derived rain area when brightness  $B > B_0(T)$  and temperature  $T < T_0(B)$

This scheme is automated.

ORIGINAL PAGES IS  
OF POOR QUALITY

5.3.1.2 CEDDA (Arkin, 1979) – This scheme describes the relationship between 6h averages of fractional cloud cover at various IR thresholds and accumulated rainfall derived from GATE C-band radars.

The functional form is:

$$[\bar{R}] = a_1 \bar{A}/Q$$

where

A = area of cloud above 10 km

Q = area of a ppi scan over which A is measured ( $\approx 10^5 \text{ km}^2$ )

The brackets indicate an area average, and the overbar indicates a time average.

5.3.1.3 Hawaii (Kilonsky and Ramage, 1976) – This technique produces rainfall estimates over large areas and time periods by relating the incidence of highly reflective cloud (HRC) on daily satellite mosaics to coral island station rainfall.

The functional form is:

$$\bar{R}_{ij} = a_0 + a_1 N$$

where

$\bar{R}_{ij}$  = mean monthly rainfall at point (i,j)

N = number of days/month with HRC at point (i,j)

5.3.1.4 NESS/CEAS (Follansbee, 1973) – This scheme is designed for estimating rains over catchments using once-daily direct-readout visible pictures. For each of three main rain-producing cloud types, the ratio of cloud to total area is multiplied by a constant coefficient. The daily area average rainrate is then given by:

$$[R] = 1/Q \sum_{i=1}^3 a_i A_i$$

where Q is the area of the catchment. Follansbee and Oliver (1975) have modified this technique to accept both VIS and IR pictures. D. LeCompte (CEAS, NOAA) uses a slightly refined version of this technique with twice-daily low-orbiter pictures to monitor drought conditions in poorer countries of the tropics.

5.3.1.5 Bristol (Barrett, 1981) – This Bristol method evaluates a satellite-viewed cloud in terms of area and type, includes gage rainfall, and adjusts coefficients by morphoclimatic weighting.

The functional form is:

$$[R] = \sum_{i=1}^6 a_i c_i$$

where  $c_i$  is the fractional cloud cover of type i, as determined by VIS or IR images or both.

5.3.1.6 NESS (Follansbee, 1976) – This technique concentrates on precipitation from synoptic rain systems of higher latitudes. It uses simple interpolation to estimate the positions of these systems between twice-daily VIS/IR satellite views and the length of time a system will bring precipitation to a station on the ground.

ORIGINAL PART OF  
OF POOR QUALITY

The functional form is:

$$P_{1/2} = 0.09 r_{1/2} E(P_{30})$$

where

$r$  = fraction of the estimation period that a point is covered by precipitating clouds

$E(P)$  = climatic normal precipitation for the point

Subscripts are periods in days.

5.3.1.7 Cropcast (Merritt, 1976) – This model provides daily estimates of precipitation for agricultural use on a 54-km-grid scale, using ground observations complemented by satellite VIS/IR analysis and nephelometry:

$$[P] = \left[ \sum_{i=1}^2 a_i(t) c_i b_i + \sum_{j=1}^4 A_j(t) C_j B_j \right] D(\tau)$$

where

$[P]$  = area averaged precipitation

$a, A$  = coefficients based on time of day

$b, B$  = cloud type

$c, C$  = fractional cloud cover

$D$  = growth/decay factor (synoptic or cloud)

$\tau$  = synoptic or cloud related condition

Indices  $i$  and  $j$  represent cloud temperature and cloud type, respectively.

5.3.1.8 NESS (Whitney and Hernan, 1979) – This scheme produces estimates of convective rainfall by a statistical model obtained through screening regression. The estimates are intended to be 6-hour, area-averaged rainfall for riverflow purposes. Among the 28 satellite and conventional variables tested are IR temperature and its various directional components and Laplacian, low-level moisture, equivalent potential temperature, moisture advection, and terrain.

The functional form is:

$$\bar{R} = a_0 + a_1 X + a_2 Y + a_3 Z + \dots$$

where  $X, Y,$  and  $Z$  identify selected variables (which rarely exceed 3 or 4 in number). Statistical stability has not been realized from time to time or area to area even in the same situation.

### 5.3.2 Time-Dependent Life-History Techniques

5.3.2.1 Wisconsin (Stout et al., 1979) – This technique relates volumetric rain rate to cumulonimbus cloud area and areal change for estimation of tropical oceanic convective rainfall.

The functional form is:

$$R_v = a_1 A + a_2 \Delta A / \Delta t$$

where

A = cloud area defined by  $B > B_0$  (or  $T < T_0$ )

t = time (typically 30 min)

VIS or IR images may be used.

In a modification to Stout et al. (Wylie, 1971), the areal change term is dropped, and a cloud model is introduced to account for different cloud environments.

The functional form is:

$$R_v = m a_1 A$$

where m is the ratio (Montreal/GATE) derived from environmental soundings input to a one-dimensional cloud model.

5.3.2.2 ERL (Griffith et al., 1981) – This technique, derived in Florida for convective rainfall, uses cloud-top temperature structure and cloud areal expansion to produce rain estimates that may be adjusted for environmental conditions by one-dimensional model output.

The functional form is:

$$R_v = a(t) \cdot b(T) \cdot A_e \text{ and } A_e = c(t, A_{\max}) \cdot A$$

where

a(t), c(t) = growth or decay coefficients

b(T) = coefficient for apportionment of rain by cloud-top temperature structure

$A_e$  = equivalent echo area

$A_{\max}$  = maximum (satellite) cloud area

This scheme is automated and uses IR data.

5.3.2.3 NESS (Scofield and Oliver, 1977) – This operationally oriented scheme uses a decision-tree technique based on commonly observed satellite-radar characteristics of thunderstorms to produce rain estimates in near-real time specifically for flash-flood storms.

The functional form is:

$$R = [a_1 (T \Delta A/\Delta t) + a_2 (\text{tower}) + a_3 (\text{merger}) + a_4 (\text{duration})] \cdot a_5 (\Delta W)$$

where

$\Delta A/\Delta t$  = expansion of coldest contour in the enhanced IR images

T = cloud-top temperature

$\Delta W$  = departure of precipitable water from a summertime normal

Other parameters relate to the occurrence of overshooting tops, merging cells or lines, and the persistence of the storm. These may be deduced from VIS as well as IR data.

5.3.2.4 NASA/GLAS (Negri and Adler, 1981) – Although it is more a case study than a technique, this approach demonstrates several relationships between the cloud-top ascent rate and minimum blackbody temperature of satellite-viewed storms to radar measured rain rates and area.

The functional form is:

$$R_v = f(\Delta T/\Delta t, T_{MIN}, \tau)$$

where

$\Delta T/\Delta t$  = cloud-top ascent rate observed in 5-minute interval infrared

$T_{MIN}$  = minimum blackbody temperature achieved by the storm

$\tau$  = parameter which identifies active convective storms in the satellite data

#### 5.4 APPLICATIONS

VIS and IR techniques are being used to estimate precipitation in support of climatology, agriculture, hydrology, flash-flood forecasting, and weather modification experiments. Several of these techniques are used in real time or near-real time. For example, the Bristol technique is employed by meteorologists in North Africa to help locate locust breeding areas. The Earth Satellite Corporation and the Center for Environmental Assessment Service of NOAA's Environmental Data and Information Service (EDIS/CEAS) compute estimates of rainfall for crop forecasting and drought relief, respectively. NOAA's Environmental Research Laboratories (ERL) estimate rainfall from landfalling hurricanes. Rainfall estimates from NESS's technique are used by Weather Service Forecast Offices and River Forecast Centers to help in evaluating flood potential and in issuing flash-flood warnings. McGill University uses its technique as an aid for forecasting precipitation in the Southern Canadian Provinces.

These techniques, and others not necessarily used in real time, are listed here according to the particular application or applications for which each was devised, together with the principal investigators involved:

- Rainfall climatology, water resource, and streamflow
  - Cloud indexing modified for different environments – E. Barrett (University of Bristol, U. K.)
  - Cloud indexing (highly reflective cloud) – B. J. Kilonsky and C. S. Ramage (University of Hawaii)
  - Cloud indexing (cold cloud) – P. Arkin (Climate Analysis Center, NWS/NOAA)
  - Life history modified for different environments – C. Griffith and W. Woodley (NOAA/ERL)
  - Life history modified for dry environments – R. Scofield and V. Oliver (NOAA/NESS)
  - Statistical association of rainfall with satellite and synoptic variables – L. Whitney and L. Herman (NOAA/NESS)
- Crop survey and forecasting, locust control, and drought assessment
  - Cloud indexing modified for different environments – E. Barrett (University of Bristol, U. K.)
  - Cloud indexing – W. Follansbee and V. Oliver (NOAA/NESS)
  - Cloud indexing – E. Merritt (Earth Satellite Corporation)
  - Cloud indexing – D. LeComte (NOAA/EDIS/CEAS)
- Mesoscale analysis of precipitation and flood forecasting
  - Life history modified for dry environments – R. Scofield and V. Oliver (NOAA/NESS)
  - Life history modified for different environments – C. Griffith and W. Woodley (NOAA/ERL)
  - Cloud indexing with cloud model – D. Wylie (University of Wisconsin)
  - Life history – D. Martin, D. Sikdar, and J. Stout (University of Wisconsin)
  - Rapid-scan life history – R. Adler and A. Negri (NASA)

- Precipitation Forecasting
  - Bispectral with radar – S. Lovejoy and G. Austin (McGill University)
  - Life history (hurricanes) – C. Griffith and W. Woodley (NOAA/ERL)
- Effects of Weather Modifications
  - Life history modified for different environments – C. Griffith and W. Woodley (NOAA/ERL)

## 5.5 ASSESSMENT OF TECHNIQUES

Pinpointing strengths and weaknesses of techniques was one of the most difficult and controversial parts of our deliberation, partly because there seemed to be at least one exception to almost every generalization. Nonetheless, we believe that VIS/IR techniques hold an advantage over other techniques in that:

- These techniques have a considerable history of scientific and practical experience
- The satellite data sets are global in coverage and are readily available
- Current techniques are applicable to most climatic regions except for the poles
- They have demonstrated capability over a considerable range of time and space scales
- They can be used with real-time, quick-look satellite data
- Most are designed to take advantage of the interpretive skill of the analyst
- They are inexpensive by-products of existing satellite systems

They are at a disadvantage compared with other techniques in that:

- Information on precipitation must be inferred from characteristics of the clouds because VIS and IR sensors "see" clouds, not the precipitation that may be embedded within them.
- Geosynchronous techniques are not applicable in high latitudes, low-orbit techniques have poor time resolution, and IR data are available only for nighttime.
- The accuracy of these techniques is not adequately specified.
- They are not readily transferrable to different areas.
- Life-history techniques are designed for convective rain estimation only.

Our general conclusion in the light of these advantages and disadvantages is that no present single VIS/IR technique can perform adequately for climatic purposes in all regions all of the time. However, no concerted effort has been made to establish such a technique.

## 5.6 IMPROVEMENTS

Improvements to the VIS/IR techniques follow from the foregoing limitations, although other factors enter as well. In terms of methodology, improvements are likely if, for each technique, the researcher:

- Expresses functional relationships in concise mathematical form
- Explains the underlying physical basis and points out the aspects that are not well-understood
- Specifies at least the mean square error
- Gives the range of the independent variables used for deriving the coefficients
- Evaluates the significance of each term or factor
- Gives an account of data processing in sufficient detail to permit repeatable testing by other scientists
- Automates the simple routine measurements.

In addition, the accuracy of all techniques depends on stable performance of satellite sensors, a dynamic range sufficient to resolve the range of contrasts implicit in bright, cold clouds viewed against dark, warm land or water surfaces, a field of view sufficient for resolving all significant precipitation systems, and sampling sufficient for resolving diurnal variations of precipitation. All techniques depend critically on the accuracy of pixel location.

## 5.7 RECOMMENDATIONS

- Continue to support efforts for producing climatologically useful estimates of rainfall over tropical oceans by simple indexing schemes.
- By rigorous statistical methods, test, evaluate and, when appropriate, compare current and proposed VIS and IR techniques. This might be done in a series of land and sea satellite precipitation ground-truth experiments.
- Develop and test simulated hybrid (active or passive VIS/IR/microwave) techniques that could be used over water and/or land.
- Increase resolution in the global digital archive to 1 to 2 km. Increase the effective coverage of low-orbiting satellites to at least four observations per day.
- Test the viability of inferring global rainfall for climatic purposes from one VIS/IR technique or a small set of VIS/IR techniques.
- Continue efforts for producing estimates of rainfall in support of flash-flood forecasting and for verifying and automating the present NESS technique. Such estimates, however, should be used with caution until further evaluated and then only to specify broad classes of rain rates or amounts.
- Continue efforts for developing, testing, and improving techniques of use in forecasting crop yields.
- Support research into convective precipitation processes and their relation to cloud-top observations for understanding the basis for statistical relations and as a basis for better applying VIS/IR techniques on shorter (1-h) time scales.
- Increase IR resolution on future geosynchronous satellites to  $\sim 1$  km.; increase VIS brightness resolution to 8 bits.
- Establish and maintain accurate absolute calibrations on all VIS and IR sensors, and record these with the data.
- Improve location accuracy to 2 km (absolute). Store location information with the data.
- Process data uniformly over long periods, especially in regard to navigation and photo reproduction.
- Maintain adequate ground-truth systems, including calibrated digital radar, and archive the data collected by these systems.
- Explore the feasibility of estimating global precipitation as part of the International Satellite Cloud Climatology Project.

## REFERENCES

- Arkin, P. A., 1979: The relationship between fractional coverage of high cloud and rainfall accumulations during GATE over the B-scale array. Mon. Wea. Rev., 107, pp. 1382-1387.
- Barrett, E. C., 1981: Satellite-improved rainfall monitoring by cloud-indexing methods; operational experience in support of desert locust survey and control. In Satellite Hydrology, (ed. M. Deutsch), American Water Resources Association (in press).
- Bellon, A., S. Lovejoy, and G. L. Austin, 1980: Combining satellite and radar data for the short-range forecasting of precipitation. Mon. Wea. Rev., 108, pp. 1554-1566.
- Follansbee, W. A., 1973: Estimation of average daily rainfall from satellite cloud photographs. Tech. Memo NESS 44, NOAA, Washington, D. C., 39 pp.



- Follansbee, W. A., 1976: Estimation of daily precipitation over China and the USSR using satellite imagery. Tech. Memo. NESS 81, NOAA, Washington, D. C., 30 pp.
- Follansbee, W. A., and V. J. Oliver, 1975: A comparison of infrared imagery and video pictures in the estimation of daily rainfall from satellite data. Tech. Memo. NESS 62, NOAA, Washington, D. C., 14 pp.
- Griffith, C. G., J. A. Augustine, and W. L. Woodley, 1981: Satellite rain estimation in the U. S. High Plains. J. Appl. Meteor., 20, pp. 53-66.
- Kilonsky, B. J., and C. S. Kamegawa, 1976: A technique for estimating tropical open-ocean rainfall from satellite observations. J. Appl. Meteor. 15, pp. 972-975.
- Merritt, E. S. (ed.), 1976: Earth satellite-spring wheat system test, 1975. Final Contract Report NAS9 14655, NASA/JSC.
- Negri, A. J., and R. F. Adler, 1981: Relation of satellite-based thunderstorm intensity to radar-estimated rainfall. J. Appl. Meteor. 20, (in press).
- Scofield, R. A., and V. J. Oliver, 1977: A scheme for estimating convective rainfall from satellite imagery. Tech. Memo. NESS 86, NOAA, Washington, D. C., 47 pp.
- Stout, J. E., D. W. Martin, and D. N. Sikdar, 1979: Estimating GATE rainfall with geosynchronous satellite images. Mon. Wea. Rev., 107, pp. 585-598.
- Whitney, L. F., Jr., and L. D. Herman, 1981. A statistical approach to rainfall estimation using satellite data. In Satellite Hydrology, (ed. M. Deutsch), American Water Resources Association, in press.
- Wylie, D. P., 1979: An application of a geostationary satellite rain estimation technique to an extratropical area. J. Appl. Meteor., 18, pp. 1640-1648.

6. MICROWAVE RADIOMETRY AND HYBRID PRECIPITATION  
MEASUREMENTS WORKING GROUP

PARTICIPANTS

Thomas T. Wilheit, Chairman  
James R. Greaves, CoChairman  
Edward B. Rodgers, CoChairman  
William R. Bandeen  
Bernard C. Diesen  
Hsaio-Hua K. Burke  
Stanley O. Kidder

Shaun Lovejoy  
Eberhard Ruprecht  
Richard C. Savage  
Thomas J. Schmugge  
James A. Weinman  
Andres S. Milman  
Norman Grody

## 6. MICROWAVE RADIOMETRY AND HYBRID PRECIPITATION MEASUREMENTS

### 6.1 INTRODUCTION

One objective of the workshop was to define a system for measuring global precipitation with an accuracy and resolution consistent with a wide variety of potential applications. To accomplish this, it was first necessary to identify the most promising measurement techniques and strategies and to understand those candidate systems in detail. The emphasis of this working group was on passive microwave remote-sensing techniques. To that end, this section: (1) provides a brief background in passive microwave and hybrid techniques for measuring precipitation, (2) discusses key problem areas and strategies for dealing with those problems, (3) proposes a precipitation measurement system, and (4) summarizes specific recommendations.

### 6.2 BACKGROUND

#### 6.2.1 Theory

Because of the validity of the Rayleigh-Jeans approximation in the microwave region, the law of radiative transfer may be expressed simply as:

$$\frac{dT_B}{dx} = a(T_B - t_0) \quad (1)$$

where  $T_B$  is the microwave radiance expressed as an equivalent blackbody temperature,  $a$  is the absorption coefficient at the point  $x$ , and  $t_0$  is the thermodynamic temperature of the medium at that point. The derivative is along the direction of propagation. Note that  $a$  is only the attenuation attributable to loss mechanisms; scattering and reflection must be accounted for by appropriate redistribution of radiation among the directions of propagation.

Figure 2 shows a typical Earth-viewing geometry to calculate the brightness temperature expected for such a situation, one first divides the atmosphere into a number of layers, each of which may be characterized by a uniform temperature and absorption coefficient. Beginning with the 3-K cosmic background, radiation is propagated from the top downwards through each layer according to equation 1. A fraction,  $r$  (the reflectivity of the radiation reaching the earth), is reflected from the surface. The surface also radiates an amount,  $\epsilon T_s$ , where  $\epsilon$  (the emissivity) is a quantity characteristic of the surface, and  $T_s$  is the thermodynamic temperature of the surface. Arguments based on thermodynamic equilibrium show that  $\epsilon$  and  $r$  are related by:

$$\epsilon + r = 1$$

Since water is a polar molecule, it has a very large dielectric constant at microwave frequencies. This results in a large reflectivity (low emissivity) for a liquid-water surface such as the ocean.

For present purposes, the atmosphere consists of three constituents: molecular oxygen, water vapor, and liquid-water droplets. Ice, as in cirrus clouds, is not a significant factor at frequencies below 40 GHz. Molecular oxygen has a series of resonances in the 50- to 70-GHz range that merge at sea-level pressure to form a band of absorption that makes quantitative determination of surface properties difficult or impossible between 40 to 80 GHz. Water vapor has a rather weak resonance at 22.235 GHz and a sequence of very strong lines at 183 GHz and higher. The tails of these lines cause the absorption attributable to water vapor to increase with frequency above 31 GHz (at sea-level pressure).

Two cases must be considered for water droplets: raining and nonraining. In the nonraining case, the small droplet (Rayleigh) limit is applicable (Gunn and East, 1954). The net absorption coefficient is then proportional to the density of liquid water and is independent of the droplet-size distribution (as long as no particles are larger than 100  $\mu$ m). A typical stratus cloud containing 20 mg  $\text{cm}^{-2}$  of liquid water would have an optical depth of about  $10^{-3}$  at 5 GHz. The optical depth increases approximately as the square of the frequency.

ORIGINAL PAGE IS  
OF POOR QUALITY

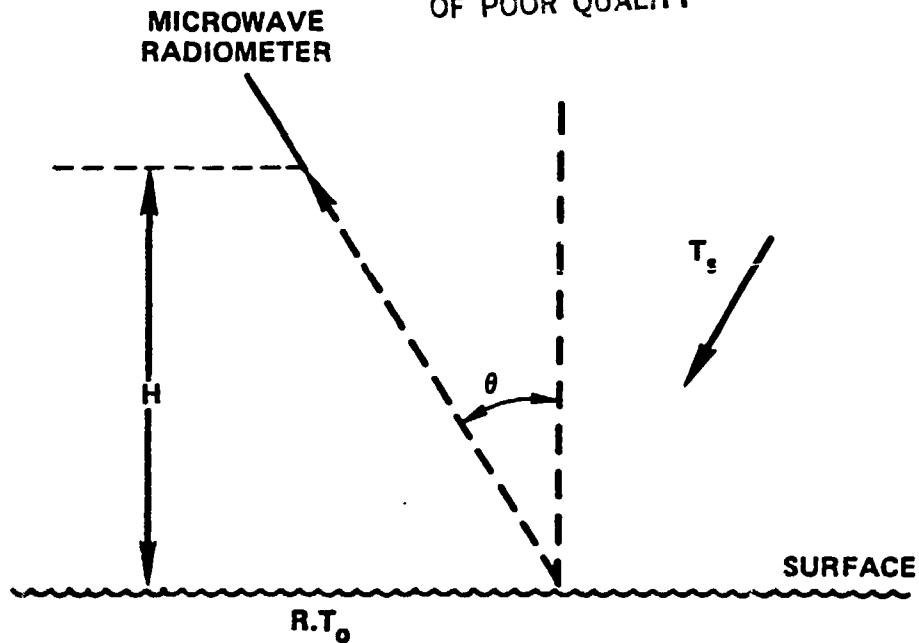


Figure 2. Typical Viewing Geometry for Microwave Remote-Sensing of Ocean Surface and Atmosphere

As larger and larger drops are considered, the absorption coefficients at first increases over the Rayleigh approximation as the drop size becomes comparable to the wavelength and then decreases below the Rayleigh approximation because of the screening of the interior of the drop. Because a rain cloud contains more water and larger drops than a nonraining cloud, it has a greatly enhanced microwave absorption. Also, as the drop size increases, scattering becomes significant.

#### 6.2.2 Previous Microwave Work

Figure 3 shows the total extinction (scattering plus absorption) and the scattering coefficients calculated for a frequency of 19.35 GHz as a function of rainfall rate for a Marshall-Palmer drop size distribution (Wilheit et al., 1977). At rainfall rates greater than a few  $\text{mm hr}^{-1}$ , the scattering becomes significant, greatly complicating the transfer computations. Wilheit et al., (1977) discusses a method for handling higher rainfall rates by using a radiative transfer model. The model relates brightness temperature ( $T_B$ ) measured at 19.35 GHz as a function of rain rate for a 4-km freezing level over an ocean background. Figure 4 shows the model results as a solid line. As a model validation experiment, simultaneous measurements of rain rate observed by the WSR-57 meteorological radar at Miami, Florida, and ESMR-5  $T_B$  were used. These data are plotted as dots in Figure 4. In addition, ground-based data consisting of measurements from an up-looking radiometer (also measuring 19.35 GHz) and two rain-rate gages are plotted as crosses in Figure 4. It is seen that the majority of the confirmation points lie between the dashed curves, which represent an envelope of a factor of 2 in rainfall rate, or  $2 \text{ mm hr}^{-1}$ , whichever is greater, about the solid line. Although this model contains uncertainties, it agrees with both the space- and ground-based data. The relationship between brightness temperature and rain rates depends on the thickness of the rain layer, which is taken to extend from the surface to the freezing level. A freezing level of 4 km provided a good approximation for both validation experiments. (See Figure 5.)

This technique of measuring rainfall intensity from ESMR-5 data was used to produce weekly, monthly, seasonally, and annually averaged rainfall maps for the world's major ocean areas for the period from December 1972 through February 1975. When the freezing level was 3 km or greater, the use of a climatological freezing level yielded reasonable results, but the results were not realistic for colder atmospheres. An *ad hoc* correction was therefore applied by using a freezing level of 3 km for climatologically colder atmospheres.

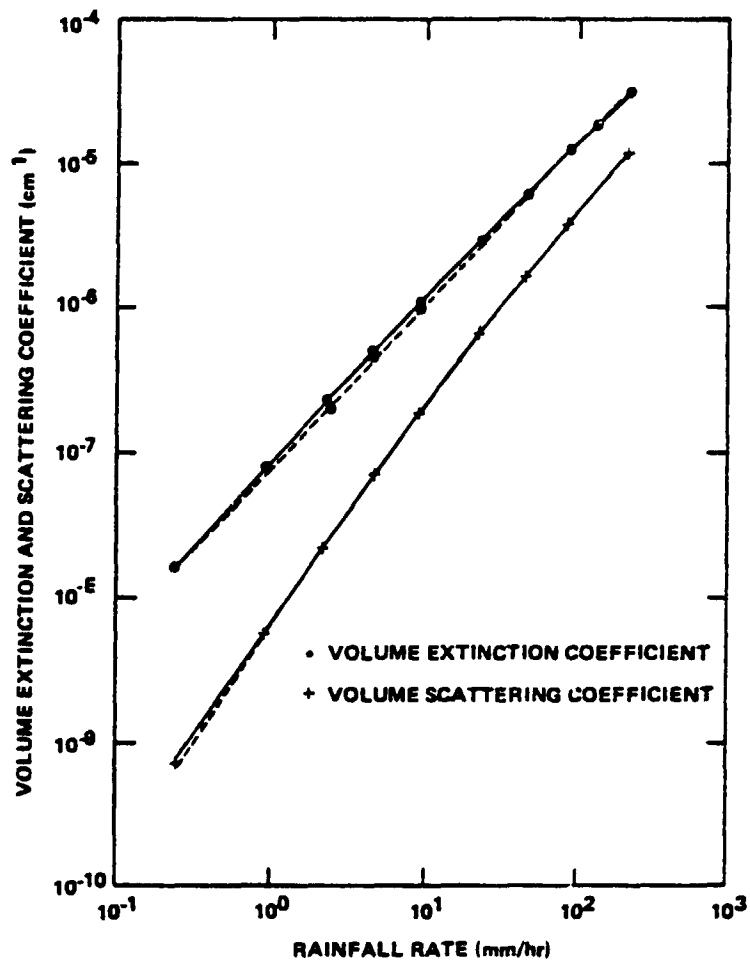


Figure 3. Scattering and Extinction (Absorption plus Scattering) by Rain at 18.35 GHz (the solid and dashed lines represent temperatures of 20° and 0°C, respectively)

The ESMR-5 technique for measuring rain rate has also been used to monitor latent heat release in tropical cyclones (Rodgers and Adler, 1981). It was found that ESMR-5 measurements could be used to monitor storm-intensity changes. Black et al., (1981 unpublished manuscript) developed a similar technique, using much lower frequencies (4 to 6 GHz), which may be applicable for airborne use in intense rain over the oceans.

Meneely (1975) demonstrated that rainfall rate and coverage cannot be delineated by using ESMR-5 measurements (19.35 GHz) over land areas because rain has only a weak effect on the upwelling  $T_B$  from the land. The effect is comparable to that of soil moisture. Thus, although rain-like patterns can be discerned in the data, they agree with both active rain areas and areas with moist soil.

However, Savage and Weinman (1975) and Savage et al. (1975) demonstrated that, at 37.0 GHz (i.e., the frequency at which the ESMR-6 measures upwelling radiance), the scattering by hydrometeors is strong enough to provide a qualitative estimate of rain coverage over land. Furthermore, Weinman and Guetter (1977) demonstrated from theoretical considerations that the upwelling radiation at 37.0 GHz emerging from rain clouds is essentially unpolarized and therefore contrasts with the radiation emanating from wet-surface background. (According to the electromagnetic theory, the addition of moisture to a surface reduces the emissivity by increasing its dielectric constant. The emissivity will then be highly polarized when the surface is viewed obliquely.) These results are demonstrated in Figure 5 which displays theoretically calculated bipolarized 37.0 GHz  $T_B$  at a 50 degree incidence angle

ORIGINAL SOURCE  
OF POOR QUALITY

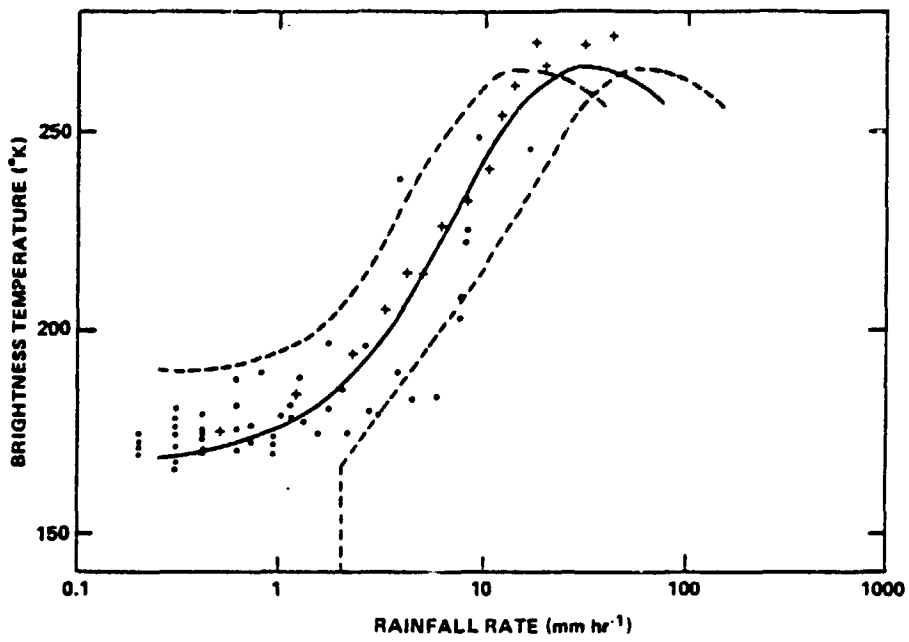


Figure 4. Brightness Temperature at 19.35 GHz as a Function of Rainfall Rate Over the Ocean

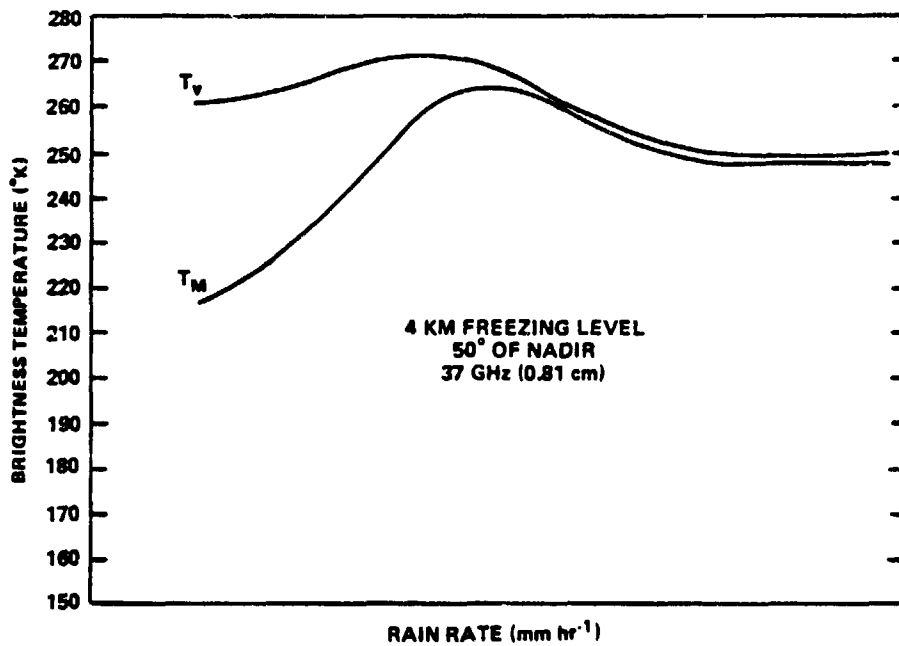


Figure 5. Computed Horizontally and Vertically Polarized Brightness Temperature at 37.0 GHz as a Function of Rain Rate

with the Earth's surface for a given rain rate. These  $T_B$ 's were derived from a radiative transfer model with Lambertian reflection (Born and Wolf, 1975) from land surfaces at a thermodynamic temperature of 299 K and with a fixed dielectric constant and an atmospheric freezing level at 4 km (Wilheit et al., 1977). Figure 5 shows that, as rain rate increases (beyond  $4 \text{ mm h}^{-1}$ ),  $T_B$  decreases because of strong backscattering by the large raindrops. Also, the polarization difference becomes smaller. Moreover, Hall et al. (1978) inferred theoretically that information analogous to that provided by the NWS radar summary charts can be produced when both the ESMR and the temperature humidity infrared radiometer (THIR) 11.5 M TR channel on board Nimbus 6 are used.

Thus, the sum and substance of these theoretical investigations is that the obliquely viewed 37-GHz radiation emitted by wet-soil surfaces is polarized ( $T_V > T_H$ ), whereas radiation emanating from dry land or heavy rainfall areas is essentially unpolarized ( $T_V \approx T_H$ ). Moreover,  $T_B$ 's upwelling from dry-land areas are distinguishably higher than those from heavy rainfall areas or wet land surfaces. Hence, according to these theoretical conclusions, rainfall over land can be at least qualitatively delineated, and its coverage and movement can therefore be monitored irrespective of the land background by employing 37-GHz measurements from the ESMR on board Nimbus 6.

Rodgers et al. (1979) analyzed several cases by using the dual-polarized 37-GHz data from ESMR-6 and statistical classification techniques. They found that the data could be classified into rain, dry ground, and wet ground, but with substantial misclassification. If the surface temperature was lower than  $15^\circ\text{C}$ , as would be the case with dew present, the technique broke down altogether. The use of infrared (IR) data to determine the presence of a cold cloud improved the performance. (At the workshop, Weinman presented data that suggested that quantitative rain measurements over land may be possible by using 37 GHz with IR observations.)

Observations from aircraft platforms have shown that, at frequencies near and above 90 GHz, the ice associated with convective rainfall scatters microwave radiation, resulting in brightness temperatures much lower than land or ocean backgrounds. Therefore, areas of active convection over land could be delineated by using these higher frequencies.

Measurements of surface soil moisture can be used as a surrogate detector of recent precipitation because, for most land surfaces, rainfall is the only mechanism for increasing surface soil moisture. The microwave emissivity of the surface soil ranges from 0.95 for dry soils to less than 0.7 for wet soils. This produces a  $T_B$  range of 80 K or more. This dynamic range has been observed by microwave radiometers operating from towers, aircraft, and spacecraft platforms. Vegetation will increase the emissivity of wet surfaces with the increase being a function of biomass and wavelength. For example, at a wavelength of 21 cm, a 2-m corn crop will decrease the dynamic range to about 40 K or less, whereas, at the 1.55-cm wavelength, pasture grass will obscure the signal from the soil.

In spite of this vegetation effect, strong correlations have been obtained between satellite observations at these two wavelengths and an antecedent precipitation index (API). Data from the 21-cm S-194 radiometer on Skylab obtained over the central United States has shown a strong correlation with API. For a pair of passes over the same track 5 days apart in June 1973, there was a 30- to 50-K increase in  $T_B$  as the soil dried following heavy rains in early June. An analysis of a set of five passes yielded an  $r^2 = 0.7$  between  $T_B$  and API for the Great Plains regions of the United States, where  $\alpha$  is the correlation coefficient. Analysis of 2 years of ESMR-5 data for the southern Great Plains has also shown high correlation with API under suitable conditions. The best correlations were obtained for the areas where a large part of the area was devoted to the production of winter wheat during the early spring and fall. These areas, which are relatively flat, have limited vegetative cover during these periods. Areas with more rugged terrain or more vegetative cover show a poor correlation between  $T_B$  and API. These results indicate that spaceborne radiometers can respond to surface-moisture changes and can be related semiquantitatively to the antecedent precipitation.

Based on the foregoing results and on modeling, the U.S. Department of Defense is building a multifrequency microwave imager called the SSMI for the Defense Meteorological Satellite Program (DMSP), (Savage, 1981). This sensor will measure radiation at 19.35, 22.235, 37, and 85 GHz with resolutions ranging from 50 km at 19.35 GHz to 12.5 km at 85 GHz. The first flight of this instrument is planned for 1984.

An instrument that was planned for the now-cancelled National Oceanic Satellite System (NOSS), the large-antenna multifrequency microwave radiometer (LAMMR), would have had radiometer channels at 18, 21, and 36.5 GHz, among others, with spatial resolutions in the 7- to 8-km range. Either this or a similar instrument would provide a valuable opportunity for oceanic rainfall mapping.

Because of resolution limitations, the use of passive microwave techniques for mapping rain from geostationary orbit must be limited to the use of frequencies above 90 GHz.

The present state of the art on which all workshop participants agree is summarized as follows:

- Passive measurements in the 10- to 40-GHz region represent a viable technique for measuring rain over the ocean. This measurement is based on a sound theoretical model in which all uncertain elements are physically measurable parameters. The problems associated with this technique are matters of detail in determining the calibration transfer function and are not fundamental limitations.
- Rain over land presents a more difficult problem. Hybrid techniques using IR and high-frequency microwave measurements (90 GHz) offer some promise, but there are no clear-cut approaches which can assure success.

### 6.3 MICROWAVE MEASUREMENT PROBLEMS

For microwave instruments, the effect of the inhomogeneity of the rain rate within the field of view (FOV) must be addressed. Because the effect is nonlinear, it is doubtful that it can be removed by using only the microwave data.

Suppose that we had the ability to obtain microwave observations of rain with unlimited spatial resolution. At any frequency, a nonlinear relationship exists between the column density of rain and the  $T_B$ . Also, there is some column density at which the  $T_B$  saturates. Above this column density, the  $T_B$  decreases because of the effects of scattering. Since the observed  $T_B$  depends on the column density of particles, the rain rate cannot be inferred unless the height of the rain column is known. Again, the effect is nonlinear.

Other problems are the effect of cloud liquid water and water vapor on the  $T_B$  and the ability to develop a technique to separate these effects from the precipitation information.

The following sections address the problems of beam-filling, rain column height, and cloud liquid water and offer some suggestions for resolving these problems.

#### 6.3.1 Beam-Filling

Because a considerable spatial variation occurs in the rain rate within the FOV of a microwave sounder, it is necessary to evaluate the effects of beam-filling. Nonuniform filling of the beam causes a bias in the rainfall estimates so that it is necessary to evaluate the magnitude of this bias. In this connection, the following steps should be taken:

- a. Statistical data must be developed concerning the size distribution of rain cells (i.e., a probability distribution function (PDF) for rainfall rates within the FOV). It would be desirable to compare the PDF's over land and ocean. The aim is to determine if there is a small enough set of parameters that describe the PDFs so that they can be determined either from the microwave data or from conventional sources. Additional experiments will be needed to expand the understanding of the statistics of rainfall distribution.
- b. Given the statistics of rainfall distribution on a scale smaller than the FOV, radiative transfer models must be used to evaluate the error in the rain-rate determination. It will be necessary to find the bias in the rain-rate estimate and the variability of the bias.
- c. IR information may be available on a much smaller spatial scale than is possible with microwave. Investigation is needed to determine how IR data can be used to estimate the beam-filling factor. This would be straightforward if the precipitation area could be defined unambiguously by IR temperature but, unfortunately, it cannot.

Data from two radar experiments, GATE and CCOPE (over ocean and land, respectively), and additional data from Kwajalein Radar and other experiments are potentially available. Analysis of these data will show the PDF's for rain-rate distribution and rain height for two climatological regimes. To the extent that the resultant PDFs are similar, the statistical approach to the beam-filling problem will work globally.



### 6.3.2 Effective Rain-Layer Height

A physical parameter essential to estimating rain from microwave radiances is the thickness of the rain column. Because the radiometer responds to the path-integrated rainfall, this thickness is best characterized by the effective rain-layer height ( $h_{\text{eff}}$ ), which is defined as the path-integrated attenuation divided by the surface attenuation coefficient.

Although radar data in GATE indicate RMS variations in  $h_{\text{eff}}$  of approximately  $\pm 60$  percent on a 1 by 1 scale, variations are considerably smoothed ( $\pm 15$  percent) when averaged over  $(200 \text{ km})^2$ . Furthermore, no systematic variation of the mean height was observed in the GATE phase III. This fact points to the probable climatological relationship of the mean  $h_{\text{eff}}$  to the mean freezing layer, which varied by  $\pm 5$  percent over the same period. The existence of such a relationship is extremely important because there is no known way of directly estimating  $h_{\text{eff}}$  by satellite.

Since nothing is known about the seasonal or geographical variation of this quantity, an intensive investigation is urgently required. Such a study could be performed by examining three-dimensional radar scans from different locations and seasons, covering as many different climates as possible. Although radar data over the oceans are clearly the most appropriate and should be used as much as possible, much could be learned from land-based observations. Observations from midlatitude radar records would be especially valuable because the freezing layer height varies considerably during the year.

A relationship may exist between  $h_{\text{eff}}$  and freezing level in stratiform and convective rain and this could be easily evaluated (particularly stratiform rain). However, meteorological parameters other than freezing-layer height should also be correlated with  $h_{\text{eff}}$  since the ultimate accuracy of the rain estimates is related to the uncertainty in  $h_{\text{eff}}$ .

An important problem related to the  $h_{\text{eff}}$  determination is the estimation of the vertically integrated water vapor. Knowledge of this quantity is important because the contribution of the water vapor to the microwave radiance must be removed so that the rain contribution can be determined. Water vapor can probably be measured by using radiances at two frequencies and by taking advantage of the extreme frequency dependence of water vapor in the 1.35-cm absorption line. This has been demonstrated by several investigators using ground-based radiometry at several frequencies.

### 6.3.3 Cloud Liquid Water

Nonprecipitating cloud liquid water (CLW) is spectrally similar to rain; it will be necessary to see how well the two can be separated. The presence of CLW will place a lower limit on the rain rate that can be detected. Steps that should be taken to minimize the problem are as follows:

- a. Experiments should be done to determine how much CLW can exist in a cloud before it begins to rain. Such experiments would consist of upward-looking radiometers in the 10- to 37-GHz range, used either alone or in conjunction with digital three-dimensional radar. Because radar and microwave radiometers measure very different moments of the drop size distribution, it is possible to simultaneously measure the amounts of rain and CLW when radar data are available.
- b. Although the spectral response of CLW is similar to that of rain, they are not identical. First, a modeling study should be performed to determine if simultaneous observations at different frequencies can be used to separate rain and CLW. If the modeling suggests that this can be done, experiments will be needed to verify this method of separating rain and CLW.
- c. The presence of variable amounts of water vapor (WV) confuses the rain determination. It has already been demonstrated that WV can be measured with microwave observation in the absence of rain. The same comments as in b apply to the problem of separating rain effects from WV (except that water vapor is spectrally very different from rain and CLW, which makes the problem somewhat easier).

- d. Much of the modeling effort depends on knowing reasonable values for the drop-size distribution of CLW and rain. In situ measurements should be made by flying aircraft into a variety of cloud types to measure particle-size distributions directly and to measure the microwave emission at the relevant frequencies in different directions.

Simultaneous data on particle size and brightness temperatures will be necessary for calibrating the radiative transfer models and for ensuring the correctness of the models.

#### 6.3.4 Rain Over Land

The use of passive microwave techniques over land, even in combination with visible (VIS) and IR data, is an extremely difficult undertaking. The large and variable emissivity of land background results in a very poor signal-to-noise ratio. Nevertheless, all the passive microwave techniques discussed in Section 6.2 involve the direct detection of precipitation-sized hydrometeors, either liquid or ice, and thus have a more direct physical connection to the rain than VIS and IR techniques.

Technique development in this area is just getting under way. A few investigators have been examining only small amounts of data for a short time as compared with other techniques under discussion. However, more data are now available, and future data will result from the DMSP/SSM/I sensor. More investigators are needed in this field, and the only requirement is that they be able to find funding and select reliable data for their analysis programs. These programs are inexpensive compared to hardware or even modeling. Some specific problems and potential solutions in connection with microwave rain-fall measurements over land are:

- a. Dew Formation – Dew on the surface of the ground and on vegetation provides large droplets that can scatter radiation in a manner similar to the scattering caused by hydrometeors. However, because dew formation is most common on cloud-free nights, the use of an IR measurement for checking the existence of clouds greatly reduces the false-rain probabilities. In fact, false-rain detection can be greatly reduced by using VIS and/or IR to check for the existence of clouds. Spatial consistency provides another filter for reducing false-rain detection.
- b. Cool Surfaces – Surface temperatures greater than 15°C are necessary for any useful rain signal in the microwave measurements. This may prove to be a fundamental limitation that will restrict the range of applicability of the passive microwave techniques to subtropical and tropical regions and to midlatitude regions during the warm months. The warm months are, of course, the most important for crop estimation purposes.
- c. Phase of Hydrometeors – When the use of higher frequencies (greater than about 85 GHz) for rain-mapping is explored, the  $T_B$  observed is determined primarily by the phase rather than the size or number of hydrometeors. Although this information is interesting, it is not directly related to rain rate. Because these high frequencies provide the only realistic hope of microwave rain-mapping from geostationary altitude, the relationship between the ice phase and rain must be better understood.
- d. Horizontal Homogeneity – The assumption of horizontal homogeneity in most radiative transfer models may be inadequate for typical convective systems. Thus, more effort is needed in the development of a finite-cell model.

#### 6.4 RECOMMENDED MEASUREMENT SYSTEM

It is premature to attempt to specify in detail what the ultimate precipitation system should be. It will be several years before any new space segment for such a system is likely to be approved; during this time, much homework must be done. However, some general conclusions can be made at this time.

Microwave radiometers offer an extremely good method of measuring rain over the ocean. Unfortunately it is only practical from a low Earth orbit. We therefore recommend a scanning multifrequency passive radiometer and a nadir-viewing radar payload for a low-Earth orbiter to complement existing instruments on geostationary satellites. As now envisioned, the microwave radiometer would have frequencies at approximately 18, 21 and 37 GHz. The

necessary ground resolution is an open issue. The radar should have as high a resolution as possible in all three dimensions. The space system must be complemented by a ground-truth benchmark system so that all measurements will ultimately be referenced to a measured volume of water.

The interaction of the components of the system would be as follows;

- a. Over ocean areas, the radiometer would provide infrequent but reliable rain measurements. On the other hand, the geostationary instrument would provide less reliable measurements almost continually. The radiometer could then be used to calibrate the geostationary instrument on a twice-daily basis. The radar would provide a limited set of high-reliability measurements with error sources independent of the radiometer errors. Further, by having high three-dimensional (x, y, z) resolution, the radar would serve as a continual check on many of the physical assumptions in the radiometer model.
- b. Over land, the radar alone would have to serve as the calibration source and the geostationary component would have to interpolate in both space and time. With the addition of the appropriate channels, the microwave measurements could possibly augment the geostationary measurements over land. It is not possible at this time to base a channel-selection recommendation on any solid result in this area.

## 6.5 RECOMMENDATIONS

Recommended activities are:

- Further study to understand rain-layer thickness effects, including airborne experiments, radar experiments, and theoretical studies.
- Statistical studies using radar data from many locations to investigate possible solutions to the beam-filling problem and to estimate requirements for future LAMMR-like instruments.
- Airborne and ground-based radiometer experiments to estimate typical nonprecipitating CLW content for both raining and nonraining situations.
- Aircraft observations at frequencies of 85 GHz and higher for various precipitation events to compare with ground-truth information.
- Cleanup of Nimbus 7 SMMR data.
- Archival of the DMSP/SSMI data with complete documentation.
- Identification of factors that affect the accuracy of hybrid methods and simulation of error budgets.
- Investigation of methods for using passive microwave techniques to estimate soil moisture and to determine if these measurements can imply rain rate over land.
- Microwave instrumentation technology studies for an advanced LAMMR-like instrument for a potential shuttle rain radar mission.

## REFERENCES

- Born, M., and E. Wolf, 1975: Principles of Optics. Pergamon Press, 182 pp.
- Gunn, K. L. S., and T. U. R. East, 1954: The Microwave Properties of Precipitation Particles. Quart. J. R. Meteorol. Soc., 80, pp. 522-554.
- Hall, C. D., R. Davies, and J. A. Weinman, 1978: The distribution of precipitation derived from Nimbus-6 data. Paper presented at 18th Conference on Radar Meteorology, Atlanta, Amer. Meteor. Soc.
- Meneely, J. M., 1975: Application of the Nimbus-5 ESMR to rainfall detection over land surfaces. Contract Rep. NAS5-20878, 48 pp.

- Rao, M. S. V., W. V. Abbott, III, and J. S. Theon, 1976: Satellite-Derived Global Ocean Rainfall Atlas (1973 and 1974), NASA X-911-76-116, Goddard Space Flight Center, Greenbelt, Maryland.
- Rodgers, E. B., and R. F. Adler, 1981: Tropical Cyclone Rainfall Characteristics as determined from a Satellite Passive Microwave Radiometer. Mon. Wea. Rev., 109, pp. 506-521.
- Rodgers, E. B., H. Siddalingaiah, A. T. C. Chang, and T. Wilheit, 1979: A statistical technique for determining rainfall over land employing Nimbus-6 measurements. J. Appl. Meteor., 18, pp. 978-991.
- Savage, R. C., and J. A. Weinman, 1975: Preliminary calculations of the upwelling radiance from rain clouds at 37.0 and 19.35 GHz. Bull. Amer. Meteor. Soc., 56, pp. 1272-1274.
- Savage, R. C., P. J. Buetter, and J. A. Weinman, 1976: The observation of rain clouds over land in Nimbus-6 electrically scanned microwave radiometer (ESMR-6) data. Preprints 7th Conference Aerospace and Aeronautical Meteorology and Symp. on Remote Sensing from Satellite, Melbourne, Amer. Meteor. Soc., pp. 131-136.
- Savage, R. C., 1981: The DMSP microwave imager (SSMI) – unfinished plans. (See Appendix D.)
- Weinman, J. A., and P. J. Guetter, 1977: Determination of rainfall distribution from microwave radiation measured by the Nimbus 6 ESMR. J. Appl. Meteor., 16, pp. 437-442.
- Wilheit, T., A. T. C. Chang, M. S. V. Rao, E. B. Rodgers, and J. S. Theon, 1977: Satellite Technique for Quantitatively Mapping Rainfall Rates over the Oceans, J. Appl. Meteor., 16, pp. 551-560.

N83 25275 D6

7. SPACEBORNE RADAR WORKING GROUP

PARTICIPANTS

Richard K. Moore, Chairman  
Jerome Eckerman, CoChairman  
Robert Meneghini, CoChairman  
David Atlas  
Wolfgang M. Boerner  
Steve Cherry  
John F. Clark

Richard J. Doviak  
Julius Goldhirsh  
Roger M. Lhermitte  
Phillipe Martin  
Carlton W. Ulbrich  
Edward A. Wolff

## 7. SPACEBORNE RADAR

### 7.1 INTRODUCTION

The spaceborne radar panel considered how radar could be used to measure precipitation from satellites. The emphasis was on how radar could be used with radiometry (at microwave, visible (VIS), and infrared (IR) wavelengths) to reduce the uncertainties of measuring precipitation with radiometry alone. In addition, the fundamental electromagnetic interactions involved in the measurements were discussed to determine the key work areas for research and development to produce effective instruments. Various approaches to implementing radar systems on satellites were considered for both shared and dedicated instruments. Finally, a research and development strategy was proposed for establishing the parametric relations and retrieval algorithms required for extracting precipitation information from the radar and associated radiometric data.

Rayleigh is the scattering process involved with centimetric radars that observe rain clouds; (i.e., the greater cross section is proportional to  $D^6/\lambda^4$  where D is particle diameter and  $\lambda$  is wavelength.) Raindrops thus produce radar returns many orders of magnitude greater than those from nonprecipitating clouds. In short, radar interacts primarily with rain and, unlike radiometry, can directly identify the presence of rain below rain clouds. It is this interaction with the rain that gives radar a good chance of measuring precipitation rates without the need for tenuous assumptions. Radar, can therefore aid substantially in measuring precipitation from space.

Nonetheless, radar measurements will be subject to certain errors involving beam-filling, propagation effects, and uncertainties in the drop-size distribution of the precipitating particles. To help reduce these errors, radiometry may be used to estimate propagation effects or to identify cloud structures that may affect the interpretation of the radar data. Combining radar and radiometry techniques (Section 6) should optimize the usefulness of precipitation measurements from space.

The relatively long wavelength of radar systems as compared with VIS and IR techniques dramatically degrades the spatial resolution. This is particularly severe if operation from geostationary satellites is to be considered. Conversely, if the radar is to image with high resolution over a large area, complex radar systems will be required. In either case, extreme demands of size and power will be placed on the carrying satellite. Therefore, the improvement in the accuracy of rainfall measurements by radar will have to be weighed against the extra complexity and cost.

### 7.2 COMBINED MEASUREMENTS

Hybrid measurements, which combine the use of radar and radiometers, have a variety of advantages. For example, the microwave radiometer when used over the ocean, can provide a measure of the path-integrated attenuation; the radar, on the other hand, can provide measurements of both the top of the precipitation and the height of the melting level. These measurements allow the radiometer-determined attenuation to be attributed to specified rain rates that are below the melting level. In addition, the profile of radar reflectivities appears to make it possible to obtain a vertical profile of rain rates. Should a radar backscattering from the sea occur, the combination of radar and radiometry can provide both the radar cross-section of the sea and the intervening attenuation required to estimate the rainfall from the attenuation.

Combinations of radar and IR/VIS measurements also appear to be useful. In one such application, the more accurate radar measurements could be used for calibrating and checking the IR/VIS precipitation maps.

Another application uses IR/VIS instruments as look-ahead sensors so that the radar could be directed toward the region of precipitation. (See paragraph 7.4.2.5.)

### 7.3 CANDIDATE SYSTEMS CONCEPTS

#### 7.3.1 Generic Systems

Among the advantages of radar, in comparison to other systems, for measuring meteorological parameters is the diversity of data acquisition techniques. Many of these techniques have been fully tested and are being used in measuring precipitation parameters with ground-based instrumentation. For example, the National Weather Service network

of weather radars combines measurements of radar backscattered power, azimuth angle, elevation angle, and range to construct a three-dimensional model of the precipitation field. Similar measurements are combined with Doppler processing in radars like those operated by the National Severe Storms Laboratory to deduce information about the motion of the hydrometeors. These are only two examples of the large variety of measurement platforms that are possible when combinations of coordinate geometry, amplitude measurement, and frequency and polarization diversity are considered. All of these are possible on satellite-borne meteorological radar. Some examples are described later in this section.

### 7.3.2 Orbit Considerations

A low Earth orbit (LEO) permits fine-scale spatial resolution with a radar system of modest size and power requirements. However, the geographical coverage of the radar footprint is limited so that a given location is covered only infrequently. Broadening the footprint provides greater geographical coverage but at the expense of resolution, increased power requirements, and accuracy. A geosynchronous orbit (GEO) permits increased temporal resolution but with less spatial resolution and power options. A highly elliptical orbit of the Molniya type combines the advantages and disadvantages of both LEO and GEO and may require a more complex measurement system. The systems considered in this report are best suited for LEO satellites. An exception is the bistatic spaceborne radar (paragraph 7.4.2.7) that is specifically designed for satellites in geostationary orbit.

## 7.4 CANDIDATE SPACEBORNE RADAR SYSTEMS

In describing the following systems, a few general assumptions about the kinds of measurements that are optimal were adopted. For example, it is assumed that the profiling of precipitation fields is best accomplished by using pulsed microwave frequencies in the X- and K-bands, either alone or in combination. Integration with respect to area and altitude is also possible in these bands. Multiple-frequency methods will permit discrimination of land surfaces from precipitation in the K-, X-, and C-bands. Introducing polarization methods should permit discrimination of rain from ice (e.g., in the identification of the bright band) and might permit discrimination of the ground echo from rain. Therefore, combinations of measurables are considered that involve coherent and incoherent polarized frequency-diversity microwave instrumentation in the aforementioned frequency bands. There are two categories of specific radar systems: (1) shared systems and (2) dedicated systems that are listed as follows:

<u>● Shared Primary Sensor</u>	<u>Systems Modifications for Precipitation</u>
- Altimeter	Early range gates
- Scatterometer	$\Delta f$ Scatrad Range-resolution Scatrad
- Multifrequency microwave radiometer (MFMR)	Doppler adaptive pointable radar Fixed simultaneous multibeam
<u>● Dedicated</u>	
- Intermediate resolution (5 to 10 km)	Multibeam Nadar Surface reference $\Delta f$ Scatrad and range resolution
- Fine resolution (1 to 3 km)	Doppler adaptive pointable radar Fixed simultaneous multibeam

The shared systems are microwave sensors developed primarily for determining geophysical parameters other than rain. Modifications of these instruments are suggested that could add a precipitation sensing mode without seriously degrading the primary performance of the sensor. However, shared precipitation sensing is not optimum for all modes. Parameters of dedicated systems are selected to improve some aspects of the sensor performance.

#### 7.4.1 Shared Systems

Several active and passive microwave sensors have been developed and flown in space for determining specific geophysical parameters:

- Altimeter – Ocean geodesy and wave height
- Scatterometer – Ocean wind speed and direction
- Multifrequency radiometer – Sea-surface temperature, ocean wind speed, water content, ice, sea, and snow

Conventional synthetic aperture radar (SAR) does not lend itself to a shared mode because the elevation beam widths needed for swath width are impediments to use of "early" precipitation gates. "Early" gates are those range gates that occur above the Earth's surface and can capture any precipitation echoes present.

In principle, it is feasible to modify each of these sensors while sharing the same antenna and obtaining additional information on precipitation. The following paragraphs describe the proposed sensor combinations.

**7.4.1.1 Nadir Altimeter for Rain (NADAR)** – Before the NOSS program was terminated, the incorporation of a rain mode on the radar altimeter was planned (Walsh, 1981), with the likelihood that future satellite-borne radar altimeters will also contain similar rain-measurement capabilities. Such a mode may be considered as a piggyback to an already existing radar system, and its implementation would require minimal cost because only minor modifications are required (Goldhirsh and Walsh, 1981). The rain altimeter would serve two purposes. First, it would provide the experimenters who are interested in establishing mean sea height and wave height with absolute levels of rain rates that degrade their measurements. Second, this piggyback scheme would provide valuable data to experimenters who are interested in precipitation and would lead to an improved design of the next generation probe which might be dedicated to measuring precipitation. The 13.5-GHz altimeter frequency enables two independent types of measurement, i.e., a relatively unattenuated power measurement at the top of the rain cell and a power difference between the top of the cell and the bottom (near ground) giving rise to the attenuation. Both measurements may be used independently to give estimates of the rain rate or may be combined to improve these estimates (Atlas and Ulbrich, 1974; Goldhirsh and Katz, 1974).

Through a preliminary analysis the ability to extract rain rate and average rain drop-size distribution using simplified assumptions has been demonstrated. Although the technique using a combination of power measurements at the storm top and attenuation measurements results in a random component of 3 to 4 mm/hr, it is superimposed on a system bias error of approximately 15 percent (Goldhirsh and Walsh, 1981). Therefore, the system should be able to be calibrated to at least this accuracy.

**7.4.1.2 Scatterometer (Scatrad)** – The scatterometer is a sensor which is based on the Scatrad S-193 principle demonstrated on the Skylab Ku-band (14-GHz) mechanically scanned parabolic reflector scatterometer-radiometer. The Scatrad is capable of viewing the ocean surface in two directions 90 degrees apart. The average scattering coefficient varies with wind speed and wind direction. The radiometer provides the precipitation loss (total attenuation) in the Scatrad beam, which is used to correct the radar signal. This wind-speed estimate is then used to improve the brightness temperature so that the iterated attenuation value is improved over the first estimate. Modifications could be made to the scatterometer to enhance precipitation measurements. Two examples are:

- a.  **$\Delta f$  Scatrad** – In this modification of the scatterometer radiometer, the radar signal is either stepped over a small frequency interval,  $\Delta f$ , or several narrowband channels are used at fixed frequencies. The ocean radar reflectivity is relatively constant whereas the rain attenuation changes significantly with frequency; the latter dependence would yield the rain rate.
- b. **Range-Resolution Scatrad** – The use of additional modulation of the Scatrad waveform (chirp, short pulse, or FM/CW) offers the capability of range-gating the precipitation-scattered signal.

**7.4.1.3 Multifrequency Microwave Radiometer (MFMR)** – The first MFMR flown on Nimbus 7 and Seasat (SMMR – 6, 10, 18, 21, 37 GHz dual-polarized channels) had a 1-meter diameter antenna with a 25-degree scan. Operational versions under consideration (e.g., large-antenna multichannel microwave radiometer) would have apertures of 2 to 4 meters in diameter and a 350-degree scan. Because the passive application of an MFMR needs only 180 degrees of



scan, it is feasible to include active channels that would use the other 180 degrees of scan. With careful RFI design, the active and passive sensors could also share the same scan directions.

Several radar configurations appear to be feasible for augmenting an MFMR. The two modifications for enhanced precipitation sensing that were outlined in the previous section could be used here also:  $\Delta f$  scatterometer channels with range resolution capabilities.

#### 7.4.2 Dedicated Systems

The shared-sensor approaches discussed in Section 7.4.1 can result in compromising some sensor performance. Dedicated sensors which are optimized for precipitation retrieval offer more accurate rain characterization. The following paragraphs briefly discuss several representative systems that have most features of the generic radar systems. These systems progress from moderate to fine spatial resolution and are accompanied by a progression in antenna size, complexity, and cost.

**7.4.2.1 Surface Target Attenuation Radar (STAR)** – The surface target radar determines the precipitation rates from radar beam attenuation. The backscattered power is directly proportional to the product of the surface scattering coefficient and the two-way attenuation through the rain to the surface. The scattering coefficient of terrain  $\sigma = -10$  db  $\pm$  2 db when the instantaneous field of view (IFOV) is large (10 km) at incidence angles greater than 30 degrees. In the ground comparison approach,  $\sigma^{\circ}$  can be determined from either measurements of nearby fields of view around the storm or average values obtained previously. The attenuation coefficient, k db/km, is calculated from the ratio of the total attenuation to the radar-measured storm height. In the 1 to 2 cm wavelength region rain rate is linearly proportional to the attenuation coefficient (Atlas and Ulbrich 1977). The surface reference target scheme can be implemented in scanning-beam and fixed-beam geometries with resolutions from 1 to 5 km. Statistical modeling results indicate that random errors of 20 percent of the true rain rate are obtained at frequencies of 36 GHz with beam widths of 4 and 1 km (Eckerman et al., 1978). This should be classified then as intermediate or high resolution.

**7.4.2.2 Frequency Agile Rain Radar (FARR)** – In the FARR approach, the radar is switched between two nearby frequencies. Ocean and land radar scattering coefficients are relatively constant in a small frequency interval. Therefore, the ratio of received power in the two channels is proportional to the differential attenuation at the two frequencies. The differential attenuation, in turn, can be related to the rain rate by means of an attenuation (k) – rainfall (R), or the k-R law.

**7.4.2.3 Scatterometer (Scatrad)** – The concept of precipitation determination using the frequency agile approach was discussed briefly in the section on shared systems. In the shared mode, the primary observation of ocean wind speed determined the scan method. In a dedicated scatterometer-based system, the beamwidth, scan modes, and frequencies can all be optimized for observing precipitation. For example, a single-beam conically scanned instrument would be adequate for the precipitation mode. The ground comparison and frequency agile surface reference techniques can be complemented at frequencies near 15 and 35 GHz.

**7.4.2.4 Fixed Simultaneous Multibeam Radar (FSMR)** – For spatial resolution on the order of 1 km, scanning-beam optics do not provide a sufficient number of independent samples to obtain accurate echo power and rainfall measurements. Broadband waveforms (Krehbiel and Brook, 1980) offer one solution to this problem but at the expense of signal-to-noise ratio, which raises the minimum detectable rain rate to higher levels. Frequency diversity also offers a possible solution. However, this method required a mechanically rotated antenna that is 1000 wavelengths in diameter. When the need for multiple beaming in elevation is factored in (to keep the rotational rate low), it is clear that a mechanically scanned 1-km IFOV precipitation radar would result in a complex system. Electronic scanning is impractical for similar reasons. One possible full-swath coverage system is the fixed simultaneous multibeam concept proposed by Technology Service Corporation (1975). This antenna system uses vertical boom array transmit and receive antennas to give conical illumination. The receive antenna is made up of many vertical sticks (or booms) with a beam-forming network forming the simultaneous azimuthal receive beams. Doppler azimuth beam-sharpening further reduces to 1 km the width of these real apertures. This configuration minimizes the antenna dimensions because synthetic aperture techniques are used. The greatest disadvantage is that two unique radars are needed to implement dual frequency, whereas, with reflector antennas, several frequencies can be integrated into a single microwave optical system.

7.4.2.5 Adaptive Pointable Multibeam Radar (APMR) – A variant of the fixed multibeam radar is a pointable approach that is in a much earlier stage of development than the fixed simultaneous multibeam. The proposed idea is to use two systems (Atlas, 1981). The first is a look-ahead radiometric system that detects and acquires storm systems ahead of the spacecraft and the second is a storm mapping radar. This latter radar has an adaptive beam which squints cross-track at selectable elevation angles that are programmed to positions of the storms as observed in the detection/acquisition system. The system's advantages are twofold because it can obtain a large sample of independent pulses and cover a wide swath. In addition, the system requires less energy and communications bandwidth because it operates only when rain events are present.

7.4.2.6 Bistatic Spaceborne Radar – A spaceborne meteorological radar in low Earth orbit is able to observe meteorological events such as hurricanes, typhoons, or specific storm fronts, but is limited as a general meteorological tool because a single satellite monitors a given area only twice a day. Coverage for these meteorological events are usually desired 5 to 10 times more frequently. Such coverage can be accomplished with a bistatic radar (Natlanson, 1981) on a single geosynchronous spacecraft.

A coherent radar transmitter with a medium-sized antenna can be placed in a geosynchronous orbit, preferably with a beam that scans the United States in a "raster" pattern with about 0.9-degree beamwidth. This scanning can be accomplished either mechanically, which is slow, electronically using multiple feeds, or by frequency-scanning techniques. The receivers are ground-based and may have Doppler capability.

Two factors make the meteorological application attractive. First, the bistatic reflections of radar signals from precipitation are omnidirectional, and the relationship of the reflectivity of the rain-to-rainfall rate can be easily derived. Second, the rain echo signal level is independent of range from a receive-only radar, and the system will work at long ranges.

The bistatic approach has the potential to provide finer resolution and more information about precipitation than other spaceborne radar techniques. Of particular significance is the low-data rate and simplicity of the bistatic system output, which lends itself to unattended receivers that are connected by telephone lines to central processors. However, this technique is limited to parts of continental areas that are within view of the receivers.

## 7.5 REQUIRED RESEARCH AND DEVELOPMENT STEPS

Several of the necessary research and development steps which will lead to the definition and implementation of a spaceborne radar are outlined here. Some of the preliminary work should focus on a detailed study of radar methods and algorithms in the context of spaceborne radars, delineating the major sources of error and determining their estimated accuracies, dynamic range, and spatial and temporal resolution. The next stage is to develop a spaceborne simulation by which the various systems and associated methods can be compared in a consistent fashion. The results of such studies will help to identify some of the most promising systems that satisfy the accuracy and sampling requirements of the major user groups. The validation of these concepts can be accomplished by means of an experimental program involving side by side flight of multiwavelength radars, radiometers, and IR/VIS instruments. Along with experimental efforts, there must be an identification of analyses and simulations which can be done with existing data bases.

### 7.5.1 Initial System Studies

A major effort is the identification of potential methods and instruments which are appropriate as spaceborne sensors. A number of systems and techniques are described in detail in Section 7.4. Nevertheless, the various methods are summarized here, emphasizing their advantages and weaknesses, to indicate studies that are needed for developing realistic options.

For spaceborne meteorological applications, the use of attenuating wavelengths is preferable because: (1) higher resolution can be attained, thereby reducing errors caused by partial beam-filling and reflectivity gradients within the resolution cell, (2) most of the attenuating-wavelength methods do not rely on the drop-size distribution dependent Z-R law, but rather use a k-R law that is less sensitive to fluctuations in DSD, and (3) several of the methods are independent of the radar calibration constant, which reduces the possibility of large offset errors in the rain-rate estimate.

The disadvantage most of these techniques have is the limited dynamic range achievable with a single attenuating wavelength. One possibility for alleviating this problem is the use of additional radar wavelengths (i.e., shorter wavelengths for estimating low rain rates and longer ones for more intense rain rates). Another possibility is the supplemental use of the conventional Z-R method. For low rain rates, this would approximate the performance of a non-attenuating wavelength radar; for high rain rates, the return from the range cell below or above the bright band (where attenuation effects would be slight) could be used to approximate the average rain rate in the vertical column just below.

Note that the attenuating-wavelength methods (dual-wavelength, attenuating-wavelength methods, and altimeters such as NADAR, STAR, and FARR) are generically the same (i.e., they depend on the assumption that over the measurement set there exists a quantity that remains essentially constant and that provides a calibration point for the total or differential attenuation). For the dual-wavelength method, this quantity is the rain reflectivity (i.e., the reflectivity of a fixed-range cell varies slowly with frequency). For NADAR, this quantity is taken to be the rain rate, in range, along a vertical column. The surface target methods depend on the invariance of the backscattering coefficient of the surface,  $\sigma^0$ . In particular, STAR relies on the small temporal or spatial fluctuations in  $\sigma^0$  (at K-band and incidence angles greater than 30 degrees), whereas FARR exploits the nearly constant nature of  $\sigma^0$  with small frequency changes. An assessment of the validity of these various assumptions should aid in assessing the accuracy and applicability of the methods.

Although combined instrument methods such as radar and radiometry are not discussed here, the contribution of passive channels to various radar techniques should form part of any feasibility study of the various spaceborne radar options.

#### 7.5.2 Modeling and Simulation

Although little active microwave data from space exists by comparison to that from microwave and VIS/IR radiometric systems, the proposed radar systems and techniques must be examined and simulated with a consistent space-oriented model. Some of the major effects to be considered with such a model are: (1) the horizontal and vertical scales of precipitation (i.e., the model must include actual three-dimensional reflectivity data or adequate models of such); (2) the effects of ground clutter and partial beam-filling; (3) the effects of ice and the bright band; (4) the effects of gain pattern, range resolution, frequency of operation, etc. so that a fairly broad parametric study can be conducted; and (5) other error sources such as calibration constant errors, receiver noise, and fluctuations in drop size distribution. The effects associated with the horizontal and vertical scales of precipitation and the effects of ice and the bright band can also be usefully investigated with ground-based and aircraft-based radar data sets. Clearly, with these kinds of data and the long history of precipitation radar development and use, we should be able to develop a space-oriented model that will provide the understanding necessary for defining realistic options for a spaceborne precipitation radar system. With such a model, it is envisioned that a comparison of the different systems and methods could be accomplished.

#### 7.5.3 Experimental Program

The development of an experimental program should be pursued in parallel with systems and modeling studies. Ground-based and airborne experiments can be used to verify, in part, the accuracies of the various measurement systems (radar design and technique) and to identify any additional problems not accounted for in the supporting modeling and analysis activities. Several sessions of the workshop emphasized the need for high-quality ground truth for assessing the accuracy of their measurements. This requirement is no less true for airborne radar experiments. The possibility of the NASA Wallops Spandar radar was suggested as a possible ground-truth site. Its advantages include high resolution and sensitivity and the existence of a supportive system of disdrometers, rain gages, and space/Earth communications links. Another advantage is that, because of its location, the Spandar can retrieve three-dimensional reflectivity profiles above both land and ocean regions.

Although little was said about the specific design requirements of an airborne radar experiment, there appears to be agreement in the basic system outline: a microwave radiometer, as well as IR/VIS instruments, should be included with any radar flight whether airborne or by shuttle. Furthermore, multiwavelength radars should be seriously considered because they will enable a verification of some of the most promising techniques and will provide a means

of selecting the near-optimum wavelengths. If an experimental program can be established early, a meaningful precipitation radar mission could be flown on the Space Shuttle within the 1985-87 timeframe.

#### 7.5.4 Algorithm Development

A strong algorithm development program should be conducted concurrently with the foregoing activities. Although such activities are inherent in modeling and simulations studies, it is important that this high-priority item receive special attention for several reasons:

- a. there is the possibility of improving precipitation data from existing passive microwave sources.
- b. in attempting to improve current algorithms, better understanding will be gained for developing a DMSP microwave precipitation algorithm and for future passive systems such as LAMMR or passive microwave channels associated with other instruments.
- c. algorithm development for passive systems should lead to better physical insights concerning corresponding algorithms for spaceborne radar, and conversely.
- d. algorithm development will be necessary for the experimental program.
- e. although fine tuning would undoubtedly be needed later, the fundamental algorithm principle for spaceborne radar must be understood early for simulations to be effective.

It is beyond the scope of this section to assess or describe current status of related algorithm development. The point here is to emphasize that this activity must be considered of equal importance and initiated at the outset of any future spaceborne radar/radiometer development studies.

#### 7.6 RECOMMENDATIONS

The Radar Working Group has considered several shared and dedicated sensors for implementing spaceborne precipitation radar. Several systems were proposed that were based on either modulated or CW systems and real- or synthetic-aperture radar modes. They all operate at rain-attenuated wavelengths. The Radar Working Group recommended precipitation science studies, experiments, and flights of these systems.

- System Studies. It is important that the shared precipitation radar/radiometer sensor be studied because these measurements can complement each other. The combined precipitation radar scatterometer would be valuable because the scatterometer is needed for both research and operational ocean missions.
- Modeling. An assessment of the accuracy, dynamic range, and applicability (over ocean and land) of the proposed techniques should be performed to identify their relative merits. Actual data or realistic models should be used in the simulations.
- Algorithm Development. There is a need to survey the algorithms that correspond to the foregoing methods and to determine whether alternative retrieval methods are possible. Studies are also required to investigate dual-polarization algorithms from space and those for combined radar/radiometer sensors.
- Measurement Techniques. To increase the ratio of dwell time to beamwidth, several strategies are available: (1) pulse compression, (2) multiple beamwidths, (3) wide-band radar, and (4) adaptive-pointing radar. These should be evaluated in terms of signal-to-noise considerations, cost, and ease of implementation. Technical and cost trade-off studies should be performed on the proposed techniques, and performance should be analyzed for the list of potential spaceborne systems outlined in Section 7.3, followed by a more detailed design of the best concepts.
- Experiments/Demonstrations. Airborne experiments are required for demonstrating the performance of the best concepts identified in this report. The majority of spaceborne precipitation radar systems operate at attenuating wavelengths. Implementation of a multifrequency airborne precipitation radar is recommended because it will provide the desired channels for an evaluation of most of the spaceborne radar methods. One of the channels should be modified to test the frequency agility mode.

- Flights should be conducted in conjunction with precision rain truth. One possibility is to develop the Spandar radar at Wallops Island, Virginia, with a facility to measure differential reflectivity at both polarization.
- Experiments must be conducted in a representative spectrum of storm types to assess the effects of variations in physical composition and structure on the accuracy of precipitation retrieval. To the greatest extent possible, these experiments should include in-situ aircraft measurements of particle types, phase, and size distribution.
- Preliminary planning should begin for a shuttle rain radar mission.
- All airborne and shuttle experiments should include selected microwave and VIS/IR channels. As a result of this workshop, several members of the Spaceborne Radar Group (Atlas, Exkerman, Meneghini, and Moore) prepared a more comprehensive paper entitled "The Outlook for Precipitation Measurements from Space". The paper, which elaborated upon many of the ideas presented here, was prepared for the Preprints of the AMS 20th Radar Meteorology Conference, but was reprinted in the present proceedings because of its relevance. (Appendix D.)

#### REFERENCES

- Atlas, D., and C. W. Ulbrich, 1974: The physical basis for attenuation rainfall relationships and the measurement of rainfall parameters by combined attenuation and radar methods, Journal De Recherches Atmospheriques, Vol. 8, pp. 275-298.
- Atlas, D., and C. W. Ulbrich, 1977: Path and area-integrated rainfall measurements by microwave attenuation in the 1 to 3 cm band, J. Appl. Meteor., Vol. 16, pp. 1322-1331.
- Atlas, D., 1981: Adaptive pointing spaceborne radar for precipitation radar (see appendix D).
- Atlas, D., J. Eckerman, R. Meneghini, and R. K. Moore, 1981: The outlook for precipitation measurements from space. Preprints 20th Radar Meteorology Conf., Amer. Meteor. Soc., Boston, November 30 - December 3, 1981.
- Eckerman, J., R. Meneghini, and D. Atlas, 1978: Average rainfall determination from a scanning beam spaceborne radar, NASA TM 79664.
- Goldhirsh, J., and I. Katz, 1974: Estimation of raindrop size distribution using multiple wavelength radar systems. Radio Science, Vol. 9, pp. 439-446, April.
- Goldhirsh, J., and E. J. Walsh, 1981: Precipitation measurements from space using a modified seasat type radar altimeter, APL Technical Report SIR81U-22, May.
- Goldhirsh, J., and E. J. Walsh, 1981: Rain rate measurement capabilities using a seasat type radar altimeter (see Appendix D).
- Krehbiel, P. R., and M. Brook, 1979: A broad-band noise technique fast-scanning radar observations of clouds and clutter targets, IEEE Trans. Geoscience Electronics, Vol. 17, pp. 196-204.
- Nathanson, F. E., J. N. Bucknam, and R. P. Dooley, 1975: A shuttle meteorological study, Final Report, Technology Service Corporation, TSC-W3-38.
- Nathanson, F. E., 1981: Bistatic radar meteorological satellite (see appendix D).
- Walsh, E. J., 1981: Altimeter rain detection (Appendix E), Performance specification for the altimeter (ALT) instrument for the national oceanic satellite system (NOSS), NASA/GSFC 485-1203-003, Revision A, February.

0017  
→  
22-1

APPENDIX A  
AGENDA  
WORKSHOP  
ON  
"PRECIPITATION MEASUREMENTS FROM SPACE"

APRIL 28 - MAY 1, 1981

NASA/GODDARD SPACE FLIGHT CENTER  
GREENBELT, MARYLAND 20771

BUILDING 8, 2ND FLOOR - AUDITORIUM

APRIL 28 TUESDAY

REGISTRATION		7:30 - 8:30
WELCOMING REMARKS:	Dr. Leslie H. Meredith Director of Applications	8:30
Precipitation Measurements from Space - Some Guiding Thoughts	David Atlas NASA/GLAS (Workshop Chairman)	
<u>FIRST SESSION</u> .....		8:45
<u>PRECIPITATION MEASUREMENT REQUIREMENTS</u>	Dudley G. McConnell, Chairman NCPO Paul H. Hwang, CoChairman NASA/GLAS	
Precipitation Measurement Requirements for Climate Model Development & Applications	Yale Mintz Univ. of Md and NASA/GLAS	9:00
Precipitation Data for Climate Diagnostics	Eugene M. Rasmusson and Phillip A. Arkin, NOAA/NWS	9:25
*Agricultural Requirements for Precipitation Measurements	Norton D. Strommen and Raymond P. Motha USDA, and Robert F. Dale Purdue University	
*Hydrological Forecasting Requirements for Precipitation	Michael D. Hudlow, Richard K. Farnsworth, Douglas R. Greene NOAA/NWS	
*Severe Storms Requirements Precipitation Information	Robert F. Adler NASA/GLAS	9:45
*Global Weather Requirements for Precipitation Measurements	John H. E. Clark Penn State University	
*Precipitation Requirements Survey	Otto W. Thiele NASA/GLAS	
COFFEE		10:30

\*Papers synopsized by Dudley G. McConnell

Elaboration/Rebuttals – Discussion		10:40
Session 1 Wrap-up	Dudley G. McConnell	11:05
<b><u>SECOND SESSION</u></b> .....		11:15
<b><u>SAMPLING PROBLEMS RELATED TO PRECIPITATION MEASUREMENTS</u></b>		
	John S. Theon, Chairman NASA Headquarters David A. Short, CoChairman NASA/GLAS	
Sampling Problems – Overview	Robert F. Crane Dartmouth College	11:15
Comparative Experimentation: Some Principles and Prescriptions	John A. Flueck Temple University	11:40
On the effect of Temporal Sampling on the Observation of Mean Rainfall	Charles R. Laughlin NASA/GLAS	12:00
LUNCH		12:20
Raingage Networks Sampling Statistics	John L. Vogel Illinois State Water Survey	1:30
Microwave Radiometry Sampling Problems Demonstrated with Nimbus 5 Rain Rates versus GATE Data	Ehrhard Raschke and Eberhard Ruprecht, Univ. of Koln	1:50
A Standard Verification for Rainfall Estimation from Remote Platforms	Jose G. Meiten, Cecilia G. Griffith, William Woodley NOAA/ERL/OWRM and John A. Augustine, CIRES	2:10
Discussion – Session 2 Wrap-up	John S. Theon NASA Headquarters	2:25
<b><u>THIRD SESSION</u></b> .....		2:55
<b><u>GROUND TRUTH MEASUREMENT SYSTEMS</u></b>		
	Robert Serafin, Chairman NCAR Gerald M. Heymsfield, CoChairman NASA/GLAS	
Satellite-Borne Dual Millimetric Wave Length Radar	Roger M. Lhermitte University of Miami	
The Differential Reflectivity Dual Polarization Method of Rainfall Measurements	Thomas A. Seliga and V. N. Bringi Ohio State University	2:55
A Survey of Radar Rain Measurement Techniques	Richard J. Doviak NOAA/NSSL	
Bistatic Radar Meteorological Satellite	Fred E. Nathanson Tech. Serv. Corp.	
Ground Truth for Oceanic Rainfall	Clive E. Dorman San Diego State University	
COFFEE		3:25

Precipitation Measurements for Earth-Space Communications: Accuracy Requirements and Ground Truth Techniques	Louis J. Ippolito, NASA Headquarters and Roger D. Kaul, ORI, Inc.	4:05
--	---	------

Discussion – Session 3 Wrap-up	Robert Serafin NCAR	4:25
--------------------------------	------------------------	------

ADJOURN		5:15
---------	--	------

APRIL 29, WEDNESDAY

<u>FOURTH SESSION</u> .....		8:30
-----------------------------	--	------

VISIBLE AND INFRARED TECHNIQUES FOR PRECIPITATION MEASUREMENTS

P. K. Rao, Chairman  
NOAA/NESS  
Robert F. Adler, CoChairman  
NASA/GLAS

*A Life History Method for Estimating Convective Rainfall	David W. Martin University of Wisconsin	
--	--	--

*Visible and Infrared Techniques	Geoffrey Austin and Shaun Lovejoy McGill University	8:30
----------------------------------	---	------

*Visible and Infrared Techniques for Flash Flood, Hydrological and Agricultural Applications	Roderick A. Scofield NOAA/NESS	
--	-----------------------------------	--

*The Estimation of Convective Precipitation from GOES Imagery with the Griffith/Woodley Technique	Cecilia G. Griffith and William L. Woodley NOAA/ERL	
---	---	--

Elaboration/Rebuttals		9:00
-----------------------	--	------

The Bristol Method of Satellite – Improved Rainfall Monitoring	Eric C. Barrett University of Bristol	9:20
---	--	------

Critique of Visible and Infrared Techniques	Colin S. Ramage University of Bristol	9:45
---	--	------

Inference of Precipitation through Thermal Infrared Measurements of Soil Moisture	Peter J. Wetzel and David Atlas, NASA/GSFC	
--	---	--

Discussion – Session 4 Wrap-up	P. K. Rao NOAA/NESS	10:10
--------------------------------	------------------------	-------

COFFEE		10:30
--------	--	-------

<u>FIFTH SESSION</u> .....		10:45
----------------------------	--	-------

MICROWAVE RADIOMETRY AND HYBRID PRECIPITATION MEASUREMENTS

William R. Bandeen, Chairman  
NASA/GLAS  
James R. Greaves, CoChairman  
NASA/GLAS

\*Papers synopsized by David W. Martin



Microwave Radiometry for Precipitation Measurements	James A. Weinman Univ. of Wisconsin and Thomas T. Wilheit, NASA/GSFC	10:45
Combined Spaceborne and Conventional Measurements for Precipitation Estimates	Thomas H. Vonder Haar and Eric A. Smith Colorado State Univ.	11:10
Combining Visible and IR Techniques with LAMMR for Daily Rainfall Estimates	Shaun Lovejoy McGill University	11:30 11:30
Using Underwater Ambient Noise Levels to Measure Rainfall Rate: A Review	Jeffrey A. Nystuen Scripps Institute of Oceanography	
*On the Measurement of Precipitation Frequencies by Microwave Radiometry	Stanley O. Kidder Laboratory for Atmospheric Research University of Illinois, Urbana	11:45
*Detection of Rainfall Rates Utilizing Spaceborn Microwave Radiometers	Hsiao-Hua K. Burke, Kenneth R. Hardy, and Nancy K. Tripp ERT, Inc.	
*The Utilization of Satellite Passive Microwave Sensors to Monitor Synoptic Scale Rainfall	Edward B. Rodgers NASA/GLAS	
Elaboration/Rebuttals		12:10
LUNCH		12:30
CONVENE		1:30
THE DMSP MICROWAVE IMAGER (SSMI) – Unfinished Plans	Richard C. Savage	1:30
Remote Sensing of Stored Precipitation (i.e., Soil Moisture and Snow)	Thomas J. Schmugge NASA/GSFC	1:45
Discussion – Session 5 Wrap-up	William R. Bandeen NASA/GLAS	2:00
<b>SESSION SIX</b> .....		2:30
<b><u>SPACEBORNE RADAR FOR PRECIPITATION MEASUREMENTS</u></b>		
	Robert A. Schiffer, Chairman NASA Headquarters Robert Meneghini, CoChairman NASA/GSFC	
**Spaceborne Precipitation Radar	Jerome Eckerman and Robert Meneghini NASA/GSFC	2:30
**Potential of Dual-Measurement Techniques for Accurate Determination of Instantaneous Rain fall Rate from Space	Carlton W. Ulbrich Clemson University	
*Papers synopsized by Shaun Lovejoy		
**Papers synopsized by Jerome Eckerman		

<b>**Rain Rate Measurement Capabilities Using Seasat Type Radar Altimeter</b>	Julius Goldhrsh Johns Hopkins Univ. and Edward J. Walsh NASA/WALLOPS Flight Center	
Elaboration/Rebuttals		3:00
COFFEE		3:20
Some Thoughts on Hybrid Radiometry and Radar Measurements of Precipitation from Space	Richard K. Moore University of Kansas	3:30
Use of the Optimal Polarization Concept in Electromagnetic Imaging of Hydrometeor Distributions	Wolfgang M. Boerner University of Illinois, Chicago	3:50
Adaptively Pointing Spaceborne Radar for Precipitation	David Atlas NASA/GLAS	4:10
Discussion – Session 6 Wrap-up	Robert A. Schiffer NASA Headquarters	4:25
General Discussion on All Sessions	David Atlas	4:50
Review Organization and assignments for writing groups – next two days	David Atlas	5:20
ADJOURN		5:30
BANQUET		7:00
Speaker	Dr. Sabatino Sofia Laboratory for Planetary Atmospheres	8:00
"Our Changing Sun"		

WRITING GROUP SESSIONS – BUILDING 99

8:30 a.m.

<u>APRIL 30 THURSDAY</u>		8:30 – 12:00
Writing Group Activities		8:30 – 12:00
<u>Requirements</u>	Room 1A	
Chairman: D. G. McConnell, NCPO		
CoChairman: P. H. Hwang, NASA/GLAS		
<u>Sampling</u>	Room 1B	
Chairman: J. A. Flueck, Temple Univ.		
CoChairman: R. K. Crane, Dartmouth College		
<u>Ground Truth</u>	Room 4	
Chairman: R. Serafin, NCAR		
CoChairman: T. A. Seliga, Ohio State Univ.		
<u>Visible and IR Techniques</u>	Room 100A	
Chairman: D. W. Martin, Univ. of Wisconsin		
CoChairman: R. A. Scofield, NOAA/NESS		

**\*\*Papers Synopsized by Jerome Eckerman**

Microwave Radiometry/Hybrid Methods  
 Chairman: T. T. Wilheit, NASA/GSFC  
 CoChairman: S. Lovejoy, McGill Univ.

Room 100C

Spaceborne Radar  
 Chairman: R. K. Moore, Univ. of Kansas  
 CoChairman: J. Eckerman, NASA/GSFC

Room 100B

LUNCH		12:00
Interactive Sessions (as required)		1:00 – 3:00
Plenary Session (Summary of Progress)		3:00 – 5:00
<u>Requirements</u>	Progress – Panel Chairman	10 minutes
	Discussion	10 minutes
<u>Sampling</u>	IBID	20 minutes
<u>Ground Truth</u>	IBID	20 minutes
<u>Visible and IR Techniques</u>	IBID	20 minutes
<u>Microwave and Hybrid Methods</u>	IBID	20 minutes
<u>Spaceborne Radar</u>	IBID	20 minutes
Overall progress review – outline of next day activities as appropriate	David Atlas	5:00
ADJOURN		5:15
<u>MAY 1 FRIDAY</u>		
Continue writing group activities (mixed sessions as required)		8:30 – 12:00
LUNCH		12:00
RECONVENE		1:00
Finalize written material and turn in working draft		1:00 – 3:00
FINAL ADJOURNMENT	David Atlas	3:00

APPENDIX B

WORKSHOP PARTICIPANTS

Robert F. Adler NASA/GLAS	Norman L. Canfield NOAA/Climate Office	Douglas R. Greene NOAA/NWS
Lewis J. Allison Consultant	Alfred Chang NASA/GSFC	Cecilia G. Griffith NOAA/ERL
Phillip A. Arkin NOAA/NWS	Steve Cherry U.K., Science Research Council	Norman Grody NOAA/NESS
Albert Arking NASA/GSFC	John H. E. Clark Pennsylvania State University	Ida Hakkarinen University of Maryland
J. E. Arnold NASA/MSFC	John F. Clark RCA Corp.	Kenneth R. Hardy ERT, Inc.
David Atlas NASA/GLAS	Robert F. Crane Dartmouth College	Richard F. Harrington NASA/LaRC
John A. Augustine CIRES	Robert F. Dale Purdue University	Arthur F. Hasler NASA/GLAS
Geoffrey Austin McGill University	Bernard C. Diesen USAF	Gerald M. Heymsfield NASA/GSFC
William R. Bandeen NASA/GSFC	James C. Dodge NASA Headquarters	Joshua Z. Holland University of Maryland
Eric C. Barrett University of Bristol, U.K.	Clive E. Dorman San Diego State University	Cheryl Horvath-Yuhas OAO Corporation
Fred L. Bartman University of Michigan	Richard J. Doviak DOC/NSSL	Michael D. Hudlow NOAA/NWS
Thomas L. Bell NASA/GSFC	Jerome Eckerman NASA/GSFC	Paul H. Hwang NASA/GSFC
Tom Blackburn NOAA/NWS	Alvin T. Edgerton Hughes Aircraft	Louis J. Ippolito NASA Headquarters
Roy Blackmer GE/MATSCO Corp.	Edward S. Epstein NOAA/NESS	Roger D. Kaul ORI, Inc
Wolfgang M. Boerner University of Illinois	Dickson J. Fang Comsat, Inc.	Stanley O. Kidder University of Illinois
D. Ray Booker Aeromet, Inc.	Richard K. Farnsworth NOAA/NWS	P. Y. Johnson NOAA/NESS/Contractor
Glen W. Brier Colorado State University	John A. Flueck Temple University	Douglas LaCompte NOAA/EDIS
V. N. Bringi Ohio State University	Julius Goldhirsh Johns Hopkins University	Charles R. Laughlin NASA/GSFC
Hsiao-Hua Burke Lincoln Laboratories	James R. Greaves NASA/GSFC	John C. Lease DOI/WORS

Roger M. Lhermitte  
University of Miami

Shaun Lovejoy  
McGill University

Robert A. Mack  
GE/MATSCO

David W. Martin  
University of Wisconsin

Phillipe Martin  
CNET France

Dudley G. McConnell  
NASA/NCPO

Wayne McGovern  
NOAA/RD/SP

Jose Meitin  
NOAA/ERL

Robert Meneghini  
NASA/GSFC

Leslie H. Meredith  
NASA/GSFC

Earl S. Merritt  
Earth Satellite Corp.

Andres S. Milman  
SASC, Inc.

Yale Mintz  
University of Md. and  
NASA/GLAS

Richard K. Moore  
University of Kansas

John F. Moses  
NOAA/NESS

Raymond P. Motha  
USDA

Marie-Jeanne Munteau  
NASA/GLAS

Fred E. Nathanson  
Tech. Services Corporation

Andrew J. Negri  
NASA/GLAS

Jeffrey A. Nystuen  
Scripps Institute of  
Oceanography

Vincent J. Oliver  
NOAA/NESS

Frank Palluconi  
NASA Headquarters

Lanning Penn  
RDS, Inc.

N. Phillips  
NOAA/NMC

Colin S. Ramage  
University of Hawaii

P. Krishna Rao  
NOAA/NESS

Ehrhard Raschke  
University of Koln  
Federal Republic of Germany

Eugene M. Rasmusson  
NOAA/NWS

David W. Reynolds  
NOAA/ERL

Peter Robinson  
NCPO

Edward B. Rodgers  
NASA/GSFC

Eberhard Ruprecht  
University Zu Koln  
Federal Republic of Germany

Richard C. Savage  
USAF

Robert A. Schiffer  
NASA Headquarters

Thomas J. Schmugge  
NASA/GSFC

Roderick A. Scofield  
NOAA/NESS

Thomas A. Seliga  
Ohio State University

Robert Serafin  
NCAR

James C. Shiue  
NASA/GSFC

David A. Short  
NASA/GSFC

Honnappa Siddalingaiah  
OAO Corp.

Joanne Simpson  
NASA/GSFC

Merrill I. Skolnik  
NRL

Eric A. Smith  
Colorado State University

Sabatino Sofia  
NASA/GSFC

Sue Steinmetz  
NOAA/NESS

David Y. Stowell  
OAO Corporation

Norton D. Stronmen  
USDA

Yogesh Sud  
NASA/GSFC

Ronald C. Taylor  
NSF

Douglas Taylor  
NOAA/NESS

Morris Tepper  
Consultant

John S. Theon  
NASA Headquarters

Otto W. Thiele  
NASA/GLAS

Gwen Thompson  
University of Maryland

Adrienne F. Timothy  
NASA/GSFC

Nancy K. Tripp  
ERT, Inc.

Carlton W. Ulbrich  
Clemson University

John L. Vogel  
Illinois State Water Survey

Thomas H. Vonder Haar  
Colorado State University

Edward J. Walsh  
NASA/Wallops

James A. Weinman  
University of Wisconsin

John E. Welker  
NASA/GSFC

Peter J. Wetzel  
NASA/GSFC

Raymond Wexler  
NASA/GSFC

Linwood Whitney  
NOAA/NESS

Thomas T. Wilheit  
NASA/GSFC

Jay Winston  
NOAA/NWS

Edward A. Wolff  
NASA/GSFC

William L. Woodley  
NOAA/ERL

John Woodruff  
NASA/GSFC

Donald P. Wylie  
University of Wisconsin

Martin Yerg  
NOAA/RD/SP

APPENDIX C  
TABLE OF ACRONYMS

ADP	Automated Data Processing
AgRISTARS	Agriculture and Resources Inventory Surveys Through Aerospace Remote Sensing
API	Antecedent Precipitation Index
APMR	Adaptive Pointable Multibeam Radar
APR	Adaptive Pointing Radar
BSR	Bistatic Spaceborne Radar
CCOPE	Cooperative Convective Precipitation Experiment
CEAS	Center for Environmental Assessment Services (NOAA-formerly CEDDA)
CEDDA	Center for Environmental Design and Data Analysis
CISK	Convective Instability of the Second Kind
CLW	Cloud Liquid Water
COSPAR	Committee on Space Programs and Research
COSS	Climate Observing System Study
CW	Continuous Wavelength
DCP	Data Collection Platform
DMSP	Defense Meteorological Satellite Program
DSD	Drop Size Distribution
EDIS	Environmental Data and Information Service
ERL	Environmental Research Laboratories (NOAA)
ESMR	Electrically Scanning Microwave Radiometer
ESSA	Environmental Satellite Services Administration
ETAC	Environmental Technical Applications Center (USAF)
FARR	Frequency Agile Rain Radar
FGGE	First Global GARP Experiment
FM	Frequency Modulation
FOV	Field of View
FSMR	Fixed Simultaneous Multibeam Radar
GARP	Global Atmospheric Research Program
GATE	GARP Atlantic Tropical Experiment

GCM	General Circulation Model
GEO	Geosynchronous Earth Orbiter
GHz	Gigahertz
GLAS	Goddard Laboratory for Atmospheric Sciences
GOES	Geostationary Operational Environmental Satellite
HRC	Highly Reflective Cloud
ICSU	International Council of Scientific Unions
IFOV	Instantaneous Field of View
IR	Infrared
ISCCP	International Satellite Cloud Climatology Project
LAMMR	Large Antenna Multichannel Microwave Radiometer
LEO	Low Earth Orbiter
LEOS	Low Earth Orbiting Satellite
MFMR	Multifrequency Microwave Radiometer
MR	Microwave Radiometry
NADAR	Nadir Altimeter for Rain
NASA	National Aeronautics and Space Administration
NCPO	National Climate Program Office
NESS	National Earth Satellite Service
NEXRAD	Next Generation of Meteorological Radars
NOAA	National Oceanic and Atmospheric Administration
NOSS	National Oceanic Satellite System
NSSL	NOAA Severe Storms Laboratory
NWS	National Weather Service
PCF	Precipitation Calibration Facility
PDF	Probability Distribution Function
RADSCAT	Radiometer-Scatterometer (Skylab)
RMS	Root Mean Square
SAR	Synthetic Aperture Radar
SCATRAD	Scatterometer-Radiometer
SEASAT	Sea Satellite
SESAME	Severe Environmental and Mesoscale Experiment



SMMR	Scanning Multichannel Microwave Radiometer
SMS	Synchronous Meteorological Satellite
SPANDAR	Space Range Radar
SSMI	DMSP Microwave Imager
STAR	Surface Target Attenuation Radar
STC	Sensitivity Time Control
THIR	Temperature Humidity Infrared Radiometer
VAD	Variable Azimuth Display
VAS	VISSR Atmospheric Sounder
VIS	Visible
VISSR	Visible and Infrared Spin Scan Radiometer
WMO	World Meteorological Organization
WV	Water Vapor

APPENDIX  
CONTRIBUTED PAPERS

<u>REQUIREMENTS TOPICS</u>	<u>Page</u>
<i>A Brief Review of the Present Status of Global Precipitation Estimates</i> Yale Mintz .....	D-1
<i>Precipitation Measurement Requirements for Climate Model Development</i> Yale Mintz .....	D-5
<i>Precipitation Data for Climate Diagnostics</i> Eugene M. Rasmusson and Phillip A. Arkin .....	D-10
<i>Agricultural Requirements for Precipitation Measurements</i> Norton D. Strommen, Raymond P. Motha and Robert F. Dale .....	D-19
<i>Hydrological Forecasting Requirements for Precipitation Data from Space Measurements</i> Michael D. Hudlow, Richard K. Farnsworth and Douglas R. Greene .....	D-23
<i>Severe Storms Requirements for Precipitation Information</i> Robert F. Adler .....	D-31
<i>Global Weather Requirements for Precipitation Measurements</i> John H. E. Clark .....	D-35
 <u>SAMPLING TOPICS</u>	
<i>Sampling Problems – Small Scale Structure of Precipitation</i> Robert F. Crane .....	D-41
<i>Some Statistical Problems Inherent in Measuring Precipitation</i> John A. Flueck .....	D-50
<i>On the Effect of Temporal Sampling on the Observation of Mean Rainfall</i> Charles R. Laughlin .....	D-59
<i>Raingage Networks Sampling Statistics</i> John L. Vogel .....	D-67
<i>Microwave Radiometry Sampling Problems Demonstrated with Nimbus 5 Rain Rates Versus GATE Data</i> Ehrhard Raschke and Eberhard Ruprecht .....	D-84
<i>A Standard Verification for Rainfall Estimation from Remote Platforms</i> Jose G. Meiten, Cecilia G. Griffith, William L. Woodley and John A. Augustine .....	D-94
 <u>GROUND TRUTH TOPICS</u>	
<i>The Differential Reflectivity Dual Polarization Method of Rainfall Measurements</i> Thomas A. Seliga and V. N. Bringi .....	D-98

APPENDIX D  
CONTRIBUTED PAPERS (Continued)

9  
Y

	<u>Page</u>
<i>A Survey of Radar Rain Measurement Techniques</i> Richard J. Doviak .....	D-105
<i>Ground Truth for Oceanic Rainfall</i> Clive E. Dorman .....	D122
<i>Precipitation Measurements for Earth-Space Communications: Accuracy Requirements and Ground Truth Techniques</i> Louis J. Ippolito and Roger D. Kaul .....	D-129
 <b><u>VISIBLE AND IR TOPICS</u></b>	
<i>A Life History Method for Estimating Convective Rainfall</i> David W. Martin .....	D-138
<i>A Combined Visible and IR Technique for the Estimation of Rain Amounts From GOES Data</i> G. L. Austin and S. Lovejoy .....	D141
<i>Visible and Infrared Techniques for Flash Flood, Hydrological, and Agricultural Applications</i> Roderick A. Scofield .....	D-145
<i>The Estimation of Convective Precipitation from GOES Imagery with the Griffith/Woodley Technique</i> Cecilia G. Griffith and William L. Woodley .....	D-154
<i>The Bristol Method of Satellite-Improved Rainfall Monitoring</i> Eric C. Barrett .....	D-159
<i>Inference of Precipitation Through Thermal Infrared Measurements of Soil Moisture</i> Peter J. Wetzel and David Atlas .....	D-170
 <b><u>MICROWAVE RADIOMETRY AND HYBRID TOPICS</u></b>	
<i>A Survey of Passive Microwave and Hybrid Remote Sensing of Precipitation</i> James A. Weinman and Thomas T. Wilhelm .....	D-173
<i>Combined Spaceborne and Conventional Measurements for Precipitation Estimation</i> Thomas H. Vonder Haar and Eric A. Smith .....	D-176
<i>Combining Visible and Infrared Techniques with LAMMR for Daily Rainfall Estimates</i> Shaun Lovejoy .....	D-184
<i>Using Underwater Ambient Noise Levels to Measure Rainfall Rate: A Review</i> Jeffrey A. Nystuen .....	D-192
<i>On the Measurement of Precipitation Frequencies by Microwave Radiometry</i> Stanley Q. Kidder .....	D-225
<i>Detection of Rainfall Rates Utilizing Spaceborne Microwave Radiometers</i> Hsiao-Hua K. Burke, Kenneth R. Hardy and Nancy K. Tripp .....	D-228

APPENDIX D  
CONTRIBUTED PAPERS (Continued)

	<u>Page</u>
<i>The Utilization of Satellite Passive Microwave Sensors to Monitor Synoptic Scale Rainfall</i> Edward B. Rodgers .....	D-234
<i>The DMSP Microwave Imager (SSM/I) – Unfinished Plans</i> Richard C. Savage .....	D-246
<i>Remote Sensing of Stored Precipitation, i.e., Soil Moisture and Snow</i> Thomas J. Schmugge .....	D-252
 <b><u>SPACEBORN RADAR TOPICS</u></b>	
<i>Spaceborne Precipitation Radar</i> Jerome Eckerman and Robert Meneghini .....	D-261
<i>Satellite-Borne Dual Millimetric Wave Length Radar</i> Roger M. Lhermitte .....	D-277
<i>Potential of Dual-Measurement Techniques for Accurate Determination of Instantaneous Rainfall from Space</i> Carlton W. Ulbrich .....	D-283
<i>Rain Rate Measurement Capabilities Using a Seasat Type Radar Altimeter</i> Julius Goldhirsh and Edward J. Walsh .....	D-288
<i>Use of Combined Radar and Radiometer Systems in Space for Precipitation Measurement – Some Ideas</i> Richard K. Moore .....	D-301
<i>Use of Optimal Polarization Concept in Electromagnetic Imaging of Hydrometeor Distribution</i> Wolfgang M. Boerner .....	D-326
<i>Bistatic Radar Meteorological Satellite</i> Fred E. Nathanson .....	D-341
<i>Adaptively Pointing Spaceborne Radar for Precipitation Measurements</i> David Atlas .....	D-351
<i>*The Outlook for Precipitation Measurements from Space</i> David Atlas, Jerome Eckerman and Robert Meneghini .....	D-353

---

\*This paper, in press for the proceedings of the American Meteorological Society 20th Conference on Radar Meteorology, is reprinted here because of its relevance to this workshop

ORIGINAL PAGE IS  
OF POOR QUALITY

LN83 25276

37

A BRIEF REVIEW OF THE  
PRESENT STATUS OF GLOBAL PRECIPITATION ESTIMATES

Yale Mintz

Department of Meteorology, University of Maryland, College Park, MD 20742  
and

Lab. Atmospheric Sciences, NASA Goddard Space Flight Center, Greenbelt, MD 20771

Introduction

This is a brief review of what is now known about the global distribution of precipitation both the "normal" distribution (i.e., the precipitation averaged over a number of years) and time-series of the precipitation. Only the most recent studies are explicitly covered. An historical account of earlier studies can be found in Jaeger (1976).

1 Jaeger (1976) produced global maps, and a corresponding machine-readable grided data set, which is the only estimate we have of the normal monthly precipitation over the entire globe.

Over the continents, the inputs were the published national and regional maps of normal monthly precipitation (Jaeger, 1976, Table 3); supplemented, where there were no maps, by station data from the World Weather Records (U.S. Dept Commerce) and other sources. In so far as the data allowed, the thirty-year period, 1931-1960, was used but where this was not possible, other time intervals were used. The globe was divided into grid areas of 5° longitude by 5° latitude and, reading from the various sources, the monthly values of the continental precipitation, averaged over the grid areas, were recorded. From these averaged values, plotted in the centers of the squares, the global maps of precipitation were drawn by hand (Jaeger, 1976, Figs 9-21).

Over the oceans, Jaeger simply took the annual precipitation, as given in the map by Geiger (1965), and distributed that precipitation over the twelve months of the year in proportion to the monthly percentage frequency of observations reporting precipitation, as given, for each 5° by 5° square, in the Manne Climatic Atlas of the World (U.S. Navy, 1955-65). Thus, over the oceans, the annual precipitation is the same as the one given by Geiger (with the exception of some small regions of the oceans adjacent to Indonesia, where Jaeger increased the annual precipitation from about 2000 to 3000 mm/year.)

Geiger's distribution of the annual precipitation over the oceans can be traced back to Schott. For the Atlantic Ocean, Schott (1926) reworked the earlier analysis of Supan (1898) in which the annual frequency of precipitation (the number of days in the year with precipitation), as reported in the logs of a large number of ships crossing the North and South Atlantic and the Indian oceans, was multiplied by an average precipitation intensity (the average amount of precipitation per rainy day) as a function of latitude, as obtained from measurements of rainfall made on a small number of ships.

For the annual precipitation in the Pacific and Indian Oceans, Schott (1933, 1935) used not only the above described frequency of precipitation multiplied by the latitude-dependent intensity of precipitation, but also extrapolated directly to the oceans the observed annual amount of precipitation at the nearest coastal and island stations.

Table 1  
Present Status of Global Precipitation Estimates

	Normal			Time Series			
	Monthly	Seasonal	Annual	Weekly	Monthly	Seasonal	Annual
Entire Globe:	1 Jaeger (1976)	continents ←-----→ oceans					
			2 Baumgartner & Reichel (1975) 3 Korzun, ed (1974)				
Continents only:		4 Korzun, ed (1974) 5 Hsu & Wallace (1976)			8 Free Univ Berlin (1963-1981)		
Oceans only:		6 Reed & Elliott (1979) 7 Dorman & Bourke (1979, 1981)			9 Rao et al (1976) (1972-1975)		

## ORIGINAL PAGES OF POOR QUALITY

[Jaeger used the same method to divide the annual oceanic precipitation into monthly amounts that Möller (1951) had earlier used to obtain the seasonal (three-monthly) precipitation amounts. Möller had available, at that time, only the seasonal frequencies of oceanic precipitation, as given in the Atlas of Climatic Charts of the Oceans, by MacDonald (1938).]

2. Baumgartner and Reichel (1975) show only the normal annual precipitation over the globe. Over the continents they used about the same input data sources as Jaeger (1976), but they retained in their map much more of the spacial detail of the original sources.

Over the oceans some unspecified combination of the global maps of Albrecht (1960), Knoch (1961) and Drosdov (1964) was used; with an adjustment of the total ocean precipitation to  $385 \times 10^3 \text{ km}^3/\text{year}$ . This adjustment was made on the assumption that the total continental precipitation is correct, and the further assumption that the estimate they had made of the total global evaporation is more reliable than any estimate that can be made of the total oceanic precipitation.

3. Korzun (ed., 1974) presents the normal annual precipitation over the continents after correcting for three systematic measurement errors: wind-effect error (which entails the largest correction), rain gauge wetting error, and rain gauge evaporation error. (See, also, Rodda, 1971.) The total correction varies with location, from about 10 mm to 200 mm/year in absolute value, and from about 3% to 70% in relative value (Korzun, ed., 1974, Figs. 19a, 19b.) The mean continental precipitation without the correction was 725 mm/year; and with the correction 800 mm/year. The input data sources were national and regional maps, derived from observations at about 42,000 stations; supplemented by about 18,000 additional stations. Thus, data from about 60,000 land stations entered into the compilation of the global map. Where possible, the data was taken from, or reduced to the 80-year period 1891-1970. The continental precipitation is shown with somewhat less detail than that given by Baumgartner and Reichel (1975). [At the present time, precipitation is measured at about 120,000 (unevenly distributed) land stations over the globe.]

Over the oceans, the annual precipitation was calculated from a new compilation of mean monthly precipitation frequencies, in  $5^\circ$  latitude by  $5^\circ$  longitude squares, taken from records in ships logs (for the period 1900-1964 in the Pacific Ocean, and 1900-1969 in the Atlantic and Indian oceans), multiplied by the mean annual intensity of precipitation (the ratio of the total amount of precipitation to the total duration of precipitation). This field of the mean precipitation intensity, which is shown on a global map (Korzun, ed., 1974, Fig. 121), was made by extrapolating to the ocean from the measured duration and measured (and corrected) amount of precipitation at the nearest of 426 island and coastal stations. [This is essentially the same method that was used by Supan (1898). It implicitly takes into account not only the effect

of the spatial variation of the air temperature, but also the effect of the different predominant weather types: giving different weights to the convective showers in the intertropical convergence zone and the western subtropical oceans, drizzle in the eastern subtropical oceans, and rain from the cyclones that move across the middle and high latitude oceans.] In addition to this product of precipitation frequency and precipitation intensity, Korzun (ed. 1974) extrapolated to the ocean directly the measured (and corrected) precipitation amounts at 173 stations on small, low islands. (See, also, Samoilenko, 1966).

4. Korzun (ed. 1974, Figs. 26, 35, 54, 66, 79, 88), using only 523 stations for all of the continents (mostly stations with long-term records), constructed maps of the percentages of the normal annual continental precipitation that occur in the four seasons of the year. Because of the small number of stations used (65 for North America, 133 for Asia), only large scale space variations are shown. Thus, whether it is so in nature or not, according to this analysis the small scale features which are seen on the annual precipitation map are features that persist throughout the year.

5. Hau and Wallace (1976) have produced an analysis of the normal precipitation over the continents (and many islands of the globe), which shows the normalized amplitude and phase of the first two annual harmonics in the precipitation. They used the precipitation data, for the period 1951-70, at about 700 of the 2000 stations in the World Monthly Surface Climatological Data Set (which they obtained on tape from the National Center for Atmospheric Research, Boulder.)

No information is given by the maps of the two annual harmonics which is not implicit in the maps of monthly precipitation, as given, for example, by Jaeger (1976). But some characteristics of the time-space variation of the precipitation are easier to see (although others are more difficult to see) when the normalized harmonics are displayed in this way.

6. Reed and Elliott (1979) produced maps of the normal seasonal and annual precipitation for the Atlantic and Pacific Oceans north of the equator, using as their input data the monthly precipitation frequencies given in the revised volumes of the Marine Climatic Atlas of the World (U.S. Navy, 1974, 1977). They divided the two oceans into tropical and extratropical domains, with the dividing line at  $20^\circ\text{N}$  in the eastern two-thirds, and at  $30^\circ\text{N}$  in the western one-third of each ocean. North of this boundary (in the extratropical domain) they used a conversion from monthly precipitation frequency to monthly precipitation amount that changed from  $0.31 \text{ (cm month}^{-1}\%^{-1}\text{)}$  in July and August to  $0.36 \text{ (cm month}^{-1}\%^{-1}\text{)}$  in December and January; and south of this boundary (in the tropical domain) they used a constant conversion of  $1.0 \text{ (cm month}^{-1}\%^{-1}\text{)}$ . These conversion factors were derived by Reed and Elliott (1977) and by Reed (1979) mainly from the work of Tucker (1961) on rainfall at land stations in Great Britain, and from measurements of precipitation that were made in the eastern Pacific, between  $60^\circ\text{N}$  and  $40^\circ\text{N}$  and between  $20^\circ\text{N}$  and  $2^\circ\text{S}$ .

in 1975-1976, by the ship "Oceanographer". Because of the discontinuity in the conversion factor, the precipitation maps show large discontinuities at the boundaries that separate the two domains.

[When compared with the measured precipitation on ships during GATs, in the summer of 1974, the calculated intertropical precipitation maximum in the eastern Atlantic is about half as large as the measured maximum.]

7. Dorman and Bourke (1979, 1981) give the normal seasonal and annual distributions of precipitation over the Atlantic and Pacific Oceans, from 30°S to 60/70°N, as obtained by the method of Tucker (1961) and a latitude-derived correction for the air temperature.

Tucker's method consists of assigning a given amount of precipitation to the different present weather types (clear sky, drizzle, showers, heavy continuous rain, etc.) that are listed in the synoptic weather code. Tucker derived the precipitation amount, for each category of the synoptic code that is associated with precipitation occurring at the time of observation, by correlating that synoptic code report with the measured precipitation at some stations on the periphery of the British Isles. Dorman and Bourke (1978a) examined the universality of Tucker's coefficients by using also coastal station data along the periphery of the Atlantic and Pacific Oceans, from south of the equator to about 75°N. They found that there was a latitudinal bias related to the local air temperature: i.e., rainfall was increasingly underestimated as air temperature increased. They found that this effect was systematic and could be corrected by empirical formulas for the annual, seasonal and monthly averages. Dorman and Bourke (1979, 1981) use the Tucker method and those correction coefficients to obtain the seasonal and annual precipitation, for 2° latitude by 5° longitude rectangles, over the Pacific and Atlantic oceans. The input data, for "present weather" and air temperature, were the synoptic observations taken by a wide variety of ships of opportunity, for the period 1950-72 in the Pacific and 1950-74 in the Atlantic, as provided by the magnetic tape data file maintained by the North Pacific Experiment (NORPAX) group at Scripps Institution of Oceanography, La Jolla. They also present maps of the normalized amplitude and phase of the first two annual harmonics of the precipitation, as derived from monthly mean precipitation estimates (which are given, for the Pacific Ocean, in Dorman and Bourke, 1978b.) For the Pacific Ocean, some information is also given about the diurnal variation of precipitation.

A detailed intercomparison and critical evaluation of these various estimates of the normal annual and seasonal precipitation distributions, though desirable, is beyond the assigned scope of this review. We should, nonetheless, note that there are large differences in these estimates, over the continents as well as over the oceans. Over large areas of the oceans some of the estimates differ by a factor of two.

8. The Free University of Berlin (1963-1981), Institute of Meteorology, has published an analysis of the precipitation distribution over the northern hemisphere continents (and extending, over Africa, to about 15°S) for each month since the summer of 1963. The field is represented by isolines for seven categories of precipitation derived from a 30-year base period, 1931-1960. (Category 1 denotes that the precipitation for the month is within the range of the amount that fell in the six driest years of the base period; and 5 denotes that it is within the range of the six wettest years of the base period. 0 denotes that it is less, and 6 that it is more than any precipitation that fell during the 30-year base period.)

9. Rao et al. (1976) derived weekly (and also monthly, seasonally and annually) averaged maps of precipitation over the oceans, for the period 11 Dec. 1972 to 28 Feb. 1975, from measurements with the Electrically Scanning Microwave Radiometer on the polar-orbiting Nimbus-5 satellite. The theoretically derived calibration of the precipitation rate as a function of the measured microwave brightness temperature, for different freezing levels, was verified in a ground-based experiment in which upward-viewing microwave brightness temperatures were compared with measured rainfall rates. In calculating the precipitation from the measured brightness temperatures, they used one of three prescribed heights of the 273°K isotherm over the globe.

[The overall pattern and general magnitudes of the seasonal and annual precipitation, as shown in these maps, conform fairly well with the normal seasonal and annual precipitation distributions given by Dorman and Bourke (1979, 1981).]

#### References

- Albrecht, F. 1960: Jahreskarten des Wärme- und Wassergehaltes der Ozeane. Ber. Dt. Wetterd., Nr. 66, Offenbach.
- Baumgartner, A., and E. Reichel, 1975: The World Water Balance. Mean Annual Global, Continental and Maritime Precipitation, Evaporation and Runoff. Elsevier Publishing Co., Amsterdam/Oxford/New York, 179 pp and plates.
- Dorman, C. E., and R. H. Bourke, 1978a: A Temperature Correction for Tucker's Ocean Rainfall Estimates. Quart. J. Roy. Meteor. Soc., 104, pp 765-773.
- Dorman, C. E., and R. H. Bourke, 1978b. Maps of Pacific Rainfall, Rep. No. 78-2, Center for Marine Studies, San Diego State University, 14 pp + 34 Figs.
- Dorman, C. E., and R. H. Bourke, 1979: Precipitation over the Pacific Ocean, 30°S to 60°N. Mon. Wea. Rev., 107, pp 896-910.

ORIGINAL PAGE 13  
OF POOR QUALITY

- Dorman, C. E., and Bourke, 1981: Precipitation over the Atlantic Ocean, 30°S to 70°N. Mon. Wea. Rev., 109, pp 554-563.
- Drosdov, O. A. (ed), 1964: Physical Geographical Atlas of the World. Moscow. Soviet Geography Review and Translation. Vol. VI. Nos. 5-6, 403 p. Amer. Geogr. Soc. New York.
- Free University of Berlin, 1963-1981: Beliage zur Berliner Wetterkarte, Welt-Wetterlage (monthly means). Institute für Meteorologie der Freien Universität Berlin.
- Geiger, R., 1965. Wandkarten 1:30 Mill., Jährlicher Niederschlag. Perthes Verlag, Darmstadt.
- Hsu, C. F., and J. M. Wallace, 1976. The Global Distribution of the Annual and Semi-annual Cycles in Precipitation. Mon. Wea. Rev., 104, pp 1093-1101.
- Jaeger, L., 1976: Monatskarten des Niederschlags für die ganze Erde. Berichte des Deutschen Wetterdienstes, Nr. 139 (Band 18). Offenbach a. M., 38 pp. and plates.
- Knoch, K. 1961: Niederschlag und Temperatur (Weltkarten). Welt-Seuchen Atlas III. 5 S., 3 K. Hamburg.
- Korzun, V. I. (ed), 1974: World Water Balance and Water Resources of the Earth. Report of the USSR Committee for the International Hydrological Decade. Studies and Reports in Hydrology, vol 25. Unesco Press, Paris, 663 pp, and Atlas with explanatory text (35 pp).
- MacDonald, W. F., 1938: Atlas of Climatic Charts of the Oceans. U.S. Weather Bureau, Wash. D.C.
- Möller, F., 1951: Vierteljahreskarten des Niederschlags für die ganze Erde. Petermanns Geogr. Mitt., 95, pp. 1-7.
- Rao, M. S. V., W. V. Abbott III, and J. S. Theon, 1976: Satellite-derived Global Oceanic Rainfall Atlas (1973 and 1974). X-911-76-116, Goddard Space Flight Center, Greenbelt, Md. 31 pp and weekly, monthly, seasonal, and annual maps.
- Reed, R. K., 1979: On the Relationship between the Amount and Frequency of Precipitation over the Ocean, J. Appl. Meteor., 18, pp 692-696.
- Reed, R. K., and W. P. Elliott, 1977. A Comparison of Oceanic Precipitation as Measured by Gage and Assessed from Weather Reports, J. Appl. Meteor., 16, pp 983-986.
- Reed, R. K., and W. P. Elliott, 1979: New Precipitation Maps for the North Atlantic and North Pacific Oceans, J. Geophys. Res., 84, pp 7839-7846.
- Rodda, J. C., 1971: The Precipitation Measurement Paradox-The Instrument Problem Reports on the WMO International Hydrological Decade Projects, No. 16 WMO No. 316, Geneva, 42 pp.
- Samoilenko, V. S., 1966. Moisture Exchange between Ocean and Atmosphere. In: The Pacific Ocean, vol I, Nauka, Moscow, pp 302-310.
- Schott, G., 1926: Geographie des Atlantischen Ozeans. Boyesen Verlag, Hamburg.
- Schott, G., 1933: Die Jährlichen Niederschlagsmengen auf dem Indischen und Stillen Ozean. Ann. Hydrogr., 6 pp 1-12.
- Schott, G., 1935: Geographie des Indischen und Stillen Ozeans. Boyesen Verlag, Hamburg.
- Supan, A., 1898: Die Jährlichen Niederschlagsmengen auf den Meeren. Petermanns Geogr. Mitt., 44, pp 179-182.
- Tucker, G. B., 1961: Precipitation over the North Atlantic Ocean, Quart. J. Roy. Meteor. Soc., 87, pp 147-158.
- U. S. Dept of Commerce: World Weather Records. Superintendent of Documents, U.S. Govt. Printing Office, Wash. D.C.
- U. S. Navy, 1955-65: Marine Climatic Atlas of the World. Vol. 1-7 NAVAER, 50-1C-528-533. U.S. Govt. Printing Office, Wash. D.C.
- U. S. Navy, 1974: Marine Climatic Atlas of the World. Vol. 1, North Atlantic Ocean. U.S. Govt. Printing Office, Wash. D.C.
- U. S. Navy, 1977. Marine Climatic Atlas of the World. Vol. 2, North Pacific Ocean. U.S. Govt. Printing Office, Wash. D.C.



ORIGINAL SOURCE  
OF PAPER QUANTITY

N83 25277

D8

## PRECIPITATION MEASUREMENT REQUIREMENTS FOR GENERAL CIRCULATION CLIMATE MODEL DEVELOPMENT AND APPLICATIONS

Yale Mintz

Department of Meteorology, University of Maryland, College Park, MD 20742

and

Lab. Atmospheric Sciences, NASA Goddard Space Flight Center, Greenbelt, MD 20771

### Introduction

A general circulation model is a set of finite-difference analogues of the equations that govern the changes in the state of the atmosphere over the global domain. With given initial state and boundary conditions, these conservation equations (for mass, momentum, energy and water substance) are integrated numerically to obtain the fields of the physical state variables: pressure, velocity, temperature, water vapor and clouds. While doing this, the calculations reveal the mass and momentum transfers, the energy productions and energy conversions, and the compositional change processes that control the distributions of the state variables. [For examples of such general circulation climate models, and of climate simulations made with these models, see, respectively, Chang (ed.), 1977, and WMO/ICSU, 1979]

Precipitation is not one of the physical state variables of the atmosphere. Unlike water vapor and clouds (or snow on the ground and moisture in the soil), it is not a part of the atmospheric (or ground) composition field. Precipitation is a process that changes the composition field.

There are two ways in which global precipitation measurements can aid in the development and use of general circulation climate models.

(1) precipitation measurements can verify the calculated precipitation and, thereby, help improve the calculation of the thermal forcing that produces the large scale atmospheric circulation, and

(2) precipitation measurements can be used to initialize one of the very important physical state variables of a climate model, the soil moisture.

#### 1. Global Measurements of Precipitation for Verifying and Improving the Thermal Forcing of the Atmosphere

The large scale motions of the atmosphere are produced by horizontal differences in the heating of the atmosphere. It is the horizontal gradient of heating that generates available potential energy, which adiabatic processes convert into the kinetic energy of the large-scale motions (Lorenz, 1955).

Figure 1 shows an example of the time-averaged and zonally-averaged heating in a climate simulation with a general circulation model. The top three panels show, respectively, the heating produced by solar and long wave radiation, by large scale condensation, and by cumulus condensation and convection. The bottom

panel shows the heating by all of these processes, together with the sensible heat transfer from the underlying land and ocean.

We see that radiation produces much smaller horizontal gradients of heating than the two kinds of condensation heating. It is especially the strong horizontal gradient of the heating by cumulus condensation and convection in the tropics that forces a strong divergent motion field within the tropics and subtropics. This motion field, by subsidence and horizontal advection of heat into the subtropics, produces the mid-latitude baroclinic zones, and, in turn, these baroclinic zones supply the available potential energy for generating the extratropical wave-cyclones. (What the figure does not show is the very large longitudinal variation of the cumulus condensation heating in the tropics, which also affects the circulation.)

The ability of a general circulation model to simulate (and predict) climate will, therefore, greatly depend on how well the model simulates the heating of the atmosphere; and especially, on how well it simulates the heating by cumulus condensation and convection.

It would be ideal if measurements could reveal how the horizontal distribution of the release of the latent heat of condensation varies with elevation. But even if we can only measure the horizontal distribution of the total latent heat release, as evidenced by the precipitation that reaches the earth's surface, that would be very useful. It would be sufficient to know the precipitation averaged over a day, averaged over areas comparable to the grid-areas of the general circulation models (which presently are about  $(200 \text{ km})^2$  to  $(400 \text{ km})^2$ , but by the end of this decade will probably be  $(50 \text{ km})^2$  to  $(100 \text{ km})^2$ ), and with an accuracy, in this time- and space-average, of about 0.5 mm/day (which, for the regions of above average precipitation, is an accuracy of about 10%).

It would be helpful if, concurrent with the precipitation measurements, there were also measurements of the distribution of the cloud top heights (and, especially, of the cumuloform clouds, which convect the released heat upwards.)

#### 2. Global Measurements of Precipitation for the Initialization of Soil Moisture

A review and intercomparison of a number of climate sensitivity experiments, made with different general circulation models, shows that the simulated fields of temperature, motion and precipitation greatly depend on the soil moisture, and that this dependence has a time scale of several months (Mintz, 1981.) It is, therefore, of utmost importance for climate simulations and

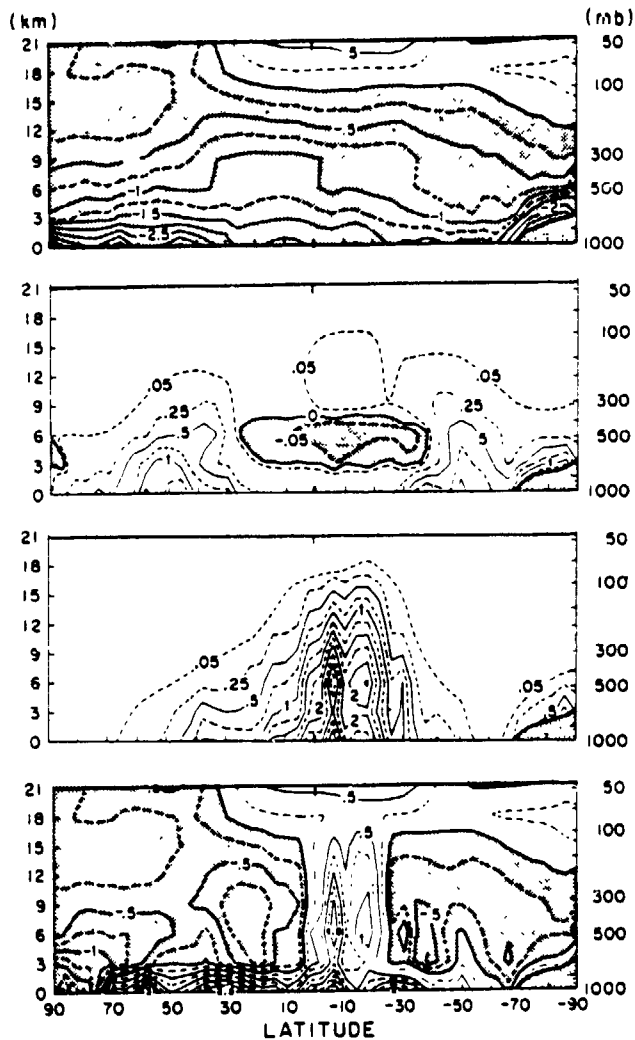


Fig. 1 Zonally-averaged heating of the atmosphere, in January, as calculated in a numerical simulation experiment (Schlesinger and Mintz, 1979). Solid line contour interval is  $0.5^{\circ}\text{C day}^{-1}$ . Top panel: Solar plus longwave radiational heating. Second panel: Large scale condensation heating. Third panel: Heating by cumulus condensation and convection. Bottom panel: Total heating (sum of the first three panels, plus sensible heat transfer from the underlying land and ocean.)

climate predictions to know the amount of moisture in the soil.

One way of determining the amount of moisture in the soil is by integration of the soil moisture continuity equation. In its most simple, but non-trivial form, this can be written

$$\frac{dw}{dt} = P - E, \quad W_{\max} = W^*$$

where

$$E = \beta E_p$$

$$\beta = \beta(W, W^*) \quad (3)$$

and

$$E_p = E_p(T) \quad (4)$$

- (1) Here,  $W$  is the amount of evapotranspiration-available moisture in the soil,  $W^*$  is the maximum available moisture that the soil can hold,  $P$  is the precipitation rate,  $E$  is the rate of evapotranspiration,  $\beta$  is the evapotranspiration coefficient,  $E_p$  is the rate of potential evapotranspiration, and  $T$  is the temperature of air near the surface.
- (2)

C-2

ORIGINAL PAGE IS  
OF POOR QUALITY

Figure 2 shows an example of the calculated soil moisture obtained by cyclic integration of equation (1) over the year, when  $P$  is the normal observed precipitation;  $W^*$  is  $15 \text{ gm/cm}^2$ ,  $\beta = 1 - \exp^{-6.8(W/W^*)}$  when  $P < E_p$ , and  $\beta = 1$  when  $P > E_p$ ; and  $E_p$  is obtained from the empirical formula of Thornthwaite, using the normal observed surface air temperature. (See Mintz and Serafini, 1981).

One can also use this method to initialize the soil moisture distribution in real time. [See, for example, Louse and Pugsley, 1981.] The global precipitation measurements that are required are a continuous time series of the measured daily (or weekly) precipitation, averaged over the computational grid areas, and with about 10% accuracy in the time and space averages. This precipitation, together with the calculated potential evapotranspiration, will produce a real-time distribution of the soil moisture.

3. Global Measurements of Detained Surface Water, for the Initialization of Soil Moisture

In the preceding section, the measured precipitation was used to obtain the infiltration of water into the soil. But there may be a better way of determining the infiltration.

Consider the water balance for the small horizontal region shown in Figure 3, where  $z_0$  denotes a level that is a few centimeters below the surface of the soil. Then we can write,

$$\frac{d}{dt}(W_{>z_0}) = P - I_{z_0} - R_{>z_0} - E_{>z_0} \quad (4)$$

where  $W_{>z_0}$  is the amount of moisture in the soil above the level

$z_0$ , together with any water that is on the surface:  $P$  is the rate of precipitation,  $I_{z_0}$  is the rate of infiltration at the level  $z_0$ ;  $R_{>z_0}$  is the rate of runoff above the level  $z_0$ , and  $E_{>z_0}$  is the rate of evaporation of the soil moisture and water that are above the level  $z_0$ . ( $E_{\leq z_0}$  is the rate of evapotranspiration of the soil moisture that is below the level  $z_0$ , and which, for the most part, is removed by the vegetation.)  $P_{>z_0}$  is the surface runoff into hills whose horizontal spacing is several times larger than the depth of the plant root zone. This is water which will not be available for evapotranspiration.

We will call  $W_{>z_0}$  the "detained surface water" (It is the water that gets your shoes wet when you walk across a field after the rain has stopped.) It is, perhaps, the water that can be measured from space by microwave radiometry (Schmugge, 1980).

Although  $R_{>z_0}$  and  $E_{>z_0}$  are functions of  $W_{>z_0}$ , for the purpose at hand we need only be concerned with the dependence of  $I_{z_0}$  on  $W_{>z_0}$ . For example, if the measured  $W_{>z_0}$  is less than the field capacity of the soil above level  $z_0$ , there will be no infiltration. If the measured  $W_{>z_0}$  is larger than field capacity, there will be infiltration. The task will be to measure  $W_{>z_0}$  and to know the function

$$I_{z_0} = I_{z_0}(W_{>z_0}, \dots) \quad (5)$$

as  $I_{z_0}$  will depend not only on  $W_{>z_0}$  but also on the properties of the soil and its antecedent wetting.

In other words, the surface of the earth and the top few centimeters of the soil would be used as a remotely-sensed "leaky rain gauge". There will be a discontinuity in the "leakage rate" when  $W_{>z_0}$  changes from being less than to being greater than the field

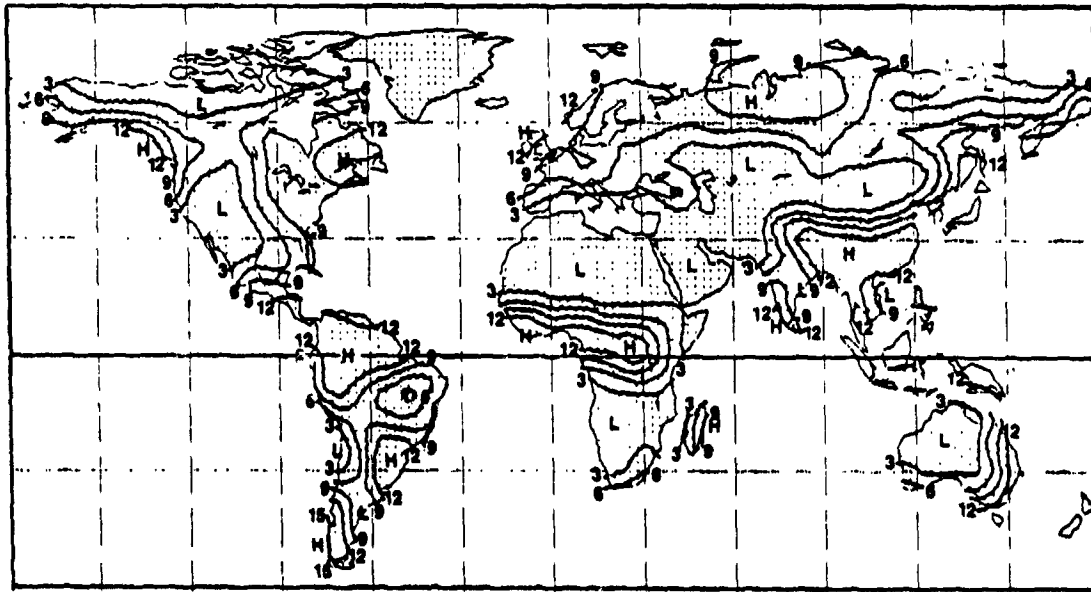


Fig. 2 Soil moisture available for evapotranspiration, in mid-July, as calculated from the observed antecedent rainfall and estimated potential evapotranspiration (Mintz and Serafini, 1981). Units:  $\text{gm/cm}^2$ . Maximum =  $15 \text{ gm/cm}^2$  (=150mm depth of water.)

ORIGINAL PAGE IS  
OF POOR QUALITY

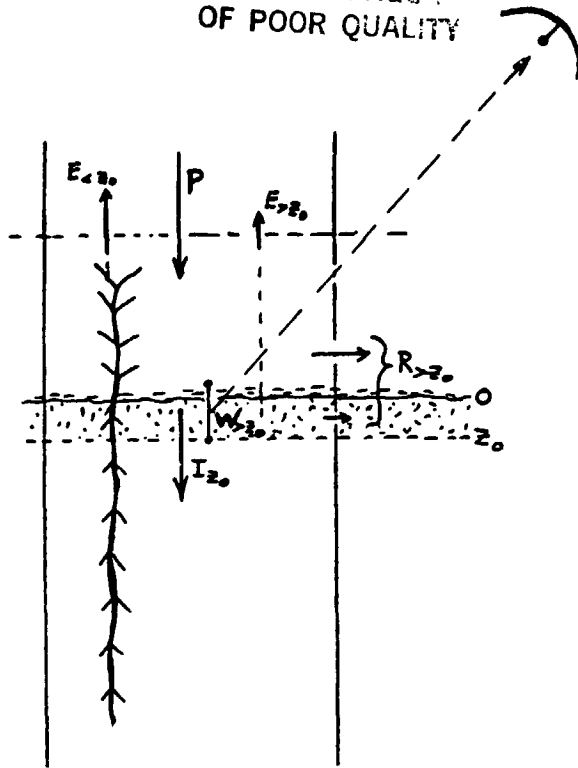


Fig. 3 Concept of the remote sensing of the earth's surface, treated as a "leaky rain gauge". Measurement of the transient water within the top few centimeters of the soil is used to calculate the infiltration into the underlying soil.

capacity of the soil above level  $z_0$ . In addition, if we measure the time rate of change of  $W_{>z_0}$ , as well as  $W_{>z_0}$  itself, on some occasions immediately subsequent to rainfall events, but at times of the day when the evaporation is negligibly small, and under various conditions for the ratio ( $I_{>z_0}/P_{>z_0}$ ), we may be able to determine the function  $I_{z_0}(W_{>z_0}, \dots)$ .

The requirement will be to measure  $W_{>z_0}$  accurately enough, and frequently enough, to determine the total daily area-averaged infiltration with an accuracy of about 10%. In this respect, there may be a practical advantage in measuring the detained surface water,  $W_{>z_0}$ , instead of measuring the precipitation,  $P$ . To obtain the daily precipitation to an accuracy of 10% may require measurements of the precipitation every few minutes. But to obtain the daily infiltration to an accuracy of 10% may require measurements of  $W_{>z_0}$  only every few hours.

#### Addendum

The above discussion was addressed to general circulation model development and the use of such models for climate simulations and climate predictions. It was not addressed to the use of general circulation models for short and medium range weather predictions, where the accuracy of the initial state of the motion field is important.

Dr. Norman Phillips has pointed out that global measurements of the precipitation, which would provide information about the horizontal distribution of the condensation heating, may make it possible to use the method of nonlinear normal mode initialization to obtain the motion field in the tropics, where there is a strong interaction between the low level velocity convergence and the heating by cumulus condensation and convection. This, in turn, will influence the prediction of the motion and weather fields in the extratropics.

It may also be possible to do this when the initialization method is four-dimensional data assimilation. (See, for example, Miyakoda *et al.*, 1976; Ghil, *et al.*, 1979). At present, because of inadequate wind observations in the tropics, it is largely the model predicted heat of condensation that forces the circulation and is the main factor in initializing the motion field in the tropics. With measurements of precipitation, we would replace the model produced condensation heating with the true condensation heating and, thereby, obtain a better initialization of the tropical motion field.

Whichever initialization method is used, the requirements are not less than 12-hourly (and preferably 3-hourly) measurements of the precipitation, averaged over the computational grid areas, and with an accuracy of about 10%. If there must be a choice (as in the satellite orbit) between 12-hourly global coverage and 3-hourly tropical coverage, it is the latter that is to be preferred for the motion field initialization.

#### References

- Chang, J. (ed.), 1977: General Circulation Models of the Atmosphere. Methods in Computational Physics, Vol. 17, Academic Press, New York/San Francisco/London, 337 pp.
- Ghil, M., M. Halem and R. Atlas, 1979: Time-Continuous Assimilation of Remote-Sounding Data and Its Effect on Weather Forecasting. Mon. Wea. Rev., 107, pp 140-171.
- Lorenz, E. N., 1967: The Nature and Theory of the General Circulation of the Atmosphere. Tech. Note No. 218, TP 115, WMO, Geneva, 161 pp.
- Louie, P. Y. T. and W. I. Pugsley, 1981: Application of Near Real-Time Water Budgets in Monitoring Climate-Related Events. Proceedings of the Fifth Annual Climate Diagnostics Workshop, University of Washington, Seattle, October 22-24, 1980. U.S. Dept. Commerce/NOAA, Wash. D.C., pp. 158-166.
- Mintz, Y., 1981: The Influence of Land-Surface Evapotranspiration on Rainfall and Circulation: A Review of Simulation Experiments. Land-Surface Processes in Atmospheric General Models. Proceedings of the Study Conference on Land Surface Processes, Greenbelt, Maryland, 5-10 Jan. 1981. GARP Publications Series, WMO, Geneva. (in press).

- Mintz, Y., and M. E. Schlesinger, 1979: Numerical Simulation of Ozone Production, Transport and Distribution with a Global Atmospheric General Circulation Model. J. Atm. Sci., 36, pp. 1325-1361.
- Mintz, Y., and V. Serafini, 1981: Global Fields of Moisture and Land-Surface Evapotranspiration. Paper submitted to Symposium on Variations in the Global Water Budget, Oxford, 9-15 August 1981
- Miyakoda, K., L. Umscheid, D. H. Lee, J. Strutis, R. Lusen and F. Pratte, 1976: The Near-real-time, Global Four-dimensional Analysis Experiment During the GATE Period. J. Atmos. Sci., 33, 561-591.
- Schmugge, T., 1980: Soil Moisture Sensing with Microwave Techniques. Proc. 14th Int. Symp. for Remote Sensing of Environment, San Jose, Costa Rica, 23-30 Apr. 1980. Environmental Res. Inst. of Michigan, Ann Arbor, pp. 487-505.
- WMO/ICSU, 1979 Report of the JOC Study Conference on Climate Models: Performance, Intercomparison and Sensitivity Studies. GARP Publication Series No. 22, Vol. I, World Meteor. Organization, Geneva, 606 pp.

ORIGINAL DOCUMENT  
OF POOR QUALITY

D9 N83 25278

ORIGINAL PAGE IS  
OF POOR QUALITY

## Precipitation Data for Climate Diagnostics

by

Eugene M. Rasmusson and Phillip A. Arkin  
Climate Analysis Center  
NMC, NWS, NOAA  
Washington, D.C. 20233

### I. Introduction

Climate diagnostics is concerned with climate fluctuations whose time scales are longer than the lifetime of typical weather systems, but shorter than the time scales of the "climate normals" used to define climate change. Examples of the phenomena of interest are slow moving weather systems such as "blocking highs" (Shukla and Mo, 1981), which may produce large regional anomalies lasting for a few weeks, pronounced seasonal anomalies, such as the abnormal winter of 1976-77 over the United States (Edmon, 1980), global scale systems of atmospheric "teleconnections" (Wallace and Gutzler, 1981) and large-scale, long period ocean/atmosphere fluctuations such as the Southern Oscillation (Rasmusson and Carpenter, 1981; Horel and Wallace, 1981).

Although initial diagnostic studies may be descriptive in nature, their ultimate goals are an understanding of the physical processes responsible for the climate fluctuations, and information on the potential predictability of the system.

Precipitation data are required in studies of both the heat and water balance of the earth-atmosphere system. Diagnostic requirements for precipitation data most frequently fall in the following range:

Temporal resolution - 1/2 - 1 month

Spatial resolution - 250 - 500 km

Accuracy - ability to identify significant year-to-year fluctuations in precipitation

Coverage - large regional to global

Diagnostic data requirements typically range around averages for spatial scales of a few hundred kilometers and time scales of a few weeks. However, both the averaging period and degree of quantification largely depends on the specific diagnostic questions being asked. In any case, the basic sampling density in time and space must greatly exceed the time/space averaging element if the episodic, small scale character of precipitation events is to be adequately resolved.

The requirement for a stable method of estimation that is accurate enough to identify significant year-to-year fluctuations is of central importance to climate diagnostics. Observations need not exceed this basic requirement to be of significant value in diagnostic studies. This fact is recognized in the GARP

ORIGINAL PAGE IS  
OF POOR QUALITY

16 requirement for a quantitative resolution of four levels of discrimination of precipitation intensity over the sea. Even "precipitation indices" which are stable but lack absolute calibration are very useful for a broad range of studies.

## 2. Global Scale Diagnostics

Precipitation data are required for global scale diagnostics to evaluate variations of the major latent energy source regions of the earth. The strongest of these regions are located in the tropics, and are clearly shown by maps of satellite observed outgoing longwave radiation (Winston et al., 1979). They consist of (1) the South American Tropics, (2) the African Tropics, (3) the Indonesian - Tropical Pacific area, and (4) the summer Asiatic Monsoon.

The Indonesian-Tropical Pacific area includes the "maritime continent" region of Indonesia, the Intertropical Convergence Zone (ITCZ) and the South Pacific Convergence Zone (SPCZ), which extends southeastward from the New Guinea-Solomon Island region. All four major latent energy source regions show a seasonal variation in location and intensity, but only the Indonesian-tropical Pacific region exhibits significant interannual variability in both intensity and location. These variations are associated with the Southern Oscillation/El Nino phenomenon (Rasmusson and Carpenter, 1981) and are linked to winter circulation anomalies in the Northern Hemisphere extratropics (Horel and Wallace, 1981). Consequently, this region, which is located largely over ocean areas almost completely devoid of conventional precipitation observations, is of major importance in the diagnosis of North American climate fluctuations.

## 3. Regional Diagnostics

Under this category we include the more detailed analysis of tropical precipitation, as well as regional precipitation fluctuations outside the tropics. Within this context we note two sampling problems which are sometimes given inadequate attention; terrain effects and diurnal variability.

Examination of a map of mean annual precipitation over the United States (e.g. Geraghty et al., 1973), clearly shows the major influence of terrain on the climatological distribution of precipitation. There is a fairly regular west to east increase in precipitation across the central part of the nation. However, over the rougher terrain of the west, and over the Appalachians and Ozark Plateau, the major spatial variance is on scales of 100-200 km or less. This small-scale variance must be adequately resolved if unbiased averages are to be obtained for larger areas. This often requires a density of surface observations beyond what is available. In such cases, the observational requirements can probably best be satisfied using a mix of surface and satellite data.

Diurnal variations of precipitation are most pronounced over land areas (Wallace, 1975). However, studies such as those of Gray and Jacobson (1977) and Short and Wallace (1980) indicate that significant diurnal variations may also be present over many low latitude ocean areas.

Rasmusson (1971) described the complex diurnal variation of summertime thunderstorm activity over the United States. Fig. 1 (from his report) shows a maximum of activity at some point in the nation at most hours of the day. Wallace (1975) made an extensive analysis of diurnal variations in precipitation

ORIGINAL PAGE IS  
OF POOR QUALITY

over the United States and found areas of significant diurnal variability even during the winter season.

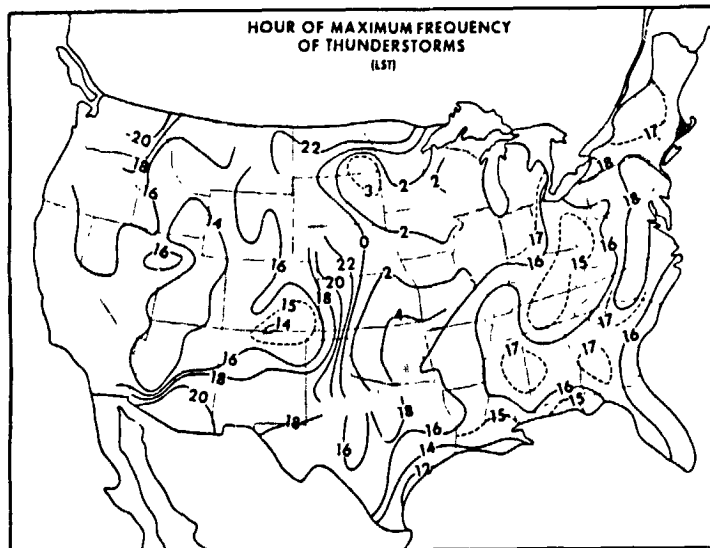


Fig. 1. Hour (local standard time) of maximum frequency of thunderstorms, June-August.

From these and many other studies, it seems apparent that frequent observations are required throughout the day to adequately resolve the diurnal cycle, particularly over regions of convective precipitation. The 12-hour resolution available from a single polar orbiter satellite may provide useful data for evaluating year-to-year variations in precipitation, particularly for averaging periods of a month or more, but is unlikely to provide reliable quantitative resolution of the diurnal cycle.

#### 4. Use of Satellite IR Data

There is at present no general technique for obtaining routine global estimates of precipitation on diagnostic time and space scales. However, a number of techniques have been developed to indirectly estimate convective rainfall using visible and/or infrared (IR) imagery from satellites. Most of these methods are based on the notion that deeper convective clouds might produce more rain and on observational findings which show that regions of rainfall tend to be correlated with bright (in visible imagery), cold (in IR), clouds (Sikdar, 1972; Griffith and Woodley, 1975; Reynolds and Von der Haar, 1975). We will not discuss these techniques here, but will briefly describe some statistical results which suggest a practical approach for estimating convective precipitation on diagnostic time and space scales.

Woodley et al. (1980) provides an example of automated rainfall estimation using IR satellite imagery. Their method estimates the instantaneous rain rate of a convective cloud by converting cloud area, which is determined by the contiguous area above (colder than) an empirically determined radiating temperature of 253K, to echo area. The conversion requires knowledge of the maximum cloud area and the cloud size and sign of change (increasing or decreasing) of the area. These are used with a set of empirically generated functions to determine echo area. Another empirical function of the cloud's life cycle is then used to convert echo area to rainfall.



ORIGINAL PAGE 19  
OF POOR QUALITY

A model such as this requires identification and tracking of individual cloud entities throughout their lifetimes in order to determine surface rainfall amounts. While this process is not necessarily too burdensome, given an appropriate interactive computer graphics system and an experienced satellite meteorologist, it is quite difficult to automate. An algorithm for automatically identifying and tracking clouds has been developed (Griffith, et al. 1978), but it is expensive to use on a large scale. Routine global application of techniques such as those of Woodley et al. might well prove impractical.

Arkin (1979) and Richards and Arkin (1981) (hereafter referred to as RA) have examined the statistical relationship between fractional cloud cover and rainfall for a variety of time and space scales during the three phases of the GARP (Global Atmospheric Research Program) Atlantic Tropical Experiment (GATE), which took place from late June through mid-September 1974. The rainfall data used in these studies were hourly accumulations in  $4 \text{ km}^2$  areas derived from digital C-band radar measurements complemented by shipboard rain gage data. A full description may be found in Hudlow and Patterson (1979). Fractional cloud cover was obtained by applying various thresholds to the frequency distributions compiled for each  $0.5^\circ \times 0.5^\circ$  area in the GATE A/B array by Polifka and Cox (1977).

In the first study, Arkin (1979) approximated the B scale hexagon with the  $0.5^\circ$  boxes and compared 6-hour averages of the fractional cloud cover above (colder than) various thresholds with 6-hour rainfall accumulations in the same area for each phase. Figure 2 (his Fig. 1) shows that correlations  $>0.8$  are found in each phase for a range of thresholds centered near 10 km (237K). A linear function of fractional cloud above 10 km was capable of explaining 75% of the variance in 6-hourly rainfall accumulations during GATE. The regression coefficients showed little variation when each phase was analyzed separately.

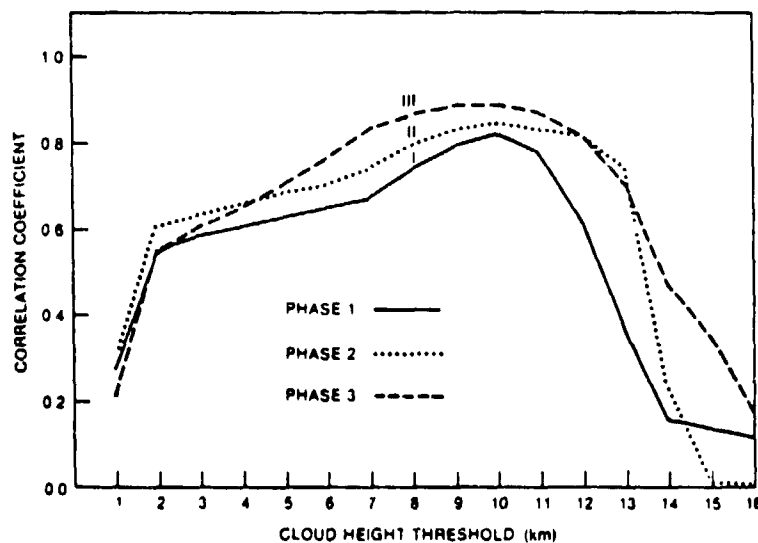


FIG. 2 Correlation between rainfall accumulation and fraction of B-scale area covered by clouds above various height thresholds.

RA computed rainfall and cloud area above several different thresholds for three regions of different sizes ( $3140$ ,  $28225$  and  $78400 \text{ km}^2$ ) for each phase of GATE. Since not all satellite observations fell on the hour, the fractional coverages were linearly interpolated in time to give hourly values. This procedure resulted in comparing instantaneous fractional coverages to rainfall accumulations during the preceding hour.

ORIGINAL PAGE IS  
OF POOR QUALITY

RA computed optimal (least squares) linear models for each combination of temporal and spatial averaging scale and several different threshold temperatures. Their results indicate that a practical trade-off exists between the spatial and temporal averaging scales. For the largest spatial scales, there is little variation of the model coefficients with temporal scale, indicating that the time averaging is relatively unimportant. For a smaller spatial averaging scale, a longer time average is required before the coefficients approach a stable value. For the hourly data, the coefficients change considerably with increasing spatial scale. They appear to be approaching constant values at the largest spatial scales examined. The phase-to-phase variation in the regression coefficients is relatively small.

The variation with threshold temperature and temporal scale for each phase and spatial scale of the linear correlation coefficient is shown in Figure 3. The patterns of the correlations for the two largest spatial scales resemble each other and the values are considerably larger than those for the smallest spatial scale. For both the 1.5° and 2.5° scales, the correlations approach or exceed 0.8 during all three phases for broad regions of the temporal scale - threshold temperature plane. The correlations generally increase with temporal scale for all three phases, but the increase becomes smaller as the spatial scale increases. It appears that averaging spatially is effectively equivalent to averaging in time. When a larger spatial average is used, a smaller time interval is generally sufficient to yield equally large correlations.

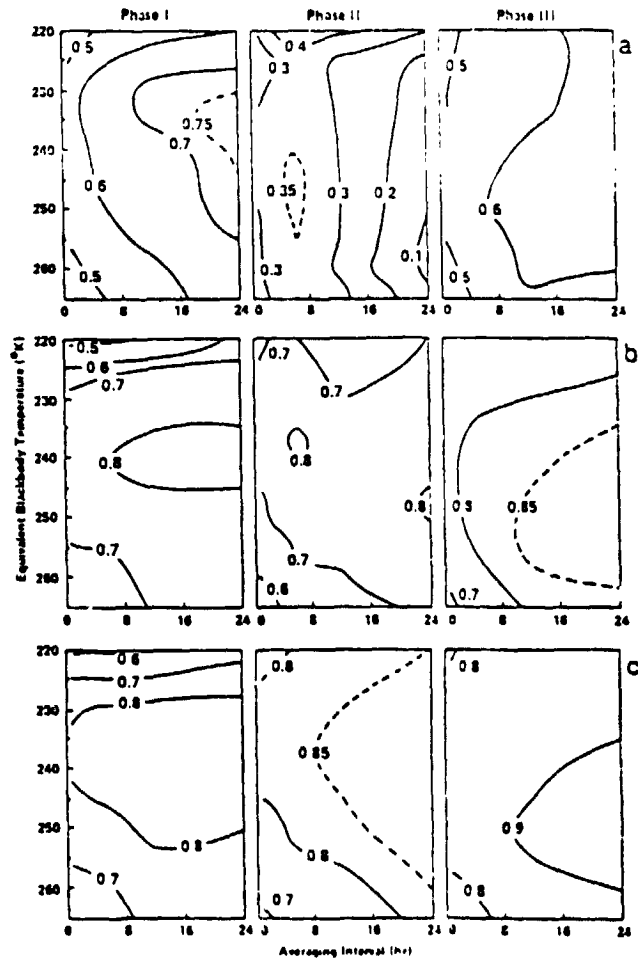


Fig. 3. Correlation between hourly radar estimated rainfall and fractional cloud coverage for each phase as a function of averaging interval and threshold temperature ( $T$ ) for the 0.5° averaging scale, (b) for the 1.5° averaging scale, and (c) for the 2.5° averaging scale.

ORIGINAL PAGE IS  
OF POOR QUALITY

Time series of rainfall estimates obtained from these optimized one-parameter linear models were compared with observed rainfall values. The estimated values generally reflected the major precipitation events. This is simply an indication that these events correspond to increases in fractional coverage at a given IR threshold. The success of the simple linear model implies that most major rain producing cloud systems in GATE, when viewed over a large enough area, had an effective mean rainfall rate that did not vary greatly from event to event. For individual convective elements, the rainfall rates change throughout the elements' lifecycles and probably vary somewhat from one cloud to another. However, when the area sampled is large enough to contain a number of individual elements at various stages of their lifecycles, these variations must approximately cancel one another.

RA also compared the estimates of the one parameter model with other results for the GATE area by Stout et al. (1979) and Woodley et al. (1980). These methods use a more sophisticated approach of tracking the clouds through their lifecycles to more accurately relate smaller scale spatial and temporal variations to time-varying rainfall rates. In these studies, estimates were made for slightly different areas than that used in RA. Stout et al. made hourly estimates for the "master array" for several rainfall events, and Griffith et al. made 6-hour estimates for a 3° square, centered on the GATE array. RA found that during the major rainfall events there was a tendency for all three methods to produce deviations from the radar estimates that were of the same sign. That is, they either over or under-estimate for the same periods.

This comparison indicates that while Woodley et al. (1980) and Stout et al. (1979) showed that the lifecycle effect, which is ignored in RA's model, is closely related to the smaller scale instantaneous convective rainfall rates, its importance is reduced for larger spatial and temporal averaging scales. When the Woodley et al., and Stout et al. GATE rainfall estimates were averaged over large areas (scales on the order of 2-3° of latitude), they are comparable to those of the one parameter model.

Indirect estimation of rainfall using visible or IR imagery requires that satellite derived parameters be empirically related to ground truth. Because of the complexity of convective precipitation, the relationship will depend on the statistical characteristics of the fields involved. Any derived relationship is strictly applicable only to the time and location for which it has been determined. The degree to which it may be applicable to other areas and times depends on the similarity of the meteorological conditions between the two locations. Whatever the relationship may be, it can ultimately be interpreted as one relating an effective mean rainfall rate to the fractional cloud cover. In this light, the results of Woodley et al. (1980) who based their estimates for the GATE area on relationships derived from observations of convective rainfall over Florida, seem to indicate that the effective rainfall rate for both areas is similar. This seems to indicate that a simple approach along the lines envisaged by Barrett (1970), who proposed assigning a mean rainfall rate to various types of cloud, may be useful for time scales of a day or more and spatial scales on the order of several degrees of latitude (200-300 km).

For applications such as climate diagnostics, where short time scales and small space scales are relatively unimportant, the results of RA suggest that

ORIGINAL PAGE IS  
OF POOR QUALITY

it may be possible to devise a useful rainfall estimation scheme in areas of predominately convective precipitation from satellite IR data based on a linear relation using a single parameter such as fractional cloud cover. Operational use of such a procedure depends on three things: an accurate IR digital counts to temperature conversion algorithm; an efficient satellite coordinate to lat/long transformation; and a transfer function for converting fractional cloud cover to rainfall estimates or indices.

Considering the broad range of threshold temperatures for which high correlations exist (Fig. 2), an error of 5K in the digital count to temperature algorithm would not pose a problem and larger errors could be tolerated. Satellite coordinate to lat/long transformations (usually referred to as navigation of the satellite image) exist (see Arkin, 1979 for a brief discussion). The navigation required to obtain cloud tracked winds (used in NMC analyses) is more accurate than would be required for climate diagnostics precipitation estimates.

The transfer function for converting from fractional cloudiness to rainfall is undoubtedly a function of position and time. For our purposes, we wish to determine long period (monthly) averages of rainfall in the tropics on large (250-500 km) space scales. The only work of which we are aware which addresses the spatial variation of such a transfer function is that of Woodley et al. (1980) who applied functions developed from data over South Florida to the entire tropical Atlantic without any modification so far as we know. Arkin (1979) and RA found little variation in transfer function from late June through mid-September in the GATE area. These results suggest that the transfer function may be a weak function of space and time. A further indication is found in the work of Heddinghaus and Krueger (1981), who examined time series of emitted IR obtained from polar orbiting satellites. They found that on monthly and longer time scales the variations in emitted IR were representative of large-scale variations in precipitation throughout the tropics.

While much more work is needed to firmly establish an appropriate form for the transfer function, a useful preliminary step for obtaining an index of rainfall variability over the tropics might be to simply assume an unvarying transfer function of the form outlined here, where rainfall is assumed a linear function of fractional cloud cover. It appears, therefore, that all the requisite elements are available for obtaining useful diagnostic precipitation indices for the convective regions of the tropics. The relative simplicity of the method which has been outlined makes it an attractive candidate for routine operational use.

## REFERENCES

- Arkin, P. A., 1979: The relationship between fractional coverage of high cloud and rainfall accumulations during GATE over the B-scale array. Mon. Wea. Rev., 107, 1383-1387.
- Barrett, E. C., 1970: The estimation of monthly rainfall from satellite data. Mon. Wea. Rev., 98, 322-327.
- Edmon, H. L., Jr., 1980: A study of the general circulation of the Northern Hemisphere during the winters of 1976-77 and 1977-78, Mon. Wea. Rev., 198, 1538-1553.
- Geraghty, J. J., D. W. Miller, F. van der Leeden, and F. L. Troise, 1973: Water Atlas of the United States, Water Information Center, Fort Washington, N. Y.
- Gray, W. M. and R. W. Jacobson, Jr., 1977: Diurnal variation of deep cumulus convection. Mon. Wea. Rev., 105, 1171-1186.
- Griffith, C. G., and W. L. Woodley, 1975: On the variation with height of the top brightness of precipitating convective clouds. J. Appl. Meteor., 12, 1086-1089.
- Griffith, C. G., W. L. Woodley, P. G. Grube, D. W. Martin, J. Stout, and D. N. Sikdar, 1978: Rain estimation from geosynchronous satellite imagery - visible and infrared studies. Mon. Wea. Rev., 106, 1153-1171
- Heddinghaus, T. R., and A. F. Krueger, 1981: Annual and intersannual variations in outgoing longwave radiation over the tropics. To be published in Mon. Wea. Rev.
- Horel, J. D. and J. M. Wallace, 1981: Planetary scale atmospheric phenomena associated with the Southern Oscillation. To be published in Mon. Wea. Rev.
- Hudlow, M.D. and V. Patterson, 1979: GATE Radar Rainfall Atlas. NOAA Special Report, Center for Environmental Assessment Services, NOAA, 155 pp.
- Kilonsky, B. J. and C. S. Ramage, 1975: A technique for estimating tropical open-ocean rainfall from satellite observations. J. Appl. Meteor., 15, 972-975.
- Polifka, M.C. and S.K. Cox, 1977: GATE SMS-1 brightness frequency distribution digital magnetic data tapes. Dept. Atmos. Sci., Colorado State University, 25 pp.
- Rasmusson, E.M., 1981: Diurnal variations in summertime thunderstorm activity over the United States. Environ. Tech. Appl. Center, Air Weather Service, U.S.A.F. Tech. Note 71-4, 12 pp.
- Rasmusson, E. M. and T. H. Carpenter, 1981: Variations in tropical sea surface temperature and surface wind fields associated with the Southern Oscillation/ El Nino. Submitted to Mon. Wea. Rev.

ORIGINAL PAGE IS  
OF POOR QUALITY

- Reynolds, D., and T.H. Von der Haar, 1975: A comparison of radar determined cloud height and reflected solar radiance measured from the geosynchronous satellite ATS-3. J. Appl. Meteor., 12, 1082-1085.
- Richards, F., and P.A. Arkin, 1981: On the relationship between satellite observed cloud cover and precipitation. Mon. Wea. Rev. (to be published May 1981).
- Short, D. A., and J. M. Wallace, 1980: Satellite-inferred morning-to-evening cloudiness changes. Mon. Wea. Rev., 108, 1160-1169.
- Shukla, J., and K. C. Mo, 1981: Seasonal variation of blocking. Paper presented at the First AMS Conference on Climate Variations, San Diego, CA.
- Sikdar, D. N., 1972: ATS-3 observed cloud brightness field related to a meso-to-synoptic scale rainfall pattern. Tellus, 24, 400-412.
- Stout, J. E., D. W. Martin, and D. N. Sikdar, 1979: Estimating GATE rainfall with geosynchronous satellite images. Mon. Wea. Rev., 107, 585-598.
- Wallace, J. M., 1975: Diurnal variations in precipitation and thunderstorm frequency over the conterminous United States. Mon. Wea. Rev., 103, 406-419.
- Wallace, J. M. and D. S. Gutzler, 1981: Teleconnections in the geopotential height field during the Northern Hemisphere winter. Submitted to Mon. Wea. Rev.
- Woodley, W., C.G. Griffith, J.S. Griffin and S.C. Stromatt, 1980: The inference of GATE convective rainfall from SMS-1 imagery. J. Appl. Meteor. 19, 388-408.
- Winston, J. S., A. Gruber, T. I. Gray, Jr., M. S. Varnadore, C. L. Earnest, and L. P. Mannello, 1979: Earth-atmosphere radiating budget analyses derived from NOAA satellite data June 1974-Feb. 1978. Vol. 1. U. S. Dept. of Commerce, Washington, D. C.

ORIGINAL PAGES  
OF FLOOR QUALITY

Agricultural Requirements for Precipitation Measurements<sup>1</sup>  
Norton D. Strommen<sup>2</sup> Robert F. Dale<sup>3</sup> Raymond P. Motha<sup>2</sup>

Agriculture is a major user of meteorological data. Precipitation data required to meet the needs of agriculture can be divided into three basic categories with very different time and spatial resolution requirements. These are strategic and tactical planning programs in support of the basic farm production unit, real time impact assessment and research programs.

Real time impact assessment requires that input data meet stringent time and cost constraints, but has a more liberal spatial resolution requirement. Strategic and tactical planning and research requirements for precipitation data include much higher spatial and time resolution at a reasonable cost.

The suggested orientation for this workshop is to consider a spatial resolution from satellite-derived data of 250 km by 250 km with a time of from 2 to 4 weeks as a most likely achievable goal. This resolution will only marginally meet agriculture's real time crop impact assessment needs and will give the U.S. farmers and researchers no additional information. Because of the proposed spatial coverage and time constraints, additional discussion in this paper will focus on the potential use for the real time crop condition impact assessment.

The Joint Agricultural Weather Facility (JAWF), staffed by NOAA meteorologists and USDA agricultural meteorologists, and the Crop Condition Assessment Division (CCAD) of the FAS are both primary agricultural users of meteorological information. JAWF is continually looking for and greatly interested in adaptation of potential new products for crop assessment. USDA's initial real time crop condition impact assessment uses soil moisture analysis where available and otherwise cumulative precipitation data to determine the likely impacts of a given series of weather events on crop condition (vigor) and for making estimates of potential yield levels. To supplement USDA's needs for surveillance of crop conditions, the CCAD is operationally using spectral-digital data from both NASA and NOAA satellite sources in its crop condition assessment work. However, both programs (i.e., JAWF and CCAD) currently heavily rely on the timely (within 24 hours of collection) flow of surface synoptic data collected from the WMO-GTS at NOAA's National Meteorological Center in Camp Springs, Maryland.

In many regions of the world, the ground observations are considered spatially too sparse to get a good indication of areal coverage for precipitation occurrences. This is particularly true in the tropics and in higher latitudes where most summer precipitation falls in the form of showers. To extend the limited ground truth data, environmental satellite photos are now used to sketch out the probable areal extent likely to have received precipitation from a storm or series of storm systems. This qualitative extension of precipitation coverage is highly subjective and the associated accuracy is sometimes less than desirable. The satellite data has, however, been extremely useful for identifying large areas that receive no precipitation, i.e. locations of regions having no cloud cover for extended periods. This is only one important application now used on an operational basis at JAWF for monitoring developing drought potential for large regions around the globe.

ORIGINAL PAGE IS  
OF POOR QUALITY

Another application, already implemented in operational work, is that of extending surface data reports into representative area coverage of significant weather events. This is particularly important when surface reports are very sparse. Such an application enhances the area estimates of precipitation for input as needed to regional type yield models and/or in the calculation of regional crop yield indices. In these cases no attempt is made to identify local conditions which may vary significantly from those of the region as a whole.

A third application used at JAWF is the verification of the extent of possible severe weather events. The NMC cooperates by scanning incoming synoptic reports for events which exceed a given list of agriculturally sensitive criteria, i.e., precipitation greater than 75 mm in 24 hours or winds in excess of 50 knots. The satellite cloud formations can often be used to help verify whether the reported event is likely to have occurred as well as the probable extent of the area covered by the event.

A fourth JAWF application involves use of satellite data to monitor the seasonal shift of the major synoptic features and their associated rainfall. The progress of the monsoons over the oceanic areas of the Pacific and Indian Oceans can be easily followed with satellite imagery.

These examples are all qualitative techniques that employ the integration of satellite cloud images to enhance available ground truth data. The next step is to provide quantification of precipitation amounts for crop growing regions from satellite imagery. The accuracy requirements of agriculture are variable. The use of the new products will, however, require that the satellite estimates show an improvement over the estimates that can be derived from aggregation of the ground data network. The satellite precipitation estimates need not be restricted from using ground derived data wherever they are available. In fact, it is encouraged that adaptation of satellite imagery for estimating area precipitation be developed and tested using both the combination of surface and satellite data and using satellite data alone. This work, however, should be done in regions where an adequately dense ground truth network exists for verification of the satellite derived precipitation estimates. To date, evaluation of efforts to use satellite data alone indicate this work generally results in over-estimation of lighter precipitation amounts and an underestimation of the heavier rainfall totals. However, the estimates between the extremes were generally clustered closer to the ground truth data network.

Agriculture users often prefer to convert precipitation data into estimates of soil moisture (SM) or plant available moisture (PAV) where PAV reflects only moisture in the root zone of the growing crop. Dale 1981, reported on work completed in Indiana using the Purdue Soil Moisture Simulator (PSMS) to predict PAV and compared these results with measured PAV using two different density precipitation data networks. The results (figure 1) show that the departures from the measured PAV in the top 105 cm of the soil generally increased with the decreasing density of ground observations. This clearly demonstrates that the research community must approach the potential use of the large region precipitation estimates with great caution. Certainly, the only potential agricultural user of the large region precipitation estimates would be for large area operational crop condition assessment, where localized departures are not critical to a successful product.



ORIGINAL BASE IS  
OF POOR QUALITY

Additional consideration from the agricultural user's viewpoint is timeliness. To be useful, the products should be available to the user within 24 hours after the end of the production period in question, be it daily, every two weeks or on a monthly time schedule, and at a cost that is competitive with the current systems, especially for the basic product. These latter points are raised to ensure that the research planning leading to the eventual satellite-derived precipitation products can be cognizant of the constraints in the three basic categories. The operational agricultural users consider precipitation data as a perishable input, and unlike the researcher, they will put timeliness and cost as well as accuracy very high in the requirements to be considered.

- 
- <sup>1</sup> Presented "Workshop on Precipitation Measurements from Space," April 28-May 1, 1981.
  - <sup>2</sup> Chief Meteorologist and Agricultural Assessment Meteorologist, WFAOSB/USDA, respectively.
  - <sup>3</sup> SEA-CR, Purdue University, W. Lafayette, Indiana.
  - <sup>4</sup> Dale, Robert F., "Existing Meteorological Networks," Anaheim, California Workshop, March 30-31, 1981.

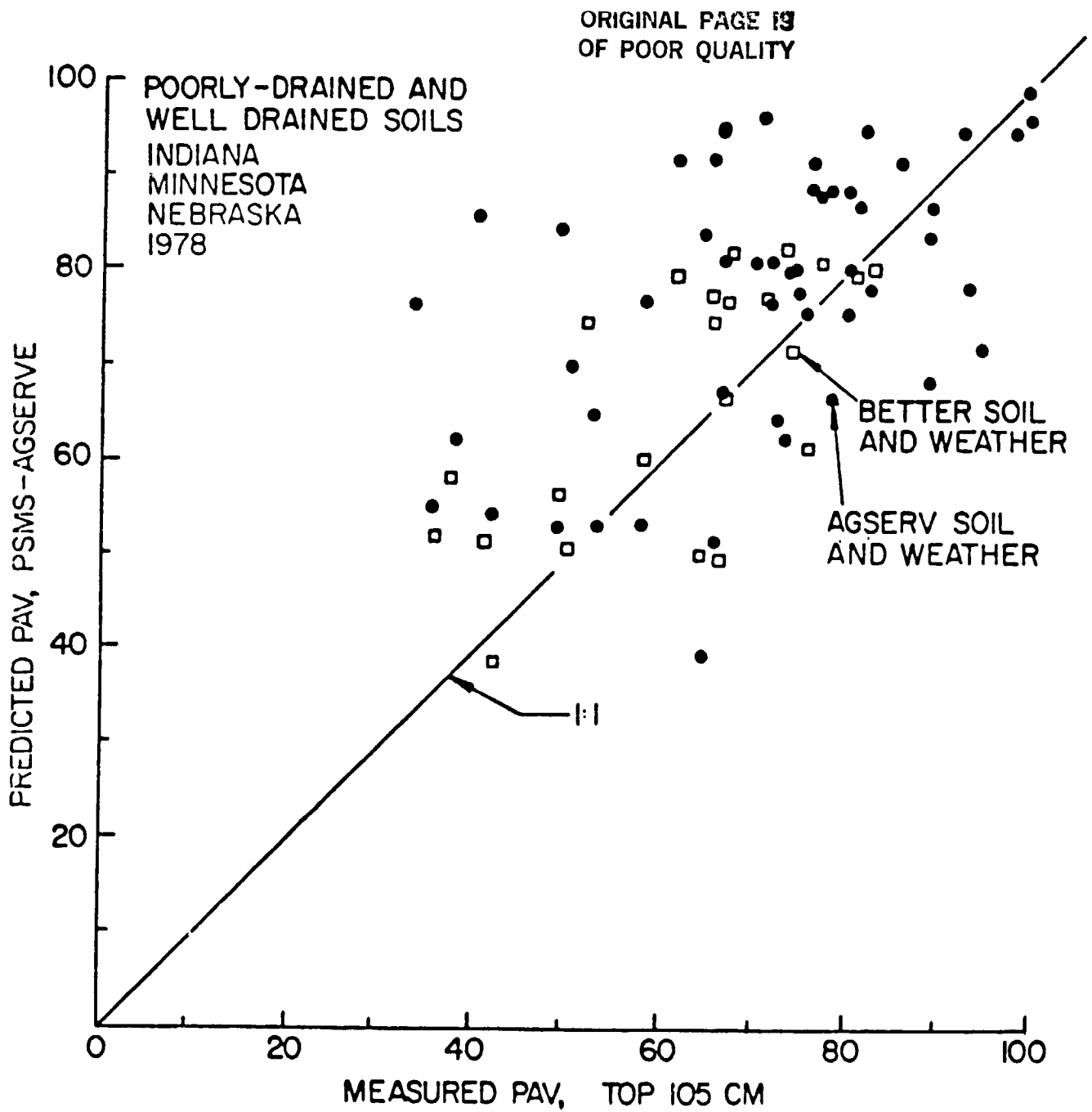


Figure 1. Measured vs. predicted soil moisture in top 105 cm using Purdue Soil Moisture Simulator (PSMS) and "county-average precipitation" interpolating linearly from first and second order station networks (●) and with precipitation measured at station within 2 km of soil moisture observation site (□).

ORIGINAL FORM IS  
OF POOR QUALITY

N83 25280

D11

Hydrologic Forecasting Requirements for  
Precipitation Data from Space Measurements

Michael D. Hudlow, Richard K. Farnsworth, and Douglas R. Greene

Hydrologic Research Laboratory  
National Weather Service, NOAA  
Silver Spring, Maryland

ABSTRACT

The requirements for precipitation measurements from space for hydrologic forecasting applications are discussed. The structure of the hydrologic forecasting service of the National Weather Service (NWS) is described, and an attempt is made to estimate the sampling and accuracy requirements for a range of spatial and temporal averaging scales corresponding to various NWS hydrologic applications. Finally, the data base requirements are addressed. The critical point is made that for the data sources to be most useful operationally at the NWS River Forecast Centers, the data must be available on-line in a format compatible with computer processing. Several data base systems are illustrated in a scenario for a multi-sensor rainfall analysis system (MSRANS). Actually, MSRANS is the software existing within the various computer environments required to preprocess, process, and analyze rainfall information from multiple sources.

1. INTRODUCTION AND BACKGROUND

Hydrologic forecasting in its broadest sense covers the prediction of the quality and quantity of all components of the hydrologic cycle (Symposium on Hydrologic Forecasting, 1980). For the purposes of this paper, however, the scope will be restricted to the requirements for precipitation measurements from space as inputs to the forecasting of quantitative streamflow amounts for scales ranging from those required to diagnose flash floods to those needed for deriving seasonal water supply forecasts. Some of the material presented also may be relevant to water quality forecasting, since water quantities have a direct effect on pollutant concentrations and thus knowledge of the quantity of water and its transport is often a prerequisite to the diagnosis or prediction of streamflow quality.

Specifically, subsequent sections of this paper will briefly cover the structure of the hydrologic forecasting service of this country and will discuss the spatial and temporal requirements for precipitation data to support the various hydrologic forecasting procedures. Accuracy and data-base structure requirements also are discussed.

2. STRUCTURE OF U.S. HYDROLOGIC FORECASTING SERVICE

The Congressional Organic Act of October 1, 1890 and subsequent reorganizations assigned to the Weather Bureau (now the National Weather Service (NWS)) the duties of the forecasting of weather, the issuing of storm warnings, the display of weather and flood signals for the benefit of agriculture, commerce, and navigation, the gaging and reporting of rivers... The NWS is the only federal organization legally authorized to disseminate river and flood forecasts and warnings directly to the public.

However, many other Federal and non-Federal organizations do become involved in various aspects of hydrologic forecasting. For example, the U.S. Army Corps of Engineers (a Federal agency) and the Salt River Project (a non-profit organization managed by landowners located in Central Arizona) produce their own specially-tailored river forecasts, which are used to supplement the NWS forecasts. These special forecasts are used in making decisions pertaining to the operation of their reservoirs and other riparian structures, but the forecasts are not disseminated directly to the public.

The hydrologic components of the NWS consist of headquarters elements and a research laboratory located in Silver Spring, Maryland; 13 River Forecast Centers (RFC's) located across the United States (Figure 1); and service hydrologists located in many of the Weather Service Forecast Offices (WSFO's). There are approximately 50 WSFO's located across the country with at least one in most states. For a further description of the relationships and interactions between the hydrologic and meteorological components of the NWS, see Clark (1977).

The current and future hydrologic procedures used by the RFC's are discussed by Ostrowski (1979). Several types of hydrologic models are currently used (Schaake, 1976). These include Antecedent Precipitation Index runoff models; conceptual hydrologic streamflow models, which use rainfall, and/or snowfall, and potential evapotranspiration as inputs to a soil moisture accounting system; streamflow routing models; reservoir operations models; and water supply forecast models. The total system of models, together with the data collection and data processing modules, is called the NWS River Forecast System (NWSRFS). Ostrowski (1979) also discusses the current types of data inputs that are available to NWSRFS. In the case of precipitation, sources range from manually read rain gages to remotely sensed measurements from land-based digital radars. In the future, the

RIVER AND FLOOD FORECAST SERVICE

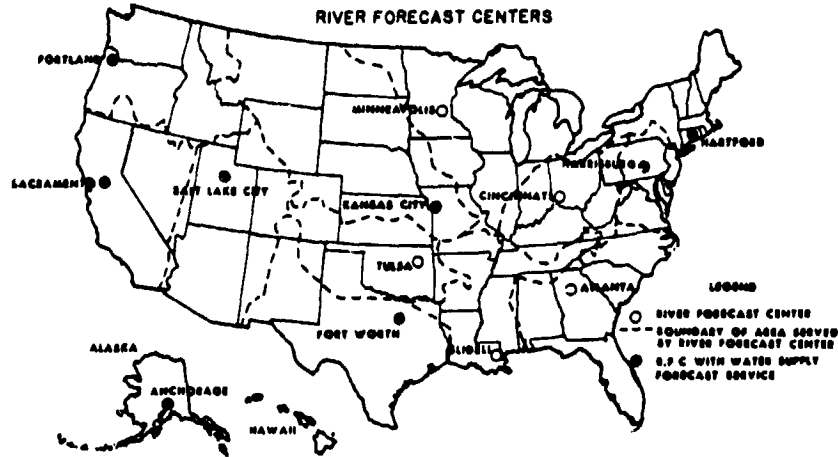


Figure 1. The 13 NWS River Forecast Centers and their respective forecast areas.

role of satellites potentially can become increasingly important if the requirements discussed in the subsequent two sections can be met.

3. SAMPLING AND ACCURACY REQUIREMENTS

As described by Kohler (1958), the operational problems confronted by the hydrologic forecaster can be partitioned according to the lead time of the forecast, which is related to the time scale for which the forecast applies. Kohler gives some of the purposes to be served by short-range hydrologic forecasts (referred to by Kohler as less than 10 days) and by forecasts for monthly or longer time periods. These include:

Short range forecasts -- usually less than 10 days

- Evacuating people and withdrawing movable property from the path of an oncoming flood.
- Fighting floods -- sand-bagging, closing of gates in levees and flood walls, planning for operation of pumps.
- Operating dams. Particularly valuable for flood control, navigation, and multiple-purpose structures.
- Planning for low-flow navigation.
- Scheduling diversion and distribution of irrigation water.
- Scheduling power production.
- Planning construction work in or near streams.

Monthly and longer forecasts

- Establishing long-range flood prevention and control operations.
- Planning for agricultural operations in irrigated areas.
- Establishing schedules of power operation.
- Planning municipal water supplies.
- Planning for long-range navigation activities.

In the short-range category, the flash-flood falls at the shortest end of the time scale, occurring in periods measured in minutes up to a few hours. At the other end of the time spectrum, it is feasible to predict with a fair degree of accuracy seasonal water supplies in those areas where a large fraction of the runoff is produced from snowmelt; for example, water stored in snowpacks provides as much as 70 percent of the water supply for the western states of the U.S. (Chang et al., 1981).

Most of the streamflow forecast models used by the NWS RFC's require precipitation averaged over a basin or sub-basin area as input. The size of the area, as well as the temporal period over which the precipitation is averaged, depend on the hydrologic application and on data availability. Quicker data availability can lead to improvements in the Mean Forecast Lead Time (MFLT) for a given size watershed; but, if the quicker data are less reliable, then the reliable MFLT can even decrease (Jettmar et al., 1979).

The frequency of samples required to achieve a desired accuracy for a given averaging domain will depend on the variability of the precipitation in time and, since rainfall generally is a nonstationary process, the variability in space is related to the variability in time. Furthermore, the precipitation variability is related to the type of precipitation which, in turn, may be related to season for a given locality. Figure 2 illustrates how the relative variability of average storm precipitation varies for a 400 mi<sup>2</sup> network in central Illinois (Changnon and Huff, 1980) for several different precipitation types. The relative variability would increase for all precipitation types for averaging increments less than those of the total storm periods.

Because the variability of rainfall varies with type and location, it is difficult to generalize the sampling requirements. However,

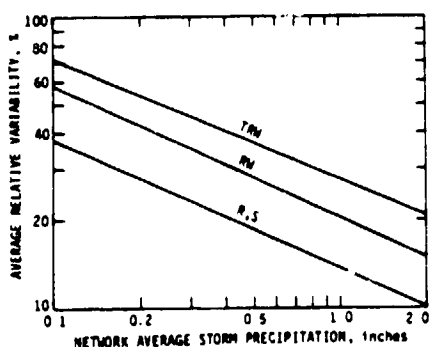


Figure 2. Relations between relative variability and precipitation type on a 400 mi<sup>2</sup> network in central Illinois (from Changnon and Huff, 1980, p.40). TRW = thunderstorm cases; RW = rain shower cases; R,S = continuous rain and snow cases.

for short-term forecasting applications, it is informative to examine some results presented in Figure 3 from Rudlow and Arkell (1978). Figure 3 gives estimates of the mean percent error that can be attributed to incomplete sampling (i.e., temporal sampling error) for various sampling intervals and size areas and for 1-hr, 2-hr, 3-hr, and 6-hr averaging intervals. The results shown in Figure 3 are based on digital radar data collected over the eastern tropical Atlantic Ocean during the GARP Atlantic Tropical Experiment (GATE). To consider these results is of value because the sampling requirements for tropical convection in the Intertropical Convergence Zone, where the GATE data were collected, may not be that dissimilar from those for thunderstorm convection in mid-latitudes and probably represent the limiting case to be met for precipitation sampling from space.

As mentioned above, the sampling frequency required depends on the application. For example, the detection of excessive rainfall at the smallest spatial scales that can produce flash floods will require samples spaced on the order of minutes while, as given by Johnson and Vetlov (1977), weekly observations are sufficiently frequent for mapping snow cover for most applications. Also, the wavelength and technique employed to estimate the precipitation may dictate even shorter sampling intervals than would be required to achieve the same accuracy from direct precipitation measurements. Negri and Adler (1980), for example, suggest that it may be necessary to collect infrared satellite data at high time resolutions (every 5 minutes) if thunderstorm-top ascent rates, estimated from the brightness temperatures, are used to infer rainfall rates. The reason for this is that the tops ascend rapidly over a short time period during the rapid growth phase of the developing stage of the storm.

Although there is very limited information available on sampling requirements for achieving necessary accuracies for various hydrologic forecasting applications, we have composed a rough summary of the requirements based on available information and the opinions of several

hydrologists in the NWS Office of Hydrology (Figure 4). The mean percent errors given in Figure 4 were arrived at by first considering the magnitude of errors tolerable for current operational techniques using conventional data from land-based precipitation systems. These initial error values were then relaxed further after considering some of the practical and technical limitations likely to be encountered in estimating precipitation from satellite measurements. We feel that users of satellite information must be realistic in specifying accuracies; the "bottom line" to keep in mind is that the hydrologic forecaster will use the best quantitative precipitation information available. Currently, the availability of such information for computer computations often is very limited, especially in real or near-real time. Precipitation measurements from space offer the potential of significantly increasing the availability of rainfall information for operational hydrologic forecasting applications.

With the above philosophy in mind, the mean percent errors given in Figure 4 are those which roughly reflect the maximum acceptable error (which we can expect to achieve once satellite techniques have been calibrated for a specific geographic area and precipitation type) from satellite estimates alone over the range of spatial and temporal averaging scales indicated. The forecaster obviously would prefer the highest accuracy achievable. Conversely, precipitation estimates from satellite data with accompanying errors larger than those given in Figure 4 would still be quite useful if the errors in the satellite patterns are largely due to systematic biases and if other independent data are available for comparison and melding with the satellite data. An example of a multi-sensor precipitation analysis system is presented in Section 4.

Also included in Figure 4 are estimates of minimum temporal sampling frequencies required to achieve the corresponding accuracies. These sampling frequency requirements are rough estimates taken from Figure 3 (for the scales covered in Figure 3). The sampling frequency estimates for the larger scales, falling outside the domain represented in Figure 3, were obtained by extrapolating the results of Figure 3 and by referring to data from other authors (for example, Johnson and Vetlov, 1977).

#### 4. DATA BASE REQUIREMENTS

The National Research Council's Space Applications Board (1980) recently concluded that recommendations made in 1974 to the National Academy of Sciences on remote sensing applications to hydrology "remain valid but mostly unmet." The Panel on Water Resources, under the Space Applications Board, optimistically views the use of remotely sensed data for resource prediction. However, the panel states that "to be useful for prediction, remotely sensed data must be compatible with mathematical modeling of hydrologic systems." This is an extremely critical point to bear in mind for hydrologic forecasting applications. All of the NWS River Forecast Centers rely heavily on numerical models and automatic data

ORIGINAL PAGE 19  
OF POOR QUALITY

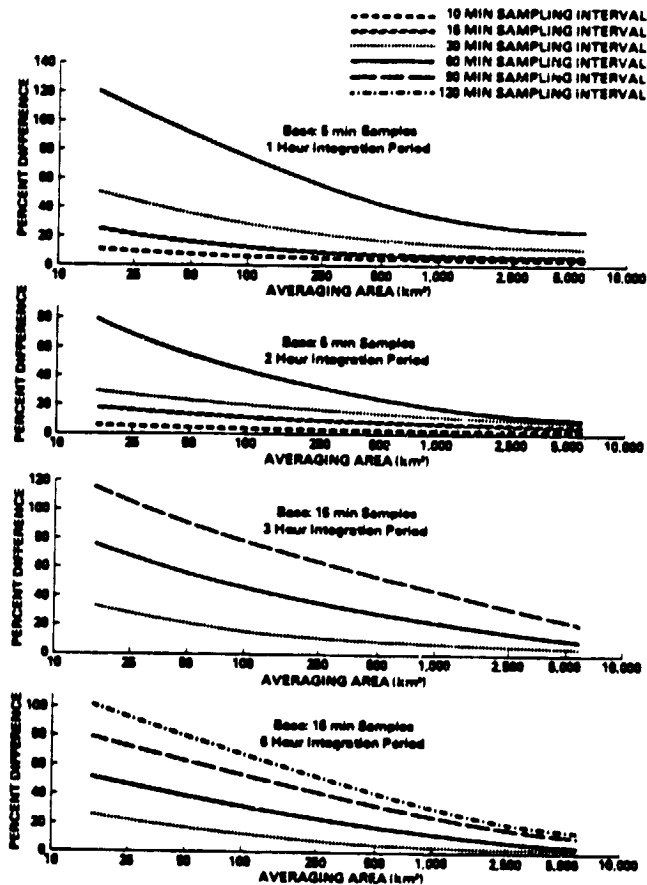


Figure 3. Upper two panels: Mean absolute percent difference between rainfall estimates using 5-min base sampling intervals and those using coarser sampling intervals for a range of spatial averaging and temporal integration scales. Lower two panels: Same as upper two, except a 15-min base sampling interval was used and longer integration periods were included. Based on analysis by Hudlow and Arkell (1978), who used digital radar data collected over the eastern tropical Atlantic Ocean during the GARP Atlantic Tropical Experiment (GATE).

processing procedures. For data sources to be most useful operationally, the data must be available on-line in a format compatible with computer processing. This becomes increasingly important as the scale of the phenomenon being forecast decreases and, correspondingly, the lead time between the occurrence of the precipitation and the hydrologic event decreases. Even for snow mapping for water supply forecasting, which usually pertains to relatively large scales (Figure 4), the large data volumes from the satellite sensors, and the informational flow that results, can be most effectively utilized only if we turn more to automatic (machine) processing of the imagery (Meier, 1980).

Progress has been made in recent years toward the computerized derivation of satellite rainfall estimates. For example, Griffith et al. (1981); Lovejoy and Austin (1979); Stout et al. (1979); Scofield and Oliver (1977); and Moses (1980) have developed procedures for estimating rainfall using data from visible and/or

infrared geosynchronous satellites. Also, Wilheit et al. (1977) have developed a technique for mapping rainfall rates over the oceans using microwave data from the Nimbus polar orbiting satellite. However, none of these procedures are currently available on-line for hydrologic forecasting. The Oliver/Scofield technique has been used on a selected basis to provide accumulated rainfall maps to field offices during critical rainfall events, and plans exist to partially automate this technique using a man-machine interactive system (Moses, 1980). This system, called an Interactive Flash Flood Analyzer (IFFA) will be used in support of the NWS Flash Flood Warning Program.

Recognizing the need to automate the use of information from multiple rainfall sensors for hydrologic applications, the NWS Office of Hydrology, through its Hydrologic Research Laboratory (HRL), initiated the ongoing Hydrologic Rainfall Analysis Project (HRAP). HRAP is aimed at improving the acquisition, preprocessing,

ORIGINAL PAGE IS  
OF POOR QUALITY

Figure 4. Maximum acceptable mean percent error (first value in the parentheses) as a function of temporal and spatial averaging scales. Also estimates of the minimum temporal sampling frequencies (samples per day) required to achieve the accuracies are given as the second value in the parentheses. Larger errors would be acceptable if the errors in the satellite patterns are primarily due to systematic biases and if other independent data are available for comparison and melding with the satellite data.

		SPATIAL AVERAGING INTERVAL					
		1 km <sup>2</sup>	10 km <sup>2</sup>	100 km <sup>2</sup>	1,000 km <sup>2</sup>	10,000 km <sup>2</sup>	100,000 km <sup>2</sup>
		Flash Flood Advisories					
Temporal Averaging Interval	0.5 hr-	(100, 144)		(75, 144)	(40, 24)	(15, 24)	
	1 hr-	(75, 96)		(60, 48)			
	2 hr-	(50, 48)		(60, 24)			
					Flash flood advisories, river forecast, soil moisture condition evaluations***		
					(20, 24)	(20, 24)	
			Soil moisture condition evaluations, reservoir operations			River forecasting, water structures design measurements***	
	6 hr-	(50, 24)		(45, 18)	(15, 48)	(15, 18)	
					GEOSYNCHRONOUS DATA POLAR ORBITER DATA		
	1 day-	(45, 24)		(40, 8)	(15, 24)	(15, 2)*	
			Soil moisture condition evaluation, reservoir operations and hydroclimatology			Crop yield, water supply forecasts, hydroclimatology, water structures design measurements***	
1 week-	(30, 4)		(15, 2)*				
		GEOSYNCHRONOUS DATA POLAR ORBITER DATA					
1 month-	Soil moisture, hydroclimatology and water structures design measurements				(10, 2)*		
1 year-	(20, 2)**		(15, 2)**				

\*Limited daily samplings (less than 4) can result in significant biases when diurnal effects are introduced either by meteorological or sensor effects.

\*\* If significant diurnal effects do not exist, data from high spatial resolution satellites such as LANDSAT could be useful even with longer intersampling intervals.

\*\*\* Estimates for these applications and corresponding scales require relatively smaller acceptable errors because they are more highly processed and are of a more quantitative nature.

quality controlling, and optimal merging of multi-sensor data bases for input to hydrologic forecasting models (Greene et al., 1979). In the foreseeable future, it seems likely that it will remain necessary to compare and combine the remotely sensed satellite data with data available from land-based remote sensors and/or in situ sensors (rain gauges) in order to achieve the quantitative accuracies required for hydrologic forecasting. Also, rain-gage data are probably one of the better "ground truth" sources for evaluating the merits of various satellite rainfall estimation procedures. Farnsworth and Centerford (1980) propose the use of an "equivalent rain-gage density" for assessing the accuracy of satellite rainfall estimates as indicated by the gage density required to give equivalent accuracies.

Figure 5 illustrates the various data components and computer facilities currently envisioned to comprise a Multisensor Rainfall Analysis System (MSRANS). Actually, MSRANS is the software that exists within the various computer environments. Some of the individual components of MSRANS are on-line now [for example, the Manual Digitized Radar (MDR) file and the Visible/Infrared Spin Scan Radiometer (VISSR) file]. For an explanation of the data acquisition and the generation of the VISSR data base from the Geostationary Operational Environmental Satellite (GOES), see McClain (1980) and Waters and Green (1979). Other MSRANS components are not now on-line (for example, the RPC Gateway Computers), but all, or at least the essential, components should be in existence within a year or two. It will be a

# MSRANS (MULTISENSOR RAINFALL ANALYSIS SYSTEM)

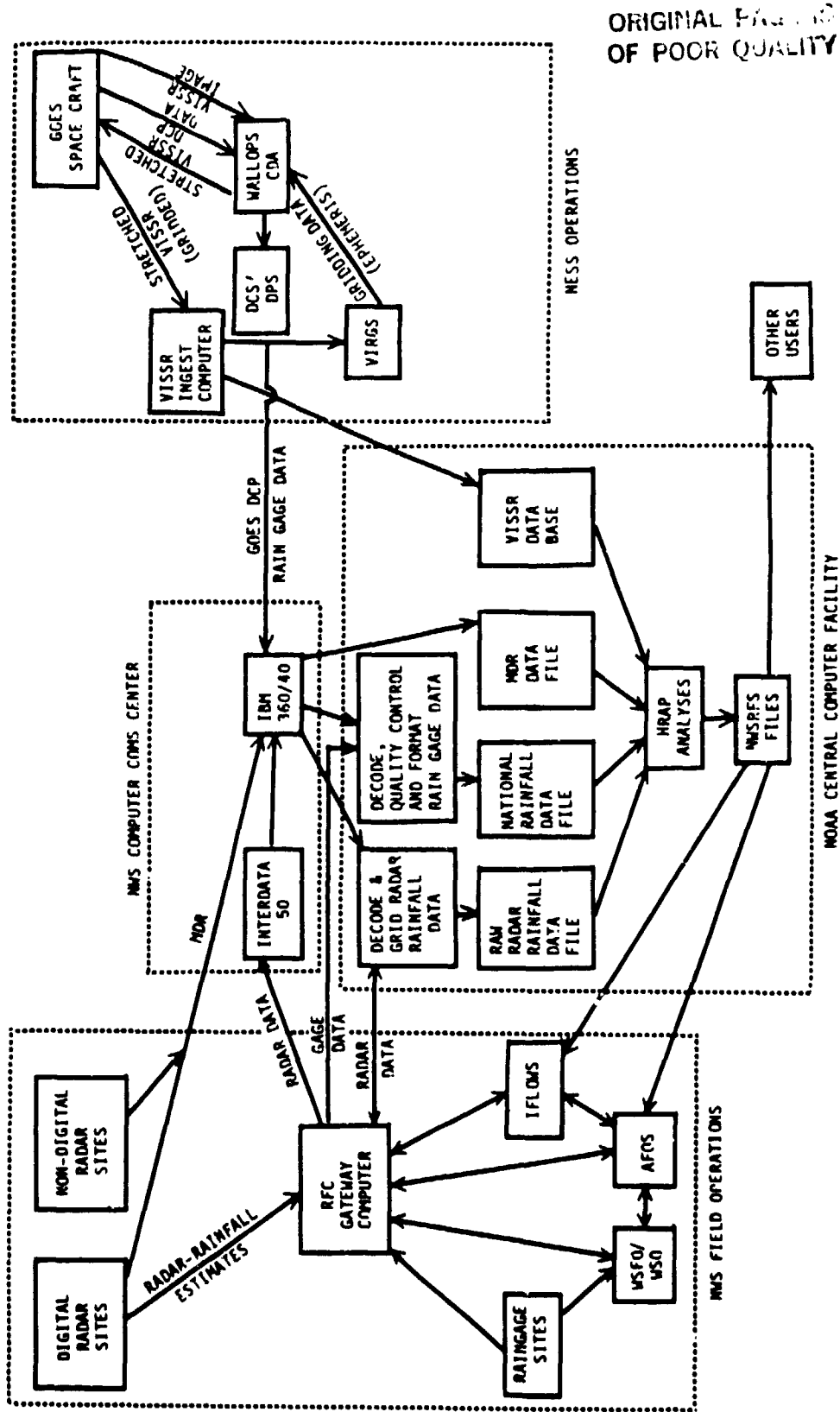


Figure 5. MSRANS -- See text for explanation of operational status of various components.



## ORIGINAL QUALITY OF POOR QUALITY

considerably longer period, however, before the total system will be functioning in an optimal multisensor analysis mode. Achieving this goal requires ongoing research and development over the next several years to implement multivariate objective analysis procedures such as those described by Crawford (1978). This is one of the objectives of HRAP (Greene et al., 1980). A similar project is under way in the United Kingdom (Collier, 1980). Satellite data base structures in the future should be planned to accommodate the types of numerical multivariate analyses being developed as part of these projects.

### 5. CONCLUDING REMARKS

In the planning for future satellite sensors and data bases, it is important to keep foremost in mind the ultimate applications for the data. In the case of most hydrologic forecasting applications, it is critical that the data bases be made available on-line in the computer environment being used by the hydrologic forecasters to perform their hydrologic computations. Achieving this will allow the strengths of the remotely sensed data to be most effectively utilized, since they can be used with data from in situ sensors in a multivariate analysis mode. As indicated in Section 3, this approach should significantly relax the accuracy requirements for the satellite precipitation estimates if the errors in the satellite patterns are largely due to systematic biases.

### 6. ACRONYMS

APOS	--	Automation of Field Operations and Services
CDA	--	Command and Data Acquisition Station
DCP	--	Data Collection Platform
DCS/DPS	--	Data Collection System/Data Processing System
GARP	--	Global Atmospheric Research Program
GATE	--	GARP Atlantic Tropical Experiment
GOES	--	Geostationary Operational Environmental Satellite
HRAP	--	Hydrologic Rainfall Analysis Project
HRL	--	Hydrologic Research Laboratory
IFFA	--	Interactive Flash Flood Analyser
IPLWS	--	Integrated Flood Observing and Warning System
MDR	--	Manual Digitized Radar
MFLT	--	Mean Forecast Lead Time
MFRANS	--	Multisensor Rainfall Analysis System
NWS	--	National Weather Service
NWRFPS	--	National Weather Service River Forecast System
RFC	--	River Forecast Center
VIRGS	--	VISIR Interactive Registration and Gridding System
VISIR	--	Visible/Infrared Spin Scan Radiometer
WSFO	--	Weather Service Forecast Office
WFO	--	Weather Service Office

### 7. REFERENCES

- Changnon, S.A. and F.A. Huff, 1980: Review of Illinois Summer Precipitation Conditions. ISWS/Bul-64/80, Urbana, Illinois, 160 p.
- Chang, A.T.C., J.L. Foster, D.K. Hall, A. Rango, and B.K. Hartline, 1981. Determination of Snowpack Properties by Microwave Radiometry: Theoretical Model and Experimental Evaluation. Earth Survey Applications Division Research Report-1980, NASA Technical Memorandum E2071, 10-14, 19.
- Clark, R.A., 1977: Adaptation of Meteorological Services to Hydrology in the United States. Preprint Volume, 2nd Conference on Hydrometeorology (Toronto), AMS, Boston, Massachusetts, 28-33.
- Collier, C.G., 1980: Data Processing in the Meteorological Office Short-Period Weather Forecasting Pilot Project. Meteorological Magazine, Vol 109, 1980, 161-177.
- Crawford K. C., 1978: On the Bivariate Objective Analysis of Surface Rainfall Using Optimum Interpolation. Preprint Volume, 18th Conference on Radar Meteorology (Atlanta), AMS, Boston, Massachusetts, 336-341.
- Farnsworth R.K. and R.P. Centerford, 1980: Satellite Rainfall Estimation for Hydrologic Forecasting. Technical Papers of the American Society of Photogrammetry ACSM-ASP Convention (St. Louis), March 1980, ASP, Falls Church, Va., 97-105.
- Greene, D.R., M.D. Hudlow, and R.K. Farnsworth, 1979: A Multiple Sensor Rainfall Analysis System. Preprint Volume, Third Conference on Hydrometeorology (Bogota), AMS, Boston, Massachusetts, 44-53.
- Greene, D.R., M.D. Hudlow, and R.E. Johnson, 1980: A Test of Some Objective Analysis Procedures for Merging Radar and Rain-gage Data. Preprint Volume, 19th Radar Meteorology Conference, April 1980 (Miami), AMS, Boston, Massachusetts, 470-478.
- Griffith C.G., J.A. Augustine, and W.L. Woodley, 1981: Satellite Rain Estimation in the U.S. High Plains. J. Appl. Meteor., Vol. 20, No. 1, January 1981, 53-66.
- Hudlow, M.D. and R.E. Arkell, 1978: Effect of Temporal and Spatial Sampling Errors and Z/R Variability on Accuracy of GATE Radar Rainfall Estimates. Preprint Volume, 18th Conference on Radar Meteorology, AMS, Boston, Massachusetts, March 28-31, 1978, 342-349.
- Jettmar, R.U., G.K. Young, R.K. Farnsworth, and J.C. Schaeke, 1979: Design of Operational Precipitation and Streamflow Networks for River Forecasting. Water Resources Research, Vol. 15, No. 6., December 1979, 1823-1831.

ORIGINAL PAGE IS  
OF POOR QUALITY

- Johnson, D.S. and I.P. Vetlov, 1977: The Role of Satellites in WMO Programmes in the 1980's. WMO, World Weather Watch Planning Report No. 36, WMO No. 494, 1977, Geneva, Switzerland.
- Kohler, M.A., 1958: Design of Hydrological Networks. WMO Technical Note No. 25, WMO No. 82, TP 32, 1958, Geneva, Switzerland, 16 p.
- Lovejoy, S. and G.L. Austin, 1979: The Delineation of Rain Areas from Visible and IR Satellite Data for GATE and Mid-Latitudes. Atmosphere-Ocean, Vol. 17, No. 1, 1979, 77-92.
- McClain, E.P., 1980: Environmental Satellites, Reprint from McGraw-Hill Encyclopedia of Environmental Science.
- Meier, M.F., 1980: Remote Sensing of Snow and Ice. Hydrologic Sciences, Vol. 25, No. 3.9, 1980, 307-330.
- Moses, J.F., 1980: Interactive Techniques for the Estimation of Precipitation from Geostationary Imagery. Preprint Volume, AMS 2nd Conference on Flash Floods, Atlanta, Ga., March 18-20, 1980, 101-108.
- National Research Council's Space Application Board, 1980: Remote Sensing for Water Resources and Hydrology. Recommended Research Emphasis for the 1980's, 34 p.
- Negri, A.J. and R.F. Adler, 1980: Detection of Heavy Convective Precipitation Using Rapid Digital Radar and Satellite Data. Preprint Volume, 19th Conference on Radar Meteorology, 1980, 264-271.
- Ostrowski, J.T., 1979: National Weather Service Products Useful for Reservoir Regulation. To be published in the Proceedings of the ASCE Workshop on Reservoir Systems Regulation held in Boulder, Colorado, August 1979.
- Schaake, J.C., 1976: Use of Mathematical Models for Hydrologic Forecasting in the National Weather Service. Proceedings of Environmental Protection Agency Conference on Modeling and Simulation, Symposium on Hydrological Forecasting, Cincinnati, Ohio, April 19-21, 1976.
- Scofield R.A. and V.J. Oliver, 1977: A Scheme for Estimating Convective Rainfall from Satellite Imagery. NOAA Technical Memorandum NESS 86.
- Stout, J.E., D.W. Martin, and D.N. Sikar, Estimating GATE Rainfall with Geosynchronous Satellite Images. Monthly Weather Review, 106, 1153-1171.
- Symposium on Hydrologic Forecasting, 1980 (Oxford, England), WMO, UNESCO, April 1980.
- Waters, M.P., III and R.N. Green, 1979: A Merged Satellite Infrared and Manually Digitized Radar Product. Preprint of talk given at the Symposium on Machine Processing of Remotely Sensed Data, Purdue University, Lafayette, Indiana, June 1979.
- Wilheit, T.T., J.S. Theon, W.E. Shenk, L.J. Allison, and E.B. Rogers, 1976: Meteorological Interpretations of the Images from Nimbus 5 Electrically Scanned Microwave Radiometer, J. Appl. Meteor., 15, 166-172.

Severe Storms Requirements  
for Precipitation Information

ORIGINAL DOCUMENT  
OF POOR QUALITY

by

Robert F. Adler

Laboratory for Atmospheric Sciences (GLAS)  
Goddard Space Flight Center  
National Aeronautics and Space Administration  
Greenbelt, MD 20771

1. Introduction

The objective of this paper is to describe the needs for precipitation information in severe storms research and in the operational detection and forecasting of such phenomena. For the purposes of this paper, the discussion will include thunderstorms, tropical cyclones, and regional and mesoscale numerical models used to analyze and forecast these and other regional scale phenomena.

This article will not cover general convective activity and the accompanying requirements for hydrological data. Instead, it will focus on the requirements for observations of two intense phenomena (flash floods and tropical cyclones) and the requirements for numerical models.

Because of the rapidly changing nature of intense mesoscale phenomena, the time and space resolutions of the necessary observations probably have the most stringent requirements of any time/space scale. The following sections describe particular phenomena and present a tentative list of observational requirements for each phenomena. The potential and limitations of current and possible future types of satellite instruments and techniques are briefly discussed.

2. Flash Flood--Detection of Heavy Convective Rain

a. Background

The observation and study of thunderstorms, especially intense thunderstorms associated with flash floods (including those associated with landed hurricanes) and other severe weather (tornadoes, hail, damaging straight line winds), require high spatial and temporal resolution data. For flash flood detection, this high resolution is needed for rainfall rate, especially at the higher rain rates. This information is usually obtained from radar data, but there have been recent attempts to obtain useful data on the necessary time and space scales from geosynchronous satellite visible and infrared (window) data (Scofield and Oliver, 1977; Griffith, et al., 1978). These techniques depend on empirical relations between satellite observation of cloud parameters and radar or rain gauge estimates of rainfall. Although clouds are correlated with rainfall, the lack of a strong physical basis for the empirical relations make

the techniques susceptible to errors when applied to various geographic, seasonal, or synoptic situations. There is some evidence (Negri and Adler, 1981) that by using short interval (5 min) GOES infrared (IR and visible) data to follow the evolution of individual thunderstorms, one could determine the relative updraft intensity of the storm and relate this parameter to storm maximum rainfall rate and maximum volume rainfall rate. Fig. 1 shows  $T_{MIN}$ , the minimum  $T_{BB}$  (maximum height) achieved during the lifetime of the storm, and storm maximum rainfall rate.  $T_{MIN}$  is a proxy variable for storm updraft intensity. A simple physical basis for such relations and the use of a one-dimensional model to study the relations among  $T_{MIN}$ , updraft intensity, and rainfall rate are being explored (Adler, et al., 1981). Although the conclusions of Negri and Adler (1981) support the effort to use satellite data to detect heavy convective precipitation and estimate its magnitude, they emphasize the need for high time resolution (3-5 minutes) data. The short interval data are necessary in order to: (1) accurately define and follow individual thunderstorms unambiguously; (2) accurately measure rate of change parameters on a time scale appropriate for thunderstorms; and (3) accurately determine the minimum  $T_{BB}$  achieved during the thunderstorm's lifetime. It must also be emphasized that the derived empirical relations between  $T_{BB}$  parameters and rainfall rate do not apply to all data points on an IR image, but only to the locations of defined thunderstorms in that image.

b. Flash Flood (Thunderstorm) Rainfall Requirements

Table 1 contains a tentative rainfall requirement listing for thunderstorm observation and research with the primary emphasis on flash flood/heavy rain analysis. The numbers should be considered "soft", and are based on the author's experience, discussions with a few individuals, and a perusal of the results of the questionnaire sent out before this conference. Although originally the numbers were to represent observational requirements irrespective of the method of observation, the values in Table 1 and the following tables are observational requirements for a positive satellite contribution.

The table is divided into three groups

ORIGINAL PAGE IS  
OF POOR QUALITY

(precipitation rate, precipitation/no precipitation, precipitation type). Desired requirements are listed, along with minimum requirements needed to obtain useful information.

The desired requirements (last column) in the precipitation rate clearly indicate the need for high time and space resolutions. The rain/no rain requirements are less stringent because we are trying to observe on the scale of whole rain cells or areas and not the scales of rainfall rate maxima or variations. Although rain/no rain information has no direct bearing on flash flood analysis, it may be a valuable contributor to a larger scheme.

Although hail detection is obviously not a part of flash flood analysis directly, it is included in this thunderstorm section. High time resolution is the key factor here.

From a satellite observation standpoint, the time resolution requirements in this section preclude anything except a geosynchronous orbit. Based on present knowledge, no direct estimate of rainfall rate can be made from that altitude, although there are possibilities for rain/no rain determination using passive microwave sensors. Rainfall rate information would then be dependent on inferences drawn from cloud data deduced from visible and/or infrared observations. For intense rainfall situations, this may be possible.

### 3. Tropical Cyclone Rainfall Over Water

#### a. Background

Observations of tropical cyclone rainfall over water are important for three reasons: 1) studying and monitoring storm latent heat release and rainfall patterns in relation to storm energetics; 2) estimating rainfall potential at landfall; and 3) model initialization of tropical cyclone models.

Adler and Rodgers (1977) and Rodgers and Adler (1981), using rainfall rate information deduced from the Nimbus-5 Electrically Scanning Microwave Radiometer (ESMR), have shown the data to be useful in determining the rainfall characteristics of these storms and the data appear to be potentially useful in monitoring and making short-term prediction of their intensity.

Comparison of the ESMR-5 derived total storm rainfall calculations with previous estimates based on moisture budget computations or composited rainfall statistics indicate good agreement for both mature systems (typhoons) and disturbances, except in the inner core where ESMR-5 measurements seem to underestimate rainfall rate. The calculations confirm that total typhoon rainfall is approximately twice that found in disturbances.

Case studies as well as composite studies indicate that the increase in the ESMR-5 derived LHR corresponds to storm intensification. In addition, the relative contribution of the heavier rainfall rates to the total storm rainfall also increases as tropical cyclones intensify. There

also is a tendency for the rainfall to concentrate toward the center during intensification. It also appears that these ESMR-5 derived rainfall parameters can be used to detect the beginning of tropical cyclone intensification. By monitoring the trend of increasing LHR, the first indication of tropical cyclone intensification may be obtained 1-2 days prior to the tropical cyclone being named and often prior to the first reconnaissance aircraft observation. Further, the time of maximum intensity may be estimated by observing the time of maximum LHR. There appears to be a 1-2 day lag relationship between maximum LHR and maximum tropical cyclone intensity.

In addition, knowledge of total storm rainfall, and rainfall distribution in the storm just before landfall, may be helpful in forecasting coastal flooding. Use of rainfall information in model initialization efforts will be discussed in Section 4.

#### b. Tropical Cyclone Requirements

Table 2 presents tentative requirements for rain information in tropical cyclones. Although high spatial resolution is desirable for good definition of rain cells, average rain rate over a larger area (20 km) would be useful in making many calculations. During the developing stage of a tropical cyclone, rainfall undergoes dramatic changes over 12 or 24 hours. To accurately monitor these changes requires time resolution of at least 6 hours. With a much higher time resolution (30 min) large cells could be tracked and their motion and evolution followed.

Although rain/no rain information would be much less valuable than rain rate, it would be useful in the developing stage of the storm where the area of rainfall expands rapidly and would also be useful in observing the motion of rainfall features, including spiral bands.

From a satellite observations standpoint, the minimum requirements are obtainable. Passive microwave sensors on low orbiting satellites can provide the time and space resolutions listed. The higher time resolution in the "desired" column calls for geosynchronous orbit, but this eliminates rain rate information at reasonable resolutions. It may be possible to provide rain/no rain information at 40 km and 30 min resolutions. The high time resolution may be achieved by a hybrid approach using occasional (6-12 hr) passive microwave/low orbit data and high time resolution visible/IR or rain/no rain data from geosynchronous orbit. Whatever approach is used, only satellite data have the potential to provide observations of tropical cyclone rainfall over open ocean.

### 4. Model Initialization and Verification

#### a. Background

Regional scale and mesoscale numerical models are important in the forecasting and understanding of precipitation events. However, precipitation information may also be important in the initialization and verification of such models.

ORIGINAL PAGE IS  
OF POOR QUALITY

Numerical models of this type are typically initialized with temperature, pressure, moisture and wind information at synoptic scales. Information at smaller scales can be added through low orbiter sounding data, geosynchronous sounding (VAS) and some "cloud-track" winds. However, rain rate data would provide indirect evidence of divergence and the ageostrophic component of the flow on sub-synoptic scales. This approach has been used by Tarbell, et al. (1981) to indicate a forecast improvement when using observed (rain gauge) rainfall against no rainfall information. Rainfall rate information may also be useful in initializing tropical cyclone models.

Rainfall information is also important in verifying regional models. This is because it is one of the most important forecast variables on this scale, and is the only variable routinely observed at the mesoscale, even with rain gauges.

b. Regional Scale Numerical Model Requirements

Table 3 presents the precipitation rate requirements for modeling. Basically, what is needed for initialization is information at every three-dimensional grid volume in the model, although the vertical distribution of latent heat release can be parameterized. Emphasis should be on the higher rainfall rates, since these will be related to significant divergences and ageostrophic components. For initialization, information is required over the model domain at one time, preferably the initial time. For model verification, observations are required with a frequency of approximately one hour.

5. Conclusions

There is a spectrum of uses and potential uses for rainfall information in the severe storms area. The spectrum ranges from the direct use of rainfall rate information in flash flood detection and study, to tropical cyclone rainfall and its relation to storm energetics and intensification, and to model initialization and verification with rainfall data.

The observational requirements vary from application to application. Although some of the requirements could be met with low-orbit satellite observations, the high time frequency (down to tens of minutes) of some of the requirements requires geosynchronous observations. This high altitude negates most ideas of a "direct" observation of rain rate with microwave techniques, but does not preclude a hybrid technique with a microwave rain/no rain sensor to give coarse rain boundaries and rain magnitude to be estimated from cloud top information derived from visible and infrared channels.

ACKNOWLEDGMENTS

The tentative requirements listed in this paper's tables are a combination of the author's views and input from the pre-meeting survey. In the section on numerical models, the listed requirements are essentially those provided by Professor Rick Anthes.

REFERENCES

- Adler, R. F., A. J. Negri, and D. Atlas, 1981: Satellite measurements of thunderstorm rainfall: possible physical foundations. To appear in Preprints Fourth Conference on Hydrometeorology, Oct. 1981.
- Adler, R. F. and E. B. Rodgers, 1977: Satellite-observed latent heat release in a tropical cyclone. Mon. Wea. Rev., 105, 957-963.
- Griffith, C. G., W. L. Woodley, P. G. Grube, D. W. Martin, J. Stout, and D. N. Sikdar, 1978: Rain estimation from geosynchronous satellite imagery-visible and infrared studies. Mon. Wea. Rev., 106, 1153-1171.
- Negri, J. and R. F. Adler, 1981: Relation of satellite-based thunderstorm intensity to radar-estimated rainfall. To appear in J. Appl. Met., March 1981.
- Rodgers, E. B. and R. F. Adler, 1981: Tropical cyclone rainfall characteristics as determined from a satellite passive microwave radiometer. To appear in Mon. Wea. Rev., March 1981.
- Scofield, R. A. and V. J. Oliver, 1977: A scheme for estimating convective rainfall from satellite imagery. NOAA Technical Memorandum NESS 86, 47 pp.
- Tarbell, T. C., T. T. Warner, and R. A. Anthes, 1981: An example of the initialization of the divergent wind component in a mesoscale numerical weather prediction model. To appear in Mon. Wea. Rev.

ORIGINAL PAGE IS  
OF POOR QUALITY

Table 1

Thunderstorm Rainfall/Flash Flood

Precipitation Rate	Minimum	Desired
Horizontal Res.	10 km	1 km
Vertical Res.	—	3 km
Time Res.	30 min	10 min
Area Coverage	500 km	1000 km
Accuracy	30%	10%

Precipitation/No Precipitation		
Horizontal Res.	40 km	10 km
Vertical Res.	—	—
Time Res.	1 hr	15 min
Area Coverage	500 km	1000 km

Precipitation Type (hail/rain)		
Horizontal Res.	10 km	1 km
Vertical Res.	—	3 km
Time Res.	15 min	5 min
Area Coverage	500 km	1000 km

Table 2

Tropical Cyclone Rainfall (over water)

Precipitation Rate	Minimum	Desired
Horizontal Res.	20 km	2 km
Vertical Res.	—	3 km
Time Res.	6 hr	30 min
Area Coverage	1000 km	1500 km
Accuracy	30%	10%

Precipitation/No Precipitation		
Horizontal Res.	40 km	20 km
Vertical Res.	—	—
Time Res.	6 hr	30 min
Area Coverage	1000 km	1500 km

Table 3

Model (Regional and Mesoscale)  
Initialization and Verification

Precipitation Rate	Minimum	Desired
Horizontal Res.	100 km	25 km
Vertical Res.	4 km	2 km
Time Res.	1 hr	15 min
Area Coverage	3000 km	5000 km
Accuracy	25%	10%

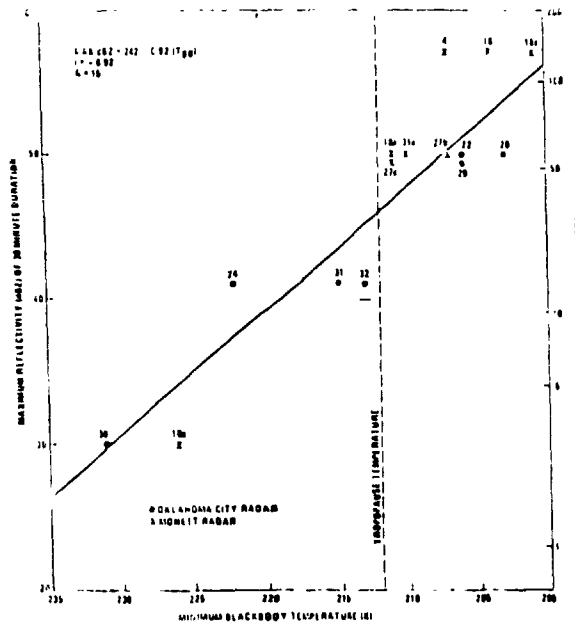


Fig. 1 Maximum observed reflectivity of 24 min duration (dbz) vs. minimum blackbody temperature. Note high reflectivities associated with tropopause penetrating storms (from Negri and Adler, 1981).

## GLOBAL WEATHER REQUIREMENTS FOR PRECIPITATION MEASUREMENTS

by

John H.E. Clark

Pennsylvania State University

Meteorologists have for a long time appreciated the fact that moisture can play an important if not dominant role in supplying energy to tropical and extra-tropical weather systems. In the tropics where the air is almost saturated only the slightest amount of uplift is required to initiate the release of vast amounts of latent heat to fuel systems as diverse as convective cloud clusters and hurricanes. The role of latent heating on extra-tropical systems is much more subtle. While the primary energy source for synoptic-scale systems is often the release of gravitational potential energy through the sinking of cold air and the rising of warm, it seems that the latent heat that is eventually realized through slow uplift of large masses of air can significantly modify the evolution of the system. We are currently performing an analysis of the energetics of the storm of March 25 to 27, 1978 over the eastern USA to understand the implications of the heat released due to the vast cloudy area associated with warm frontal overrunning. Figs. (1) and (2) illustrate the energetics of the storm with and without the effect of latent heating on the vertical motion field and thus the horizontal convergence field accounted for. Note the large changes in the transformation between available potential and kinetic energy. For instance, the conversion between zonal mean potential and kinetic energy has reversed sign and almost increased by a factor of twenty in magnitude due to the latent heating. Clearly the latent heat will play an important role in determining the evolution of this mature system.

Mid-latitude meso-scale systems are also fueled by latent heat release but in a different manner. The dominant mode of uplift is convective such as that associated with convective cells in a squall line. In many cases the systems, once initiated, are mainly driven by the convective heat release and larger scale baroclinic energy conversions play only a minor role.

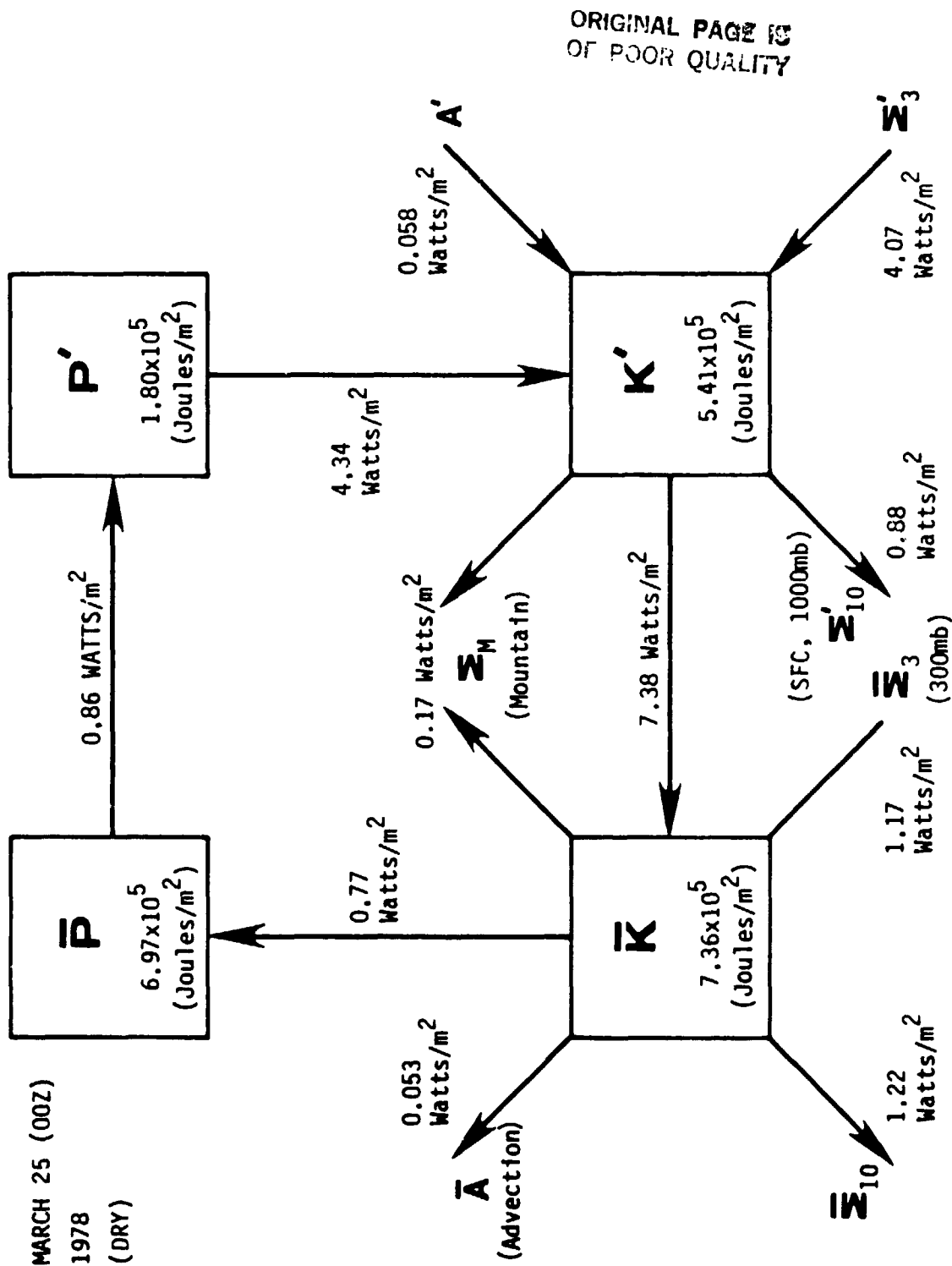


Figure 1. Energetics of East coast storm of March 25, 1978 where effects of latent heating are not accounted for. P and K represent available potential and kinetic energies.



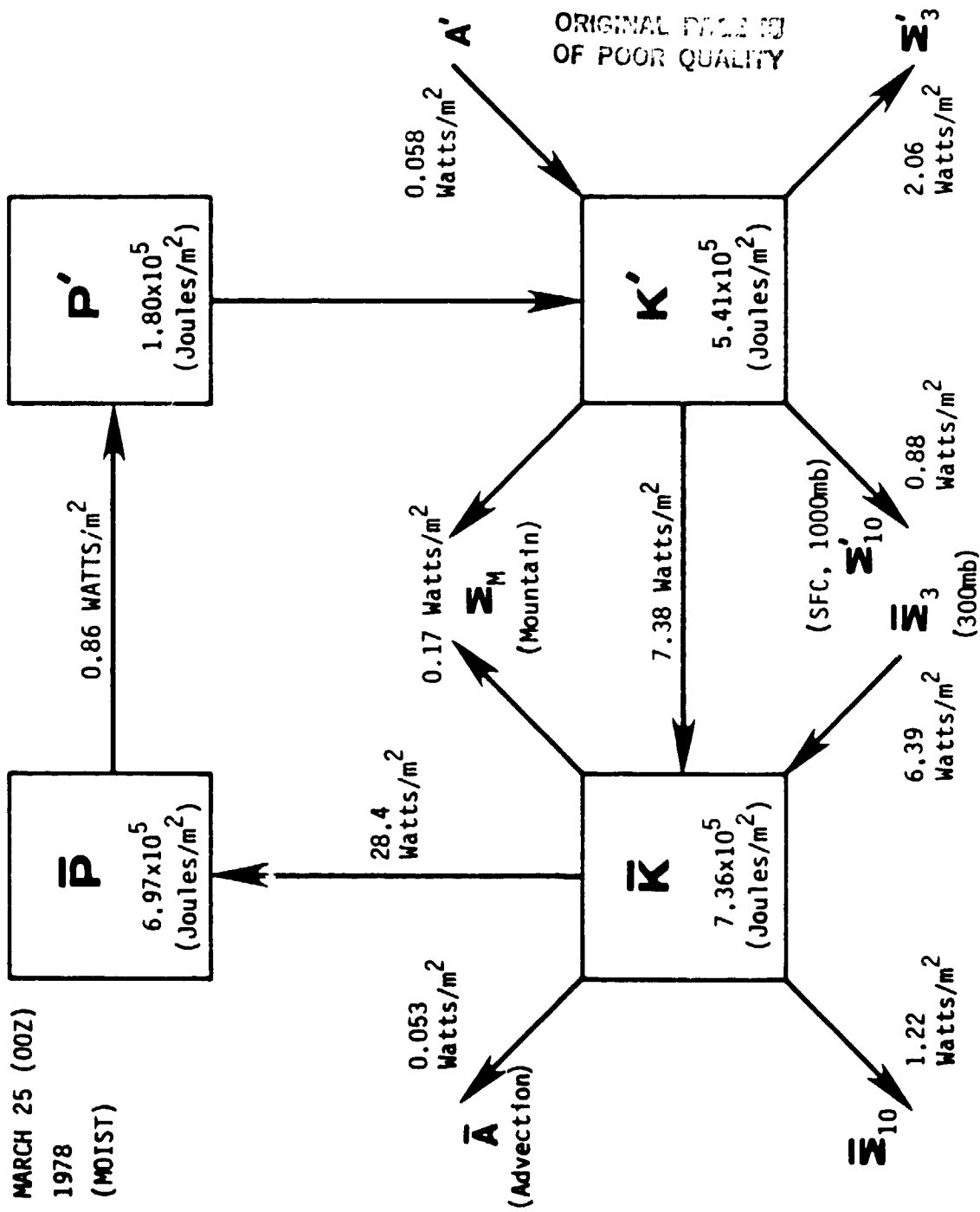


Figure 2. Energetics of East coast storm of March 25, 1978 including effects of latent heating.

Through the use of conceptual models such as CISK, dynamicists have been able to understand the consequences of latent heat release on tropical systems despite the paucity of rainfall and moisture data. The more subtle effects of latent heating on extra-tropical systems will require much more extensive observational coverage of moisture and precipitation to help us understand it's consequences. Consider the flow chart in

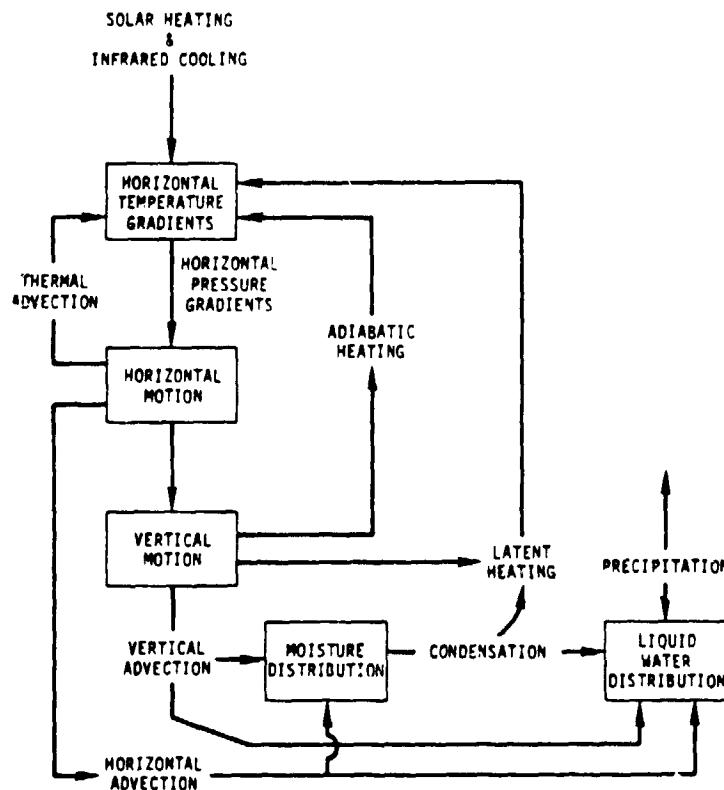


Figure 3. Schematic illustration of the role of moisture and liquid water in a synoptic system.

Fig. (3) that will help us in understanding some of the effects of water on a synoptic scale system. Horizontal and vertical motions both affect the distributions of liquid water and water vapor. When vapor condenses the resulting latent heating can in turn create horizontal temperature gradients and vertical motions result to maintain a state of geostrophic and hydrostatic balance. Thus there is a complicated nonlinear interaction between the moisture and liquid water distributions on one hand and the motion field on the other via the agency of latent heating. An indication of how much condensation and thus latent heating is occurring is

ORIGINAL DESIGN  
OF POOR QUALITY

provided by the field of precipitation. This is more clearly illustrated by considering the total mass of liquid water ( $M_w$ ) and vapor ( $M_v$ ) in a vertical column. We can write the following equations:

$$\frac{dM_w}{dt} = \text{Horizontal Advection of Liquid Water} - \text{cloud } \frac{\alpha q_s}{Z} \rho dz$$

(Evaporation of Rain) - (Precipitation) (1)

$$\frac{dM_v}{dt} = \text{Horizontal Advection of Vapor} + \text{cloud } \frac{\alpha q_s}{Z} \rho dz$$

+ (Evaporation of Rain) (2)

where the evaporation from the ground has been neglected. The integral term measures the condensation associated with the cooling of rising saturated air in the clouds. From Eq. (1) we see that if steady state is assumed and the horizontal advection and evaporation of rainfall is neglected, the precipitation is a measure of condensation in the cloud. On the other hand if Eqs. (1) and (2) are added and the less restrictive assumption made that the total storage of water substance in the column is small, we see that the precipitation reflects the total advection of vapor and liquid water into the column. The conclusion is that precipitation measurements by themselves will not be adequate to enable us to unravel the effects of latent heating on synoptic scale systems or for that matter the general circulation of the atmosphere. Satellites in conjunction conventional observations must provide us with simultaneous distributions of water vapor, liquid water, and precipitation if the complex interactions between the motion fields and the moisture fields are to be understood.

There are simple methods of discerning the immediate effects of latent heating on vertical motion fields derived by solving the thermodynamic equation or the quasi-geostrophic omega equation, but it is impossible to check the accuracy of these techniques without the ground truth provided by reliable moisture, liquid water, and precipitation measurements.

A problem that frequently arises in the analysis of precipitation data is that they tend to be very spotty. Local values of rainfall rates are strongly influenced by orography and thus a single station can be very unrepresentative of regional rainfall rates. Furthermore if convective precipitation is occurring in a system, the proximity of a station to a cell can completely influence the rainfall rate and mean rates over an area are difficult to evaluate. Thus it is often essential to measure precipitation with a very dense network.

If we are going to develop a thorough understanding of moisture as it affects not only the general circulation but synoptic and meso-scale systems, we must have the capability of sensing precipitation over a fairly dense network of station and simultaneously sense vapor and liquid water distributions. Unfortunately over oceanic regions where satellite microwave measurements of total liquid water content of the atmosphere are apparently straightforward, precipitation measurements are lacking. Over land microwave measurements of liquid water are difficult because of the rapidly varying brightness temperature of the ground, but precipitation measurements are possible.

Global requirements for precipitation measurements are 3-hourly measurements with an average separation between stations of no more than 100 km at least initially. The present network of stations over North America could probably be beefed up to satisfy this requirement. Coarser scale measurements of vapor and liquid water must also be available however. The conventional radiosonde network could provide the vapor data but the technology does not exist to provide the liquid water data unless the NOAA radar network could be utilized for this purpose.

D14  
N83 25283

SAMPLING PROBLEMS: THE SMALL SCALE STRUCTURE  
OF PRECIPITATION

R. K. Crane  
Thayer School of Engineering  
Dartmouth College  
Hanover, New Hampshire 03755

ABSTRACT

Results of a radar study of summertime convection in the high plains of Kansas are presented which demonstrate the importance of the small scale structure of precipitation to the overall production of precipitation in a storm. The smaller scale structure must be modeled to develop valid relationships between satellite observables and precipitation amount. The Kansas results suggest that just the observation of the number and spacings of the active regions of convection (thunderstorms) is sufficient to provide an estimate of water flux with an uncertainty of less than a factor of two.

INTRODUCTION

Satellite systems proposed for precipitation measurement suffer from a variety of defects. Observables, such as reflectivity or attenuation for satellite borne radar systems, brightness temperature for microwave radiometers, or radiance for infrared radiometers, are not linearly related to rainfall rate and the areal integration of the observable over the field-of-view of the satellite system is not proportional to water flux (area integrated rain rate). Due to the non-linear dependence of an observation parameter on rain rate, or single value of the parameter can correspond to a number of different values of water flux. As a result, the water flux value can be estimated only statistically. The smaller-than-the-field-of-view scale rain rate variations must be taken into account before a water flux estimate can be made and, lacking observations on the

smaller scale, a statistical guess must be made to transform an observation into a water flux estimate.

Precipitation amount, not water flux, is the goal of most precipitation measurement systems. Precipitation amount can be obtained by integrating a time series of water flux measurements but, with the exception of observations from a geostationary satellite, satellite observations are made only infrequently. The estimate of precipitation amount from infrequent samples of water flux must be made statistically.

The statistical estimation of water flux from satellite observations and precipitation amount from a sparse set of water flux estimates requires the use of models developed from an understanding of the small scale structure of precipitation and from an understanding of the diurnal, seasonal and geographical variation of the precipitation process. In this paper, information is presented on the small scale structure of precipitation. The data were obtained in the high plains of Kansas during the afternoon and evening hours of three consecutive summer observation periods. Similar data are not currently available from other times of day, seasons, or geographical locations to provide the complete set of data required to generate the models necessary for the extraction of precipitation amounts from satellite observations.

#### SMALL SCALE STRUCTURE

A C-band weather radar was employed to routinely observe the small scale structure of precipitation during the 1976-1978 measurement seasons of the Kansas HIPLEX Program (Crane and Hardy, 1981). The radar data were processed to provide statistical data on the small, three dimensional radar cells evident in the radar observations. Radar volume cells were automatically detected using a half scattering value to define the cell boundaries (Crane, 1979). The small regions of higher reflectivity, and therefore rain rate, are the regions that contribute to the uncertainty in the estimation of water flux averaged over the field-of-view of the satellite.

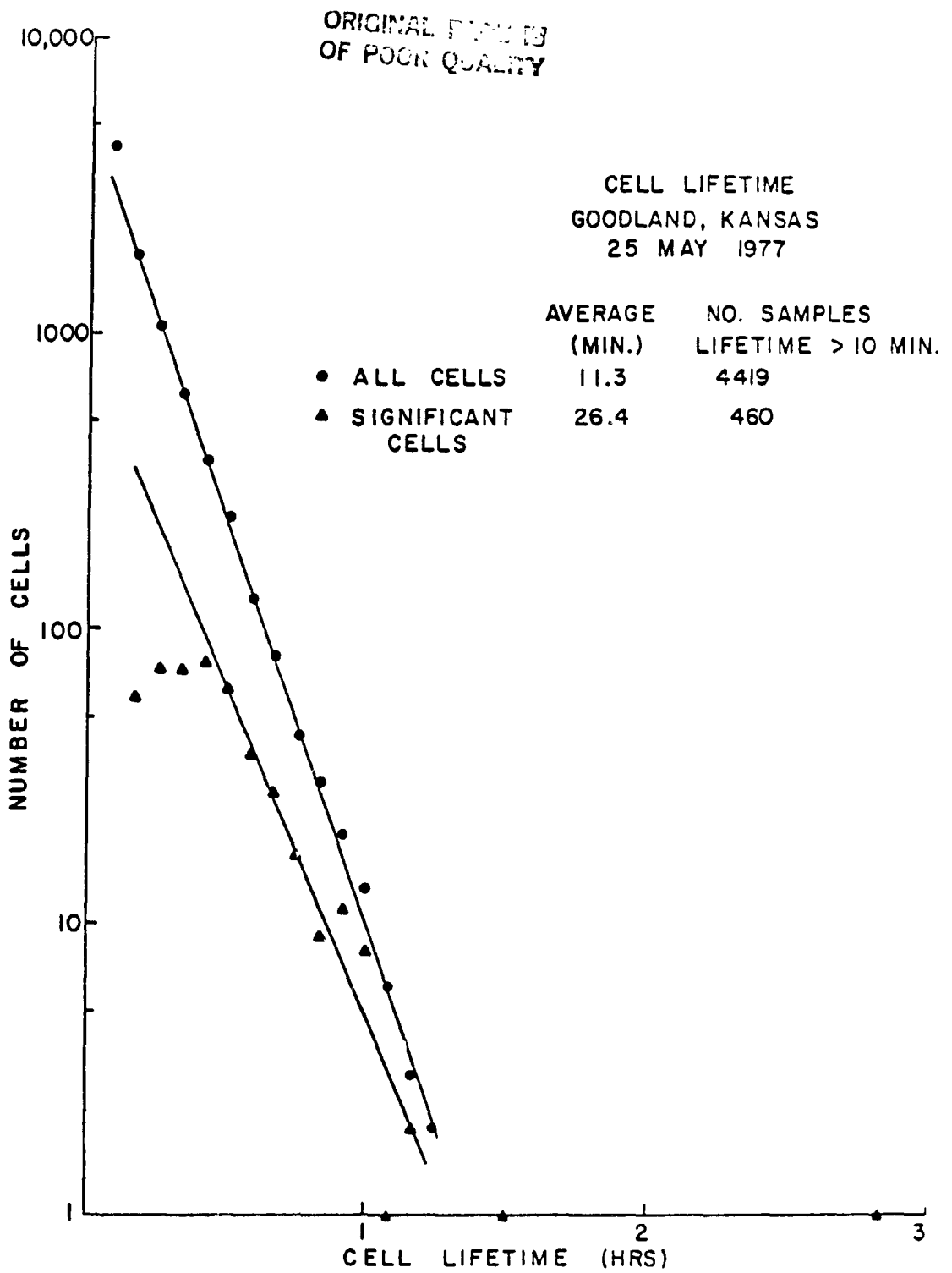


Figure 1. Number density distribution of volume cells and significant volume cells over the range of lifetime values, Day 7144

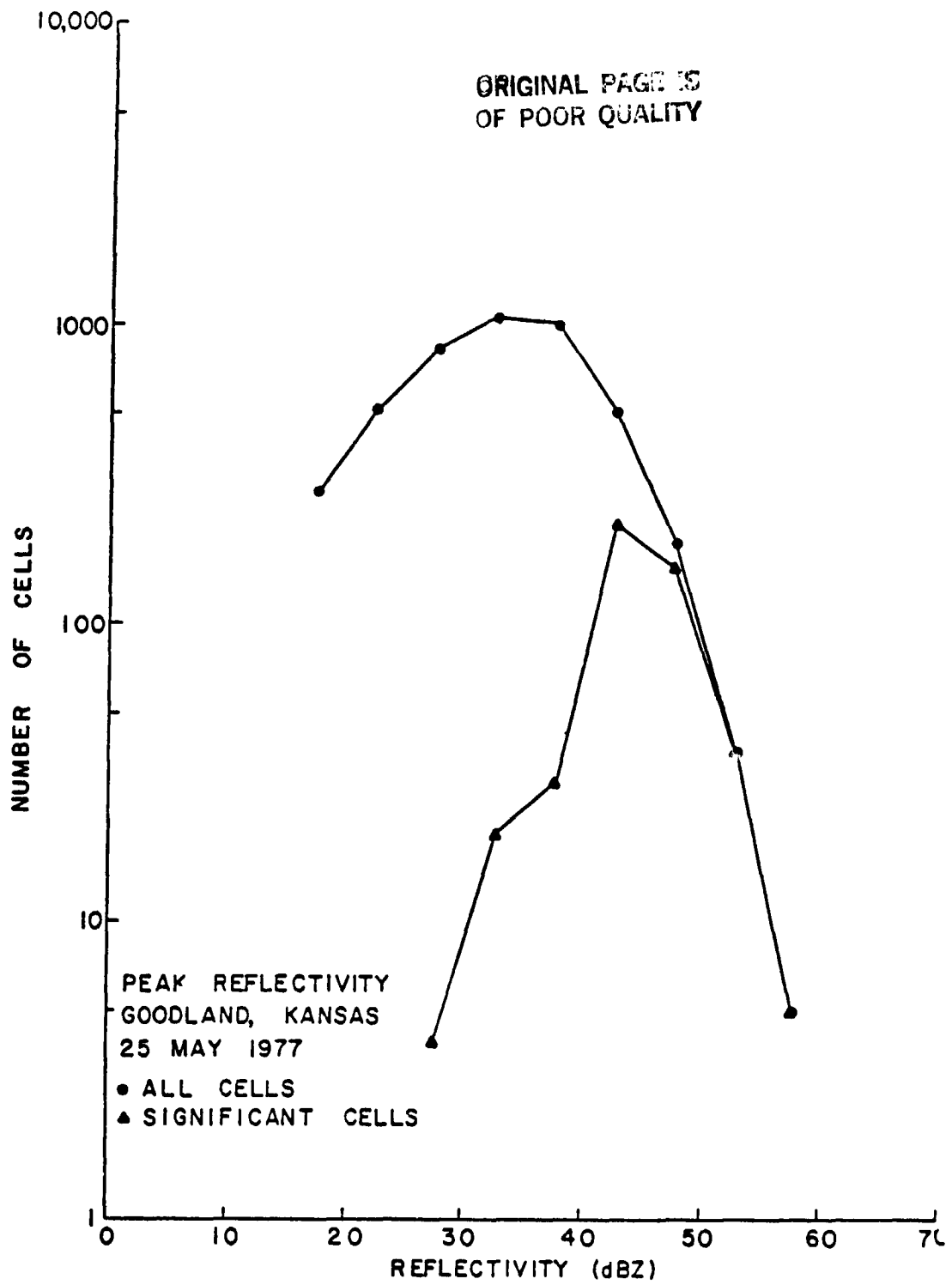


Figure 2. Number density distribution of volume cells and significant volume cells over the range of peak reflectivity values, Day 7144



ORIGINAL PAGE IS  
OF POOR QUALITY

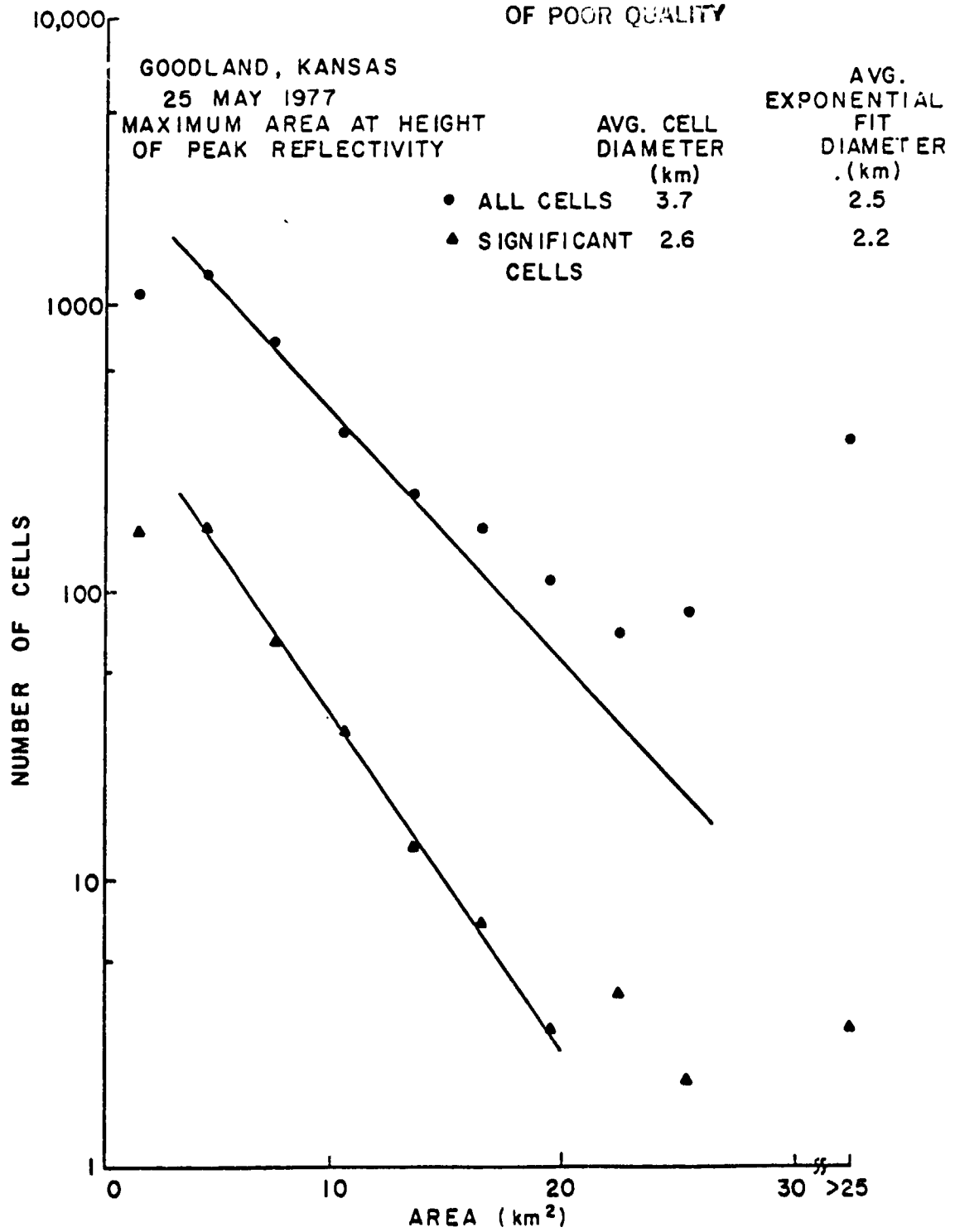


Figure 3. Number density distribution of volume cells and significant volume cells over the range of peak area values, Day 7144

ORIGINAL PAGE IS  
OF POOR QUALITY

TABLE 1

			RADAR DATA					VOLUME CELL ATTRIBUTES		
Year and Day	Start Time UT(h)	Stop Time UT(h)	No of Vol. Cell Tracks	No of Cluster Tracks	No of Fixed Contour Tracks	Total Water Mass (MT) <sup>1</sup>	First Echo Height (km)	Avg. Area (km <sup>2</sup> )	Life-time (min)	Avg. (dBZ)
6140	2130	0655	1687	239	206	2.6	4.6	5.0	14.9	21.6
6141*	2245	0655	5078	606	378	16	4.2	3.6	13.1	24.8
6162	2045	2335	3409	432	57	34.5	5.6	4.1	12.3	29.9
6169*	2150	0750	10000 <sup>†</sup>	1240	254	43	3.6	5.9	13.0	21.7
6226	1740	0330	10000 <sup>†</sup>	2484	2562	58	3.6	5.1	11.4	23.2
7144*	1930	0925	10000 <sup>†</sup>	1757	177	150	3.3	4.7	12.8	27.4
7161*	1820	2040	64	4	18	0.04	-	5.7	13.9	18.1
7173	2100	0655	10000 <sup>†</sup>	1861	1170	44	4.9	4.4	10.5	21.9
7174	1930	0825	10000 <sup>†</sup>	2623	2293	73	4.0	3.9	14.8	22.4
7194	2310	0725	1776	166	407	8	4.3	7.0	11.7	20.5
7196	2225	1025	10000 <sup>†</sup>	1152	1162	78	3.3	3.4	15.1	23.5
7208	2210	0720	487	42	53	2.5	3.5	4.7	15.9	21.6
7209	1415	2330	5377	546	303	17	3.7	4.7	11.3	23.8
7216*	2300	0305	6896	706	66	44	3.9	6.1	10.9	25.5
7220	1650	0520	4349	579	205	6.0	4.4	5.3	14.9	18.5
7236*	1425	0730	10000 <sup>†</sup>	1702	268	106	4.8	4.7	12.5	28.3
7237	1925	2210	125	8	20	0.68	-	4.6	14.3	20.9
8124	1640	0550	3443	507	93	8.0	2.1	5.5	15.2	16.1 <sup>Δ</sup>
8143*	2055	0135	5874	830	158	24	4.3	5.1	12.3	20.6 <sup>Δ</sup>
8144	2000	0510	9734	1418	382	42	M	4.0	13.1	22.7 <sup>Δ</sup>
8145	1940	0555	6441	507	75	32	5.9	6.9	11.5	20.6 <sup>Δ</sup>
8146	2120	0555	10000 <sup>†</sup>	1060	334	49	4.3	5.1	11.5	22.0 <sup>Δ</sup>
8170	1935	0510	10000 <sup>†</sup>	1865	583	74	4.3	5.4	11.4	21.2 <sup>Δ</sup>
8177	2340	0155	1980	230	18	20	M	6.2	11.2	24.1 <sup>Δ</sup>
8181	1855	0555	9897	1111	791	11 <sup>‡</sup>	3.8	4.1	13.2	18.6 <sup>Δ</sup>
SUM			~240,000	23,675	12,033	943				
AVI RAGL						37		5.0	12.9	22.0
STANJARI III VJAJJL								0.9	1.6	4.2

\* Duration limited by length of observation

† 10000 - Greater than 10<sup>4</sup>

Δ Adjusted 5.3 dB to correct calibration error

### ORIGINAL BASIS OF POOR QUALITY

Empirical density functions for the volume cell descriptors, reflectivity, area at the height of peak reflectivity, and lifetime are presented in Figures 1 through 3 respectively for one of the observation days are presented in Table 1. Two types of cells are described in the figures, significant cells and all cells. The all category includes all the observed cells with lifetimes of 10 or more minutes. Significant cells are cells with a pronounced vertical development or a high reflectivity (see Crane, 1979 for a detailed description).

The volume cells were not uniformly distributed throughout the rain (radar echo) region. Cell clustering was evident with clusters of 3 or more cells corresponding to regions of active convection (thunderstorms). The number and spacings of the clusters was found to be an important indicator of the water flux produced by a storm during its most active period of production as observed by a single radar.

### OBSERVED WATER FLUX

Water flux estimates were obtained from the radar data using a single fixed reflectivity vs. rain rate relationship for all the data. The time integral of the water flux, the water mass, was calculated for each of the storm days and is presented in Table 1. The water flux at the time of maximum production as observed by the radar was used to explore possible relationships between the numbers of cells, their spacings, and the water flux. The water flux normalized by the number of cluster (isolated significant cells and clusters-SC - see Crane and Hardy, 1981 for a detailed analysis) was found to display little day-to-day variation. The observed distribution of water flux per SC values could be approximated by a log-normal distribution as shown in Figure 4. The observed variance was about the same as the day-to-day variance expected for radar calibration. To first order, a count of the number of SC (thunderstorms) could be used to estimate the water flux.

A more detailed analysis of the variation in water flux per SC showed that it depended on the observed nearest-neighbor spacing

ORIGINAL RECORDS  
OF POOR QUALITY

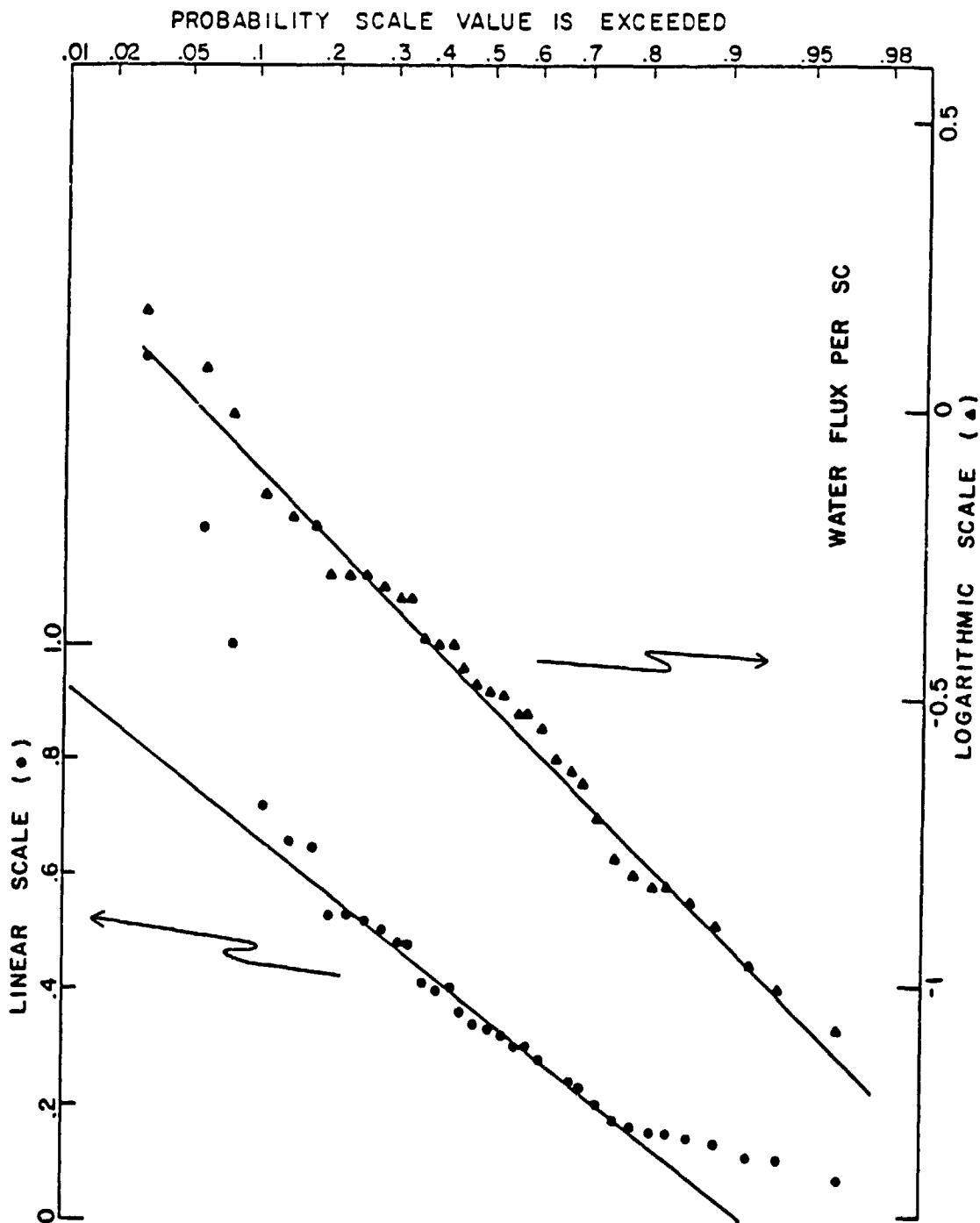


Figure 4. Cumulative distribution of water flux per isolated significant cell and cluster (SC) for 36 storm elements

between SCs. The data indicate that if the nearest neighbor distance to mixed layer depth ratio approximated the width-to-depth ratio expected for Rayleigh - Benard convection the water flux per SC values were higher than for other width-to-depth values. This observation is consistent with the expectation that Rayleigh-Benard convection operates to maximize vertical transport and therefore to maximize water flux.

### CONCLUSIONS

The radar data from Kansas indicate that the small scale organization of the convective elements (volume cell clusters) is important to the amount of precipitation produced by a storm. In Kansas summertime precipitation, a count of the number of thunderstorms (SCs) and a measure of their spacing is sufficient to obtain an estimate of water flux within a factor of 2. The water flux estimate from just counting the thunderstorms is of comparable accuracy to the estimate obtainable from a well calibrated radar. This result suggests that further work be done on the counting and classification of active regions of convection within a storm system to see if the number of countable entities could be used as a proxy variable for water flux and, by an appropriate sampling strategy, for precipitation amount.

### REFERENCES

1. Crane, R.K. and K.R. Hardy, (1981), "The HIPLEX Program in Colby-Goodland, Kansas: 1976-1980", ERT Report P-1552-F, Environmental Research & Technology, Inc., Concord, Massachusetts.
2. Crane, R.K., (1979), "Automated Cell Detection and Tracking", IEEE Trans. Geoscience Elect., GE-17, 250-262.

D15

N83 25284

ORIGINAL PAGES  
OF POOR QUALITY

## SOME STATISTICAL PROBLEMS INHERENT IN MEASURING PRECIPITATION

John A. Flueck  
Department of Statistics  
Temple University  
Philadelphia, Pa. 19122

### I. Introduction

The quantitative measurement of precipitation characteristics for any area on the surface of the earth is not an easy task. First, precipitation is rather variable in both space and time, and the distribution of surface rainfall at a given location typically is substantially skewed. Second, it now appears that there are a number of precipitation processes at work in the atmosphere, and even today few of them appear to be well understood. Third, the formal theory on sampling and estimating precipitation appears to be considerably deficient. Convenience sampling and simple means or totals seems to have been the norm. Also, it appears that little systematic attention is given to non-sampling errors (e.g. sample point location errors, instrument errors, data storage errors, data reduction errors, etc.) that always arise in utilizing any measurement system. In short, although the precipitation measurement problem is an old one, it continues today to be one that is in need of systematic and careful attention. A brief history of the presently competing measurement technologies should aid us in understanding the problems inherent in this measurement task.

#### I.A. Gages

The earliest attempts at measuring surface precipitation were by rain gages and it is reported that in India in about 400 B.C. bowls of about 46 cm in diameter apparently were regularly used to collect rainfall measurements for determining the annual crop to be sown. By the 13th century the Chinese (and later the Koreans, 15th century) apparently were using bronze cylinders of about 14 cm diameter and 30 cm depth, with an attendant scale, to measure rainfall in numerous provinces and cantons (Needham and Ting, 1959; Frisinger, 1977). The first English rain gage reportedly was designed by Sir Christopher Wren in 1662, but it was Richard Townley who initiated the idea of the weighing rain gage in 1677. He also apparently assembled the first extensive rainfall record for England, 1677 to 1703. However, it was not until Rev. Horsley in 1722 related the diameter of the catch to the diameter of the container, and scaled the container accordingly, that a rain gage similar to our present non-recording one was achieved. Finally, it should be noted that the remarkable weather clock, presumably designed by Sir Christopher Wren about 1663 and implemented by Robert Hooke in about 1673, clearly was the forerunner to our present recording rain gage (Middleton, 1969) and its more recent digitized output.

#### I.B. Radar

The next technology that was brought to bear on the precipitation measurement problem was radar. Its start apparently is traceable to February 20, 1941 when a small shower was tracked by radar, up to a distance of seven miles, off the English coast. This and other related meteorological uses of radar in the period of 1935 to 1945 led to the development of the field of radar meteorology (Battan, 1973). An important topic in this discipline is the quantitative measurement of rainfall.

In the late 40's a theoretical relation between backscatter energy (i.e. radar reflectivity factor,  $Z$ ) and rainfall rate ( $R$ ),  $Z = aR^b$ , was developed. However, this simple polynomial function assumed that; (1) the drop size distribution was of the exponential family, unchanging and known, and (2) the vertical air motions were zero. Subsequent experimentation showed that neither of these assumptions were upheld in the atmosphere, and thus the so-called "Z-R" relation is at best, a crude approximation to the actual relation. At present, researchers either rely on a popular version of this crude approximation (e.g.  $Z = 200 R^{1.6}$ ) or attempt to estimate the values of  $a$  and  $b$  for their particular conditions (see Battan, 1973, for an extended list of utilized Z-R relations).

The comparison of radar and gage estimated precipitation in the 1960's and early 70's indicated that the radar estimates tended to have systematic errors (e.g. Wilson, 1964; Woodley et al, 1975). For example, radar appears to overestimate "light" rain and underestimate "heavy" rain. Also, it became apparent that the variability both between and within storms was sizeable, and hence conditional Z-R relations were needed. However, useful conditioning events proved difficult to find (e.g. Wilson, 1966). Clearly a new approach was needed.

The "new approach" was to follow an old suggestion of Hitschfeld and Borden (1954) and adjust the radar estimated rainfall solely by rain gages. This method allows the radar to define the distribution of precipitation over an area and the gages to define the magnitude. The evidence to date suggests that this method is a clear improvement over unadjusted radar estimated rainfall (e.g. Wilson, 1970; Woodley et al, 1975, Thomas et al., 1981). In fact, this method has developed to the point where today a number of researchers believe radar estimated rainfall is the preferred method for assessing rainfall over large areas which are not instrumented with a high density ( $\geq 1$  gage per 250 to 400 km<sup>2</sup>) gage network (Wilson and Brandes, 1979). It also should be noted that more recent radar developments (e.g. digitized doppler) appear to offer further advances.

### I.C. Satellite

The third and most recent technology to be applied to the precipitation measurement problem is that of satellite data. One of the first efforts with this technology was to estimate the probability of precipitation as a function of the "window temperature" (i.e. 8-12  $\mu\text{m}$  or .55 to .75  $\mu\text{m}$  or both) using TIROS IV data (Lethbridge, 1967). Rainbird (1969) apparently had less success extending this approach to estimating 24 hour surface rainfall in the Mekong River basin using TIROS III "window temperature." By the 1970's a number of researchers were investigating the possibilities of estimating areal mean surface rainfall depths by establishing relations with infrared and/or visible radiances collected by satellites, and many of these pioneers are attending this conference. Martin and Scherer (1973) present a useful review of this early work and its attendant problems.

In the mid 70's another satellite estimation method appeared, the microwave technique. This technique related the Nimbus 5 electronically scanning microwave radiometer (ESMR) brightness temperatures (a measure of upwelling radiation emitted by the earth and its atmosphere) with hourly rain rates. Wilheit et al. (1977) presented a technique for estimating rainfall rates over the oceans and more recently others (e.g. Rodgers et al, 1979) are attempting to extend this technique to measuring over land. Today, useful qualitative results (i.e. probability of rain) seem probable, but the quantitative picture still is rather uncertain.

## II. Some Sampling Problems

The sampling problems that inherently arise in attempting to measure surface precipitation stem from three principal causes:

- (1) the variability of the natural process,
- (2) the lack of understanding of this process, and
- (3) the lack of a comprehensive formal theory of precipitation measurements.

Let us briefly indicate some of these problems.

### II.A

For many years it has been believed that precipitation events have substantial spatial and temporal variability. However, it only is more recently that quantitative measures have been offered for these two types of variability (e.g. Huff, 1971; Longley 1974; Woodley et al; 1975; Osborn et al., 1979). As an example, Woodley et al, (1975) indicate a spatial precipitation gradient of approximately 330 mm in 10 km for two months of south Florida summer-time (14 June to 14 August, 1973) rainfall within the FACE-1 target area. For a single day (22 July 1973) the spatial gradient is even steeper becoming 94 mm in 1 km.

ORIGINAL PAGE IS  
OF POOR QUALITY

Peck (1980) has sub-divided both spatial and temporal variability into long and short-term categories, and he provides a useful general summary of work in each of the categories. The indication is that all four categories contain substantial precipitation variability. Furthermore, Vogel and Huff (1978) and others have shown that precipitation also varies with storm or synoptic type.

Those who have attempted to model or fit statistical distributions to temporal or spatial precipitation also are much aware of the rather substantial inherent variability. One quickly learns that most precipitation data sets are highly skewed toward the larger values, and distributions such as the Gamma, Log-normal, and Weibull become the candidates of choice (e.g. Flueck and Boik, 1980). Furthermore, it is not unusual to find one or more extreme events ("outliers") in the data. Figure 1 presents an example of both of these points using a back-to-back stem and leaf plot (Tukey, 1977) of the Florida Area Cumulus Experiment (FACE-1) 6 hour rainfall (Note that in spite of substantial efforts to prevent skewness in this experiment it still occurred). These results begin to well explain the often heard statement that only a small portion of the storms or rainfall events (e.g. 10 to 15%) provide the majority of the total rainfall (e.g. Riehl, 1954; Garstang, 1972; Woodley et al, 1975). Huff (1970) has made an important start on modeling this sampling variability as a function of other factors.

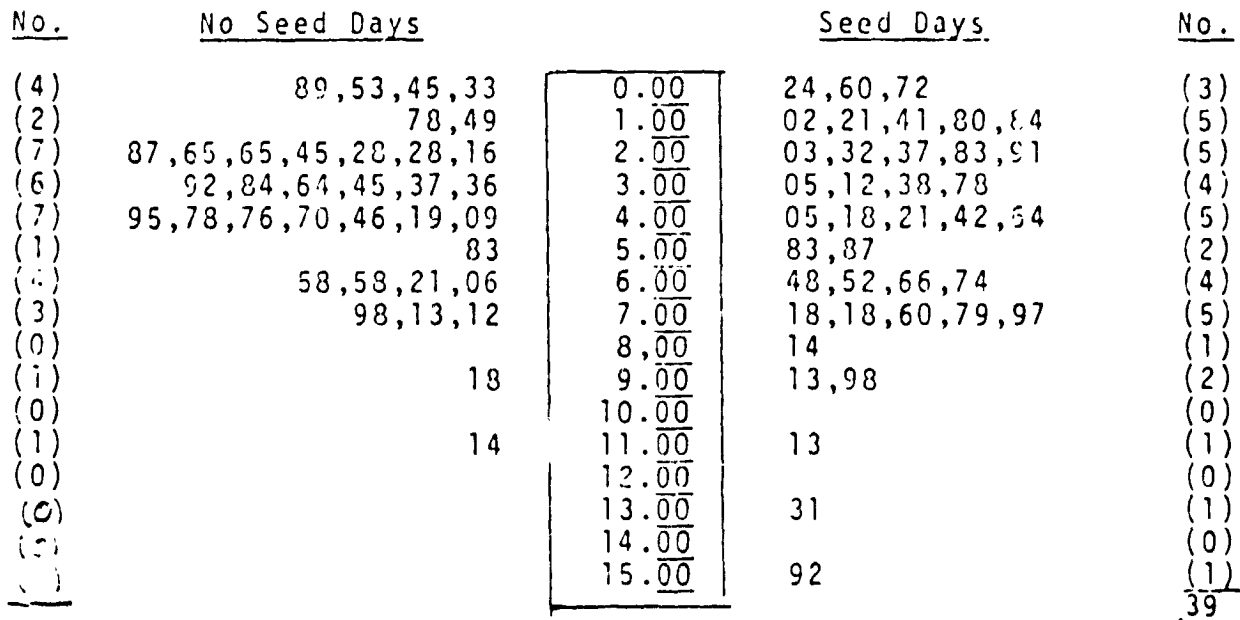


Figure 1. A back-to-back stem-and-leaf plot of the FACE-1 total target radar-estimated, gage adjusted rainfall for all no-seed type B days, 1970-76. All units are mm per 6 h.

The impact of the above findings on the estimation of surface precipitation is five-fold;

- (1) one must sample rather than take a complete count,
- (2) the sample must be in both space and time,
- (3) the sharp precipitation gradients demand more frequent sampling both in space and time,
- (4) some form of stratification appears to be needed to handle the changes in precipitation due to synoptic and other factors, and
- (5) the substantial skewness and presence of "extreme events" requires great care and thought (possibly some new theory) in designing and implementing the sampling and estimation plans for precipitation measurement.



## II.B. Lack of Valid Models

Given the substantial natural variability of surface precipitation, one might attempt to "control" this variability by utilization of one of the following four techniques (Flueck, 1978);

- (1) prescreening,
- (2) blocking,
- (3) covariating, or
- (4) replication

In this situation, only (2), (3), and (4) appear useable: (1) requires the selection and measurement of only a subset of events. However, blocking would require a priori classification of each precipitation event into a known category. Different categories could then invoke different precipitation measurement schemes. Unfortunately, the ability to predict the type and other characteristics of a precipitation event with enough certainty and lead-time is minimal. Trustworthy models presently are not available. Covariating, or the use of auxiliary information, also has its modeling problems. There is very little evidence that validated models of the precipitation processes currently exist. It is interesting to note that in the late 40's and early 50's at least one statistician (Le Cam, 1961) began attempts to stochastically model precipitation. One use of such models is to identify useful predictor or auxiliary variables that could be used in estimation to dampen the sampling variability. Thus, although there have been numerous searches for useful covariates, very little success has resulted from these efforts. As Peck (1980) and others have well stated the relations between surface precipitation and synoptic meteorology is very limited (null set?).

This leaves us with the final technique, that of replicating or increasing the spatial and temporal sampling points. Although this may be the only alternative at this stage in the development of the theory and methods of precipitation measurement, it typically is not an easy solution and certainly is an expensive one. In short, one attempts to overcome the sampling variability by "brute force" (large numbers).

## II.C. Lack of Formal Theory

All three previously mentioned surface precipitation measurement systems (i.e. network of raingages, radar, and satellites) explicitly utilize some form of systematic sampling. All three techniques sample precipitation systematically in either space or time or both. However, I am unaware of any formal statistical theory on space-time systematic sampling. Nor am I aware of any formal work on comparisons of alternative sampling techniques for precipitation. We seem to have adopted the "convenient" without much thought as to why.

In the interest of stimulating a formal theory of precipitation sampling and estimation, let me briefly pose a simple sampling problem. Figure 2, panel (a), presents a systematic or square grid (aligned) sampling point design of  $d$  units between sampling points. Note how this simple design provides "alleys" of width  $d$  through which west-east or north-south moving cells of diameter  $< d$  can pass completely undetected. Panel (b) presents an unaligned systematic sampling point design in which the  $X, Y$  coordinates in each row and each column are systematically (but separately) selected. Now the "systematic alleys" have disappeared and the strict west-east or north-south cells will not escape detection or sampling. Which of the two designs is preferred and when? See Cochran (1977) for some partial theoretical answers and Silverman et al. (1981), for some interesting simulation results.

Now, let's add the elevation and time dimensions to the above problem. Very quickly we see that we have constructed a complex sampling problem in need of formal theory. At the very least, this sampling problem is five dimensional, i.e.  $(x, y, z, t, r)$  where  $x, y,$  and  $z$  are surface location,  $t$  is time, and  $r$  is some rainfall characteristic of interest. Furthermore, rainfall is correlated over a number of these dimensions. Now the fun begins! We may need to rely on simulation derived results when the formal theory is intractable or advances slowly. However, it is time to get "marching."

## III. Estimation Problems

A number of estimation problems also arise in the measuring of surface precipitation. Some of them are system related and others are more general. We will briefly review both types.

ORIGINAL :  
OF POOR Q

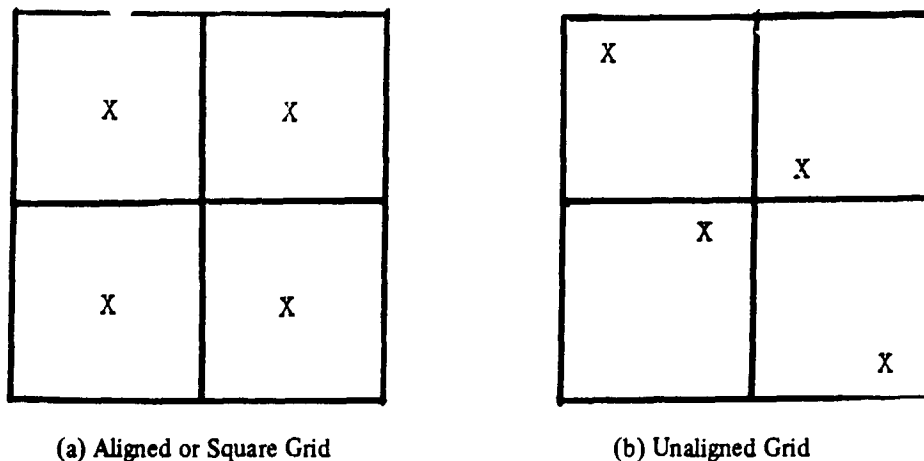


Figure 2. Two examples of systematic sampling in two dimensions.

### III.A. Estimators

A number of precipitation characteristics are available for point rainfall, and they include total amount, rate, duration, frequency, and others. Usually the context indicates the desired characteristic (e.g. total rainfall in 24 hours or rain rate per hour), but if not, an appropriate characteristic must be selected. Clearly it should be that characteristic which is most "closely-tied" to the problem of interest.

However, even given that point rainfall characteristics are of interest, there typically are a number of estimators available. As an example, hourly rainfall rate can be estimated by the time-honored mean, the more stable median, a trimmed mean, or one of the newer so-called robust estimators. These different estimators can give very different estimates (Stigler, 1977). Certainly the two guardians of useful measurement, accuracy and precision, must be heard.

Thus far we only have mentioned the estimation of point rainfall. However, for many situations (e.g. hydrology), it is areal precipitation that is desired. How should this characteristic be estimated? When sampling in space or time, some type of weighting and/or interpolation scheme is needed. Many techniques have been advanced for estimating areal precipitation under spatial sampling (e.g. Thiessen, 1911; Cressman, 1959; Hatch, 1976; Bras and Rodriguez-Iturbe, 1976). However, I am unaware of any formal study which systematically examined the theory and results of these different techniques. Clearly some careful comprehensive comparative studies are needed.

### III.B. Measurement Errors

Finally, we must face the problem of measurement errors in both the sampling and estimation stages. Although a number of the well-known measurement errors should be dealt with in the sample design (e.g. shielding rain gages to lessen wind effects), it is the estimation stage that must systematically correct or adjust for the detected errors that were not eliminated in the design.

Ratio and regression type estimators are standard statistical approaches to these estimation problems, and hence local or regional auxiliary information becomes important (e.g. wind speed and direction at each gage site – particularly for snow which indicates an efficiency of only 50% for an unshielded gage at a wind speed of only 10 mph – or for each sector of the network). Here again, validated relations or models between the surface precipitation and intervening variables are needed. The gage catch efficiency versus wind speed work of Larson and Peck (1974) is an example of the type of results that are urgently needed in all precipitation measurement systems.

Obviously errors can and do arise in any stage of the measurement process. The three most important antidotes for this problem are checking, checking, and checking. In short, there is no substitute for careful attention to all stages (i.e. measurement, collection, reduction, handling, estimation, etc.) of the measurement (estimation) process.

### III.C. Linkage Function

We mentioned above the problem of rain gage efficiency or how well a gage captures the true precipitation occurring at the site. In truth, the observed precipitation is some function (typically unknown) of the actual precipitation. Hence the precipitation estimate is linked by some function to the actual precipitation. The type and characteristics of this "linkage" (sometimes termed transfer) function are important.

In the radar and visible/IR satellite measurement systems the linkage is less direct. Both of these systems measure a proxy variable which then must be functionally related to rainfall. The standard radar measurement technique is to measure Z (a reflectivity factor) and then attempt to link it to R (the rainfall rate) through the popular physically based "Z-R" function. Needless to say, this approach has not always been well received and present evidence appears to suggest that the current popular "Z-R" function is too crude and in need of further work.

The current operational satellite measures of precipitation typically use enhanced brightness and/or infrared radiation as their "starting" variables. Then through various specialized empirical linkage functions one ultimately arrives at estimates of rainfall rates. It appears that at times the linkage is rather "ad hoc" and not physically based. The approach of Gruber (1973) appears to be an exception to this general picture. He does attempt to estimate and use well-known physical processes and relations in his linkage function.

### IV. Comparative Experiments

Three types of potentially competing precipitation measurement systems (i.e. rain gage network, radar, and satellite) have been presented. Furthermore, within each type there are competing designs and techniques. Each of the candidates has its own measurement, sampling, collection, retrieval, equipment and servicing constraints with the result that it is difficult to determine which system performs best in general and specific situations.

The only scientifically acceptable approach to the above dilemma is to perform some comparative experiments. We need to allow the various measurement systems a chance to compete fairly in field trials in order to evaluate properly their current performances and to plan for future improvements. This comparative approach requires that useful, unambiguous and comprehensive "ground-rules" be established prior to any comparative experiment and that the tenants of proper comparative experimentation (Flueck, 1981) be followed.

#### IV.A. Great Precipitation Evaluation Experiment

A number of methods have recently been advanced for estimating surface precipitation based on satellite data. Furthermore, numerous claims typically have been made for each method. The time has come for a comparative field experiment of the various competitors. It seems that the science of precipitation measurement would be well served by an assessment of the comparative strengths and weaknesses of the various competitors. Hence, I propose that we undertake the Great Precipitation Evaluation Experiment (GPEE).

This experiment should be limited to those methods that presently are able to present a comprehensive detailed document on their design and implementation. This design document would have to be presented to the GPEE committee prior to the experiment and followed in every detail. Thus an entrant would have to present the details of how the method estimated surface precipitation and exactly follow this method in the experiment.

The experiment should be conducted in a "blind" manner in that the days and locations selected for precipitation evaluation should be unknown to the experimenters. Furthermore, the actual surface rainfall values (probably based on a dense rain gage network) for the days of the experiment would be withheld from all participants.

I would tentatively propose that two or three areas of varying size (e.g. 200, 2000 & 10,000 km<sup>2</sup>) be selected as the "playing fields" of the experiment, and the goal would be to estimate 24 h total precipitation for each of the areas. It would seem useful to select about seven days in the 1981 growing season for this task. One could satisfy the days such that light, medium, and heavy rainfall days are present in the experiment. One might also include a zero rainfall day.

ORIGINAL DOCUMENT  
OF POOR QUALITY

Following their design document, each research team should perform the required precipitation estimations based on the satellite data received from the GPEE committee. At the end of the experimental period (probably 6 months to 1 year), each team should submit their daily estimates to the GPEE committee for evaluation. Any missing days (days with no estimate) should be assigned the value of zero. In addition, I would recommend that one randomly selected day be fully checked by the committee for compliance with the submitted design document.

The question of what statistic should be used to evaluate the overall performance of the competing methods should be settled prior to the experiment. My current preference would be to use mean square error ( $MSE = \text{Variance} + \text{Bias}^2$ ) with the raingage network value as the standard or population value. This would allow both the precision and accuracy of competing methods to be assessed. The other often mentioned evaluation statistics (i.e.  $\rho$ ,  $a + bx$ , and  $R^2$ ) appear to have clear deficiencies.

#### IV.B. Further Experiments

Once we have succeeded in selecting the best performing satellite based precipitation estimation methods (we may not find a uniformly best one), we should be able to more effectively develop the new competitors. I would propose that new methods also be theoretically and experimentally compared with the present "King or Kings of the Hill." This should be done by subsequent GPEE's (1,2, . . . ,k).

It also would seem useful to empirically compare various radar based precipitation estimation methods via an experiment. A few selected comparison case studies are not a substitute for a GPEE.

Lastly, the opportunity for comparison within an experiment of all three general types of precipitation measurement systems should not be overlooked.

#### V. Concluding Comments

The opportunities for substantial advancement in precipitation measurement and estimation appear to be at hand. The uses for improved estimates appear to be many and extend from flash flood and severe storm warnings to weather modification results and water and energy budgets.

This paper has advocated a systematic and scientific approach to improving surface precipitation measurements. In truth, all present surface precipitation measurements are really estimates. We need to recognize this fact and strive for improved estimators.

#### References

- Battan, L. J., 1973. Radar Observation of the Atmosphere, The Univ. of Chicago Press, Chicago, Ill., 324 pp.
- Bras, R. L. and I. Rodriguez-Iturbe, 1976. Network design for the estimation of real mean of rainfall events. Water Resource. Res., 12, 1185-95.
- Cochran, W. G., 1977. Sampling Techniques, 3rd edition, J. Wiley, N.Y., N.Y., 428 pp.
- Cressman, G. P., 1959. An operational objective analysis system. Mon. Wea. Rev. 87, 367-74.
- Flueck, J. A., 1978. The role of statistics in weather modification experiments. Atmos-Ocean, 16, 337-95.
- \_\_\_\_\_, 1981. Comparative experimentation: some principles and precipitations. To appear in the Teaching Statistics and Statistical Consulting, J. S. Rustagi and Wolfe, eds., Academic Press, N.Y., N.Y.
- \_\_\_\_\_ and R. J. Boik, 1981. A randomization study of the FACE-1 results and the FACE-2 design. Draft, NOAA-ERL tech. rpt., Boulder, Col.

ORIGINAL PAGE IS  
OF POOR QUALITY

- Frisinger, H. H., 1977. The History of Meteorology: to 1800., Am. Met. Soc. Hist. Mono. Series, Science History Publications, N.Y., N.Y.
- Garstang, M., 1972. A review of hurricane and tropical meteorology. Bull. Amer. Meteor. Soc., 53, 612-30.
- Gruber, A., 1973. Estimating rainfall in regions of active convection. J. Appl. Meteor. 12, 110-18.
- Hatch, D. J., 1976. Estimation of local rainfall by sampling gauging. Weather, 31, 79-83.
- Hitschfeld, W. and J. Bordan, 1954. Errors inherent in the radar measurement of rainfall at attenuating wavelengths. J. Appl. Meteor. 11, 58-67.
- Huff, F. A., 1970. Sampling errors in measurement of mean precipitation. J. Appl. Meteor. 9, 35-44.
- \_\_\_\_\_, 1971. Evaluation of precipitation records in weather modification experiments. Advances in Geophysics, 15, Academic press, N.Y., N.Y., 59-134.
- Larson, L. W., and E. L. Peck, 1974. Accuracy of precipitation measurements for hydrologic modeling. Water Resour. Res., 10, 857-63.
- LeCam, L., 1961. A stochastic description of precipitation. Proc. 4th Berkeley Symp. Math. Stat. & Prob., Univ. of Calif. Press, Vol. 3.
- Lethbridge, M., 1967. Precipitation probability and satellite radiation data. Mon. Wea. Rev., 95, 487-90.
- Longley, R. W., 1974. Spatial variation of precipitation over the Canadian prairies. Mon. Wea. Rev., 102, 307-12.
- Martin, D. W. and W. D. Scherer, 1973. Review of satellite rainfall estimation methods, Bull. Amer. Meteor. Soc., 54, 661-74.
- Middleton, W. E. K., 1969. Invention of the Meteorological Instruments, Johns Hopkins Press, Balt., Md.
- Needham, J. and W. Ting, 1959, Science and civilization in China. Mathematics and the Sciences of the Heavens and the Earth, Vol. 3, Cambridge Univ. Press, London.
- Osborne, H. B., K. G. Renard, and J. R. Simanton, 1979. Dense networks to measure convective rainfall in the southwestern United States, Water Resour. Res., 15, 1701-1711.
- Peck, E. L., 1980. Design of precipitation networks. Bull. Amer. Meteor. Soc., 61, 894-902.
- Rainbird, A. F., 1969. Some potential applications of meteorological satellites in flood forecasting. Hydro. Forecasting, Proc. of the WMD-UNESCO Symp. on Hydrological forecasting, WMD, Tech. note No. 92, WMD-No. 122, TP. 122, 73-80.
- Riehl, H. 1954. Tropical Meteorology, McGraw-Hill, 392 pp.
- Rodgers, E., H. Siddalingaiah, A. T. C. Chang, & T. Wilheit, 1979. A Statistical techniques for determining rainfall over land employing Nimbus 6 ESMR measurements. J. Appl. Meteor., 18, 978-91.
- Silverman, B. A., L. K. Rogers, & D. Dahl. 1981. On the sampling variance of raingage networks. To appear in J. Appl. Meteor.
- Stigler, S. M., 1977. Do Robust estimators work with real data? The Ann. of Stat., 5, 1055-98.
- Thiessen, A. H., 1911. Precipitation averages for large areas. Mon. Wea. Rev., 39, 1082-84.

- Thomas, J. L., A. G. Barnston, W. L. Woodley, & J. A. Jordan, 1981. A comparison of radar and raingage rainfall estimates in FACE-2 Submitted to J. Appl. Meteor.
- Tukey, J. W., 1977. Exploratory Data Analysis, Addison-Wesley, Reading, Mass., 506 pp.
- Vogel, J. L. and F. A. Huff, 1978. Relations between St. Louis urban precipitation anomaly and synoptic weather factors. J. Appl. Meteor., 17, 1141-52.
- Wilheit, T. T., A. T. C. Chang, M. S. V. Rao, E. B. Rodgers, & J. S. Theon, 1977. A satellite technique for quantitatively mapping rainfall rates over the oceans. J. Appl. Meteor. 16, 551-60.
- Wilson, J. W., 1964. Evaluation of precipitation measurements with the WSR-57 weather radar. J. Appl. Meteor., 3, 164-74.
- \_\_\_\_\_. 1966. Storm-to-storm variability in the radar reflectivity-rainfall rate relationship. Proc. 12th Conf. on Radar Meteor., AMS, Boston, Mass. pp. 229-233.
- \_\_\_\_\_, 1970. Integration of radar and raingages data for improved rainfall measurements. J. Appl. Meteor., 9, 489-97.
- \_\_\_\_\_ and E. A. Brandes, 1979. Radar measurement of rainfall – a summary. Bull. Amer. Meteor. Soc., 60, 1048-58.
- Woodley, W. L., A. R. Olsen, A. Herndon, & V. Wiggert, 1975. Comparison of gage and radar methods of convective rain measurement, J. Appl. Meteor., 14, 909-928.

ORIGINAL PAGE IS  
OF POOR QUALITY

N83 25285

D/6

ORIGINAL FACSIMILE  
OF POOR QUALITY

ON THE EFFECT OF TEMPORAL SAMPLING ON THE OBSERVATION OF MEAN RAINFALL

Charles R. Laughlin

Goddard Laboratory for Atmospheric Sciences (GLAS)  
NASA/Goddard Space Flight Center  
Greenbelt, Maryland 20771

ABSTRACT

A formula permitting calculation of the mean-square error of the mean value of a random variable due to periodic sampling is derived and applied to estimating the sampling error for satellite observation of the mean rainfall during the GARP Atlantic Tropical Experiment (GATE). The effects of both spatial resolution and frequency of observation on the sampling error are summarized in graphs. It is found that four observations per day are sufficient to determine the monthly mean rainfall over an area of 2.5° square (280km X 280km) to within a standard deviation of 5 percent of its mean value, two samples per day would yield an error with a standard deviation slightly less than 10 percent of the mean. A satellite instrument with less frequent sampling may produce significantly greater error in the estimate of monthly mean rainfall.

1.0 INTRODUCTION

Satellite borne instruments offer the opportunity to globally measure meteorological parameters. Such instruments on near earth satellites are however intrinsically constrained by their orbits on non-continuous observations. This observational constraint introduces an error, called sampling error, into the mean value of meteorological parameters calculated from satellite observations. For example, mean rainfall estimates obtained from surface radars during the GATE<sup>1</sup> and the Electronically Scanned Microwave Radiometer (ESMR), have shown substantial differences (Austin, 1978)<sup>2</sup> which in part may be due to inadequate sampling. A method of estimating the bias introduced by inadequate sampling of ESMR and other satellite instruments used to obtain meteorological averages would be useful.

Formulas which permit evaluation of the error in the mean value of a parameter due to periodic as opposed to continuous sampling are developed here. They are applied to estimating the sampling required to obtain an accurate estimate of the mean rainfall over tropical oceans, and assess the potential magnitude of sampling error on mean rainfall estimates derived from the ESMR during the GATE.

The statistical relationships needed to obtain the mean-square error of the mean value of a random variable due to periodic sampling are presented in Section 2. In Section 3 the Gate radar data used in this study are described. The

autocovariance functions needed to evaluate sampling errors for mean rainfall during GATE are examined in Section 4, and estimates of the sampling error for mean rainfall are given in Section 5. Section 6 contains a discussion and conclusions of this paper.

2.0 SAMPLING ERROR ESTIMATION

In order to derive an estimate of the variance of the mean value of a random variable due to discrete uniform sampling the sampling problem is formalized as follows. For a fixed interval of time, beginning at some arbitrary time  $t_1$ , and extending to  $t_2$ , the mean value,  $M(T)$ , for a random variable  $X(t)$ , over a time interval,  $T = t_2 - t_1$  is

$$M(T) = \frac{1}{T} \int_{t_1}^{t_2} X(t) dt. \quad (1)$$

In practice, a continuous record of  $X(t)$  is seldom available. In particular, for satellite observations, we can at best only estimate  $M(T)$  from the average of a sequence of measurements. Specifically, we may have only samples taken at say, times  $t_1 + t_0, t_1 + 2t_0, \dots, t_1 + Nt_0$ , where  $N$  represents the number of samples taken at times separated by intervals of length  $t_0$  with  $Nt_0 = T$ . The mean,  $M(T, t_0)$ , of such a sample sequence is,

$$M(T, t_0) = \frac{1}{N} \sum_{k=1}^N X(t_1 + kt_0). \quad (2)$$

With measurements taken by an ideal instrument every  $t_0$  hours, the expected value of the square of the difference between the  $M(T, t_0)$  and  $M(T)$ ,  $E\{[M(T, t_0) - M(T)]^2\}$ , may be taken as a measure of sampling error.

The expected value of a random variable  $Q$ ,  $E\{Q\}$ , may be calculated by means of the ergodic theorem (Margenau and Murphy, 1964) by

$$E\{Q\} = \lim_{L \rightarrow \infty} \frac{1}{L} \int_0^L Q dt \quad (3)$$

if the limit exists. In Appendix A it is shown that the mean square sampling error  $\sigma^2$  is given by

$$\sigma^2 = \frac{2}{T} \int_0^T \left(1 - \frac{r}{T}\right) R(r) dr + \frac{R(0)}{N} + \frac{2}{N} \sum_{k=1}^{N-1} \left(1 - \frac{k}{N}\right) R(kt_0) - \frac{2}{NT} \sum_{k=1}^N \int_0^T R(r - kt_0) dr \quad (4)$$

provided  $\bar{X}$ , the true mean, and  $R$ , the autocovariance function

<sup>1</sup>GATE (Global Atmospheric Research Program) Atlantic Tropical Experiment.

<sup>2</sup>Austin, P. M. and S. G. Geotis, 1978: Evaluation of Quality of Precipitation Data from a Satellite-Borne Radiometer, Department of Meteorology, Massachusetts Institute of Technology, 77 Mass Ave., Cambridge, MA 02139.

ORIGINAL PAGE IS  
OF POOR QUALITY

given by

$$\bar{X} = \lim_{L \rightarrow \infty} \frac{1}{L} \int_0^L X(L)dL \quad (5)$$

and

$$R(\tau) = \lim_{L \rightarrow \infty} \frac{1}{L} \int_0^L X(L) X(L + \tau)dL \quad (6)$$

exist.

It is recognized that  $\bar{X}$ , and  $R(\tau)$  may not exist in a climatological sense (Brooks, 1929), however it will be assumed that these limits are sufficiently well satisfied to permit the use of the derived expression for the mean square sampling error (Yaglom, 1962), (Leith, 1973).

Application of the expression for mean square error to the GATE radar derived rainfall measurements permits an estimate of sampling error on ESMR derived mean rainfall, and provides a means of estimating sampling requirements for measurements of tropical oceanic rainfall. The Gate data will be briefly described.

### 3.0 THE GATE AREA RADAR DATA

The GATE experiment conducted during the summer of 1974 provided detailed measurements of rainfall from both gauges and radars on an array of ships (Oceanographer, Researcher, Gillis, and Quadra) over an area called the B-scale, located approximately 1000km off the West Coast of Africa. Stationed within this area (centered at 8° 30' N latitude and 23° 30' W longitude), these ships collected rainfall data over three approximately tri-weekly, periods called phases. Figure 1 illustrates the experiment area and Table 1 describes the three phases of the GATE experiment. The ships carried 5cm

radars which measured rain-echo intensities. Patterson et al. (1979)<sup>1</sup> calculated rainfall rates from these observations, and presented them in the form of cartesian scans over the B-scale area with mean equivalent rainfall given in 4 km X 4 km data bins. The processing included elimination of questionable data, interpolation to fill missing data, and application of corrections that included those for atmospheric attenuation and antenna elevation.

Table 1 Three Phases of GATE

Phase	Dates	Total Time
I	28 Jun - 16 Jul 1974 (Julian Day 179-197)	450 hrs. (19 days)
II	28 Jul - 15 Aug 1974 (Julian Day 209-227)	455 hrs. (19 days)
III	30 Aug - 19 Sep 1974 (Julian Day 242-262)	499 hrs. (21 days)

Only data from Phases I and II were utilized in this study. Both degradation of Phase III data resulting from antenna stabilization problems on the Oceanographer, and its incompatibility with Phases I and II precluded the use of the Phase II data. GATE radar data at its original 15-minute intervals was made available by the National Oceanic and Atmospheric Administration (NOAA) for use in this study.

Though, the derivation of the rainfall amounts in GATE was preceded by very careful calibration of the radars and by intercomparisons between radars and between radar and gauge measurements, it is recognized that radar measurements of rainfall are subject to uncertainties (Hudlow and Patterson, 1979)<sup>2</sup>. These uncertainties may arise, for example, in the relationship between radar reflectivity and rainfall rate or in the difference between radar observed precipitation and that which actually reaches the surface. The GATE rainfall data is assumed to be typical of rain in the Equatorial Atlantic and to possess its statistical properties.

### 4.0 AUTOCOVARANCE FUNCTIONS

GATE rain-rate time series data, at 15 minute intervals provided the mean values and autocovariance functions. Means and autocovariances were computed for five of the 4 X 4 km<sup>2</sup> time series with one in the center of the GATE area and one in each of the four quadrants. Areal estimates were obtained by averaging the five values. Similarly, in order to study the dependence of autocovariance on area size, means and autocovariance values were computed for time series for other area sizes: 8 X 8 km<sup>2</sup>, 16 X 16 km<sup>2</sup>, 32 X 32 km<sup>2</sup>, 64 X 64 km<sup>2</sup>, 96 X 96 km<sup>2</sup>, 128 X 128 km<sup>2</sup>, 176 X 176 km<sup>2</sup>, 224 X 224 km<sup>2</sup> and the total GATE area of 280 X 280 km<sup>2</sup>. For each area size beyond 64 X 64 km<sup>2</sup>, the mean and autocovariance were computed only from time series corresponding to the center of the GATE area, since the quadrants in all such cases are smaller than the area size under consideration.

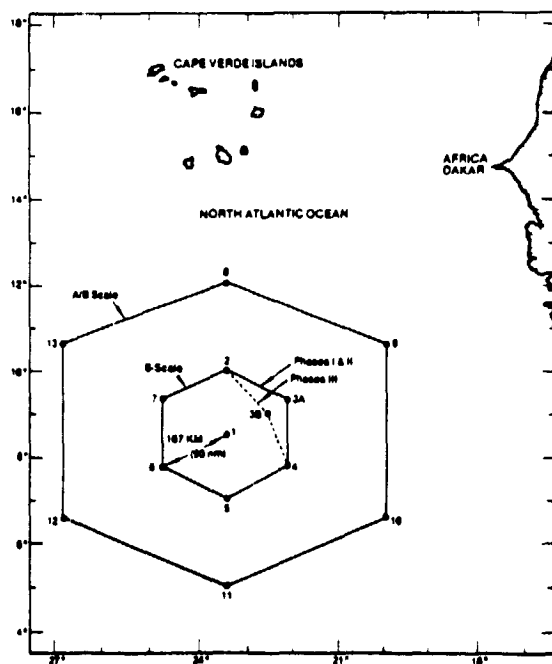


Figure 1. The GATE Observation Network Showing the Relationship with the B-Scale Area

<sup>1</sup>Patterson, V. et al., 1979: GATE Radar Rainfall Processing System, NOAA Technical Memo. EDIS 26, Federal Bldg., Silverhill Rd., Suitland, MD 20233.

<sup>2</sup>Hudlow, M. and V. Patterson, 1979: Gate Radar Rainfall Atlas, NOAA Special Report, Center for Environmental Assessment Services, NOAA, 6010 Executive Blvd., Rockville, MD 20852.



The autocovariance functions calculated for Phases I and II are presented in Figures 2 and 3, respectively. The empirically derived curves all appear to be examples of exponential decay. Each was least squares fitted to a function of the form  $B \exp(-\alpha |r|)$ . In all cases, the goodness of fit (measured as the mean square error) between the empirical data and the analytic form was found to be better than 2.5 percent. The parameters of the exponential forms and other statistics of the rainfall are tabulated in Table 2. The analytic form obtained for the autocovariance functions allows a closed form evaluation of the sampling error

### 5.0 RAINFALL SAMPLING ERRORS

The mean square sampling area for the GATE rainfall observations is shown in Appendix B to be given by

$$\sigma_e^2 = \frac{2B}{T/\tau_0} \left[ -1 + \frac{t_0}{2\tau_0} \left( \frac{e^{t_0/\tau_0} + 1}{e^{t_0/\tau_0} - 1} \right) + \left( \frac{e^{-T/\tau_0} + 1}{T/\tau_0} \right) \left\{ 1 - \frac{t_0}{\tau_0} \left( \frac{e^{t_0/\tau_0} + 1}{e^{t_0/\tau_0} - 1} \right) + \left( \frac{t_0}{\tau_0} \right)^2 \frac{e^{t_0/\tau_0}}{(e^{t_0/\tau_0} - 1)^2} \right\} \right] \quad (7)$$

The sampling error can be computed as a function of  $t_0$ , the sampling interval, once the measurement interval,  $T$ , and the area size over which the rainfall is averaged are selected. This was done for Phases I and II (for the entire GATE area) with results shown in Figures 4 and 5.

The graphs in Figures 4 and 5 indicate that measurements of temporal rainfall, when spatially averaged over an area

commensurate with GATE radar data, is entirely practical from a sampling point of view. Still, comparisons that have been made between ESMR-5 measurements and GATE data show a disappointing difference. This can be explained in part by recognizing that ESMR-5 scan angle was limited to  $\pm 30^\circ$  from nadir as opposed to its nominal  $\pm 50^\circ$ . Thus, the ground coverage was reduced by almost one-half in the equatorial regions and operational limitations resulted in further losses of data over the GATE area. The net result was that during the GATE, the averaging time between ESMR-5 observations was on the order of once every 36 hours, so that we should expect about 24 percent sampling error on the average, and not be particularly surprised by considerably larger errors for any one particular such experiment.

Equation (7) was also used to compute the sampling error as a function of  $t_0$  with  $T =$  one month for area sizes  $32 \times 32 \text{ km}^2$ ,  $64 \times 64 \text{ km}^2$ ,  $128 \times 128 \text{ km}^2$  and  $280 \times 280 \text{ km}^2$ . The results for Phases I and II are plotted in Figures 6 and 7, respectively. From these figures and Table 2 it is clear that for  $\tau_0$  sampling errors are relatively insensitive to averaging area size and that the sensitivity, however small, decreases as the average size is increased

### 6.0 CONCLUSIONS

From a sampling point of view, a single earth orbiting satellite system capable of measuring rainfall should not be expected to provide useful estimates of the monthly mean rainfall on a spatial scale of less than  $100 \times 100 \text{ km}$  in tropical oceanic regions if the GATE observations are considered typical. A practical satellite instrument that is significantly limited in scan angle (and hence whose revisit time is

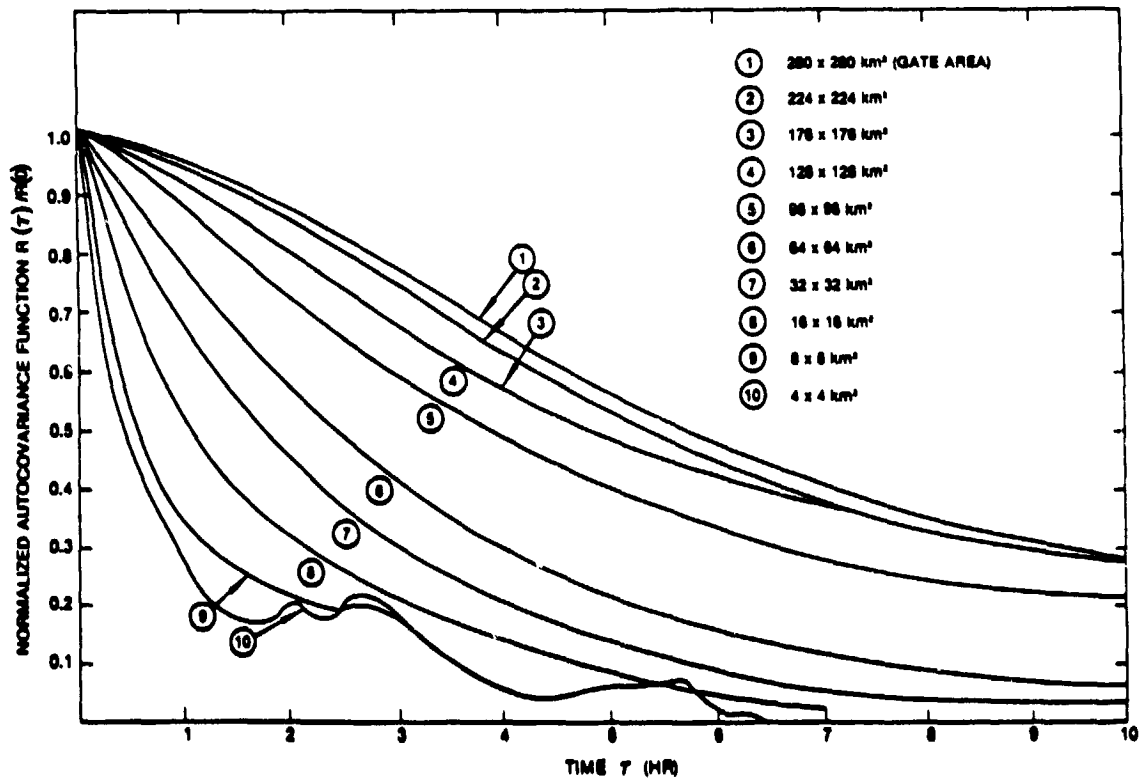


Figure 2. Autocovariance Functions for Phase I

ORIGINAL PAGE IS  
OF POOR QUALITY

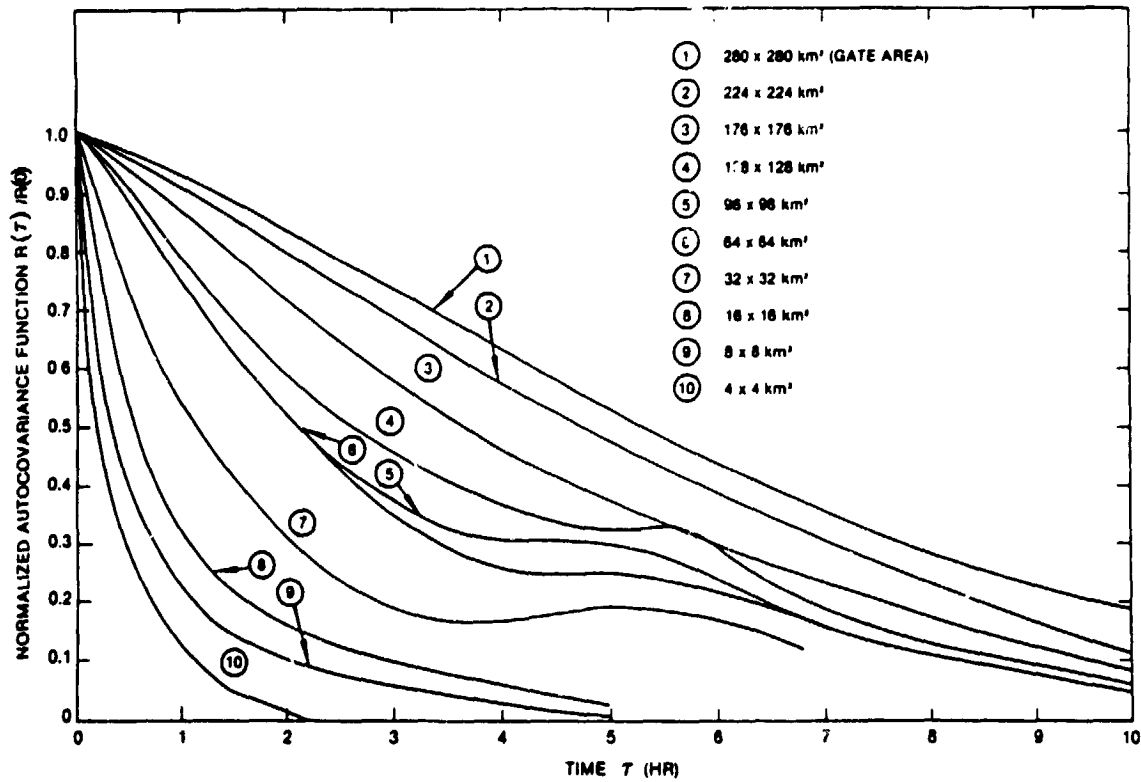


Figure 3. Autocovariance Functions for Phase II

Table 2. Best Fit Autocovariance Functions

Area Size (km <sup>2</sup> )	Phase I - 450 Hrs.			Phase II - 455 Hrs.		
	Autocovariance Function	Mean mm/hr	$\tau_0$ hrs	Autocovariance Function	Mean mm/hr	$\tau_0$ hrs
4 x 4	$8.85 \exp(-1.55  \tau )$	0.46	0.65	$10.63 \exp(-2.13  \tau )$	0.40	0.47
8 x 8	$6.17 \exp(-1.06  \tau )$	0.45	0.95	$5.92 \exp(-1.67  \tau )$	0.38	0.60
16 x 16	$3.37 \exp(-0.49  \tau )$	0.44	2.06	$3.76 \exp(-0.96  \tau )$	0.38	1.03
32 x 32	$2.25 \exp(-0.42  \tau )$	0.44	2.36	$1.84 \exp(-0.55  \tau )$	0.36	1.80
64 x 64	$1.37 \exp(-0.32  \tau )$	0.43	3.10	$1.01 \exp(-0.34  \tau )$	0.34	2.94
96 x 96	$0.87 \exp(-0.20  \tau )$	0.51	5.13	$0.20 \exp(-0.31  \tau )$	0.21	3.23
128 x 128	$0.87 \exp(-0.15  \tau )$	0.55	6.63	$0.21 \exp(-0.22  \tau )$	0.27	4.59
176 x 176	$0.73 \exp(-0.15  \tau )$	0.52	6.68	$0.24 \exp(-0.21  \tau )$	0.32	4.82
224 x 224	$0.63 \exp(-0.15  \tau )$	0.50	6.72	$0.25 \exp(-0.16  \tau )$	0.36	6.23
280 x 280	$0.51 \exp(-0.14  \tau )$	0.49	7.16	$0.24 \exp(-0.16  \tau )$	0.39	6.37

ORIGINAL RESULTS  
OF FOOD QUALITY

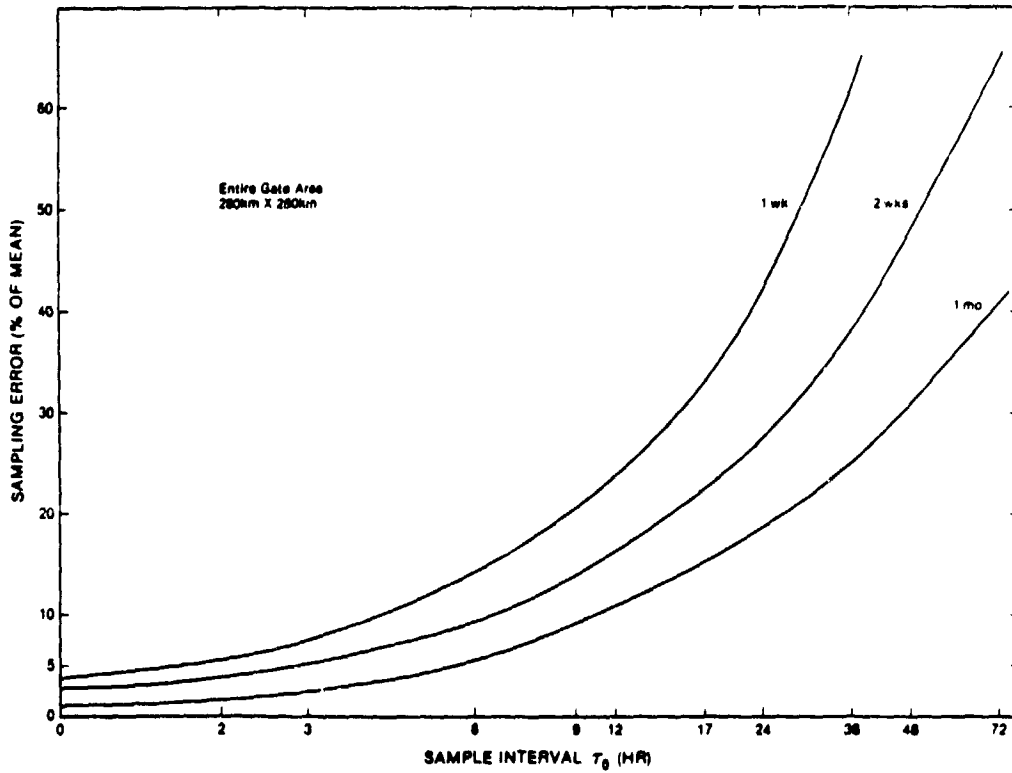


Figure 4. Sampling Error (Standard Deviation  $\sigma_e$  in Percent of Mean) vs. Sampling Interval for Phase I for Measurement Intervals  $T = 1 \text{ wk}, 2 \text{ wks}, 1 \text{ month}$

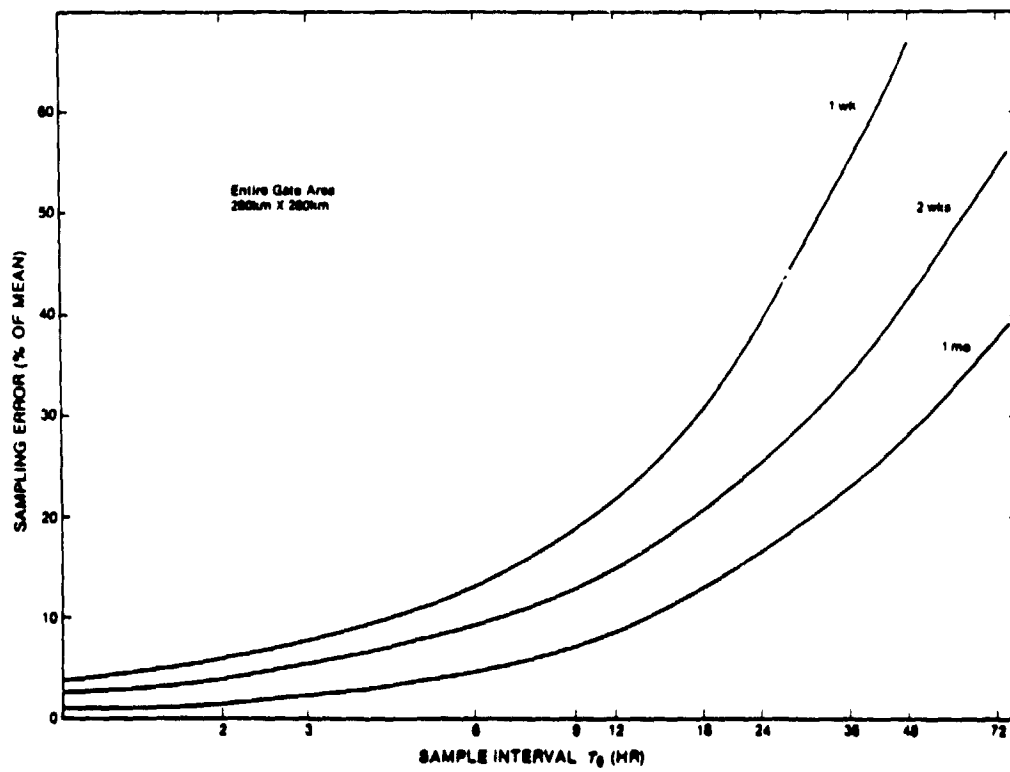


Figure 5. Sampling Error (Standard Deviation  $\sigma_e$  in Percent of Mean) vs. Sampling Interval for Phase II for Measurement Intervals  $T = 1 \text{ wk}, 2 \text{ wks}, 1 \text{ month}$

ORIGINAL PAGE IS  
OF POOR QUALITY

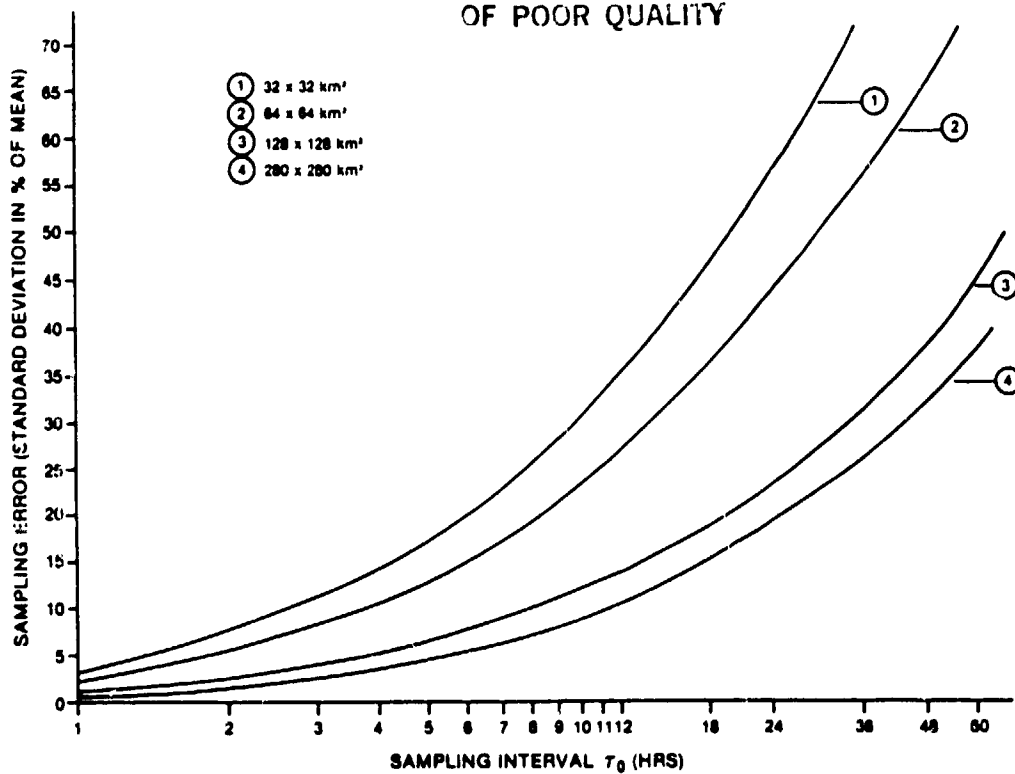


Figure 6. Sampling Error (Standard Deviation  $\sigma_s$  in Percent of Mean) vs. Sampling Interval for Phase I for Measurement Interval T = 1 Month

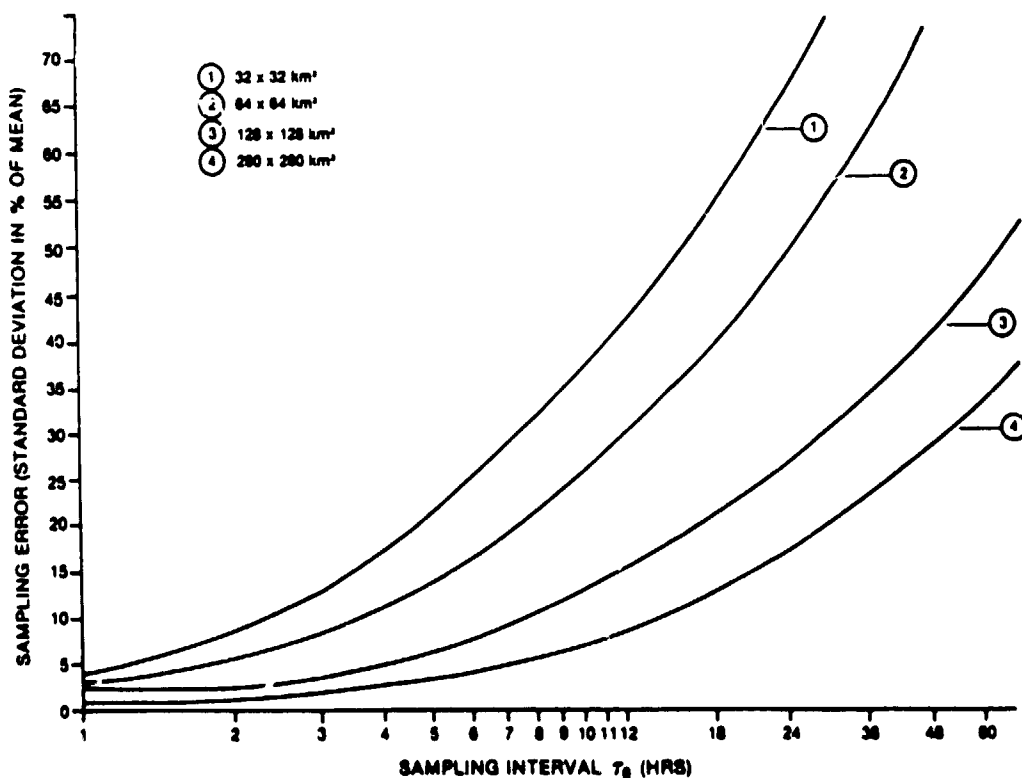


Figure 7. Sampling Error (Standard Deviation  $\sigma_s$  in Percent of Mean) vs. Sampling Interval for Phase II for Measurement Interval T = 1 Month

## ORIGINAL PAPER OF POOR QUALITY

significantly increased beyond 12 hours) should be flown simultaneously on more than one satellite to obtain accurate monthly means.

In any event, the results presented here provided a quantitative basis for such judgements, insofar as the GATE radar data permits. It is emphasized that the methods used were based on the actual data in a way that assured any diurnal variation that may have existed during the GATE period was included within the sampling error estimates. Therefore, it can be concluded that any diurnal variation that may have been present in the GATE data certainly was an insignificant factor.

Since the frequency of the sampling by an earth orbiting satellite system increases for latitudes away from the equator, it seems likely that a practical satellite system providing adequate sampling over equatorial regions would also be adequate for other areas. However, the statistical model presented should be useful for any comparisons derived with rainfall processes at other areas of the globe.

### REFERENCES

- Brooks, C. E. P., 1929: *Climate Through the Ages*, Dover Publications, 180 Varick St., New York, NY 10014.
- Leith, C. E., 1973: The Standard Error of Time-Average Estimates of Climatic Means, *Journal of Applied Meteorology*, Vol. 12, 1973, p. 1066.
- Margenau, H. and G. Murphy, 1964: *The Mathematics of Physical Chemistry*, Van Nostrand Reinhold Co., 135 North 50th St., New York, NY 10020.
- Yaglom, A. M., 1962: *Stationary Random Functions*, Prentice Hall, Inc., Route 9W, Englewood Cliffs, NJ 07632.

### APPENDIX A

#### DERIVATION OF SAMPLING ERROR

The sampling error is given by

$$\sigma^2 = E[(M(T, t_0) - M(T))^2] \quad (A-1)$$

or, upon expansion,

$$\sigma^2 = E[M^2(T)] + E[M^2(T, t_0)] - 2E[M(T, t_0)M(T)] \quad (A-2)$$

where

$$E[M^2(T)] = E\left[\frac{1}{T^2} \int_{t_1}^{t_2} X(t)dt \int_{t_1}^{t_2} X(s)ds\right], \quad (A-3)$$

$$E[M^2(T, t_0)] = E\left[\frac{1}{N^2} \sum_{k=1}^N X(t + Kt_0) \sum_{l=1}^N X(t + lt_0)\right] \quad (A-4)$$

and

$$E[M(T, t_0)M(T)] = E\left[\frac{1}{NT} \sum_{k=1}^N (t + Kt_0) \int_{t_1}^{t_2} X(t)dt\right] \quad (A-5)$$

with  $T = t_2 - t_1$  and  $Nt_0 = T$ .

An assumption of ergodicity permits the evaluation of  $E[Q]$  as the limit of a time average of  $Q$ , if the limit exists; that is

$$E[Q] = \lim_{L \rightarrow \infty} \frac{1}{L} \int_0^L Q(s)ds \quad (A-6)$$

with  $L$  representing time. The true mean of  $X(t)$ , denoted by  $\bar{X}$ , may be calculated as

$$\bar{X} = \lim_{L \rightarrow \infty} \frac{1}{L} \int_0^L X(t)dt. \quad (A-7)$$

The autocovariance function,  $R(\tau)$ , may be calculated as

$$R(\tau) = \lim_{L \rightarrow \infty} \frac{1}{L} \int_0^L (X(t) - \bar{X})(X(t + \tau) - \bar{X})dt. \quad (A-8)$$

Upon expanding the terms in the integrand, the following relationships are demonstratable.

$$R(\tau) = \lim_{L \rightarrow \infty} \frac{1}{L} \int_0^L X(t)X(t + \tau)dt - \bar{X}^2. \quad (A-9)$$

With the assumption of the existence of  $\bar{X}$ , and  $R(\tau)$  the expected values of each of the expressions in equations A-3, A-4, and A-5 are evaluated in turn.

$$E[M^2(T)] = \lim_{L \rightarrow \infty} \frac{1}{L} \int_0^L \frac{1}{T^2} \int_0^T X(t+a)dt \int_0^T X(s+a)dsda. \quad (A-10)$$

Upon interchanging the order of integration and letting  $U = t + a$

$$E[M^2(T)] = \frac{1}{T^2} \int_0^T \int_0^T \left[ \lim_{L \rightarrow \infty} \frac{1}{L} \int_0^L X(U)X(U+s-t)dadt \right] \quad (A-11)$$

or

$$E[M^2(T)] = \frac{1}{T^2} \int_0^T \int_0^T [R(s-t) + \bar{X}^2]dadt.$$

This equation may be simplified further through inspection of the area in the  $s, t$  plane over which the integration is performed.  $R(s-t)$  is constant along lines of the form  $s = t + c$ . These lines have a slope of 1 and an intercept of  $c$ . Choosing a coordinate system with one axis parallel to these lines simplifies evaluation of the integral, for  $R$  will be constant on all lines parallel to the axis. Letting  $X = (s+t)/\sqrt{2}$ ,  $y = (t-t)/\sqrt{2}$ ,

$$E[M^2(T)] = \frac{1}{T^2} \int_0^{T/\sqrt{2}} \int_{X-\sqrt{2}y}^{X-\sqrt{2}y} [R(\sqrt{2}y) + \bar{X}^2] dx dy$$

and substituting  $U = \sqrt{2}y$ , after integration yields

$$E[M^2(T)] = \frac{2}{T} \int_0^T \left(1 - \frac{U}{T}\right) (R(U) + \bar{X}^2) dU. \quad (A-12)$$

Reordering the sums in equation A-4 yields

$$E[M^2(T, t_0)] = \lim_{L \rightarrow \infty} \frac{1}{L} \int_0^L \frac{1}{N^2} \sum_{k=1}^N \sum_{l=1}^N X(L+Kt_0)X(L+lt_0)dL \quad (A-13)$$

ORIGINAL ...  
OF POOR QUALITY

and upon interchanging the order of integration and summation, letting  $U = L + Kt_0$ , and using equation A-9,

$$E[M^2(T, t_0)] = \frac{1}{N^2} \sum_{K=1}^N \sum_{J=1}^N (R((L-K)t_0) + \bar{X}^2) \quad (A-14)$$

Evaluation of the double sum using the relationship  $R(r) = R(-r)$  yields

$$E[M^2(T, t_0)] = \frac{R(0)}{N} + \frac{2}{N} \sum_{J=1}^{N-1} \left(1 - \frac{J}{N}\right) (R(Jt_0) + \bar{X}^2) \quad (A-15)$$

Equation A-5 may be evaluated with the same techniques as used in evaluation of equations A-3 and A-4 to obtain.

$$E[M(T, t_0) M(T)] = \frac{1}{NT} \sum_{K=1}^N \int_0^T (R(t - Kt_0) + \bar{X}^2) dt \quad (A-16)$$

Substitution of equations A-12, A-14, and A-15 into equation A-2 yields

$$\sigma^2 = \frac{2}{T} \int_0^T \left(1 - \frac{r}{T}\right) R(r) dr + \frac{R(0)}{N} + \frac{2}{N} \sum_{K=1}^{N-1} \left(1 - \frac{K}{N}\right) R(Kt_0) - \frac{2}{NT} \sum_{K=1}^N \int_0^T R(r - Kt_0) dr. \quad (A-17)$$

APPENDIX B

The sampling error for an exponential autocovariance function of the form  $R(r) = B \exp(-|r/\tau_0|)$  may be evaluated using the following relationships:

$$\int_0^T R(r) dr = B\tau_0(1 - e^{-T/\tau_0})$$

$$\int_0^T rR(r) dr = B[\tau_0^2 - \tau_0^2 e^{-T/\tau_0} - T\tau_0 e^{-T/\tau_0}]$$

and,

$$\begin{aligned} \int_0^T R(r - Kt_0) dr &= \int_{-Kt_0}^{T-Kt_0} R(s) ds \\ &= \int_{-Kt_0}^0 R(s) ds + \int_0^{T-Kt_0} R(s) ds \\ &= 2B\tau_0 - B\tau_0 e^{-Kt_0/\tau_0} - B\tau_0 e^{-T/\tau_0} e^{Kt_0/\tau_0} \end{aligned}$$

In addition, note that

$$\sum_{i=1}^N A^i = \frac{A(1 - A^N)}{(1 - A)}$$

Substitution of these relationships into equation A-17 after simplification yields

$$\begin{aligned} \sigma_e^2 &= \frac{2B}{(T/\tau_0)} \left[ -1 + \frac{\tau_0}{2\tau_0} \left( \frac{e^{t_0/\tau_0} + 1}{e^{t_0/\tau_0} - 1} \right) \right. \\ &\quad \left. + \frac{e^{-T/\tau_0} - 1}{(T/\tau_0)} \left\{ 1 - \frac{t_0}{\tau_0} \left( \frac{e^{t_0/\tau_0} + 1}{e^{t_0/\tau_0} - 1} \right) \right. \right. \\ &\quad \left. \left. + \left( \frac{t_0}{\tau_0} \right)^2 \frac{e^{t_0/\tau_0}}{(e^{t_0/\tau_0} - 1)^2} \right\} \right] \end{aligned}$$

## RAINGAGE NETWORK SAMPLING STATISTICS

John L. Vogel

Illinois State Water Survey  
Champaign, Illinois 61820

## 1. INTRODUCTION

Studies of rainfall characteristics using data from dense recording raingage networks will be reviewed. Data from such networks have quantified temporal and spatial rainfall distributions, and have supplied specialized information about local and orographic effects. The natural variability, temporally and spatially, for annual, seasonal, monthly, and individual events will be treated. Especially important are the spatial variations of precipitation as a function of synoptic type, precipitation type, amount, and duration. Much of this review will concentrate on results from dense raingage networks in Illinois, but some data from other climatic regions will also be treated.

A major portion of the data analysis of the dense raingage networks in Illinois has defined the natural variability of annual, seasonal, and individual rain events. Early in the analysis of network data in the 1950s, the Water Survey coined the term 'storm' to describe a discrete period of rainfall within a fixed network area. Huff (1966), in a study of rainfall on a dense raingage network of 1000 km<sup>2</sup>, developed an objective definition of storm as "any rain period separated by more than 6 hours without rain on the network." This definition of 'storm' allowed discrete rain periods to be identified with specific weather systems. The operation of larger networks with areas greater than 5000 km<sup>2</sup> necessitated an altered storm

definition (Vogel and Huff, 1978), consisting of time-space delineations for individual rain events. For these larger networks a storm was considered to be a rain period identified with a specific synoptic weather event and separated from other rain areas by 32 km and more than 1 hr between rain events at any gage.

## 2. RAINFALL VARIABILITY

An important measure of rainstorm climatology is the natural variability of rainfall with duration. Table 1 from Huff (1969) shows how the climatological distribution of storm mean precipitation is related to storm duration based on an assessment of 12-years of data from a 1000 km<sup>2</sup> network in east central Illinois. For example, reading horizontally in the upper portion of the table it is seen that with durations of 3 hr or less on the network, 28% of the total precipitation, on the average, will result from a network mean exceeding 12.7 mm, whereas this percentage increases gradually to 95% with durations in excess of 24 hr. Reading vertically in the upper portion of Table 1 an estimate of the distribution of storm mean rainfall in each duration category is obtained. Thus, for storms with durations of 3 hr or less, 80% of the rainfall, on the average, results from a network means exceeding 2.5 mm compared with 7% in storms exceeding 25.4 mm. The lower part of Table 1 shows how storm duration affects the relation between storm mean rainfall and the frequency distribution of storm occurrences. For example, it indicates that for a duration of 3 hr or less that only 26% of the storms, on the average, have an areal mean rainfall greater than 2.5 mm, and that only 26% of the storms with durations less than 3 hr account for 80% of the rain associated with these storms. This



ORIGINAL PAPER  
OF POOR QUALITY

table stresses the importance of the storm duration factor in the establishment of the distribution characteristics of storm precipitation in this climatic region.

TABLE 1. Average 12-yr Distribution of Network Storm Precipitation Grouped by Storm Duration

Network mean storm precipitation (mm) exceeded	Cumulative percent of total precipitation for given duration (hrs)					Cumulative percent, all storms combined
	$\leq 3$	3.1-6.0	6.1-12.0	12.1-24.0	24.1-48.0	
25.4	7	22	29	54	80	41
12.7	28	52	61	85	95	70
6.3	52	79	87	96	99	86
2.5	80	93	96	99	>99	95

Network mean storm precipitation (mm) exceeded	Cumulative percent of total storm occurrences for given duration (hrs)					Cumulative percent, all storms combined
	$\leq 1$	1.1-2.0	2.1-4.0	4.1-8.0	8.1-16.0	
25.4	<1	4	8	26	53	7
12.7	2	15	26	56	78	19
6.3	9	34	52	80	89	33
2.5	26	60	80	95	96	50

The last column in Table 1 indicates that 7% of the storm accounted for 41% of all precipitation, and that only half of all storms account for 95% of the total rainfall. Garstang (1972) notes that in the Tropics, 10% of the time during which precipitation falls produces 50% or more of the total precipitation. Thus, even though there are many storms associated with precipitation, a small number of these storms are responsible for most of the precipitation.

Equally important is the distribution of total precipitation by warm and cold-seasons. Warm-season (May to September) rainfall is characterized synoptically by scattered showers, semi-organized to organized mesoscale systems, and a few large-scale cyclonic storms (Vogel and Huff, 1978). The cold season (October-April) precipitation typically is dominated by

organized large-scale cyclonic motions and well-organized mesoscale systems, such as squall lines (Huff and Schickedanz, 1970). In Table 2, the percent of total precipitation and percent of total storm occurrences for the warm and cold seasons are given for various storm durations (Huff, 1971). During both seasons, storm durations of 3 hr or less were most frequent. However, over 20% of all precipitation falls from these storms during the warm season and less than 10% of the precipitation occurs within these storms during the cold season. In the warm season 63% of the precipitation occurs with storms of less than 12-hr duration, whereas 59% of the precipitation during the cold season occurs with storms greater than 12-hr. This reflects the difference in the synoptic weather regimes from the warm to the cold season. The warm season rains are mainly convective and often occur within a tropical air mass; during the cold season the precipitation occurs in cyclonic storms near or in the boundaries of cold air masses. Thus, there are major differences between the durations of warm- and cold-season precipitation.

TABLE 2. Average Distribution of Precipitation on a 1000 km<sup>2</sup> Raingage Network in East-Central Illinois Grouped by Storm Duration.

<u>Storm Duration</u>	<u>Percent of total precipitation</u>		<u>Percent of storms</u>	
	<u>May-Sept</u>	<u>Oct-April</u>	<u>May-Sept</u>	<u>Oct-April</u>
≤3	22	9	57	35
3.1- 6.0	21	11	20	19
6.1-12.0	20	21	12	22
12.1-24.0	23	40	8	19
24.1-48.0	13	16	3	5
>48	1	3	0+	0+

Precipitation type helps to define the spatial and temporal characteristics of precipitation. Thunderstorms dominate summertime warm-season precipitation, frequently being the major producer of rainfall intermingled with light rainshowers. During a 12-yr period (1955-1966) over a 1000-km<sup>2</sup> network in east-central Illinois, Huff and Schickedanz (1970) found that the combination of thunderstorms and rainshowers accounted for 88% of the May-September rainfall and were associated with 87% of the storm occurrences. From October to April the thunderstorm-rainshower combination were observed with 40% of the storm occurrences, but 55% of the total precipitation. Stable-type rains accounted for about 30% of all precipitation and storm occurrence in the cold season. Snow and rain mixed with snow were associated with 30% of the cold-season storms, but only 14% of the total seasonal precipitation.

### 3. PRECIPITATION GRADIENTS

The variation of point rainfall with distance is another method of evaluating spatial variability of precipitation. Results from studies in Illinois (Huff, 1967), Florida (Woodley et al., 1975), and the southwest United States (Osborn et al., 1980) are presented (Table 3). The Illinois analysis had a total of 186 storms in the period 1950-1954 from two networks over flat agricultural lands. One network consisted of 25 gages in 260 km<sup>2</sup> and the other had 50 gages in 260 km<sup>2</sup>. All analysis were confined to convective rainfall occurring from spring to fall with durations of 24 hours or less. Synoptically, the precipitation ranged from air mass showers to organized mesoscale systems to some large-scale precipitation events. The Florida data consisted of 127 storms collected during the summers of 1971

and 1973 as part of the Florida Area Cumulus Experiment. This raingage network had 186 separate gage locations spread over 570 km<sup>2</sup> of flat agricultural land. The dominant rain type during the period was air mass showers. The Southwest United States data was derived from the 150 km<sup>2</sup> Walnut Gulch Experimental Watershed in southeastern Arizona with 95 gages and the 174 km<sup>2</sup> Alamogordo Creek Experimental Watershed in eastern New Mexico with 65 gages. The precipitation gradient presented from the last two networks represent individual air mass thunderstorms.

Table 3 presents the percent changes in rainfall with distance normalized by dividing from a central gage. The Illinois data was stratified by areal average rainfall and showed that the relative variability decreased with increased rainfall volume. This is reflected by the changes in the rainfall gradient for those storms which had network average rainfall of 2.5, 6.3, and 25 mm which are average curves. Huff, also, calculated extreme precipitation gradients which are expected to occur less than 5% of the time. Such a gradient for a 25-mm storm is given in Table 3. The extreme gradient decreases much more rapidly than the average curve. For example, at 10 km for an average gradient the precipitation would be expected to be 74% of the central gage, whereas in an extreme gradient situation the precipitation at 10 km is 36% of the central gage. The extreme gradients are about 2.5 times the average values.

The Florida data was analyzed for N-S and E-W profiles of precipitation change with distance. These profiles were averaged for Table 3, since the results suggested symmetry in all directions and the differences were minor. The variation of precipitation with distance changes rapidly, and by 10 km only 17% of the point maximum precipitation is expected, on the average.

The average Florida gradient is more extreme than the average Illinois curves, and are more comparable to the extreme Illinois curves. This reflects the predominate air mass shower activity in Florida.

The Arizona and New Mexico data presented in Table 3 represent the precipitation gradients from extreme air mass thunderstorms derived from area-depth curves (Osborn et al., 1980). As a result, the values represent smoothed gradients for these extreme events. The gradient for the storm over Walnut Gulch, Arizona, resembles the extreme 25-mm gradient in Illinois for the first 6 km, but then the gradient changes sharply and resembles the average Florida curve. The precipitation gradient over Alamogordo Creek, New Mexico, is relatively smooth and falls between the 6.3- and 25-mm Illinois gradients. Thus, for individual storms extremely sharp changes in precipitation gradient can be anticipated.

Average monthly and seasonal precipitation gradients have been calculated by Huff (1971) for Illinois. The percent change of precipitation with distance depended upon the average precipitation for the area, with the sharper gradients occurring with lighter rainfalls. Extreme percent differences of as much as 65% over 16 km for monthly values and 15 to 20% over 16 km for seasonal values can be expected. On the average, in Illinois monthly differences of 25 to 35% can be expected in the warm season (May to September) and 10 to 15% differences are found in the cold season (October to April). Woodley et al. (1975) for 3 months of data in Florida measured an extreme gradient of 355 mm in 6 km. Thus, individual months or seasons, especially in those regions characterized by convective rainfall, can expect extreme changes in precipitation amounts over relatively short distances for individual storms, months, or seasons.

TABLE 3. Precipitation Gradients for Illinois, Florida, and Southwest United States Expressed as Percent Change

Distance	Illinois				Florida	Arizona	New Mexico
	Average		Extreme		Average	Storm	Storm
	2.5 mm	6.3 mm	25 mm	25 mm			
1	57	83	90	76	73	80	95
2	37	71	86	66	59	69	90
3	24	63	83	57	48	60	85
4	14	57	80	53	40	50	80
5	0	52	79	49	33	45	76
6	0	48	78	45	28	42	71
7	0	45	77	43	24	35	67
8	0	43	76	40	21	25	63
9	0	42	75	38	19	17	60
10	0	41	74	36	17	11	57

#### 4. CORRELATION ANALYSIS

Annual--Annual correlation patterns were obtained for Illinois using 36 long-term stations (Huff, 1979). The results showed that the correlation between raingages decreases faster in some direction than in others. These directional differences were primarily due to prevailing storm movements, but the correlations can also be affected by topography and other factors. These results indicated that the optimum raingage spacing for the measurement of annual precipitation in Illinois would require a greater density of raingages in north and south directions than in west and east directions to maintain an equivalent degree of measurement accuracy in all directions.

Table 4 shows median correlation coefficients in each of 8 directions for all stations combined over distances of 40 to 240 km. The largest correlation coefficients at all four distances occurred with NE, E, SW, and W directions, which is in agreement with expectancies from the standpoint of prevailing storm movement. However, differences among directions are not

exceptionally large. For example, the highest correlation at 80 km was 0.76 and the lowest was 0.68. These account for 58% and 46%, respectively, of the variance between point precipitation measurements separated by this distance. For all directions combined, the coefficients of 0.90, 0.72, 0.58, and 0.45 at distances of 40, 80, 160, and 240 km account for 81%, 52%, 46%, and 20% of the variance. Thus, the correlation decay with distance, and, therefore, the representativeness of point precipitation measurements, decreases quite rapidly.

TABLE 4. Correlation Decay of Annual Precipitation with Distance and Direction for Illinois

<u>Direction</u>	Median coefficient at given distance (km)			
	<u>40</u>	<u>80</u>	<u>160</u>	<u>240</u>
NE	0.93	0.76	0.63	0.52
E	0.92	0.75	0.60	0.55
SE	0.89	0.71	0.57	0.38
S	0.88	0.69	0.53	0.38
SW	0.90	0.73	0.62	0.53
W	0.90	0.73	0.60	0.50
NW	0.85	0.68	0.51	0.33
N	0.89	0.72	0.55	0.38
All directions combined	0.90	0.72	0.58	0.45

Monthly and Seasonal--Huff (1979) used data from two dense networks in east central and southern Illinois to investigate monthly and seasonal correlation patterns. Analyses were restricted to the May-September period. Convective precipitation dominates in this period and the spatial variability in rainfall was obtained (Huff, 1966). Correlation coefficients were calculated for distances of 3.2 to 32 km. Results of the monthly and seasonal analyses combining data from both networks are summarized in

Table 5. Only small differences occurred between monthly and seasonal correlation relations so that a total storm sampling network would satisfy sampling for both periods.

TABLE 5. Average Monthly and Seasonal Correlations for May-September in Illinois

Period	Average correlation coefficient at given distances (km)							
	3.2	6.4	9.6	12.8	16.0	19.2	24.0	32.0
Monthly	0.95	0.91	0.89	0.86	0.84	0.83	0.81	0.78
Seasonal	0.95	0.91	0.89	0.87	0.86	0.85	0.84	0.81

Storm--Huff (1979) analyzed the spatial correlation relationships in storms, using data from two Illinois dense raingage networks to provide a range of measurements that included 1-min and 10-min average rainfall rates in addition to total storm rainfall. The two networks were 260 and 1000 km<sup>2</sup>. Analyses were made of the effects synoptic weather type, storm intensity, and duration have upon the spatial distribution of storm precipitation, and are summarized in Table 6.

The data were separated into three basic synoptic storm types through use of published synoptic weather maps of the National Weather Service. Types included frontal storms, low center passages, and air mass storms. Analyses did not show substantial differences in the patterns associated with the various frontal types and squall lines, so all were combined in the frontal storm group (Huff and Shipp, 1969). Low center storms shows little variation with distance, frontal storms decrease somewhat with distance, and the correlation in air mass storms decreases to 0.74 at 16 km. The correlation patterns for the synoptic conditions (not shown) indicate striking differences between air mass storms and low centers. With low



centers the correlation coefficient exceeds 0.90 over the entire 1000 km<sup>2</sup> network, whereas in air mass storms it decreases to less than 0.60 in some directions only 16 km from the central gage.

The storm duration relations in Table 6 are interesting. Correlation decay decreases with increasing duration with storms lasting up to 12 hours, then the trend reverses. A similar behavior was observed in the October-April storms and on other networks, the reversal appears to be real rather than a sampling vagary present in this particular sample of storms. A possible explanation is that the long duration storms are usually associated with extensive synoptic storm systems, and storm movements across the network are more likely to shift during these lengthy storm periods as the weather system approaches and passes.

The mean rainfall groupings in Table 6 indicate that average precipitation within a sampling area has very little effect upon point-to-point correlations. The trend of correlation is very erratic with increasing mean rainfall, and is relatively low in three of the five data groups. Erratic trends and relatively low correlation coefficients were also found during the October-April period.

At the bottom of Table 6 relations are shown for 1-min and 10-min rainfall rates for comparison with grouped storm relations. The 1- and 10-min correlations show rapid decay with distance indicating the great variability in rainfall rates within storms.

## 5. SYNOPTICS

Generally, summer or warm season storms provide the most rainfall variability in the mid latitudes (Huff and Schickedanz, 1970), because of

TABLE 6. Variation of Correlation Coefficient with Distance about Central Gage in Illinois during May-September Storms

Group	Average correlation coefficient for given distance (km)						
	N	1.6	3.2	6.4	9.6	12.8	16.0
Fronts	195	0.98	0.96	0.94	0.91	0.88	0.86
Low centers	28	1.00-	0.99+	0.99	0.98	0.97	0.96
Air mass storms	73	0.97	0.94	0.87	0.79	0.76	0.74
≤ 3 hour	184	0.96	0.91	0.82	0.75	0.70	0.65
3.1-6.0 hour	61	0.97	0.95	0.90	0.86	0.81	0.76
6.1-12.0 hour	29	0.98	0.96	0.93	0.91	0.89	0.87
12.1-24.0 hour	19	0.97	0.95	0.82	0.72	0.69	0.66
0.01-0.10 inch	111	0.96	0.93	0.90	0.88	0.87	0.82
0.11-0.25 inch	53	0.64	0.22	0.05	-0.02	-0.06	-0.10
0.26-0.50 inch	33	0.86	0.69	0.32	0.11	0.06	0.03
0.51-1.00 inch	36	0.84	0.68	0.38	0.22	0.12	0.06
>1.00 inch	19	0.96	0.93	0.88	0.82	0.77	0.71
1-min rain rate							
(Goose Creek)	3142	0.77	0.60	0.40	0.31		
10-min rain rate	2892	0.76	0.61	0.44	0.38		

the convective nature of many of the rain events. A study of the general weather types and of some of the pertinent summertime precipitation characteristics was done for METROMEX (Vogel, 1977; Vogel and Huff, 1978) using available synoptic and mesoscale data for each of the 330 rain events or "storms" which occurred during the 5-summer period from 1971 to 1975. Each storm was classified into general weather types which best defined the rain-producing mechanism of each storm. The eight storm types are given in Table 7. A complete definition of each storm type is given in Vogel (1977). The METROMEX raingage network consisted of 222 raingages distributed evenly over 5100 km<sup>2</sup> surrounding St. Louis. The network was circular and had a radius of 40 km.

The storm type with the greatest frequency of occurrence were air mass storms which made up 27% of all the storms. Air mass storms had no apparent large-scale or mesoscale support and were usually widely scatter to

scattered and weak. However, these storm, even though they were observed most frequently, accounted for only 2% of the total precipitation. The average network mean rainfall for air mass storms was 0.2 mm and the average rainfall recorded in only those gages with rain was 2.8 mm. These storms covered about 7% or 360 km<sup>2</sup>. The individual convective entities covered an area between 20 and 70 km<sup>2</sup>. At a point these storm can provide some locally heavy rains, in excess of 12 mm, but they made up only a small percentage of the storm rainfall over the region for individual events or for a summer. In southwestern United States, which is a semi-arid to arid area, extreme spatial variability has been observed over small areas (Osborn et al., 1980). Such air mass rains typically make up a large part of the annual rainfall.

The next most frequent storm type was squall zones which consisted of semi-organized to organized clusters or groups of showers and/or thunderstorms with motion continuity in time and space. Squall zone storms comprised 25% of the storms and 25% of the total summer rainfall. On the average, they covered slightly more than half of the network, had a network areal average rainfall of 3.4 mm, and those gages with rain in the network averaged 6.4 mm. Squall line storms were the next most frequent storm type over METROMEX. The squall lines were usually intense, well organized lines of convection accompanied by strong, upper-air impulses. Even though these storms only made up 15% of the storms, 51% of all the rainfall was recorded during these storms. The average network rainfall in squall lines was 11.9 mm, for only those gages with rain the average gage amount was 15.7 mm, and 76% of the network had rainfall amounts of 0.25 mm or more. Squall line and squall zone storms were the only two storm types which, on the average, covered more than

half of the network. Cold fronts occurred almost as frequently as squall lines (14%). The rains associated with these storms were often well organized, but occasionally cold fronts moved across the network with only widely scattered convective elements and light rain amounts. Cold front storms accounted for 12% of the total rainfall, had network average rains of 3.1 mm, in only those gages with rain the average point rainfall was 9.4 mm, and the average areal coverage was 33%. Overall, squall lines, squall zones, and cold front storms were often well organized, covered large portions of the network, and consisted of convective elements with locally intense rain rates with large spatial and temporal variations in time and space within the storm and for the whole storm.

In addition, squall line, squall zone, and cold front storms accounted for 54% of all storms which traversed the network, but 88% of the total summer rainfall. For reasonable measurements of climatic precipitation amounts in the Midwest or in regions with a similar climate, it is necessary to be able to measure the rainfall within these storms. Other areas receive a significant portion of monthly, seasonal, or annual rainfall from air mass storms, and to adequately measure rainfall in these regions, it is necessary to be able to delineate rainfall amounts from these storms. Thus, to represent the precipitation amounts from convective storms it is necessary to resolve rainfall amounts from widely scattered air mass storms to well developed showers and thunderstorms organized into meso- and large-scale atmospheric disturbances.

TABLE 7. Summary of Precipitation Results from Synoptic Analysis of 1971-1975 METROMEX Summers

<u>Weather Type</u>	<u>Percent frequency of weather types</u>	<u>Percent of total precipitation</u>	<u>Storm point average precipitation (mm)</u>		<u>Percent of storm area with precipitation</u>
			<u>All gages</u>	<u>Gages with precipitation</u>	
Squall line	15	51	11.9	15.7	76
Squall zone	25	25	3.4	6.4	52
Cold front	14	12	3.1	9.4	33
Stationary front	6	7	3.9	10.9	38
Warm front	4	2	1.6	4.1	36
Pre & Post frontal	8	1.5	0.7	3.3	20
Air mass	27	1.5	0.2	2.8	7
Low	1	+	1.3	5.1	25

Acknowledgments

This paper was prepared under the direction of Bernice Ackerman, Head of the Meteorology Section, and Stanley A. Changnon, Jr., Chief, Illinois State Water Survey. The typing was ably done by Rebecca Runge.

## REFERENCES

- Garstang, M., 1972: A review of hurricane and tropical meteorology.  
Bull. Amer. Meteor. Soc., 53, 612-630.
- Huff, F. A., 1979: Spatial and temporal correlation of precipitation in Illinois. Circular 141, Illinois State Water Survey, Champaign, IL, 14 pp.
- Huff, F. A., 1971: Evaluation of precipitation records in weather modification experiments, in Advances in Geophysics, 15, Academic Press, New York, 59-135.
- Huff, F. A., 1969: Climatological assessment of natural precipitation characteristics for use in weather modification. J. Appl. Meteor., 8, 401-410.
- Huff, F. A., 1967: Rainfall gradients in warm season rainfall. J. Appl. Meteor., 6, 435-437.
- Huff, F. A., 1966: The effect of natural rainfall variability in verification of rain modification experiments. Water Resources Res., 2, 791-801.
- Huff, F. A., and P. T. Schickedanz, 1970: Rainfall Evaluation Studies, Final Report-Part II Description of Individual Studies. Illinois State Water Survey, Champaign, IL, 224 pp.
- Huff, F. A., and W. Shipp, 1968: Mesoscale spatial variability in midwestern precipitation. J. Appl. Meteor., 7, 886-891.
- Osborn, H. B., E. D. Shirley, D. R. Davis, and R. B. Koehler, 1980: Model of Time and Space Distribution of Rainfall in Arizona and New Mexico. Southwest Range and Watershed Research Center, Tucson, AZ, 27 pp.
- Vogel, J. L., 1977: Synoptic weather relations in Summary of METROMEX, Volume 1: Weather Anomalies and Impacts, Bull. 62, Illinois State Water Survey, Champaign, IL, 85-112.

- Vogel, J. L., and F. A. Huff, 1978: Relations between the St. Louis urban precipitation anomaly and synoptic weather factors. J. Appl. Meteor., 17, 1141-1152.
- Woodley, W. L., A. R. Olsen, A. Herndon, and V. Wiggert, 1975: Comparison of gage and radar methods of convective rain measurement. J. Appl. Meteor., 14, 909-928.

18  
N83 25287

Microwave Radiometry Sampling Problems Demonstrated With Nimbus 5  
Rain Rates versus GATE Data

E. Raschke and E. Ruprecht  
Institut für Geophysik und Meteorologie,  
Universität Köln, F.R.G.

1. Introduction

Sampling problems raise large difficulties for the precipitation measurements from space. In the main rain producing area, the tropics, rainfall processes are organized in scales which can be hardly resolved by the microwave radiometers on board of satellites. Even in the cloud clusters, which mark significant, large extended signals in the visible and infrared images, the precipitation areas cover only a small region. Our analysis of the cloud clusters over the W-Pacific Ocean revealed that more than 50% of the area of a typical Western Pacific cluster are without rain (Ruprecht and Gray, 1976). The concentration of the rainfall is seen from the two figures of that analysis (fig. 1 + 2). The radar observations during GATE generally confirmed those results (Houze and Cheng, 1977).

In this study the rainfall was calculated from Nimbus V microwave data at 19.35 GHz and the results were compared with the GATE radar rainfall. It will be shown how the results can be improved if the rain areas within the field of view of the ESMR are determined by additional observations and lead to a correction of the microwave brightness temperature. A first order method is developed which uses simultaneous IR data for the determination of the rain areas. The method will be demonstrated on a few case studies.

2. Data

Five days (Aug. 31, Sept. 2, 4, 5, 7, 1974) are chosen out of the 21 days of phase III of GATE. During these days the subsatellite path of Nimbus V was direct over or very close to the GATE B-area.



ORIGINAL PAGE IS  
OF POOR QUALITY

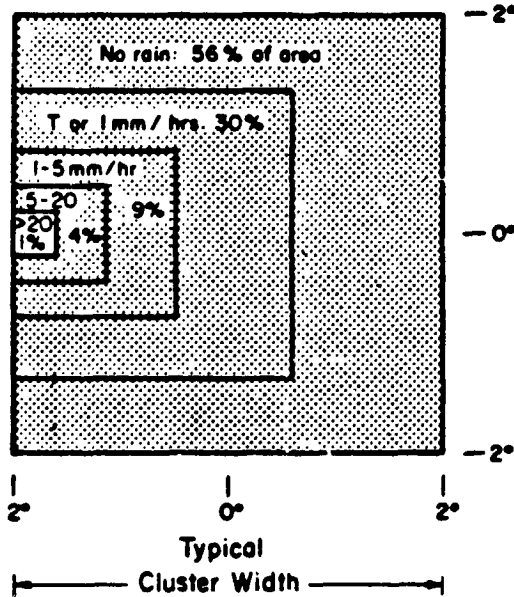


Fig. 1 Area distribution of rainfall intensity within the typical Western Pacific cloud cluster (Ruprecht and Gray, 1976)

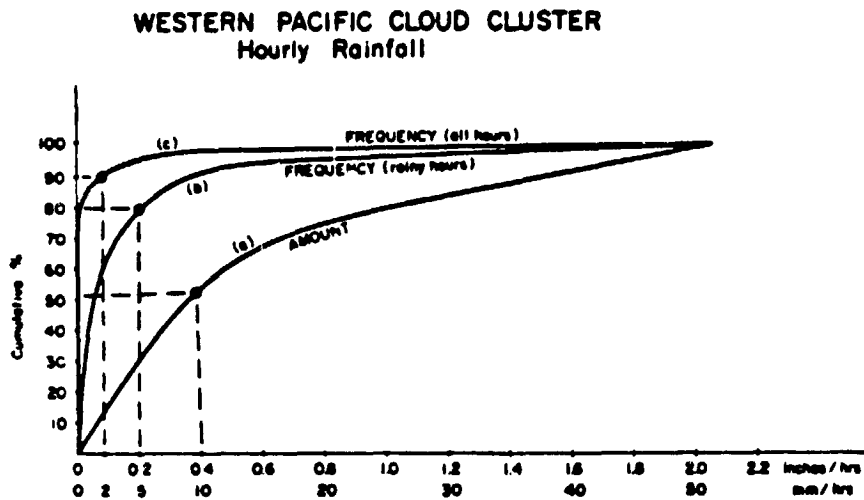


Fig. 2 Western Pacific cloud cluster cumulative rainfall vs. hourly rainfall intensity rainfall amount. Curves b and c portray the cumulative frequency of rainfall vs. rain hours (curve b) and for all hours (curve c) (Ruprecht and Gray, 1976)

The microwave radiances are available once a day at noon with a spatial resolution of 25 x 25 km near nadir.

The rainfall data are derived from radar observations (Hudlow and Patterson, 1979). They are given for each hour with a spatial resolution of 28 x 28 km. All 148 data fields of the so called "Master Array" are used.

The Nimbus V data are rearranged in a grid system with a spatial resolution similar to the radar rainfall data. For the 3 days - Aug. 31, Sept. 2 and 7 - the resolution is 28 x 28 km. For the other two days when the subsatellite path not directly cross the "Master Array" the observations of 2 data fields are averaged to give a resolution of 28 x 56 km.

### 3. Theoretical aspects

The equation of radiative transfer for the microwave region is iteratively solved (Jung, 1980) with the following assumptions and parameters.

- a) The vertical profiles of temperatures and humidities are given by the GATE B-scale mean of phase III. A small correction was applied to the temperature profiles in the rain area given by Gray (1977). Constant mixing ratios are assumed for CO<sub>2</sub> and O<sub>2</sub>.
- b) During the observation period the surface winds were not stronger over the GATE area than 7 m/s, thus we assumed a smooth ocean surface and undisturbed Fresnel-reflection.
- c) The rain clouds are modelled with 2 layers: the lower layer is a pure rain cloud with a Marshall-Palmer rain drop distribution, the upper layer has a thickness of 1 km and contains either cloud drops with a liquid water content of 0.1 g/m<sup>3</sup> or a Marshall-Palmer ice particle distribution for an equivalent rain rate of 5 mm/h. The top heights of the clouds, that is the top of the upper layer, is determined from the radiation temperature in the IR.

#### 4. Correction method

The first test of the derived rainfall rates was done with averaged data. The rainfall rates were calculated for each data field of the "Master Array" and then averaged. These mean rainfall rates for each of the 5 days are compared with the mean radar rainfall in Fig. 3. The curve depicts the theoretically derived relation between microwave brightness temperatures and rainfall rates for clouds with top heights above 5 km.

It is obvious that the rainfall rates will be underestimated if the theoretical curve is applied. That is also true for all individual data fields as shown by the error bars (standard deviation). The results in Fig. 3 can also be interpreted in this way that the observed brightness temperatures are too small for the given rainfall rates. We believe that the main reason for this underestimation is due to the fact that the microwave data with a spatial resolution of 25 x 25 km cannot resolve the individual rain clouds or cells but give an average over an area with rain and large portions without rain (beam filling problem).

It is assumed that the observed brightness temperature  $T_{RG}$  consists of 2 components: the brightness temperature of the rain area  $T_{RR}$  and of the non-raining area  $T_{RK}$ . It is further assumed that  $T_{RG}$  is an area-weighted mean of these two components:

$$T_{RG} = f T_{RR} + (1 - f) T_{RK} \quad (1)$$

$f$  = horizontal fractional area of the rain clouds.

From Eq. (1)  $T_{RR}$  can be calculated with the knowledge of  $f$ .

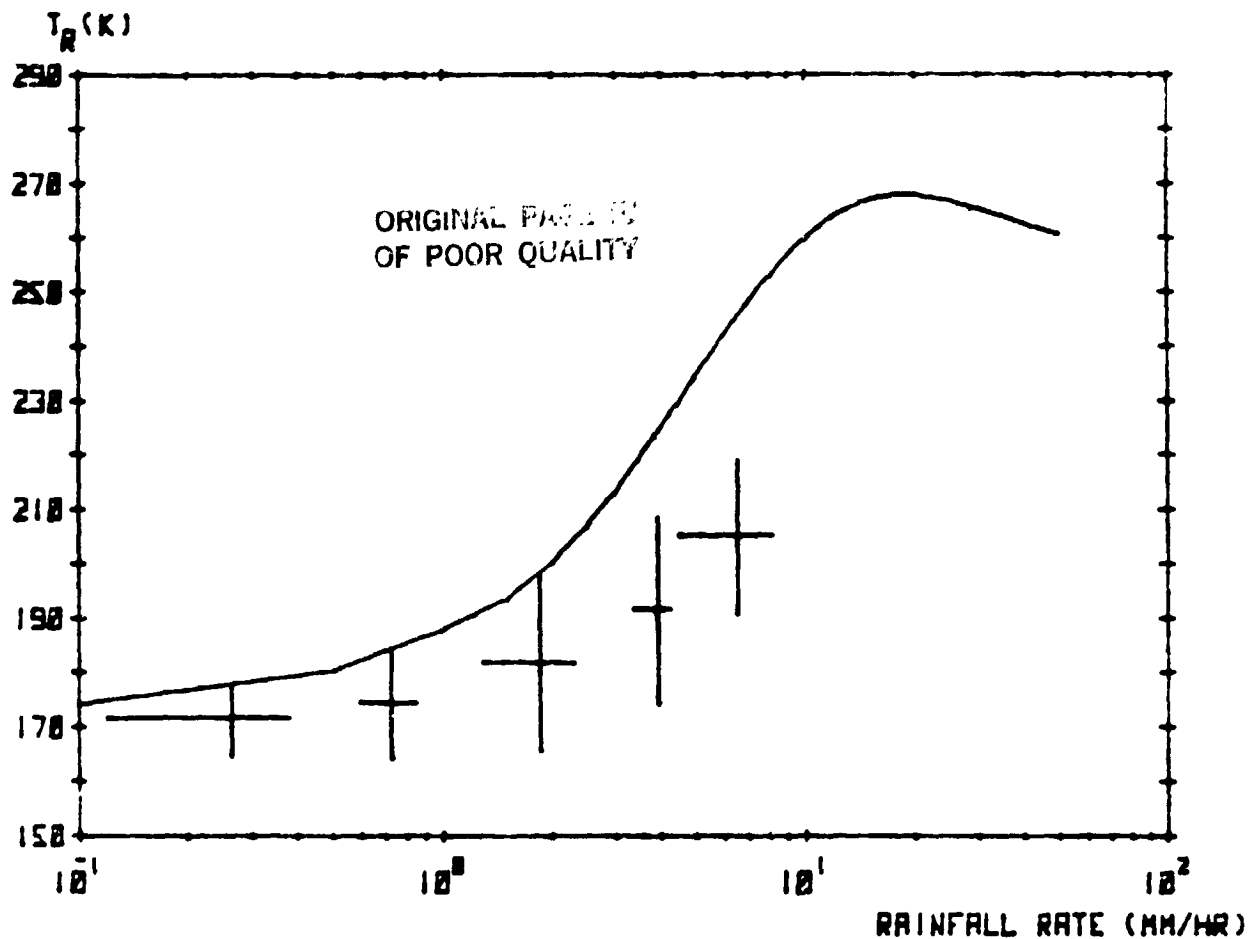


Fig. 3: Mean brightness temperatures against mean radar rainfall rates averaged over all data fields with mean cloud top heights greater than 5.5 km. The bars give the standard deviation (full lines = theoretically derived curve).

The determination of  $f$  is based on the general knowledge about the nature and the distribution of clouds in the tropics and especially on the observations during GATE. The following information can be used:

- a) Clouds with tops below 3.5 km produce no rain (e.g. Riehl, 1979),

ORIGINAL DATA  
OF POOR QUALITY

- b) During Phase III of GATE only 0.2% of the total rain was observed in areas with echo top heights below 5.5 km (Cheng and Houze, 1979).
- c) In the presence of deep convective clouds in the GATE B-area rain occurred only beneath those clouds with top heights above 8.8 km. ( $T_{IR} < 247 K$ ) (Stout et al., 1979).
- d) Nearly 50% of the area with deep convective clouds is non-raining (Cheng and Rodenhuis, 1977).
- e) From the radar observations the fractional coverage of each data field with rain rates greater than 0.5 mm/h is given.

Based on these informations four criteria are assumed to determine the horizontal fractional area of rain cloud f:

Criterion	Information	Assumption about the cloud distribution	Fractional coverage f
1	a)	no	fractional coverage of all clouds with $h > 3.5$ km
2	b)	no	fractional coverage of all clouds with $h > 5.5$ km
3a)	a)+c)	shallow clouds are predominant fractional coverage of deep cloud $h > 8.8$ km is less than 20 %	fractional coverage of all clouds with $h > 3.5$ km
3b)	d)	deep clouds are predominant fractional coverage of deep clouds $h > 8.8$ km is greater than 80 %	50 % of the fractional coverage of all clouds with $h > 8.8$ km
3c)	c)	fractional coverage of deep clouds ( $h > 8.8$ km) is between 20 and 80 %	fractional coverage area of all clouds with $h > 8.8$ km
4	e)	no	fractional coverage of radar rainfall rate $> 0.5$ mm/hr
h = cloud top height			

The threshold (80%) to distinguish the different cloud types in criterion 3 were chosen after a careful study of our data. The brightness temperature for the non-raining areas  $T_{RK}$  was derived from the observed temperatures for the data fields without radar rainfall. The average of 160 K was adopted as a constant value for all non-raining areas.

## 5. Results

For each data field the observed brightness temperature is corrected applying criterion 1 to 4. The top heights of the clouds are determined from the IR observations from SMS 1 with a spatial resolution of 7.5 x 3.5 km. The rainfall rates are computed with the corrected temperatures for each data field. The results are shown in Tab. 1. The first 3 columns give the technical informations, in the 4th and 5th column the comparison is shown between the calculated rainfall rates and the radar rainfall given as total water output over the "Master Array" in absolute (column 4) and relative (column 5) values.

With the uncorrected brightness temperatures the rainfall rates are underestimated by more than 50%. The correction method 3 gives a drastic improvement although then a large deficit is sometimes encountered.

The frequency distributions shown in column 6 give a hint, why the calculated rainfall is underestimated: the frequencies of the intense and low rainfall rates are too small.

It is remarkable that the correction 4, based on the radar rainfall itself, does not give an improvement. The horizontal movement of the disturbances increases the rain area at the surface when averaging is done over a finite time period, thus  $f$  is still too large after the correction.

The results have shown that it is principally possible to overcome some of the sampling problems by applying such a simple

correction method to the brightness temperatures. The method will be further tested with more GATE data and if data available for other regions. Besides the space sampling problem there exist also time sampling problems. In Cologne we are working on that problem although not yet with rainfall data but with radiation observations. I shall show a result which may also be applied to rainfall. The global radiation measurements

Table 1: Comparison of the total water output over the "Master Array" calculated by the radar rainfall and the computed rainfall rates with different correction schemes.

Description of the data	Date Time (GMT)	Ground resolution (km)	Total water output over the GATE Master Array		Frequency distribution of the rain rates				
			10 <sup>6</sup> kg/s	mm	0.1-0.5	0.5-1	1-3	3-5	>5 mm/h
radar rainfall uncorrected T <sub>RR</sub> T <sub>RR</sub> correction to 1 T <sub>RR</sub> correction to 2 T <sub>RR</sub> correction to 3 T <sub>RR</sub> correction to 4	31.08.74 12-13.00	28 x 28	5.2		18	1	3	2	1
			2.0	38	4	4	3		
	12.43		3.0	58	6	9	3		
			2.5	49	1	7	5		
			4.3	84	3	8	6	1	
			3.0	59	2	5	6		
radar rainfall uncorrected T <sub>RR</sub> T <sub>RR</sub> correction to 1 T <sub>RR</sub> correction to 2 T <sub>RR</sub> correction to 3 T <sub>RR</sub> correction to 4	02.09.74 12-14.00	28 x 28	34.4		35	25	45	10	6
			14.2	41	26	15	19	2	
	13.00		14.8	43	27	17	19	2	
			16.5	48	21	26	21	2	
			20.9	61	27	17	23	7	1
			16.8	49	23	24	21	4	
radar rainfall uncorrected T <sub>RR</sub> T <sub>RR</sub> correction to 1 T <sub>RR</sub> correction to 2 T <sub>RR</sub> correction to 3 T <sub>RR</sub> correction to 4	07.09.74 12.-13.00	28 x 28	5.3		42	6	6		
			2.2	42	5	3	4		
	12.47		3.0	57	5	4	6		
			3.1	59	2	6	6		
			3.1	60	4	5	6		
			3.6	68	5	4	6		
radar rainfall uncorrected T <sub>RR</sub> T <sub>RR</sub> correction to 1 T <sub>RR</sub> correction to 2 T <sub>RR</sub> correction to 3 T <sub>RR</sub> correction to 4	04.09.74 13.-14.00	56 x 28	14.6		11	6	3	4	1
			7.2	49	4	10	2	1	
	13.16		8.1	55	5	9	3	1	
			8.5	58	5	10	4	1	
			12.9	88	5	7	9	2	
			10.9	75	2	9	7	1	
radar rainfall uncorrected T <sub>RR</sub> T <sub>RR</sub> correction to 1 T <sub>RR</sub> correction to 2 T <sub>RR</sub> correction to 3 T <sub>RR</sub> correction to 4	05.09.74 12.-13.00	56 x 28	37.5		16	3	15	4	5
			37.2	73	4	8	17	5	
	12.31		38.2	75	9	8	18	5	
			39.7	79	7	9	19	5	
			42.1	112	9	4	17	11	3
			39.7	106	4	5	15	8	4

for 2 years every minute at Zurich are used to derive a simple model which is applied to calculate the daily sum of the radiation with only a few individual observations. Fig. 4 shows the relative error with the integration time for 1 and 3 sampling points per day. The error for actual cases can be large but they decrease after a week of integration. Similar studies are planned for the precipitation thus it will be possible to derive realistic climatological rainfall patterns with only a few observations per day.

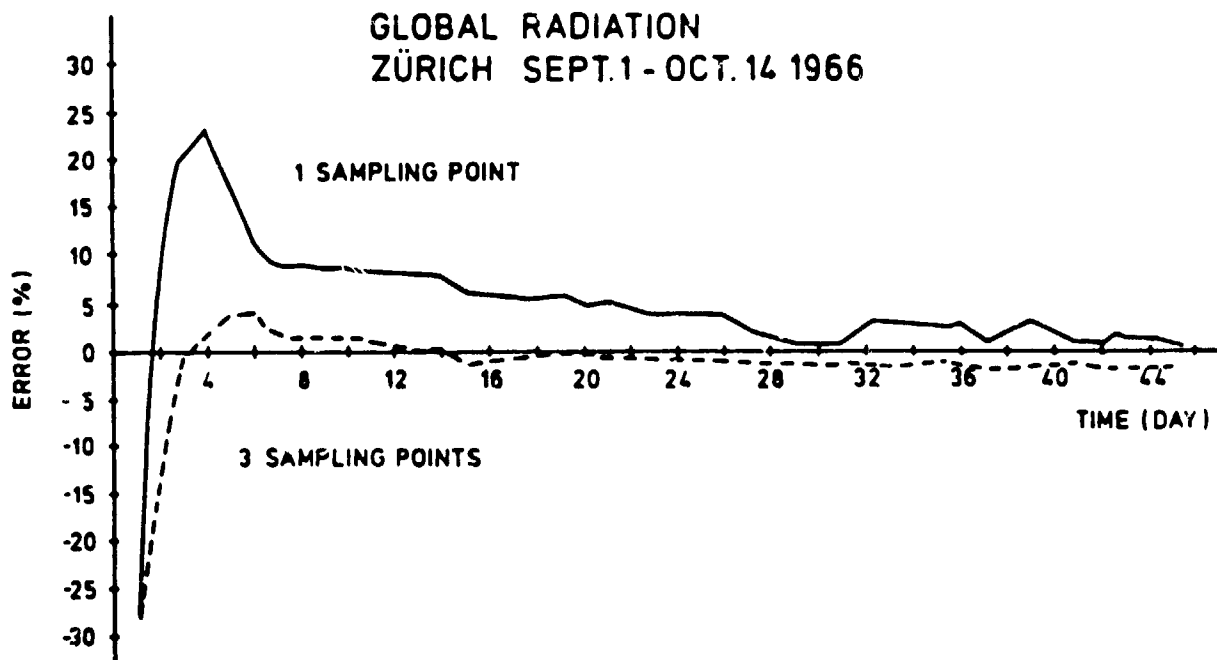


Fig. 4: Relative errors with integration time of the global radiation derived from 1 and 3 observations per day.



## References

- Cheng, C.-P. and R.A. Houze, Jr., 1979: The Distribution of Convective and Mesoscale Precipitation in GATE Radar Echo Patterns.  
Mon. Wea. Rev., 107, 1370 - 1381
- Cheng, N. and D. Rodenhuis, 1977: An Intercomparison of Satellite Images and Radar Rainfall Rates.  
Proceeding of the 11th Technical Conference, Hurricanes and Tropical Meteorology, Dec. 13 - 16, 1977, Miami Beach, Fla., USA
- Gray, W.M., 1977: Tropospheric Mean State and Variability.  
Report of the U.S. GATE Central Program Workshop; Boulder, Colorado, 199 - 213
- Houze, R.A. and C.-P. Cheng, 1977: Radar Characteristics of Tropical Convection observed during GATE: Mean Properties and Trends over the Summer Season.  
Mon. Wea. Rev., 105, 964 - 980
- Hudlow, M.D. and V.L. Patterson, 1979: GATE radar rainfall atlas.  
NOAA Special Report, Center for Env. Ass. Serv., NOAA, 155 pp.
- Jung, H.J., 1980: The determination of rainfall from satellite measurements of the thermal microwave emission.  
Beitr. Phys. Atm., 53, 366 - 388
- Riehl, H., 1979: Climate and Weather in the Tropics.  
Academic Press, London, New York, San Francisco, 611 pp.
- Ruprecht, E. and W.M. Gray, 1976: Analysis of satellite-observed tropical cloud clusters.  
II Thermal, moisture and precipitation fields.  
Tellus, 28, 414 - 426
- Stout, J.E., D.W. Martin and D.N. Sikdar, 1979: Estimating GATE rainfall with geosynchronous satellite images.  
Mon. Wea. Rev., 107, 585 - 598

D19

N83 25288

ORIGINAL SOURCE  
OF PUBLICATION

A STANDARD VERIFICATION FOR RAINFALL ESTIMATION FROM REMOTE PLATFORMS

José G. Meitín<sup>1</sup>, Cecilia G. Griffith<sup>2</sup>, John A. Augustine<sup>2</sup>, and William L. Woodley<sup>2</sup>

<sup>1</sup> Cooperative Institute for Research in Environmental Sciences, Boulder, CO.

<sup>2</sup> Office of Weather Research and Modification, NOAA/ERL, Boulder, CO.

1. INTRODUCTION

Rain estimation from space affords the hydrologic community the opportunity to monitor precipitation over time and space scales not before possible from in situ means. To be able to estimate accurately the precipitation over very large areas and for long periods of time offers the agriculturalist a solid input of the most crucial variable in crop prediction models. Likewise, hydrologists can better assess the water supply through estimates of precipitation over large uninstrumented watersheds. Climatologists also have an interest. Through monthly precipitation estimates over the tropical oceans, climatologists can more accurately determine the energy budget of the earth's climate machine. There is indeed a wide range of interest in rain estimation, and, as a consequence, just as wide a range of scales of interest. This leads to the question of whether or not existing techniques supply the required accuracies at the various scales of interest.

In this paper a method which objectively analyzes the performance of rain estimation techniques is described. It is applicable to any form of rain estimates but, for the sake of brevity, only results from the Griffith/Woodley satellite rain estimation technique are tested in this study. Rain estimates over south Florida are compared over a 9350 km<sup>2</sup> area equipped with rain gages at a 11 km spacing. Several statistical tests, outlined by Flueck (1981) and Huff (1970) are conducted on the error (S-G) for various space and time scales. Results, although preliminary, allow the community to objectively determine the feasibility of the use of satellite rain estimates at various scales of interest.

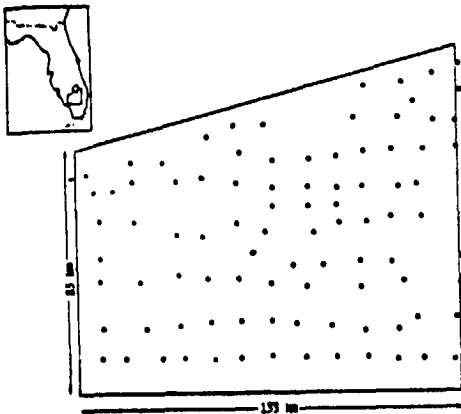


Figure 1. Recording rain gauge locations in the FACE target area.

2. DATA BASE

In conjunction with the Florida Area Cumulus Experiment (FACE), a weather modification project, raingages were deployed over a 13000 km<sup>2</sup> area in south, central Florida. The approximate gage locations are shown in figure 1. There were 100 raingages operating in the quadrilateral area of the FACE target during the summer of 1978.

Data are recorded in 5-minute increments and for this exercise were integrated over 30 minute periods. The analysis was carried out from 1200 to 2100 local daylight time.

For the purpose of this analysis, the data points were transferred to an evenly-spaced grid. This was done by applying objective analysis routines described by Cressman (1959). Basically the scheme works as follows: The area is subdivided into a grid system with points spaced every 11 km. These represent centroids to areas of influence of each raingage value. A computer program is used to search out the two raingage locations closest to the gridpoint and a weighting function is derived based on the relative distance of these gages. If a raingage falls within 2 km of the gridpoint, the actual gage value is assigned to that gridpoint. The distribution of gridpoints using such a scheme is depicted in figure 2. Bi-linear interpolation is then used to derive 2 intervening values; leading to one ground value every 3.7 km.

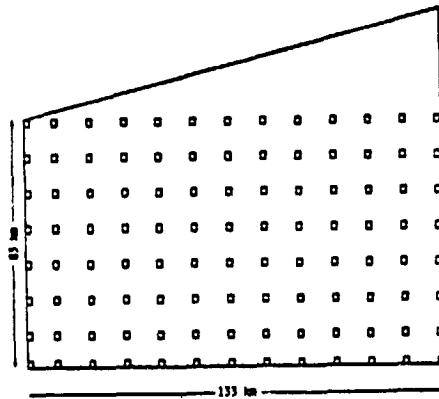


Figure 2. Grid for the Cressman-interpolated raingage values

Nominally, infrared satellite imagery is recorded every 30 minutes. Full resolution grid spacing is approximately 8 km (i.e. two objectively analysed gage values on a side). This allows us to compare, one to one, ground values and satellite derived values over common area and time scales.

The satellite technique used for this demonstration is the Griffith/Woodley convective rain estimation technique. It is a computer-automated, life history technique described in these proceedings (Griffith & Woodley, 1981). This technique was empirically derived over south Florida and applicability of the results of these error analyses to areas climatically dissimilar to Florida should be questioned. Ultimately, the performance of any rain estimation technique should be tested over various climate regimes.

For the purpose of this workshop, 13 FACE cases in 1978 were processed. Comparisons were made over 4 subareas beginning with the single pixel resolution at 55 km<sup>2</sup>. It should be noted that all error analyses are the combined effect of errors due to the satellite technique and errors inherent in the sampling of rainfall at this raingage density. Work by Huff (1970) suggests that in basins (<1500 km<sup>2</sup>) instrumented with one gage every 55 km<sup>2</sup>, the sampling error due to raingage density can be as large as 40% in light rain cases (< 2 mm).

The grid array used for the satellite estimates is shown in figure 3. Note the area is within the boundaries of the ground network in order to eliminate any trending caused by the objective analysis scheme. The subareas of comparison between the satellite-inferred and raingage-derived rainfalls are also shown; these areas are: 1) each full resolution pixel (55 km<sup>2</sup>), 2) four pixels combined (220 km<sup>2</sup>), 3) the four quadrants of the target area (2200 km<sup>2</sup>), and 4) the full rectangular area covering most of the target (9350 km<sup>2</sup>). The temporal resolution is similarly degraded from the best satellite resolution of 1/2 hr through 1-1/2, 3, and 6 hr comparisons.

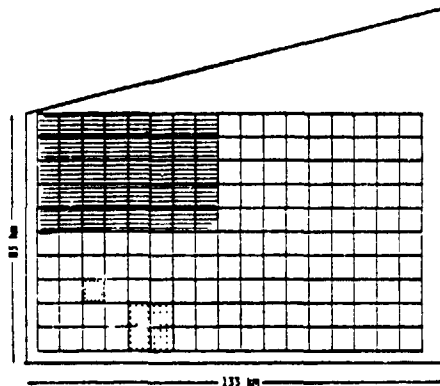


Figure 3. Satellite imagery grid spacing and subareas of comparison in the FACE target area.

#### STATISTICAL ANALYSES AND RESULTS

The data were analyzed by fitting a linear regression and by computing the mean square error. For the linear regression analyses the slope, intercept and correlation coefficient were computed in the usual manner. The mean square error, MSE, is defined as

$$MSE(d) = (d_1)^2 / (n-1) \quad (1)$$

and

$$d = S - G \quad (2)$$

where S is the mean satellite and G is the mean gage estimate. The mean square error can be decomposed into the standard deviation (Var) and the bias (B) of the difference, d:

$$MSE(d) = Var(d) + B^2(d). \quad (3)$$

Because we used only a small subset of the total FACE sample, all results shown here should be viewed as preliminary.

In performing the linear fits we regressed the satellite-inferred rainfall as the dependent variable and the gage-estimated rainfall as the independent variable. In order to present the worst possible case, points for which both the satellite and gage values were zero were not used. Both the satellite and gage estimates were accumulated over the 16 combinations of the 4 space and 4 time scales discussed in section 2. Results of the linear fits are shown in Figure 4 and Table 1. Figure 4 is a plot of the correlation coefficient as a function of area (along the abscissa) and period of accumulation (the family of curves). As can be seen, the correlation coefficient improves as either the length of the calculation or the area of interest increases, and ranges from 0 at half-hourly estimates for one pixel to .92 for 6-hourly estimates over 9350 km<sup>2</sup>. The values in Table 1 show that the slope approaches 1.00 as the space and time parameters increase. For a given time period the regression intercept decreases as a function of network size. For a given area, though, the preliminary results show a different trend. At the two smallest areas the intercept increases with time, whereas for the two largest areas the intercept initially increases and then decreases as the period of calculation lengthens. It is possible that the intercept results for the two smallest areas would show the same trend if longer time periods were included in the analysis.

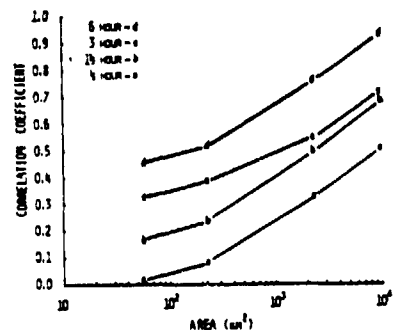


Figure 4. Correlation coefficients over varying time and space scales.

The results for the mean square error are shown in Figures 5 and 6 for the bias and standard deviation of the difference respectively. In these figures, both the bias and the standard deviation have been normalized by the mean gage value for the basin of interest.

## ORIGINAL PAPER OF POOR QUALITY

Mean gage values are shown in Table 2. The mean bias of the error is roughly 0.15 for all network sizes at 1/2, 1-1/2 and 3 hours; that is, the satellite estimates are systematically 15% higher than the mean gage value. The mean bias decreases to 0 for all network sizes accumulated over 6 hours. Similar to what was seen with the linear regressions, the standard deviation of the error again decreases as time and space increase.

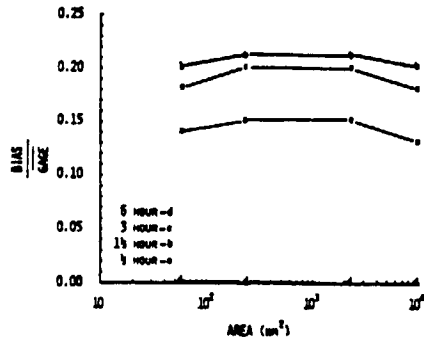


Figure 5. Systematic error over varying time and space scales.

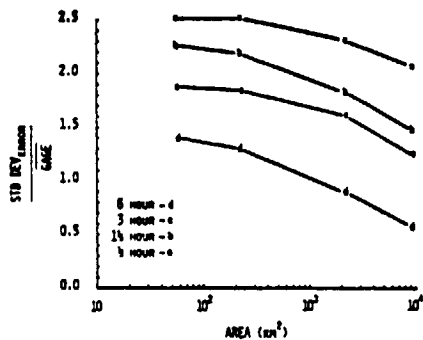


Figure 6. Sampling error over varying time and space scales.

#### 4. FUTURE WORK

We intend to use the Statistical Package for the Social Sciences (SPSS) (Nie et al., 1975) to fit a multivariate regression to these mean square error data. The regression would take the form

$$E = b_0 + b_1\bar{R} + b_2A + b_3T + b_4\bar{R}A + b_5\bar{R}T + b_6AT + b_7X^2 + \dots \quad (4)$$

where  $E$  is mean square error,  $\bar{R}$  is mean rain in the network,  $A$  the area of the network,  $T$  the length of the calculation and  $X^2$  represents higher order terms in these variables. This regression would summarize the results shown in Figures 5 and 6 and, moreover, would permit any potential user to ascertain the error inherent in using our satellite technique over the time and space scales of the user's interest.

TABLE 1

Slope (top line) and intercept (bottom line) values for the linear regressions as a function of space ( $A \text{ km}^2$ ) and time ( $T \text{ h}$ ).

T \ A	55	220	2220	9350
1/2	.01	.06	.37	.80
	1.63	1.18	.46	.14
1-1/2	.13	.21	.62	1.07
	3.10	2.33	.87	.15
3	.28	.37	.66	.97
	4.2	3.33	1.63	.56
6	.38	.47	.92	1.23
	4.90	3.80	.42	-1.50

Before an accurate assessment of the errors in the Griffith/Woodley satellite technique can be made, all 51 experimental case days of FACE will be processed. At that time, work by Barnston and Thomas (NOAA/ERL) will provide a ground truth data set based on a hybrid system of raingages and radar which will potentially achieve a density of one value every 12  $\text{km}^2$ , thus reducing any errors attributed to the sampling of rainfall from ground-based systems. Ultimately, an accurate analysis must be performed separating the errors derived from the ground measurements and those derived from the satellite estimation technique.

TABLE 2

Mean gage rainfalls (mm) as a function of space ( $A \text{ km}^2$ ) and time ( $T \text{ h}$ ).

T \ A	55	220	2220	9350
1/2	1.44	1.10	0.59	0.42
1-1/2	2.86	2.33	1.48	1.18
3	4.72	4.00	3.01	2.74
6	8.10	7.36	6.29	6.07

ORIGINAL PAGE IS  
OF POOR QUALITY

5. SUMMARY

A verification method to assess the relative error in rainfall techniques over a spectrum of spatial and temporal resolutions has been proposed. Initial results from the verification analysis show an average systematic error of 15% for the Griffith/Woodley rain estimation technique. An improvement was found for increasing temporal and spatial scales. A useful data set is offered for other experimenters to compare their results over a densely instrumented area. Lastly, we acknowledge the need to quantify the errors in techniques to estimate rainfall from remote platforms.

6. REFERENCES

- Cressman, G.P., 1959: An operational analysis system. Mon. Wea. Rev., 87, 367-374.
- Flueck, J.A., 1981: Some statistical problems inherent in measuring precipitation. NASA Workshop on Precipitation Measurements from Space. April 28 - May 1, 1981.
- Griffith, C.G. and W.L. Woodley, 1981: The estimation of convective precipitation from GOES imagery with the Griffith/Woodley technique. NASA Workshop on Precipitation Measurements from Space. April 28 - May 1, 1981.
- Huff, F.A., 1970: Sampling errors in measurement of mean precipitation. J. Appl. Meteor., 9, 35-44.
- Nie, N.H., C.H. Hull, J.G. Jenkins, K. Steinbrenner and D.H. Bent, 1975: SPSS, Statistical Package for the Social Sciences. McGraw-Hill, New York, 675pp.

D20

N83 25289

ORIGINAL PAPER  
OF POOR QUALITY

THE DIFFERENTIAL REFLECTIVITY DUAL POLARIZATION METHOD  
OF RAINFALL MEASUREMENTS

Thomas A. Seliga and V. N. Bringi

Atmospheric Sciences Program and Department of Electrical Engineering  
The Ohio State University  
Columbus, OH 43210

ABSTRACT

Measurements of reflectivity at horizontal ( $Z_H$ ) and vertical ( $Z_V$ ) polarizations provide adequate information necessary to infer the two parameters of an exponential raindrop size distribution ( $N_0, D_0$ ) where the distribution is given by  $N(D) = N_0 \exp(-3.67 D/D_0)$ . This distribution in turn enables one to compute water content or still air rainfall rates. The physical basis of the radar technique is outlined and illustrated theoretically, and experimental results, comparing radar-derived rainfall rates with raingauge and disdrometer measurements, are reviewed. The technique should prove useful for many meteorological and hydrological purposes, including ground truth measurements of rainfall rate over the ocean for comparison with satellite-related observations.

1. INTRODUCTION

The accurate measurement of rainfall by remote sensing, especially by satellite, is fundamentally important to an improved understanding of climate, earth resources and atmospheric-oceanic processes. [Martin and Scherer, 1973; Wilhelm et al., 1977; Vizee et al., 1978; Izrael, 1979]. Although a number of satellite measurement schemes have been devised for this purpose, they all suffer from one or more attendant problems as outlined by Atlas (1980). These problems result from effects of clouds and variations in humidity, variations in effective rain layer extent, limited spatial resolution and limited temporal resolution. In addition, every technique employed thus far depends upon empirical hypotheses which require ground truth observations for testing and evaluation. This paper addresses this latter need through the consideration and exploitation of the recently developed differential reflectivity ( $Z_{DR}$ ) radar technique introduced by Seliga and Bringi (1976) for the quantitative ground-based measurement of rainfall.

2. REVIEW OF THEORY

The  $Z_{DR}$  radar technique utilizes measurements of reflectivity factor at horizontal ( $Z_H$ ) and vertical ( $Z_V$ ) polarizations to quantify rainfall intensity and estimate drop size distributions.  $Z_{DR}$  is given by

$$Z_{DR} = 10 \log Z_H/Z_V \text{ dB} \quad (1)$$

$$Z_{H,V} = \frac{\lambda^4}{\pi^3 |K|^2} \int_0^{D_m} \sigma_{H,V} N(D) dD \text{ cm}^6 \text{ m}^{-3} \quad (2)$$

and, when combined with either reflectivity

factor, yields estimates of the two parameters ( $N_0, D_0$ ) of an assumed exponential drop size distribution.

$$N(D) = N_0 \exp(-3.67 D/D_0) \text{ m}^{-3} \text{ cm}^{-1} \quad (3)$$

$D$  is the equivalent spherical diameter of the drops in cm and  $D_m$  is the maximum drop size diameter. Also, although this distribution is not always applicable, it has been found to be representative of most rainfall events and is commonly used by meteorologists.

Rainfall rate ( $R$ ) and volumetric water content ( $M$ ) are related to  $N(D)$  as follows:

$$R = 0.6\pi \int_0^{D_m} D^3 v(D) N(D) dD \text{ mmh}^{-1} \quad (4)$$

$$M = \frac{\pi}{6} \int_0^{D_m} D^3 N(D) dD \text{ g} \cdot \text{m}^{-3} \quad (5)$$

where  $v(D)$  is the terminal velocity of the drops ( $\text{m} \cdot \text{s}^{-1}$ ). Note that  $N(D)$  or equivalently rainfall is described by two parameters and, therefore, at least two radar observables are required to obtain estimates of them. It is for this reason that the conventional radar method of measuring rainfall using Z-R relationships [Battan, 1973; Wilson and Brandes, 1979] fails to quantify rainfall rate adequately.

The  $Z_{DR}$  signal derives from the non-spherical shape and nearly common alignment of raindrops falling at terminal velocity in the atmosphere. Furthermore, since each raindrop has its own characteristic oblate spheroidal shape [Pruppacher and Beard, 1971],  $Z_{DR}$  is uniquely a measure of drop size, or, as in the case of an

## ORIGINAL PAPER OF POOR QUALITY

exponential distribution, it can be used to estimate  $D_0$ . Introducing either reflectivity factor  $Z_{H,V}$  then gives  $N_0$  as illustrated in Fig. 1.

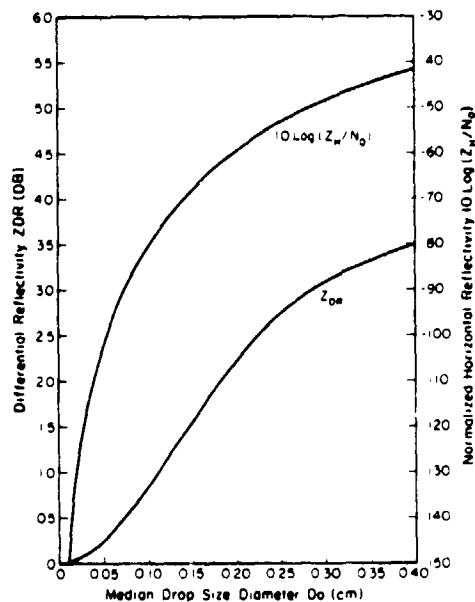


Figure 1. Theoretical basis for the ZDR radar technique.

This theory can be used to derive an equation for R

$$R = \frac{6.82 \times 10^{-3} Z_H}{(Z_{DR} + 0.47)^{4.45}} \quad \text{mm h}^{-1} \quad (6)$$

$0.5 \leq Z_{DR} \leq 4.8\text{dB}$

where  $Z_H(\text{mm}^6\text{m}^{-3})$  and  $Z_{DR}(\text{dB})$ .

### 3. THE ZDR RADAR SIGNAL

Several schemes are available to measure  $Z_{DR}$  [Bringi et al., 1980]. The most desirable scheme utilizes pulse-to-pulse switching between polarizations and a square-law or power estimator.

$$Z_{DR} = 10 \log \left[ \frac{\frac{1}{m} \sum_{i=1}^m A_{H1}^2 / \frac{1}{m} \sum_{i=1}^m A_{V1}^2}{\frac{1}{m} \sum_{i=1}^m A_{H1}^2 / \frac{1}{m} \sum_{i=1}^m A_{V1}^2} \right] \quad (7)$$

where  $A_{H1}, V_1, i=1, m$  are pairwise sets of independently correlated samples of the scattered signal amplitudes at horizontal and vertical polarizations, respectively, and  $m$  is the number of independent sample pairs available. This estimator is asymptotically unbiased and has a theoretical standard deviation as given in Fig. 2. Note that the greater the correlation between the amplitude samples the better the estimator of  $Z_{DR}$ . Data obtained with the Chilbolton Radar facility, operated by the Science Research Council of the United Kingdom, showed that this correlation is consistently high (>0.90) and not very dependent on  $Z_{DR}$  when pulse-to-pulse measurements of  $Z_{H,V}$  are used. These results indicate that it is reasonable to expect standard errors for  $Z_{DR}$  in

the range 0.1 - 0.3dB when around 60 or more independent pairs of highly correlated samples are employed. Thus, a typical 10cm meteorological radar should be capable of measuring  $Z_{DR}$  to very good accuracy in 0.4 - 1.0s at a single range gate, corresponding to times for independence between pulse pairs ranging between 7 - 15ms. Spatial averaging and frequency diversity techniques may be employed to reduce the time period required for measuring  $Z_{DR}$ . A corresponding standard error of  $Z_{H,V}$  would be 1.dB.

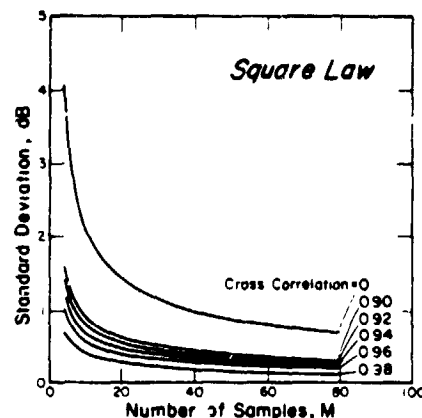


Figure 2. Standard deviation of the square law estimator for measuring  $Z_{DR}$ .

### 4. THEORETICAL STANDARD ERRORS OF RAINFALL RATE ESTIMATES

It is of interest to estimate the standard or random error of the rainfall rate derived from  $Z_{DR}$  measurements. Applying analysis of variance [Barford, 1967] to Eq. (6) gives a fractional standard deviation (FSD) of R

$$\text{FSD} = \left\{ 0.053 \text{Var}(10 \log Z_H) + \frac{(2.45)^2 \text{Var}(Z_{DR})}{[\langle Z_{DR} \rangle + 0.47]^2} \right\}^{1/2} \quad (8)$$

Var represents variance and  $\langle \rangle$  refers to the sample mean. Thus, a typical FSD of a single radar-derived rainfall estimate would be 24% for a  $\langle Z_{DR} \rangle = 2\text{dB}$ ,  $\text{Var}(10 \log Z_H) = 1$  and  $\text{Var}(Z_{DR}) = 0.04$ . Introduction of time and/or spatial averaging would further reduce FSD by  $1/\sqrt{N}$  where  $N$  is the total number of independent contiguous samples. This result implies that random errors in radar R's should be insignificant when applied to most spatial and temporal scales of radar meteorological or climatological importance.

### 5. OTHER ERRORS

In addition to the statistical variability discussed above, systematic biases in the estimate of R may also occur. These may be due to many sources, but the most important ones are expected to be calibration errors in  $Z_{H,V}$  and  $Z_{DR}$ . Deviations from the exponential drop size distribution, raindrop oscillation, raindrop canting and beam-filling problems, could also lead to errors, both statistical and systematic. All of

ORIGINAL PAGE IS  
OF POOR QUALITY

these factors require attention and care in radar design and operation in order to understand completely the limitations of the method. Nevertheless, results to date are very encouraging as are shown in the following sections.

6. CHILL RADAR: RAINGAUGE COMPARISONS

Following the first measurements of Z<sub>DR</sub> [Seliga and Bringi, 1979] in Oklahoma with the CHILL radar, operated by the Illinois State Water Survey, to confirm the existence and practicality of measuring Z<sub>DR</sub>, a comparative radar-raingauge experiment was planned in the Chicago metropolitan area during August 1978. On August 3 this Chicago experiment led to an opportunity to compare time-averaged radar rainfall rate esti-

mates over two separate 550 km<sup>2</sup> areas (see Fig. 3) which contained 26 and 27 gauges each. This gauge density is expected to produce around a 5% standard error in the average rainfall rate over these areas when averaged over a 1 h time period. Therefore, the gauge results provide a good standard for comparison if a rainfall event over the two areas lasts for around 1 h. These conditions were met on this day and produced the results shown in Tables 1 and 2 which compare rainfall rates in each of the two 550 km<sup>2</sup> sectors and their seven subsectors. R obtained from the Z<sub>DR</sub> technique and two Z - R relationships [ $Z = 486 R^{1.37}$  due to Jones (1956) and  $Z = 187 R^{1.27}$  a calibrated relationship] are also listed along with the raingauge values and the ratios of radar-derived values to the raingauge values.

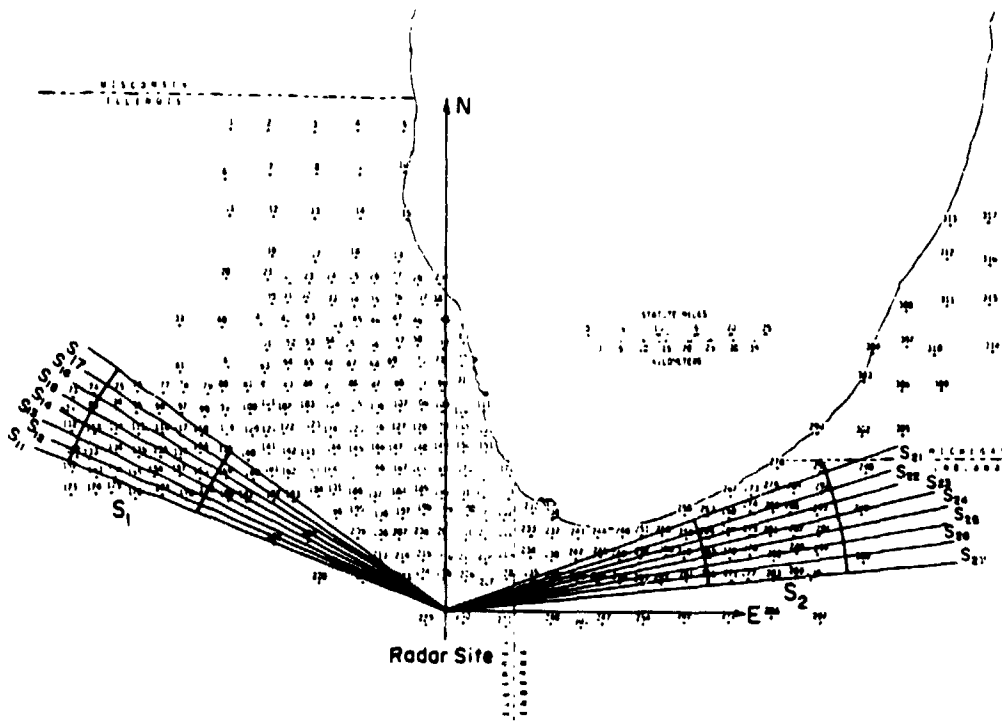


Figure 3. Location of CHILL radar and raingauges near Chicago.

Table 1

Rainfall Rate (mm hr<sup>-1</sup>) Based on the Z<sub>DR</sub> Technique (R<sub>ZDR</sub>), Jones' (1956) Z-R Relationships (R<sub>ZR</sub>), Raingauge Calibrated Z-R Relationship (R<sub>ZR</sub><sup>C</sup>) and the Raingauge Network (R<sub>G</sub>) for Region S<sub>1</sub> and its Subsector Areas S<sub>1j</sub>. Storm duration was 1h 20 min.

Area (km <sup>2</sup> )	No. of Gauges	R <sub>G</sub>	R <sub>ZDR</sub>	R <sub>ZR</sub> <sup>C</sup>	R <sub>ZR</sub>	R <sub>ZDR</sub> /R <sub>G</sub>	R <sub>ZR</sub> <sup>C</sup> /R <sub>G</sub>	R <sub>ZR</sub> /R <sub>G</sub>
S <sub>11</sub>	6	5.6	4.8	7.2	2.8	0.86	1.28	0.50
S <sub>12</sub>	6	4.2	2.8	3.3	1.4	0.67	0.79	0.33
S <sub>13</sub>	5	2.0	1.4	2.1	0.9	0.70	1.05	0.45
S <sub>14</sub>	5	1.9	2.0	3.5	1.4	1.05	1.84	0.74
S <sub>15</sub>	5	2.9	2.0	3.7	1.5	0.69	1.28	0.52
S <sub>16</sub>	4	3.0	1.8	3.6	1.5	0.60	1.20	0.50
S <sub>17</sub>	5	2.4	2.0	3.6	4.5	0.83	1.50	0.63
S <sub>1</sub> (550)	26*	2.80*	2.40	3.66	1.57	0.77	1.28	0.52

\* In S<sub>1</sub>, 10 gauges were common to 2 adjacent subsectors (see Fig. 3)

Table 2

Rainfall Rate (mm hr<sup>-1</sup>) Based on the Z<sub>DR</sub> Technique (R<sub>ZDR</sub>), Jones' (1956) Z-R Relationships (R<sub>ZR</sub>), Raingauge Calibrated Z-R Relationship (R<sub>ZR</sub><sup>C</sup>) and the Raingauge Network (R<sub>G</sub>) for Region S<sub>2</sub> and its Subsector Areas S<sub>2j</sub>. Storm duration was 40 min.

Area (km <sup>2</sup> )	No. of Gauges	R <sub>G</sub>	R <sub>ZDR</sub>	R <sub>ZR</sub> <sup>C</sup>	R <sub>ZR</sub>	R <sub>ZDR</sub> /R <sub>G</sub>	R <sub>ZR</sub> <sup>C</sup> /R <sub>G</sub>	R <sub>ZR</sub> /R <sub>G</sub>
S <sub>21</sub>	5	1.2	1.5	1.9	0.9	1.25	1.58	0.64
S <sub>22</sub>	5	1.3	1.5	1.9	0.9	1.15	1.58	0.75
S <sub>23</sub>	4	1.2	1.3	1.7	0.8	1.08	1.46	0.69
S <sub>24</sub>	4	1.3	1.3	1.5	0.7	1.00	1.42	0.67
S <sub>25</sub>	4	1.3	1.5	1.5	0.9	1.07	1.15	0.54
S <sub>26</sub>	6	1.2	1.4	1.6	0.8	1.17	1.33	0.58
S <sub>27</sub>	5	1.0	1.4	1.5	0.7	1.40	1.50	0.70
S <sub>2</sub> (550)	27*	1.20*	1.41	1.66	0.81	1.16	1.37	0.64

\* In S<sub>2</sub>, 7 gauges were common to 2 adjacent subsectors (see Fig. 3).



ORIGINAL PAGE IS  
OF POOR QUALITY

Comparative statistics of the rainfall data presented in Tables 1 and 2 are given in Table 3.

Table 3  
Comparative Statistics of Rainfall  
Data Presented in Tables 1 and 2

Ratio Estimates	S <sub>1</sub>	S <sub>2</sub>	Average
$\langle R_{ZDR} \rangle / \langle R_G \rangle$	0.86	1.17	1.02
$\langle R_{ZR}^C \rangle / \langle R_G \rangle$	1.36	1.33	1.35
$\langle R_{ZR} \rangle / \langle R_G \rangle$	0.57	0.66	0.62
$\langle R_{ZDR} / R_G \rangle$	0.77	1.16	0.965
$\langle R_{ZR}^C / R_G \rangle$	1.28	1.37	1.32
$\langle R_{ZR} / R_G \rangle$	0.52	0.64	0.58
Average difference*			
$R_1 = R_{ZDR_1}$	24%	20%	22%
$R_1 = R_{ZR_1}^C$	40%	43%	41.8%
$R_1 = R_{ZR_1}$	56%	38%	47%
Fractional Standard Deviation**			
$R = R_{ZDR}$	20%	11.5%	15.8%
$R = R_{ZR}^C$	26%	12.5%	19.3%
$R = R_{ZR}$	24.8%	14%	19.4%

$$\frac{1}{N} \sum_{i=1}^N \frac{|R_{G_i} - R_i|}{R_{G_i}} \quad N = 7$$

\*\* FSD = Standard Deviation of  $(R/R_G) / \langle R/R_G \rangle$  where  
 $R = R_{ZDR}, R_{ZR}^C$  or  $R_{ZR}$ .

Two different ratio estimates are considered, viz.,  $\langle R \rangle / \langle R_G \rangle$  and  $\langle R/R_G \rangle$  where R now refers to  $R_{ZDR}, R_{ZR}^C$  or  $R_{ZR}$ . Averages of these were obtained from Tables 1 and 2 for areas S<sub>1,2</sub>. The combined average is also shown in the last column of Table 3 which demonstrates the superiority of the ZDR technique over use of Z-R relationships. Note that Jones' Z-R relationship systematically underestimates the gauge rainfall rate while the calibrated Z-R relationship overestimates the gauge rainrate. An estimate of the relative average difference between gauge and radar derived rainfall rates is also given in Table 3. This difference is defined as

$$\frac{1}{N} \sum_{i=1}^N \frac{|R_{G_i} - R_i|}{R_{G_i}} \quad \text{and } R_i = R_{ZDR_i}, R_{ZR_i}^C \text{ or } R_{ZR_i}$$

The ZDR technique yields considerably lower average differences (22%) than either of the two Z-R relationships. This same statistic was estimated at 63% by Wilson and Brandes (1979) based on data from 14 storms using Z-R relationships to estimate rainrates. Finally, Table 3 lists the fractional standard deviations (FSD) of radar to gauge ratios defined as  $\sigma(R/R_G) / \langle R/R_G \rangle$  where  $R = R_{ZDR}, R_{ZR}^C$  or  $R_{ZR}$  and  $\sigma^2(R/R_G)$  is the variance of  $R/R_G$ . Again, the ZDR technique gives a lower FSD than either Z-R relationship though these values are also quite small. Wilson and Brandes (1979) obtained an estimate of 30% for the same statistic based on data from 14 storms. Note

that their analysis is based on storms of considerably longer duration (typically 5 hours or longer) than considered here.

7. CHILL RADAR: DISDROMETER COMPARISONS

On August 2, 1978, at approximately 17:40 CST, a strong convective storm approached the radar site directly from the West. The radar was operating in the ZDR mode, step-scanning at elevation at 1° steps every 8 s. During the course of radar measurements, three distinct low elevation angle data sets of Z<sub>H</sub> and Z<sub>DR</sub> were obtained from which rainfall rate profiles with range can be derived. Simultaneously, the disdrometer, which was located at the radar site, recorded the rainfall intensity as the storm moved over the site from West to East. This combination of measurements provided an opportunity to compare the radar-derived range-dependent, rainfall rates with the time-dependent, disdrometer-derived rainfall rates. In this event, a meaningful comparison is possible, if the storm is in steady state and if both measurements can be translated into a common range or time axis through an appropriate transformation.

Fig. 4 shows Z<sub>DR</sub> and Z<sub>H</sub> as a function of range for the last (storm nearest to the radar) scan prior to the storm reaching the site. Also shown is Z<sub>H</sub> for the previous scan which occurred 4 min earlier. Comparison of the Z<sub>H</sub> profiles constitutes a test of whether the storm was in steady state. Clearly, both were very similar in structure, supporting the steady state assumption.

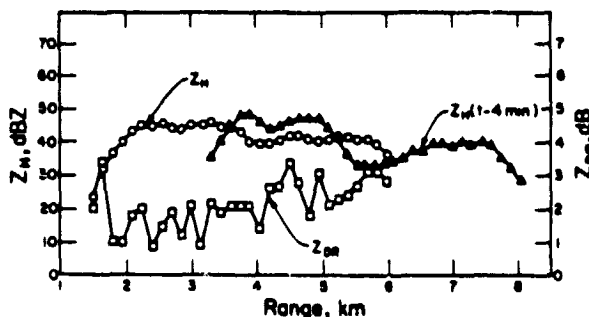


Figure 4. ZDR and Z<sub>H</sub> as a function of range. Z<sub>H</sub> at t-4 minutes is also shown to compare with Z<sub>H</sub> in support of steady state assumption.

The rainfall rate comparisons are shown in Fig. 5 where the disdrometer time data is transformed uniformly over range according to the mean estimate of the storm's speed, 18 km hr<sup>-1</sup>. Note that the disdrometer data is lagged so as to co-locate the two peaks of R at ranges 2.85 and 3.15 km. Also shown in the figure is R derived from the relationship Z<sub>H</sub> = 300 R<sup>1.5</sup>. The correlation between the radar and disdrometer profiles in the range interval 2 - 4 km is very good. On the other hand, the Z-R relationship is unable to reproduce the large variability of R recorded by the disdrometer.

The first two disdrometer peaks in R at 100 and 38 mm hr<sup>-1</sup> are in excellent agreement with the first two radar peaks at 100 and 52 mm hr<sup>-1</sup>.

ORIGINAL PAGE IS  
OF POOR QUALITY

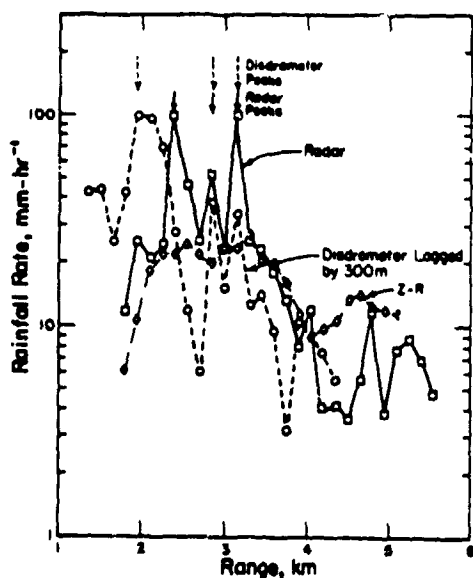


Figure 5. Radar and disdrometer rainfall rates. Note  $Z_{DR}$ 's ability to produce the variability of  $R$  as compared to a  $Z-R$  relationship-derived rate.

The third peak, however, is considerably different with the disdrometer and radar values being 34 and 100  $\text{mm hr}^{-1}$ , respectively. Considering the time delay between the disdrometer and radar observations, this single major discrepancy out of three peak values could easily occur because of the natural variability of the storm between the time of the radar measurements and the time the storm passed over the radar (disdrometer) site.

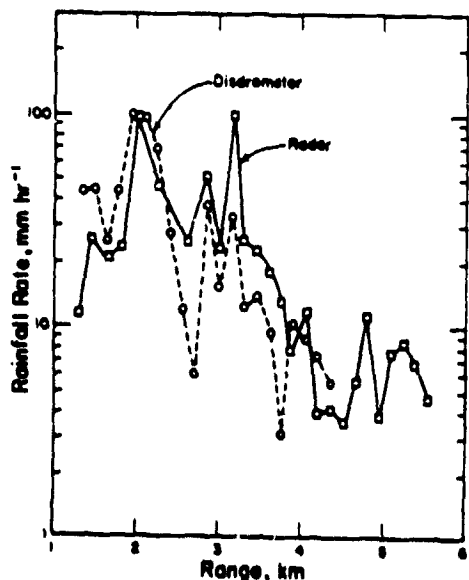


Figure 6. Comparison of radar  $Z_{DR}$  and disdrometer rainfall rates when the radar results are slightly adjusted in range to accommodate the main disdrometer peaks.

Overall comparison of the storm structure would be very good if a spread between the front and rear of the storm as seen by the radar occurred. Such an effect is not unreasonable in convective storms and could explain the discrepancies in the profiles with range. Fig. 6 illustrates the two measurements when the radar data (three peaks) are extended over range to accommodate such spreading. This figure clearly illustrates that a very good comparison between the radar and disdrometer measurements resulted.

#### 8. CHILBOLTON RADAR: DISDROMETER COMPARISONS

A current cooperative research program between Ohio State University and the Rutherford-Appleton Laboratory resulted in measurements of disdrometer-derived rainfall drop size distributions at a fixed site with the radar beam directed over the disdrometer. Although this effort has yielded a limited data set which has not been completely analyzed yet, the results are very encouraging in that calculated values of  $Z_{DR}$ , obtained from the disdrometer measurements and Pruppacher and Beard's drop shapes, correlate very well with the radar measurements of  $Z_{DR}$ . This result is shown in Fig. 7 and provides strong confirmation that  $Z_{DR}$  actually does estimate drop size. It is clear from these measurements and the limited CHILL results, presented previously, that the  $Z_{DR}$  technique has great potential for producing a significant improvement in radar's ability to quantify rainfall.

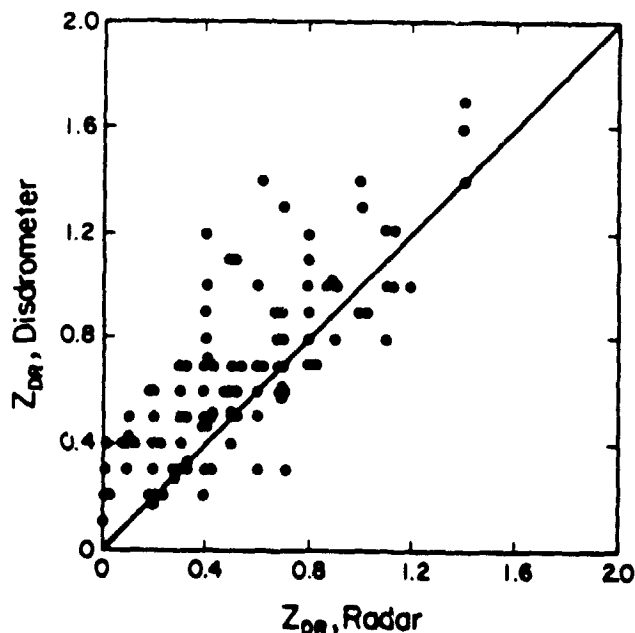


Figure 7. Comparison of disdrometer-derived and radar-measured  $Z_{DR}$ 's.

ORIGINAL PAGE IS  
OF POOR QUALITY

9. RADAR MEASUREMENTS FOR GROUND TRUTH

Should future experiments continue to support the Z<sub>DR</sub> radar technique as an accurate, reliable method of measuring rainfall, radar would then be ideally suited for ground truth observations of rainfall for comparison with satellite observations. The benefits of this approach would include:

- Large spatial coverage from a single site.
- Real time, centralized data handling capability.
- Continuous monitoring.
- Both land and oceanic coverage.
- Adaptability to different spatial and temporal scales.
- Availability of other radar observables such as Doppler, hydrometeor phase and storm structure data.
- Relative ease with which existing radars can be modified for Z<sub>DR</sub> measurements.
- Raingauges would be required only for periodic verification of proper radar system performance.

Obviously, the radar measurements themselves could contribute greatly to the needs of climatic and hydrological research and operations as well.

10. OTHER APPLICATIONS OF THE Z<sub>DR</sub> RADAR TECHNIQUE

In addition to rainfall measurement for ground truth, several other important applications of the Z<sub>DR</sub> radar technique have been identified [Seliga, 1980]:

- Hydrology--flash flood forecasting; improved description and classification of storms; better understanding of topographical influences on rainfall; development and testing of watershed and stream flow modeling.
- Cloud Physics--organization and structure of clouds and precipitation on the meso-scale and microscale; evolution of drop size distributions in storms; validation and development of cloud models; discrimination of hydrometeor phase; hail detection; melting layer processes.
- Climatology--accurate rainfall measurement over large areas; correlation of rainfall with cloud structure; parameterization of rainfall for applications in general circulation and climate models; regional rainfall statistics.
- Weather Modification--accurate rainfall measurement; hydrometeor phase detection; statistical and deterministic evaluation of seeding effects; tracing of seeding materials within and outside of clouds.
- Other--effects of precipitation and storms on satellite-ground and ground-ground communication links; erosion of land surfaces and the surfaces of airborne

vehicles; scavenging of gaseous and particulate air pollutants.

11. CONCLUSIONS

The concept of employing dual linear polarization measurements of radar reflectivity factor was examined as a possible means of providing ground truth rainfall rate data to compare with satellite observations. The theory of this differential reflectivity technique was reviewed along with the results of several experimental comparisons obtained with two different radars. Although the available data are limited, all the results obtained to date support the hypothesis that the technique can be used for the accurate measurement of rainfall and, thus, should be considered for ground-truth applications in any future satellite programs designed to monitor precipitation. Finally, the advantages of this approach are identified and, although not specifically dealt with here, numerous other applications of the radar technique are listed.

ACKNOWLEDGEMENTS

This research was supported by the Atmospheric Research Section, National Science Foundation, under Grants No. ATM-7908666 and ATM-8003376 and by a NATO Research Grant (No. RG 054.80) which partially supported the disdrometer-radar comparisons obtained using the Chilbolton radar. The collaboration of S. M. Cherry, M. P. M. Hall and J. W. F. Goddard of the Rutherford and Appleton Laboratories is gratefully acknowledged.

REFERENCES

- Atlas, D., 1980: Precipitation Measurements. In Chapter on Heat Sources and Sinks, COSPAR Panel on Climate Observing Systems, England, March 1980.
- Barford, N. C., 1967: Experimental Measurements: Precision, Error and Truth. Addison-Wesley Pub. Co.
- Battan, L. J., 1973: Radar Observations of the Atmosphere. The Univ. of Chicago Press.
- Bringi, V. N., T. A. Seliga and M. G. Srinam, 1980: Statistical characteristics of the differential reflectivity radar signal. Preprints, 19th Conf. on Radar Meteor., Miami Beach, Fla., 15-18 April, 692-696.
- Izrael, Ju. A., 1979: Climate monitoring and climatic data collection services for determining climatic changes and variations: Monitoring data relevant to climate. Proc. World Climate Conf., Geneva, 12-23 Feb. 1979, 154-169.
- Jones, D. M. A., 1956: Rainfall drop size distribution and radar reflectivity. Res. Rept. No. 6, Illinois State Water Survey, Univ. of Illinois, Urbana.
- Martin, D. W. and W. D. Scherer, 1973: Review of satellite-rainfall estimation methods. Bull. Amer. Meteor. Soc., 54, No. 7, 661-674.
- Pruppacher, H. R. and K. V. Beard, 1970: A wind tunnel investigation of the internal circulation and shape of water drops falling at terminal velocity in air. Quart. J. Roy. Meteor. Soc., 96, 247-256.

ORIGINAL PAGE IS  
OF POOR QUALITY

Seliga, T. A., 1980: Dual polarization radar. *Nature*, 285, 191-192.

Seliga, T. A. and V. N. Bringi, 1976: Potential use of radar differential reflectivity measurements at orthogonal polarizations for measuring precipitation. *J. Appl. Meteor.*, 15, 69-76.

Seliga, T. A. and V. N. Bringi, 1979: Differential reflectivity measurements in rain: First experiments. *Trans. IEEE Geosci. Elect.*, GE-17, No. 4, 240-244.

Viezee, W., P. A. Davis and D. E. Wolf, 1978: Technique to use satellite microwave spectrometer data in moisture budget studies of cyclones. *Mon. Wea. Rev.*, 106, No. 11, 1627-1633.

Wilheit, T. T., A. T. Chung, M. S. V. Rao and E. B. Rodgers, 1977: A satellite technique for quantitatively mapping rainfall rates over the ocean. *J. Appl. Meteor.*, 16, 551-560.

Wilson, J. W. and E. A. Brandes, 1979: Radar measurement of rainfall--a summary. *Bull. Amer. Meteor. Soc.*, 60, 1048-1058.

ORIGINAL PAGE IS  
OF POOR QUALITY

## A SURVEY OF RADAR RAIN MEASUREMENT TECHNIQUES

R. J. Doviak  
National Severe Storms Laboratory  
1313 Halley Circle  
Norman, OK 73069

### Abstract

Several methods used to estimate rainfall rate  $R$  are surveyed. The distribution  $N(D)$  of dropsizes is of central importance in determining the reflectivity factor  $Z$ , attenuation rate  $K$ , and  $R$ . With single parameter measurement techniques either of the remotely sensed parameters  $Z$  or  $K$  can be used to estimate  $R$  when gross assumptions on  $N(D)$  can be made. If  $N(D)$  can be described by a two parameter distribution, dual measurement techniques can better estimate  $R$  without invoking these coarse assumptions. A review is made of three techniques whereby two variables might be measured: (1) dual wavelength in which  $Z$  and  $K$  are remotely measured, (2) dual polarization in which reflectivity is measured with two orthogonal polarizations and (3) rain gage-radar combinations whereby in situ point measurements of  $R$  and radar measurement of  $Z$  or  $R$  are combined to obtain a better assessment of rain over areas between gages.

### 1. INTRODUCTION

Accurate estimates of rainfall rate  $R$  and/or cloud liquid water content  $M$  requires detailed knowledge of the liquid water droplet size distribution  $N(D)$ . Although radar techniques have practical limitations and its accuracy in rainfall rate estimation is highly suspect, it has the decided advantage of remotely surveying vast areas and making millions of measurements in minutes. Radars in combination with satellites, rain gages, and other instruments may give the sought for accuracy of rainfall estimate with the ease of data collection inherent in remote sensing.

To accurately characterize relations between water density and cloud dynamics with good spatial resolution, and to reliably sense the threat of unusual but significant events such as floods, there have been and still are efforts under way to improve the accuracy by which radar can better estimate rainfall.

### 2. RAINDROP SIZE DISTRIBUTION

Srivastava (1971) has determined the steady state  $N(D)$  for raindrops generated by their breakup and coalescence (Fig. 1). He shows that the steady state  $N(D)$  is independent of the assumed initial distribution but depends upon the liquid water content. Calculations by Srivastava (1967) show that exponential distributions are quasi-stable with respect to coalescence in that they change rather slowly whereas narrow distributions tend rather rapidly toward the exponential shape. Although the steady-state distributions shown on Fig. 1 are not exponential, they can be fitted by truncated exponential functions at least over the droplet size range which contributes most to  $Z$ ,  $R$ , and  $M$ . Thus, the use of exponential distributions in radar estimates of rainfall is justified, and two parameters of the exponential function would only need to be estimated. At larger  $R$  a third parameter,  $D_{max}$ , may be required to accurately estimate  $R$ ,  $Z$ , and  $M$ .

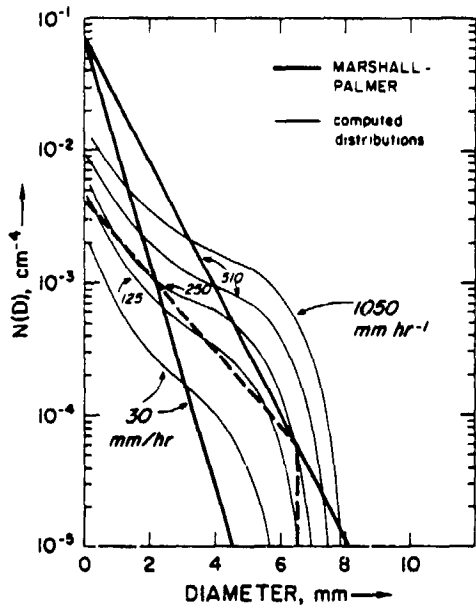


Figure 1. Steady state raindrop size spectra assuming coalescence and spontaneous breakup of large drops. The Marshall-Palmer exponential distributions for two rain rates are shown for comparison. Dashed line is an exponential spectrum truncated at  $D_{max} = 6.5$  mm. After Srivastava (1974).

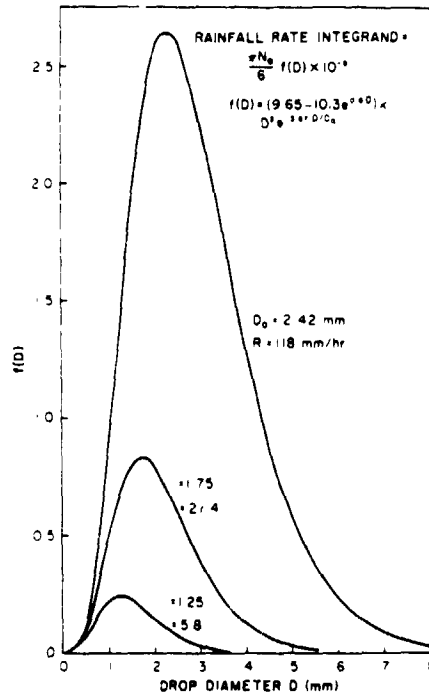


Figure 2. The integrand of the rainfall rate equation (3) showing which drops contribute most for an exponential dropsize distribution.

### 3. RAINFALL RATE

Gunn and Kinzer (1949) made precise measurements on the terminal velocity  $w_{t0}$  of water droplets in stagnant air at sea level. These data are commonly used in calculating the rainfall rate, on the ground, from  $N(D)$ , and in deriving the Doppler velocity power spectra for vertically pointed radars. A useful approximation to the data for  $w_{t0}$  is

$$w_{t0}(D) = 9.65 - 10.3 \exp[-600D] \quad (\text{m} \cdot \text{s}^{-1}) \quad (1)$$

(Atlas et al. 1973), where  $D$  is drop diameter (m). If  $D$  lies between  $6 \times 10^{-4}$  and  $5.8 \times 10^{-3}$  m, there is less than 2 percent error from the measured values of Gunn and Kinzer. We shall find it useful to have a power law fit for  $w_t(D)$  data. Atlas and Ulbrich (1977) show that

$$w_{t0}(D) \approx 386.6D^{0.67} \quad \text{for } 5 \times 10^{-4} < D < 5 \times 10^{-3} \text{ m} \quad (2)$$

fits the data of Gunn and Kinzer in the indicated range of  $D$ . An exponent of 0.5 in (2) would be expected from theory, but this holds true only for the very smallest diameter (0.3 mm) drops which remain spherical. Rainfall rate  $R$  is obtained from

$$R = \frac{\pi}{6} \int D^3 N(D) w_t(D) dD \quad (3)$$

We can derive a relation between  $R$  and the two parameters of an exponential distribution of drop diameters by substituting (1) into (3) which gives, after integration, the following formula for  $R$

ORIGINAL PAGE IS  
OF POOR QUALITY

$$R = \frac{\pi N_0 D_0^4}{(3.67)^4} \left\{ 9.65 - \frac{10.3}{(1+163 D_0)^4} \right\} (\text{m} \cdot \text{s}^{-1}) \quad (4)$$

where  $D_0$  is the median volume drop diameter and MKS units are implied throughout.  $N_0$  is the number density per unit diameter for  $D \rightarrow 0$ . This formula applies only if the exponential  $N(D)$  is steep enough so that contributions to  $R$  from diameters larger than  $D_{\max}$  are insignificant.

It is instructive to show the drop diameters that contribute most to the rain. So we have plotted on Fig. 2 the rainfall rate integrand of (3) assuming an exponential dropsize distribution. We see that even for the highest rain rate shown in the figure, most contribution to rain comes from drops having diameters less than 6 mm. Thus, significant rain comes from a narrow range of dropsizes (0.5-6 mm). This fact is of importance when power law equations are fitted to scatter cross section-drop diameter curves. However,  $R$  has been computed using the M-P distribution, and this is steeper than the steady state spectra especially at large  $R$ . Flatter spectra, as shown in Fig. 1, may have important contribution from drops of diameter near  $D_{\max}$ .

#### 4. SINGLE PARAMETER MEASUREMENT TO ESTIMATE RAINFALL RATE

In this section, we discuss methods whereby remote measurement of one parameter such as reflectivity factor  $Z$ , or attenuation rate  $K$ , is used to estimate rainfall rate.

##### 4.1 R, Z Relations

The remote measurement of  $R$  has considerable practical interest. For many years radar meteorologists have attempted to find a useful formula that relates  $R$  to the radar measured parameter  $Z$ . Unfortunately, there is no universal relationship connecting these parameters although it is common experience that larger rainfall rates produce more intense echoes. By examining Eq. (4) we see that, for the exponential dropsize distribution, we need to measure 2 parameters in order to obtain  $R$ . Thus, the radar determined value of  $Z$  alone cannot provide a unique measurement of  $R$  unless either  $N_0$  or  $D_0$  was uniquely related to  $R$  or to one another.

There has been considerable effort to establish whether some of the dropsize distribution parameters might be known given the type of rain (i.e., stratiform, thunderstorm, etc.). Measurement of dropsize distributions around the globe under different climatic conditions were made, and Battan (1973) lists no less than 69 different  $R, Z$  relations! Even when rain conditions were supposedly the same (stratiform), Atlas and Chmela (1957) show considerable variability in the  $R, Z$  relations. For example, their data show the same reflectivity factor  $Z$  could be associated with an  $R$  of 33 mm/hr or 11 mm/hr, a possible 300 percent error depending upon which measured dropsize distribution is used.

It is quite difficult to calibrate radars to within  $\pm 1$  dB so there could be a systematic bias in the radar measured reflectivity. Some of this error can be compensated by choosing an appropriate  $R, Z$  relation. According to Cain and Smith (1976), the relation  $Z=155 R^{1.88}$  removed any pervasive bias in the radar estimated rainfall RER, whereas in Florida Woodley et al. (1975) reported the Miami  $R, Z$  relation  $Z=300 R^{1.4}$  worked better. We should recognize that even if the dropsize distribution was the same at two different locations, errors in

radar calibration can lead the meteorologist to develop an appropriate, but different R, Z relations that apply to each region. In order to develop an appropriate R, Z relation, radars need to be accurately calibrated so that other radars can use a common Z, R relation that may depend only upon different meteorological conditions and not upon the radar used.

In spite of the superfluity of R, Z relations, many of them do not differ greatly at rainfall rates between 20 and 200 mm/hr (for further illustrations and discussion, see Fig. 5 and Sec. 5.1). For stratiform rain, the Marshall-Palmer (M-P) relation (1948)

$$Z = 200 R^{1.6} \quad (5)$$

with R in mm/hr and Z in  $\text{mm}^6 \text{m}^{-3}$  has proven quite useful. Laws and Parsons (1943) dropsize spectral measurements give

$$Z = 400 R^{1.4} \quad (6)$$

More recently Joss and Waldvogel (1970) have used

$$Z = 300 R^{1.5} \quad (7)$$

and showed a 42 percent standard deviation (S.D.) between radar and disdrometer measured daily rainfall accumulations for 47 days of rain events throughout the 1967 year. When they considered those 25 days in which rain accumulation was larger than 10 mm, the S.D. reduced to 28 percent. The use of three different R, Z relations (one for drizzle, one for widespread rain, and one for thunderstorms) doubled the accuracy of radar measured amounts of precipitation (S.D.  $\approx$  13 percent)!

Although the use of (5), (6), or (7) may produce large dispersion from the actual rain rate measured by a gage, the accuracy of rainfall measurements can be greatly improved by averaging in space or time. Leber, Merritt, and Robertson (1961) used (5) to obtain hourly averages of 10-cm radar rain rate during extremely heavy rain, and integrated these hourly averages to produce a 24-hour isohyetal map that compared very well with accumulated rainfall obtained from a dense network of rain gages.

#### 4.2 Attenuation Method

Communication engineers and radar meteorologists have observed, for a wide range of rainfall rates and rain type, a consistent relationship between microwave attenuation and rainfall rate measured with rain gages along the path of communication. Thus, accurate measure of attenuation might be used to obtain reasonable estimates of R without apriori information on N(D).

It can be shown that if the extinction cross section  $\sigma_t(D)$  is well approximated by a power law dependence upon D in the range of diameters which contribute significantly to K, then liquid water content M and K would also be related by a power law, a result that is consistent with many experiments. Moreover, it can be demonstrated that the power law approximation,

$$\sigma_t(D) = CD^n \quad (8)$$



COMPARISON OF  
OF POOR QUALITY

9  
Y

for  $\sigma_t(D)$  leads to a rainfall rate versus attenuation rate that can be independent of drops size distribution! Atlas and Ulbrich (1974) first illustrated that the power law dependence between microwave attenuation and rainfall rate implies the "effective" power law dependence given by (8).

Now let's examine again the rainfall rate formula (3). In order to have R expressed as an integral of a power law function of D, we are motivated to use the approximation (2) for terminal velocity  $w_{t0}$ . Using (2) in (3) yields

$$R = \frac{\pi(386.6)}{6} \int_0^{\infty} D^{3.67} N(D) dD \quad (9)$$

Substitution of (8) into the attenuation rate formula

$$K = 4.34 \times 10^3 \int_0^{\infty} N(D) \sigma_t(D) dD \quad \frac{dB}{km} \quad (10)$$

gives

$$K = 4.34 \times 10^3 C \int_0^{\infty} N(D) D^n dD \quad (11)$$

Comparison of (9) and (11) immediately shows that if the power exponent n had a value equal to 3.67 then R and K would be linearly related and, moreover, this relation would be independent of drops size distribution!

Atlas and Ulbrich (1974) fitted Waldteufel's (1973) numerically computed K, R values with a power law in the R interval 1-100 mm/hr. From these fitted curves, they have obtained values of C and n for a wide range of wavelengths (0.1-10 cm) and temperature (0-40°). These data (Fig. 3) show that n = 3.67 for  $\lambda = 0.88$  cm.

Any wavelength near 1 cm would similarly show that attenuation and rainfall rate relations are relatively independent of the drops size distributions. This conclusion is quickly accepted if one refers to Fig. 4 which plots attenuation rate versus rainfall rate for 4 wavelengths. The circles are K and R values numerically computed using measured drops size distributions (204 of them for 3 days) and the exact attenuation cross sections for each drop diameter at T = 10°C. These numerical values form the scattergram and lines are best fit of a log-log regression to the equation  $K = \alpha R^\beta$ . The regression equations and the average percent deviation of R are shown in the upper inset table of Fig.4. Note how closely packed the data are for  $\lambda = 0.86$  cm in spite of the large number of different drop spectra used and that at  $\lambda = 3.22$  cm, a larger scatter that might be attributed to differences in drops size spectra.

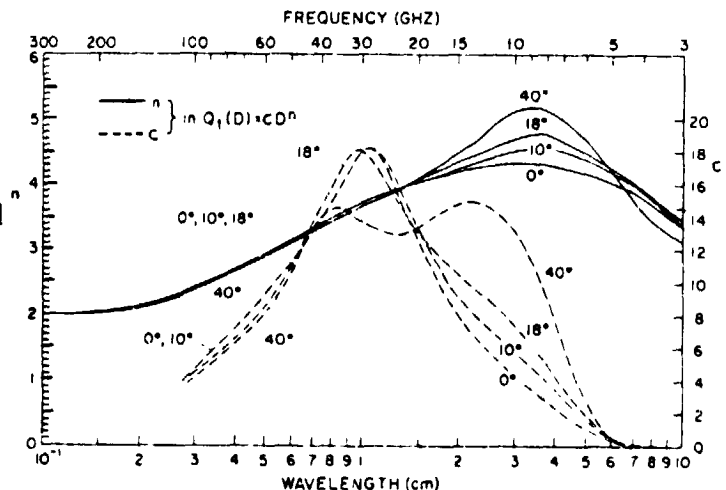


Figure 3. Curves of "effective" C and n in attenuation cross section  $Q_t = CD^n$  versus wavelength and temperature.  $Q_t$  is in units of  $cm^2$  if D is in cm (from Atlas and Ulbrich, 1974).

ORIGINAL PAPER  
OF POOR QUALITY

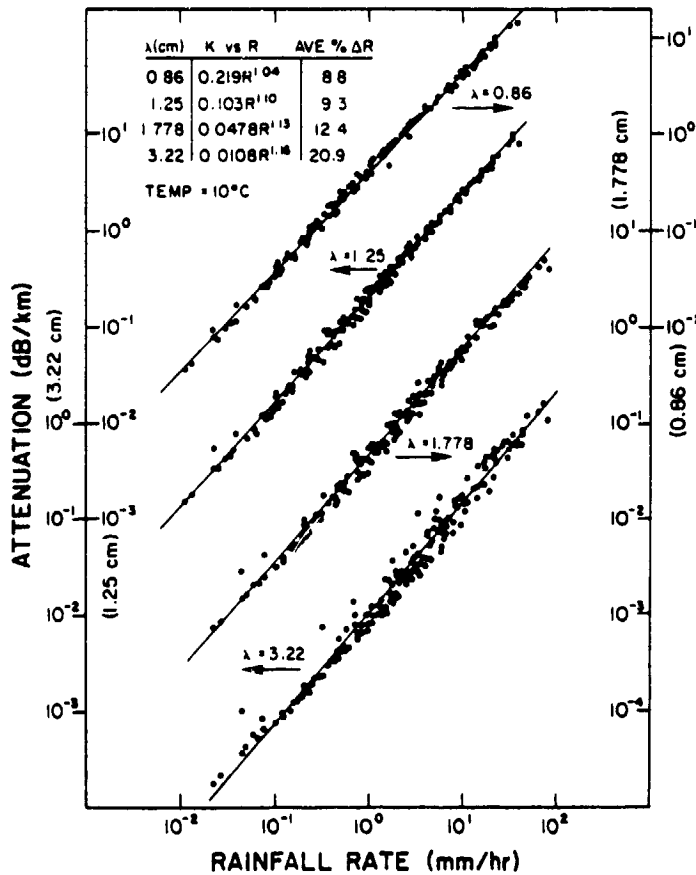


Figure 4. Scattergrams and regression lines of K versus R at indicated wavelengths. Inset table gives regression equations and average errors in R (from Atlas and Ulbrich, 1977).

5. DUAL PARAMETER MEASUREMENT TO ESTIMATE RAINFALL RATE

We now turn our attention to methods whereby measurement of two variables can be used to deduce others. For example, measurement of the two remotely sensed variables, attenuation rate and reflectivity, can in principle be used to infer rainfall rate, liquid water content, or any other variable that is derived from a two parameter dropsize distribution. Atlas and Chmela (1957) were first to develop a rain parameter diagram which permits one to obtain the rain parameters R, M,  $D_0$ , and Z from any pair of the set. Atlas and Ulbrich (1974) and

Ulbrich and Atlas (1978) developed a more general and accurate rain parameter diagram which added microwave attenuation K and optical extinction rate  $\Sigma$  ( $m^{-1}$ ) to the other four parameters, thus permitting one to deduce all six parameters from measurement of any pair. The underlying principle is that measurement of any two variables can be used to completely specify a two parameter dropsize distribution.

5.1 Rain Parameter Diagram

Before we proceed, it is well to examine one of the rain parameter diagrams (Fig. 5). Although Fig. 5 is specialized for  $\lambda = 3.22$  cm and  $T = 10^\circ C$ , it does illustrate the interrelationships between K, Z, R, and  $D_0$  for an assumed exponential dropsize distribution. For example, a measurement of  $K = 10^{-1}$  dB/km and  $Z = 2 \times 10^3$   $mm^6/m^3$  gives a rainfall rate estimate slightly larger than 10 mm/hr and a  $D_0$  slightly smaller than 1 mm. The heavy lines in the figure are approximate rain parameter curves:

$$K = 8.61 \times 10^{-4} Z^{0.405} R^{0.595} \quad (\text{dB/km}) \quad (12)$$

where Z is in  $mm^6 m^{-3}$  and R in mm/hr units. The agreement is good in those regions (shaded) within which most measured dropsize distributions fall and at high rainfall rates.

For accuracy we may need to estimate K over long paths and thus we consider path averaged values  $\bar{Z}$ ,  $\bar{K}$  to estimate  $\bar{R}$ . Because K, Z, and R are invariant with

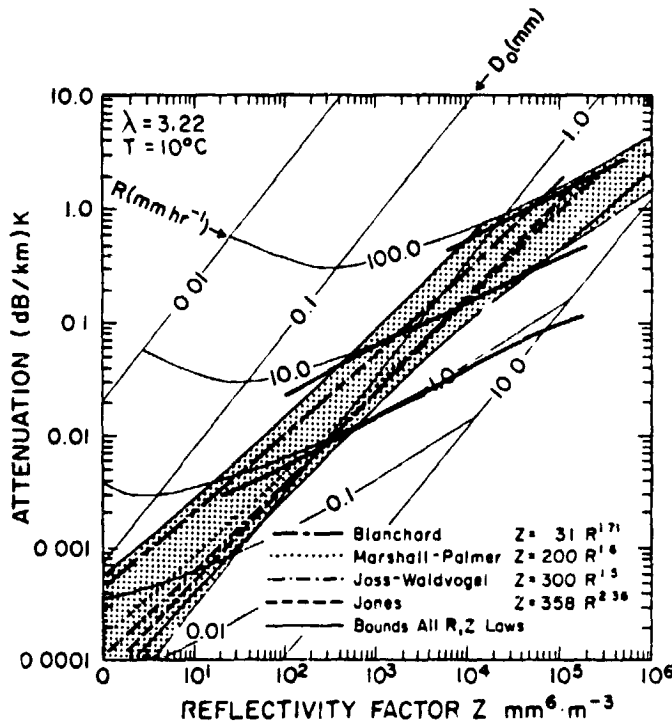


Figure 5. The rain parameter diagram for exponential dropsize spectra (from Atlas and Ulbrich, 1974). The shaded area contains the 69  $Z, R$  relations of Battan (1973). The heavy solid lines are approximate rain parameter curves given by Eq. (12).

respect to the placement of drops along the path (provided the number and sizes of drops remain the same although placed anywhere along the path and the range interval over which the average is taken is small compared to the range to it), we might expect the path averaged  $\bar{R}$  could be retrieved from  $\bar{Z}$  and  $\bar{K}$ . The use of path averages  $\bar{Z}, \bar{K}$  in a rain parameter diagram will not, in general, give  $\bar{R}$  but at a wavelength of 0.88 cm this is true.

Apart from the weighting given by the beam pattern function, the measured reflectivity factor  $Z_e$  does not depend on how the scatterers are distributed across the beam. This is not so for measured attenuation rates which requires a measure of echo power change between two colinear resolution volumes, and this will depend on how drops are placed across the beam. For example, if scatterers have nonuniform density across the beam and the more distant ones were behind a group of nearer ones, the measured  $K$  would be different than if those same distant scatterers were displaced transversely to the beam to a position aside the clump of nearer ones. Thus, any dual parameter measurement method

that uses measured  $K$  as one of the parameters will have an estimated  $R$  strongly dependent upon the distribution of dropsize density across the beam. Upon further study, it can be deduced that this is not so for methods such as the dual polarization technique (see Sec. 3) for which the measured reflectivity and differential reflectivity do not depend as strongly upon the distribution of drop density.

## 5.2 Dual Wavelength Method

Because of the practical limitations that direct attenuation measurements impose on areal coverage of rain, investigators have turned to dual wavelength ( $\lambda$ ) radars in an attempt to remotely measure  $K$ . The dual  $\lambda$  technique does not limit attenuation measurements to  $\lambda$  near 1 cm. Rather, it allows remote measurement of  $Z$  and  $K$  from which one can determine two parameters of the dropsize spectra.

Alternately, we can measure effective reflectivity factor at two wavelengths in which one involves Rayleigh scatter whereas the other wavelength could be sufficiently short that substantial Mie scatter (i.e.,  $D > \lambda/16$ ) occurs for the larger drops that comprise the scatter domain. From the differences in measured reflectivity factors, one can deduce dropsize parameters (Wexler and Atlas, 1963). Although we have several techniques that could be discussed, we shall confine our attention to one promising dual wavelength method, i.e., the independent measurement of  $Z$  and  $K$ .

For sake of illustration, we shall assume  $N(D)$  exponential to show how the parameters  $N_0$  and  $D_0$  can be determined from measurement of reflectivity factor  $Z$  and attenuation rate  $\bar{K}_s$ . We will arrive at two simultaneous equations containing  $N_0$  and  $D_0$  along with measured samples of backscattered power at two wavelengths, one long ( $\lambda_l$ ) and nonattenuating and the other ( $\lambda_s$ ) short and attenuating. One equation represents the attenuation at  $\lambda_s$ ; the other the other the reflectivity factor at  $\lambda_l$ . We select a nonattenuating wavelength ( $\lambda_l$ ) in order to simplify the problem although two attenuating wavelengths can be used (Goldhirsh and Katz, 1974).

The path averaged short wavelength attenuation rate  $\bar{K}_s$  is,

$$\bar{K}_s = N_0 \int e^{-3.67D/D_0} \sigma_t(D) dD \quad (\text{m}^{-1}) \quad (13)$$

For precision, (13) needs to be numerically evaluated because  $\sigma_t(D)$  is not an analytic function. But, as we have discussed previously, it can be approximated by a power law in the range of drop diameters that contribute significantly to rainfall rate. Thus substituting (8) into (13) and integrating, we obtain

$$\bar{K}_s = \Gamma(n+1) C' N_0 D_0^{n+1} / (3.67)^{n+1} \quad (14)$$

where  $C' = 10^{2n-4} C$ , and  $D_0$  is in meters. Likewise, the path averaged reflectivity factor is

$$\bar{Z} = N_0 (6!) \left( \frac{D_0}{3.67} \right)^7 \quad (15)$$

We thus have two equations and two unknowns. Let's divide (14) by (15) to eliminate  $N_0$

$$\frac{\bar{K}_s}{\bar{Z}} = \frac{4.34 \times 10^3 (n+1) C'}{6!} \left( \frac{D_0}{3.67} \right)^{n-6} \frac{\text{dB}}{\text{km} \cdot \text{m}^3} \quad (16)$$

and thus  $D_0$  (in meters) is determined directly from the ratio of  $\bar{K}_s$  to  $\bar{Z}$ . The 4.34 factor in (16) arises because we have expressed  $\bar{K}_s$  in decibel (dB/km) units. The ratio (16) is plotted on Fig. 6 for two attenuating wavelengths  $\lambda_s = 5$  and 3 cm at  $T = 18^\circ\text{C}$  using  $C$  and  $n$  values obtained from Fig. 3.

We observe that  $\bar{K}_s/\bar{Z}$  changes by a factor of 5 over the range (2-300 mm/hr) of significant path averaged rainfall rate  $\bar{R}$ . This is not a very large span considering errors in  $\bar{Z}$  and  $\bar{K}_s$  less than 1 dB are difficult to achieve and at this level could cause significant error in  $\bar{R}$ .

For more detailed discussion on errors and requirements on the radar, see Goldhirsh (1975). But, it is important to note here that we are focusing our attention on path averaged values and these might be estimated with greater accuracy

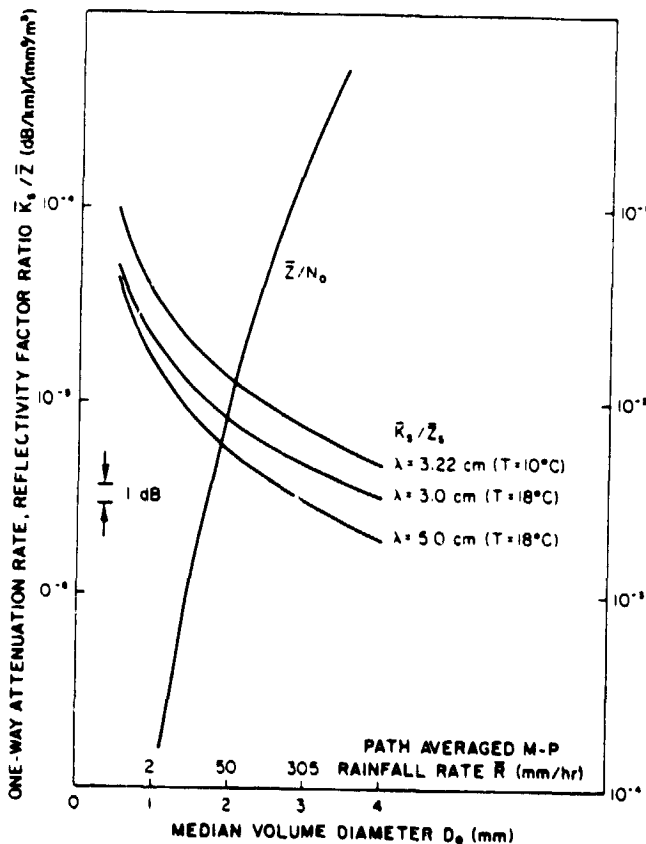


Figure 6. Path integrated attenuation rate reflectivity factor ratio  $\bar{K}_s/\bar{Z}$  and normalized reflectivity factor  $\bar{Z}/N_0$  vs median volume drop diameter. Rainfall rate scale is only for the M-P value of  $N_0 = 8 \times 10^6 \text{ m}^{-4}$ .

than point (i.e., resolution volume) estimates of  $Z$  and  $K_S$ . Still the radar needs to be well calibrated and the dual wavelength radar might well be supplemented with a small number of rain gages for purposes of calibration. However, if one considers the measurement of attenuation at two wavelengths, precise absolute calibration is not required, but relative powers need to be accurately measured. Then path averaged estimates can be used to considerable advantage.

### 5.3 Dual Polarization

This scheme, which also attempts to estimate two parameters of the drops size distribution, uses information of echo intensity of two orthogonally polarized waves. Each transmitted pulse has alternate horizontal and vertical polarizations, and echoes received in the respective principal plane of polarization are processed.

The basis for the dual polarization scheme is the observation that drops are not spherical, but have an oblate spheroidal shape. In still air, without strong static electric fields, the drops fall with their minor axis vertical. Thus, for particles satisfying the Rayleigh conditions for scatter, we expect larger power echoes for horizontally polarized waves. It can be shown that the ratio of reflectivities  $Z_H/Z_V$  for horizontally and vertically polarized waves, is a direct measure of  $D_{0t}$ , the parameter that specifies the steepness of the truncated exponential distribution.

A simplified theory attributed to Gans (1912), and employed by Seliga and Bringi (1976) determines the reflectivity of oblate spheroids for incident waves of either horizontal or vertical polarization. Gans' work is essentially an extension of the Rayleigh theory for spheres applied to the case of oblate and prolate spheroids.

Seliga and Bringi (1976) have evaluated the differential reflectivity factor  $Z_{DR} \equiv 10 \log Z_H/Z_V$  for  $D_{max}=10$  mm and  $T=20^\circ\text{C}$ . Their results are plotted on Fig. 7 where, for comparison, the more recent  $Z_{DR}$  values are plotted using an exact theoretical formulation evaluated by Al-Khatib et al. (1979). We see that the simplified theory agrees well with the more exact formulation. The large difference for  $D_{0t}$  greater than 2.5 mm is mostly caused by the difference in  $D_{max}$ . When both limits are equal, there is relatively little difference in the entire indicated range of  $D_{0t}$  (Seliga and Bringi, 1978).

Once we have  $D_{0t}$ , we need to determine  $N_0$  in order to completely specify the drops size distribution.  $N_0$  can be determined from measurements of  $Z_H$  or  $Z_V$ . The

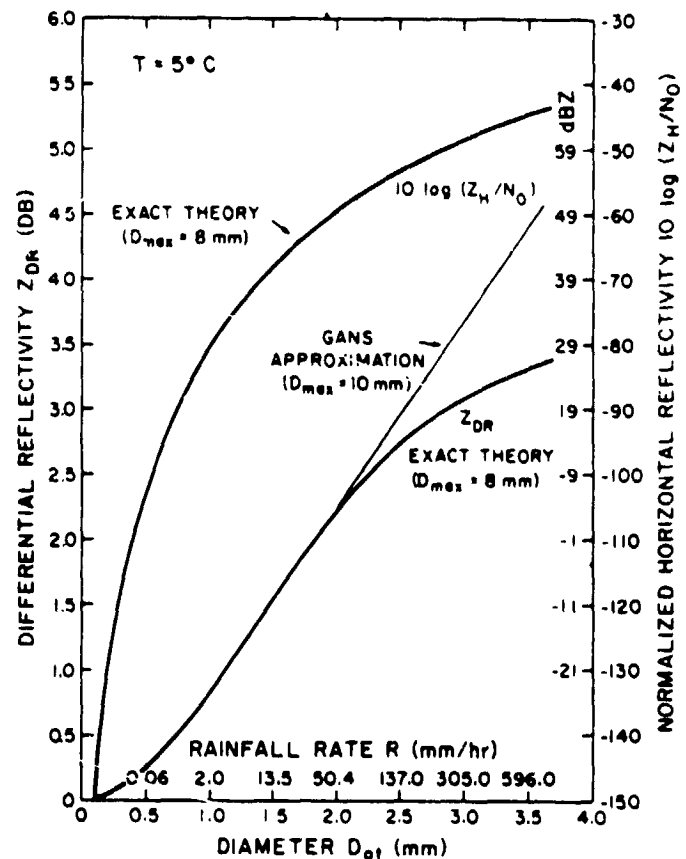


Figure 7. Variations of  $Z_{DR}$  and normalized horizontal reflectivity  $10 \log (Z_H/N_0)$  with  $D_{0t}$ .  $N$  is in units of  $m^{-3} cm^{-1}$  and  $Z_H cm^6/m^3$ .  $R$  and dBZ scale for  $N_0=8 \times 10^4 m^{-3} cm^{-1}$  (from Al-Khatib, 1979).

reflectivity factors  $Z_{H,V}$  have been evaluated by Al-Khatib et al. (op.cit) using the exact formulation for scattering. We also plot  $Z_H$  on Fig. 7. Now both parameters of the drops size distribution can be computed from  $Z_H$  and  $Z_{DR}$  measurements and henceforth rainfall rate.

### 5.3.1 Sample Results

We show here some sample results using the dual polarization technique. The results (Fig. 8) are for times when the radar elevation angle was low enough to insure that the radar beam was well below the freezing level so that scatterers are most likely raindrops.

Figs. 8a,b are the measured values of  $Z_H$  and  $Z_{DR}$  along a radial through, what appears to be, several cells. Reflectivity factor extends up to 45 dBZ, and  $Z_{DR}$  is always positive and lies within the expected range as predicted by the theoretical values given in Fig. 7. These results immediately show that significant errors (i.e., > 1 dB) would be made if reflectivity factor values were deduced from the equivalent spherical diameters. For example, vertically polarized measurements of reflectivity in rain will tend to underestimate the equivalent spherical drop reflectivity.

Figs. 8c,d show the value of  $D_{0t}$  and  $N_0$  for the same data set. Of particular importance is the large variability of  $N_0$  measured with this technique. The M-P value of  $N_0$  can be seen to be a poor approximation to the effective values of  $N_0$  computed from  $Z_H$  and  $Z_{DR}$ . Fig. 8e shows the rainfall rate computed from the  $N_0$  and  $D_0$  values. Even though  $N_0$  and  $D_{0t}$  have highly irregular spatial dependence, the rainfall rate is quite systematic and suggests that only two cells produce significant rain.

## 5.4 Rain Gage and Radar

Technically, the simplest and most direct way to measure rainfall rate is to use rain gages--a catchment that measures the depth of water per unit time. Although tipping buckets and weighing gages are commonly used, they are subject to significant errors caused by wind (Neff, 1977). The most accurate gage is one that is flush to the surface (e.g., pit gage). However, even when rain gages are accurate, they only measure rainfall at a point. Because there may be large errors in the rain depth at any one gage representing the areal average, hydrologists have resorted to a network of rain gages and radar to improve areal average rainfall estimates.

Although radar accuracy of rainfall rate is highly suspect, it has the decided advantage of surveying ramotely vast areas and making millions of measurements in minutes. The cost of a gage network to match these capabilities in spatial continuity and rates of data sent to a central location would be prohibitive. Therefore, meteorologists have combined radar and rain gage data to take advantage of the best of the two: (1) the accuracy of gage data and, (2) the spatial coverage of radar data. The improvement, using radar gage combinations, to estimate areal average rain, is discussed in Sec.5.4.2. The combination adjusts radar rainfall estimates with gage samples sprinkled throughout the area surveyed by radar.

### 5.4.1 Gage Accuracies for Areal Average Rainfall Depth

Because there is no easy way to establish a true areal average of rainfall depth, rain gage network accuracy is determined relative to the most dense network

ORIGINAL PAGE IS  
OF POOR QUALITY

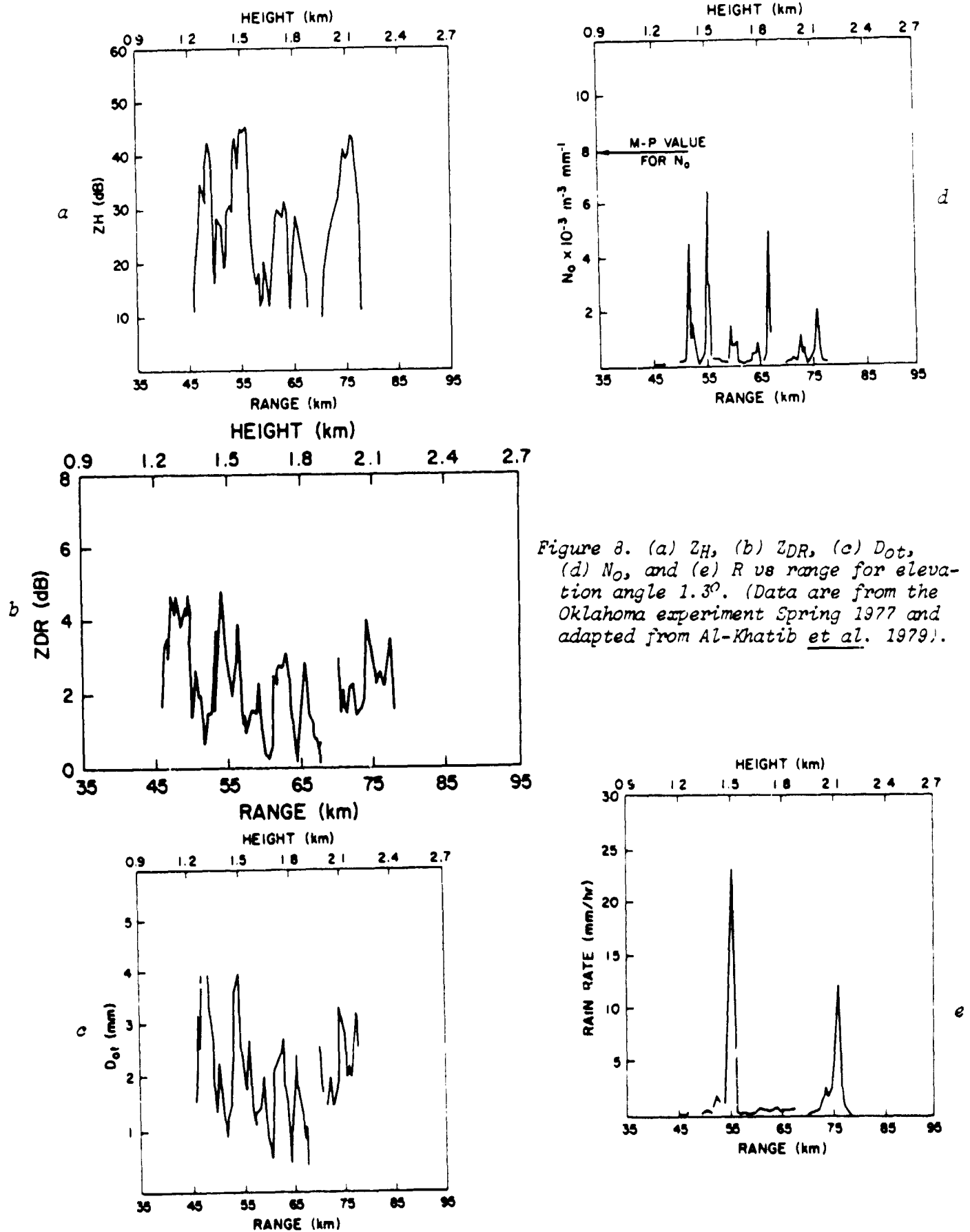


Figure 8. (a)  $Z_H$ , (b)  $Z_{DR}$ , (c)  $D_{ot}$ , (d)  $N_0$ , and (e)  $R$  vs range for elevation angle  $1.3^\circ$ . (Data are from the Oklahoma experiment Spring 1977 and adapted from Al-Khatib et al. 1979).

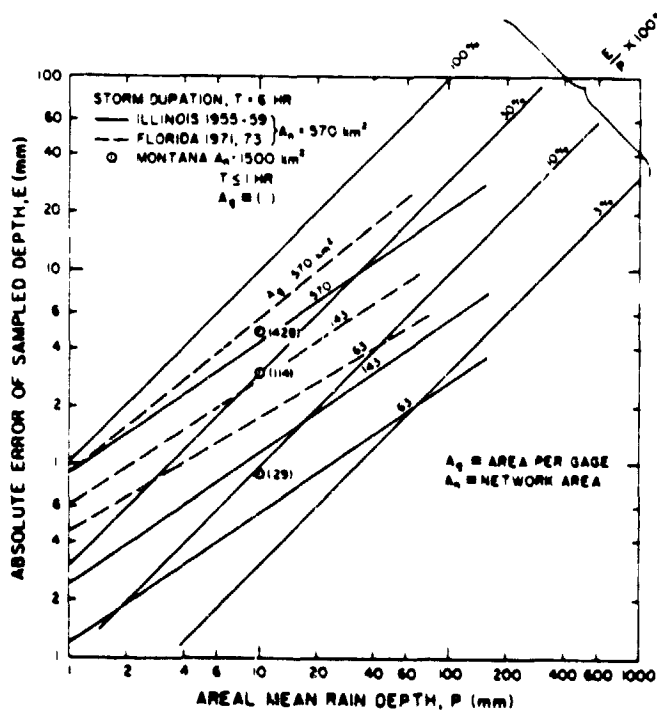
ORIGINAL PAGE IS  
OF POOR QUALITY

that can be economically deployed at the time. Huff (1970) used a 49 gage network in Illinois for the years 1955-1964, and these gages were deployed over a 100 km<sup>2</sup> area. In 1971 and 1973, Woodley et al. (1975) deployed 220 gages over a 510 km<sup>2</sup> area in Florida. More recently, Hildebrand et al. (1979) analyzed gage accuracies for a network of 109 gages on a 1500 km<sup>2</sup> area in Montana during the summer of 1976.

The sampling error E in mm of water represents the absolute difference between the best estimate of the true mean P of precipitation depth (mm) obtained from the maximum density of gages and the sample mean precipitation P<sub>g</sub> calculated from the gage amounts for less dense network of gages. This is a measure of how accurately a network of gages estimates areal averages of rain depth. In his study of 10 years of rain gage data, Huff found the error E to be a function of mean precipitation P, mean area per gage or gage area A<sub>g</sub> (km<sup>2</sup>), area of the network A<sub>n</sub> (km<sup>2</sup>), and duration T (hr) of the storm. The regression equation

$$\log E = -0.51 + 0.68 \log P + 0.94 \log A_g - 0.01 \log T - 0.75 \log A_n \quad (17)$$

fits quite well the data for 1955-59, a period in which there was a relatively large percentage (33 percent) of air mass storms with considerable spatial variability. The data for 1960-64 had 23 percent air mass showers and consequently show somewhat smaller error (Huff, 1970). Higher spatial variability suggests larger natural dispersion of rainfalls and hence a larger error for any given network. The regression equation (17) is plotted on Fig. 9 and shows that error increases with increasing mean precipitation depth although the percent error (E/P) x 100 is seen to decrease. As gage density increases, A<sub>g</sub> decreases and error decreases. Also, plotted in this figure are data from Woodley et al. (1975) for Florida in which the predominant rain was from air mass showers and may explain why errors were larger than the Illinois data which were dominated by frontal storms, squall lines, and low center storms.



Nevertheless, for those regions where air mass thunderstorms may contribute appreciably to the rainfall, Fig. 9 shows that in order to have an accuracy in areal average rainfall of 30 percent for precipitation greater than 10 mm, a gage area less than 143 km<sup>2</sup> should be adequate. However, even this spacing may be too dense for an economical measurement of rain over large areas.

Figure 9. Absolute difference of mean areal average rain depth computed for a thinned network of gages having indicated area per gage A<sub>g</sub> and the depth computed for the full dense network.



ORIGINAL PAGE IS  
OF POOR QUALITY

Also plotted on this figure are data from Montana as reported by Hildebrand et al. (1979). He combined several data sets to give a percent error independent of P, but we have arbitrarily plotted this percent error at a P=10 mm. The brackets next to the Montana data are the mean areas per gage. Based upon this Montana data, a gage area of 114 km<sup>2</sup> gives an accuracy of 30 percent, a somewhat larger gage density (smaller A<sub>g</sub>) than required in Florida or Illinois for the same accuracy.

The data accuracy exhibited in Fig. 9 could serve as a guide for determining gage deployment in absence of radar. Hildebrand suggests that radar used in conjunction with gages as outlined in the next section only improves gage estimates when gage areas are larger than 300 km<sup>2</sup>.

5.4.2 Radar, Rain Gage Combinations

Before we can confidently accept radar estimates of rainfall, we should be aware of the phenomena that can cause variance from gage estimates. If only reflectivity factor measurements are available, one needs to choose an appropriate R, Z relation. As we saw in Fig. 8, parameters N<sub>0</sub> and D<sub>0t</sub> of an assumed exponential dropsize distribution vary considerably from point-to-point so one may also expect the R, Z relation to vary. On the other hand, for areal averages of rain, there is suggestive evidence that N<sub>0</sub> and D<sub>0t</sub> may be appropriately chosen to produce an R, Z relation that, in the mean, predicts the average rainfall measured by a network of gages.

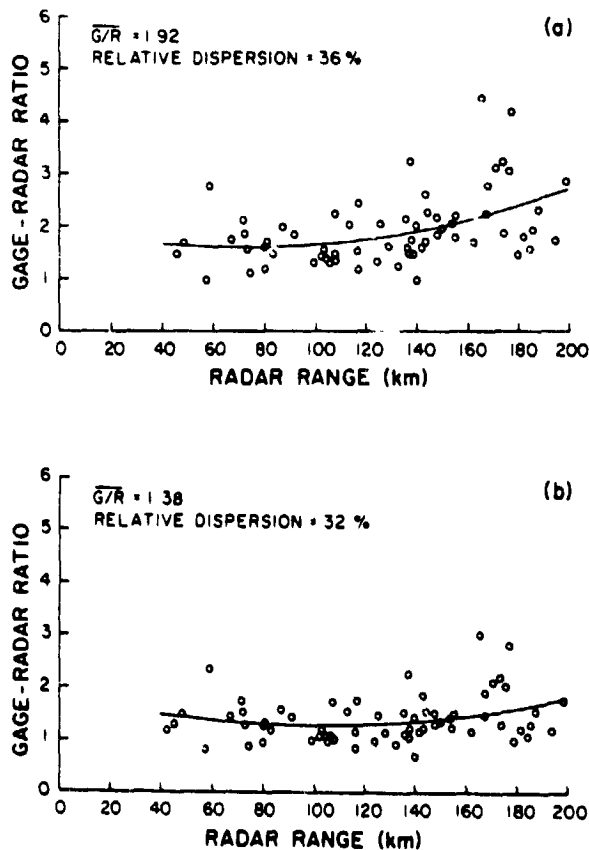


Fig. 10 shows comparison of gage to radar estimate of water depth  $\frac{GER}{RER}(\frac{G}{R})$  at 65 gage locations for a shower observed with the National Severe Storms Laboratory's WSR-57 radar located in Central Oklahoma. Although, for this day, the GER was 1.38 times higher than the RER, the average ratio  $\frac{G}{R}$  for 14 rain events was 1.05 when the M-P relation  $200 R^{1.6}$  was used (Brandes and Sirmans, 1976). Because daily radar calibrations can be in error, as well as different R, Z relations might be appropriate for different locations being surveyed by the radar, it becomes mandatory to adjust radar rain estimates in accordance with the in situ gage measurements. But, as can be deduced by examining Fig. 10, if few rain gages were used, large errors could result!

Figure 10. Range distribution of G/R ratios using radar measurements (a) uncorrected and (b) corrected for atmospheric absorption, rainfall attenuation, and biases due to reflectivity gradients. (Convective precipitation, Oct. 10-11, 1974). Relative dispersion is the standard deviation expressed as a percentage of the mean (from Brandes and Sirmans, 1976).

An objective of the gage-radar rainfall estimation technique is to combine sparse gage and radar rainfall data to produce a rainfall estimate with the point accuracy of the gages and the spatial resolution and coverage of the radar. The technique would work quite well if the radar measured the spatial variability of  $R$ , but in fact it only measures  $Z$  variability (compare Figures 8(a) and (e)). Secondly, the technique assumes that the gage measures an  $R$  that fills the resolution volume at the individual gage location. The capability of the radar to measure  $R$  variations is not well verified but is reasonable only if dropsize distribution does not change appreciably from storm cell to storm cell or within the cell. However, if the radar measures  $Z_{DR}$  and  $Z_H$  or  $Z_V$ , it will map better the spatial variations in  $R$ . Then a few rain gages would be helpful in removing the pervasive bias due to radar calibration error.

Even if the radar poorly measures the actual variation of rain rate, there may still be value in gage-radar combinations if the horizontal scales of  $N(D)$  are large compared to gage spacings. In the studies of Wilson (1970) and Brandes (1975), the gage-radar mean rainfall estimates were more accurate than the gage only estimates for large area (29,000 km<sup>2</sup>), low-gage density ( $\leq 1$  gage per 700 km<sup>2</sup>), long duration rainfall cases. Brandes (1975) shows that radar measured rain corrected by gage data improved the accuracy from 24 percent for gage alone measurements to 14 percent for radar-gage combined measurements with gage density of 1 gage per 1600 km<sup>2</sup>.

When gage spacings are large compared to the scales of  $N(D)$ , then large errors can be made using radar and rain gage combinations if radar only measures the spatial variability of  $Z$ . However, if it also measures  $Z_{DR}$ , then radar should measure better the spatial variability of  $R$ , and few gages would be required to remove bias errors.

## 6. CONCLUSION

Several techniques for rain rate measurement have been reviewed. It is concluded that after many years of technique development there is still no satisfactory proven method in use to accurately estimate rain rate when high spatial resolution is required. Dual parameter measurement techniques appear to offer the best possibility for rain rate estimation.

If  $N(D)$  is controlled by coalescence and drop breakup and is in steady state, Srivastava's (1971) results show that  $N(D)$  is only a function of liquid water density. Hence, a one-parameter radar measurement, for example  $Z$ , would suffice to estimate  $R$ . If  $N(D)$  were not in steady state, this brings us to some interesting questions. Assuming that the initial cloud dropsize spectra are known, could one use time of measurement in the evolution of the rain cell as a second measurement parameter to estimate  $R$  or  $M$  from  $Z$ ? If so, then the parameters time and  $Z$  are two parameters that could be used to deduce the spatial variability of  $R$  and  $M$ , and a few rain gages would only be required to remove any pervasive bias due to inaccurate radar calibration. Since the theoretical results of Srivastava (1971) suggest that the time to reach steady state depends upon the initial distribution, could rates of change of  $Z$  be useful to estimate  $N(D)$  in evolving rain cells?

Observed cloud drops often appear in exponential distributions and evolve into the steady-state rain spectra shown on Fig. 1. Although these spectra are not exponential, they can be fitted by truncated exponential functions. With this view, we see that as rain spectra are evolving, they can continuously be fitted by an exponential function but, in contrast to a fixed  $N_0$  as in the M-P

distribution,  $N_0$  and  $D_{0t}$  would both be variables that need to be measured. Hence, for low rain rates, a two parameter radar measurement should satisfactorily describe the dropsize distribution. But as steady state is approached at large  $R$ , it will be important to at least truncate the spectrum because large drops significantly contribute to  $R$ . We then can no longer describe  $N(D)$  by 2 parameters unless there is some deterministic relation between  $D_0$ ,  $N_0$ , and  $D_{max}$  at large  $R$ .

## 7. ACKNOWLEDGMENTS

I fully appreciate the dedication of Mss. Walton and Tyo who did an excellent job in typing and editing this paper. The graphic work reflects the patience and care of Ms. Kimpel and Mr. Clark.

## 8. REFERENCES

- Al-Khatib, H.H., T.A. Seliga, and V.N. Bringi, 1979: Differential reflectivity and its use in the radar measurement of rainfall. Rpt. AS-S-106, Atmos. Sci., Prog., The Ohio St. Univ.
- Atlas, D., and A.C. Chmela, 1957: Physical-synoptic variations of dropsize parameters. Proc. Sixth Wea. Radar Conf., Am. Meteor. Soc., Boston, Mass., 21-30.
- \_\_\_\_\_, and C. W. Ulbrich, 1974: The physical basis for attenuation-rainfall relationships and the measurement of rainfall parameters by combined attenuation and radar methods. J. De Recherches Atmospheriques, Vol.VIII, Jan.-Jun., Nos. 1-2, 275-298.
- \_\_\_\_\_, 1977: Path- and area-integrated rainfall measurement by microwave attenuation in the 1-3 cm band. J. Appl. Meteor., 16, 1322-1331.
- \_\_\_\_\_, R. C. Srivastava, and R.S. Sekhon, 1973: Doppler radar characteristics of precipitation at vertical incidence. Rev. Geophys. Space Phys., 2, 1-35.
- Battan, L.J., 1973: Radar Observation of the Atmosphere. Chicago, IL: Univ. Chicago Press.
- Brandes, E., 1975: Optimizing rainfall estimates with the aid of radar. J. Appl. Meteor., 14, 1339-1345.
- \_\_\_\_\_, and D. Sirmans, 1976: Convective rainfall estimation by radar: Experimental results and proposed operational analysis technique. Preprints, Conf. Hydro-Meteor., Apr. 20-22, Am. Meteor. Soc., Boston, Mass., 54-59.
- Cain, D. E., and P. L. Smith, Jr., 1976: Operational adjustment of radar estimated rainfall with rain gage data: A statistical evaluation. Preprints, 17th Conf. Radar Meteor., Oct. 26-29, Seattle, Am. Meteor. Soc., Boston, Mass., 533-538.
- Gans, R., 1912: Uber die form ult ramikroskopischer goldteilchen. Aun. Phys., 37, 881-900.
- Goldhirsh, J., 1975: Improved error analysis of raindrop spectra, rain rate, and liquid water content using multiple wavelength radars. IEEE Trans. Antennas Prop., Vol. AP-23, Sept., 718-720.

- \_\_\_\_\_, and I. Katz, 1974: Estimation of raindrop size distribution using multiple wavelength radar systems. Radio Sci., 9, (4), 439-446.
- Gunn, R., and G. D. Kinzer, 1949: The terminal velocity of fall for water droplets in stagnant air. J. Meteor., 6, 243-248.
- Hildebrand, P.H., N. Towery, and M.R. Snell, 1979: Measurement of convective mean rainfall over small areas using high-density rain gages and radar. J. Appl. Meteor., 18, 1316-1326.
- Huff, F.A., 1970: Sampling errors in measurement of mean precipitation. J. Appl. Meteor., 9, 35-44.
- Jones, P.M.A., 1956: Rainfall dropsize distributions and radar reflectivity. Res. Rept. No. 6 Urbana: Meteor. Lab, Illinois St. Water Survey.
- Joss, J., and A. Waldvogel, 1970: A method to improve the accuracy of radar measured amounts of precipitation. Preprints, 14th Radar Meteor. Conf., Am. Meteor. Soc., Boston, Mass., 237-238.
- Laws, J. O., and D. A. Parsons, 1943: The relationship of raindrop size to intensity. Trans. Am. Geophys. Union, 24th Annual Mtg., 452-460.
- Leber, G. W., C. J. Merritt, and J.P. Robertson, 1961: WSR-57 analysis of heavy rains. Proc. Ninth Wea. Radar Conf., Am. Meteor. Soc., Boston, Mass., 102-105.
- Marshall, J.S., and W. Palmer, 1948: The distribution of raindrops with size. J. Meteor., 5, 165-166.
- Neff, E.L., 1977: How much rain does a rain gage gage? J. Hydrology, 35, 213-220.
- Seliga, T. A., and V. N. Bringi, 1976: Potential use of radar differential reflectivity measurements at orthogonal polarizations for measuring precipitation. J. Appl. Meteor., 15, 69-76.
- \_\_\_\_\_, 1978: Differential reflectivity and differential phase shift: Applications in radar meteorology. Radio Sci., 13, 271-275.
- Srivastava, R. C., 1967: On the role of coalescence between raindrops in shaping their size distribution. May, J. Atmos. Sci., 287-292.
- \_\_\_\_\_, 1971: Size distribution of raindrops generated by their breakup and coalescence. J. Atmos. Sci., 28, 410-415.
- Ulbrich, C. W., and D. Atlas, 1978: The rain parameter diagram: Methods and applications. J. Geophys. Res., 83, (C3), 1319-1325.
- Waldvogel, A., and B. Federer, 1976: Large raindrops and the boundary between rain and hail. Preprints, 17th Conf. on Radar Meteor., Am. Meteor. Soc., Boston, Mass., 167-172.
- Waldteufel, P., 1973: Attenuation des ondes hyperfréquence par la pluie: une mise au point. Ann. Telecommunic, France, 28, 255-272.

Wexler, R., and D. Atlas, 1963: Radar reflectivity and attenuation of rain, J. Appl. Meteor., 2, 276-280.

Wilson, J.W., 1970: Integration of radar and gage data for improved rainfall measurement. J. Appl. Meteor., 9, 489-497.

Woodley, W.L., A.R. Olsen, A. Herndon, and V. Wiggert, 1975: Comparison of gage and radar methods of convective rain measurement. J. Appl. Meteor., 14, 909-928.

D22

N83 25291

ORIGINAL PAGE IS  
OF POOR QUALITY

## GROUND TRUTH FOR OCEANIC RAINFALL

Clive E. Dorman  
Department of Geological Sciences  
San Diego State University

### 1. INTRODUCTION

In the past, oceanic rainfall was extrapolated from land and island measurements. It was uncertain how representative the land measurements were in local and remote oceanic areas. There were even suggestions that orographic effects raised land measurements significantly higher than oceanic values. Now, however, several independent oceanic rainfall analyses are available. Although these analyses are based upon different techniques, they produce similar values. This agreement suggests that island and coastal measurements are suitable to calibrate satellite oceanic rainfall measurements.

### 2. CLIMATIC RAINFALL ESTIMATES

There are several independent oceanic rainfall analysis techniques that agree in details. Perhaps one of the best and most up-to-date land based measurement analyses is by Baumgardner and Reichel (1975). This modern work has the advantage of additional data from the expanded station network after World War II and satellite cloud patterns to guide analysis in remote areas with no observations. Because of the superior data base, this analysis is significantly better than earlier land based analyses still cited in literature, although some were produced in the 1920's and 1930's.

Studies based only upon low island and atolls agree with land stations analysis. These include studies by Stoddart (1971) and Taylor (1973). Experienced meteorologists feel that atolls are representative of the open ocean rainfall. This instinct is confirmed by the plotting of lines of low island measurements when these islands cross large rainfall gradients in the tropical Pacific. Such plotting yields smooth curves. These curves confirm that low islands have an insignificant effect on the measured rainfall (See Figures 1 and 2, and Table 1).

Satellite cloud analysis correlates well with land and island measured rainfall patterns, particularly in the lower latitudes. Examples of such cloud analysis may be found in Sadler, Oda, and Kilonsky (1976). Kilonsky and Ramage (1976) took advantage of the strong relationship between tropical clouds and rainfall by using atoll measurements to calibrate satellite cloud analysis and calculate Pacific tropical ocean rainfall.

Open ocean rainfall intensity has been estimated from satellite radar microwave measurements (Rao, *et al*, 1977). If it is assumed that these intensities are related to the total rainfall, then this analysis correlates with the others. Unfortunately these radar measurements were coarsely averaged over intensity and over  $10^{\circ}$  by  $10^{\circ}$  of latitude and longitude. Still, some limited confidence of the radar analysis may be gained since large areas are correlated into patterns.

ORIGINAL PAGE 13  
OF POOR QUALITY

Ships of opportunity present weather observations have been used to estimate rainfall. Dorman and Bourke (1979, 1981) and Dorman (1981c) have constructed estimates for the open ocean based upon temperature corrected Tucker estimates. A composite may be seen in Figure 3.

Reed and Elliott's (1979) recent analysis disagrees with the above analyses in pattern and amounts. This analysis uses the uncorrected Tucker estimates to regress present weather observation to one frequency of rain value. The fact that single frequency of precipitation is not well correlated with peak rainfall at islands (Lavoie, 1963) is a significant problem for the technique. Reed and Elliott's analysis increasingly underestimates even low atoll measurements, exceeding a factor of two or three in the Pacific Inter-Tropical Convergence Zone (See Figures 1 and 2, Table 1). Reed and Elliott's rainfall patterns conflict with the corrected Tucker ship based patterns (Dorman and Bourke, 1979, 1981), satellite cloud patterns (Sadler, Oba, Kilonsky, 1976), and satellite radar measurements. These and other criticisms are discussed in Dorman (1980, 1981a, 1981b).

### 3. GENERAL CLIMATOLOGY

We can use instead the data from the collection of studies which are in agreement to define the general climatology of oceanic rainfall. Figure 3 shows an annual map composited from Dorman and Bourke (1979, 1981) and Dorman (1981c). This could be used for general testing of satellite estimates.

It is important to recognize that suitable averaging scales for the oceanic rainfall vary considerably. The Pacific has a significantly longer east-west scale than the Atlantic or the Indian and is more amenable to coarser averaging. However, the maximum scales are  $2^{\circ}$  of latitude by  $5^{\circ}$  of longitude for the open ocean in general. But a  $1^{\circ}$  of latitude by  $5^{\circ}$  of longitude would be the maximum for the tropical Atlantic and Indian Oceans with their shorter scales. Resolving complicated coastal rainfall requires averaging areas certainly no more than one degree square. In higher rainfall coastal areas, as on the east side of Central America, even this is too coarse. Averaging over scales larger than those mentioned here will mask significant variations and significantly degrade the usefulness of any product.

### 4. LOCAL VARIATIONS

It would be useful to see if future satellite estimates can successfully replicate shorter term variations in rainfall. Coastal and island stations could be used to compute time series of the deviation from the mean to be compared to a time series of the satellite estimate for that local area. For such an investigation, the local area should be restricted to a physically sensible region. Such an investigation would be feasible since most oceanic climatic areas have reporting meteorological stations from which the data is readily available.

For variations, a month is perhaps optimal for the basic averaging in time. In length, a time series of the order five years is appropriate for the mid-latitudes. However, for areas of high variability and low rainfall, such as the subtropics, a time series of 10 years would be more appropriate.

ORIGINAL POINT  
OF POOR QUALITY



REFERENCES

- Baumgartner, A. and E. Reichel, The World Water Balance: Mean Annual Global, Continental, and Maritime Precipitation, Evaporation, and Runoff. Elsevier, New York, 1975.
- Dorman, C. E., 1980a: Comments on 'The Relationship between the Amount of Frequency of Precipitation over the Ocean.' J. Appl. Meteor., 19, 0131-0133.
- Dorman, C. E., 1981a: Comments on 'New Precipitation Maps for the North Atlantic and North Pacific Oceans.' Accepted by J. Geophys. Res.
- Dorman, C. E., 1981b: Comments on 'Comparison of Ocean and Island Rainfall in the Tropical Pacific.' Submitted to J. Appl. Meteor.
- Dorman, C. E., 1981c: Indian Ocean Rainfall. Submitted to Mon. Wea. Rev.
- Dorman, C.E., and R. H. Bourke, 1978: A temperature Correction for Tucker's Ocean Rainfall Estimates. Quart. J. Roy. Meteor. Soc., 104, 765-773.
- Dorman, C. E., and R. H. Bourke, 1979: Precipitation over the Pacific Ocean, 30°S to 60°N. Mon. Wea. Rev., 107, 896-910.
- Dorman, C. E., and R. H. Bourke: Precipitation over the Atlantic, 30°S to 70°N. Mon. Wea. Rev., 109, 148-157.
- Kilonsky, B. J., and C. S. Ramage, 1976: A technique for estimating tropical open-ocean rainfall from satellite observations. J. Appl. Meteor., 15, 972-975.
- Lavoie, R. L., 1963: Some aspects of the meteorology of the tropical Pacific viewed from an atoll. Atoll Research Bulletin, 96, 1-77.
- Rao, M. S. V., and J. S. Theon, 1977: New features of global climatology revealed by satellite-derived oceanic rainfall maps. Bull. Amer. Meteor. Soc., 58, 1285-1288.
- Reed, R. K., and W. P. Elliott, 1979: New Precipitation maps for the North Atlantic and North Pacific Oceans. J. Geophys. Res., 84, 7839-7846.
- Stoddart, D. R., 1971: Rainfall on Indian Coral Islands, Atoll Res. Bull., 147, Smithsonian Inst.
- Sadler, J. C., L. Oda and B. J. Kilonsky, 1976: Pacific Ocean Cloudiness from Satellite Observations. Rep. UHMET 76-C1, U. of Hawaii.
- Taylor, R. C., 1973: An Atlas of Pacific Islands Rainfall. Rep. HIG-73-9, Hawaii Institute of Geophysics, 7 pp. + 13 fig.

Table 1. Island Stations plotted.

ORIGINAL PAGE IS  
OF POOR QUALITY

JOHNSTON - PUKA PUKA				
NO.	STATION	LATITUDE	LONGITUDE	MEASURED (mm)
1	Johnston	16°44N	169°31W	710
2	Palmyra	5°52N	162°06W	4162
3	Washington	4°43N	160°25W	2903
4	Fanning	3°55N	159°23W	2086
5	Christmas	1°59N	157°22W	766
6	Malden	4°01 S	155°01W	689
7	Phoenix	9°01S	158°03W	1893
8	Puka Puka	10°53S	165°49W	2853
MIDWAY - KAPINGAMARANGI				
36	Midway	28°13N	177°22W	1100
9	Wake	19°17N	166°39E	965
37	Eniwetok	11°21N	162°21E	1470
38	Ujelang	9°42N	161°02E	1980
39	Mokil	6°41N	159°47E	3056
40	Kapingamarangi	1°05N	154°48E	2808

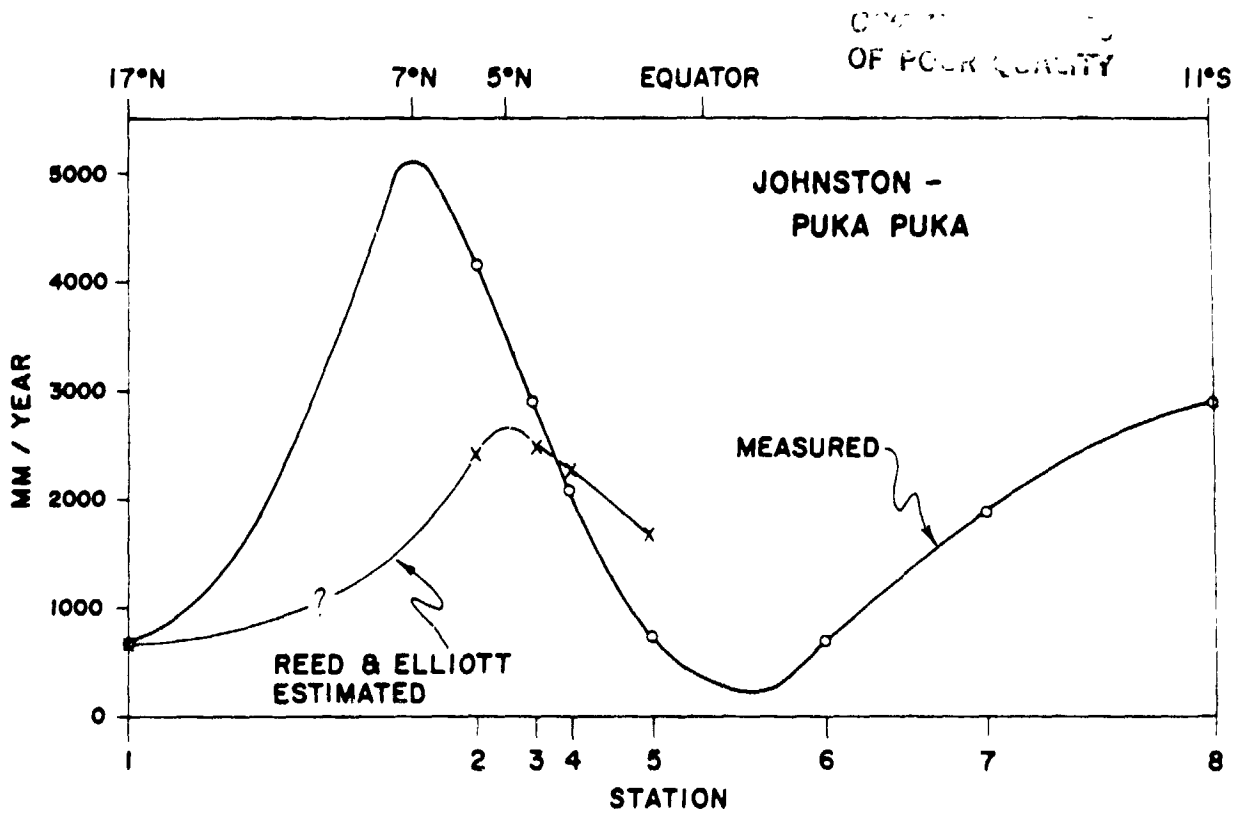


Figure 1. Annual rainfall measured at the Line Islands in the central equatorial Pacific. The smoothness of the fit suggests that small island measurements are representative of open ocean rainfall. Reed and Elliott's rainfall estimate is also plotted for comparison.

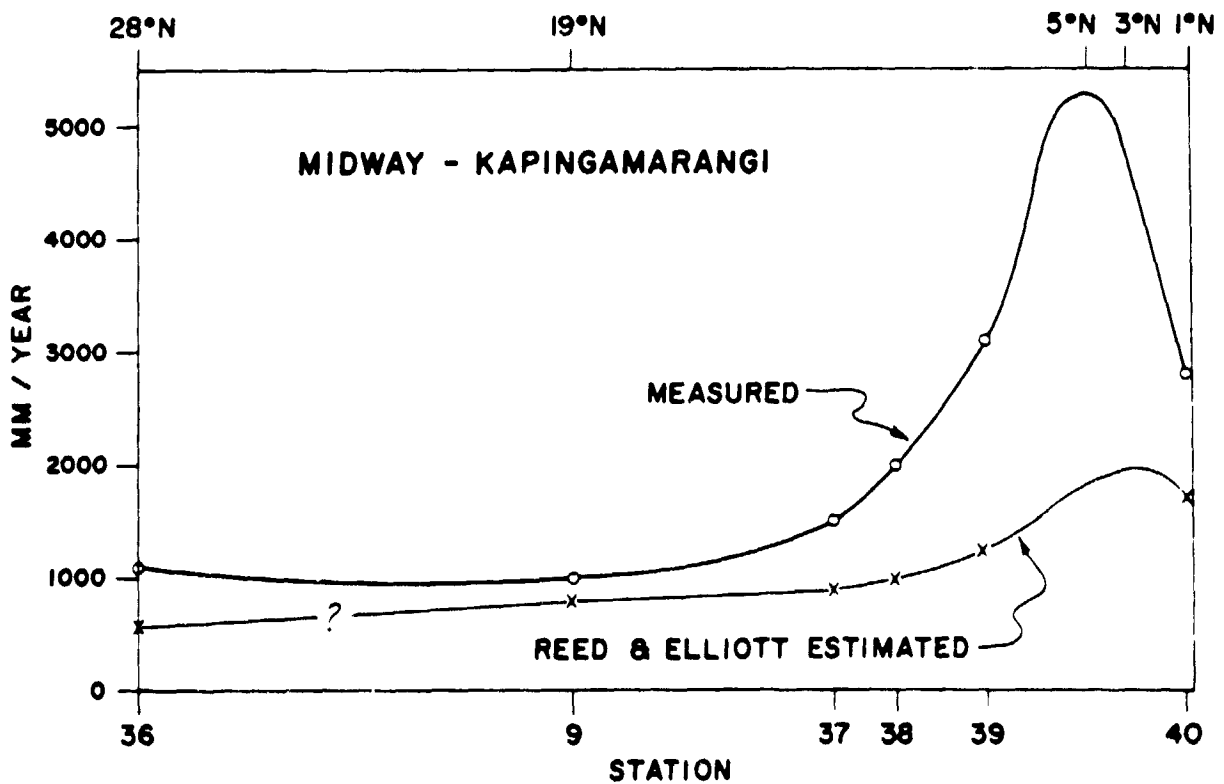


Figure 2. Midway-Kaplingamarangi. See Figure 1 caption for explanation.

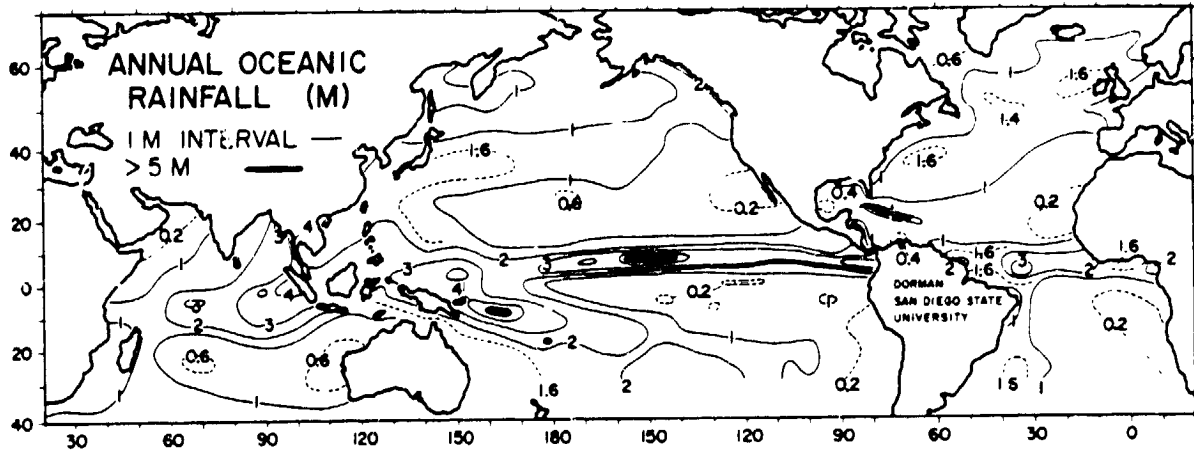


Figure 3. Annual oceanic rainfall.

ORIGINAL PAGE IS  
OF POOR QUALITY

OFFICE OF  
OF PROGRAMS  
ITY

PRECIPITATION MEASUREMENTS FOR EARTH-SPACE COMMUNICATIONS:  
ACCURACY REQUIREMENTS AND GROUND-TRUTH TECHNIQUES

L. J. Ippolito, NASA Headquarters  
R. Kaul, ORI, Inc.

I. INTRODUCTION

The Role of Rain on Communication Links

Communications systems operating at frequencies in excess of 10 GHz are degraded significantly by rainfall. To provide the information needed for design of these millimeter wave systems (defined in this paper as 10 to 100 GHz) NASA has been developing rain attenuation models and accumulating data bases of propagation related information. These data bases have, for the most part, been developed based on the signal level measurements of geostationary satellite beacons at selected frequencies (Kaul, et al, 1977). Recently, ground-based radar reflection measurements have been shown to be able to develop data bases for system design (Goldhirsh, 1978). The rain attenuation models have now allowed accurate correlation between the rain rate and the attenuation.

Generally, the system designer is concerned with the annual cumulative attenuation statistics to be expected along the selected path. The path may be part of either a terrestrial or earth-space system. This paper will emphasize earth-space systems, but similar considerations apply to terrestrial systems. These cumulative rain attenuation statistics identify, for a given system rain margin, what percentage of the average year the system will operate to a specified performance level. In addition, in some instances, worst month system performance requirements and/or the maximum outage time are also specified for the system designer. The designer is then confronted with utilizing the most stringent requirement to select the system margin. In the case of earth-space systems, system margin on the downlink can be quite expensive. This arises because the prime power for powering the satellite-borne transmitter is quite expensive and the design of large space-qualified antennas is also quite expensive.

Large Scale Rain Models

The Rice-Holmberg Model (Rice and Holmberg-1973) is based upon two rainfall types: convective (thunderstorm) rains and stratiform (uniform) rains. The statistical model is based upon the sums of individual exponential terms for each mode of rainfall. An independent parameter,  $B$ , is utilized to select the amount of total annual rainfall,  $M$ , associated with each mode. In their original paper they provide plots of  $B$  and  $M$  throughout the world based on meteorological data. In general it is anticipated that millimeter

meter wave communication systems will be designed to operate during most stratiform rainfall periods, but not during heavy convective rainfall periods.

Recently, a Global Model (Crane - 1980) has been developed based on meteorological observations. Eight median point rainrate cumulative distributions have been developed to describe the world's rainfall characteristics. In Europe and the U.S. where more data is available, these regions have been expanded into higher resolution regions. These distributions cover the range from 2% (175 hours/year) to 0.001% (5.3 minutes/year). Typically, domestic communication systems operate at 99.5 to 99.99% availability on a path, so the attenuations associated with the range 0.01 to 0.5% of the year are of most interest to designers.

Specific Attenuation and Effective Path Length

Given the rain rate distribution models or measurements, the designer must develop the estimate of the total attenuation distribution for his specific system configuration. Alternatively, he can make direct attenuation measurements of satellite-borne beacon or radiometric measurements of sky temperature. Generally these direct measurements are not available so the designer develops the attenuation statistics from the rain statistics.

The attenuation associated with a microwave signal passing through a specified volume of rain has been estimated using Mie scattering theory (Olsen, et al - 1978) for various drop size distributions. These calculations, along with experimental measurements (Ryde and Ryde - 1945), have resulted in the empirical relation.

$$\alpha = a(f)R^{b(f)} \text{ dB/km}$$

where  $\alpha$  is the specific attenuation,  $R$  is the rain rate in mm/hr and  $a$  and  $b$  are frequency (and to some degree rain rate) dependent parameters (Olsen, et al - 1978).

The effective path length  $L_e$  has been developed to extend the attenuation associated with one kilometer of rain to the total attenuation along the earth-space path. It assumes that the rain rate  $R$  is uniform over the hypothetical path length  $L_e$ . Of course, uniform rain is not the case, but to a first approximation the total attenuation  $A$  is

$$A = \alpha R^b L_e \text{ dB.}$$

ORIGINAL DATA IN  
NOT QUALITY

For frequencies up to 30 GHz L appears to be relatively independent of frequency.

Total Attenuation Implies Rain Rate

Based on the above relations it is clear that an empirical statistical relation exists between the total attenuation and the rain rate measured at a point on the surface of the earth. By inverting this relation

$$R = \left( \frac{A}{aL_e} \right)^{\frac{1}{b}}$$

and considering the attenuation measurements made to date it is possible to provide ground truth measurements of the rain rate being observed by a space-borne meteorological monitoring system (see Section III). In addition, this relation can be utilized to estimate the accuracy required of the rain rate measurements to provide meaningful design information for system builders (see Section II).

Attenuation and Precipitation Measurements

Extensive experimental research has been performed by direct measurement of rain effects on earth-space paths beginning in the late 1960's with the availability of orbiting propagation beacons on geostationary satellites (Kaul et. al. - 1977, 1980 and Ippolito - 1981). The satellites include ATS-5, ATS-6, CTS, the three COMSTAR satellites, ETS-II, CS, BSE, SIRIO and OTS. Table I lists the launch date, orbit location and frequencies for each of the satellites.

TABLE I  
SATELLITES UTILIZED FOR PROPAGATION  
STUDIES ON EARTH-SPACE PATHS

SATELLITE	LAUNCH DATE	ORBIT LOCATION	FREQUENCIES (GHz)	
			UPLINK	DOWNLINK
ATS-6 (USA)	8-68	10°W	21.6 GHz	16.2 GHz
ATS-6 (USA)	8-74	8°W 3°E (BSE) 10°W (CTS)	16.2 17.7	12
CTS (CANADA)	1-76	11°W	16.162	11.7 16.2
COMSTAR (USA)	6-76 (BSE) 7-76 (BSE) 6-76 (BSE)	10°W 10°W 10°W	-	16 20.4 20.4
ETS-II (JAPAN)	3-77	10°E	-	17 11.8 16.2
BSE (ITALY)	6-77	10°W	17.4	11.8
CS (JAPAN)	10-77	10°E	27.28-28.28	17.76-18.28
BSE (JAPAN)	4-78	11°E	16.162	11.7 16.2
OTS (USA)	6-78	10°E	16.2 16.2	11.8 11.8

Table II summarizes the results of 11 GHz measurements observed in the United States, Europe and Japan utilizing the CTS, SIRIO, BSE and ETS-II satellite beacons at 11.7, 11.6, 11.7, and 11.5 GHz respectively. The U.S. slant paths tend to exhibit more severe attenuation than the European slant paths for a given percent time. This is to be expected since the rain conditions are more severe in the U.S. regions, particularly for thunderstorm occurrence periods, which account for most of the attenuation observed for less than

TABLE II

SUMMARY OF 11 GHz ANNUAL  
ATTENUATION MEASUREMENTS

LOCAL ON	ELEVATION ANGLE	TIME PERIOD	ATTENUATION (dB) FOR GIVEN PERCENT OUTAGE							
			1%	0.5%	0.1%	0.05%	0.01%	0.005%	0.001%	0.0001%
USA - NEW YORK	20°	FEB 77 - JAN 78 FEB 78 - JAN 79	2.7	2.7	7.5	7.5	15.8	15.8	15.8	15.8
EUROPE - NETHERLANDS	27°	JAN 78 - JAN 77 JAN 77 - JAN 78 JAN 78 - JAN 79	2.1	2.1	3	3	12.5	12.5	12.5	12.5
EUROPE - GERMANY	20°	JAN 78 - JAN 77 JAN 77 - JAN 78 JAN 78 - JAN 79	2.1	2.1	6	6	12	12	12	12
EUROPE - BLACKSBURG, VA	30°	JAN 78 - DEC 78 JAN 77 - DEC 77	2	2	3.7	3.7	9.9	9.9	9.9	9.9
USA - ALBANY, NY	40°	FEB 78 - JAN 79	4.1	4.1	3	3	13	13	13	13
EUROPE - BERNICA, ITALY	20°	JAN 78 - DEC 78 (BY COMSTAR)	3	3	6.8	6.8	-	-	-	-
USA - PUEBLO, CO	30°	JAN 78 - DEC 78	-	-	3	3	13	13	13	13
USA - LAKE O HAVEN, OHIO	30°	JAN 78 - DEC 78	-	-	2	2	17	17	17	17
EUROPE - BERNICA, ITALY	27°	JAN 78 - OCT 78 JAN 78 - JAN 77 JAN 78 - JAN 79	6	6	11	11	18	18	18	18
USA - ALBANY, NY	40°	FEB 78 - JAN 79	-	-	2.7	2.7	7.5	7.5	7.5	7.5
USA - ALBANY, NY	40°	FEB 77 - JAN 78	-	-	1.2	1.2	11	11	11	11

INCLUDES HAZARDOUS DATA

about 0.05 percent of the time. The Japanese data tends to fall between the U.S. and European results. The mean attenuation for the time (53 minutes per year) is 11.2 dB for the U.S. paths, 4 dB for the European paths, and 5.8 dB for Japan. Some variability between locations is to be expected because of the different observation periods and elevation angles, however, the data does exhibit a fairly consistent trend and gives a good indication of expectations for an operational communications link.

The five U.S. locations have acquired nearly 15 station-years of 11.7 GHz satellite attenuation data and the long term attenuation distributions are shown Figure 1 (Ippolito, 1981). The multi-year distributions demonstrate the 'dual mode' characteristic of rain induced attenuation, where the low attenuation values, below about 5 dB in amplitude, are caused by stratiform rainfall and the higher attenuation 'tails' of the distribution are produced by the more severe convective rain usually associated with thunderstorm activity. The resulting rain margins for the four U.S. stations which have elevation angles near 30° are 2.5 + 1dB, 11.2 + 2.2dB, and 14.5 dB + 3 dB for link reliabilities of 99.9, 99.99, and 99.995 percent respectively.

A large data base of rain attenuation measurements in the 20/30 GHz bands also is available in the U.S., beginning with measurements in 1974 utilizing the ATS-6 satellite. Tables III and IV present listings of attenuation statistics at 20 and 30 GHz respectively, for several slant paths with elevation angles ranging from 18.5 to 54.4 degrees. The attenuation is, as expected, more severe with increasing frequency, reaching very high levels at 30 GHz for percent times less than 0.05. The mean attenuations for 0.5 percent of the time are 2.7 dB and 5.7 dB for 20 and 30 GHz, and for 0.1 percent of the time are 8.7 dB and 15.8 dB.

A large portion of the slant-path locations listed above have also acquired rain rate distributions coincident with the attenuation distributions.

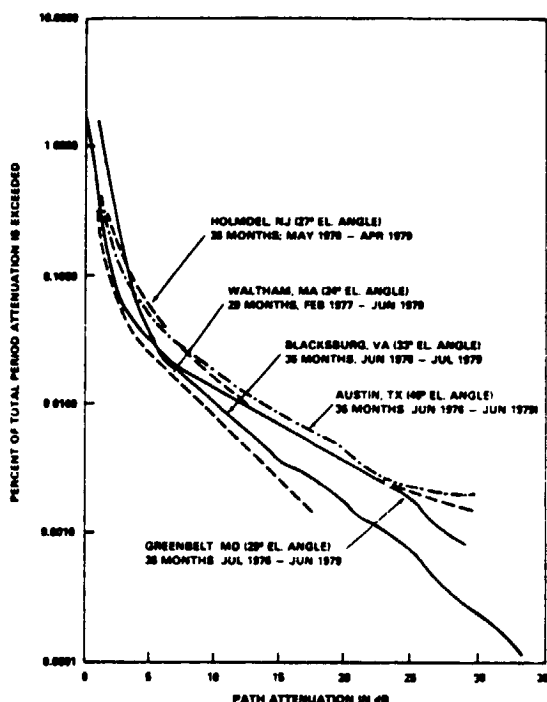


FIGURE 1. MULTI-YEAR 11.7 GHz ATTENUATION DISTRIBUTIONS MEASURED IN THE UNITED STATES

Similar results are observed for most of the U.S. locations where the rain rate data have been processed and analyzed. The measurements are obtained from tipping bucket rain gauges, and annual distributions are developed for comparison with the measured attenuation distributions. The next section discusses accuracy requirements for measurements of this type.

TABLE IV  
SUMMARY OF 30 GHz ANNUAL ATTENUATION MEASUREMENTS

LOCATION	ELEVATION ANGLE	TIME PERIOD	ATTENUATION IN DB FOR GIVEN PERCENT OUTAGE							
			1%	0.5%	0.1%	0.05%	0.01%	0.001%	0.0001%	
GRANT PARK, AL	27.2°	JUL 76 - JUN 77	-	6.5	17	>20	-	-	-	-
PALMETTO, GA	29.0°	JUN 76 - JUL 77	-	7.5	20	>20	-	-	-	-
WALTHAM, MA	29.2°	JAN 76 - DEC 76**	<2	2.8	7.5	11	>20	-	-	-
HOLMDEL, NJ	28.0°	MAY 77 - MAY 78	3.5	5.5	14.5	21.5	46	-	-	-
WALLOPE IS., VA	41.0°	APR 77 - MAR 78	2.3	4	12.5	26	-	-	-	-
GRANT PARK, AL	27.2°	AUG 77 - AUG 78	-	9	20	>20	-	-	-	-
BLACKSBURG, VA	40°	JAN 76 - DEC 76	2	5.4	17.8	14.9	24	25	26	-
ROSMAR, NC	40°	JAN 74 - DEC 74	3.9	9	23	26	-	-	-	-
PALMETTO, GA	29.0°	AUG 77 - AUG 78	-	6.5	16	>20	-	-	-	-
AUSTIN, TX	39°	OCT 76 - OCT 76	1.8	3.8	17	27.5	-	-	-	-

\*SEPTEMBER EXCLUDED \*\*FEBRUARY EXCLUDED

TABLE III  
SUMMARY OF 20 GHz ANNUAL ATTENUATION MEASUREMENTS

LOCATION	ELEVATION ANGLE	TIME PERIOD	ATTENUATION IN DB FOR GIVEN PERCENT OUTAGE							
			1%	0.5%	0.1%	0.05%	0.01%	0.001%	0.0001%	
HOLMDEL, NJ	28.0°	JUN 76 - JUN 77	7.5	4	12	18	140	-	-	
GRANT PARK, AL	27.2°	JUL 76 - JUN 77	-	5	6.5	16	>20	-	-	
PALMETTO, GA	29.0°	JUN 76 - JUL 77	-	5	16	18	>20	-	-	
WALTHAM, MA	29.2°	JAN 76 - DEC 76**	<2	<2	3.8	5.2	20	-	-	
HOLMDEL, NJ	28.0°	MAY 77 - MAY 78	1	2.8	6.5	9	22	33	>44	
GRANT PARK, AL	27.2°	AUG 77 - AUG 78	-	2.4	9	17	>20	-	-	
BLACKSBURG, VA	40°	JAN 76 - DEC 76	1.7	3.4	6.9	8.7	11.2	14.9	24	
BLACKSBURG, VA	40°	JAN 76 - DEC 76**	1	3.5	9	-	12.9	19	25	
ROSMAR, NC	40°	JAN 74 - DEC 74	1	3.8	10	11	-	-	-	
PALMETTO, GA	29.0°	AUG 77 - AUG 78	-	2	9	17	>20	-	-	
AUSTIN, TX	39°	OCT 76 - OCT 76	1	1.8	7.5	12.2	23	34	-	
TAMPA, FLA	34.1°	JAN 76 - DEC 76	<1	<1	2.1	>20	-	-	-	

\*SEPTEMBER EXCLUDED \*\*FEBRUARY EXCLUDED

Figure 2 presents three measured rain rate distributions for Greenbelt, Maryland observed during CTS observations for a three year period. (The solid and dashed prediction curves on the figure will be discussed in a later section.)

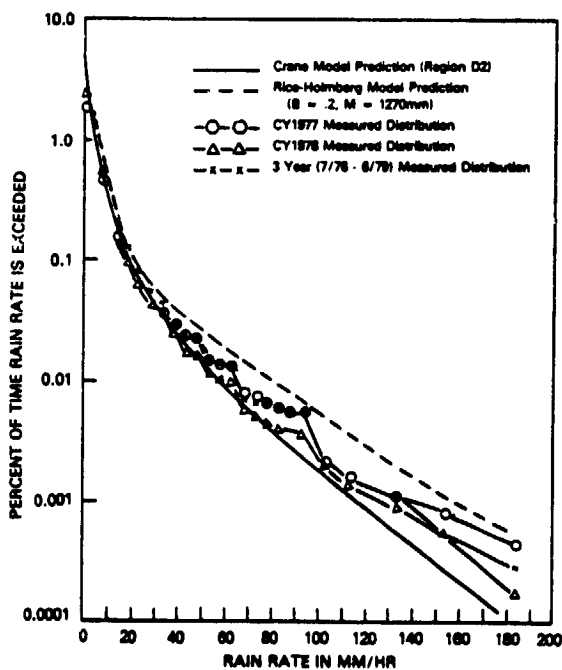


FIGURE 2. RAIN RATE DISTRIBUTIONS - GREENBELT, MARYLAND

II. ACCURACY REQUIREMENTS FOR PRECIPITATION MEASUREMENTS

Designers of future communication systems operating above 10 GHz will desire knowledge about the long term statistics of rain rates at a location. Based on the effective path length model, or other models, these statistics can be extended to attenuation statistics. However, it is reasonable to ask what accuracy of rain rate information the designer seeks. This accuracy in turn establishes the accuracy required of a spaceborne measurement system. As a first estimate of the accuracy required, the following system design will be described.

Availability Analysis Approach - Commercial

Most domestic satellite systems operating in the frequency range from 10 to 30 GHz will seek 99.5% system availability (on two links). Therefore each earth-space path will require about 99.8% availability. This level of availability corresponds to approximately 18 hours or 3/4 day of cumulative outage each year. Based on the economic considerations of loss of tariff for periods of time exceeding 18 hours, it seems logical that an upper bound of 24 hours would be acceptable.

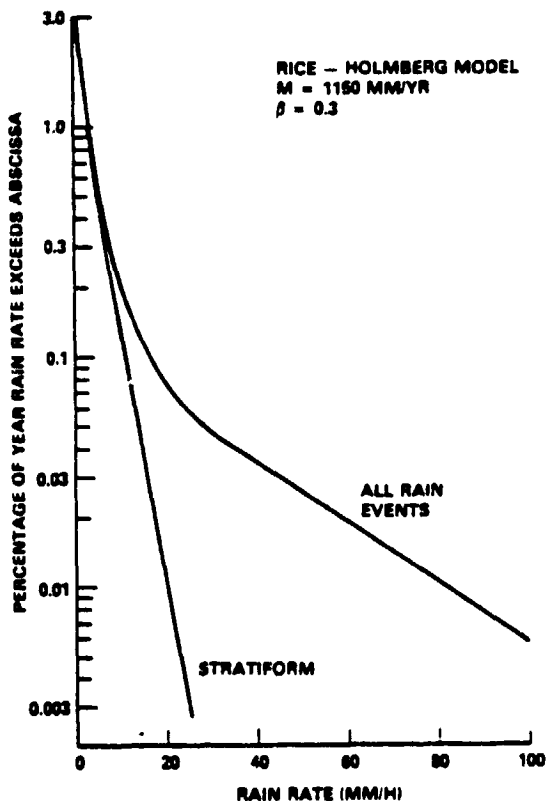


FIGURE 3. CUMULATIVE DISTRIBUTION OF RAIN RATE FOR UNIFORM AND ALL RAIN EVENTS

The corresponding availability is approximately 99.7% of a year per link. Using the cumulative rain rate distribution model developed by Rice-Holmberg (1973) applied to Washington, D.C. (see Figure 3), it appears that measurement accuracies approaching 3 mm/hr at an average rain rate of 10 mm/hr are required over a long period to develop the statistical accuracy required.

Note that the attenuation associated with this 10 mm/hr rain rate can be significant. Using the Crane model for a 40-degree elevation angle, the rain attenuation at 30 GHz is about 15 dB. Clearly this is a significant amount of system power gain required to assure system operation at the 99.5% level. In addition, a small change in the rain rate makes a significant change in the gain required for system operation.

Availability Analysis Approach - Military

For many military applications, the desired two-link availability is significantly lower than for domestic commercial users. Typical values are 95% overall or about 97% for each link. If one requires only this value of availability, then for Washington, D.C. (Figure 3) a measurement of the presence or lack of rain is required. This measurement is much less critical than the commercial case and probably could be accomplished with a space-borne radiometric monitoring system.

Maximum Outage Time Design

An alternative approach to millimeter wave system link availability synthesis is to design the system to not fail more than a given number of contiguous minutes in the average year. Using the Weather Services (U.S. Dept. of Commerce - 1955) rain rate-duration-frequency charts, the rain rate associated with this rain event can be estimated. For Washington, D.C. if an outage length exceeding 30-minutes per year is not acceptable, the system should be capable of operating through a 60 mm/h rain rate. For a 30 GHz signal at 40-degrees elevation angle, 70 dB of attenuation is encountered.

If this 30-minute period is to be accurate in the average year within  $\pm 5$  minutes, the rain rates must be measured to  $\pm 5$  mm/h during a rain event of 60 mm/h. If the accuracy is only  $\pm 10$  minutes, the error bounds on the rain rate are about  $\pm 10$  mm/hr. Note that for only 1-3/4 hours per year does the rain rate in Washington, D.C. exceed 60 mm/h.

To obtain data of the type required for this system design approach nearly continuous spaceborne observations will be required. At a minimum two observations would be made in each 5-minute period to be able to resolve the duration of a rain event to the resolution needed for this system design approach.



Diversity System Design Approach

Currently many proposed millimeter wave systems are considering utilizing site diversity ground stations in order to raise the availability of a communication system for a given level of system rain margin. A site diversity communication system utilizes two or more ground stations to simultaneously observe the same satellite from different geographic location. The locations are selected so the probability of an intense rain cell(s) simultaneously attenuating two or more links is low. This system design results in more system availability and/or the requirement for less system signal margin. However, for these systems to be effective they must operate in the region of the cumulative statistic curves where the spatially-dependent convective storms are prevalent. Referring to Figure 3, this means for periods of times less than 0.3% (about 24 hours) per year of total system down time. This time value is highly dependent on geographic location, being significantly higher where the ratio of thunderstorm rain to total rainfall is high (Kaul - 1980).

If a diversity system is desired to increase the availability by a factor of 10 (2.4 hours of down time per year) it must be able to operate at rain rates near 48 mm/h (see Figure 3). If the accuracy of the factor is to be  $10 \pm 2$ , then the rain rates must be known to  $\pm 6$  mm/h. Based on the results presented elsewhere (Kaul - 1980) at 30 HGz and 40 degree elevation angle, the maximum possible diversity gain available is about 25 dB. Since the attenuation on the worst link will be about 60 dB, a minimum rain margin of over 35 dB is required in each link assuming the ground stations are sufficiently separated to give optimum diversity gain.

In summary, the precipitation accuracy requirements required for communication system design is highly dependent on the system requirements. The broad range of possible accuracy requirements is summarized in Table V.

TABLE V  
TYPICAL RAIN RATE ACCURACIES REQUIRED FOR  
COMMUNICATION SYSTEM DESIGN

Type of System	Rain Rate*
Commercial Systems	$10 \pm 3$ mm/h
Military Systems	presence of rain
Outage Time ( $30 \pm 5$ min)	$60 \pm 5$ mm/h
Diversity System ( $I = 10 \pm 2$ )	$48 \pm 6$ mm/h
*Rain rates measured at surface	

III. SATELLITE BEACONS FOR GROUND TRUTH  
PRECIPITATION MEASUREMENTS

The evaluation of rain attenuation for satellite link system design requires a detailed knowledge of the attenuation for each ground terminal location at the specific frequency of interest. Direct long-term measurements of path attenuation for all potential ground terminal locations in an operational domestic satellite network are not feasible. Over the past several years extensive efforts have been undertaken to develop reliable techniques for the prediction of path rain attenuation for a given location and frequency, and the recent availability of satellite beacon measurements has provided for the first time a data base for validation and refinement of the prediction models.

Attenuation Prediction Models

Virtually all the prediction techniques proposed use surface-measured rain rate as the statistical variable and assume the  $aR^b$  relationship described earlier to determine rain-induced attenuation. In general, the prediction models can be expressed in the form

$$A = aR^b L(R) \quad \text{dB}$$

where R is the rain rate, a and b are the frequency-dependent constants and L(R) is an "effective" path length parameter, usually a specified function of R. The path length parameter L(R) is the coupling function that develops an attenuation distribution from a specified rain rate distribution, through the above equation. The major difference between the various rain attenuation prediction methods available is in the rationale used to develop the path length parameter L(R).

An empirical method for estimating rain-induced outage probabilities on radio-wave paths was developed by Lin (1977, 1979). The Lin method is based on a 5-min point rain rate rather than the 1 min or less rain gage integration times of other prediction techniques. Two arguments are presented to justify the use of the 5-min averaging time. First, the available long-term rain rate data published by the National Climate Center have minimum integration times of 5 min, and attempts to estimate shorter times from the original strip chart data produce significant uncertainty. Second, the 5-min averaging time effectively develops a path average rain rate distribution from a point rain rate distribution; i.e., the spatial average of the rain rate along the radio-wave path can be represented by a 5-min average of the rain rate at a single point on the path.

The effective path length from the Lin method is

$$L(R_5) = \frac{2636}{R_5 - 6.2 + \frac{2636 \sin \theta}{4 - 6}}$$

ORIGINAL PAGE IS  
OF POOR QUALITY

where  $R_5$  is the 5 minute point rain rate,  $\theta$  is the slant-path elevation angle, and  $G$  is the ground terminal elevation above sea level.

Figure 4 presents a comparison of the attenuation prediction model as calculated by Lin with measured attenuation statistics for four locations in the eastern United States at frequencies from 11.7 to 28.56 GHz. The prediction curves are seen to give very good agreement with the measured data throughout the range of comparison.

A rain attenuation prediction model recently developed by R. K. Crane provides, for the first time, a completely self-contained prediction procedure that is applicable on a global basis (Crane-1980). The global model is based upon the use of geophysical data to determine the surface point rain rate, point-to-path variations in rain rate, and the height dependency of attenuation given the surface point rain rate or the percentage of the year the attenuation value is exceeded. The model also provides estimates of the expected year-to-year and station-to-station variations of the attenuation prediction for a given percent of the year.

Surface point rain rate data for the United States and global sources were used to produce 10 rain rate climate regions for the land and water surface areas on Earth. The boundaries for each climate region were adjusted for expected variations in terrain, storm type, storm motion, and atmosphere circulation. The continental United States climate region (region D) was further subdivided into regions  $D_1$ ,  $D_2$ , and  $D_3$  because of the extensive amount of surface rain data available and the wide variations observed throughout the region.

The Crane model relates the surface point rain rate  $R_p$  to a path-averaged rain rate  $\bar{R}$  through an effective path average factor determined empirically from terrestrial measurements of rain rate at path lengths up to 22.5 km. The resulting relationship was modeled by a power law expression:

$$\bar{R} = \sigma(D) R_p^{1+\delta(D)}$$

where  $D$  is the horizontal path length and  $\sigma$  and  $\delta$  are determined from a best-fit analysis of the terrestrial path data. Relative path profile curves for rain rate as a function of  $D$  were determined by numerically differentiating  $\gamma$  and  $\delta$ , then represented by two exponential functions, over the range of  $D$  from 0 to 22.5 km. The effective path length for the Crane model is:

$$L(R_p) = \frac{1}{\cos\theta} \left( \frac{e^{Ubd} - 1}{Ub} \right) \quad 0 < D \leq d$$

$$= \frac{1}{\cos\theta} \left( \frac{e^{Ubd} - 1}{Ub} - \frac{X^b e^{Ybd}}{Yb} + \frac{X^b e^{Ybd}}{Yb} \right) \quad d < D \leq 22.5$$

where  $d$ ,  $U$ ,  $X$ , and  $Y$  are empirical constants that depend on  $R_p$ .

Upper and lower bounds on the annual attenuation distribution prediction were developed by combining the statistical variances of each step in the model development. Figure 5 presents the global model mean prediction and bounds for several locations and frequencies, compared with measured attenuation distributions at those locations. All of the predictions show excellent correlation with the measured data, except for the Blacksburg, Va., distributions at 28.56 GHz. The global model develops a prediction curve down to 0.001 percent and tends to reproduce the tails of the curve consistently well. The sharp dropoffs in the measured data from Austin, Tex. are most likely caused by the noise characteristics of the receiver systems as the rain attenuation drives the receiver signal level down to its threshold.

The global model has yet to be extensively validated by direct measurements from other regions of the world such as Europe or Asia; however, the results from over a dozen U.S. locations at frequencies from 11 to 30 GHz have shown very good results to date.

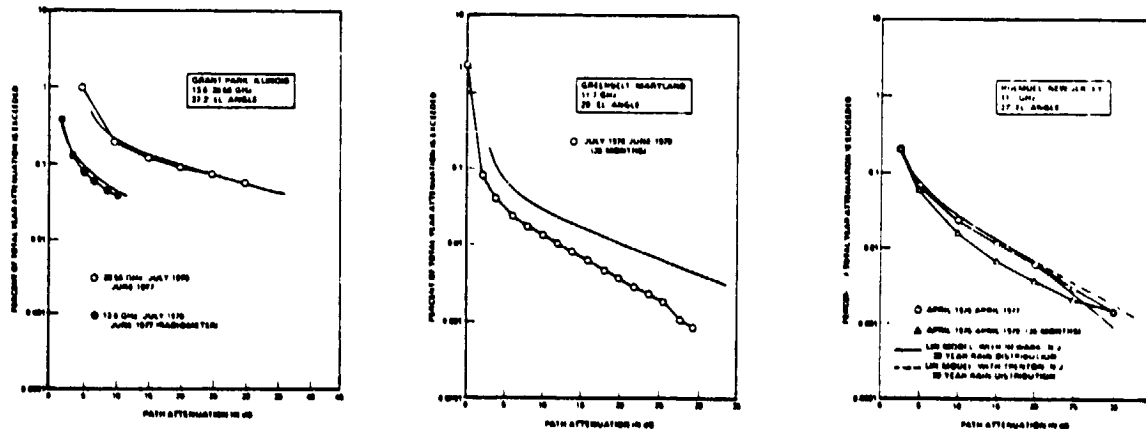


FIGURE 4. COMPARISON OF LIN MODEL WITH MEASURED DATA

Ground Truth Measurements

The availability of satellite beacons on geostationary communications satellites and the recent success in the development rain rate provides an interesting opportunity to measure precipitation quantities from slant-path attenuation measurements. That is, if the processes described in the previous section are reversed, then rain rate distributions should be derivable from attenuation measurements on a slant path.

Single Frequency Beacon Method

Consider a single beacon at frequency  $f_1$ , received at the surface at an elevation angle  $\theta$ . The measured attenuation can then be modeled as

$$A = aR^b L_e \quad (1)$$

translating this result to the vertical direction ( $\theta = 90^\circ$ ),

$$A_v = aR_v^b H \quad (2)$$

where  $H$  is the vertical storm height predicted from the effective path length  $L_e$ . Since

$$A_v = \sin \theta A \quad (3)$$

the predicted path average rain rate in the vertical direction,  $R_v$ , is given by solving for  $R_v$  in eq. (2) and using Eq's. (1) and (3), i.e.

$$R_v = \left[ \frac{A}{aL_e} \right]^{1/b} = \left[ \frac{\sin \theta A}{aH} \right]^{1/b}$$

Therefore, the rain rate can be predicted as long as  $L_e$  (or  $H$ ) is available. These can be found from one of the prediction models described above, such as the  $L(R_S)$  of Lin or the  $L(R_p)$  of Crane.

The prediction error, or uncertainty, of the path average rain rate caused by the measurement uncertainty of the attenuation can be determined by assuming typical values for  $a$ ,  $b$ ,  $H$  and  $\theta$ . Table VI shows the expected % error for a given value of path average rain rate,  $R_v$ , for an assumed Marshall-Palmer rain distribution at  $20^\circ\text{C}$ ,  $H = 4$  km, and  $\theta = 30$  degrees. The attenuation measurement error is set at  $\pm 1$  dB, which is a realistic number based on operating beacon receiver systems. Values are given for three frequencies, 11.7, 20 and 30 GHz. The errors are seen to be quite large for low rain rates, but become acceptable at rates above about 20 mm/h at 11.7 GHz, and about 5 mm/h at 30 GHz. The upper bound of the measurement is determined by the dynamic range of the receiver system, but typically a 30 dB margin is a reasonable value.

Dual Frequency Beacon Method

The path length dependence of  $R_v$  can be eliminated by employing dual frequency beacons in place of the single frequency system described

TABLE VI  
SINGLE FREQUENCY BEACON METHOD

ASSUMPTIONS: MARSHALL-PALMER DISTRIBUTION AT  $20^\circ\text{C}$   
 $H = 4$  KM,  $\theta = 30$  DEGREES  
ATTENUATION MEASUREMENT ERROR:  $\pm 1$  DB

PATH AVERAGE RAIN RATE (mm/hr)	11.7 GHz			20 GHz			30 GHz		
	A DB	$\Delta R$ (mm/hr)	% ERROR	A DB	$\Delta R$	% ERROR	A DB	$\Delta R$	% ERROR
1	13	11.3	1130	5	5.1	510	1.4	1.4	139
5	1	9	180	3	2.8	56	7	1.3	26
10	2	7.2	72	7	2.6	26	15	1.3	13
20	5	6.3	32	15	2.4	12	31	1.2	6
30	9	5.7	19	24	2.2	7	48	1.2	4
50	17	5	10	42	5	10	-	-	-
100	39	4	4	91	1.9	2	-	-	-

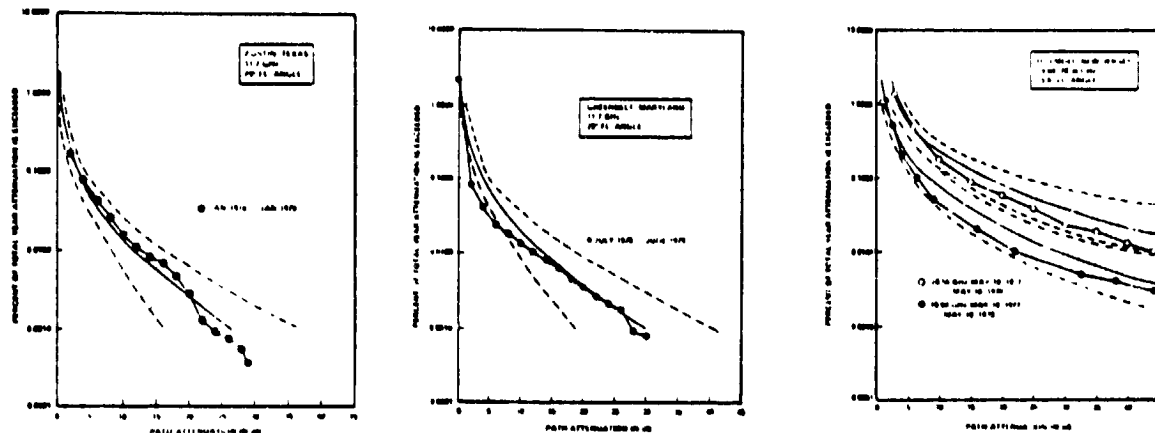


FIGURE 5. COMPARISON OF CRANE MODEL WITH MEASURED DATA

ORIGINAL PAGE IS  
OF POOR QUALITY

above. Consider a dual frequency beacon transmission, at frequencies  $f_1$  and  $f_2$  ( $f_2 > f_1$ ), received at the surface at an elevation angle  $\theta$ . The measured attenuations are then

$$\text{at } f_2: A_2 = a_2 R^{b_2} L_{e2}$$

$$\text{at } f_1: A_1 = a_1 R^{b_1} L_{e1}$$

Taking the ratio and solving for  $R_V$ , as before

$$R_V = \left[ \frac{A_2 a_1 L_{e1}}{A_1 a_2 L_{e2}} \right]^{\frac{1}{b_2 - b_1}}$$

For  $L_{e1} = L_{e2}$ , which is not strictly true, but is a reasonable first order approximation for  $f_2$  and  $f_1$  close to each other:

$$R_V = \left[ \frac{a_1 A_2}{a_2 A_1} \right]^{\frac{1}{b_2 - b_1}}$$

The path average rain rate is seen to be a function of the attenuation ratio only, with the frequency dependent constants  $a_1$ ,  $a_2$ ,  $b_1$  and  $b_2$ .

The prediction error of the dual frequency beacon method is much greater than the single frequency method, as shown by Table VII. The uncertainty in path average rain rate,  $\bar{R}$ , is unacceptably large for the  $\pm 1$  dB attenuation measurement error, and is still excessive even when a  $\pm .5$  dB error is assumed. The problem occurs because the ratio of two attenuations is required, and the worst case additive error can be quite high, particularly for low path rain rates.

TABLE VII  
DUAL FREQUENCY BEACON METHOD

ASSUMPTION: MARSHALL-PALMER DISTRIBUTION AT 20°C

PATH AVERAGE RAIN RATE $\bar{R}$ MM/HR	$A_{30}$ DB	$A_{20}$ DB	$\Delta R$ (MM/HR)	
			FOR $\pm 1$ DB ERROR	FOR $\pm .5$ DB ERROR
10	15	7	156	38
20	31	15	69	29
30	48	24	59	27

Ground Truth Measurements Summary

Table VIII presents a summary of ground truth precipitation measurements from satellite beacons, for both the single and dual frequency methods discussed above. The measurement range for the single frequency system, is defined at the lower

end by a 25% maximum error, and at the upper end by a 30 dB system rain fade margin. The range is frequency dependent, with 11.7 GHz covering a higher range, up to 82 mm/h, and 30 GHz covering down to 6 mm/h. A frequency can be selected to meet the range of coverage desired, or multiple frequencies can be selected to cover the complete range of expected rain rates. The upper limit can be extended somewhat, however, measurements for rain rates above 100 mm/h would be quite difficult to achieve with present and projected near term technology.

The dual frequency method, employing 30/20 GHz beacons, is seen to produce unacceptably high errors at all rain rate values, and does not appear as an attractive alternative.

TABLE VIII  
SUMMARY  
SATELLITE BEACONS FOR GROUND TRUTH  
PRECIPITATION MEASUREMENTS

SINGLE FREQUENCY METHOD	
•	MEASUREMENT RANGE FOR 25% OR LESS ERROR IN R WITH A 30 dB RAIN MARGIN:
	11.7 GHz → 24 TO 82 MM/HR
	20 GHz → 10 TO 37 MM/HR
	30 GHz → 6 TO 19 MM/HR
DUAL FREQUENCY METHOD	
•	UNACCEPTABLY HIGH ERRORS IN R FOR A 30/20 GHz BEACON SYSTEM

IV. LONG-TERM STATISTICS OVER LARGE AREAS

A space-borne precipitation monitoring system has decided advantages over ground-based systems. The primary advantages are the ability to make measurements over a long period without the need to manually collect the data and to uniformly observe large areas. The measurements required are the surface point rain rate over a spatial dimension smaller than the dimension of convective cells (less than several kilometers in the eastern U.S.).

Long-Term Statistics

The year-to-year variability of the rain rate statistics is significant enough to introduce significant error in rain rate data bases made over a period of less than 10 years. For example, hurricane Belle significantly shifted the annual statistic during the period June 1976 to May 1977 in New Jersey (Cox, et al - 1979).

Based on measurements both by the weather service and researchers sponsored by NASA, it is believed that at least a 10-year data base is required to develop median annual statistics of sufficient accuracy to be meaningful in communication system link calculations. Of course, if worst month or longest outage statistics are needed, the data base must be able to generate these for use by the system designer.

#### World-Wide Statistics

To date the models developed for estimating communication system link attenuations have been quite coarse in being able to discriminate between the rain rates in various regions. The climate region D of the Global model (Crane - 1980) is separated by a ratio of 3.5 at 0.01 percent of the year from climate regions C and E. At 12 GHz this results in a variation in attenuation of 4.3 dB, with a higher variation at higher frequencies. Because of this wide variation and the availability of ground-based rain rate data, the climate region D has been resolved into 3 regions in the U.S. In most areas of the world, this is not possible because of the lack of data.

#### Orographic Effects

The ability of a space-borne precipitation monitoring system capable of resolving convective rain cells would be of significant value to link designers planning site diversity systems. Measurements made in Florida (Block, et. al. - 1978) and in Germany (Rucker - 1980) have shown a wide variation between the cumulative attenuation statistics observed at different sites and in different azimuthal directions, respectively. If it is true that the rain rate distribution varies significantly with geographic location while the total amount of precipitation is uniform, then the sites with the most low rain rate precipitation are more desirable. In the case of Tampa, Florida the presence of the city's heat and the cool Tampa Bay made some sites much more desirable than others. In the case in Germany, the link on the east side of the Rhine Valley showed less attenuation.

A spaceborne monitor could map these desirable locations, and if sites which had low rain rates could be found, it might eliminate the need for an additional ground station. The savings associated with one less ground station in most high-availability systems would be very substantial.

#### V. SUMMARY

This paper has identified typical rain rate measurement accuracies required for communication system design. In addition, the accuracies attainable from satellite beacon measurements have been estimated and a sample of the experimental data has been presented.

#### REFERENCES

- Bloch, S.C., D. Davidson and D. D. Tang (1978), "Rain-Attenuation Experienced With the Tampa Triad Using 19-GHz COMSTAR Satellite Beacon Signals," Conference Record, EASCON 78, Arlington, VA, p. 379.
- Cox, D.C., H.W. Arnold and A.J. Rustako, Jr. (1979), "Attenuation and Depolarization of Rain and Ice Along Inclined Radio Paths Through the Atmosphere at Frequencies Above 10 GHz," Conference Record, EASCON 79, Arlington, VA, p. 56.
- Crane, R.K. (1980), "Prediction of Attenuation by Rain," IEEE Trans. Comm., Vol. COM-28, No. 9, September 1980, p. 1717.
- Goldhirsh, J. (1978), "The Use of Radar at Non-Attenuating Wavelengths as a Tool for the Estimation of Rain Attenuation at Frequencies Above 10 GHz," EASCON 79 Record, Arlington, VA, September 25-27, p. 48.
- Ippolito, L.J. (1981), "Radio Propagation for Space Communications," Proc. IEEE, Vol. 69, No. 6, June.
- Kaul, R. (1980), "Extension of an Empirical Site Diversity Relation to Varying Rain Regions and Frequencies," URSI Comm. F Open Symposium, Lennoxville, Quebec, Canada, p. 4.13.1.
- Kaul, R., D. Rogers and J. Bremer (1977), "A Compendium of Millimeter Wave Propagation Studies Performed by NASA" ORI, Inc., TR 1276, November.
- Kaul, R., R. Wallace and G. Kinal (1980), "A Propagation Effects Handbook for Satellite System Design," NASA Headquarters, Washington, D.C., ORI TR 1679, March.
- Lin, S.H. (1977), "Nationwide Long Term Rain Rate Statistics and Empirical Calculations of 11 GHz Microwave Rain Attenuation," B.S.T.J., Vol. 56, No. 9, p. 1581.
- Lin, S.H. (1979), "Empirical Rain Attenuation Model for Earth-Satellite Paths," IEEE Trans. Comm., Vol. COM-27, May, p. 812.
- Olsen, R.L., D.V. Rogers and D.B. Hodge (1978) "The  $\alpha_D$  Relation in the Calculation of Rain Attenuation," IEEE Trans. Ant. Prop., Vol. AP-26, p. 318.
- Rice, P.L. and N.R. Holmberg (1973), "Cumulative Time Statistics of Surface Point-Rainfall Rates," IEEE Trans. Comm. Tech., Vol. COM-21, No. 10, October.
- Rucker, F. (1980), "Simultaneous Propagation Measurements in the 12-GHz Band on the SIRIO and OTS Satellite Links," URSI Comm. F Open Symposium, Lennoxville, Quebec, Canada, p. 4.1.1.
- Ryde, J.W. and D. Ryde (1945), "Attenuation of Centimeter and Millimeter Waves by Rain, Hail, Fogs and Clouds," Rpt. No. 8670, Res. Lab. of the General Electric Co., Wembley, England.
- U.S. Dept. of Commerce (1955), "Rainfall Intensity-Duration-Frequency Curves," Technical Paper No. 25, Washington, D.C.

D24

N83 25293

ORIGINAL PAGE IS  
OF POOR QUALITY

## A LIFE HISTORY METHOD FOR ESTIMATING CONVECTIVE RAINFALL

David W. Martin

Space Science and Engineering Center  
Madison, Wisconsin

## 1. INTRODUCTION

Rainfall was regarded from the very beginning as one of the more important observations to be made for the Global Atmospheric Research Program Atlantic Tropical Experiment:--but one of the most difficult too, for the measurements of this most variable parameter had to be made continuously, across large areas and over the sea. Ships could not provide the needed resolution nor could available radars provide the needed breadth of coverage. Microwave observations from the Nimbus-5 satellite offered some hope. Another possibility was suggested by the results of many comparisons between rainfall and the clouds seen in satellite pictures. Of particular interest were those comparisons made by Sikdar (1972) and by Woodley and Sancho (1971), who employed sequences of pictures from the first geostationary satellites. Both found a general correspondence between rain and the convective clouds visible in satellite pictures. Woodley and Sancho demonstrated in addition that the agreement was best for growing clouds. This began a collaboration between the University of Wisconsin and the Environmental Research Laboratory to develop methods to infer GATE rainfall from geostationary satellite images. The present paper summarizes the method which evolved at Wisconsin and is described in the paper by Stout *et al.* (1979).

## 2. BASIS OF THE WISCONSIN APPROACH

We assume that 1) most GATE rain comes from cumulonimbus clouds, 2) cb's can readily be identified--on the basis of growth, movement and texture, in addition to temperature or brightness--in a sequence of infrared or visible images, and 3) cb area can be approximated by a single threshold contour of temperature or brightness. To a first approximation, the rainrate  $R$  for a cb then is given by

$$R = a_0 \cdot A + a_1 \cdot \Delta A / \Delta t.$$

$A$  is cloud area,  $\Delta A / \Delta t$  is time rate of change of area,  $a_0$  and  $a_1$  are empirical coefficients, and the units of  $R$  are volume divided by time. Area is defined by thresholds of temperature and albedo: 245 K and 45%. These were selected (mainly on the basis of observations near Miami) to exclude the bulk of cloud material which contributes only a trivial amount to total rainfall.

## 3. APPLICATION IN GATE

To calculate the coefficients  $a_0$  and  $a_1$ , two days of SMS-1 visible and infrared images were matched in time and space to calibrated radar observations from the GATE ship Oceanographer. Using an interactive image processing system, cumulonimbus clouds in each sequence were identified. Their areas and the corresponding rainrates then were measured, picture by picture, for the whole lifetime of the cloud. Results are summarized in Table 1.

Table 1

Coefficients of the Visible and Infrared Rainfall Relations

	Infrared	Visible
Number of clouds	34	23
Number of image pairs	329	219
$a_0$ [ $10^{-7} \text{m s}^{-1}$ ]	5.4	5.2
$a_1$ [ $10^{-3} \text{m}$ ]	2.8	2.5
$a_0 \cdot A$ [ $10^3 \text{m}^3 \text{s}^{-1}$ ]	3.3	2.3
$a_1 \cdot  \Delta A / \Delta t $ [ $10^3 \text{m}^3 \text{s}^{-1}$ ]	1.9	1.3

The last two lines of Table 1 compare the average contribution of each term to the total rainfall. For the clouds measured, area change accounted for about 1/3 of the total variance in rainfall, a fraction which might be significant in flash flood forecasting, for example, where timing is important. The correlation of area with rainfall increased for area lagging rainfall up to 1 to 1 1/2 h (Fig. 1), and ranged up to 0.9. The standard error is 60% for visible, 75% for infrared. Thus for one cloud for one-half hour the expected error is 60 to 75% of the rain estimate. This error would tend to diminish in proportion to the inverse of the square root of the sample size.

As a test of this method rainfall was estimated for four days of GATE, including one of the calibration days (overlap amounted to 1/6 of the test data). The correlation of satellite rainfall regressed against radar rainfall, both averaged over an area of  $\sim 10^5 \text{km}^2$ , was 0.84 (see Fig. 2). Minus 0.05 mm is the intercept value, 0.91 is the slope and the standard error of estimate is 1/4 mm, about 30% of the hourly average rainrate. Satellite rainfall tended to be smoother than radar rainfall and displaced slightly toward the north and northwest (Fig. 3). Otherwise patterns of 24 h rainfall were in remarkable agreement.

# CORRELATIONS OF RAIN QUALITY

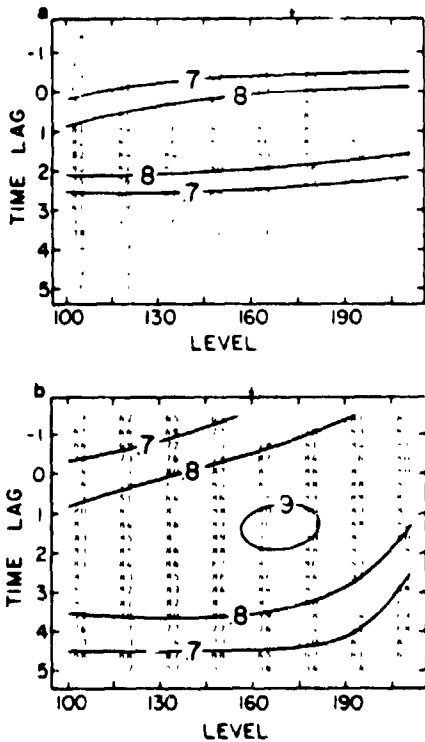


Figure 1. Correlations between volumetric rainrate and cloud area. Area is measured at threshold levels, in digital counts, varying along the abscissa. Correlations are calculated for time lags, indicated in hours along the ordinate. Arrows along the upper ordinate mark digital counts corresponding to threshold levels for raining clouds. a) Visible. b) Infrared.

## 4. SUMMARY

The main weaknesses of this method aside from those intrinsic to the visible--infrared methods, are as follows:

- a. It was designed for GATE and so far has only been applied in the GATE area.
- b. It ignores rain from stratiform and warm convective clouds. Augustine *et al.* (1981) have shown that under some regimes this can be a large part of total rainfall.
- c. It is inflexible.
- d. It demands much skill and concentration from the user.

The strengths of the method lie in the simplicity of the algorithm. In addition, this method makes full use of the high time and space resolution and large dynamic range of geostationary satellite data. Finally, it yields a volumetric rather than a point estimate of rainfall.

## 5. OUTLOOK

This review and comparisons with other techniques suggest several possibilities for improving the scheme described here. First, the growth term could well be dropped in applications at synoptic and larger scales, for a great gain in simplicity. Second, the measurement of cloud area could be automated. This ought to significantly speed the processing of images. Third, where accuracy is critical, the addition of mean cloud temperature or brightness, standard deviation of temperature or brightness and cloud thickness terms might significantly improve the estimate for any particular cloud.

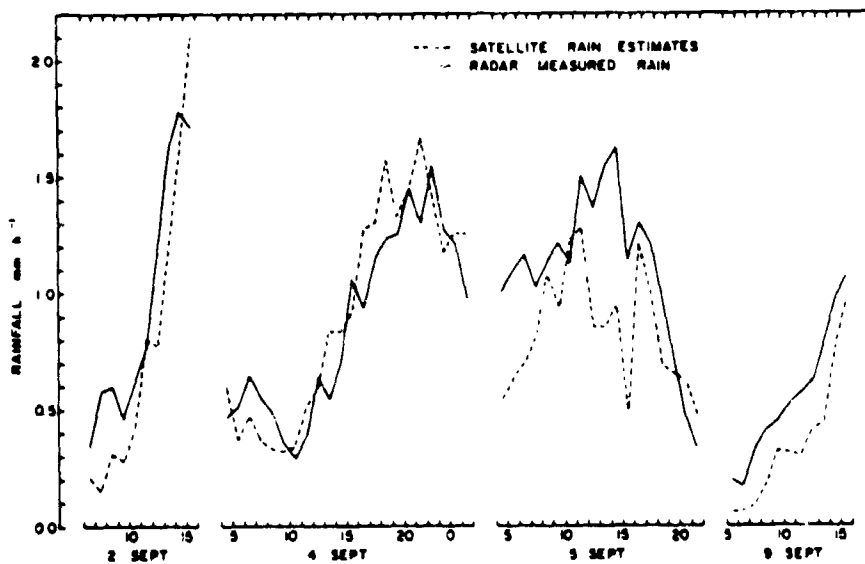


Figure 2. Satellite and radar hourly rainrates averaged over a disc 204 km in radius centered at 08°30'N, 23°30'W. Hours in GMT are plotted along the abscissa.

5 SEPT 1974

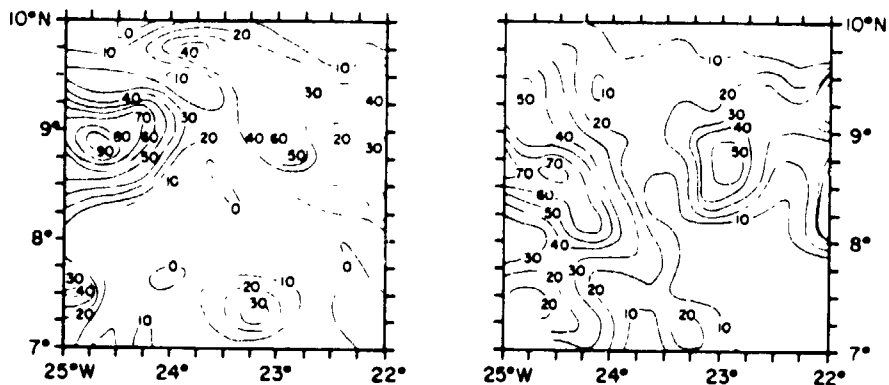


Figure 3. Maps of satellite rainfall (left) and radar rainfall (right). Periods are 0400 to 2200 GMT for the satellite estimate; 0000 to 2345 for the radar estimate.

6. REFERENCES

Augustine, J. A., C. G. Griffith, W. L. Woodley and J. G. Maitin, 1981: Physical insights into satellite-derived rainfall underestimates in GATE. Submitted to J. Appl. Meteor.

Sikdar, D. N., 1972: ATS-3 observed cloud brightness field related to a meso-to-subsynoptic scale rainfall pattern. Tellus, 24, 400-413.

Stout, J. E., D. W. Martin, and D. N. Sikdar, 1979: Estimating GATE rainfall with geosynchronous satellite images. Mon. Wea. Rev., 107, 585-98.

Woodley, W. L., and B. Sancho, 1971: First step toward rainfall estimation from satellite cloud photographs. Weather, 279-289.



ORIGINAL PAGE IS  
OF POOR QUALITY

A COMBINED VISIBLE AND IR TECHNIQUE FOR THE ESTIMATION  
OF RAIN AMOUNTS FROM GOES DATA

G. L. Austin and S. Lovejoy

McGill Radar Weather Observatory  
Macdonald College, Ste. Anne de Bellevue, Que., Canada H9X 1C0

1. INTRODUCTION

The remote sensing of rain amounts is clearly of great interest not only to those concerned with climate modelling but also for a great variety of operational applications, including hydrology, hydroelectricity and agriculture. While the microwave radiometer represents the most obvious technique in that the hydrometeors are sensed directly, we believe that poor spatial and temporal resolution, together with the problems associated with the estimation of effective rain layer height make visible and IR techniques more promising at the present time.

A comprehensive review of satellite rainfall estimation methods up to 1973 was gathered by Martin and Scherer (1973). Significant work was subsequently published by Reynolds and Vonder Haar (1973), Griffith and Woodley (1973), Follansbee and Oliver (1975) and Kilonsky and Ramage (1976). More recently, Stout et al (1979) and Griffith et al (1978) introduced the concept of the rate of areal change in refining rainfall measurements. Scofield and Oliver (1977) devised a procedure in the form of a flow diagram in order to ascribe a rainfall rate to cumulonimbus clouds. Wylie (1979) attempted, with some success, to apply the Stout et al technique to the Montreal region.

Of significant importance are the concluding remarks of the review paper by Martin and Scherer (1973): "Based on bivariate frequency distribution of brightness versus temperature, Gruber concluded that brightness enhancing or infrared technique alone may be inadequate to deduce details of convective activity... This implies that better estimates of rainfall will come from visible and IR observations *combined* than from either used alone". However, with the exception of a note on image differencing by Reynolds (1978) this recommendation had been ignored until the two wavelength pattern recognition technique of Lovejoy and Austin (1979a) was introduced.

The latter technique identifies clouds with high probability of rain as those which have large optical and presumably physical thickness as measured by the visible albedo in comparison with their height, determined by the intensity of the IR emission.

2. DATA BASE

The radar data used in this analysis are from the GATE experiment from CCGS Quadra and from Montreal from the McGill Radar Weather Observatory. The digital GOES data for the appropriate times and locations were obtained from the University of Wisconsin, through the good offices of Dr. Don Wylie.

3. ANALYSIS

We believe the estimation of rain amount from satellite data depends upon two separable steps: 1) the delineation of the areas of rain, and 2) the estimation of the rain rate given that the area is known. A problem with this type of analysis is that it is necessary to compare error statistics for different techniques and there seems to be no generally accepted best statistic to characterize the errors. The main possibilities seem to be the bias (B) or mean ratio, the error factor ( $E_R$ ) and the root mean square error ( $E_{rms}$ ). For a perfect technique

$$B = E_R = 1 \quad \text{and} \quad E_{rms} = 0$$

4. THE RAIN AREA ESTIMATION SCHEME

The satellite visible and IR data were remapped onto the radar coordinate system with a spatial resolution of 4 km x 4 km and an intensity resolution of 25 levels. The two-dimensional frequency matrix was then calculated separately for the raining and non-raining locations as defined by radar. Typical samples are shown in Figs. 1a and 1b. The ratio of raining to non-raining points was then found and plotted as a percentage accuracy or probability of rain as shown in Fig. 1c, where the greater-than-50% contour has been plotted. Errors as described above were then calculated for GATE and Montreal data. Figure 2 shows the resulting satellite and radar rain maps for GATE and Montreal.

5. THE RAIN RATE ESTIMATION SCHEME

Several techniques for the estimation of instantaneous rainfall rate were tried. For example, the probability of rain is slightly correlated with the rainfall rate. However, we have concluded that, since the visible and IR wavelengths primarily respond to the relative abundance of cloud droplets and not to precipitation sized particles, that it is unrealistic to expect good, or even half-sensible, rainfall rate estimates.

ORIGINAL PAGE IS  
OF POOR QUALITY

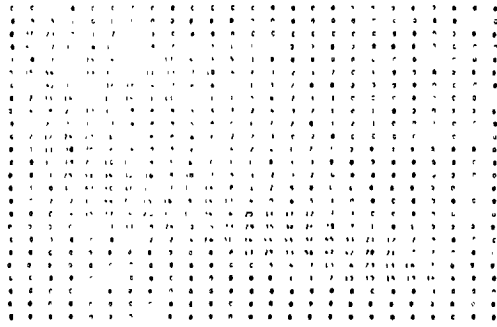


Fig. 1a

Frequency plot of no-rain distribution for GATE day 1300 GMT. Horizontal axis is visible data on scale 0-1, and vertical axis temperature also normalized on scale 0-1.

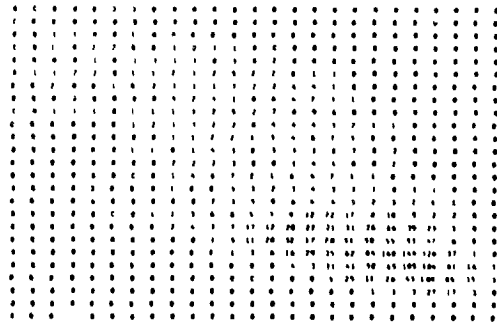


Fig. 1b

Similar to 1a, for rain data.

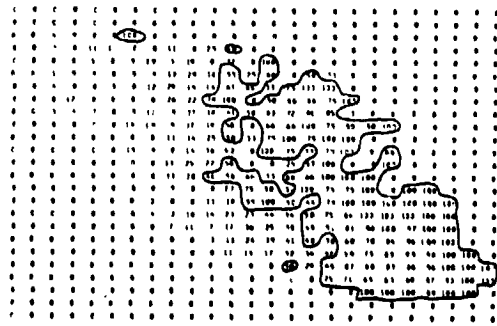


Fig. 1c

Elements of Fig. 1b as a percentage of Fig. 1a plus Fig. 1b, with the resulting optimum boundary sketched in. Any combination of visible and IR values within this boundary resulted in a satellite rain point. Anything outside resulted in a no-rain point. The resulting map is shown in Fig. 2.

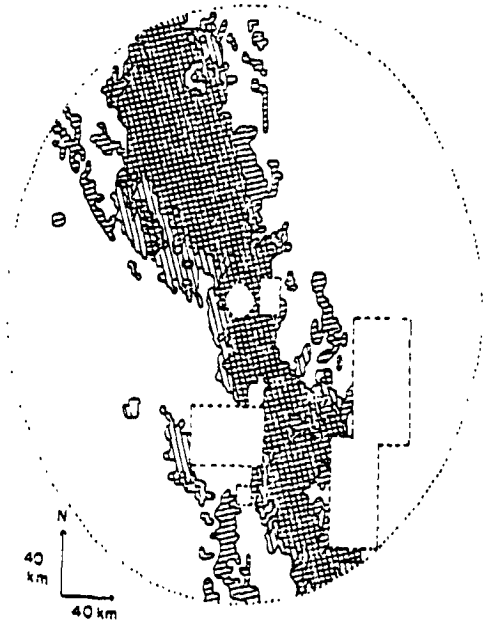
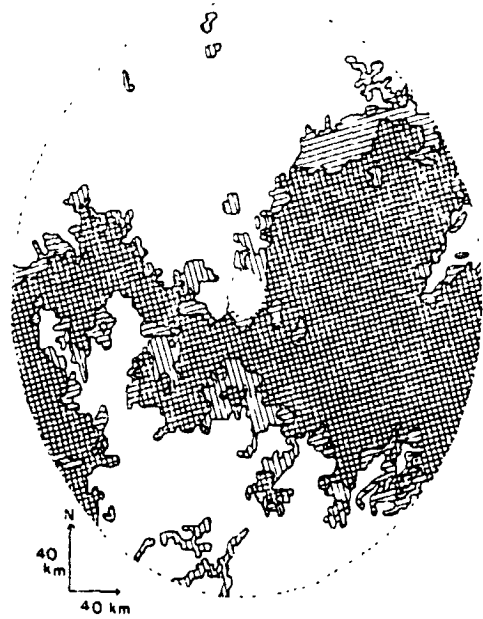


Fig. 2

(top) The satellite rain map produced by the optimization of the data in Fig. 1. Vertical lines are radar rain areas, horizontal lines are satellite rain areas. The radar range is 180 km. Note that the percentage error (in this case = 15.2%) is not the percentage of the striped areas to cross-hatched areas, but is the percentage of the striped areas to areas cross-hatched or blank (the latter represented satellite and radar agreement on no-rain).  
(bottom) A satellite rain map of Montreal, day 180, 1977, at 1630 GMT, showing an active cumulus band. The radar range is 180 km.

Consequently, we sought to answer the question for a radar sized (400 km x 400 km) piece of real estate how great an error was introduced by assuming a constant or climatological rainfall rate for those areas which were raining and zero elsewhere. Single images (each half-hour) and two-hour accumulations for GATE and Montreal were attempted. The technique was to assume that the radar data delineated the raining area exactly and then to compute the flux of rain based on this area and a climatological rain rate and compare with the flux from the full radar data (3-km CAPPI).

## 6. RESULTS

Table 1 indicates the magnitudes of the errors inherent in the techniques described in (4) and (5) above.

For comparison, error statistics by different authors for satellite rain estimation schemes are shown in Table 2

Number of consecutive hours of data accumulated	Number of sequences of accumulated data					
	1	2	4	7	10	15
$\rho_{rs}$	0.91	0.91	0.91	0.91	0.94	0.93
$\rho_{rs}$	0.15	0.64	0.63	0.72	0.62	0.72
$E_{rms}$	0.41	0.37	0.33	0.33	0.22	0.20
$\sigma_e$	1.02	0.79	0.71	0.66	0.39	0.40
$B$	1.53	1.41	1.35	1.34	1.17	1.16
$E_e$	1.74	1.56	1.49	1.47	1.29	1.29
$\sigma_s$	1.30	0.70	0.64	0.58	0.33	0.33

Table 1

Statistics determined by the Quadra radar for Phase III of GATE accumulated for various lengths of time.

## 7. CONCLUSIONS

In agreement with other researchers, we have found that GOES infrared and visible imagery can be used both for rain area and amount estimation. By using data for long time periods in both GATE and Montreal, the variability of rain amount estimates from known areas of rain can be computed, and, due to the high correlation (correlation coefficient = 0.88, 0.91 respectively) between rain area and rain amount, this variability is shown to be of the same order of magnitude when compared to the errors involved in the existing satellite rain amount estimation techniques. When this variability is coupled with errors in the area estimation by two-dimensional pattern matching, reasonable accuracy for rain amount estimation is obtained. These facts support the hypothesis that GOES IR and visible data are good for determining rain areas, but poor for determining rain rates.

For Montreal, we may roughly estimate the contributions to  $E_{rms}$  from different sources as follows: 5% from the gauge to radar measurement, 22% for radar area to satellite area, and 44% for the satellite area to the satellite amount, yielding, for independent processes, 49% for the total process, for estimates based on single sets of IR and visible images.

## 8. ACKNOWLEDGEMENTS

Helpful discussions with Don Wylie, Fred Mosher and Dave Martin, of the University of Wisconsin, are acknowledged. The project was supported by AES through the good offices of Mr. Graham Morrissey

Author	Follansbee and Oliver (1975)*			Scofield and Oliver (1977b)**		Griffith <i>et al.</i> (1978)				Wylie (1978)*		Stout <i>et al.</i> (1979)	
Technique	Nephelyses			History and synoptic data		Lifetime measurements				Expanding anvils		Expanding anvils	
Region	Alabama, Georgia, South Carolina			North Carolina		Florida				Montreal		GATE	
Size of area (km <sup>2</sup> )	~10 <sup>6</sup>			~10 <sup>6</sup>		~10 <sup>6</sup>				~10 <sup>6</sup>		~6 x 10 <sup>6</sup> ~10 <sup>6</sup>	
Number of sequences examined	255			1		8				5		2 4	
Number of data points used	255			4		53 8 37 43 5 5				35		219 329 62 8	
Time of accumulation	"daily"			6 h		"hourly" "daily" "hourly" "daily"				1/2 h		1/2 h 1 h 6 h	
Type of data used	vis	IR	both	IR and vis	vis	vis	vis	IR	vis	IR	vis	IR	IR
$E_{rms}$	1.31	1.51	1.22	0.44	—	—	—	—	—	—	58	46	62 76 32 23
$B$	—	—	—	1.18	1.11	0.83	1.15	2.70	1.13	1.90	—	—	—
$E_e$	—	—	—	1.86	2.61	1.68	2.38	3.71	1.39	1.95	—	—	—

\* The error figures have been computed from Follansbee and Oliver (1975, Tables 2, 3, 4)  
 \*\* This column has been computed on the basis of the only rainfall amount statistics contained in either Scofield and Oliver (1977a or 1977b), that is, from Fig. 11 of Scofield and Oliver (1977b)  
 \* These are the average  $E_{rms}$  figures for the five sequences, taken from Wylie (1978 Table 2)

Table 2.

Comparison of the error statistics obtained by various researchers in satellite rain amount estimation.

ORIGINAL PAGE IS  
OF POOR QUALITY

9. REFERENCES

- Follansbee, W. and V.J. Oliver, 1975: A comparison of infrared imagery and video pictures in the estimation of daily rainfall from satellite data. NOAA Tech. Memo. NESS 62.
- Griffith, C. and W.L. Woodley, 1973: On the variation with height of the top brightness of precipitating convective clouds. J. Appl. Meteor. 12, 1086-1089.
- Griffith, C. et al, 1978: Rain estimation from geosynchronous satellite imagery - visible and infrared studies. Mon. Wea. Rev., 106 1153-1171.
- Kilonsky, B.J. and C.S. Ramag 1976. A technique for estimating tropical open-ocean rainfall from satellite observations. J. Appl. Meteor., 15, 972-975.
- Lovejoy, S. and G.L. Austin, 1979a: The delineation of rain areas from visible and IR satellite data for GATE and mid-latitudes. Atmos-Ocean, 17, 77-92.
- Martin, D.W. and W.D. Scherer, 1973: Review of satellite rainfall estimation methods. Bull. Amer. Meteor. Soc., 54, 661-674.
- Reynolds, D. and T.H. Vonder Haar, 1973: A comparison of radar-determined cloud height and reflected solar radiance measured from the geosynchronous satellite ATS-3. J. Appl. Meteor., 12, 1082-1085.
- Reynolds, D. et al, 1978: Cloud type separation by spectral differencing of image pairs. Mon. Wea. Rev., 106, 1214-1218.
- Scotfield, R.A. and V.J. Oliver, 1977: A scheme for estimating convective rainfall from satellite imagery. NOAA Tech. Memo. NESS 86.
- Stout, E.J., D.W. Martin and D.N. Sikdar, 1979: Estimating GATE rainfall with geosynchronous satellite images. Mon. Wea. Rev., 107, 585-598.
- Wylie, D.P., 1979: An application of a geostationary satellite rain estimation technique to an extra-tropical area. Mon. Wea. Rev. (in print).

ORIGINAL PAGE IS  
OF POOR QUALITY

VISIBLE AND INFRARED TECHNIQUES FOR FLASH FLOOD,  
HYDROLOGICAL, AND AGRICULTURAL APPLICATIONS

Roderick A. Scofield

Applications Laboratory  
National Earth Satellite Service, NOAA  
Washington, D.C.

1. Introduction

This paper discusses the use of visible and infrared techniques for estimating precipitation for flash flood, hydrological, and agricultural applications. The visible and infrared technique discussed was developed by Scofield and Oliver. Satellite-derived rainfall estimates may supplement other data or, in some important cases, may be the only data available. In this paper, the Scofield/Oliver convective rainfall technique is used for analyzing a half-hour period of heavy rainfall during a Chicago flash flood event. The results of a real-time hydrological application of the Scofield/Oliver technique for the Hurricane Allen event are also presented. Finally, the paper very briefly discusses visible and IR techniques for agricultural applications.

2. Scofield/Oliver Technique

Scofield and Oliver (1976, 1977, 1978, and 1980) have developed a technique that gives half-hourly or hourly rainfall estimates from convective systems by using GOES IR and high resolution visible pictures. The Scofield/Oliver technique is presented in the form of a decision tree which an analyst uses to determine rainfall estimates. The technique was designed for deep convective systems that occur in tropical air masses with high tropopauses, and it is applied using IR pictures displayed according to the digital enhancement curve (Mb curve).

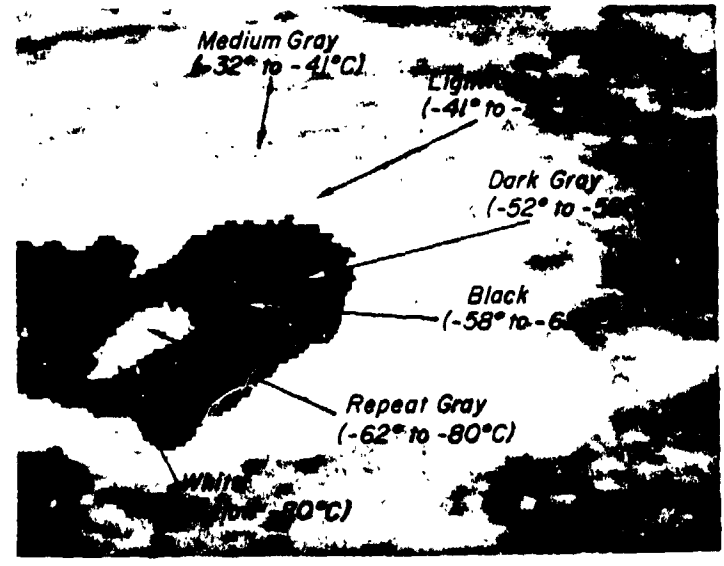


Figure 1. Enhanced infrared imagery (Mb curve),  
0900 GMT, September 12, 1978.

ORIGINAL PAGE IS  
OF POOR QUALITY

An example of a thunderstorm system displayed with such a curve is shown in Figure 1. The picture shows the temperatures associated with each of the contours in the Mb curve: medium gray (-32 to -41°C) represents the warmest tops, white (below -80°C), the coldest.

Estimates of convective rainfall are done by comparing the changes in two consecutive pictures, both IR and high resolution visible. The technique is divided into two main parts: (1) the active portion of the convective system is identified, and (2) the half-hourly convective rainfall estimate is computed for the active portion from the meteorological factors in the following equation:

$$\text{Rainfall Estimate (inches)} = (\text{Cloud-top temperature and cloud growth factor or divergence aloft factor} + \text{overshooting top factor} + \text{merger factor} + \text{saturated environment factor})$$

X

$$\frac{\text{Observed surface to 500 mb precipitable water}}{1.5 \text{ (standard surface to 500 mb precipitable water for the technique)}}$$

Details on how to compute these meteorological factors are found in the following references: Scofield and Oliver, 1977 and 1980.

3. The Chicago Rainstorm, June 13-14, 1976

An unusually good opportunity for a test of this technique was presented by a severe thunderstorm that dumped torrential rains over an area around Chicago; the area contains 300 rain gauges at a 2-nm spacing belonging to the Illinois State Water Survey.

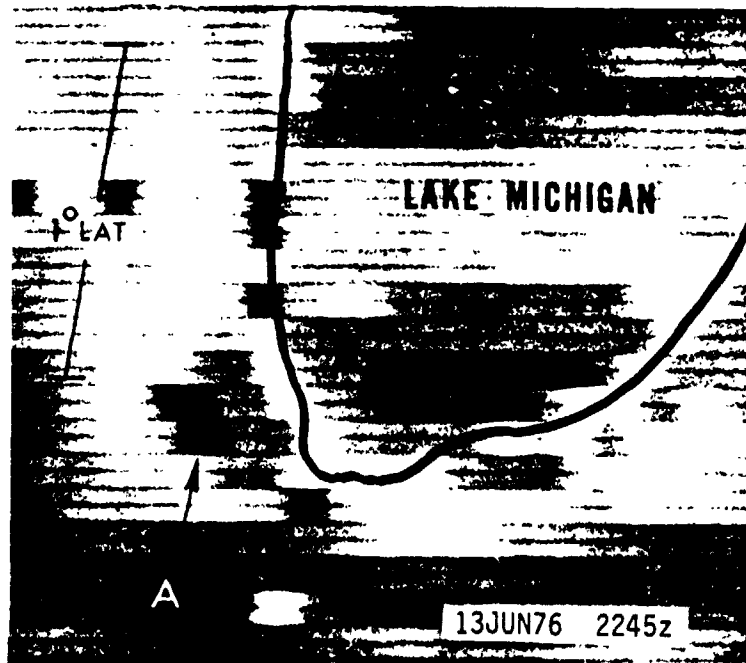


Figure 2. Enhanced infrared imagery (Cb curve), 2245 GMT, June 13, 1976.

ORIGINAL PAGE IS  
OF POOR QUALITY

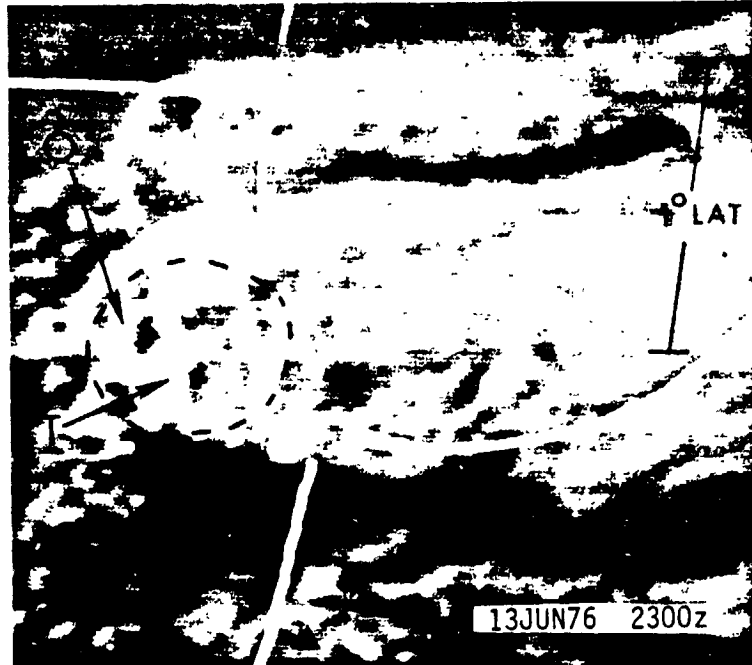


Figure 3. One-km visible imagery, 2300 GMT, June 13, 1976.

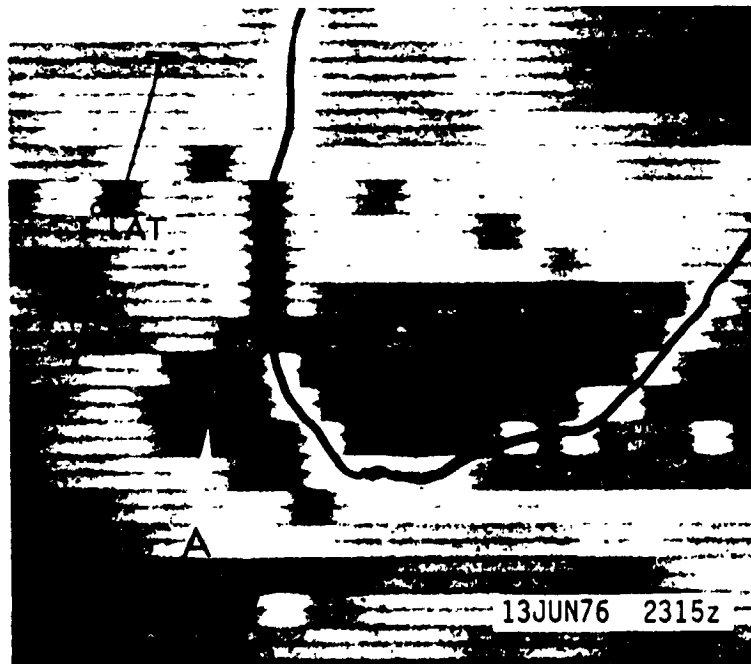


Figure 4. Enhanced infrared imagery (Cb curve), 2315 GMT, June 13, 1976.

A 30-minute period between 2245 and 2315 GMT was selected for comparing the estimated isohyets with the 300 rain gauge observations. The enhanced IR imagery for 2245 and 2315 GMT is shown in Figures 2 and 4; the 1-km visible imagery for 2300 GMT is displayed in Figure 3. The enhanced IR imagery in Figure 2 shows the active area of the thunderstorm at A is very cold (black contour:  $-58$  to  $-62^\circ\text{C}$ ); rainfall estimates were computed over this active area. At 2300 GMT (Figure 3), the 1-km visible imagery shows the active area of the storm as bright and textured; this active area is dashed. Overshooting tops are observed at O and T. The enhanced IR imagery at 2315 GMT in Figure 4 shows that the temperatures have become colder at A (around  $-65^\circ\text{C}$ ) and have reached the repeat gray level enhancement ( $-62$  to  $-80^\circ\text{C}$ ). This repeat gray level area grew in size,  $<1/30$  latitude during the half-hour interval. A circular black area surrounds the repeat gray level area.

The half-hourly estimated isohyetal analysis between 2245 and 2315 GMT superimposed on the rain gauge observations is shown in Figure 5 where the dots locate the rain gauges. The rain gauge values are in inches and "M" means the rain gauge observation is missing. The overshooting tops in Figure 3 were used to produce the small areas of maximum rainfall in Figure 5 whose sizes range from near  $2\times 2$  nm at O to near  $5\times 5$  nm at T. In this case, the estimates compared to the observed appear to be good.

#### 4. Hurricane Allen, August 9-12, 1980

On August 9-12, 1980, the Scofield/Oliver technique was applied in real-time to Hurricane Allen as he moved westward from the Gulf of Mexico through southern

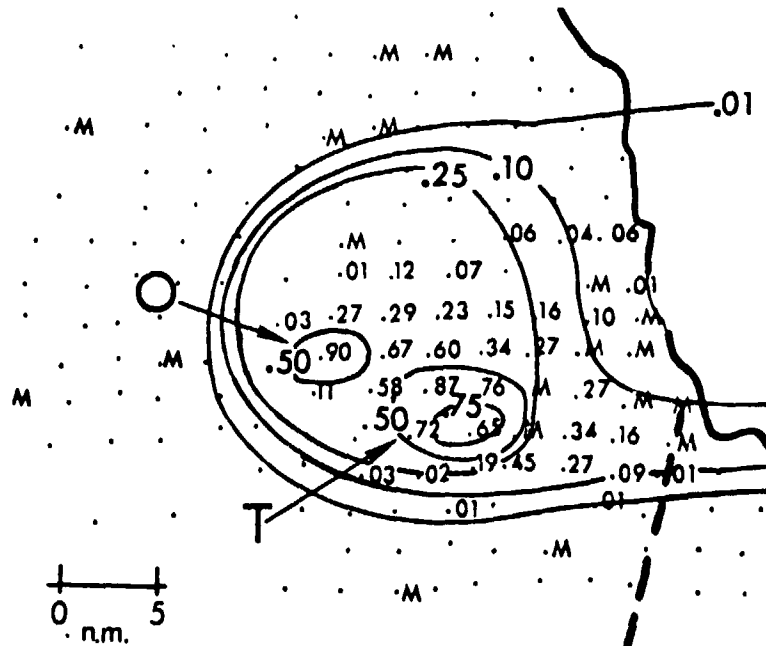


Figure 5. Estimated/observed rainfall, 2245-2315 GMT, June 13, 1976; isolines represent estimated isohyets (inches); dots locate the rain gauges; rain gauge values are in inches; "M" means the rain gauge observation is missing.



CONTAINS COPIES OF  
OF POOR QUALITY



Figure 6. Enhanced infrared imagery (Mb curve),  
0130 GMT, August 11, 1980.

Texas and into northern Mexico. As an aid in evaluating the flood potential, estimated isohyets were produced by NESS meteorologists in the Synoptic Analysis Branch in Washington, D.C., and transmitted to the River Forecast Center in Dallas-Fort Worth and the Weather Service Forecast Offices in San Antonio and Lubbock. The period of heaviest rainfall occurred along a convective cloud band shown in Figure 6 between A and A'. Twenty-four hour observed and estimated rainfall amounts ending at 1200 GMT, August 11, are displayed in Figures 7 and 8, respectively. As can be seen from comparing the figures, the estimated rainfall pattern and amounts over southern Texas were quite good especially along the heavy rainfall band between A and A'.

##### 5. Agricultural Applications

AgRISTARS (Agriculture and Resources Inventory Surveys Through Aerospace Remote Sensing) requires that visible and infrared precipitation estimation techniques be developed for agriculture application around the world. Such an effort encompasses four regimes: convective, tropical storm, monsoon, and extratropical storm. Therefore, precipitation estimation techniques must be developed for rainfall events occurring from cumuliform clouds, stratiform clouds, and stratiform clouds with embedded cumuliform clouds. Both geostationary and polar-orbital satellite data are to be used in the technique development. However, for the countries where geostationary satellite data are not available, techniques using polar-orbital data alone will be developed. The principal ongoing precipitation estimation technique research and development activities using visible and IR data are shown in Table 1. Of course,

the techniques in Table 1 will eventually be combined with microwave techniques in order to develop the best overall global precipitation estimation algorithms.

## 6. Conclusions

In this paper, the Scofield/Oliver technique was applied successfully to a flash flood producing thunderstorm over Chicago and to Hurricane Allen as he crossed southern Texas. Despite these successes, additional research is required before the technique becomes completely operational. We have plans to apply, develop, test, and verify this technique on NESS's Interactive Flash Flood Analyzer.

NESS has the mission to develop precipitation estimation techniques for the agricultural community. Therefore, a goal of AgRISTARS is to implement the best and most efficient techniques into pilot operation and a large-scale applications test for agricultural users by 1984.

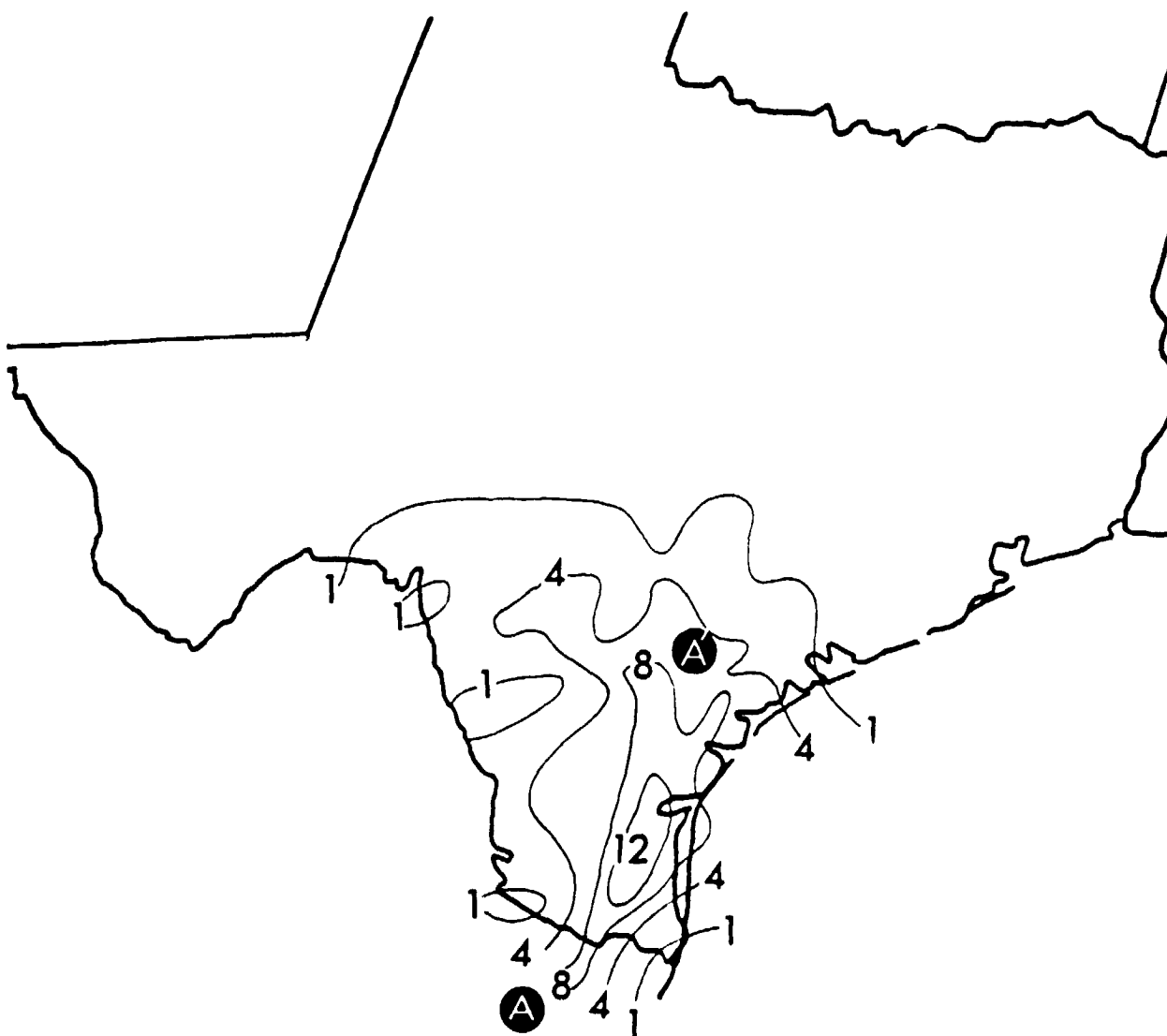


Figure 7. 24-hour observed rainfall in inches ending at 1200 GMT, August 11, 1980.

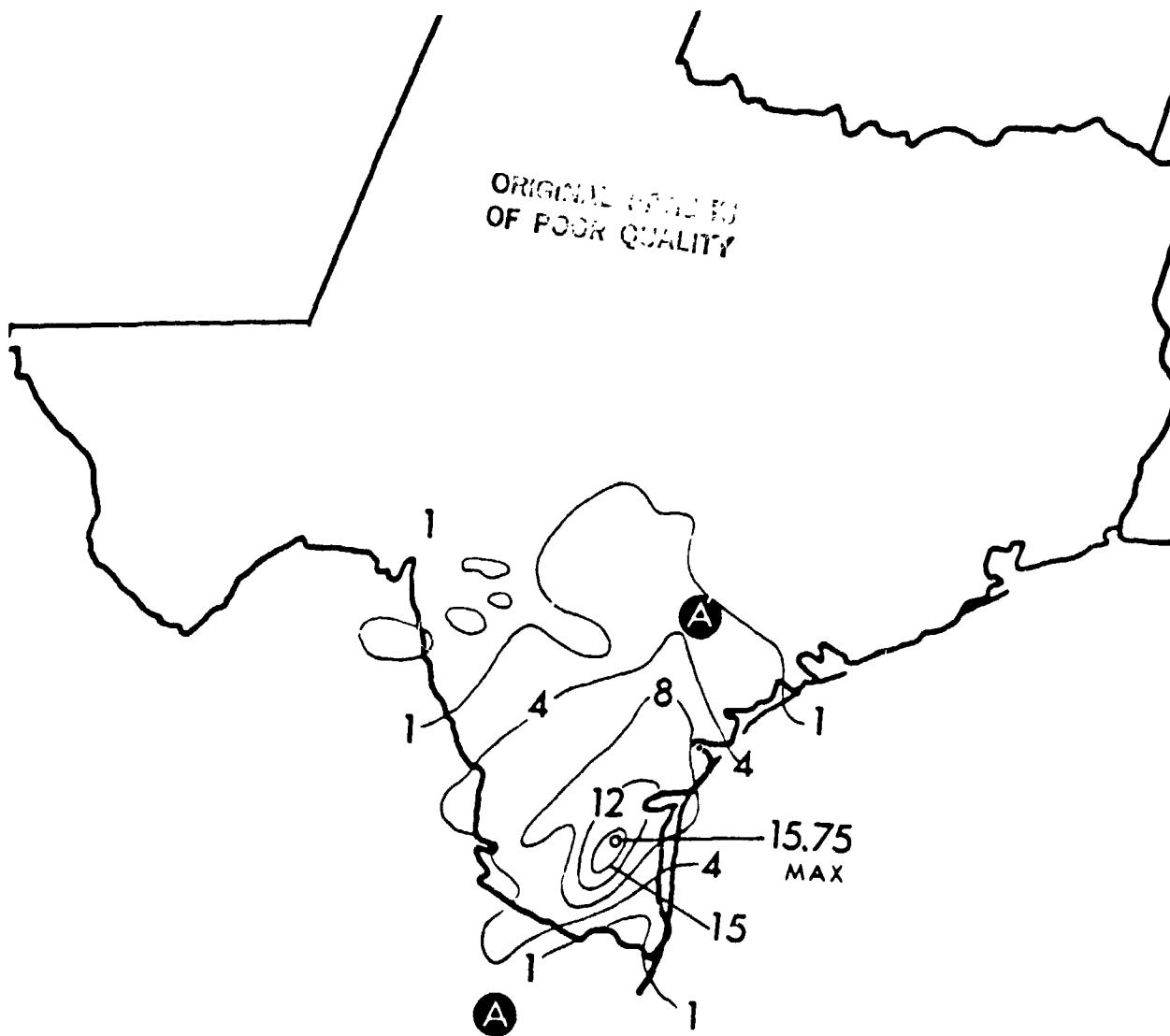


Figure 8. 24-hour satellite-derived rainfall estimate in inches ending at 1200 GMT, August 11, 1981.

#### 7. Acknowledgments

The author would like to thank Vincent J. Oliver, Applications Laboratory, NESS, for his constructive criticism in the preparation of the manuscript. Finally, I thank Sheila Collin for the typing and the layout of this manuscript, and John Shadid for the final draft of the figures and illustrations.

#### 8. References

Oliver, Vincent J. and R.A. Scofield, 1976: Estimation of Rainfall from Satellite Imagery. Published in the preprint volumes from both the Conference on Hydro-Meteorology, April 20-22, 1976, Ft. Worth, TX, and the Sixth Conference on Weather Forecasting and Analysis, May 10-14, 1976, Albany, NY, AMS, Boston, MA, 242-245.

Scofield, Roderick A. and V.J. Oliver, 1977: A Scheme for Estimating Convective Rainfall from Satellite Imagery. NOAA Technical Memorandum NESS 86, 45 pp.

Scofield, Roderick A., 1978: Using Satellite Imagery to Detect and Estimate Rainfall from Flash Flood Producing Thunderstorms. Seventh Conference on Weather Forecasting and Analysis October 16-19, 1978, Silver Spring, MD, AMS, Boston, MA, 132-141.

Scofield, Roderick A. and V.J. Oliver, 1980: Some Improvements to the Scofield/Oliver Technique. Second Conference on Flash Floods, March 18-20, 1980, Atlanta, GA, AMS, Boston, MA 115-122.

TABLE 1. VISIBLE AND INFRARED PRECIPITATION TECHNIQUES  
FOR AGRICULTURE APPLICATIONS

Platform	Cloud Types From Which Precipitation is Occurring	Technique	Principal Investigators	Countries
Geostationary	Cumuliform	<ul style="list-style-type: none"> <li>• Pattern Interpretation (empirical, dynamical, and physical reasoning)</li> <li>• Estimates modified for different environments</li> <li>• Observed Precipitation (including radar)</li> <li>• Cumulus Cloud Model</li> </ul>	<ul style="list-style-type: none"> <li>• Griffith et al. (ERL)</li> <li>• Scofield et al. (NESS)</li> <li>• Wylie (SSEC)</li> <li>• Martin et al. (SSEC)</li> <li>• Austin (McGill)</li> <li>• Ramage (Hawaii)</li> </ul>	The Americas
Geostationary	Stratiform and Stratiform with embedded Cumuliform	<ul style="list-style-type: none"> <li>• Pattern Interpretation (see above)</li> <li>• Estimates modified for different environments</li> <li>• Precipitation mechanisms in the atmosphere (warm air advection, vorticity advection, jet maxima, upslope flow, etc.)</li> <li>• Observed Precipitation (including radar)</li> </ul>	<ul style="list-style-type: none"> <li>• Scofield et al. (NESS)</li> <li>• Wylie (SSEC)</li> <li>• Austin (McGill)</li> <li>• Follansbee</li> </ul>	The Americas
Polar	Cumuliform, Stratiform, and Stratiform with embedded Cumuliform	<ul style="list-style-type: none"> <li>• Cloud Indexing modified for different environments</li> <li>• Some limited pattern interpretation (see above)</li> <li>• Precipitation mechanisms in the atmosphere (see above)</li> <li>• Observed Precipitation</li> </ul>	<ul style="list-style-type: none"> <li>• Barrett (Bristol)</li> <li>• Earth Satellite Corporation</li> <li>• Follansbee</li> </ul>	The Remainder of the World

THE ESTIMATION OF CONVECTIVE PRECIPITATION FROM GOES  
IMAGERY WITH THE GRIFFITH/WOODLEY TECHNIQUE

Cecilia G. Griffith and William L. Woodley

Office of Weather Research and Modification  
NOAA/ERL, Boulder, Colorado

1. INTRODUCTION

Agriculturalists, climatologists, hydrologists and meteorologists have many research and operational needs. A common requirement of these diverse fields is the accurate and timely estimation of precipitation. Yet, it is often difficult to obtain such estimates by conventional means. The advent of satellite remote sensing however has opened the possibility of making rain estimates over time and space scales never before available. This paper gives an overview of a computer-automated technique that estimates summertime convective rainfall from the thermal infrared imagery of geosynchronous satellites. The rudiments of the technique, the applications to date and future studies are reviewed in this paper.

2. TECHNIQUE

The derivation and verification of a technique to estimate summertime convective rainfall from geosynchronous satellite data has been described in detail in Griffith et al. (1978). Briefly, thermal infrared images were calibrated by a combined system of gage and radar data in south Florida to produce an empirical, diagnostic satellite rain estimation scheme. Satellite clouds and radar echoes were found to follow a life cycle in which each grew to a maximum area and then decreased in area until it disappeared below the cloud or echo definition threshold of  $-20^{\circ}\text{C}$  for clouds or  $1 \text{ mm h}^{-1}$  for echoes. There is an offset between the echo life history and the cloud life history which is important because it compensates for contamination from cold but inactive cirrus.

Radar echoes within 90 n mi of Miami were matched to clouds on the corresponding infrared image for a number of sequences of satellite pictures. The resulting empirical relationships between parameters measured from the satellite image and rainfall have the following properties:

- o Raining clouds are those which are as cold or colder than  $-20^{\circ}\text{C}$ .
- o Rainfall is directly proportional to cloud area on any given picture.
- o Rainfall is inversely proportional to cloud top temperature.
- o Rainfall is a function of cloud life cycle, that is, more rain is inferred in the early stage of a cloud's history than in the later stage.

The technique is fully automated so that estimates can be made routinely over large areas from digital satellite data. The four computer

programs required to produce the estimates are 1) the image navigation program (NAVIGATION), ii) the cloud isolation and tracking program (TRACK); iii) the program which compiles cloud life histories and calculates volumetric rain production for each cloud (TRACER) and iv) the rain mapping program (RAINMAP).

Although the technique was derived in south Florida, it has been successfully used for extra-tropical convection, once environmental differences have been accounted for.

3. VERIFICATION

Verification of the satellite estimates is made with the best ground data available. This has been gages, radar or a combination of the two. Verification is judged on three aspects:

- o correspondence between satellite-inferred and ground estimates of the amount of rain (usually area average depth) over a given region (Figure 1).
- o temporal coincidence of the rain maxima and minima in the time series of the satellite and ground rainfall (Figure 2) and
- o spatial coincidence of the rain cores and no rain areas of the satellite- and ground-derived isohyets (Figure 3).

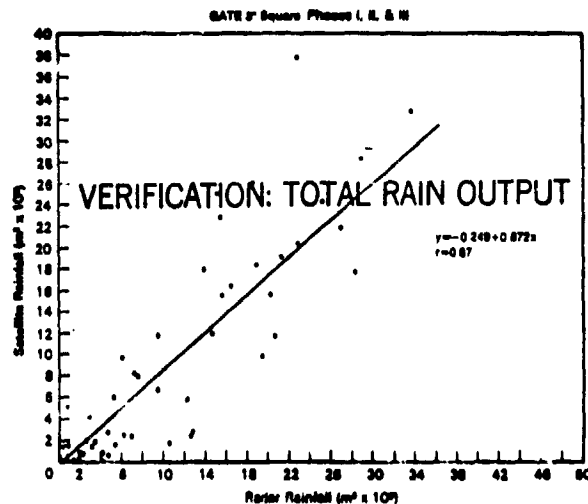


Figure 1. An example of verification on the basis of satellite and gage amount. The linear fit and correlation coefficient are shown on the scatter diagram.

ORIGINAL RESEARCH  
OF THE U.S. ARMY

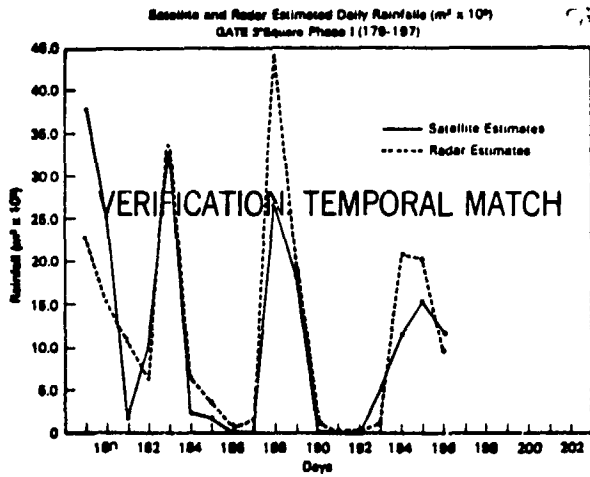


Figure 2. An example of verification on the basis of temporal coincidence of the satellite (solid) and radar (dashed) time series.

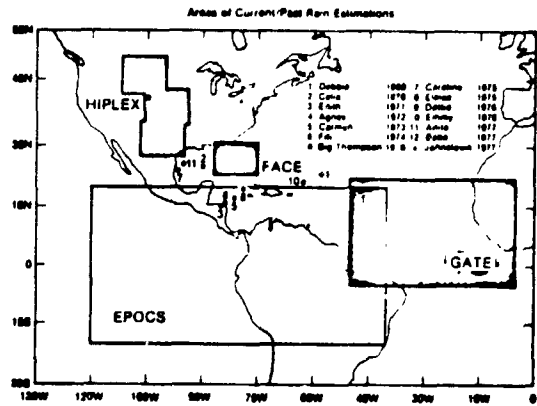


Figure 4. Areas over which the Griffith/Woodley technique has been applied. Refer to Table 1 for the acronyms and period of calculation.

The first two are relatively easy to achieve with this technique, the latter is more difficult because there is not a unique relationship between instantaneous cloud top temperature and integrated surface rainfall.

4. APPLICATIONS

Rain estimates have been made over a number of time and space scales shown in Table 1 and Figure 4, respectively. (For more detail the reader is referred to Waters et al., 1978; Woodley et al., 1978; Woodley et al., 1979; Woodley et al., 1980; Griffith et al., 1981; Augustine et al., 1981; and Jarvinen and Griffith, 1981.) With the exception of the EPOCS work and several calculations for

hurricanes, comparison with ground data are possible for all of these. Several statistics for the amount comparisons are shown in Table 2. The number of cases represented by "N" in the table are days for GATE, period for HIPLEX and FACE (which ranges from 3.5 to 16 hours) and storm event for hurricanes and flash floods. The bias, root mean square error and linear least squares fit parameters are shown for each sample. Ground data are radar for GATE, a combination of gages and radar for the Johnstown flash flood and gage data for the remaining samples. Bias (B) is defined as  $\sum S / \sum G$  where S is the total satellite-inferred rain depth (mm) over the period of calculation and G is the total ground rainfall for the same period. The root mean square error ( $E_{RMS}$ ) is

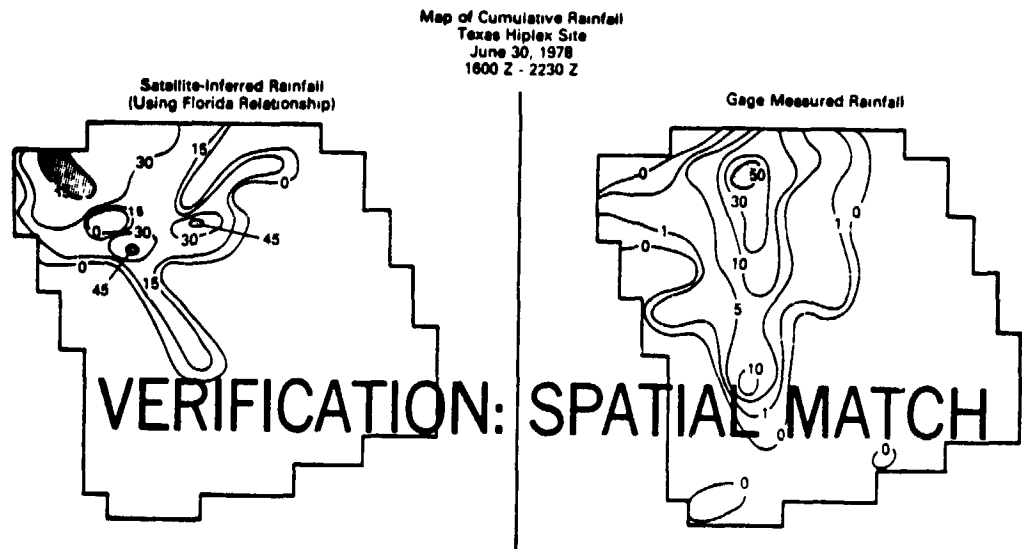


Figure 3. An example of verification on the basis of isohyets for satellite (left) and gage (right) estimates of rainfall.

ORIGINAL PAGE IS  
OF POOR QUALITY

TABLE 1  
APPLICATIONS OF THE GRIFFITH/WOODLEY TECHNIQUE

AREA	PERIOD
Global Atmospheric Research Project's Atlantic Tropical Experiment (GATE)	June 27 to Sept. 20, 1974
Florida Area Cumulus Experiment (FACE)	Selected days June to September 1972 to 1980
Equatorial Pacific Ocean Climate Studies (EPOCS)	2-1/4 days November, 1978 30 days November, 1979
High Plains Experiment (HIPLEX)	Selected days, May to July 1976 to 1978
Hurricanes	Selected storms 1969 to present
Flash floods	Big Thompson, CO 7/31 - 8/1, 1976 Johnstown, PA July 19-20, 1977

$$\left[ \frac{\sum (S-G)^2}{n} \right]^{1/2}$$

for S and G as before. In calculating the linear fits, the ground data have been used as the independent variable, and both satellite and ground rainfalls are mean rainrates (mm/h) averaged over the period of calculation and the area of interest of each case. In the dense HIPLEX networks the gage spacing ranges from 20 to 150 km<sup>2</sup>/gage, while the sparse gage networks have a spacing an order of magnitude larger (1400 to 2700 km<sup>2</sup>/gage). In FACE the spacing is 120 km<sup>2</sup>/gage, whereas the balance of the gage data are available climatological data at a coarser spacing.

The data in Table 2 indicate that on the average the technique approximates fairly well the ground data. The biases are close to 1.00, the value for a perfect correspondence and, with the exception of the GATE and dense HIPLEX results, the root mean square error is small. (This technique consistently underestimated the radar rainfall during Phase 2 of GATE, due to rain from shallow convection. The root mean square error for the dense HIPLEX data is dominated by one light rain case in which the average rain in the gage network was 0.001 mm/h and the satellite inferred 0.01 mm/h. Without this case, the root mean square error is 0.78.) In the linear fits, the correlations are all 0.8 or greater. With the exception of the sparse

TABLE 2

ERROR STATISTICS FOR APPLICATIONS OF THE GRIFFITH/WOODLEY TECHNIQUE						
LOCATION	N	R	R <sub>RMS</sub>	R	SLOPE	INTERCEPT
GATE	53	0.84	0.79	0.87	0.97	-1.47
HIPLEX (dense)	15	0.77	2.81	0.90	0.62	0.07
FACE	11	0.88	0.42	0.95	1.18	-0.23
HIPLEX (sparse)	9	0.90	0.55	0.78	1.81	-0.27
HURRICANES	3	1.08	0.06	1.00	0.89	0.18
FLASH FLOOD	2	1.39	0.48	0.99	0.89	23.93
PERFECT CORRESPONDENCE		1.00	0.00	1.00	1.00	1.00



HIPLEX network, the slopes are all close to 1.00. (The relatively large slope for the dense network results may be more indicative of sampling errors due to the ground data than to errors inherent in the satellite technique.) The intercepts of the GATE and flash flood data show the effects of the satellite's underestimation of GATE Phase 2 (noted above) and overestimation of the flash flood cases. All other intercepts are close to zero.

There is also evidence that the technique performs better on heavier rain than on light rains. (See Griffith et al., 1981.) In comparing 12 heavy rains to 12 light rains from the HIPLEX data set, we found that the bias and root mean square error were much larger for the light rain cases. The bias was 2.38 for light rains, but 1.28 for heavy; the root mean square error was 3.62 for the light rains and 1.58 for the heavy.

Temporal comparisons of satellite and ground rainfall time series show that satellite estimates are usually within 30 to 60 minutes of the ground rainfall maxima and minima. (Note that the temporal resolution of the satellite data is usually 30 minutes, so that this quoted figure is for the nominal resolution of the satellite data. The lag naturally is a function of the temporal resolution of the satellite imagery.) The satellite offset shows no bias toward preceding or lagging the ground data.

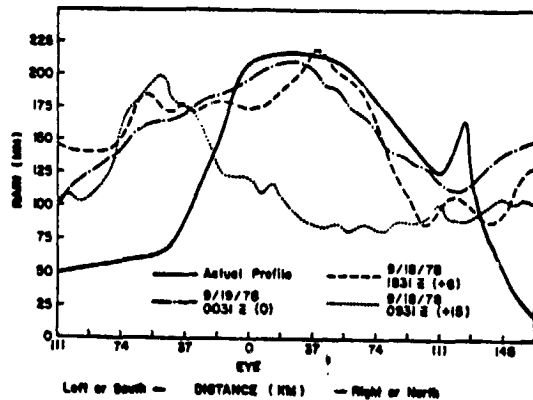


Figure 5. Coastal rain profiles for a landfalling hurricane. Profiles derived from gage and satellite data are shown for hurricane Greta, 9/19/78. Gage results are shown by the solid line and three satellite-inferred profiles for 0, 6, and 15 hours prior to landfall are shown in the remaining curves.

During the last several hurricane seasons the technique has been used quasi-operationally for landfalling hurricanes. The product for this application was a temperature contoured satellite image and three gross measures of storm rainfall which were computed on the basis of a single image: total volumetric output, area-average depth and average rain potential of the storm. The hurricane verification results previously shown indicate such a close correspondence between satellite and gage estimates that much confidence can be given to these

measures of gross rainfall. This past season a new product has been added. It shows a satellite-inferred rain profile along a hypothetical coastline which is perpendicular to the direction of storm motion (Figure 5). In this figure distance from the storm's eye along the hypothetical coastline is plotted on the abscissa and rainfall in inches is plotted along the ordinate. Actual gage data for the passage of Greta (1978) through the country of Belize, Central America are given in the solid line and three satellite estimates at 0, 6 and 15 h prior to landfall are shown in the remaining curves. Initial results (for Greta and Allen, 1980) indicate that peak rainfalls and total rainfalls inferred by the satellite are remarkably close to gage results, but that the satellite technique tends to calculate too much rain to the left of the hurricane's eye and too little in the region immediately to the right of the eye. These discrepancies may be due to the effect of the land on the storm's low-level circulation.

#### 5. CURRENT AND FUTURE STUDIES

Ongoing research is involved in assessing the applicability of the technique to several different problems. In the context of AgRISTARS we are determining the applicability of the technique to agricultural users for both summertime and wintertime precipitation. Secondly, the extra-area effects of cloud seeding will be quantified by use of this technique for the area surrounding the Florida Area Cumulus Experiment (FACE). Thirdly, a study to determine the accuracy of the technique as a function of space and time is addressed in another paper for this workshop (Woodley, Griffith and Meitin, 1981). And lastly, initial efforts have been made to use satellite rain estimates from this technique for the determination of microwave attenuation in the SEASAT SASS sensor (Figure 6). On the left of this figure is rainfall for hurricane Fico derived from the SEASAT 36 GHz passive microwave radiometer (SMPR). The right side shows rainfall inferred with the Woodley/Griffith technique by using the SEASAT thermal infrared channel on the VIRR. With the exception of the 1/2° latitude displacement, the extent and location of the cores in the patterns are similar, although the intensities of the cores are higher for the SMPR data. Comparisons such as this one will be used to assess the accuracy of our inferred isohyets in hurricanes.

#### 6. REFERENCES

- Augustine, J.A., C.G. Griffith, W.L. Woodley and J.G. Meitin, 1981: Insights into errors of SMS-inferred GATE convective rainfall. Accepted for publication, *J. Appl. Meteor.*, 20, June.
- Griffith, C.G., W.L. Woodley, P.G. Grube, D.W. Martin, J. Stout and D.N. Sikdar, 1978: Rain estimation from geosynchronous satellite imagery - visible and infrared studies. *Mon. Wea. Rev.*, 106, 1152-1171.
- Griffith, C.G., J.A. Augustine and W.L. Woodley, 1981: Satellite rain estimation in the U.S. High Plains. *J. Appl. Meteor.*, 20, 53-66.
- Jarvinen, B.R. and C.G. Griffith, 1981: Forecasting

ORIGINAL PAGE IS  
OF POOR QUALITY

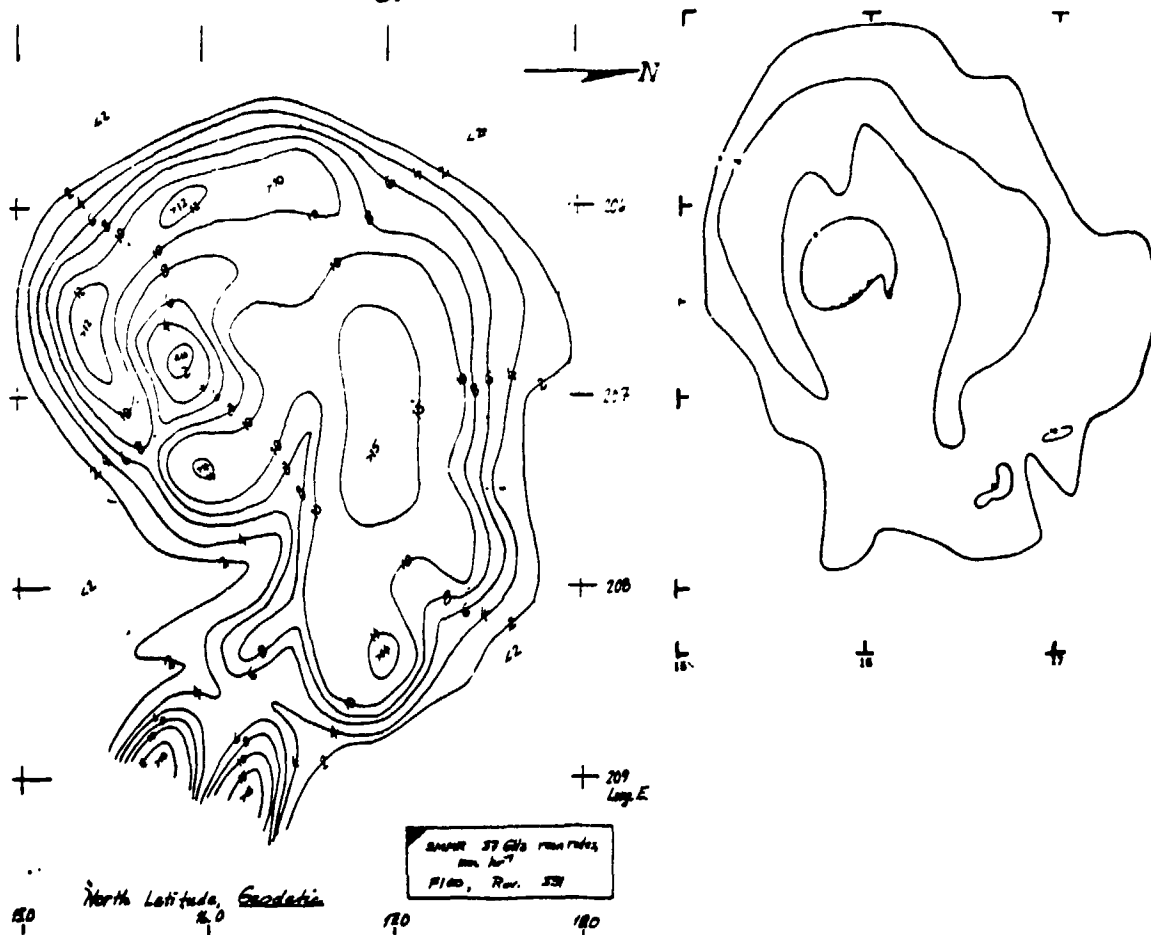


Figure 8. Rain rates inferred from passive microwave (left) and thermal infrared (right) channels on the SEASAT for hurricane Fico (1979) in the Pacific Ocean. Contours are incremented by 2 mm/h for the microwave and 5 mm/h for the IR data.

rainfall in tropical cyclones using digitized infrared satellite data. Submitted to Mon. Wea. Rev.

Waters, M.P., III, C.G. Griffith and W.L. Woodley, 1978: Use of digital geostationary satellite imagery for real-time estimation of hurricane rain potential in landfalling storms. Vol. of Conf. Papers: 11th Tech. Conf. on Hurricanes and Tropical Meteor., Amer. Meteor. Soc., Boston, MA, 198-203.

Woodley, W.L., C.G. Griffith, J. Griffin and J. Augustine, 1978: Satellite rain estimation in the Big Thompson and Johnstown flash floods. Preprint Vol.: Conf. on Flash Floods: Hydrometeorological Aspects, Amer. Meteor. Soc., Boston, MA, 44-51.

Woodley, W.L., J.A. Augustine, S.P. Browner and C.G. Griffith, 1979: Inference of rainfall in weather modification experiments using satellite imagery. Preprint Vol.: 7th Conf. on Inadvertent and Planned Weather Modification, Amer. Meteor. Soc., Boston, MA, 104-105.

Woodley, W.L., C.G. Griffith, J.S. Griffin and S.C. Stromatt, 1980: The inference of GATE convective rainfall from SMS-1 imagery. J. Appl. Meteor., 19, 388-408.

Woodley, W.L., C.G. Griffith and J.G. Meitin, 1981: A standard verification for rainfall estimation from remote platforms. Workshop on Precipitation Measurement from Space, NASA/Goddard, Greenbelt, MD.

N83 25297

D28

The Bristol Method of  
Satellite-improved Rainfall Monitoring

by

Eric C. Barrett  
University of Bristol,  
Bristol U.K.

Paper presented to the NASA Workshop on  
"Precipitation Measurements from Space", GSFC, Washington, D.C.

May, 1981.

ORIGINAL PAGE IS  
OF POOR QUALITY

I Introduction

Since 1969 we have had an active interest in the University of Bristol in improved rainfall monitoring using satellite and conventional data. Our research has aimed to design and develop a method to:

- (a) Provide rainfall evaluations more uniform, accurate and complete than could have been derived from satellite or conventional data alone;
- (b) Serve current operational environmental programmes in countries with special needs for improved rainfall data;
- (c) Invoke either polar-orbiting &/or geostationary imagery as the satellite inputs;
- (d) Utilise Global Telecommunication System (GTS) SYNOP messages as the basic conventional data inputs;
- (e) Be applicable to any and all types of weather situations in the operational areas;
- (f) Be undemanding in hardware and software so as to be an option available for use even by nations or agencies with very limited financial resources.

Our most basic intention has been to capitalise simultaneously on the more desirable characteristics of raingauge and satellite cloud-image data in our attempts to achieve these goals. These characteristics involve the following considerations:

- (a) Raingauge data are relatively accurate measurements of rainfall accumulated through time, but are notoriously location-specific. This is a serious disadvantage where such a spatially noisy weather parameter is concerned.
- (b) Satellite data give spatially complete and detailed pictures of the distributions of clouds, from which useful assessments of rainfall may be deducible. However, rain areas and amounts can be very difficult to evaluate with confidence owing to wide variations in rain rates from apparently similar cloud fields.

We have sought to make the best possible use of the two types of base data, and to compensate for the inherent deficiencies of each, by using raingauge data as the bases for our rainfall maps, and improving the shapes of isohyets in conventional data-sparse areas through extrapolations of observed cloud/rainfall relationships from gauged into ungauged areas. We have developed "floating" schemes to help us make suitable allowances both for climatological variations, and day-to-day differences in cloud/rain relationships.

Although the present Bristol Method (Mark IV) retains the climatological

/statistical heart of its predecessors, it relies heavily upon the meteorological knowledge and skill of the analyst. Consequently, it has been described recently as "an extension of classical synoptic meteorology, involving as it does a strong element of qualitative judgement, based on a variety of types of weather observations, and executed as it is within a framework of rules and practices evolved largely through practical experience". (Barrett, in press).

## II Significant stages in the development of the Bristol Method.

The Bristol Method of improved rainfall monitoring through the integration of conventional data and polar-orbiting satellite imagery (see Fig. 1) had its origins in a climatological (monthly accumulated rainfall) technique described by Barrett (1970, 1971). Estimation and mapping of rainfall within shorter, meteorological, time-frames using such a cloud-index technique in which satellite-viewed cloud is evaluated in terms of cloud area and type, and the likely associated intensities and frequencies of rain, was attempted first for Northern Sumatra (Barrett, 1975a, 1977a). Subsequently other studies have been undertaken in North-east Oman (Barrett, 1977b & 1978), and most extensively and continuously, in North-west Africa (Barrett 1976, 1977c, 1977d, and Barrett & Lounis, 1979, Barrett 1980; for a general summary see Barrett, in press). Significant stages in the development of the Bristol approach from its early experimental stages to its current operational use in North-west Africa may be summarised as follows:

### 1. The Bristol Method, Mark I.

Calibration of cloud indices was undertaken for grid squares lacking rainfall stations (satcells) through the cloud-index: observed rainfall relationships established for a series of squares containing individual rainfall stations (gacells) through a selected "historic" period on a once-daily sampling basis. Unlike similar methods developed in the USA (see e.g., Follansbee, 1973; Follansbee & Oliver, 1975), the Bristol Method incorporated, from its outset, a "floating" device to accommodate the variable relationship between satellite-imaged cloud and surface-measured rainfall. In Mark I the historic cloud-index:observed rainfall regressions were contoured by confidence limits to achieve suitable floats of rainfall estimates for each satcell as required.

### 2. The Bristol Method, Mark II.

This differed from Mark I in two important respects. First, cloud-index: observed rainfall regressions were prepared for ("morphoclimatic") regions, each embracing several gacells, not for individual gacells as in Mark I.

**ORIGINAL FACTORS  
OF POOR QUALITY**

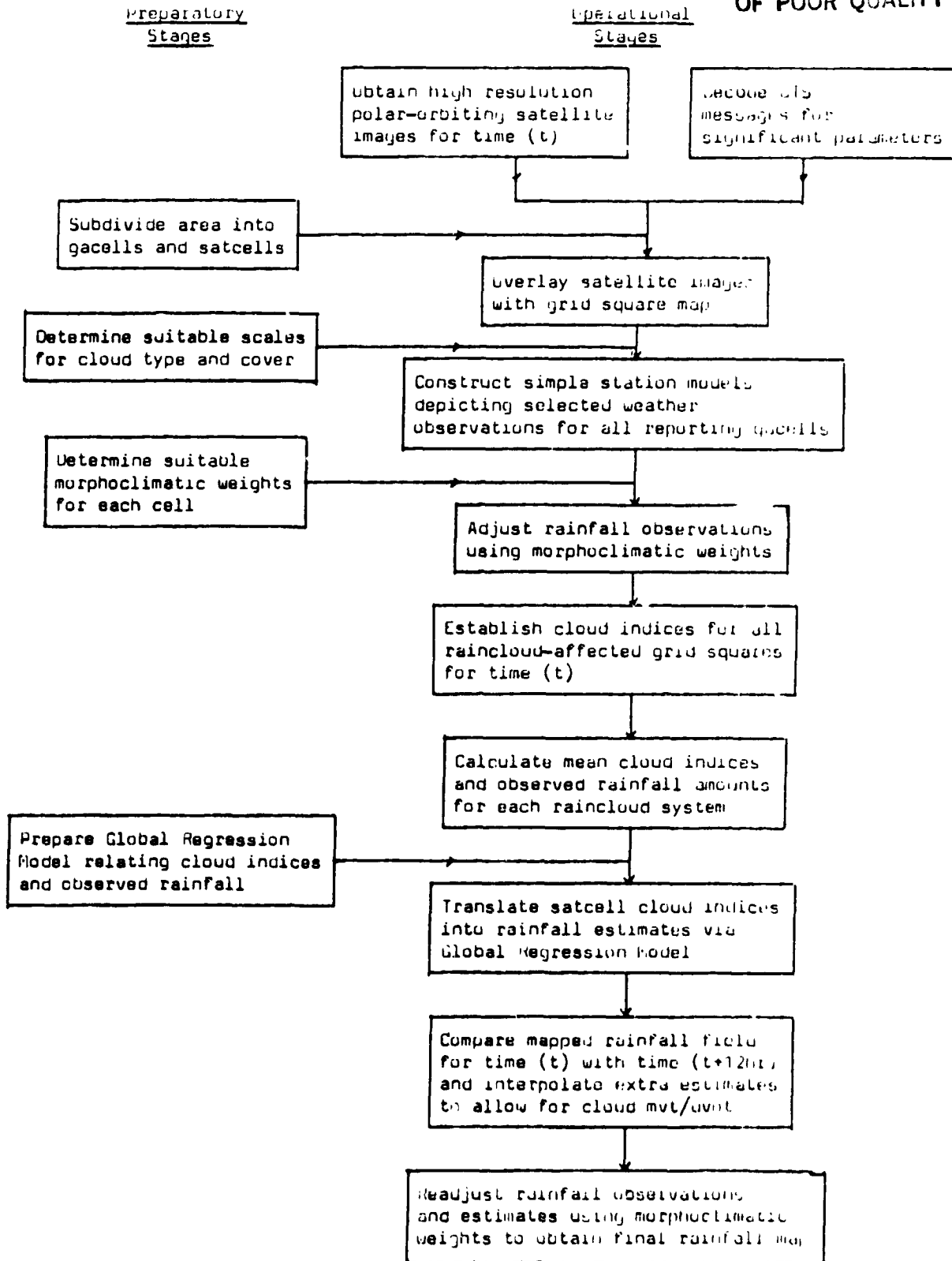


Figure 1. Flow diagram for the Bristol Method in its most recent form (Mark IV).

## GENERAL OF POLAR QUALITY

This was necessitated by the much lower number of rain days at each gauge in the semi-arid environment of North-east Oman than had been recorded in North-west Sumatra. Second, "floating" of daily rainfall estimates for satcells was achieved through the use of regressions contoured parallel to the computed regression lines (Fig. 2), not sub-parallel &/or oblique as the confidence limits in Mark I had been. The change was made partly to achieve more realistic estimates at the intense end of the rain-rate spectrum, and partly to avoid certain questionable statistical assumptions necessitated by the confidence limit approach. However, the new meteorological assumption (that rain-cloud systems might be expected to precipitate everywhere more or less heavily than the norm) were also open to question, especially where rain-rates were low.

### 3. The Bristol Method, Mark III.

This again advanced on its immediate predecessor in two ways, necessitated by its application over much wider, less well-gauged areas than Marks I & II. First, its temporal resolution was doubled in order to give 12 hr rainfall data. Second, its spatial performance was improved through routines following, but more flexible than those suggested first by Follansbee (1976) to accommodate as well as possible the implications of rain-cloud system movement &/or development between the times of the "set-piece" analyses based directly on twice-daily satellite imagery. Although applied usually to polar-orbiting (visible &/or infrared imagery, tests have demonstrated that Mark III is (even more) viable if based on more frequent Meteosat imagery (Barrett, 1980).

4. Germane work of a similar nature was undertaken in the early 1970s with the aim of not estimating, but predicting, rainfall totals. (Barrett, 1973, 1975b). This work was not carried forward because of the greater interest exhibited by the user community in post-event data. However, the pre-event results are of significance in the present context because they were derived from mid-latitude studies covering parts of south-west Ireland and south-west England.

### III The Bristol Method Mark, IV

Current work under the umbrella of the AGHISTAMS project (NESS, 1980) seeks to:-

- (a) Demonstrate the viability of the Bristol approach in middle latitude (cyclonic frontal) areas;
- (b) Review the requirements and bases for local regional calibration; and
- (c) Move towards a form of the Method which could be transferred conveniently to an interactive system so that it might be more rapidly applied to

ORIGINAL PRESENTATION  
OF POOR QUALITY

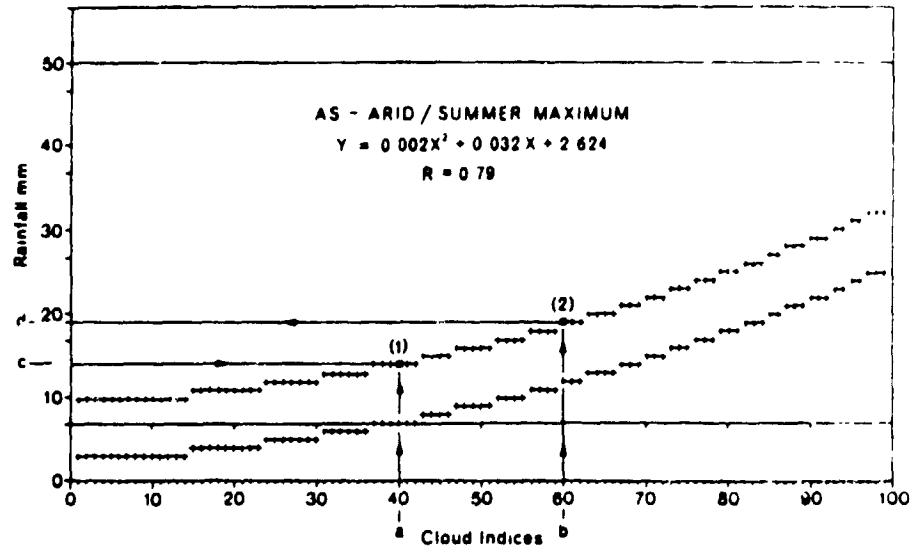


Figure 2. A regression diagram for part of north-west Africa as used to "float" rainfall estimates for satcells in relation to gacell-evidence. In this example a gacell cloud index (a) and rainfall observation (c) locates point (1) on the operative regression surface. A transparent overlay is moved up so that the climatic regression (marked by the tagged line) intersects (1). For an associated satcell, the cloud index (b) is translated into a rainfall estimate (d) through point (2), which, like (1), lies on the operative regression surface.

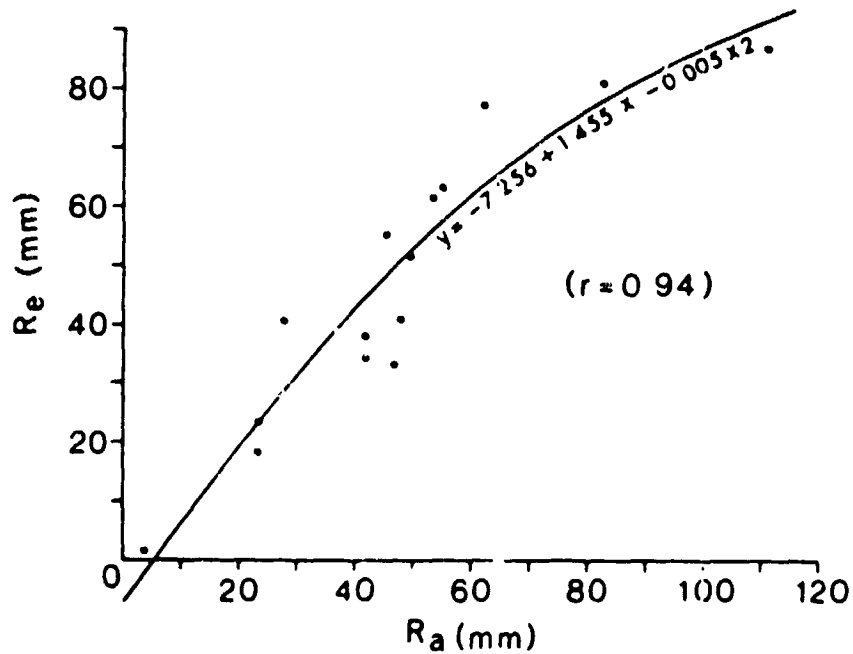


Figure 3. Annual verification statistics for 15 stations in north-east Oman, 1975.



ORIGINAL PAPER  
OF POOR QUALITY

large areas by a minimum of analysts and support staff.

Although our present studies are, as yet, incomplete, it is not too early to propose that:

1. A "Global Regression Model" can be used to obviate the need for time-consuming calibration of the method for each new area of application;
2. The first results of the use of Mark IV in a mid-latitude test area (Spain - France - England) appear very promising; and
3. Running a derivative of the Bristol Method, Mark IV, on a suitable interactive system would yield better results than the longhand ("eye-ball") Method, for this would permit more flexible contouring for obvious rainfall gradients than at present.

IV Verification of Results.

The forms of the results have been dictated mainly by the purposes for which they were compiled. They may be represented as follows:

- (a) Mark I: Annual run-off data from river gauging stations at the outlets of two basins in northern Sumatra showed that satellite rainfall estimates over those basins provided 79.2 & 87.8% of basin average rainfall.
- (b) Mark II: Data from 15 reserved verification stations in north-east Oman showed that annual rainfall estimates from satellite evidence were strongly correlated with observed rainfall (Fig. 3); annual rainfall estimates for the 13 stations averaged 97.9% of observed rainfall.
- (c) Mark III: Satellite indications of significant rainfall events in north-west Africa have been verified mostly by vegetation response: we have evidence of no major rainfall events in over 2 years that we have not identified in our satellite-improved rainfall maps. (See Fig. 4).
- (d) Mark IV: First results in our AgRISTARS study in Western Europe are represented in Fig. 5. We have yet to establish how much of an improvement these data represent over those which would have been achieved through standard interpolation techniques.

V Problems and prospects.

The biggest problem we have grappled with is how we might best accommodate the changes which take place in cloud fields from one imaging time to another, especially when these are as much as 6 or 12 hr apart. This poses special problems for automation: mean brightness (averaged through time) tells us relatively little about cloud types, whilst texture, which is so informative on cloud type in instantaneous images, would be undependable in composite images. Such difficulties lead us to believe that full automation of a method

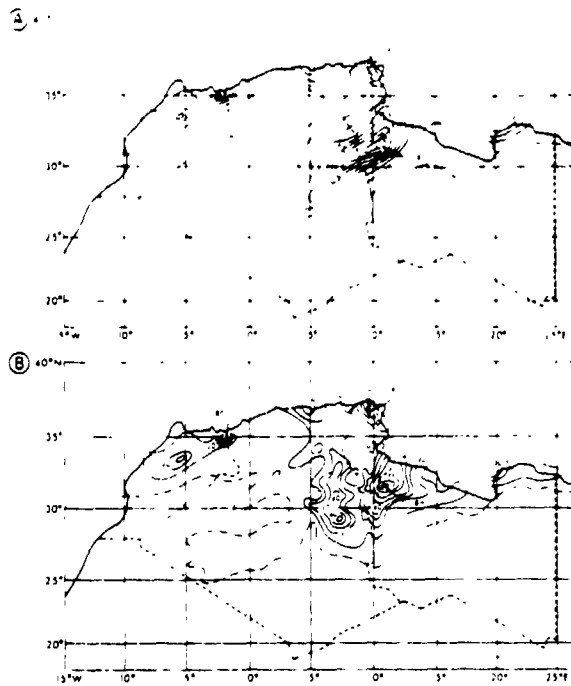


Figure 4. Rainfall in north-west Africa, for the week of 29 March - 4 April 1977, from (A), GTS data alone, and (B) GTS plus twice-daily satellite evidence.

		$R_e$										
		0	0-24	25-49	50-74	75-99	100-124	125-149	150-174	175-199	≥ 20	Totals
$R_o$	0	236	23	3		1						263
	0-24	22	29	10	3							64
	25-49	4	9	4	5	1						23
	50-74		6	2	8	4	2	2				24
	75-99		1		3	2		1				7
	100-124	1		1	1	2	1		1			7
	125-149						1	1	1			4
	150-174						1	2	4			9
	175-199								1			1
	≥ 20										1	1
Totals		263	68	20	20	10	5	6	7		4	403

Figure 5. Contingency table of 12 hourly satellite-estimated ( $R_e$ ) rainfall versus observed ( $R_o$ ) rainfall for verification stations in a western Europe test area, 1 - 8 May, 1978.

like ours cannot be contemplated yet.

Further problems involve the ways in which we might increase the physical directness of the Bristol Method, and improve our assessments of errors in the absence of ground truth. Physical models of key weather structures are generally unhelpful in analyses of day-to-day situations, in which the atmosphere usually behaves in a subdued and relatively nondescript way. Additional parameters (e.g. precipitable water) might usefully guide the analyst using an interactive system for his operations: but no operational method can utilise data or data types which are unavailable locally or through local channels.

In conclusion, we see the Bristol Method as an organically-evolving optimization technique for rainfall monitoring in conventional data-sparse areas, to be used until a more physically-direct method (microwave, radar?) becomes available to every user. However, we are also confident that much of our experience will continue to be relevant to the future problems of calibration of new satellite rainfall data, and the integration of satellite data with ground truth.

VI References.

- Barrett, E.C. (1970): "The estimation of monthly rainfall from satellite data", Monthly Weather Review, 98, p.322-27.
- Barrett, E.C. (1971): "The tropical Far East: high season climatic patterns derived from ESSA satellite images", Geographical Journal, 137, p.535-55.
- Barrett, E.C. (1973): "Forecasting daily rainfall from satellite data", Monthly Weather Review, 101, p.215-22.
- Barrett, E.C. (1975a): Rainfall in Northern Sumatra: analyses of conventional and satellite data for the planning and implementation of the Krueng Irene/Krueng Baro irrigation schemes. Final Report to Binnie & Partners (Consulting Engineers), London, 50 pp.
- Barrett, E.C. (1975b): "Analyses of image data from meteorological satellites", in Processes in Human and Physical Geography: Bristol Essays, (ed. R.F.Peel), Heinemann (London), p.170-92.
- Barrett, E.C. (1976): Pilot project in desert locust survey and control using remote sensing techniques: Results of the estimation of rainfall from weather satellite imagery for southern Africa. Consultant's Report to F.A.O., Rome, 21 pp.
- Barrett, E.C. (1977a): "Applications of weather satellite data to mapping rainfall for the solution of associated problems in regions of sparse conventional observations", in Remote Sensing of the Terrestrial Environment, (eds. E.C.Barrett, L.F.Curtis, & R.F.Peel), Butterworths, (London).
- Barrett, E.C. (1977b): The assessment of rainfall in north-eastern Oman through the integration of observations from conventional and satellite sources. Consultant's Report, F.A.O., Rome, w/k 7629, 55 pp.

ORIGINAL PAGE IS  
OF POOR QUALITY

- Barrett, E.C. (1977c): Mapping rainfall from conventional data and weather satellite imagery across Algeria, Libya, Morocco and Tunisia, Desert Locust Satellite Application Project, Stage II, Consultant's Report, F.A.O., Rome, AGP/DL/RS/1, 13 pp.
- Barrett, E.C. (1977d): Rainfall monitoring in the region of the North-west African Desert Locust Commission in 1976-77 (with French translation: Surveillance des precipitations dans la zone de responsabilite de la Commission du Criquet Pelerin pour l'Afrique du Nord-Ouest F.A.O., Rome, AFP:LCC/77/9, 44 pp.
- Barrett, E.C. (1978): The use of weather satellite data in the evaluation of national water resources with special reference to the Sultanate of Oman, Space Research, 19, p.41-46.
- Barrett, E.C. (1980): An operational method for rainfall monitoring in north-west Africa, Desert Locust Application Project, Stage IV, FAU, Rome, AGP:LCC/80/6, 43 pp.
- Barrett, E.C. (in press): Satellite-improved rainfall monitoring by cloud-indexing methods; operational experience in support of desert locust survey and control. In Satellite Hydrology (ed. M.Deutsch), American Water Resources Association.
- Barrett, E.C. and Lounis, M. (1979): Progress towards the establishment of an Operational Remote Sensing Unit for Desert Locust monitoring and control in north-west Africa, Desert Locust Application Project, Stage III, F.A.O., Rome, AGP:LCC/79/11, 40 pp.
- Follansbee, W.A. (1973): Estimation of average daily rainfall from satellite cloud photographs. NOAA Technical Memorandum, NESS 44, Washington, D.C., 39 pp.
- Follansbee, W.A. (1976): Estimation of daily precipitation over China and the USSR using satellite imagery. NOAA Technical Memorandum, NESS 81, Washington, E.C., 30 pp.
- Follansbee, W.A., & Oliver, V.J. (1975): A comparison of infrared imagery and video pictures in the estimation of daily rainfall from satellite data. NOAA Technical Memorandum, NESS 62, Washington, D.C., 30 pp.
- NESS (1980): NESS AgRISTARS Program Development Plan, NESS, Washington, D.C., 28 pp.

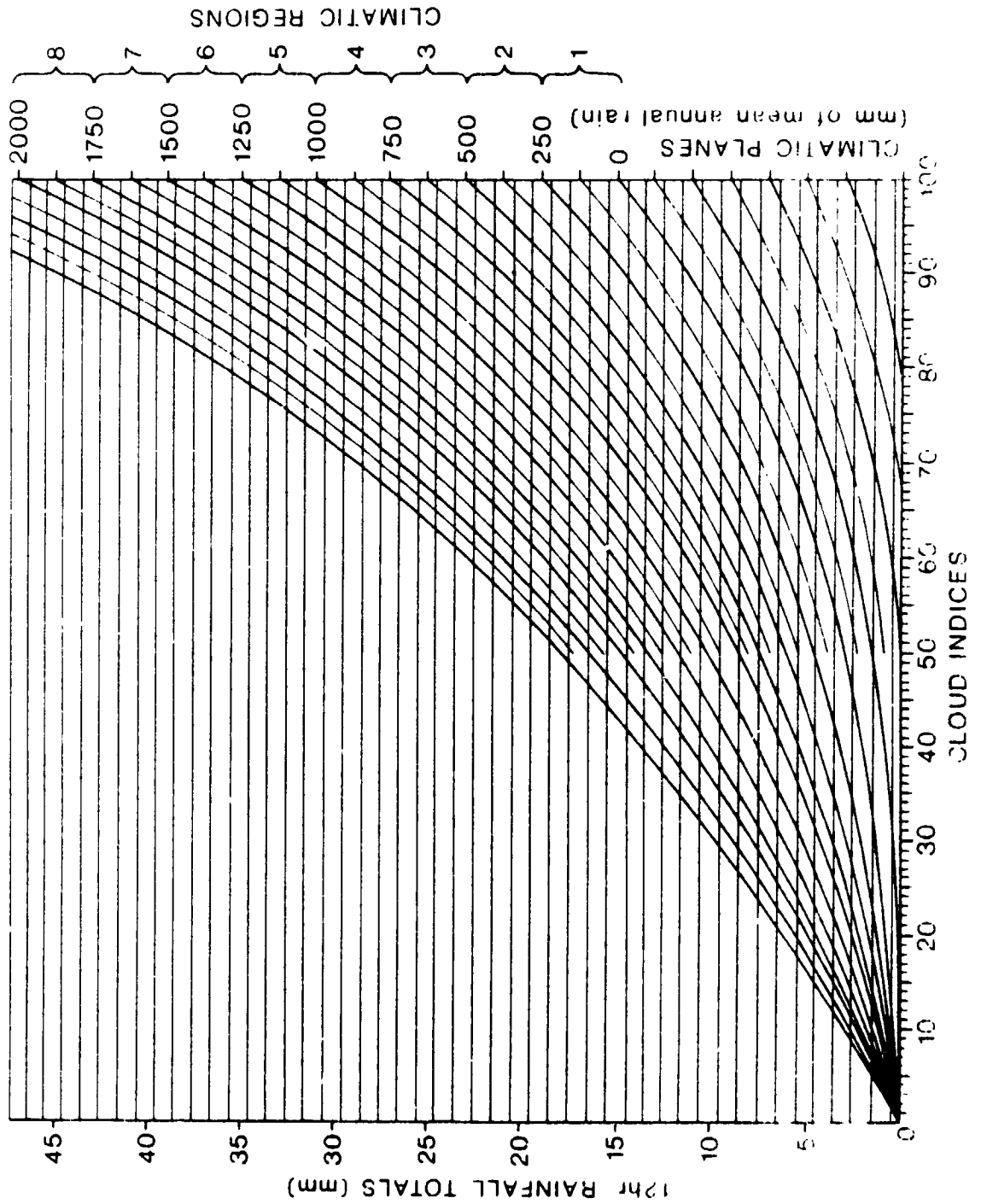


Figure 6. "Global Regression Model" for instant use in a wide range of climatic regions, developed from computed regressions in several more local studies in different parts of the world.

D29 N83 25298

DIURNAL VARIATION  
OF SURFACE TEMPERATURE

INFERENCE OF PRECIPITATION THROUGH THERMAL INFRARED  
MEASUREMENTS OF SOIL MOISTURE

BY

Peter J. Wetzel  
David Atlas  
NASA/Goddard Space Flight Center  
Laboratory for Atmospheric Sciences  
Greenbelt, Maryland 20771

Remote sensing estimates of area average precipitation have particular usefulness to agricultural and climatological applications. Estimates obtained by means of active or passive microwaves, infrared and visible sensors may be augmented and improved using indirect measures of precipitation, such as the change in near-surface soil moisture content caused by a particular event. Obviously, measurements of soil moisture using infrared radiances do not provide precipitation information in real time since the sky must clear at least partially before the observation can be made. However, the resultant estimate of precipitation is a time-integrated value which can provide a significant savings in data handling and can overcome virtually all of the sampling problems associated with the monitoring of precipitation through storms of long duration.

Thermal infrared observations of soil moisture have been attempted in the past using sun-synchronous polar orbiting satellite data, such as the Heat Capacity Mapping Mission (HCMM, e.g., Harlan, 1980), however, such observations are limited by twice-daily temporal resolution of the surface temperature wave. As shown in Figure 1, there are a wide variety of signatures sensitive to soil moisture which polar orbiters cannot detect, but which are observable from geosynchronous satellites. Figure 1, extracted from Schmugge et al. (1978), represents in-situ observations of surface temperature over a bare soil field in Arizona which was monitored during the drying cycle

following irrigation. The data suggest that soil moisture information is contained in such parameters as the area integral under the diurnal curve, the slopes at various times, the difference between maximum and minimum temperatures, and the lag time of the maximum behind local noon.

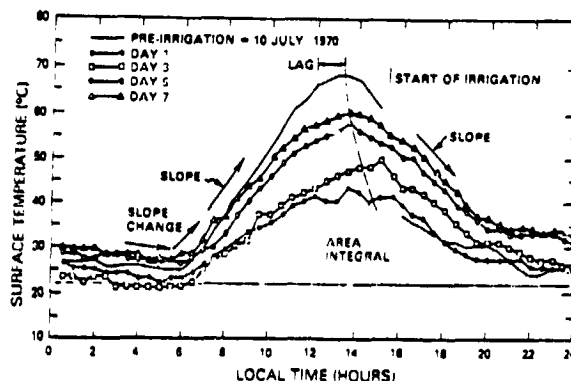


Figure 1. Diurnal variation of surface temperature over a bare soil field as measured by a Thermocouple. Indicated are some of the parameters measurable from geosynchronous satellites which are sensitive to soil moisture. Data reproduced from Schmugge et al. (1978).

In order to determine which physical parameters are most sensitive to soil moisture and which are less prone to interference by seasonal changes, atmospheric effects, vegetation cover, etc., a numerical model was employed. The model is an updated version of the boundary layer/earth's surface model of

ORIGINAL SOURCE  
OF POOR QUALITY

Wetzel (1978). Results of the modeling effort have shown that a normalized morning slope parameter,

$$B = \frac{(dT_s/dH_s)}{(dT_s/dH_s)_{dry}} \quad (1)$$

has the optimum characteristics for detecting soil moisture. Here  $dT_s/dH_s$  is the change of surface temperature with solar radiation absorbed by the surface, as measured at mid-morning (0800-1000 local time). This slope parameter, when normalized by its dry soil value, is quite insensitive to surface characteristics for non-forested surfaces. Figure 2 is a plot of model calculations of B vs. fractional soil water content, where  $W_s$  is the saturation or field capacity value of water content for a unit soil column of specified depth adjacent to the surface. Calculations for several wind speeds and two generalized surface cover types are shown. These results, as well as the results of many other experiments in which atmospheric, surface and soil variables were systematically varied, indicate that the parameter B is primarily sensitive only to soil moisture and wind speed.

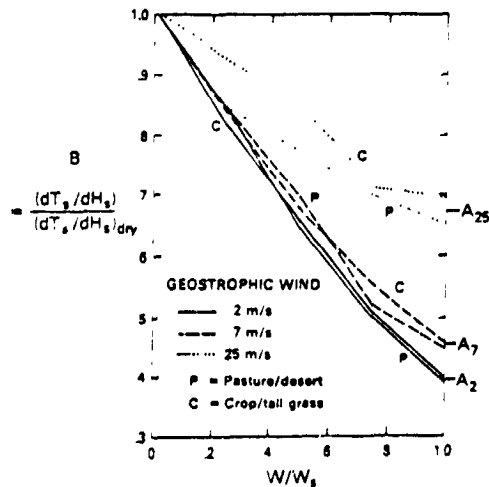


Figure 2. Normalized morning slope parameter vs. soil moisture. Note that A, the limiting value of B for saturated soil is dependent on geostrophic wind speed. W is the slab soil moisture content ( $g/cm^2$ ) for the top 15 cm of soil,  $W_s$  is the saturation value of W.

A simple algorithm has been developed relating an average value of B for all surface types, along with the observed geostrophic wind speed, to soil moisture content  $W/W_s$ . Model results show that there is a parameter, to be called A, which has a simple linear relationship to geostrophic wind speed as follows:

$$A = \frac{(dT_s/dH_s)_{s \text{ wet}}}{(dT_s/dH_s)_{s \text{ dry}}} = 0.37 + 0.012 V_g \quad (2)$$

where  $V_g$  is the surface geostrophic wind velocity in meters per second. When B is normalized by the parameter A in the manner shown in Figure 3, the resulting family of curves for all wind speeds fall within a narrow range which can be closely represented by a single mean curve. Thus, when A is determined using (2) and B is measured from the satellite (using a predetermined value of  $(dT_s/dH_s)_{dry}$  from a library of previous measurements), the soil moisture may be obtained from a single regression equation fit to the curve in Figure 3.

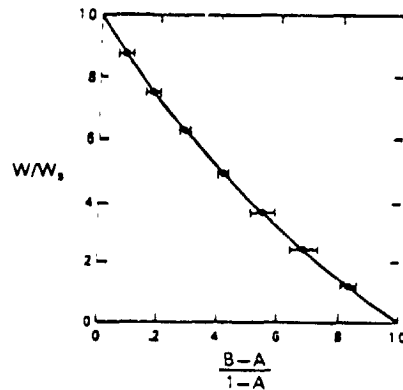


Figure 3. Morning slope parameter averaged for all non-forested surfaces and normalized to both dry and wet soil extreme values. Curves for all wind speeds are represented by the mean curve and standard deviation shown.

ORIGINAL PAGE IS  
OF POOR QUALITY

In order to then estimate precipitation, one invokes the assumption that the soil moisture content is directly proportional to the antecedent precipitation index, API, which is defined by Blanchard et al. (1981):

$$API_i = P_i^{.829} + API_{i-1}k, \quad (3)$$

where  $P$  is the 24-hour precipitation for day  $i$ . Based on data from an Oklahoma watershed, the exponent of  $P$  is reduced from unity to account for direct surface runoff. The API value is related to the water content in a soil layer, the thickness of which is dependent on specification of the depletion coefficient  $k$ . One then measures API through a series of days during which precipitation fell and inverts (3) to obtain  $P$ .

Using precipitation data from a rain gauge network in Oklahoma, Harlan (1980) found a correlation between API and the difference between pre-rain and post-rain afternoon infrared surface temperatures measured from the HCMM satellite (see Figure 4). At the network stations which received the most precipitation, the same regression slope appears to apply even 8 days after the precipitation. Having established the existence of a correlation between surface temperature and API, the next step is to attempt to estimate API quantitatively by applying the algorithm described above on the NASA/GLAS interactive image processing system. This process is currently underway using geosynchronous satellite and rain gauge data for the same case studied by Harlan (1980). At the minimum, it is expected that several classes of soil moisture can be distinguished which will provide useful area-average information for input to climate models and agricultural data sets.

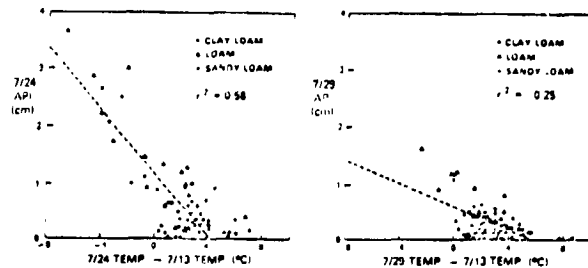


Figure 4. From Harlan (1980). Wet minus dry soil daytime HCMM IR temperature vs. antecedent precipitation index. Rain fell 7/21.

REFERENCES

- Blanchard, B. J., M. J. Farland, T. J. Schmugge, and E. Rhoades, 1981: Estimation of soil moisture with API algorithm and microwave emission. Accepted for publication in Water Resour. Bull.
- Harlan, J. C., 1980: Dryland pasture and crop conditions as seen by HCMM, Report to HCMM investigators meeting, November 24-26, 1980, NASA/GSFC, Greenbelt, MD.
- Schmugge, T., B. Blanchard, A. Anderson, and J. Wang, 1978: Soil moisture sensing with aircraft observations of the diurnal range of surface temperature. Water Resour. Bull., 14, 169-178.
- Wetzel, P. J., 1978: A detailed parameterization of the atmospheric boundary layer, Atmospheric Science Paper No. 302, Colorado State University, 195 pp.



A Survey of Passive Microwave and Hybrid Remote Sensing of Precipitation

J. A. Weinman  
Department of Meteorology  
University of Wisconsin (Madison)

and

T. T. Wilheit  
Microwave Sensor Branch  
NASA/Goddard Space Flight Center  
Greenbelt, MD 20771

Introduction

Rainfall is a key element in our understanding of climate because the release of latent heat affects the energy budget of the atmosphere. Climate zones are frequently classified by their rainfall patterns, Koppen (1918) because the availability of rain water has a profound effect on vegetation patterns and on crop yields. The economic benefit of accurate crop yield forecasts has been widely recognized in recent years, see AgRISTARS (1979), and rainfall is the major determinant which fluctuates from one year to the next. Microwave radiometry from satellites has been used to remotely measure rainfall from Nimbus-5 (19 GHz H polarization), Nimbus-6 (37 GHz H and V polarization) and Nimbus-7 (6.6, 10.7, 18, 21, 37 GHz).

The physics of microwave radiative transfer is well understood so that causal models can be assembled which relate the observed brightness temperatures to assumed distributions of hydrometeors (both liquid and ice) non-precipitating cloud (only liquid needs to be considered), water vapor oxygen and surface conditions. Present models assume a Marshall Palmer (1948) size distribution of liquid hydrometeors from the surface to the freezing level (near the 0°C isotherm) and a variable thickness of frozen hydrometeors above that with various reasonable distribution of the other relevant constituents. The validity of such models is a critical issue here. All uncertainties in the rain rate retrieval algorithms can be expressed in terms of specific model uncertainties which can be addressed through appropriate measurements. Those factors which must be known to achieve unambiguous results can be identified so that rainfall measuring algorithms can be developed and improved. The emissivity of the underlying surface significantly affects the contrast that may be measured between areas covered by rain and those which are dry so that rainfall estimates over land and sea must be investigated with somewhat differing algorithms.

Rain Over Ocean

Microwave radiometry offers a particularly quantitative method of measuring rain over the ocean. The emissivity of the ocean surface is low and not highly variable; it thus provides a good background for observing rain. The theory and initial validation of this concept was given by Wilheit et al. (1979). They predicted brightness temperature/rain rate relationships

based on the previously described model for 19.35 GHz down receiving and for both 19.35 and 37 GHz upward viewing. All three combinations compared very favorably with observations with the freezing level at 4 Km; the model was not verified at any other freezing level. The freezing level dependence of the model has not been verified and remains an open issue. Rao *et al.* (1976) found in using climatological freezing levels in producing an oceanic rainfall atlas that the freezing level dependence of the model seemed excessive and were forced to make ad hoc adjustments to the freezing levels to obtain reasonable results. The open issues are:

- a. The effect of partial beam filling
- b. Typical non-precipitating cloud liquid content and temperature
- c. The use of multiple frequencies to address model uncertainties

#### Rain Over Land

The large and variable emissivity of land surfaces makes microwave measurement of rain rate over land much more difficult. However, rainfall estimates may be derived over land from 37 GHz measurements obtained at both polarizations. Besides rainfall rate, the measured brightness temperatures depend significantly on soil moisture, surface temperature, height and horizontal distribution of the hydrometeor column and the distributing non-precipitating water. Rogers *et al.* (1979), Hall *et al.* (1980) and Weinman and Guetter (1977) showed that both water on the ground and precipitation have low brightness temperatures; however, the brightness temperature emerging from wet ground is polarized, whereas that from precipitation is unpolarized. Further discrimination has been achieved by utilizing colocated infrared images to identify cold high clouds so that wet surfaces are not erroneously classified as rain. Radiative transfer theory suggests that the brightness temperature at 37 GHz becomes insensitive to changes in rainfall rate once rainfall rates exceed 8 mm/hr. Regions where rainfall is heavy can be identified, but quantitative inferences are difficult to make. Hall *et al.* (1980) attempted to overcome this limitation by empirically incorporating infrared cloud top brightness temperatures in his rainfall algorithm to estimate heavy rainfall.

Besides the problems posed by satellite remote sensing techniques, reliable quantitative radar data was difficult to obtain at the time that data from Nimbus-6 was obtained. Nimbus-7 should provide data of comparable quality, but the quality of radar data that NOAA can provide should now be considerably better. It should be borne in mind that a valid test of the efficacy of microwave radiometric measurements requires that the limited number of Nimbus overflights must coincide with the occurrence of rainfall in an area that is monitored by a calibrated digital radar. The coincidence of these events has limited the opportunities to test rainfall measuring algorithms in the past.

In an attempt to expand the tempting successes at 37 GHz, higher frequency measurements (92, 183 GHz) have been made from aircraft platforms. Here a basic qualitative difference has been noted. In convective precipitation extremely low (<150°K) brightness temperatures have been noted which can

ORIGINAL DATA IS  
OF POOR QUALITY

be accounted for in the radiative transfer models by the frozen hydrometeors above the 0°C isotherm. The observations near the strong water vapor line at 183 GHz also give information as to the height of the frozen hydrometeors and have indicated heights of at least 9 Km. On the basis of these observations, the 85 GHz channel on the microwave imager which is to be launched in 1984 on the DMSP satellite should provide excellent maps of convective rainfall.

References

1. AgRISTARS (1979), "Preliminary Technical Program Plan," Agriculture and Resources Inventory Surveys through Aerospace Remote Sensing (AgRISTARS) USDA-NASA-USDC-USDI-AID.
2. Hall, C. D., R. Davies, J. A. Weinman, (1980), "The Determination of Rainfall Distributions by Means of Passive Microwave on Nimbus-6," 18th Conference on Radar Meteorology, Atlanta, GA.
3. Koppen, W., (1918), "Klassifikation der Klima nach Temperatur, Niederschlag und Jahreslauf," Petermanns Mitt 64, 193-203, 243-248.
4. Marshall, T. S., and W. McK. Palmer, 1948: "The distribution of raindrops with size," J. Meteor., 5, 165-166.
5. Rao, M. S. V., Abbott, W. V., III, and Theon, J. S.: 1976, "Satellite-Derived Global Oceanic Rainfall Atlas' (1973 and 1974)," NASA X-911-76-116, Goddard Space Flight Center, Greenbelt, Maryland.
6. Rodgers, E. B., Siddalingaiah, H., Chang, A. T. C., Wilheit, T., (1979), "A Statistical Technique for Determining Rainfall over Land Employing Nimbus-6 ESMR Measurements," J. App. Met., 18, 978-991.
7. Weinman, J. A., Guetter, P. J., (1977), "Determination of Rainfall Distribution from Microwave Radiation Measured by Nimbus-6 ESMR," J. App. Met., 16, 437-442.
8. Wilheit, T. T., A. T. C. Chang, M. S. V. Rao, E. B. Rodgers, J. S. Theon: 1977, "A Satellite Technique for Quantitatively Mapping Rainfall Rates over the Oceans," J. App. Met., 16, 551-560.

COMBINED SPACEBORNE AND CONVENTIONAL  
MEASUREMENTS FOR PRECIPITATION ESTIMATION

Thomas H. Vonder Haar  
Eric A. Smith

Department of Atmospheric Science  
Colorado State University  
Fort Collins, CO 80523

1. INTRODUCTION

For practical realization of new information on precipitation during this decade, satellite observing systems must be coupled into surface-based observations and computer models of weather systems as they develop. Objections of the precipitation estimation methods vary from local scale applications related to floods and agriculture; to problems of the climatology of latent heat release in the atmosphere over the oceans. In all cases methods are available to combine the satellite/surface-based/model capabilities. This paper outlines and proposes several such Precipitation Estimation Pilot Studies (PEPS). The combined methods provide opportunity for near-term data sets needed for climate research and weather forecasting (COSPAR, 1980).

Challenges in the implementation of combined methods are analogous to those encountered in the assimilation of remote temperature soundings from satellites with conventional rawinsondes. Namely, "smart" analysis methods are required. These are often optimized when "guided" by pre-existing climatologies or by near-real-time physical model output.

Of course, combined methods of precipitation estimation do not circumvent the need for thorough sampling studies and well calibrated instrumentation. These key topics are addressed by other papers in the workshop. Our paper does emphasize the use of satellite measurements in the 1980's to determine precipitation frequencies (see Kidder, 1981, this workshop) rather than rates or amounts. Given the frequencies from the satellites we rely on the ground-based and/or models to ascribe rates and thus estimate amounts of precipitation.

2. PHYSICAL UNDERSTANDING OF PRECIPITATION ESTIMATION AT THE LOCAL SCALE

Kidder and Vonder Haar (1976), Scherer and Hudlow (1971) and others began case study of combined satellite visible, infrared, and passive microwave measurements from satellites with weather radar data in the early 1970's as the satellite data became available. Using data

over the tropical oceans from the 1974 GATE experiment Smith and Kidder (1978) studied the improvement of precipitation estimation by use of concurrent infrared measurements to correct for microwave field-of-view "smearing". They used 5 cm ship radar estimates of precipitation as "truth". A sequence of their results are shown in Figures 1 to 4.

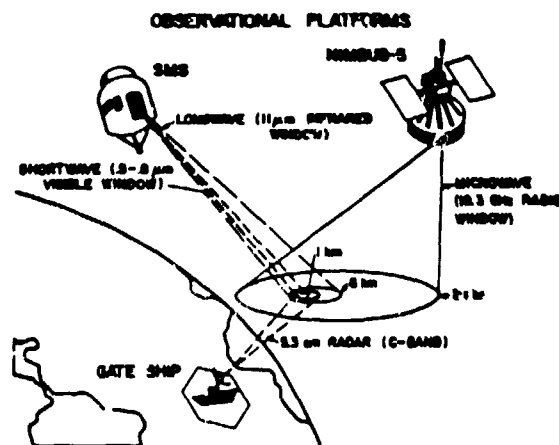


Figure 1. Depiction of first trispectral study of satellite data and ship radar data from the GATE.

ORIGINAL FIGURES  
OF POOR QUALITY

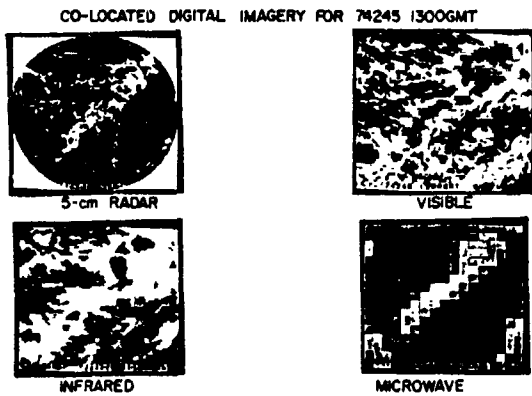


Figure 2. Display of co-located 0.5 $\mu$ m, 11 $\mu$ m, 1.55 cm satellite data and 5 cm radar using the C.S.U. man-computer-interactive ADVISAR system.

MULTI-SPECTRAL DIAGNOSIS OF PRECIPITATING REGION

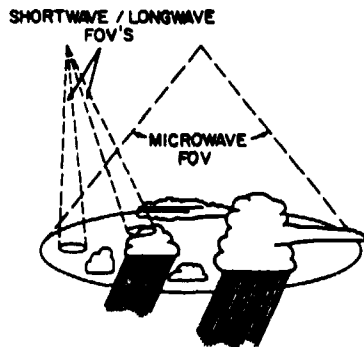


Figure 3. The microwave FOV problem and a solution.

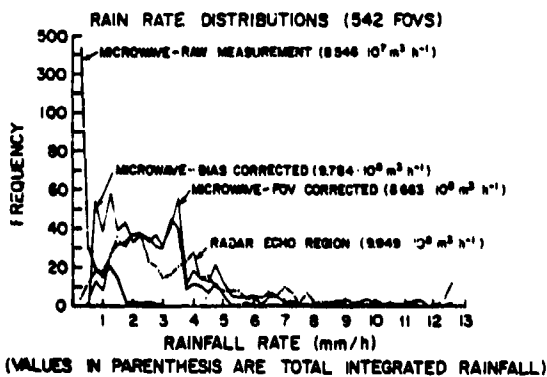


Figure 4. Results of the FOV correction presented by Kidder and Smith (1978).

Rogers et al. (1979), Durkee (1980) and others have addressed the complexities of use of passive microwave measurements from satellites over land. During the 1980's visible and infrared radiance measurements from satellites (especially the geostationary) will continue to be the most common satellite data set. Reynolds and Smith (1979) pioneered the quantitative computer combination of high time frequency concurrent satellite and radar data sets. Figures 5 to 7 display examples of such satellite/radar combinations during a local scale storm system in western Kansas.



Figure 5. Digital GOES image of severe convective storm over Western Kansas (Reynolds, private communication).

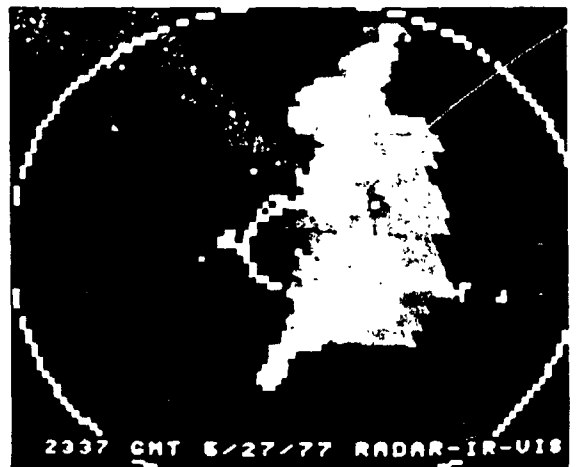


Figure 6. Superimposed digital radar and GOES data noted in Figure 5 illustrating the combined radar/satellite approach for precipitation estimation.

ORIGINAL PAGE IS  
OF POOR QUALITY



Figure 7. A second image following Figure 6 in time to illustrate the time-dependent capability of the method.

Physical interpretation of the satellite data for precipitation purposes is presently under study at C.S.U. Sophisticated radiative transfer models are coupled with a 2-D cloud model [Hall, (1980)] in order to better interpret the remote measurements from the satellites. Smith et al. (1981) describe the simulated radiances that would be measured by a satellite viewing precipitating clouds having certain physical characteristics and rates of change. Figures 8 and 9 from this study describe the spectral reflectance (near visible wavelengths) and spectral emittance (wavelengths in the microwave) from clouds simulated as in Figures 10 to 12.

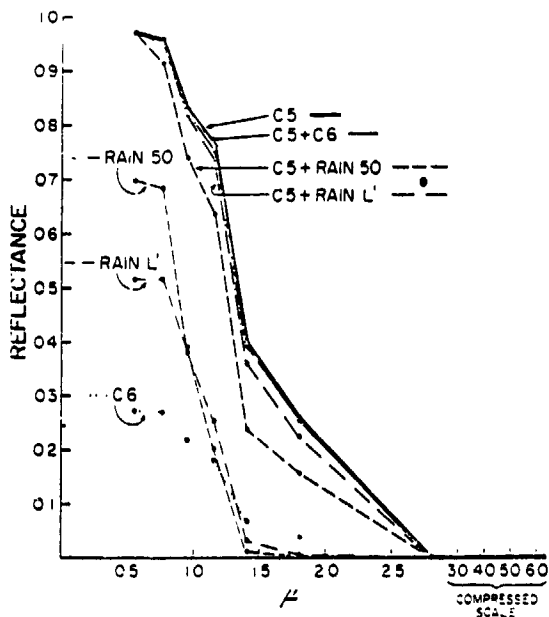


Figure 8. Spectral reflectance of monomodal and bimodal droplet distributions to simulate satellite measurements (after Smith et al., 1980).

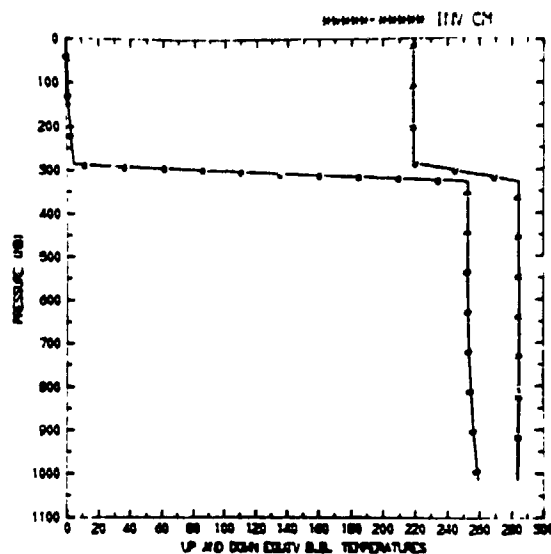


Figure 9. Equivalent black-body temperatures at 1.55 cm as would be viewed from a satellite; based on cloud model and radiative transfer model calculations.

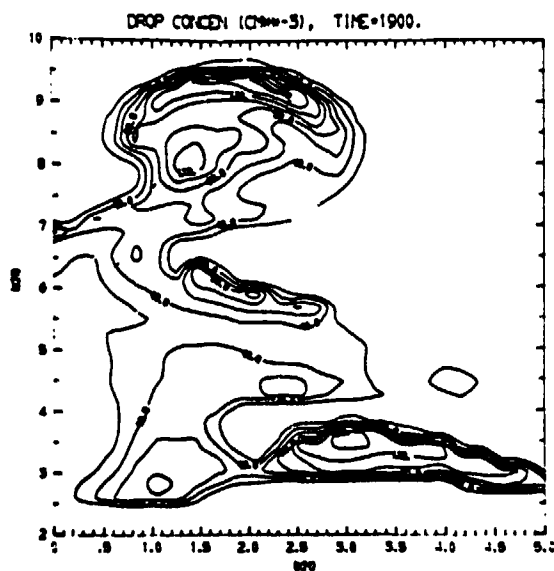


Figure 10. Cloud droplet concentration (per  $\text{cm}^3$ ) at  $t = 1900$  sec produced from the Hall 2-D cloud model.

ORIGINAL PAGE 19  
OF POOR QUALITY

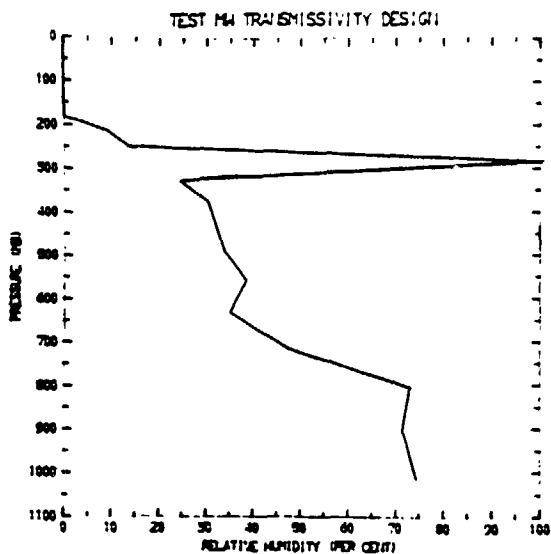


Figure 11. Relative humidity vs. height from the Hall cloud model.

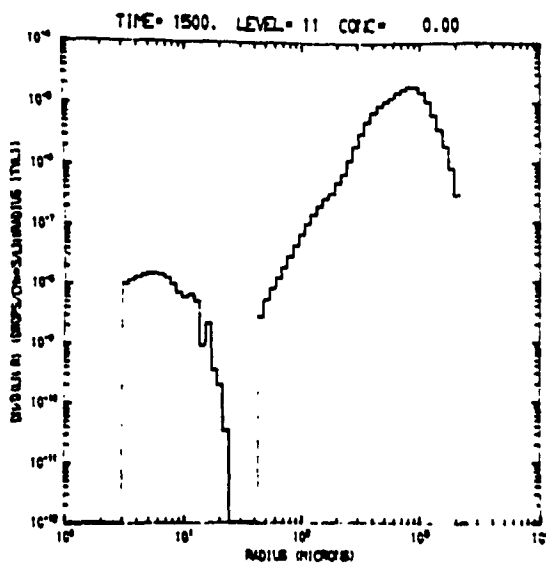


Figure 12. Example of the cloud model's time-dependent droplet size distribution.

The next step in a combined estimation method is to incorporate the surface based rain gauge networks into the techniques. Figure 13 displays the density of such ground data over a typical agricultural area. In certain cases, for research or special local needs, a very high spatial resolution network is available. Figure 14 displays infrared satellite measurements of major convective storms over the 1979 Texas HIPLEx "mesonet". At this small scale the combined use of satellite and surface data is apparent. We use gauges located at designated points to determine localized rain rate and satellite data to ascribe these rates to a specific area.

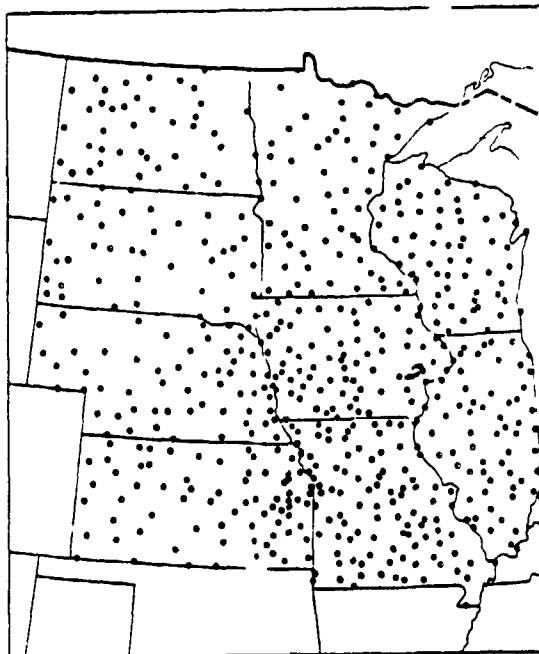


Figure 13. Existing distribution of surface rain gauges over U.S. corn belt. All could report hourly or more frequently via satellite data collection platforms. This illustrates the potential of combined satellite/surface site precipitation determination methods.

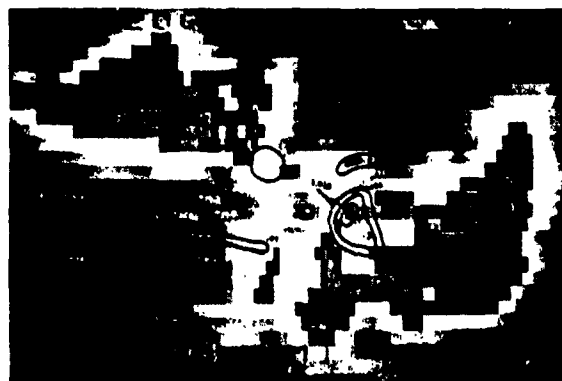


Figure 14. Digital image of concurrent GOES infrared data and surface mesonet stations with isohyets of precipitation during merging storm situation (after Reynolds).

ORIGINAL PAGE IS  
OF POOR QUALITY

Of special note in the case of this Texas mesonet is that the surface gauges report their data in near-realtime via satellite. These satellite Data Collection Platforms are shown in Figures 15 to 18. At Colorado State University a small satellite earthstation receives both the satellite imagery and DCP data (from more than 100 stations). This important breakthrough insures practical near-realtime processing of combined system data into the precipitation estimates. The central U.S. raingauge network discussed in Figure 13 is a candidate for data collection via satellite.

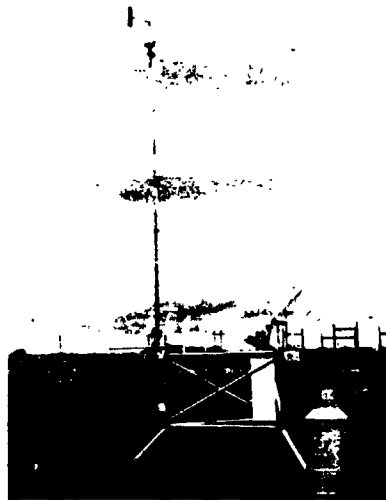


Figure 15. One of the satellite data collection platforms of the Water and Power Resources Service.

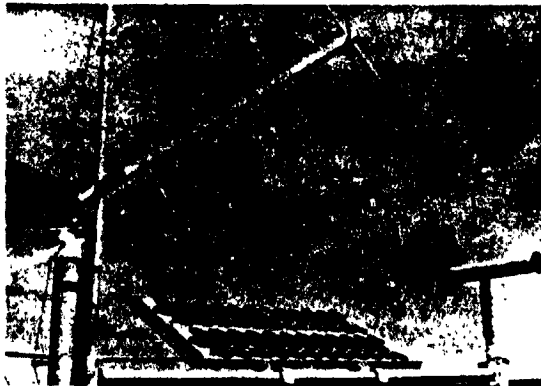


Figure 16. Close-up of the WPRS solar cells and satellite transmitter antenna.



Figure 17. The C.S.U. earthstation.

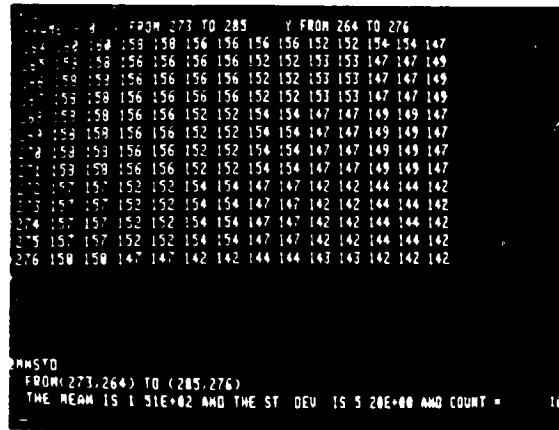


Figure 18. Display of DCP weather data after reception via satellite at C.S.U.'s satellite earthstation.

In summary, the "smart" or optimum precipitation estimation method at the local scale during the 1980's should include multi-spectral satellite measurements combined with surface gauge networks and radar where available. Radar data and computer models of clouds can guide the interpretation of the remotely sensed, yet spatially contiguous, satellite data as well as the "in situ" point data from the raingauges.

3. CLIMATOLOGICAL ESTIMATES OF PRECIPITATION OVER LARGER REGIONS

The U.S. Climate Program (1980) and the World Climate Research Program express strong requirements for the monthly, seasonal and annual averages and variances of precipitation over land and ocean. These provide estimates of important diabatic heating processes in the atmosphere. Interannual variability information is the primary goal. Thus,



ORIGINAL PAGE IS  
OF POOR QUALITY

stable estimates over 10-20 years with high relative accuracy are required. Before considering combined satellite/surface/model system contributions to those objectives it is useful to review the state-of-the-art of the non-satellite precipitation estimates. Figure 19 and Table 1 from Reed and Elliott (1979) and Dorman and Bourke (1980) are representative of the ocean case. For climate purposes their mean annual and seasonal results are useful over those oceans where a modest sample of ship and small island data are available. Their method uses only precipitation frequency values from these surface data sets and ascribes a rate assumed to represent the region and season to determine the average amount of precipitation.

ON THE ANNUAL AND SEASONAL DISTRIBUTION  
OF OCEANIC PRECIPITATION

REED AND ELLIOTT (1979, J. GEOPHYS. RES.)

"RANDOM ERROR IN THESE DATA --- MAY APPROACH  $\pm 10\%$  FOR MIDLATITUDES WITH A GREATER UNCERTAINTY IN TROPICAL REGIONS --- SYSTEMATIC BIAS --- HAS BEEN ELIMINATED"

(FOR THE NORTH ATLANTIC AND NORTH PACIFIC)

Figure 19. The state-of-the-art of non-satellite precipitation estimation methods over the ocean.

TABLE 1. A COMPARISON BETWEEN REED AND ELLIOTT'S (1977) REASONED VALUES AND DORMAN AND BOURKE'S (1979) ESTIMATED VALUES OF PRECIPITATION

REGION	REED AND ELLIOTT'S ESTIMATED REASONED ANNUAL RAINFALL (MM)	DORMAN AND BOURKE'S ESTIMATED ANNUAL RAINFALL (MM)
40°N-60°N E of 180°W (7)	1080	1000
2°N-20°N 125°W-157°W	1840	1700

Obviously, over the oceans satellite estimates of frequency alone can play a very significant role when combined with the surface data. This would allow all world oceans to be observed each season in contrast to the present non-satellite situation which yields only seasonal averages for northern oceans.

It should be noted that in the mid-1980's the earth will be girdled once again with a network of 5 geostationary satellites, as was the case for the first time during the 1979 Global

Weather Experiment. An International Satellite Cloud Climatology Program (ISCCP)(1981) under the WCRP will be underway using these satellites and will preprocess the vast amounts of data ( $>5 \times 10^6$  BPS) they transmit. This will provide an excellent opportunity for the pilot studies on precipitation estimation proposed in the conclusion to this paper.

Over land the reader is referred to the various atlases and tabulations of precipitation commonly available. Note that the U.S. network displayed in Figure 13 is the most dense raingauge network deployed over any large land region. Thus, again a combined satellite/surface systems for precipitation estimation is required (see also papers by Barrett and Ramage in this workshop).

In summary, the improved precipitation estimates over land and ocean can be obtained from a combination of satellite precipitation frequencies [Kidder and Vonder Haar (1977)] with the "ship-plus" or "land-gauge-plus" methods. Examples of the individual maps are shown in Figure 20. Their combination by a "smart" method can provide an excellent mean and variance data set for climate models and diagnostics.



(a) Frequency of precipitation (in percent of observations) for the season December 1972 through February 1973 as derived from Nimbus II SSM data. The noon and midnight observations have been averaged [after Kidder and Vonder Haar (1977)].



(b) Frequency of precipitation (in percent of observations) for the season December-February from ship observations taken at noon, universal time [after McDonald (1958)].



(c) The winter (December, January, February) distribution of precipitation over the tropical portions of the North Pacific and North Atlantic Oceans [after Reed and Elliott (1979)].

Figure 20. Comparison of quasi-global estimates of precipitation frequency from a satellite and ship data and precipitation amount from non-satellite sources, illustrating the potential of combination of the existing methods.

4. SPECIAL USE OF FORECAST MODEL OUTPUT

The climatology of specific forecast variables output by high resolution primitive equation forecast models should be examined as potential contribution to a combined precipitation estimation technique. The grid mesh (potential data set) of the U.S. LFM is superimposed in an infrared satellite image sequence in Figures 21 to 23. This illustrates the density of potential data. A Quantitative Precipitation Forecast (QPF) is

ORIGINAL PAGE IS  
OF POOR QUALITY

produced by this model every 6 hours. Do these data compose a valuable input to precipitation climatologies when aggregated on a daily, weekly or seasonal basis? Can they be adjusted for model bias?

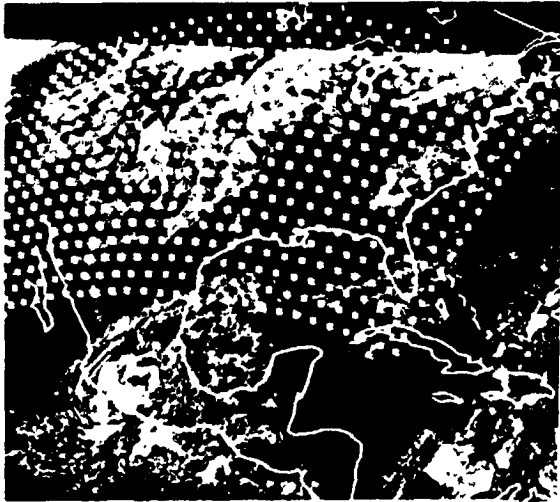


Figure 21. Digital display of the LFM gridmesh on a GOES infrared image (after Buss and Laybe, personal communication), illustrating the potential of combined satellite and numerical model output for precipitation estimation.

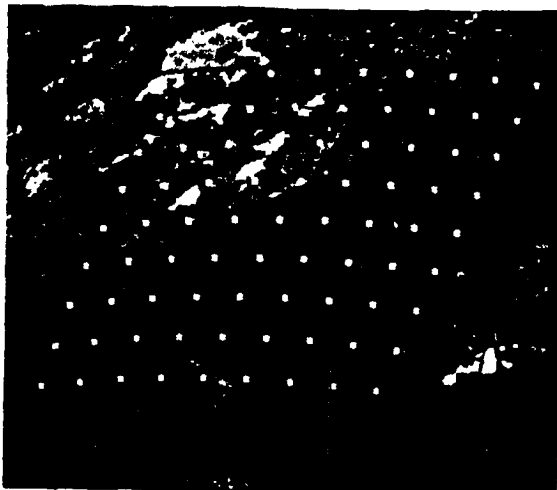


Figure 22. A computer zoom of Figure 21 illustrating the potential satellite/weather model method at the local scale.

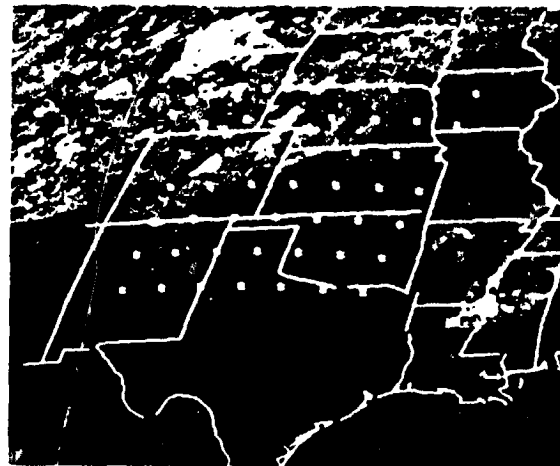


Figure 23. Another zoom of Figure 21.

#### 5. SUMMARY

Optimum analysis methods are needed to combine satellite, surface and model data into the improved estimates of precipitation needed in the 1980's. Such combined systems provide the best opportunity for nearterm improvements beyond present methods described in this workshop. At local scales satellite, digital radar and gauge mesonet values might be combined optimally using a computer-man-interactive approach. The man may be guided by a 2-D cloud model output during the interactive process to overcome the inherent physical variabilities and cloud conditions encountered.

For practical processing of the combined system data, raingauges on land (and perhaps ship reports) should be transmitted via present-day satellite Data Collection Systems.

The potential use of relatively high resolution model forecasts of quantitative precipitation should be explored as an addition to the combined system for all scales greater than the local area hourly.

Two Precipitation Estimation Pilot Studies (PEPS) should be initiated under the Hydro/Agro and National Climate Program auspices to define, develop and test the new methods of precipitation estimation using combined spaceborne and conventional data sets. One study at the local scale and one at the regional climate scale should define the concept of subdivision of the problem into those situations encountered over specific regions of the world ( $2 < n < 10$ ). For both the nearterm and longterm the best combination of data sets to estimate precipitation over each distinct region should be selected and demonstration experiments developed.

#### 6. ACKNOWLEDGEMENTS

This paper is supported by the Goddard Space Flight Center, National Aeronautics and Space Administration, Contract Number NAS5-26343.

ORIGINAL PAGE IS  
OF POOR QUALITY

REFERENCES

- COSPAR, 1980: Space-based observations in the 1980s and 1990s for climate research: A planning strategy. Report to the Joint Scientific Committee for the WMO/ICSU World Climate Research Program. November, 1980.
- Dorman, Clive E. and Robert H. Bourke, 1979: Reply to comments by Elliott and Reed. Quart. J. A.M.S., Vol. 105, p. 1082-1083.
- Durkee, Philip, 1980: Summer precipitation frequency of the north central U.S. from satellite microwave observations. Presented at the AGU Spring Meeting, Toronto, Canada, 22-27 May.
- Hall, William D., 1980: A detailed microphysical model within a two-dimensional dynamic framework: Model description and preliminary results. J. Atmos. Sci., Vol. 37, p. 2486.
- International Satellite Cloud Climatology Project, 1981: World Climate Programme. Geneva, January, 1981.
- Kidder, Stanley Q., 1981: On the measurement of precipitation frequencies by passive microwave radiometry. Proceedings of the Climate Observing System (COS) Workshop on "Precipitation Measurements from Space", Goddard Space Flight Center, NASA, April 28 - May 1, 1981.
- Kidder, Stanley Q. and Thomas H. Vonder Haar, 1976: A comparison of satellite rainfall estimation techniques over the GATE area. Proceedings of the Symposium on Meteorological Observations from Space: Their Contribution to the First GARP Global Experiments, 8-10 June, 1976, Philadelphia, PA, pp. 123-125.
- Kidder, Stanley Q. and Thomas H. Vonder Haar, 1977: Seasonal oceanic precipitation frequencies from Nimbus-5 microwave data. J. Geophys. Res., 6 pp.
- Reed, R.K. and W.P. Elliott, 1979: New precipitation maps for the North Atlantic and North Pacific oceans. J. of Geophys. Res., Vol. 84, No. C12, December 20, 1979, pp. 7839-7846.
- Reynolds, David and Eric Smith, 1979: Detailed analysis of composited digital radar and satellite data, Bull. Amer. Meteor. Soc., Vol. 60, No. 9, pp. 1024-1037.
- Rogers, E., H. Siddalingaich, A.T.C. Chang, and T.T. Wilheit, 1979: A statistical technique for determining rainfall over land employing Nimbus-6 ESMR measurements. J. Appl. Met., 18, 8, pp. 978-991.
- Scherer, W.D. and M. D. Hudlow, 1971: A technique for assessing probable distributions of tropical precipitation echo lengths for x-band radar from Nimbus 3 HRIR data. BOMEX Bull., No. 10, BOMAP Office, NOAA, Rockville, MD, pp. 63-68.
- Smith Eric, A. and Stanley Q. Kidder, 1978: A multi-spectral satellite approach to rainfall estimates. Preprint 18th Conference on Radar Meteorology. A.M.S., Atlanta, GA. 28-31 March, 1978.
- Smith, Eric A., Thomas H. Vonder Haar, Ronald Welch and Warren J. Wiscombe, 1980: The development of a multi-spectral radiative signature technique for estimation of rainfall from satellites. Monthly Progress Reports No. 4 & 5. Contract No. NA-80-SAC-00246. National Center for Atmospheric Research, November and December, 1980.
- U.S. National Climate Program, 1980: Five-Year Plan. National Oceanic and Atmospheric Administration. September, 1980.

D32 EN83 25301

ORIGINAL PAGE IS  
OF POOR QUALITY.

COMBINING VISIBLE AND INFRARED TECHNIQUES WITH LAMMR FOR  
DAILY RAINFALL ESTIMATES

Shaun Lovejoy  
Stormy Weather Group, McGill University, Montreal, Canada

1. INTRODUCTION

The production of rainfall maps from satellite imagery would have a significant impact on many branches of meteorology, climatology and hydrology. To be successful, a remote sensing device would have to have both high spatial and temporal resolution in order to be commensurate with the extraordinary variability of rainfall. An obvious candidate for such a device, is the geostationary visible and IR satellite system (GOES, Meteosat, for example), which have high temporal spatial resolution (30 min, ~1 km respectively). Because these wavelengths chiefly respond to cloud drops, rather than rain drops, inferring rain amounts is an indirect process, primarily skillful in determining rain areas rather than rates. Considerable interest has therefore been shown in alternative rain-estimating techniques which respond directly to rain drops, such as the microwave radiometers presently flying on NIMBUS 7.

However, as discussed in detail elsewhere (Lovejoy and Austin (1980)), and in outline in the first part of this paper, existing radiometers have neither adequate temporal nor spatial resolution. Furthermore, they are inherently incapable of measuring the effective rainlayer height, without which no direct rain estimates are possible. In order to overcome the limitations of both IR/visible and microwave radiometer-based techniques, we therefore suggest a 'hybrid' scheme whose accuracy is investigated using radar-based simulations. Such a scheme could potentially combine the high temporal resolution of the vis/IR imagery with the anticipated rain rate estimating ability of the next generation of satellite-borne microwave radiometers. A solution to the problem of estimating the effective rain layer height is an important unsolved problem, not addressed here.

2. HISTORICAL REVIEW

Ever since the launch of a four-channel microwave radiometer on Cosmos-243 in 1968, a research goal has been the determination of surface rainfall rates from satellite-determined microwave brightness temperatures. While investigating microwave determination of integrated liquid water, Akvilonova et al (1971) reported that regions with high values of this parameter were "regions likely to produce precipitation". However, following an extensive ground-based measuring program investigating the variability of the effective rain-layer height (Gorelik and Kalashnikov (1971), rain attenuation coefficient (Gorelik et al (1971a)), integrated cloud water content (Gorelik et al (1971b)), humidity (Gore-

lik et al (1971c)), etc., the Russians concluded that the accuracy of radiometer estimates of rainfall rate were low (44-70% depending on the wavelength: Basharinov et al (1970)). They further concluded that using multiple wavelengths would not increase accuracy significantly (Kalashnikov and Frolov (1971)).

In the United States, rainfall rates were sought directly. Allison et al (1974) used an ESMR (Electrically Scanning Microwave Radiometer) launched on Nimbus 5 in 1972 to determine rainfall rates in the following categories: 2 mm/hr, 2-7 mm/hr, 7 mm/hr, using a cloud model. Wilheit et al (1977) used a more complicated model (with negligible cloud) to produce a 1:1 relationship between microwave brightness, temperature and rainfall rate and obtained agreement to within  $\pm 100\%$  for rainfall in the range 1-25 mm/hr when comparing averaged radar data for four satellite passes. Smith and Kidder (1978) tried to improve the Wilheit et al (1977) technique by field of view (FOV) characterization. Recently Viezee et al (1979) have assumed the more modest task of correlating area- and time-averaged vertically-integrated cloud-water content with subsequent rainfall. Here the vertically-integrated cloud-water content was determined by assuming no rain and ignoring the ice phase. Another indirect approach is that of Rodgers et al (1979) who use a 2-D pattern-matching technique to distinguish rain areas from wet and dry soil. This paper attempts to evaluate and compare these diverse approaches to the problem of rainfall estimation from microwave radiometers.

3. BRIGHTNESS TEMPERATURE AND RAINFALL RATE

3.1 Theoretical considerations

Following the standard method of solution of the radiative transfer equation (see Stepenevko (1968a), for example), we may deduce the following:  
a) the satellite brightness temperature is extremely sensitive to the surface reflection coefficient (which is reliably known only over the ocean),  
b) to a good approximation, the temperature depends on the integrated path attenuation ( $\tau$ ) and not on the distribution of attenuating substance along the path. For the atmosphere,  $\tau$  is made up of four components: ozone, water vapor, cloud water, rain water. (Ice is essentially transparent at wavelengths in the microwave 'window' 0.8-1.0 cm.) Of these four, ozone can be subtracted because of its small value and small variability. The water vapor contribution can similarly be removed either using climatology or other microwave or IR channels (Smith and Howell (1971)). The resulting attenuation which is due to rain and cloud only may be written

ORIGINAL PAGE IS  
OF POOR QUALITY

$$\tau = a R h + k Q$$

where  $h$  is the thickness of the raining layer,  $Q$  is the total integrated cloud water content,  $R$  is the rainfall rate,  $k$  is the mean cloud attenuation coefficient (as a function of wavelength) and  $a, b$  are rain attenuation parameters (Olsen et al (1978), Atlas and Ulbrich (1977), for example). Since  $b$  is virtually constant for the wavelengths in our microwave 'window' (and is very dependent on the large drop part of the drop-size distribution), it is clear that no quantity of microwave channels can separate the rain-layer height and rain rate components especially since experimentally there is an RMS error in  $\tau$  of about  $\pm 30\%$  (Crane (1971)) and Gorelik et al (1971d)). Other channels, i.e., IR or visible, suffer from severe scattering with the result that only the top part of the cloud can be sensed (Reynolds et al (1976, 1978) and Bunting (1978)). Scattering, and thus cloud geometry, is also an important complication for microwave wavelengths smaller than 0.8 cm.

In particular, it is expected that radiances from the 85 GHz channel (0.35 cm) will be very sensitive to the detailed structure of the raining region. For example, according to figures in Shifrin and Chernyak (1968) at 3 mm/hr the mean free path for scattering is 57, 5.3, 1.0 km for wavelengths of 1.6, 0.8, 0.4 cm respectively. This should be compared with the distance through the rain layer at a  $50^\circ$  viewing angle, which at 3 mm/hr is 6.3 km in GATE (taking  $h = 4.0$  km from Table 2). Therefore at 0.4 cm we can not ignore the detailed structure of the raining region.

It is worth briefly mentioning the question of the polarization of the emitted radiation. If we ignore the tiny anisotropy due to the elliptical deformation of falling rain drops, then

clearly the absorption and emission processes taking place in the rain layer are indifferent to polarization. In such a case, polarization data will yield information only on surface polarization (i.e., land or calm water) but no independent information on the rain layer. In this paper we therefore ignore the polarization question since it can yield rainfall information only as a second order effect, i.e., when scattering is important. Furthermore, Weinman and Guetter (1978) have shown that even when scattering is important that it produces polarization effects of only 1-2%, even at high rain rates. Discussion of polarization beyond the question of measuring surface properties is therefore misleading.

### 3.2 Models

With the exception of the Wilhelm et al (1977) model, all observations and models have cloud attenuations comparable with rain attenuations, although there is virtually no actual data during precipitation (see, however, Gorelik and Kalashnikov (1971)). To evaluate the models, we used GATE radar data to determine the rain-layer heights and variabilities (Table 1), adding in the best published values for the rain attenuation coefficient and its variability, as well as best values for cloud components and average GATE Phase III sounding data for the water vapour contribution (Table 2). The result is compared with the Wilhelm et al (1977) model and the Kalashnikov and Frolov (1971) model in Fig. 1. Both of these models substantially over-estimate the rain-layer thickness and the Wilhelm et al (1977) model severely under-estimates the cloud contribution. Also visible in Fig. 1 are best estimates of the variabilities at a level of 1 standard deviation. We conclude (Table 2) that microwave radiometer-based estimates of instantaneous rainfall rates have an RMS

TABLE 1. RADAR-DETERMINED ZENITH ATTENUATIONS AT DIFFERENT RAINFALL RATES AND TWO FREQUENCIES FOR A SAMPLE OF 28 GATE PHASE III 3-D RADAR SCANS

Wavelength:	$\lambda = 1.55 \text{ cm}$				$\lambda = 0.81 \text{ cm}$				Echo top mean ht (km)	Std. deviation (km)	Variation (%)	
	Rainfall rate mm/hr	Mean attenuation (dB)	Std. deviation (dB)	Effective rainlayer ht (km)	Variation (%)	Mean attenuation (dB)	Std. deviation (dB)	Effective rainlayer ht (km)				
	1±0.5	0.27	0.33	4.00	118	1.16	1.24	4.58	107	4.25	2.45	38
	3±0.5	0.79	0.59	4.02	74	3.17	1.94	4.27	61	5.36	2.02	38
	5±0.5	1.13	0.68	3.39	60	4.37	2.41	3.52	55	5.37	2.02	38
	7±0.5	1.49	0.91	3.03	61	5.60	3.18	3.24	57	5.71	2.39	42
	10±0.5	1.92	1.12	2.61	58	7.04	3.85	2.86	55	5.89	2.64	45
	15±1	2.89	1.53	2.55	53	10.17	5.09	2.79	50	5.97	2.57	43
	20±1	3.19	1.69	2.04	53	11.06	5.58	2.27	50	6.66	2.78	42
	30±1	4.10	2.18	1.68	53	13.79	7.30	1.90	53	5.27	2.81	53

TABLE 2. TOTAL ATMOSPHERIC ATTENUATION AT 1.55 CM AND 0°C WITH: (a) RAIN LAYER THICKNESS ACCORDING TO TABLE 1, (b) CLOUD WATER CONTENT AS:  $Q = 1.52 \pm 0.33$  FOR  $R < 3 \text{ mm h}^{-1}$  AND  $Q = 1.52 \pm 0.71$  FOR  $3 < R < 7$  (FROM GORELIK AND KALASHNIKOV 1971) AND  $Q = 1.52 \pm 1.00$  FOR  $7 < R$  (EXTRAPOLATION), (c) OXYGEN COMPONENT OF 0.1 dB (MEEKS AND LILLEY 1963) AND WATER VAPOUR ASSUMING A GATE PHASE III LAPSE RATE ( $5.86 \text{ K km}^{-1}$ ) UP TO THE MEAN BLIND TOP HEIGHT WITH RELATIVE HUMIDITY LINEARLY VARYING FROM 80% AT SURFACE TO 100% AT SCND TOP HEIGHT (FROM TABLE 1)

Rainfall rate (R) in mm h <sup>-1</sup>	Rain attenuation in dB (a)		Cloud attenuation in dB (b)		Water vapour and O <sub>2</sub> attenuation in dB (c)		Total attenuation in dB			Approx. resultant uncertainty in estimation of R (%) <sup>a</sup>
	Average	Std. deviation	Average	Std. deviation	Average	Std. deviation	Average	Std. deviation	Std. dev as % of average	
0	0.0	0.0	0.61	0.17	0.30	0.06	1.11	0.18	16	—
1	0.27	0.32	0.61	0.17	0.30	0.06	1.37	0.37	27	80
3	0.79	0.59	0.64	0.19	0.71	0.08	2.24	0.62	25	55
5	1.13	0.68	0.64	0.32	0.71	0.09	2.47	0.76	31	63
7	1.49	0.91	0.67	0.34	0.85	0.10	3.01	0.98	33	70
10	1.92	1.12	0.71	0.48	0.90	0.11	3.52	1.22	35	80
15	2.89	1.53	0.70	0.48	0.95	0.11	4.54	1.61	35	60
20	3.19	1.69	0.74	0.51	0.99	0.12	4.92	1.77	36	55
30	4.10	2.18	0.74	0.51	1.05	0.12	5.87	2.24	38	65

<sup>a</sup> Estimated from Fig. 1.

ORIGINAL PAGE IS  
OF POOR QUALITY

error of  $\pm 70\%$ , which agrees well with the Basharinov et al (1970) experimental values ( $\pm 44\text{--}\pm 70\%$ ).

We have not plotted our rain rate against microwave brightness temperature, since the latter depends on a variety of subsidiary model conditions such as surface emissibilities and atmospheric temperatures and lapse rates, and for large rain rates, where scattering is important, on the details of the rain cell geometry. Uncertainties in all of these independent parameters can only increase the error in an operational scheme predicated on the conversion of a microwave brightness temperature into a rain rate. If a temperature is required, approximately  $\pm 10\%$  accuracy can be achieved by using the attenuations in Fig. 1 in the following formula (if scattering is unimportant, i.e.,  $\tau \ll 3$  dB).

$$T_R = T_{av}(1 - e^{-\tau}) + T_s(1 - R)e^{-\tau} + RT_{sv}(1 - e^{-\tau})e^{-\tau}$$

where  $T_R$  is the microwave brightness temperature,  $T_{av}$  is the average atmospheric temperature of the emitting layer,  $T_s$  the surface temperature,  $R$  is the surface reflection coefficient (approx 0.6 for water at 1.55) and  $\tau$  the net attenuation in the viewing direction.

4. The effect of low radiometer spatial and temporal resolution

The variability of  $R$  for a given  $\tau$ , discussed in the previous section, was computed over an area about as small as radar resolution permits, i.e.,  $\approx 1$  km<sup>2</sup>. Although such variation is substantial it may be hoped that averaging cloud water content and effective rain layer height over larger areas would yield a large reduction in the variation of these quantities about their long term means. To

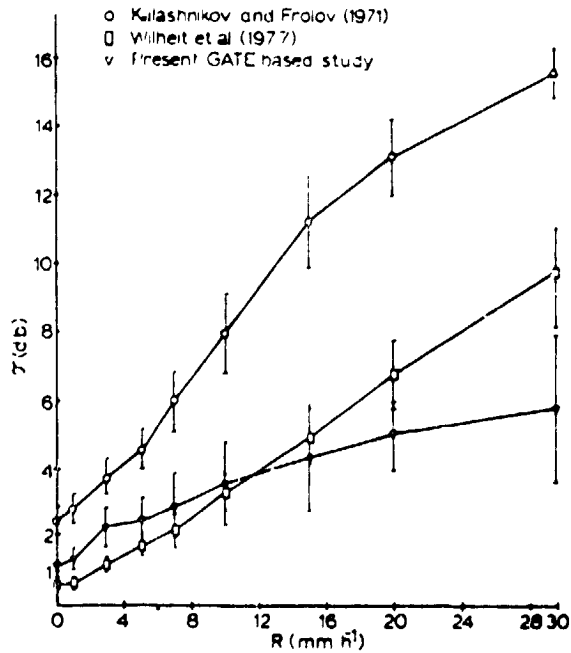


fig. 1: attenuation ( $\tau$ ) as a function of rain rate ( $R$ ) with estimated one standard deviation error bars.

get a feel for the variability of these parameters, readers should examine the example shown in Fig. 2 calculated from radar data on day 251 of GATE. This figure shows the surface rain rate map (Fig. 2a), the effective rain layer height (Fig. 2b)

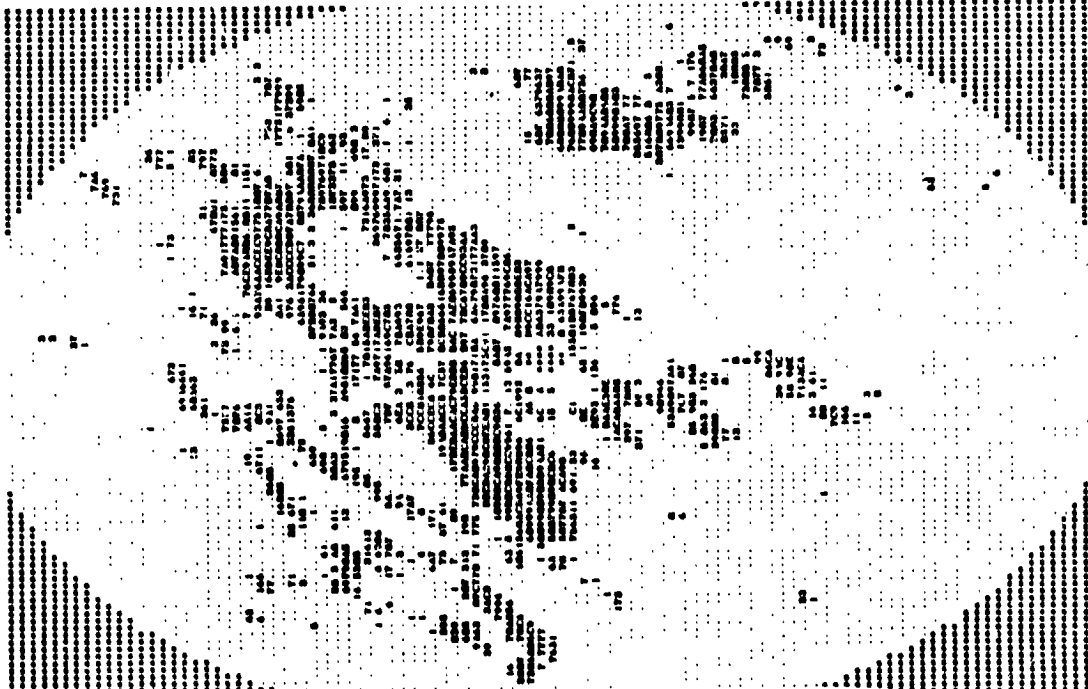


fig. 2a: surface rain map (1 km CAPPI), at 4x4 km resolution, scale in units of 1.25 dBZ, starting at "1" = 0.2 mm/hr. Letters in alphabetic order follow number symbols.

ORIGINAL PAGE IS  
OF POOR QUALITY

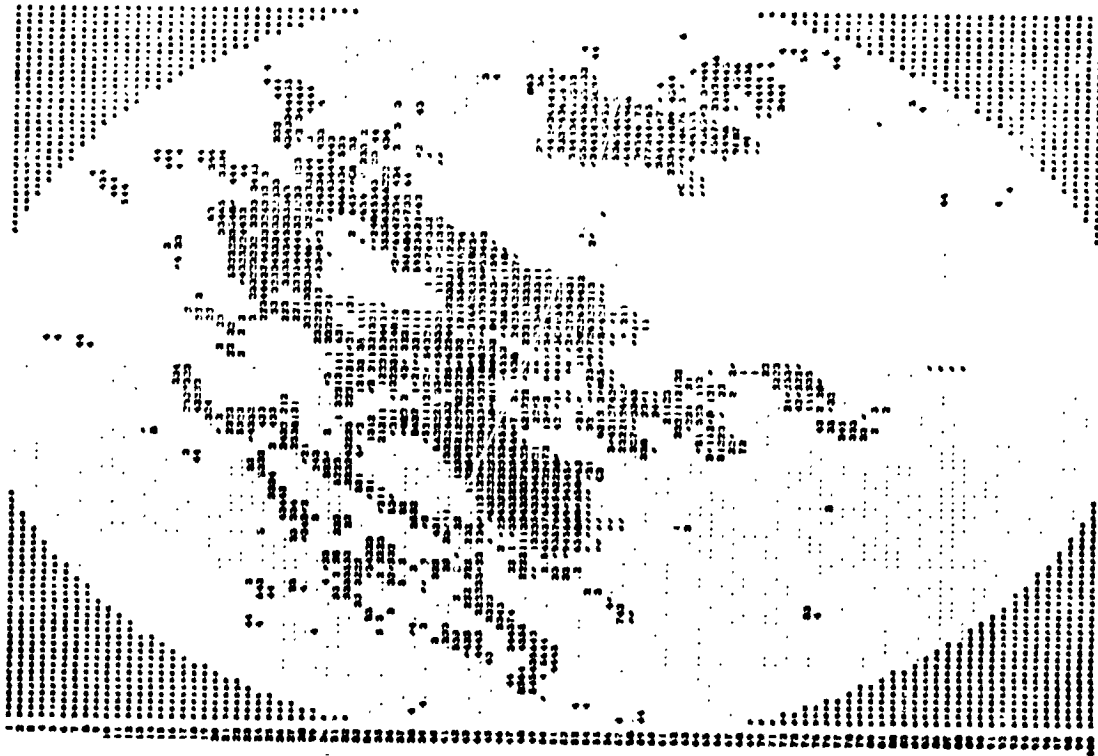


fig. 2b: effective rain layer height map. Units are in km. "0", "0" indicate no rain at ground.

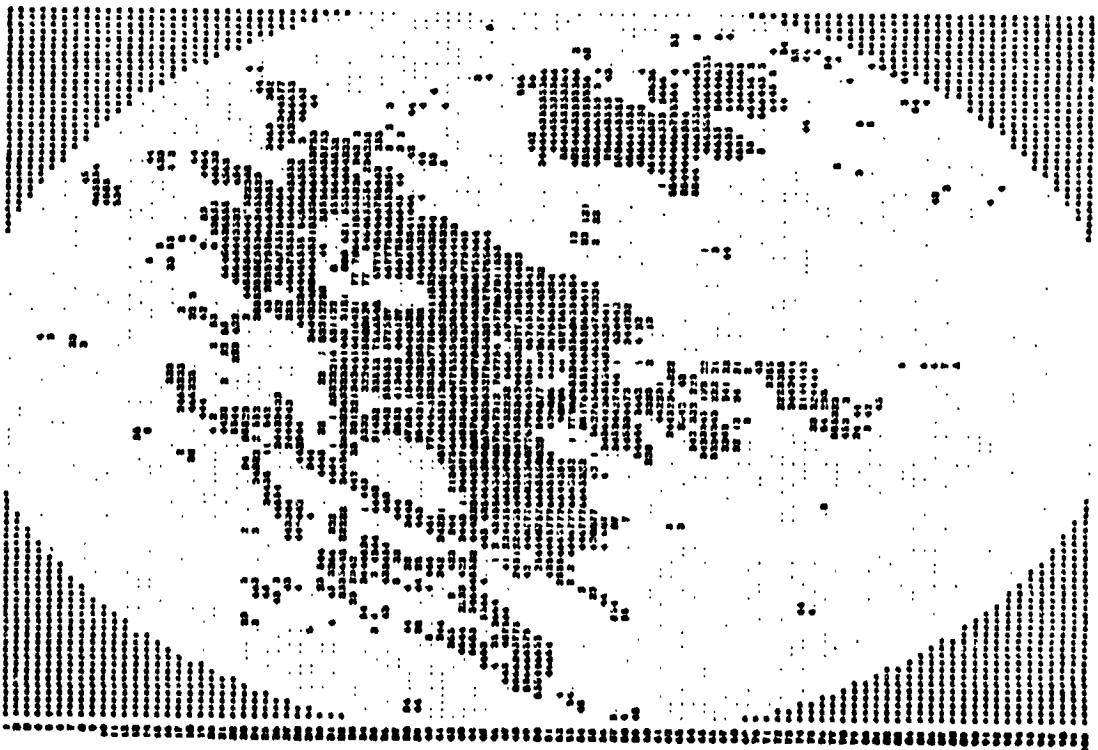


fig. 2c: echo top height map. Units are in km.

ORIGINAL PAGE IS  
OF POOR QUALITY

and the echo top height (Fig. 2c), the latter being a measure of the cloud vertical extent. There is so much structure in each of these that an assumption of constancy in any of these parameters - even averaged of large areas - would not seem to be adequate.

In considering the effect of the rain structure on various radiometer FOV's, two rather different effects must be considered. The first is that referred to above, where the microwave temperature field is averaged over cloud and rain areas, an effect which smooths variations in cloud amount and rain layer height. The other effect, of greatest importance in the present generation of microwave radiometers, e.g., the Scanning Multi-channel Microwave Radiometer (SMMR on NIMBUS 7) is that of incomplete coverage of FOV by rain. For example, in GATE Phase III, we found that for FOV's of 20x44 km which is the best resolution currently available (at 0.81 cm), that only 37% had some rain, and of these, on average, only 29% of their area was covered by rain. In comparison, the next generation of satellite-borne microwave radiometer, LAMMR, is expected to have an FOV of 7x14 km at 0.81 cm. We therefore expect the effect of incomplete FOV coverage to be relatively unimportant compared to that of intrinsic rain layer height and cloud amount variations.

In order to verify this conjecture, we simulated both SMMR and LAMMR performance using GATE radar data.

4.2a SMMR simulation

In this case, it appeared that the key source of error in rain estimates would be the variation of fractional FOV coverage of emitting substance other than background known as the "duty factor" (Stepanenko (1968b)). We therefore ignored variations in effective rain layer height and cloud amounts, and directly applied the Wilheit et al (1977) rain-rate/brightness temperature relationship for a 4-km freezing layer. The simulation was made by using this relationship to convert 4x4 km radar PPI scans into brightness temperature fields, and then integrating these over the radiometer antenna beam pattern down to a 6 dB level.

We were thus able to evaluate the accuracy of the "direct" technique (assuming uniform rain over the entire FOV) as well as that of "FOV" technique (which assumes rain only over the fraction actually raining). This latter technique was suggested by Smith and Kidder (1978), and could only be practical if some independent "FOV" characterization or determination of  $K_d$  was possible.

Using random number generators, we could simulate antenna noise and duty factor errors. Statistics giving the results are shown in Table 3 after empirical removal of bias (over 30%) resulting from non-uniform rain. Advantages of this method are the enormous data base available (in our study we used 30,000 data points) as well as the absence of navigation and calibration problems (since the radar data 'verified' the simulation). We concluded that for individual FOV's, errors of  $\pm 200\%$  result, with scant improvement with FOV characterization for errors in estimating  $K_d$ ,  $\pm 15\%$ , since this technique amplifies the errors.

TABLE 3 THE RMS ERRORS OF VARIOUS RAIN AMOUNT ESTIMATION TECHNIQUES IN %

Antenna error of 2K <sup>2</sup>	no	yes	yes	yes	yes
Error in estimate (%)	0	0	$\pm 10$	$\pm 20$	$\pm 50$
Individual FOV's	'direct'	180	200	200	200
	'FOV'	160	170	180	220
	'area times constant'	240	240	250	270
Entire PPI's	'direct'	26	39	39	39
	'FOV'	32	33	35	46
	'area times constant'	57	57	62	72

Many researchers who have worked with SMMR data find these errors very high in view of the fact that the observed brightness temperatures show considerable spatial homogeneity and even continuity between satellite passes 12 hours apart. On closer examination, this situation is not as paradoxical as it seems: the primary characteristic of convective rainfall is precisely its fantastic temporal and spatial variability; and thus any measuring device whose response is not highly variable is unlikely to be an accurate estimator of rainfall.

4.2b LAMMR simulation

It was anticipated that the partial FOV coverage problem would be largely overcome by the improved LAMMR resolution. We therefore included the cloud and rain layer height variations in the LAMMR simulation since these were likely to be the principle causes of error if LAMMR is used for rainfall estimates.

To make the simulation, we made the following assumptions: 1) an 8x8 km FOV, 11) a 1.55 cm wavelength, 111) a 50° viewing angle. The other wavelengths were included only implicitly by assuming that they could accurately estimate the total cloud and humidity attenuations. As the detailed discussion in Lovejoy and Austin (1980) indicates, such a determination is theoretically possible, although should be quite difficult in practice due primarily to the difficulty in accurately measuring the effective cloud temperature. Neither did we take into explicit account the polarization of the radiances, since we only considered the case of emission over an ocean surface where the surface emissivity is well known, and is nearly constant.

To perform the simulation, we used 4x4 km resolution radar data of the types shown in Figs. 2a, b, c: 1 km CAPPI's, effective rain layer height maps, and echo top height maps. These were converted to 4x4 km attenuation fields by assuming a cloud density of 0.3 kg/m<sup>2</sup> extending from the echo top down to 1 km above the ground, and a humidity profile varying from 80% at ground to 100% at the echo top. The 4x4 km attenuation field was converted to an 8x8 km field by averaging the resulting microwave temperature and converting the average temperature back into attenuation. The relationship used was the simple isothermal - no scattering model, fairly appropriate for this case. The resulting rain rate-attenuation relationship is graphed in Fig. 3 with 1 standard deviation error bars. For a given rain rate, the attenuation error is about  $\pm 35\%$  for  $R \leq 5$  mm/hr, and for a given attenuation, the resulting error in R is about  $\pm 70\%$ . For the slightly different model used to construct Table 2 on a 1x1 km scale



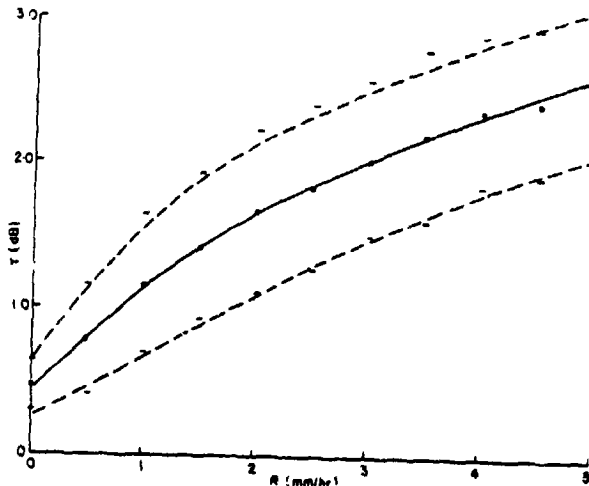


Fig. 3  
The rainrate ( $R$ )-attenuation ( $\tau$ ) curve with one standard deviation error bars (dashed lines) for the LAMMR simulation

the corresponding values are  $\pm 30\%$ ,  $\pm 70\%$ . This indicates that the LAMMR antenna size does not significantly contribute to the error in a single FOV. The limiting error is the rain layer height variability, which is about  $\pm 60\%$  at a 1x1 km scale. It should be stressed that this is the accuracy assuming that data of the type shown in Fig. 3 is available - i.e., assuming some source of calibration such as a radar or raingage.

As a very minimum - even if direct rainfall ground truth is not available - some estimate of the effective rain layer height is required. As discussed earlier, such estimates cannot be supplied by any known remote sensing technique other than radar.

For estimates of the accuracy of the LAMMR over a large area (here 40,000 km<sup>2</sup>), we need to investigate the spatial variability of the effective rain layer height. In our sample of 21 GATE, Phase III 3-D radar scans, we determined  $h = 3.50 \pm 0.52$ , i.e.  $\pm 15\%$ . There was no apparent diurnal variation although this is a small sample to estimate such a variation. This variation represents a much smaller variation than the 1x1 km  $\pm 60\%$  variation and also shows that  $h$  shows little systematic variation as a function of time. These conclusions are not surprising since  $h$  is a measure of the average rainfall rate gradient, not the rainfall rate itself. To estimate the LAMMR accuracy over a PPI, we assumed  $h = 3.50$  km, and the cloud height = mean echo top = 5.32 km. These assumptions lead to an RMS error of  $\pm 28\%$  for the LAMMR rain estimate over a 40,000 km<sup>2</sup> area. This may decrease to  $\pm 20\%$  for 10<sup>5</sup> km<sup>2</sup>. Since  $h$  apparently varies randomly about the mean, we may expect LAMMR estimates to quickly approach the correct value when they are accumulated over successive satellite passes - providing that the average effective rain layer height is known.

#### 4.3 Temporal resolution

In the present and in the foreseeable future, satellite-borne microwave radiometers will have

sun-synchronous orbits. The geometry is such that for the regions between  $\pm 60^\circ$  latitude, the satellite covers 25% of the region twice a day, 50% once a day, and the remainder not at all. This low sampling rate raises two separate questions. The first is the accuracy of daily rainfall amount estimates if only one or two instantaneous rainfall rate estimates are available. The second problem is that of estimating seasonal or climatological rainfall (e.g., Rao et al (1976)). In this case, the chief problem is that of the diurnal variation in rain rate and the fact that sun-synchronous satellites always pass a given point at the same (local) time of day. The size of the bias in climatological rain rates from this source was found to be approximately a factor 3 in GATE Phase III. Frank (1979) found a variation of approximately factor 1.5 for the entire GATE experiment, indicating that averaging even over fairly long time periods (approx. 3 months) will not remove this effect. Furthermore, we may expect the diurnal variation to be a function of geographical location as well as season. Probably the most pertinent data on this effect is to be found in Jordan (1980), who used ship reports to investigate oceanic rainfall off the west coast of Africa, for four regions. For all regions, all seasons, he obtained an average diurnal variation factor of 1.7. For a given season, however, variations between 1.3 and 4.4 were found depending on the location and for a given location variation with season was of a similar magnitude. These results unambiguously indicate that the diurnal variation is not only large, but also variable in time and space.

The size of the diurnal variation in rainfall suggests that a once or twice daily rainfall rate estimate will give little idea of total rainfall during a 12- or 24-hour period. This suspicion was verified by comparing 12-hour accumulations of rainfall over approximately 10<sup>3</sup> km<sup>2</sup> with that estimated by assuming a constant rain rate for 12 hours: average accuracies of approx.  $\pm 300\%$  were found, depending somewhat on the time of day of the satellite pass.

#### 5. COMBINING LAMMR WITH VIS/IR TECHNIQUES

In order to overcome the problem of low sampling rate, either many (perhaps 10) LAMMR's will be required or some other high temporal resolution data source must be used as a supplement. Here we propose that the visible/IR data available every half hour from the GOES satellites is an attractive possibility. First, because a variety of visible/IR rain estimating schemes already exist (Griffith et al (1978), Stout et al (1979), Lovejoy and Austin (1979a) and Bellon et al (1980)), and second, because as argued in Lovejoy and Austin (1979b) they require for calibration the mean rain rate for raining areas, a number which the LAMMR could supply every 12 or 24 hours.

In order to see if the idea is worth pursuing, we first calculated the diurnal variation in the mean rain rate for raining areas (averaged over 10<sup>5</sup> km<sup>2</sup>). For 12, 24 hours, the variation about the mean was  $\pm 2\%$ ,  $\pm 4\%$  respectively. In other words, almost all of the diurnal variation in rainfall was accounted for in the diurnal variation in raining areas. In Lovejoy and Austin (1979a) errors of  $\pm 25\%$  were obtained for estimates of rain areas from vis/IR data for regions  $\sim 10^5$  km<sup>2</sup> for single

vis/IR image pairs (at night time, with IR data only, errors of  $\sim \pm 70\%$  were obtained). If rain areas were estimated every half hour and accumulated for 12 or 24 hours fairly accurate total area estimates should be obtained. These accumulated areas could then be used to estimate rain accumulations by multiplying by a mean rain rate for raining areas.

In outline, a LAMMR-vis/IR hybrid scheme might work as follows: the LAMMR would estimate the mean rain rate for raining areas at every pass and the vis/IR data the total rain areas. The final step in estimating rain amounts could be to combine the two pieces of information in the optimum manner. If neither datum had errors, and the mean rain rate for raining areas did not vary in time then rain amounts could be obtained by simply multiplying the mean rain rate for raining areas with the total area. However, the mean rain rate for raining areas does fluctuate around the long term mean on a time scale of several days. Furthermore, the LAMMR rain rate estimate will be in error by an amount  $\sim \pm 20\%$  due to the variation of the effective rain layer height about its long term average. The error in total rain areas is expected to be smaller than this because of the very high temporal resolution of the GOES data, although this point needs further investigation. Using the fact that both the long term mean rainfall rate for raining areas, and the mean effective rain layer height appear to be well defined (i.e., no systematic variation was observed over GATE Phase III) we applied the following autoregressive order 1 model to estimate the optimum rain rate for raining areas for the next 12 hour period ( $R_1$ ):

$$R_1 = (R_0 - \bar{R})a + \bar{R}$$

where  $\bar{R}$  is the long term (in this case, 20 day) mean rain rate, and  $R_0$  is the last LAMMR rain rate estimate. 'a' is a constant chosen to minimize the error in  $R_1$ . When  $a = 0$ , we obtain an RMS error of  $\pm 28\%$ , i.e., we use only the long term average rain rate. When  $a = 1$ , we obtain an RMS error of  $\pm 40\%$ , i.e., when only the most recent LAMMR rain rate is used. The optimum 'a' was  $\sim 0.3$  which resulted in RMS errors of  $\pm 24\%$ . Since this puts a small weight on the most recent LAMMR rain rate, we expect little increase in this error if a random  $\pm 20\%$  rain rate error is added to  $R_0$  as we would expect in an operational scheme. Indeed, computer simulations of this procedure yield an RMS error of  $\pm 25\%$  when such an error is added. Since this figure holds for a  $40,000 \text{ km}^2$  area, it is likely to be reduced to  $\pm 20\%$  for an area of  $\sim 10^5 \text{ km}^2$ . This is probably a good estimate of the error of rain accumulation estimates since it is expected that the total rain areas will be estimated considerably more accurately than this. Since these estimates are likely to be independent they ought to add as a sum of squares, and therefore result in total errors of the same order. It should be remembered that these figures correspond to areas of approx  $10^5 \text{ km}^2$  and that the method is entirely dependent on the assumption that the long term average effective rain layer height is known. A consequence of this fact is that the accuracy of, for example, monthly rainfall will be limited not by the random errors discussed here, but by biases introduced from insufficient knowledge

of the rain layer height. Since virtually nothing is known about the relationship of the rain layer height to other meteorological parameters (such as the freezing level), or of its variations with season and location, it is clearly premature to expect LAMMR to be the most practical method of obtaining rain amounts by remote means. For example, it may ultimately prove simpler and more accurate to calibrate the vis/IR techniques directly from a sparse rain gage network, rather than via LAMMR.

## 6. CONCLUSIONS

It has been argued that a fundamental limitation on the accuracy of microwave radiometer based rainfall estimation is the extreme variability of both cloud amount and effective rain layer height. This accuracy is estimated to be of the order of  $\pm 70\%$  in point rain rate estimates, and is unlikely to be improved upon by using other wavelengths or polarizations. Using a simulation based on GATE data, it was shown that for FOV's  $\sim 880 \text{ km}^2$ , that errors  $\sim \pm 200\%$  result primarily due to partial FOV coverage by rain, and that scant improvement was effected by FOV characterization. However, this effect is of secondary importance in the case of  $64 \text{ km}^2$  FOV's (e.g., the LAMMR). In this case, errors of  $\sim \pm 20\%$  over an area  $\sim 10^5 \text{ km}^2$  are obtained if the long term average effective rain layer height is known.

It was argued that for the purposes of either daily accumulations or climatological sampling that a single LAMMR was insufficient. It was proposed that vis/IR data from GOES satellites be used as a natural supplement since these have high temporal resolution and require the mean rain rate for raining areas as calibration. It was estimated that for areas of  $\sim 10^5 \text{ km}^2$ , that such a hybrid scheme could achieve accuracies of the order of  $\pm 20\%$  in total 12 hour rainfall accumulations - if the long term average effective rain layer height was known. However, if it proves more accurate, and simpler to estimate the mean rain rate for raining areas directly

Spatial scale	PPI ( $\sim 10^4 \text{ km}^2$ )	FOV ( $\sim 10^5 \text{ km}^2$ )
Rain rate-temperature conversion accuracy	20*	70
Error due to low spatial resolution	40	200
Combined (instantaneous) accuracy†	50	210
Error due to low temporal resolution (every 12 hours)	80	310
Combined (total) accuracy‡	90	370
Climatology (12 hours)	90	200
Area times constant (12 hours)	20	120
Area times constant (instantaneous)	60	240

\*This figure depends on how the effective rain-layer height varies as a function of space. The effective rain-layer height averaged over a PPI was determined to be  $3.50 \pm 0.52 \text{ km}$  or  $\pm 15\%$  (at  $1.55 \text{ cm}$ ). Since this is the chief source of variability in rain estimates, we have rounded this to the nearest 10% and used it directly.

†Combination of errors from rows 1, 2.

‡Combination of errors from rows 1, 2, 4.

Table 4: A comparison of rain estimation accuracy for different spatial scales (in %) estimation techniques and for each principal source of error, rounded to the nearest 10%.

ORIGINAL PAGE 19  
OF POOR QUALITY

than to estimate the effective rain layer height, this hybrid scheme would clearly be unnecessary. Table 4 compares some of these errors, including those of an "area x constant" technique which estimates rainfall by multiplying the rain area by the long term mean rain rate for raining areas. This is the likely accuracy of a vis/IR technique given that the mean rain rate for raining areas is known. This is a convenient benchmark by which the accuracy rain estimating techniques may be judged, since it is probably not far from what is currently available by combining vis/IR data with rain gauge or radar calibration.

7. ACKNOWLEDGEMENTS

We would like to thank Eric Smith, of Colorado State University, for helpful communication regarding FOV characterization. Useful discussions with David Atlas, of NASA, are also acknowledged. We would like to thank Alamelu Kilambi for her aid with the data processing.

8. REFERENCES

- Akvilonova, A.B., M.S. Krylova, B.G. Kutuza and L.M. Mitnik, 1971: SHF Radiometric characteristics of frontal cloudiness as measured from Cosmos-243. *Advances in Satellite Meteorology*, Wiley & Sons, N.Y., 65-73.
- Allison, L.J., E.B. Rodgers, T.T. Wilheit and R.W. Fett, 1974: Tropical cyclone rainfall as measured by the Nimbus 5 Electrically Scanning Microwave Radiometer. *Bull. Amer. Met. Soc.* 55, 1074-1089.
- Atlas, D., C.W. Ulbrich (1977): Path- and area-integrated rainfall measurement by microwave attenuations in the 1-3 cm band. *J. Appl. Meteor.*, 16, 1322-1331.
- Basharinov, A.E., A.G. Gorelik, V.V. Kalashnikov and K.G. Kutuza, 1970: Joint radio emission and radar measurements of meteorological parameters of cloud formations. *IZV, AN SSSR, Ser. "Fiz. Atm. i Okeana"*, 5, 526-530.
- Bellon, A., S. Lovejoy, G.L. Austin, 1980: Combining satellite and radar data for the short range forecasting of precipitation. *Mon. Wea. Rev.*, 108, 1554-1566.
- Bunting, J.T., 1978: Cloud measurements from satellites and aircraft. 3rd Conf. on Atmos. Radiation, June 28-30, Davis, Calif. A.M.S. 45 Beacon St., Boston, Mass. 02108.
- Crane, R.K., 1971: Propagation phenomenon affecting satellite communication systems operating in the centimeter and millimeter wavelength bands. *Proc. I.E.E.E.*, 59, 173-188.
- Gorelik, A.G., V.V. Kalashnikov, B.G. Kutuza, V.F. Logunov and I.S. Skuratove, 1971a: Dependence of attenuation coefficients in the 0.8 to 3.2 centimeter band on rain intensity and drop size distribution. *Advances in Satellite Meteorology*, Wiley & Sons, N.Y. 48-57.
- Gorelik, A.G., V.V. Kalashnikov, B.G. Kutuza and V.I. Semiletov, 1971b: Measurements of space distribution of brightness temperatures of clouds and rain at 0.8 and 1.35 centimeter wavelengths. *Advances in Satellite Meteorology*, Wiley & Sons, N.Y. 19-28.
- Gorelik, A.G., V.V. Kalashnikov and Yu. A. Frolov, 1971c: Determination of total atmospheric moisture content from atmospheric emission. *Advances in Satellite Meteorology*, Wiley & Sons, N.Y. 3-18.
- Gorelik, C.G., V.V. Kalashnikov and Yu.A. Frolov, 1971d: Possibility of precipitation zone identification from meteorological satellites. *Advances in Satellite Meteorology*, Wiley & Sons, N.Y. 29-39.
- Griffith, C.G., W.L. Woodley, P.G. Grube, D.W. Martin, J. Stout and D.N. Sikdar, 1978: Rain estimation from geosynchronous satellite imagery. *Mon. Wea. Rev.*, 106, 1153-1171.
- Jordan, C.L. 1980: Diurnal variations of precipitation in the eastern tropical Atlantic. *Mon. Wea. Rev.*, 108, 1065-1067.
- Kalashnikov, V.V. and Yu.A. Frolov, 1971: Prospects for determining rain intensities by the thermal atmospheric emission in the millimeter and centimeter bands. *Advances in Satellite Meteorology*, Wiley & Sons, N.Y. 40-47.
- Lovejoy, S. and G.L. Austin, 1979a: The delineation of rain areas from visible and IR satellite data for GATE and mid-latitudes. *Atmos-Ocean*, 17, 77-92.
- Lovejoy, S. and G.L. Austin, 1979b: The sources of error in rain amount estimating schemes from GOES visible and IR satellite data. *Mon. Wea. Rev.*, 107, 1048-1054.
- Lovejoy, S. and G.L. Austin, 1980: The estimation of rain from satellite-borne microwave radiometers. *Quart. J. Roy. Met. Soc.*, 106, 255-276.
- Rao, M.S.V., W. Abott III, and J.S. Theon, 1976: Satellite derived global oceanic rainfall maps. 6th Conf. Wea. Fore. and Anal., May 10-13, A.M.S., Boston, Mass.
- Reynolds, D.W., T.B. McKee and K.S. Danielson, 1976: Effects of cloud size and cloud particles on satellite-observed reflected brightness. Intern. Conf. on Cloud Physics, Boulder, Colo., July 26-30 (preprints).
- Reynolds, D.W., T.B. McKee and K.S. Danielson, 1978: Effects of cloud size and cloud particles on satellite-observed reflected brightness. *J. Atmos. Sci.*, 35, 160-164.
- Rodgers, E., H. Suddalingaiah, A.T.C. Chang, T. Wilheit, 1979: A statistical technique for determining rainfall over land employing NIMBUS 6 ESMR measurements. *J. Appl. Meteor.* 18, 978-991.
- Smith, W.L. and H.B. Howell, 1971: Vertical distributions of atmospheric water vapour from satellite infrared spectrometer measurements. *J. Appl. Meteor.*, 10, 1026-1034.
- Smith, E.A. and S.Q. Kidder, 1978: A multi-spectral satellite approach to rainfall estimates. Sept. of Atmos. Sci., Colo. State Univ., Fort Collins, Colo. 80523 (preliminary draft).
- Stout, J., D.W. Martin and D.N. Sikdar, 1979: Estimating rain with geosynchronous satellite images. *Mon. Wea. Rev.*, 107, 585-598.
- Viezee, W., H. Shigeishi and A.T.C. Chang, 1979: Relation between west coastal rainfall and Nimbus 6 SCAMS liquid water data over the northeastern Pacific ocean. *J. Appl. Meteor.* 18, 1151-1157.
- Weinman, J.A., P.J. Guetter, 1978: Determination of rainfall distributions from microwave radiation measured by the NIMBUS 6 ESMR. *J. Appl. Meteor.* 17, 437-442.
- Wilheit, T.T., A.T.C. Chang, M.S.V. Rao, E.B. Rodgers and J.S. Theon, 1977: A satellite technique for quantitatively mapping rainfall rates over the ocean. *J. Appl. Meteor.*, 16, 551-560.

D37 EN83 25302

ORIGINAL PAGE IS  
OF POOR QUALITY

Using Underwater Ambient Noise Levels  
to Measure Rainfall Rate: A Review

Jeffrey A. Nystuen  
Scripps Institution of Oceanography  
April 1981

Abstract

A brief description of other methods of rainfall measurement at the sea surface is given. The general underwater ambient noise background of the ocean is described. The physics of noise generation by bubbles and splashes is reviewed. Monitoring underwater ambient noise levels to measure rainfall rate requires that the spectral shapes of the noise from wind and rain be different or at least distinguishable. This would allow the rain noise to be separated from the wind noise and then hopefully it can be correlated with rainfall rate. Different spectral shapes are observed experimentally.

Introduction

Rainfall is one of the parameters most often cited when one describes the climate of a region. Accurate rainfall measurements are needed for such things as local weather forecasting, measuring latent heat release and assessing flood potential from individual storms. Intense rainfall is also an indication of upward mass flux. These are important parameters for the global heat and water budgets and are vital inputs into circulation models.

Unfortunately because of the extreme spatial and temporal variability of rain, accurate rainfall measurements are hard to make. This is especially true on a global scale since roughly 80% of the earth's precipitation occurs over the ocean where only 10% of the weather stations are located (Kidder and VanderHaar, 1977). Satellite techniques using visible and infrared imagery, microwave radiometers and satellite-mounted radars have been proposed. These techniques should be able to improve global rainfall measurements dramatically as they provide relatively complete and uniform coverage. One of the current limitations is the lack of accurate ground truth needed for calibration. This is especially true over the ocean.

There are several methods that are used to measure rainfall at the sea surface. Ship-board raingages are widely used but are affected by sea spray, platform instabilities and ship-induced wind effects. Other ship measurements, such as the measurement of the dilution of seawater or attenuation from lidars, haven't been widely used. Data from island weather stations can also be used to estimate oceanic rainfall. Unfortunately there are very few islands and vast areas of open ocean. In addition, orographic effects, especially in the tropics, bias the results. Nevertheless extrapolations using rain rates and weather reports from ships and nearby land stations to map rainfall over the ocean have been made (Reed and Elliot, 1973).

Land or ship based radars can also give an estimate of rainfall. Conventional weather radars measure the radar reflectivity factor, Z. The radar reflectivity factor is dependant on the drop size distribution of the rain:

$$(1) \quad Z = 10^6 \int_0^{\infty} D^6 N(D) dD ,$$

where  $N(D)$  is the drop size distribution and  $D$  is the drop diameter. Rainfall rate is also dependant on the drop size distribution, but it is a different moment of the drop size distribution.

$$(2) \quad R = 0.6\pi \int_0^{\infty} D^3 N(D) v(D) dD \approx 0.006\pi \int_0^{\infty} f(D) N(D) dD ,$$

where  $v(D) \approx 965 - 1030 \exp(-6D)$  in cm/sec is the raindrop fall velocity and

ORIGINAL PAGE IS  
OF POOR QUALITY

$f(D) = 1767D^{3.67}$  is an approximation proposed by Atlas and Ulbrich (1977). The drop size distribution is usually defined by two parameters, typically

$$(3) \quad N(D) = N_0 \exp(-\Lambda D) ,$$

where  $\Lambda = 3.67/D_0$  and  $D_0$  is the median diameter of the distribution. Ulbrich and Atlas (1978) note that there are other measurable quantities (optical extinction, liquid water content and attenuation) that are moments of the drop size distribution. They suggest that in order to measure rainfall rate accurately independent measurements of at least two of the above quantities are required. Once two are determined then all of the rest are determined.

x Unfortunately weather radars measure only one quantity, radar reflectivity, with a resulting error in rainfall rate of roughly 25-50%.

One possible method to measure rainfall rate over water is to monitor the ambient noise level underwater. This method has not been developed although there are reports of significant increase in ambient noise during rain storms (Heindsman, Smith and Arneson, 1955 and Bom, 1968). Franz (1959) proposed a theory of sound generation from splashes which will be reviewed in this paper. Other mechanisms for sound production will also be discussed. Potentially this method would allow rainfall measurements to be made at any location in the oceans where it is possible to moor a hydrophone.

ORIGINAL PAGE IS  
OF POOR QUALITY

The Underwater Sound Spectrum

The underwater ambient noise spectrum of the ocean has been extensively studied. Wenz (1962) describes it and suggests possible noise sources in different frequency bands. His summary is given in figure one.

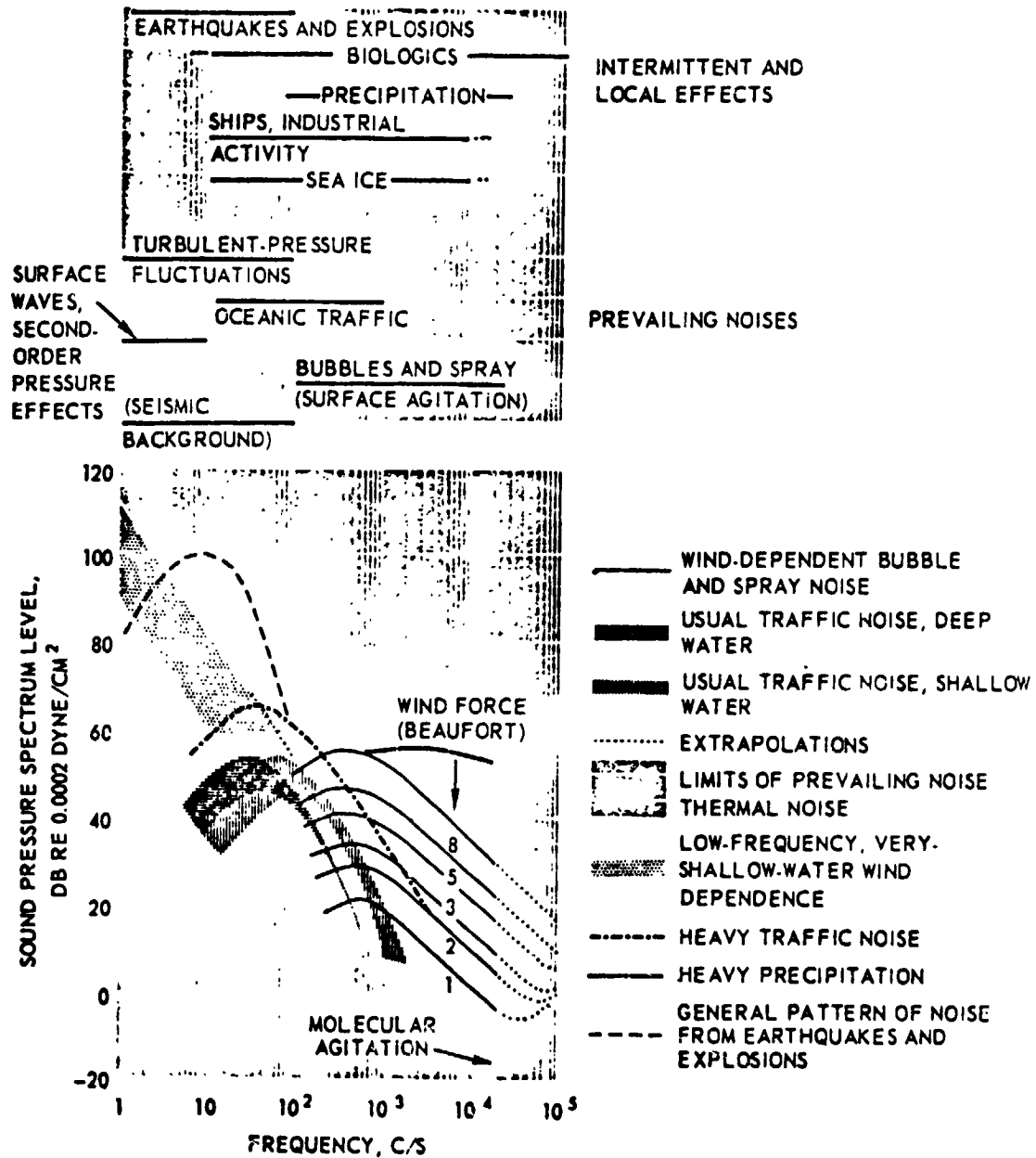


Figure 1.

Figure 1. Ambient-noise spectra, summarizing results and conclusions concerning spectrum shape and level and probable sources and mechanisms of the ambient noise in various parts of the spectrum between 1 c/s and 100 kc/s.

from Frish (1966)

Turbulent pressure fluxuations in the atmosphere near the ocean surface and in the turbulent ocean surface layer are the most often cited sources of noise below 20 hertz. This can be attributed to the wind (Wilson, 1979). For slightly higher frequencies, twenty to several hundred hertz, shipping or industrial noise is often dominant, even in the deep ocean. As frequency increases shipping noise diminishes until, at roughly one kilohertz, wind noise due to "surface agitation" becomes dominant. Nearby ships can still contribute significant noise as high as 15 kHz (Evans, 1980).

The Knudsen relation is used to describe the noise due to wind between 500 Hz and 25 kHz (Knudsen, Alford and Emling, 1948; Wenz, 1971). Roughly, the relation states that the ambient noise spectrum levels decrease 5 dB per octave with increasing frequency and increase 5 dB with each doubling of the wind. In figure one various spectrum levels are shown for different Beaufort wind forces, usually spectrum levels are given for different sea states. A typical measured ambient noise spectrum is shown in figure two. One to 25kHz

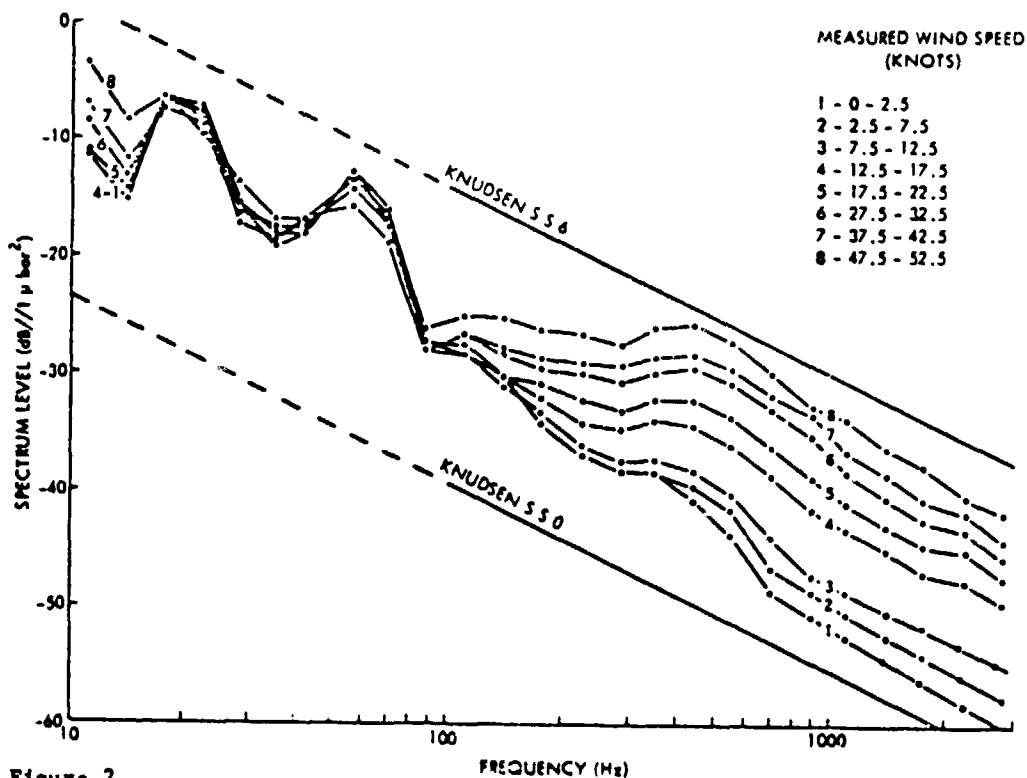


Figure 2

Fig. 8. Variation of deep-ocean ambient-noise spectra with wind speed. from Perrone (1969)

is the frequency band where rainfall measurement is possible. Figure one shows heavy rain is the dominant noise source when it is present at these frequencies.



ORIGINAL PAGE 19  
OF POOR QUALITY

Heindsman et al. (1955) noted a 25 dB increase in the ambient noise level during a heavy thunderstorm in the Long Island Sound. Bom's results of ambient noise level increase during four rain periods in a small lake in Italy are shown in figure three.

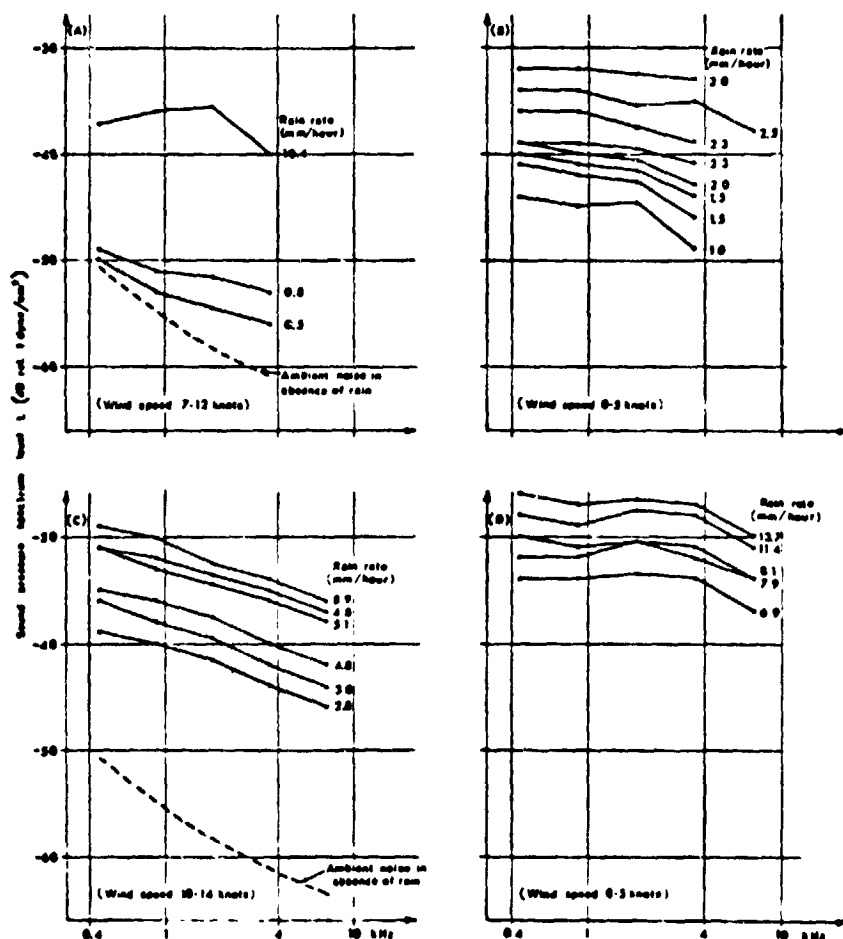


FIG. 3. Noise spectrum levels as measured during four precipitation periods.

Figure 3.  
Bom (1968)

Above 25 kHz there are very few measurements. In fact the curves shown in figure one are extrapolated from lower frequencies. Between 50 and 100 kHz molecular thermal agitation obscures other noise sources. The spectrum level due to thermal agitation was predicted by Mellen (1952). He used classical statistical mechanics to derive the following relation for mean squared pressure per unit frequency:

$$(4) \quad \langle P^2 \rangle df = \frac{4}{c^2} f^2 kT (\rho c) df$$

where  $f$  is frequency,  $c$  is the speed of sound in water,  $T$  is temperature,  $\rho$  is density and  $k = 1.37 \times 10^{-23}$  joules/deg. When appropriate values are inserted into (4), it becomes

(5)  $L = -35 + 20 \log f$  in dB re  $1 \mu\text{Pa}$ ,

where  $f \gg 1$  kHz and  $L$  is the sound pressure spectrum level. The thermal noise spectrum has a slope of +6 dB/octave.

ORIGINAL PAGE IS  
OF POOR QUALITY.

## Noise from Wind and Rain

In order to use ambient noise levels to measure rainfall rate, it is necessary to choose a frequency band where the wind has a red Knudsen spectrum and rain has a "white-ish" spectrum. This fact would allow separation of the two noise sources and permit quantification of rainfall rate. Above a few kilohertz these spectral shapes are observed, however the mechanisms by which the rain and the wind generate acoustic noise are not well defined. This is especially true for noise generation by wind.

Breaking waves are the most obvious possible source for wind noise although as wind speed increases the ambient noise level begins to rise even before whitecaps are present. Studies have been made that show a relationship between the fraction of the ocean surface covered by whitecaps,  $W$ , and the ten meter elevation wind speed,  $U_{10}$ . Monahan and Muircheartaigh (1980) summarize the experimental results as shown in figure 4 and determine the following relationship.

$$(6) \quad W = 3.84 \times 10^{-6} U_{10}^{3.41}$$

Monahan and Davidson (1979) suggest that whitecap coverage may be slightly greater when the atmosphere is thermally unstable. Shaw, Watts and Rossby (1978) measured the underwater noise level,  $L$ , with respect to the wind speed. They determined that at 5 kHz

$$(7) \quad 20 \log V = 1.01 L - 30.4 \quad ,$$

where  $V$  is wind speed in knots and  $L$  is in dB re 1 Pa. Equations (6) and (7) can be combined to give

$$(8) \quad L = 5.88 \log W + 68.2$$

The ambient noise data at 1 kHz shown in figure 2 was converted to whitecap coverage using equation (6). It is presented in figure 5 with equation (8) superimposed. These figures suggest that whitecaps are a major source for wind-generated noise.

Whitecaps generate noise from bubble formation and spray. Bubbles generate acoustic waves when agitated. In addition as bubbles break, small water droplets are created. Wu (1981) summarizes several studies of bubble populations in the ocean surface waters. These studies show bubbles are present in large numbers even at low wind speeds or calm conditions. As wind speed increases the total number of bubbles present increases and the bubble size distribution shifts. At higher wind speed the bubble population has proportionally more large bubbles. This may be due to coalescence of small bubbles or more efficient entrainment of air by breaking waves. Figure 6 shows data from Medwin (1970).

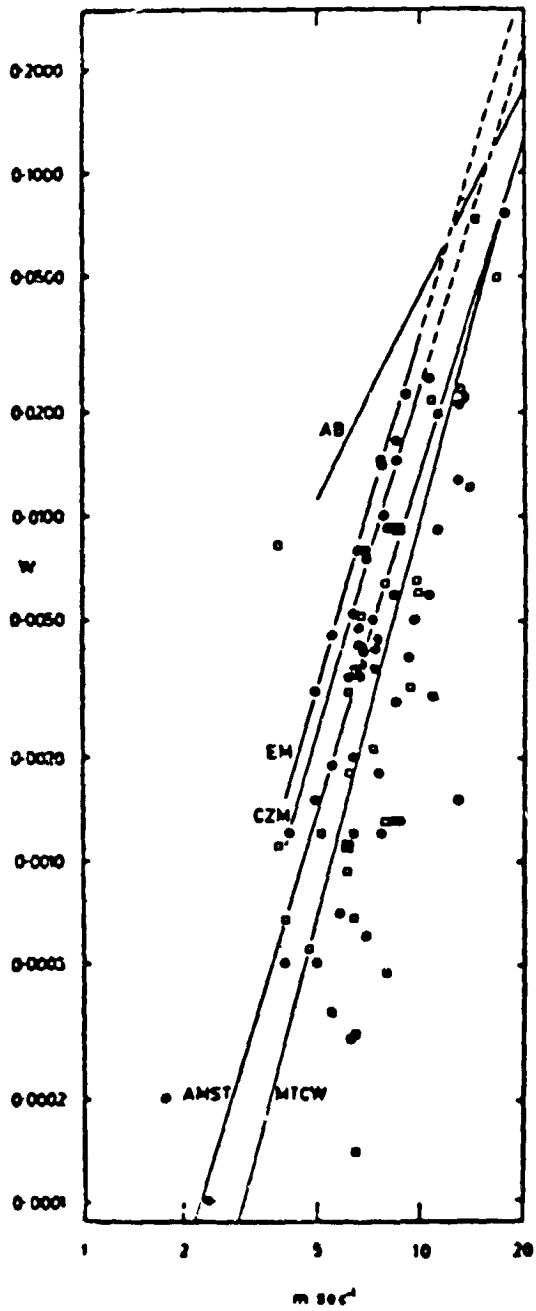


FIG. 1. The fraction  $W$  of the ocean covered by whitecaps versus the 10 m elevation wind speed  $U$ . Filled circles, mean whitecap coverage fractions for specific observation intervals from Monahan (1971); open squares, whitecap coverage values from Toba and Chen (1973). Labeled lines represent various power-law expressions for  $W(U)$  described in the text.

Figure 4. Monahan and Muirchoartaigh (1980)

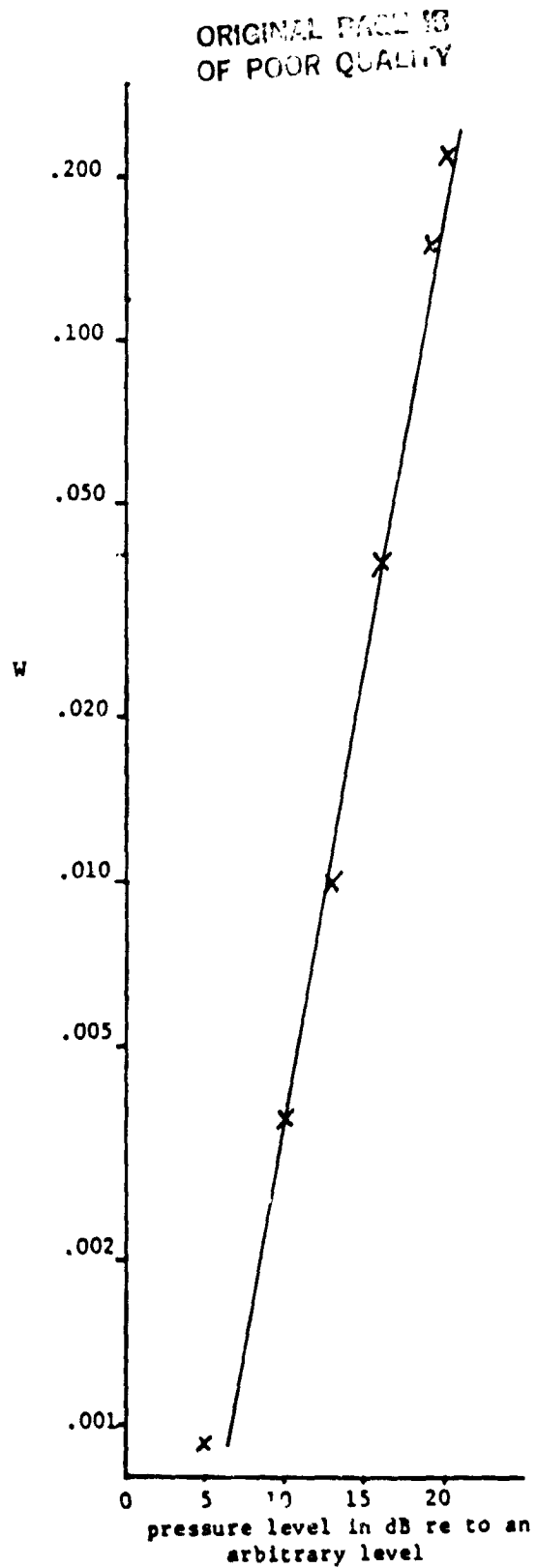


Figure 5

ORIGINAL PAGE IS  
OF POOR QUALITY

Figure 7 is a summary from Wu (1981). Blanchard and Woodcock (1957) attempted to measure bubble populations in the surf. Their technique deliberately excluded large millimeter sized bubbles which rise to the surface quickly. Results from Blanchard and Woodcock appear in figure 6. Thorpe and Stubbs (1979) used bubble clouds from breaking waves to attempt to measure a vertical velocity for mixing of surface water. They determined that the depth,  $d$ , that a bubble cloud penetrates is related to the wind speed.

$$(9) \quad d = 0.4 (U_{10} - 250) ,$$

where  $U_{10}$  is in cm/sec.

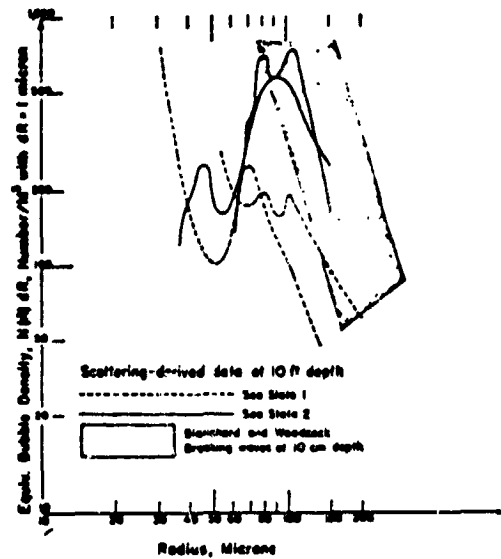


Fig. 6. Four runs showing distribution of numbers of equivalent bubbles per cubic meter in 1-micron-radius bands inferred from pulse-scatter measurements at depth 10 feet during sea states one and two. Range of Blanchard and Woodcock data (taken at 10-cm depth near breaking wave) is also shown. Figure 6. Medwin (1970)

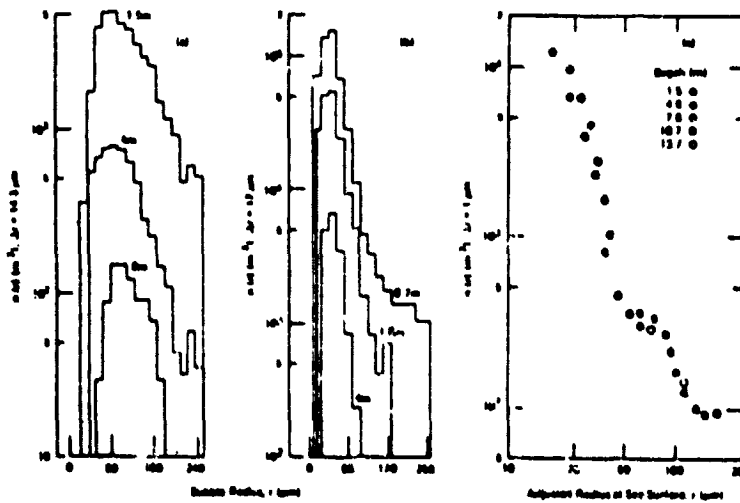


Fig. 7. Distributions of bubbles measured (a) by Kalogezov (1976) at depths of 1, 3, 4, and 8 m, (b) by Johnston and Cooke (1979) at depths of 0.7, 1.2, and 4 m, and (c) by Medwin (1970). The data in 1a and 1b were obtained at  $U_{10} = 11-13 \text{ m s}^{-1}$ , and those in 1c at  $U_{10} = 1-4 \text{ m s}^{-1}$ . Figure 7. Wu (1981)

Most bubbles are created by entrainment of air by breaking waves however several other mechanisms have been suggested (Blanchard and woodcock, 1957; Medwin, 1970). These mechanisms include: bubbles entrained from falling drops, bubbles created from "floating" water drops skimming across the surface when the water has been violently agitated, bubbles created from biological sources such as during photosynthesis and bubbles entrained by continental aerosols. Generally surface waters are supersaturated with air and so it might be possible for pressure fluxuations due co surface waves to generate bubbles, although Blanchard and Woodcock note that even in supersaturated conditions bubbles with diameters less than 300 $\mu$ m tend to dissolve.

The generation of an acoustic signal from bubbles has been investigated by several authors. A very extensive study was done by Strasberg (1956). He notes that there are many different modes of oscillation for each bubble. While any mode can by excited only the zeroth mode, a volumetric pulsation, contributes significantly to the acoustic field. The contribution to the sound spectrum by any given bubble is likely to be at that bubble's resonant frequency. The resonant frequency,  $f_o$ , is derived in Appendix B an is given as

$$(10) \quad f_o = \left( \frac{3\gamma P_o}{\rho} \right)^{1/2} (1/2\pi a_o) ,$$

where  $P_o$  is the ambient pressure at the bubble's depth,  $\gamma$  is the ratio of specific heats in the bubble and is equal to 1.4 for air in water,  $\rho$  is the water density and  $a_o$  is the mean bubble radius. The bubble response is sharply peaked at the resonant frequency as shown in figure 8.

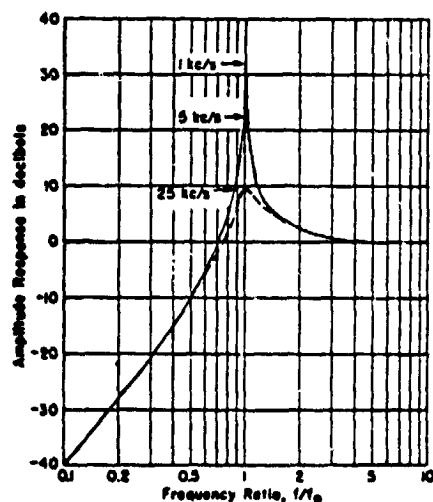


FIG. 8. Amplitude response of a bubble to a steady-state sinusoidal external pressure.

Figure 8.

Strasberg (1956)

ORIGINAL PAGE IS  
OF POOR QUALITY

The magnitude of the bubble oscillation is a much more difficult problem. Strasberg suggests that the appropriate equation to consider is

$$(11) \quad M\ddot{v} + R\dot{v} + K(v - V_0) = p_e(t) - P_0,$$

where  $v = v(t)$  is the bubble volume,  $V_0$  is the equilibrium bubble volume,  $p_e(t)$  is an external pressure forcing term,  $P_0$  is the equilibrium pressure,  $M = \rho/(4\pi a_0)$  is an inertial coefficient,  $K = \gamma P_0/V_0$  is a stiffness coefficient and  $R$  is a resistive coefficient that has a complicated form which varies with bubble size and frequency. The sound pressure radiated by the bubble, at a distance  $r$  from the bubble, is

$$(12) \quad p_s = e\ddot{v}/(4\pi r)$$

Equation (12) is derived in Appendix B. Equation (11) suggests that the form of the external forcing,  $p_e(t)$ , is important. Strasberg considered a short pulse, a somewhat longer pulse and an external pressure that fluctuates sinusoidally. His solution for a short pulse is

$$(13) \quad p_s = P^* \exp(-\pi f_0 t) \cos(\omega t - \phi),$$

where

$$P^* = \frac{e f_0}{2r} \left[ \dot{v}^2 + 4\pi f_0^2 (v - V_0)^2 \right]^{1/2},$$

$$\phi = \arctan \left[ -\dot{v} / 2\pi f_0 (v - V_0) \right] \quad \text{and}$$

$$\delta = \text{dissipation constant} = 0.014 + 4.5 \times 10^{-4} f_0^{1/2}.$$

The solution for the longer pulse is

$$(14) \quad p_s = (a_0/r) \left[ P'(t) - 2\pi f_0 \int_0^t P'(\tau) \exp(-\pi f_0 \delta (t - \tau)) \sin 2\pi f_0 (t - \tau) d\tau \right]$$

where  $P'(t) = p_e(t) - P_0$ . Finally the solution for a sinusoidal external pressure fluctuation of the form  $p_e(t) = P_0 + p_a \cos(2\pi f t)$  is

$$(15) \quad p_s = p_a \left\{ \delta^2 + \left[ (f_0/f)^2 - 1 \right]^2 \right\}^{-1/2}$$

Equation (15) is determined by another method in Appendix B.

The relationship that the above solutions have with the real ocean is currently speculative. Surface gravity waves and turbulent pressure fluctuations certainly provide a fluctuating external pressure field but at much lower frequencies than the resonant frequency of a typical bubble. Turbulent pressure fluctuations may extend as high as 20 Hz however a 100 $\mu$  bubble resonates at 35kHz. A pressure pulse is possible from "crashing" waves and maybe the pressure pulses from smaller splashes or even other bubbles is enough to make a bubble resonant. The most likely source of bubble agitation is from the violent injection of air bubbles into the water by crashing waves. Thorpe and Stubbs (1979) note occasional bubble clouds extending much deeper into the water column than the mean bubble cloud level suggested by their equation (eqn. (9)). These bubble clouds are likely to be caused by breaking waves.

ORIGINAL PAGE IS  
OF POOR QUALITY

If external forcing is ignored and we assume a bubble is oscillating, it is possible to predict the amplitude of that oscillation and thus predict a root mean square pressure at a distance  $r$  from the bubble. This calculation is done in Appendix B with the following result:

$$(16) \quad P_{\text{rms}} = \frac{3 \gamma P_o (\epsilon a_o)}{2r}$$

where  $\epsilon a_o$  is the amplitude of the oscillation of the bubble radius. In order to make a prediction for the underwater pressure spectrum from bubbles it is necessary to make a few assumptions. A bubble size distribution per unit area,  $D(a_o)$ , is required. Bubble size distributions are given in figure 7, however not all of the bubbles are actively resonating and so an active bubble size distribution,  $\delta(a_o)D(a_o)$ , where  $\delta(a_o)$  is a small parameter, will be assumed. The bubble field needs to be uniform at the ocean surface. This might not be true since Arase and Arase (1968) note a directional dependence of ambient noise and other authors claim to be able to detect individual breaking waves. However if the hydrophone measuring the pressure spectrum is deep enough this should be a good assumption. A frequency dependant signal attenuation factor,  $e^{-mr}$ , is required. This is discussed in Appendix C. Finally equation (10) is used to relate bubble radius to frequency.

Applying all of these assumptions the measured rms pressure should be

$$(17) \quad (P-P_o)_{\text{rms-hydro}} = \int_{\text{BSD}} \int_{\text{surface}} (P-P_o)_{\text{rms-bub}} \delta(a) D(a) e^{-mr} dA da$$

This calculation is done in Appendix B and gives

$$(18) \quad (P-P_o)_{\text{rms-h}} = \int_{\text{BSD}} (3\gamma P_o \pi) \epsilon a \delta D(a) (1/m) e^{-mh} da$$

The pressure per unit frequency,  $L$ , is

$$(19) \quad L = (3\gamma P_o \pi) \epsilon \delta D a e^{-mh} (1/m) ,$$

where  $\epsilon$ ,  $\delta$ ,  $D$ ,  $a$  and  $m$  are all frequency dependent.

$L/(\epsilon \delta)$  is graphed in figure 9 using the bubble size distributions of Medwin at sea state one and Johnson and Cooke at sea state five (figure 7). Except possible between 10 and 20 kHz, figure 9 does not look like the measured spectrums for wind noise, however  $\delta$  and  $\epsilon$  are likely to be increasing functions of frequency and so they may "straighten out" a graph of  $L$  vs. frequency. Furthermore measured spectrums do not extend above 20 kHz. Measured spectrums show an influence of wind as low as 400 Hz. If bubbles are responsible for wind noise then bubbles much larger than those measured in the bubble populations discussed in this paper are needed. To resonant at 400 Hz. a bubble has to have a radius of 9 mm. Such large bubbles could be formed but they would rise



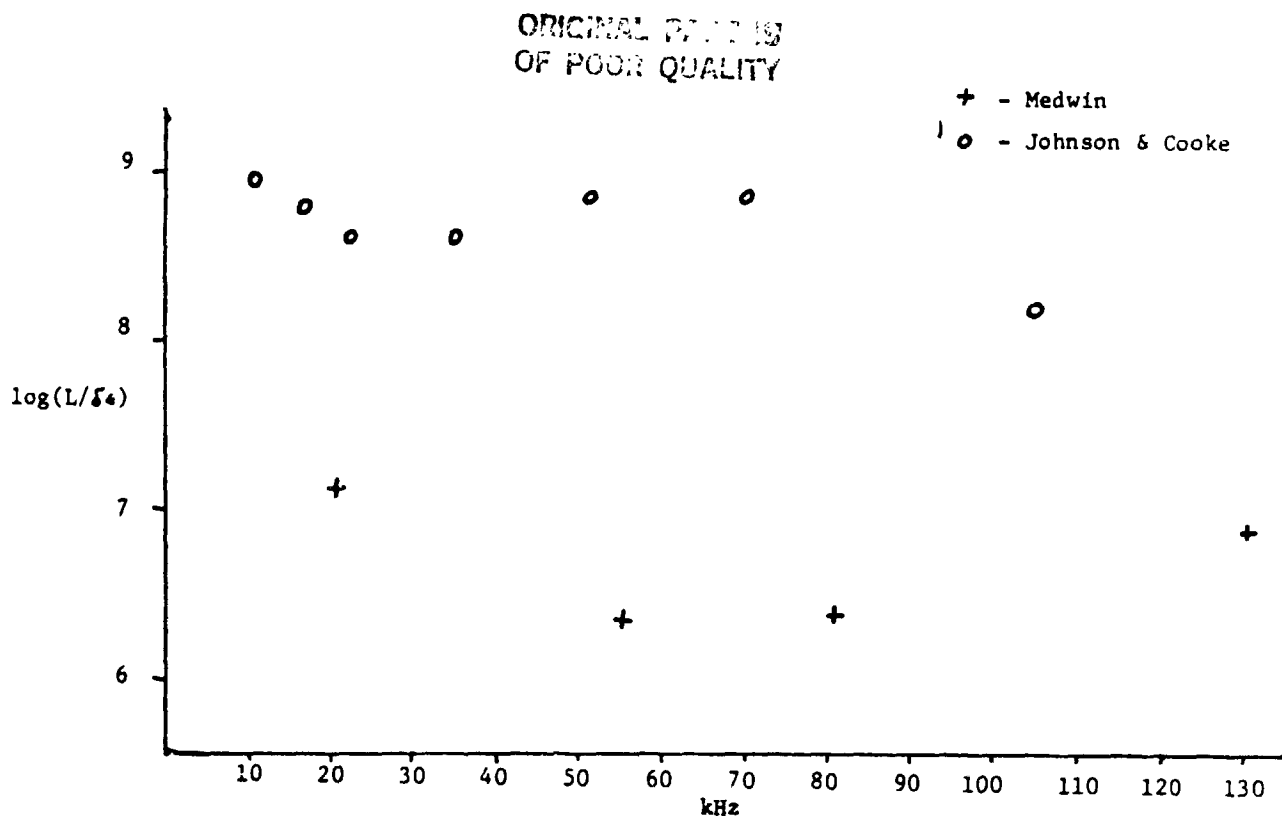


Figure 9. Pressure spectrum from bubbles divided by  $(\delta_a)$

quickly to the surface. The bubble populations mentioned in this paper were measured at depths between 0.7 and 1.8 meters. Large bubbles may not penetrate that deep into the water column. Blanchard and Woodcock deliberately excluded large bubbles from their measurements.

In addition to bubbles there are two other explanations for noise due to wind. Marsh (1963) suggests the Knudsen spectrum is due to pressure fluctuations from surface waves. If this is a mechanism for noise generation it is only applicable at very low frequency. In addition other authors note that the sound spectrum is better correlated with wind speed than wave height. Wilson (1980) suggests the noise from wind is due to sea spray striking the surface. This is a definite noise source but does not have a Knudsen spectral shape. It seems likely that the noise from wind is due to a combination of bubble oscillation and splashing.

The theory of noise generation due to splashing was worked out by Franz (1959). This is obviously the source of noise from rain. Franz studied the entry of individual drops into the water and considered sound production from the impact at the surface, the vibration of the drop as it enters the water, secondary splashes from droplets thrown up by the initial drop, resonant vibration of cavities open to the air and the oscillation of air bubbles entrained by the

ORIGINAL PAGES  
OF POOR QUALITY

drop. He concluded that only the impact at the surface and the oscillation of entrained air bubbles contribute significantly to the observed underwater noise. The magnitude of the impact component varied with fall velocity and drop size, however it was reproducible if those two parameters were fixed. The bubble contribution was not predictable varying in both magnitude and frequency. For a given drop, if a bubble occurs, then the bubble contribution to the sound field is equal to the impact contribution, however bubbles are not usually formed, especially at high impact velocities. For this reason Franz developed a theory for splashes considering only the impact at the surface.

Franz claims that there are two stages to consider for the impact of a raindrop. These are a "supersonic" stage when the drop acts as a simple sound source and a "subsonic" stage when the drop is a dipole source. The duration of the "supersonic" phase is "the time which the rate of growth of the wetted area is supersonic" and is given by

$$(20) \quad t = \frac{au}{2c^2}$$

where  $u$  is the vertical impact velocity,  $a$  is the radius and  $c$  is the speed of sound in water. For an average raindrop  $t = 2 \times 10^{-9}$  seconds. Franz uses geometry to predict the pressure from a drop because of "supersonic" flow:

$$(21) \quad P - P_0 = \left( \frac{e a u^2}{r} \right) \left[ 1 - (t - r/c) \frac{u}{a} \right]$$

The duration of this phase is so short that its influence on the pressure field is questionable.

A drop hitting the surface quickly passes through the phase when it can be considered a simple source. Instead the surface must be considered. The drop looks like a distributed sound source just below the surface (introducing volume) and an image (sink) just above the surface. This may be thought of as a set of simple sources on the rapidly expanding splash and a set of out of phase reflections off the surface which look like a set of sinks just above the surface. The entire splash can be approximated as a dipole source with a vertical axis. If a drop enters the water at an angle then Franz suggests that it be considered a quadrupole source.

The expected pressure at a hydrophone due to splashes is derived in Appendix D as

$$(22) \quad p^2 = \int_{\text{surface}} \frac{3ecI}{2\pi r^2} \cos^2 \Theta \left[ 1 + \left( \frac{c}{2\pi fr} \right)^2 \right] dS$$

where  $\Theta$  is the angle between the vertical and the path connecting the surface patch  $dS$  with the hydrophone. The intensity,  $I$ , is defined as the total water-

borne sound energy per unit time per unit area at the surface. If the hydrophone is directly beneath a circular spray area then (22) can be integrated (Appendix D) to give the mean square pressure as

$$(23) \quad p^2 = \left( \frac{3\rho c I}{2} \right) \left[ (1 - \cos^2 \alpha) + \frac{c^2 (1 - \cos^4 \alpha)}{8 \pi^2 f^2 h^2} \right]$$

where  $h$  is the hydrophone depth and  $\alpha$  is the angle between the vertical and the path between the edge of the splash zone and the hydrophone. The second term in the brackets is a near field correction that can be neglected if the hydrophone is at a sufficient depth below the surface.

The rate at which sound pressure is produced in water is proportional to the kinetic energy of the falling drops. Franz uses

$$(24) \quad I = (1/2) \rho R u^2 M^3 (E/TM^3) ,$$

where  $u$  is the impact velocity,  $R$  is the volume of the drops striking the surface per unit time per unit area,  $M = u/c$  is the mach number,  $E$  is the total sound energy transmitted into the water and  $T$  is the kinetic energy of the drop at impact times the ratio of the liquid density to the droplet density,  $T = (1/2) \rho R u^2 d S d t$ . The ratio  $E/TM^3$  is a measure of the conversion of kinetic energy to acoustic energy and is a function of drop radius, impact velocity and frequency. Franz's experimental determination of this ratio is shown in figure 10.

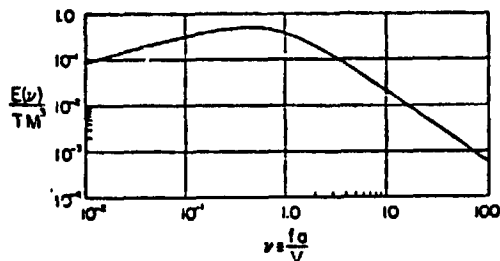


Figure 10.  
Franz (1959)

FIG. 10. The dimensionless spectral density of the sound energy radiated into the water by the impact of single droplets of water or by the splashes of a spray of water droplets.

Neglecting the near field correction term equation (23) can be written in terms of pressure per unit frequency,  $L$ , where  $L$  is in dB relative to  $1 \mu Pa$ .

$$(25) \quad L = 120 + 10 \log \left\{ (3/4) \frac{\rho^2 R u^4 a}{c^2} \left( \frac{E(\omega)}{TM^3} \right) (1 - \cos^2 \alpha) \right\}$$

Equation (25) is for a circular spray area directly above the hydrophone. It can be generalized to give the sound pressure per unit frequency for a small spray area,  $S$ , where the distance between the spray area and the hydrophone is large compared to a linear dimension of  $S$ . It is

ORIGINAL PAGE IS  
OF POOR QUALITY

$$(26) \quad L = 120 + 10 \log \left\{ \frac{3 \rho^2 R u^4 a}{4 c^2} \frac{E(\nu)}{T M^3} \frac{\Omega \cos \theta}{\pi} \right\}$$

where  $\Omega$  is the solid angle subtended by the spray area S. (see Appendix D)

Franz's theoretical prediction for the sound pressure spectrum due to rain is shown in figure 11. The levels in figure 11 are lower than the ambient noise levels observed by Bom (1969) and Heindsman et al. (1955). This may be because those measurements were made in shallow water. The sound spectrum is usually 5 - 10 dB higher in shallow water than in deep water probably because of bottom effects.

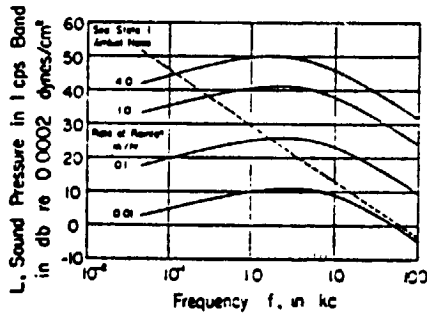


Figure 11.

Franz (1959)

FIG. 11. The estimated sound-pressure-spectrum levels of the underwater sound from the impact of rain on the surface, at depths greater than a wavelength from the surface.

Other Considerations

There are several other influences on the underwater noise levels. One of these is the noise due to marine life, principally snapping shrimp and croakers (a type of fish). Figure 12 shows that over shrimp beds this noise is significant.

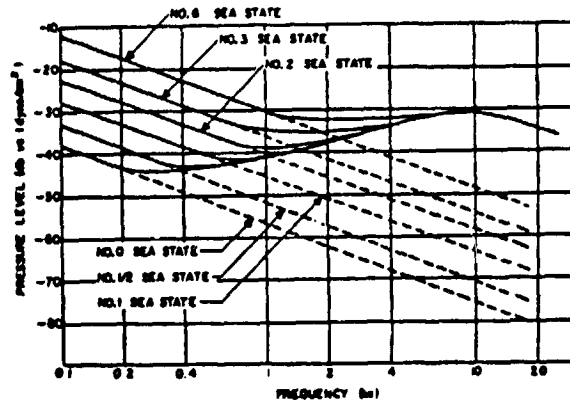


Figure 12.  
Albers (1965)

Fig. 12.8—Average noise spectra over a shrimp bed.

Snapping shrimp and croakers are found mostly in shallow water or harbors and so to eliminate this sound source ambient noise should be monitored in deep water or in locations where these organisms are not active. It is possible that other marine organisms such as porpoises might make an occasional noise at high frequency, however these sounds are usually distinctive and can be easily removed from data.

Ambient noise does show some depth dependence. Perrone (1970) notes that deep ( 5 km) hydrophones record noise levels 4 - 8 dB less than shallower ones, especially at higher frequencies. This is probably due to attenuation (Appendix C). Deep hydrophones would also tend to "average out" the influence of individual breaking waves or very intense, very local rain patches.

Monohan and Zietlow (1969) note that whitecaps last longer in salt water than in fresh water, roughly 50% longer. This may be because there are relatively more small bubbles formed in salt water. As a result the ambient noise levels in fresh and salt water may be different. Temperature also effects the lifetime of whitecaps. As a result of this fact the ambient noise level in cold water may be higher than in warm water.

Noise from breaking surf has not been considered. It is likely to be a large signal where it is present.

ORIGINAL PAGE IS  
OF POOR QUALITY

Conclusion

Monitoring underwater noise levels can be used to detect rain. To quantify rainfall rate requires that we assume the noise due to wind has a well defined spectral shape, the Knudsen spectrum, and that rain noise has a different spectral shape, a white-ish spectrum. The difference in spectral shapes would allow these two noise sources to be separated. Rainfall rate could then be correlated to underwater noise. These spectral shapes have been observed experimentally but a better understanding of the physics of sound generation by wind and rain is desirable.

Appendix A : General Acoustic Theory (Lighthill, 1978)

1. Wave Equation

The momentum and continuity equations are given as

$$(A1) \quad \frac{\partial \bar{u}}{\partial t} + \bar{u} \cdot \nabla \bar{u} = -\frac{1}{\rho} \nabla P$$

$$\frac{\partial \rho}{\partial t} + \nabla \cdot (\rho \bar{u}) = 0$$

These can be linearized to give

$$(A2) \quad \rho_0 \frac{\partial \bar{u}}{\partial t} = -\nabla P$$

$$\frac{\partial \rho}{\partial t} = -\rho_0 \nabla \cdot \bar{u}$$

Introduce a velocity potential,  $\phi$ , such that

$$(A3) \quad \bar{u} = \nabla \phi$$

Use (A3) to rewrite (A2) as

$$(A4) \quad P - P_0 = -\rho_0 \frac{\partial \phi}{\partial t}$$

$$\frac{\partial \rho}{\partial t} = -\rho_0 \nabla^2 \phi$$

Now assume  $P = P(\rho)$  and expand about  $\rho_0$ .

$$(A5) \quad P = P(\rho_0) + (\rho - \rho_0) P'(\rho_0) + \dots \quad \text{which means}$$

$$(A6) \quad \frac{\partial P}{\partial t} = P'(\rho_0) \frac{\partial \rho}{\partial t}$$

Use (A6) to convert (A4) into the wave equation

$$(A7) \quad \frac{\partial^2 \phi}{\partial t^2} = c^2 \nabla^2 \phi$$

where  $c = \sqrt{P'(\rho_0)}$  is the speed of sound.

2. Simple Source

An oscillating bubble may be thought of as a simple sound source. For a simple source

$$(A8) \quad \phi = \phi(t, r)$$

Using (A8), equation (A7) can be written in spherical coordinates as

$$(A9) \quad \frac{\partial^2}{\partial t^2} (r\phi) = c^2 \frac{\partial^2}{\partial r^2} (r\phi)$$

which has the general solution

ORIGINAL PAGE IS  
OF POOR QUALITY

$$(A10) \quad r\phi = f(r - ct) + g(r + ct)$$

The bubble is a source (outward moving wave) and so let  $g = 0$ . Our solution is

$$(A11) \quad \phi = \frac{-m(t - r/c)}{4\pi r}$$

where  $m(t)$  signifies the volume outflow from the source (source strength).

Combining (A4) with (A11) gives

$$(A12) \quad P - P_0 = \dot{q}(t - r/c) \frac{1}{4\pi r}$$

$$q(t) = \rho_0 m(t)$$

This is the fundamental equation for a simple source.

### 3. Acoustic Intensity, Dipole Source

At a distance  $r$  from the source the flow through the area  $4\pi r^2$  is

$$(A13) \quad 4\pi r^2 \frac{\partial \phi}{\partial r} = m(t - r/c) + (r/c) \dot{m}(t - r/c) \quad \text{by eqn. (A11)}$$

Combining (A13) with (A12) gives

$$(A14) \quad u_r = \frac{\partial \phi}{\partial r} = (\rho_0 c)^{-1} \frac{1}{4\pi r} [ \dot{q}(t - r/c) + (c/r) q(t - r/c) ]$$

Far from the source only the first term in brackets is important and so

$$(A15) \quad u_r = (\rho_0 c)^{-1} (P - P_0)$$

Acoustic intensity,  $I$ , is defined as the rate of transport of acoustic energy and is given as

$$(A16) \quad \bar{I} = (P - P_0) \bar{u}$$

In the far field the acoustic intensity of a simple source is

$$(A17) \quad I = (\rho_0 c)^{-1} (P - P_0)^2$$

This equation is also valid as an linearization of the far field acoustic intensity of a dipole. The far field pressure from a dipole source is found by considering a simple sink and a simple source separated by a small distance  $l \ll r$ .

$$(A18) \quad P - P_0 = [ \dot{q}(t - r/c) \frac{1}{4\pi r} ] - [ \dot{q}(t - r'/c) \frac{1}{4\pi r'} ]$$

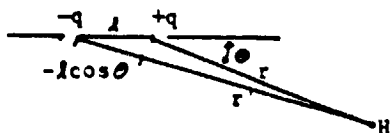


Figure A1.

By geometry (figure A1), the distance  $r - r'$  is approximated by  $-l \cos \theta$  and so (A18) can be expressed as a derivative.

$$(A19) \quad P - P_0 = (-l \cos \theta) \frac{\partial}{\partial r} [ \dot{q}(t - r/c) \frac{1}{4\pi r} ] \quad \text{or}$$



ORIGINAL PAGE IS  
OF POOR QUALITY

$$(A19) \quad P - P_0 = \cos \theta \left[ \lambda \dot{q}(t - r/c) \frac{1}{4\pi r^2} + \lambda \ddot{q}(t - r/c) \frac{1}{4\pi r c} \right]$$

In the far field ( $\omega r/c \gg 1$ ), (A19) reduces to

$$(A20) \quad P - P_0 = \frac{\cos \theta}{4\pi r} \frac{\lambda \ddot{q}}{c}$$

Appendix B : Acoustic Theory of Bubbles

1. Sound Pressure from a Bubble

Lighthill suggests that for sound from an oscillating bubble that equation (A13) be written as

$$(B1) \quad m(\dot{r}) = 4\pi r^2 \frac{\partial \phi}{\partial r} = \dot{v}(t)$$

where  $v(t)$  is the volume of the bubble.

When (B1) is combined with (A12) we get the form given in the text.

$$(B2) \quad P - P_0 = \frac{\rho \dot{v}(t)}{4\pi r}$$

2. Resonant Frequency of a Bubble

If the bubble is small enough the pressure outside the bubble will be equal to the pressure inside the bubble. Consider a fluctuating external pressure field of the form

$$(B3) \quad P_e(t) = P_0 + P_a e^{-i\omega t}$$

The velocity potential outside an oscillating bubble has the form

$$(B4) \quad \phi = \frac{A}{r} e^{i(kr - \omega t)}$$

which is related to pressure by equation (A4). Inside the bubble

$$(B5) \quad PV^\gamma = \text{constant}$$

where  $\gamma$  is the ratio of specific heats in the bubble.  $\gamma = 1.4$  for air bubbles in water. Differentiating (B5) gives

$$(B6) \quad \frac{dP}{dt} = -\frac{P_0 \gamma}{V_0} \frac{dv}{dt} = -\frac{3\gamma P_0}{a_0} \frac{da}{dt}$$

where  $a(t)$  is the bubble radius and  $a_0$  is the equilibrium bubble radius.

Substituting (B3) into (B6) the pressure inside the bubble is

$$(B7) \quad P_{\text{inside}} = P_0 - i \frac{3\gamma P_0 \dot{a}}{a_0 \omega}$$

Continuity of pressure at the surface of the bubble implies

$$(B8) \quad P_0 - i \frac{3\gamma P_0 \dot{a}}{a_0 \omega} = P_{\text{outside}} \Big|_{r=a} = P_0 + P_a e^{-i\omega t} + i \frac{\rho A \omega}{a} e^{ika - i\omega t}$$

which simplifies to

$$(B9) \quad -i \frac{3\gamma P_0 \dot{a}}{a_0 \omega} = (P_a + \frac{\rho A}{a} i\omega) e^{-i\omega t}$$

if we assume  $e^{ika} = 1$ .

The radial velocity,  $\dot{a}$ , at the bubble surface is also continuous and so from (B4)

$$(B10) \quad \ddot{a} = \frac{\partial^2 p}{\partial r^2} \Big|_{r=a} = A(ik/a - 1/a^2) e^{-i\omega t}$$

Combining (B9) and (B10) gives

$$(B11) \quad P_a + \frac{\rho i \omega}{a} A = \frac{3\gamma P_0}{a^2 c} A + i \frac{3\gamma P_0}{a^3 \omega} A$$

where  $c = \omega/k$  is the sound velocity. Solving for A gives

$$(B12) \quad A = \frac{P_a \left( \frac{a}{i\omega \rho} \right)}{\left( \frac{\omega_0}{\omega} \right)^2 - 1 - \frac{B}{\omega}}, \quad \text{where}$$

$$(B13) \quad \omega_0 = \frac{1}{a} \sqrt{\frac{3\gamma P_0}{\rho}} \quad \text{and}$$

$$(B14) \quad B = \frac{3\gamma P_0}{ac \rho} \quad \text{is the radiation resistance load on a}$$

spherical surface. Equation (B13) defines the resonance frequency for a bubble and is mentioned as equation (10) in the text. Equation (15) is derived by substituting (B12) into (A4).

### 3. Amplitude of Oscillation

Assume that the radius of an oscillating bubble is given by

$$(B15) \quad a = a_0 + (\epsilon a_0) e^{-i\omega t}$$

where  $\epsilon a_0$  is the amplitude of oscillation and  $\epsilon$  is a small parameter that is probably frequency dependant. The pressure inside the bubble can be written as

$$(B16) \quad P_{\text{inside}} = P_0 + P_1 e^{-i\omega t}$$

Using (B6) this is equal to

$$(B17) \quad P_{\text{inside}} = P_0 + \frac{3\gamma P_0}{a i \omega} \dot{a}$$

From (A4) and (B4) the pressure outside the bubble is

$$(B18) \quad P_{\text{outside}} = P_0 + \frac{\rho A}{r} i \omega e^{-i\omega t}$$

Applying continuity of pressure at  $r = a$  and substituting for  $\dot{a}$  using (B15), it is possible to solve for A using (B17) and (B18).

$$(B19) \quad A = \frac{3\gamma P_0 a \epsilon}{\rho \omega} i$$

Therefore from (A4) and (B4) the pressure due to an oscillating bubble at a distance  $r$  from the bubble is given as

$$(B20) \quad P = - \frac{3 \gamma P_0 a_0 \epsilon}{r} e^{i k r - i \omega t}$$

This means that the amplitude of oscillation is

$$(B21) \quad P_s = \frac{3 \gamma P_0 (\epsilon a_0)}{r}$$

which is a form mentioned by Strasberg (1956) and Wenz (1962). The root mean square pressure is

$$(B22) \quad P_{rms} = \frac{3 \gamma P_0 \epsilon a_0}{2r}$$

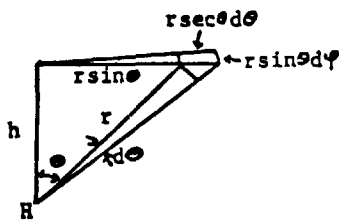
#### 4. Sound Spectrum due to Bubbles at the Ocean Surface

Starting with equation (17) of the text.

$$(B23) \quad (P - P_0)_{rms-h} = \int_{BSD} \int_{surface} (P - P_0)_{rms-b} \delta(a) D(a) e^{-mr} dA da$$

Substituting for  $(P - P_0)_{rms-b}$  (equation B22) and for  $dA$ , (B23) becomes

$$(B24) \quad P - P_0 = \int_{BSD} \int_0^{2\pi} \int_0^{\pi/2} \left( \frac{3}{2} \gamma P_0 \epsilon a_0 \right) \frac{1}{r} \delta(a) D(a) e^{-mr} (r^2 \tan \theta d\theta d\varphi) da$$



The hydrophone depth,  $h$ , equals  $r \cos \theta$   
and so

Figure B1.

$$(B25) \quad P - P_0 = \int_{BSD} \left( \frac{3}{2} \gamma P_0 \epsilon a_0 \right) \delta D(a) \int_0^{2\pi} \int_0^{\pi/2} \frac{h \sin \theta}{\cos^2 \theta} e^{-mh \sec \theta} d\theta d\varphi da$$

By substitution,  $x = \sec \theta$ , this becomes

$$(B26) \quad P - P_0 = \int_{BSD} 3 \gamma P_0 \epsilon a_0 \pi \delta D(a) \int_1^{\infty} h e^{-mhx} dx da$$

and so

$$(B27) \quad P - P_0 = \int_{BSD} (3 \gamma P_0 \pi) \epsilon a \delta D(a) (1/m) e^{-mh} da$$

Note: BSD = bubble size distribution

ORIGINAL PAGE IS  
OF POOR QUALITY

Appendix C : Attenuation of Sound in Sea Water (Urlick, 1975)

Attenuation of acoustic intensity is exponential.

$$(C1) \quad I_2 = I_1 e^{-nr}$$

Urlick describes attenuation as total intensity loss (TL) in decibels.

$$(C2) \quad TL = 10 \log (I_1/I_2) = 10 \log_{10} e (nr)$$

Urlick defines a logarithmic absorption coefficient,  $\alpha$ , as

$$(C3) \quad \alpha = 10 n \log_{10} e = 4.35 n$$

Attenuation of sound in sea water is primarily from three processes. These are shear viscosity, volume viscosity and the ionic relaxation of magnesium sulfate ions. Shear viscosity accounts for one third of the absorption actually measured in distilled water. It was first studied by Rayleigh who concluded that

$$(C4) \quad \alpha = \frac{16 \pi^2 \mu_s}{3 \rho c^3} f^2$$

where  $\mu_s$  is the shear viscosity coefficient = 0.01 in water. Volume viscosity accounts for two thirds of the absorption in distilled water and is given by

$$(C5) \quad \alpha = \frac{4 \pi^2}{\rho c^3} \mu_v f^2$$

where  $\mu_v$  is the volume viscosity coefficient = 0.028. The ionic relaxation of  $MgSO_4$  is a dissociation - reassociation process, involving a finite time interval called the relaxation time, in which the  $MgSO_4$  ions in solution dissociate under the pressure of a sound wave. Urlick gives the total absorption coefficient for sea water as

$$(C6) \quad \alpha = A \frac{S f_T f^2}{f_T^2 + f^2} + B \frac{f^2}{f_T^2} \quad \text{in dB/kyd}$$

where

$A = 1.86 \times 10^{-2}$ , a constant  
 $B = 2.68 \times 10^{-2}$ , a constant  
 $S$  = salinity in parts per mille (‰)  
 $f$  = frequency in kilohertz  
 $f_T = 21.9 \times 10^{(6 - 1520/T)}$ , the relaxation frequency in kilohertz  
and  $T$  = temperature in degrees Kelvin

Figure C1 is a graph of theoretical curves.

Figure C1.  
Urlick (1975)

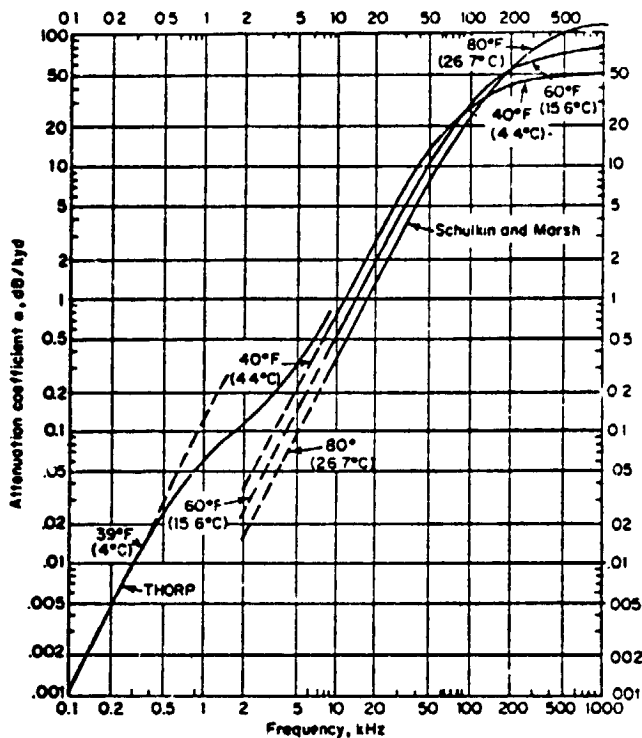


fig. 88 Attenuation coefficient in seawater as a function of frequency and temperature, according to the formulas of Thorp and Schulkin and Marsh for a salinity of 35 ppt.

For this paper attenuation is expressed as

$$(C7) \quad (P_2 - P_{20}) = (P_1 - P_{10}) e^{-mr} \quad \text{or}$$

$$(C8) \quad TL = 20 \log \left( \frac{P_1 - P_{10}}{P_2 - P_{20}} \right) = 20 mr \log_{10} e = \alpha r$$

and so

$$(C9) \quad m = 0.115 \alpha$$

Appendix D : Acoustic Theory of Spray (Franz, 1959)

1. Energy Radiated by a Single Splash

A splash striking the water surface acts like an acoustic dipole source (Appendix A). The intensity (energy flux) measured at a hydrophone at a distance  $r$  from the drop is determined from equations (A17) and (A20):

$$(D1) \quad I_s = \frac{1}{\rho c} \left( \frac{\cos^2 \theta}{16 \pi^2 r^2} \right) \left( \frac{1}{c^2} \frac{d^2 q}{dt^2} \right)$$

where  $\theta$  can now be thought of as the angle between the vertical and a path connecting the hydrophone and the splash. The total energy radiated into the water is found by integrating  $I_s$  over a hemisphere of radius  $r$ .

$$(D2) \quad E_s = \int_{-\infty}^{\infty} \int_{\text{hemisphere}} \frac{1}{\rho c} \left( \frac{\cos^2 \theta}{16 \pi^2 r^2} \right) \left( \frac{1}{c^2} \frac{d^2 q}{dt^2} \right) dS dt$$

$$= \int_{-\infty}^{\infty} \int_0^{2\pi} \int_0^{\pi/2} \frac{1}{\rho c} \left( \frac{1}{c^2} \frac{d^2 q}{dt^2} \right) \frac{\cos^2 \theta \sin \theta}{16 \pi^2} d\theta d\varphi dt$$

since  $dS = r^2 \sin \theta d\theta d\varphi$ . Equation (D2) is integrated to give

$$(D3) \quad E_s = \frac{1}{\rho c} \frac{1}{24 \pi} \int_{-\infty}^{\infty} \left( \frac{1}{c^2} \frac{d^2 q}{dt^2} \right) dt$$

Substituting back in for  $(P - P_0)^2$  (eqn. A20) we get

$$(D4) \quad E_s = \frac{1}{\rho c} \frac{2 \pi r^2}{3 \cos^2 \theta} \int_{-\infty}^{\infty} (P - P_0)^2 dt$$

where  $(P - P_0)$  is the pressure measured at the hydrophone.

2. Mean Square Pressure from Spray

The total acoustic energy radiating into the water from a spray can be written as

$$(D5) \quad E = \int_t \int_S I dS dt$$

where  $I$  is the total water-borne sound energy per unit area per unit time at the free surface. Equations (D4) and (D5) can be combined to give

$$(D6) \quad (P - P_0)^2 = \int_{\text{surface}} \frac{3 \rho c I}{2 \pi r^2} \cos^2 \theta dS$$

We have integrated over all drops hitting the surface. Franz included a near-field correction term in his equation. His experimental apparatus required such a

ORIGINAL PAGE IS  
OF POOR QUALITY.

term. When the near-field correction term is included (D6) becomes

$$(D7) \quad (P - P_0)^2 = \int_{\text{surface}} \frac{3 \rho c I}{2 \pi r^2} \cos^2 \theta \left[ 1 + \left( \frac{c}{2 \pi f r} \right)^2 \right] dS$$

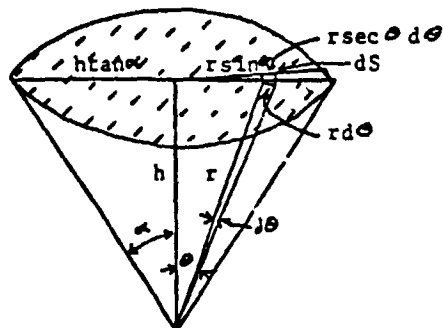


Figure D1.

A circular splash area of radius  $h \tan \alpha$  as show in figure D1 is the first case considered. In this case

$$(D8) \quad dS = (r \sec \theta d\theta)(r \sin \theta d\phi)$$

Equation (D7) becomes

$$(D9) \quad (P - P_0)^2 = \frac{3 \rho c I}{2} \int_0^\alpha \int_0^{2\pi} \frac{\sin \theta \cos \theta}{\pi} \left[ 1 + \left( \frac{c}{2 \pi f r} \right)^2 \right] d\theta d\phi$$

$$= \frac{3 \rho c I}{2} \left[ (1 - \cos^2 \alpha) + \frac{c^2 (1 - \cos^4 \alpha)}{8 \pi^2 f^2 h^2} \right]$$

Again, the second term in (D9) is a near field correction term that can be neglected if the hydrophone is many wave lengths under the surface,  $h \gg c/2 \pi f$ .

L is defined as the sound pressure in an one hertz band relative to 1  $\mu$ Pa. The sound energy in an one hertz band can be written as  $E(f)df$ . This can also be written as

$$(D10) \quad E(\nu) d\nu = E(\nu) \frac{a}{u} df$$

where  $\nu = \frac{af}{u}$ . From the definition of L

$$(D11) \quad L = 20 \log \frac{P_2}{P_1} = 20 \log P_2 - 20 \log P_1 = -35 + 20 \log P_2$$

Equation (25) of the text is derived by combining the far field approximation of equation (D9) with equations (24) and (D11).



ORIGINAL PAGE IS  
OF POOR QUALITY

$$(D12) \quad L = 120 + 10 \log \left[ \left( \frac{3}{4} \right) \frac{e^{2R} u^4 a}{c^2} \left( \frac{E(\omega)}{TM^3} \right) (1 - \cos^2 \alpha) \right]$$

In order to calculate the ambient noise from a small spray area, S, we need to assume that r is large compared to a linear dimension of S.

Equation (D6) becomes

$$(D13) \quad (P - P_0)^2 = \frac{3ec}{2\pi} I \cos^2 \theta \frac{S}{r^2}$$

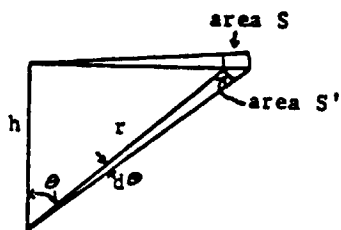


Figure D2.

The solid angle subtended by the rain area is

$$(D14) \quad \Omega = \frac{S''}{r^2} = \frac{S \cos^3 \theta}{h^2}$$

Solve (D14) for S and substitute into equation (D13) to get the sound pressure spectrum from a small patch of spray.

$$(D15) \quad L = -35 + 10 \log \left\{ \frac{3e^{2R} u^4 a}{4c^2} \left( \frac{E(\omega)}{TM^3} \right) \frac{\Omega \cos \theta}{\pi} \right\}$$

## REFERENCES

ORIGINAL PAGE IS  
OF POOR QUALITY

- Albers, V.M., 1965: Underwater Acoustics Handbook II, Penn State Press.
- Arase, E.M. and T. Arase, 1965: Correlation of Ambient Sea Noise.  
J. Acous. Soc Amer. 40, 205-210.
- Arase, T. and E.M. Arase, 1968: Deep Sea Ambient Noise Statistics.  
J. Acous. Soc. Amer. 44, 1679-1684.
- Atlas, D. and C.W. Ulbrich, 1977: Path and Area-integrated Rainfall Measurements by Microwave Attenuation in the 1-3 cm Band. J. Applied Meteor. 16, 1322-1331.
- Blanchard, D.C. and A.H. Woodcock, 1957: Bubble Formation and Modification in the Sea and its Meteorological Significance. Tellus 9, 145-158.
- Bom, N., 1968: Effect of Rain on Underwater Noise Level. J. Acous. Soc. Amer. 45, 150-156.
- Evans, D., 1980: personal letter.
- Foote, G.B. and P.S. duToit, 1969. Terminal Velocity of Raindrops Aloft. J. Applied Meteor. 8, 249-253.
- Franz, G.J., 1959: Splashes as Sources of Sound in Liquids. J. Acous. Soc. Amer 31, 1080-1096.
- Frish, W.L., 1965: Sea Noise vs. Near and Distant Wave Height and Wind Speed. NEL Report #1390.
- Glotov, V.P., P.A. Kolobaev and G.G. Neumin, 1962: Investigation of the Scattering of Sound by Bubbles Generated by an Artificial Wind in Sea Water. Soviet Physics-Acoustics 7, 341-345.
- Heindsman, T.E., R.H. Smith and A.D. Arneson, 1955: Effect of Rain upon Underwater Noise Levels. J. Acous. Soc. Amer. 27, 378-379.

ORIGINAL PAGE IS  
OF POOR QUALITY

S  
Y

- Johnson, B.D. and R.C. Cooke, 1979: Bubble Population and Spectra in Coastal Waters: A Photographic Approach. *J. Geophys. Res.* 84, 3761-3766.
- Kidder, S.Q. and T.H. Vanderhaar, 1977: Seasonal Oceanic Precipitation Frequencies from Nimbus 5 Microwave Data. *J. Geophys. Res.* 82, 2083-2086.
- Knudsen, V.O., R.S. Alford and J.W. Emling, 1948: Underwater Ambient Noise. *J. Mar. Res.* 1, 410-429.
- Lighthill, J., 1978: Waves in Fluids, Cambridge Univ. Press.
- Marsh, H.W., 1963: Origin of the Knudsen Spectra. *J. Acous. Soc. Amer.* 35, 409-410.
- Medwin, H., 1970: In situ Acoustic Measurements of Bubble Populations in Coastal Ocean Water. *J. Geophys. Res.* 75, 599-611.
- Mellen, R.H., 1952: The Thermal Noise Limit in the Detection of Underwater Acoustic Signals. *J. Acous. Soc. Amer.* 24, 478-480.
- Monahan, E.C., 1971: Oceanic Whitecaps. *J. Phys. Ocean.* 1, 139-144.
- Monahan, E.C., 1979: Whitecapping: A Manifestation of Air-Sea Interaction with Implications for Remote Sensing. Primars-1 workshop, Univ. of Manchester, June 1979.
- Monahan, E.C. and K.L. Davidson, 1979: Preliminary Intercomparison of JASIN Wind, Whitecap and Aerosol Observations. JASIN Data Display Meeting, WHOI, 21-25 May 1979.
- Monahan, E.C. and I.O. Muircheartaigh, 1980: Optimal Power Law Description of Oceanic Whitecap Coverage Dependence on Wind Speed. *J. Phys. Ocean.* 10, 2094-2099.
- Monahan, E.C. and C.R. Zietlow, 1969: Laboratory Comparison of Freshwater and Salt-water Whitecaps. *J. Geophys. Res.* 74, 6961-6966.

- Morris, G.B., 1978: Depth Dependence of Ambient Noise in the Northeastern Pacific Ocean. *J. Acous. Soc. Amer.* 64, 581-590.
- Morse, P.M. and H. Feshback, 1953: Methods of Theoretical Physics, McGraw-Hill Book Co.
- Perrone, A.J., 1969: Deep-Ocean Ambient Noise Spectra in the Northeast Atlantic. *J. Acous. Soc. Amer.* 46, 762-770.
- Perrone, A.J., 1970: Ambient Noise Spectrum Levels as a Function of Water Depth. *J. Acous. Soc. Amer.* 48, 362-370.
- Piggott, C.L., 1965: Ambient Sea Noise at Low Frequencies in Shallow Water of the Scotian Shelf. *J. Acous. Soc. Amer.* 36, 2152-2163.
- Reed, R.K. and W.P. Elliott, 1973: Precipitation at Ocean Weather Stations in the North Pacific. *J. Geophys. Res.* 78, 7087-7091.
- Shaw, P.T., D.R. Watts and H.T. Rossby, 1978: On the Estimation of Oceanic Wind Speed and Stress from Ambient Noise Measurements. *Deep Sea Res.* 25, 1225-1233.
- Strasberg, M., 1956: Gas Bubbles as Sources of Sound in Liquids. *J. Acous. Soc. Amer.* 28, 20-26.
- Thorpe, S.A. and D.N. Humphries, 1980: Bubbles and Breaking Waves. *Nature* 283, 463-465.
- Thorpe, S.A. and A.R. Stubbs, 1979: Bubbles in a Freshwater Lake. *Nature* 279, 403-405.
- Ulbrich, C.W. and D. Atlas, 1978: The Rain Parameter Diagram: Methods and Applications. *J. Geophys. Res.* 83, 1319-1325.
- Urick, R.J., 1975: Principles of Underwater Sound, McGraw-Hill Book Co.
- Wenz, G.M., 1962: Acoustics Ambient Noise in the Oceans: Spectra and Sources. *J. Acous. Soc. Amer.* 34, 1936-1956.

ORIGINAL PAGE IS  
OF POOR QUALITY

N83 25303

D34

ORIGINAL PAGE IS  
OF POOR QUALITY

ON THE MEASUREMENT OF PRECIPITATION FREQUENCIES  
BY PASSIVE MICROWAVE RADIOMETRY

Stanley Q. Kidder

Laboratory for Atmospheric Research  
University of Illinois  
Urbana IL 61801

1. INTRODUCTION

Knowledge of global precipitation is of fundamental importance to the study of climate and climate dynamics. Any program to observe climate with satellite instrumentation must include precipitation measurements. Many such attempts have been made, starting from the earliest observation of reflected solar radiation. Since rain falls from clouds, knowledge of cloud location is a first step toward precipitation estimation. However, most clouds are not raining. One must look, then, to information other than simply the presence of clouds to determine precipitation. Among the attributes utilized for this purpose are visible brightness, cloud type, cloud area, and cloud growth rate. With the introduction of infrared observations, more parameters became available for study: cloud top temperature, time rate of change of temperature, and growth rate the area enclosed by selected isotherms. Martin and Scherer (1973) have summarized many of these techniques. The principal difficulty with these methods of estimating precipitation is that none of them directly sense raindrops. The instruments sense only the top-most part of the cloud, and precipitation must be inferred. With the launch of Nimbus 5 in December 1972 and Nimbus 6 in June 1975, observations became available in a new window, the radio window. In the vicinity of 1 cm clouds are nearly transparent, but raindrops interact strongly with the radiation stream. Thus it is possible to directly sense the presence of precipitation-size drops. The thesis of this paper is that these simple, direct measurements of precipitation should be part of any future climate observing system.

2. PRECIPITATION FREQUENCIES

The first microwave images of the earth (e.g. Theon, 1973; Allison et al., 1974; Wilheit et al., 1976) offered the exciting possibility of measuring precipitation over the ocean.

Precipitating areas such as the ITCZ and frontal systems appeared distinctly grey against the white background of the ocean. Scattering calculations soon appeared (Wilheit et al., 1977) which gave the rainfall rate over the ocean as a function of microwave brightness temperature and freezing level (used as an indicator of the thickness of the rain layer.) The initial enthusiasm waned somewhat, however, when it was discovered that rainfall was being underestimated, largely because of the beam filling problem. The footprint of the Nimbus 5 Electrically Scanning Microwave Radiometer (ESMR5) is about 500 km<sup>2</sup>--much larger than the scale of many precipitation shafts. Due to the nonlinearity of the calibration curve, this results in an underestimation of the rainfall rate. Adler and Rodgers (1977) were forced to use an empirical (higher) calibration curve to estimate precipitation in tropical storms, for example.

Frequently overlooked, however, is the fact that passive microwave observations do a good job in defining the area of precipitation. Comparison with radar echos showed that ESMR5 data matched the echo areas well (Fig. 1). Kidder and Vonder Haar (1977), using a simple thresholding technique, analyzed three months of ESMR5 data during the period December 1972 through February 1973 to calculate the frequency of precipitation in the tropical oceans (Fig. 2). Their calculations compared favorably with both climatology and independent observations of the frequency of highly reflective clouds (Ramage, 1975).

Detecting precipitation over land is complicated by nonuniformity of background and lack of contrast; light rain and warm ground both appear dark (warm) in ESMR5 images. These problems were partially solved by the ESMR on Nimbus 6 (ESMR6). It had a higher frequency (37 GHz versus 19 GHz) which caused brightness temperature to decrease rapidly with rainfall rate. Thus rain appears bright (cold) against the background of warm earth. ESMR6 also

ORIGINAL PAGE IS  
OF POOR QUALITY

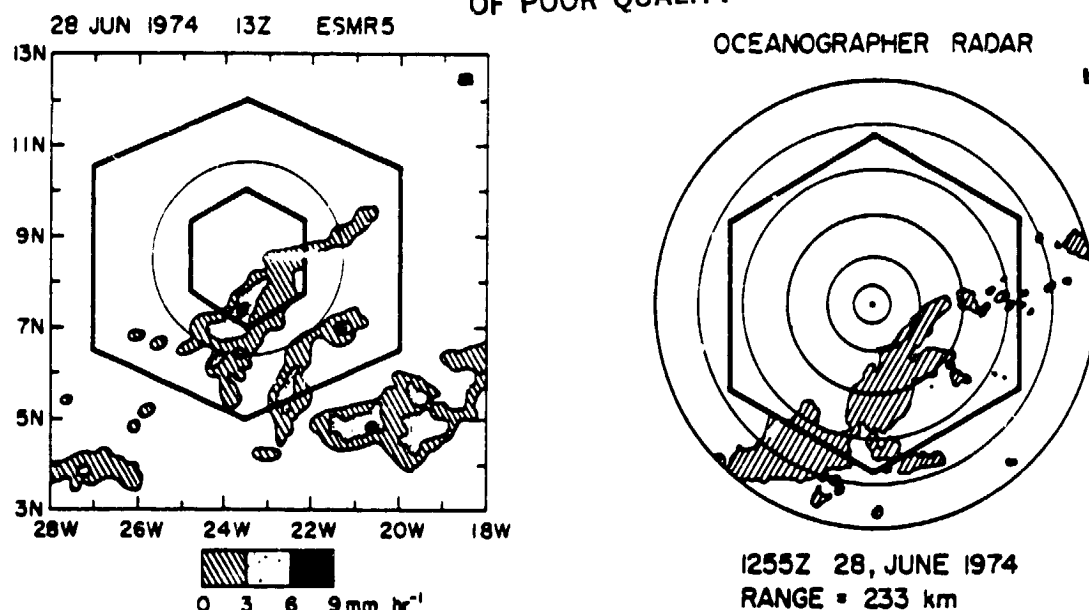


FIGURE 1. (a) Precipitation rate over the GATE array as estimated from Nimbus 5 ESMR data. (b) Nearly-coincident radar data from the ship Oceanographer. The

circle in (a) is the 233 km range of the radar. (After Kidder and Vonder Haar, 1976.)

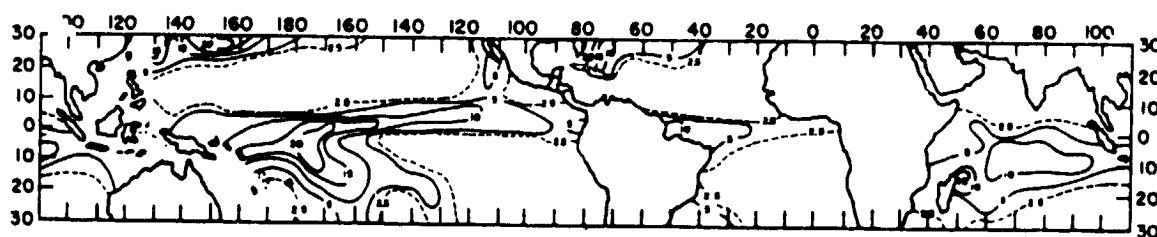


FIGURE 2. Precipitation frequencies from the period December 1972 through February 1973 as estimated from Nimbus 5 ESMR

data. (After Kidder and Vonder Haar, 1977.)

made dual polarization measurements, which could be used to separate rain from standing water. Durkee (1980), using a statistical technique to determine a threshold temperature and polarization differences to eliminate water surfaces, was able to define raining areas in the north central U.S. during the summer of 1975 (Fig. 3). He also was successful at determining precipitation frequencies (Fig. 4). Rodgers et al. (1979), also using a statistical technique, mapped raining areas in the southeastern U.S. They found, however, that dew and wet ground could cause problems.

There still remain situations in which passive microwave radiometry has not been used to detect precipitation. Frozen precipitation is not well-detected, and liquid precipitation over cold land ( $T$  less than 288 K) has not been measured. It is hoped, however,

that new instruments such as LAMMR (Large Antenna Multifrequency Microwave Radiometer) plus additional research will solve these problems.

### 3. CONCLUSIONS

For climate monitoring it is necessary to employ stable, accurate, long-lived instruments. Electrically scanning microwave radiometers, which have no moving parts, have shown themselves to be such instruments on Nimbus 5 and Nimbus 6. In addition, there must exist proven retrieval algorithms which yield useful parameters. Precipitation frequency is not as immediately attractive as precipitation amount, but it is adequate for many climate purposes. The statistical retrieval algorithms for precipitation frequency have shown good results in two

ORIGINAL PAGE IS  
OF POOR QUALITY

situations, and may be expected to yield adequate results in others. Based on all of these factors, it is reasonable to suggest that whatever instrumentation is chosen for the climate observing system, one of its major goals should be the measurement of precipitation frequencies by passive microwave radiometry.

References

- Adler, R.F., and E.B. Rodgers, 1977: Satellite-observed latent heat release in a tropical cyclone. Mon. Wea. Rev., 105, 956-963.
- Allison, L.J., E.B. Rodgers, T.T. Wilheit, and R.W. Fett, 1976: Tropical cyclone rainfall as measured by the Nimbus 5 electrically scanning microwave radiometer. Bull. Amer. Meteorol. Soc., 55, 1074-1089.
- Durkee, P.A., 1980: Summer precipitation frequency of the North Central U.S. from satellite microwave observations. M.S. Thesis, Colorado State Univ., 67 pp.
- Kidder, S.Q., and T.H. Vonder Haar, 1976: A comparison of satellite rainfall-estimation techniques over the GATE area. Proceedings Vol., COSPAR Symposium on Meteorological Observations from Space, Philadelphia, 123-125.
- Kidder, S.Q., and T.H. Vonder Haar, 1977: Seasonal oceanic precipitation frequencies from Nimbus 3 microwave data. J. Geophys. Res., 82, 2083-2086.
- Martin, D.W., and W.D. Scherer, 1973: Review of Satellite rainfall estimation methods. Bull. Amer. Meteor. Soc., 54, 661-674.
- Ramage, C.S., 1975: Preliminary discussion of the meteorology of the 1972-1973 El Nino. Bull. Amer. Meteorol. Soc., 56, 234-242.
- Rodgers, E.B., H. Siddalingaiah, A.T.C. Chang, and T.T. Wilheit, 1979: A statistical technique for determining rainfall over land employing Nimbus 6 ESMR measurements. J. Appl. Meteorol., 18, 978-991.
- Theon, J.S., 1973: A multispectral view of the Gulf of Mexico. Bull. Amer. Meteorol. Soc., 54, 934-937.
- Wilheit, T.T., J.S. Theon, W.E. Shenk, L.J. Allison, and E.B. Rodgers, 1976: Meteorological interpretations of the images from the Nimbus 5 electrically scanning radiometer. J. Appl. Meteorol., 15, 166-172.
- Wilheit, T.T., A.T.C. Chang, M.S.V. Rao, E.B. Rodgers, and J.S. Theon, 1977: A satellite technique for quantitatively mapping rainfall rates over the oceans. J. Appl. Meteorol., 16, 551-560.

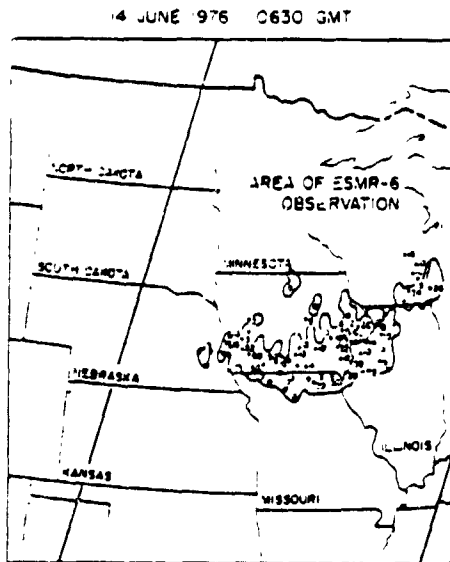


FIGURE 3. A comparison of precipitation area (solid line) determined from Nimbus 6 ESMR data with raingage data (hundredths of an inch) for the hour during which the satellite passed. (After Durk 1980.)

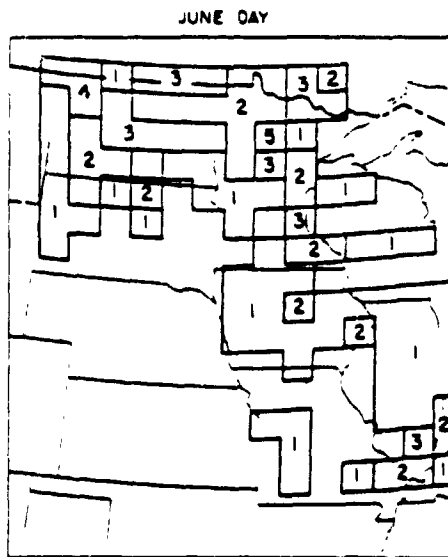


FIGURE 4. Precipitation occurrences during June 1976 as determined from Nimbus 6 ESMR data. (After Durkee, 1980.)

D35  
N83 25304

ORIGINAL PAGE 19  
OF POOR QUALITY

DETECTION OF RAINFALL RATES UTILIZING  
SPACEBORNE MICROWAVE RADIOMETERS

Hsiao-hua K. Burke  
Kenneth R. Hardy, and  
Nancy K. Tripp

ENVIRONMENTAL RESEARCH & TECHNOLOGY, INC.  
696 Virginia Road, Concord, Massachusetts 01742

ABSTRACT

Over most of the microwave spectrum, raindrops both absorb and scatter radiation producing large changes in brightness temperatures relative to clear or cloudy conditions. Since the structure of rain varies substantially for different rain rates and climatological backgrounds, the raindrop size distribution, the rain layer thickness and the ice clouds above the rain layer are all important inputs to the model computations. The subsequent modeling involves applying the Mie theory to derive the absorption and scattering effects and the radiative transfer computations to derive the brightness temperature. The radiative transfer calculation is based upon a variational iterative approach which takes account of the multiple scattering effect of the rain layer. Results over both ocean and land backgrounds are demonstrated. It is shown that over ocean background, which is "cold" in the microwave region, lower frequencies are sufficiently sensitive to rain conditions. Over land background, higher frequencies have to be utilized in order to obtain the sensitivity to rain rates.

It is also demonstrated that by using discrimination tests of the radiometric data, the rain/no rain decision can be made and the rainfall rate can be retrieved from a statistical inversion technique. The shortcomings of this technique are: (1) the assumption of a homogenous field of view at different wavelengths can be erroneous, (2) the actual physical structure of the rain layer may be significantly different from the one used in the climatological approach, and (3) the additional uncertainty which may be introduced because of the limitations of the radiative transfer algorithm.

1. INTRODUCTION

The basic concept of rain determination utilizing passive microwave measurements relies upon increases in absorption and/or increases in scattering of the raindrops which produce signatures very different from those found in the absence of rain. At lower frequencies, such as 19.35 GHz, rain is highly absorptive and produces increasingly warm brightness temperatures over cold backgrounds such as the oceans. Wilheit et al. (1977) developed a technique of interpreting rain rate over oceans from data sensed by the Electrically Scanning Microwave Radiometer on-board Nimbus-5 (ESMR5); this instrument has a frequency of 19.35 GHz and senses the upwelling



radiation emitted by the earth and its atmosphere. At higher frequencies, scattering effects from the rain become more pronounced and can produce cooling effects relative to warm backgrounds such as land (Savage 1978). Since the effects of absorption and scattering increase with increasing rainfall rates at microwave frequencies, there is a basis for the hypothesis that proper utilization and interpretation of multifrequency microwave measurements will permit estimation of rain rate values over both ocean and land surfaces.

## 2. THEORETICAL MODEL

### 2.1 Physical Model

The structure of a rain layer varies substantially for different rain rates and climatological backgrounds. Therefore, physical properties of the precipitation layer have to be carefully defined prior to model simulation. Drop size distribution, rain layer thickness, and the existence of water or ice clouds of the rain layer are all factors which can have a considerable impact on the radiative signature.

To accommodate the variety of raindrop size distributions, the distribution derived by Deirmendjian (1964) was used to fit the empirically observed spectra of Laws and Parsons (1943). At low rain rates, the distribution is usually narrower with fewer large drops. Similarly, the mode radius generally increases with increasing rain rate. These characteristics are incorporated into the model distribution by calculating the shape parameters as a function of rain rate.

The thickness of the rain layer and its coexistence with water and the clouds are considered next. For weak storms with low rain rates, the top of the rain layer generally does not exceed the 0°C isotherm. However, for more intense convective storms with high rain rate, the thickness of the effective rain layer grows with the addition of supercooled water above the freezing level. The height of this supercooled layer is primarily a function of the convective forces at work in the storm. These forces are variable, but in general, are correlated with rain rate as well as climatological factors. For example, the potential for convection is typically greater over land than water. In addition, the convective forces vary with latitude, reaching maximum strength over the mid-latitudes.

### 2.2 Radiative Transfer Model

The effects of hydrometeors on microwave radiation can now be carried out. Calculation of the absorption and scattering effects of rain are based on the Mie theory. The approach of Gaut and Reifstein (1971) incorporates the Mie theory, computes the efficiency factors, and integrates across specified drop size distributions to determine the total extinction, absorption and single scattering albedo for each atmospheric layer. The computation of brightness temperatures for rain conditions then involves solving the radiative transfer equation. The variational-iterative approach

(Sze 1976; Burke and Sze 1977) is used. This method provides a direct way for construction of an approximate solution for the source function, and then through iterations, a solution to the desired accuracy is obtained. Using this approach, it was possible to compute brightness temperatures for a wide range of rain and atmospheric conditions and to determine the sensitivity of microwave radiometers to realistic precipitation situations.

### 3. RESULTS

#### 3.1 Results of Inversion from Simulated Precipitation Data

The basic tool used for retrieving rain rate estimates from the brightness temperatures is the Statistical Parameter Inversion Method (e.g., Gaut 1967). The method seeks out significant statistical correlations between the simulated brightness temperatures and their associated parameters. It starts from an ensemble of simulated scenes. These scenes are represented by brightness temperatures associated with the physical parameters. The resulting correlations are contained in an inversion matrix.

Tests for rain rate inversion are carried out by utilizing brightness temperatures of 19 GHz H (Horizontal), 22 GHz V (Vertical) and 37 GHz (V and H) over the ocean and 37 GHz and 85.5 GHz (both V) over land. These are the channels to be used on a microwave radiometer sensor on-board a future Defense Meteorological Satellite Program (DMSP) satellite. The sensor's look angle with respect to the earth's surface is a constant of 53°.

A no rain or maybe rain decision test is carried out first. An example is demonstrated for a summer tropical ocean background. If either  $T_B(37 \text{ GHz V}) - T_B(37 \text{ GHz H}) < 25^\circ\text{K}$  or  $T_B(19 \text{ GHz H}) > 190^\circ\text{K}$ , inversion for rain rate estimate will be carried out. The simulated brightness temperatures as a function of rain rate for four different channels are presented in Figure 1. The scatter of the simulated data is mainly due to surface variabilities (temperature and wind speed) at lower rain rates and various cloud and ice contaminations at higher rain rates. The overall rms error of inversion is approximately 1.5 mm/hr.

Similar procedures are carried out for a mid-latitude land background of spring and fall. If  $T_B(37 \text{ V}) < 270^\circ\text{K}$ , inversion for the rain rate estimate will be carried out. The simulated brightness temperatures as a function of rain rate are presented in Figure 2. The scatter of the simulated data is greater than that for an ocean background. The reasons are twofold. First, the land background is much warmer in the microwave range and thus produce more relative noise in the data. Secondly, the mid-latitude region (25° - 55° latitude) includes a wider range of climate variations which results in different physical structures of the rain layers. The overall rms error of inversion is close to 3 mm/hr.

#### 4. DISCUSSION AND CONCLUSION

The results of this investigation show that it is feasible to map surface rainfall rates using a multifrequency passive microwave satellite sensor system. Over an ocean background, the rainfall retrieval is more accurate due to the fact that thermal emission from rain is more pronounced against the radiometrically cold ocean background. Over land background, higher frequency sensors are needed in order to observe radiometric cooling due to the scattering effect from precipitation-size droplets.

Many aspects of the remote sensing of rainfall using passive microwave sensors still require further investigation. One example is the model for rain layer thickness as a function of the rainfall rate and climate region. In this paper, the model was adopted from Crane and Blood (1979); it is based on long-term statistics which indicate that the thickness of the rain layer (or the region of wet particles) increases as more intensive convective storms with higher rain rate develops. However, there are also other controversial theories; for example, Wilheit et al. (1977) assumed constant rain layer thickness and Lovejoy and Austin (1980) defined an effective rain layer thickness which decreases significantly with rainfall rate and becomes much less than the height of the freezing level. Thus, detailed studies of the physical structures of the rain layer at various rain rates for different climates are urgently required since these structures impact substantially on the response of microwave radiometers.

Another problem arises because a typical satellite field of view for microwave sensors can be larger than the rain cell size. Moreover, there is usually only one antenna for the multi-channel radiometer system which results in different ground resolutions for different frequencies. Rosenkranz (1978) has attempted to use a space filter technique to characterize the resulting remote sensing system by an impulse response matrix in ordering space or by a transfer matrix in frequency space. Improvement of the sensor spatial resolution or the use of higher frequencies can also be a solution to this partial beamfill problem.

In addition to the physical rain model and the field of view problems, the radiative transfer algorithm can also be a challenging area especially at higher frequencies due to the more complex scattering effects of rain droplets and the lack of data. The rms inversion errors presented are only meant for mathematical consistency and may not be true for the real world because of the above problems. Further research efforts should include both theoretical and experimental programs in order to evaluate more completely the value of radiometric techniques for the monitoring and mapping of rainfall over both ocean and land surfaces.

## REFERENCES

- Burke, H.K. and J.D. Sze (1977), A Comparison of Variational and Discrete Ordinate Methods for Solving Radiative Transfer Problems, J. Quant. Spectrosc. Radiat. Transfer, 17, 783.
- Crane, R.K. and D.W. Blood (1979), Handbook for the Estimation of Microwave Propagation Effects, Final Report, Contract No. NAS5-25341, Environmental Research & Technology, Inc.
- Deirmendjian, D. (1964), Scattering and Polarization Properties of Water Clouds and Hazes in the Visible and Infrared, Applied Optics, 3 (2), 187.
- Gaut, N.E. (1967), Studies of Atmospheric Water Vapor by Means of Passive Microwave Techniques, Ph.D. Thesis, Dept. of Meteor., MIT, Cambridge, Mass.
- Gaut, N.E. and E.C. Reifstein, III (1971), Interaction Model of Microwave Energy and Atmospheric Variables, Final Report, Contract No. NAS8-26275 (NASA CR-61348), Environmental Research & Technology, Inc.
- Laws, J.O. and D.A. Parsons (1943), The Relation of Raindrop-Size to Intensity, Amer. Geophys. Union Trans., 24, 452.
- Lovejoy S. and G.L. Austin (1980), The Estimation of Rain from Satellite-Borne Microwave Radiometers, Quart. J.R. Met. Soc., 106, 255.
- Rosenkranz, P. (1978), Inversion of Data from Diffraction-Limited Multi-wavelength Remote Sensors, Radio Sci., 13, 1003.
- Savage, R.C. (1978), The Radiative Properties of Hydrometeors at Microwave Frequencies, J. Appl. Met., 17, 904.
- Sze, N.D. (1976), Variational Methods in Radiative Transfer Problems, J. Quant. Spectrosc. Radiat. Transfer, 16, 763.
- Wilheit, T.T., A.T.C. Chang, M.S. Rao, E.B. Rodgers and J.S. Theon (1977), A Satellite Technique for Quantitatively Mapping Rainfall Rates Over the Oceans, J. Appl. Meteor., 16, 551.

ORIGINAL PAGE IS  
OF POOR QUALITY

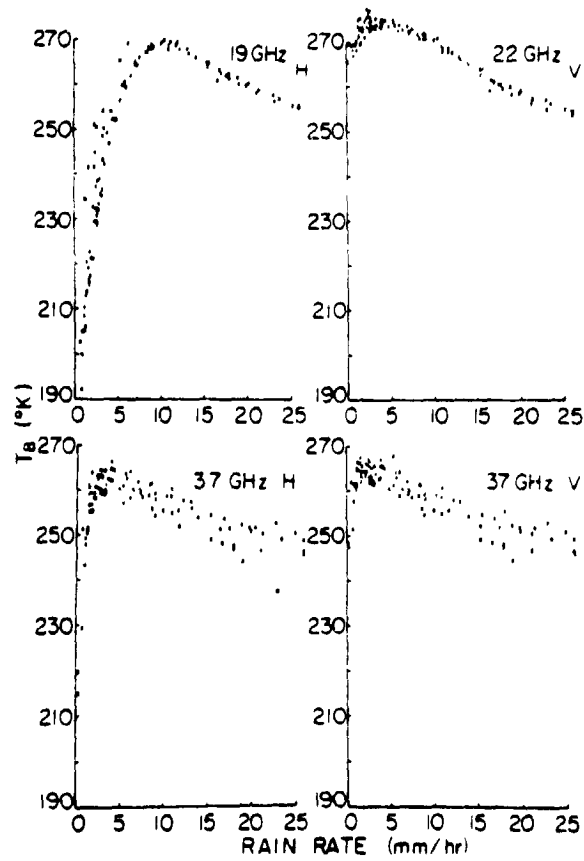


Figure 1. Simulated brightness temperatures at 19.35 GHz (H), 22.235 GHz (V), 37 GHz (V and H) for a look angle of  $53^\circ$  as a function of rain rate over a tropical ocean background during the summer.

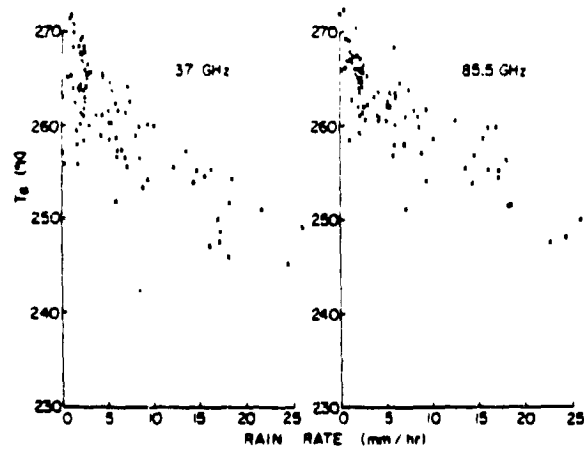


Figure 2. Simulated brightness temperatures at 37 GHz (V) and 85.5 GHz (V) for a look angle of  $53^\circ$  as a function of rain rate for a mid-latitude land background during the spring or fall season.

D36

N83 25305

ORIGINAL PAGE 19  
OF POQR QUALITY

The Utilization of Satellite Passive  
Microwave Sensors to Monitor  
Synoptic Scale Rainfall

by

Edward Rodgers

Laboratory for Atmospheric Sciences (GLAS)  
Goddard Space Flight Center  
National Aeronautics and Space Administration  
Greenbelt, MD 20771

## 1. Introduction

Considering today's satellite technology, the only realistic method of monitoring synoptic scale (approximate time scale of 10 h and space scale of 1000 km) rainfall, particularly over water, is through the utilization of passive microwave sensors flown on the polar orbiting satellites. It has not been vigorously demonstrated that visible and infrared sensors flown on the polar orbiting satellites can be used to monitor rainfall from measurements of cloud top temperature or brightness. There is sometimes very little difference between the visible and infrared signatures of precipitating and non-precipitating clouds, particularly the upper and middle tropospheric clouds producing stratified rainfall. However, there appears to be more promise in using the infrared and visible sensors to monitor convective rainfall if the cloud signatures are measured at a shorter interval from geosynchronous satellites (Negri and Adler, 1980; Scofield and Oliver, 1979; Griffith et al., 1978) although this technique again fails for stratiform rain.

To demonstrate the success of utilizing passive microwave sensors in monitoring synoptic scale rainfall, two studies will be highlighted in which Electrically Scanning Microwave Radiometer (ESMR-5 and 6) on board Nimbus 5 and 6 were employed using a Lagrangian frame of reference for the purpose of monitoring rainfall and monitoring and predicting storm intensity. The first study suggests a method of utilizing ESMR-5 measurements to quantize rainfall over water within tropical and extratropical storms and to use these measurements to monitor and possibly predict storm intensity (Adler and Rodgers, 1975; Adler and Rodgers, 1977; and Rodgers and Adler, 1981).

The second study suggests a method of monitoring the coverage and movement of synoptic rain over land by employing ESMR-6 (Rodgers et al., 1979).

## 2. ESMR-5 Study

The release of latent heat through condensation and precipitation is important in the energetics of both tropical and extratropical

cyclones. The intensification of tropical cyclones are related to the interaction of convection-scale precipitation and the synoptic scale flow field (Morrey and Eliassen, 1964). Without the energy provided by latent heat release, tropical cyclones could not be maintained and hurricanes and typhoons could not be generated. The observation of precipitation in tropical disturbances is therefore, of obvious importance.

Latent heat release in extratropical storms is not related so closely to storm energetics as is the case with tropical systems. Extratropical cyclogenesis can be modelled successfully using a dry model atmosphere. Baroclinic instability is the principal mechanism of development. However, rapid cyclogenesis and intensification appears to be related to the release of latent heat, which enhances the upward vertical motions and thereby accelerates the conversion of potential to kinetic energy (Danard, 1964). In addition, if adequate moisture is available, the magnitude of the latent heat release in the rain shield of an extratropical storm should be an indicator of the intensity of the upward vertical motion and hence, also an indicator of the energy conversion which leads to intensification.

Estimates of rainfall rate over oceans can be made with data from Nimbus 5 Electrically Scanning Microwave Radiometer (ESMR-5). This instrument is a passive microwave radiometer measuring emitted radiation in the 19.35 GHz (1.55 cm) region with a spatial resolution of 25 km at nadir. A description of the instrument and a discussion of the relevant physical relationships are given by Wilheit (1972). Over water, the microwave radiation emitted by the earth and atmosphere (expressed in terms of brightness temperature,  $T_b$ ) is affected primarily by the state of the sea surface, atmospheric water vapor, and atmospheric liquid water. Liquid water, in the form of drops of the size associated with rain, is the dominating factor in the variation of  $T_b$  over water.

a. Tropical Cyclones

- i. Data preparation and calculation method
- o Brightness temperature-rainfall rate relationship

Wilheit et al. (1977) derived an ESMR-5  $T_B$  rainfall relationship for 19.35 GHz using a radiative transfer model. The model assumes a Marshall-Palmer drop size distribution and limits the vertical extent of the rain to the height of the 0°C isotherm (freezing level height). A layer of  $25 \times 10^{-3} \text{ g cm}^{-2}$  liquid water content (LWC) is assumed for 0.5 km layer just below the freezing level. A relative humidity profile linearly decreasing from 100% at the freezing level to 80% at the surface is used. Upwelling radiance is then calculated for various rainfall rates and for various freezing level heights. The calculated radiance, convertible to  $T_B$ , also contains the implicit assumption that from a satellite data perspective, the Instantaneous Field of View (IFOV) is filled with rain at a constant rainfall rate. The beam-filling problem, the lack of information on amount of cloud LWC and water vapor contribute to errors and uncertainties in estimating rainfall rate from ESMR-5  $T_B$  values (Lovejoy and Austin, 1980).

Preliminary calculations indicated that the total storm rainfall calculated using the model-derived relationship for the appropriate freezing level heights gave values systematically too low in comparison with previous studies using in-situ measurements. This was true even for cases of typhoons where the scale of the precipitation was large enough so that the field of view problems were minimized. In order to avoid these problems, an empirical relationship derived by comparing ESMR-5  $T_B$  values with radar-estimated rainfall rates was used.

The ESMR-5  $T_B$ -radar comparisons were made on June 20 and July 7, 1973, and June 24 and 25, 1974, when disturbed, with synoptic-scale rain, was occurring off the Florida coast. The rain rates in these disturbances were measured by a calibrated digitized National Weather Service WSR-57 radar at Miami. The rain systems observed by the ESMR-5 and the radar had many features in common with the disturbances and depressions observed in the western Pacific. The average temperature (the average freezing level is ~4.5 km) and moisture profiles for the rain-comparison used were quite similar to what is found in the average western Pacific disturbance or depression (Gray et al., 1975). Although the freezing level height is not a very good measure of rain-layer depth, especially in convective situations where liquid water droplets can exist at temperatures at least as cold as -10 to -15°C, it may be a good relative measure of rain-layer depth averaged over a large area (such as a tropical disturbance or typhoon). Since the temperature and moisture profiles for the ESMR-5  $T_B$ -radar comparison cases appear similar to those for western Pacific disturbances and depressions, the assumption that

the rainfall characteristics (e.g., LWC, rain rates, height of the effective rain layer) are similar appears justifiable. Therefore, an empirical relationship derived from a data set taken under similar environmental conditions should be valid for use in calculations of rainfall for western Pacific Ocean disturbances.

However, to estimate rain rate in western Pacific typhoons where the average freezing level is ~5 km (Frank, 1977; Bell and Kar-Sing, 1973), the height of the effective rain layer must be raised. Since there are no simultaneous ESMR-5  $T_B$  and radar measurements of rain rate in western Pacific typhoons, the derived empirical relationship was adjusted according to calculations of Wilheit et al. (1977).

Another advantage of the empirical approach is that it helps alleviate the field of view problem. The radar-estimated rainfall rate values were available with a much higher horizontal resolution than the ESMR-5 data. Each satellite data point is compared to the average rainfall rate within the ESMR-5 IFOV rather than assuming a constant rainfall rate over the area as was done in the model calculations.

o Method of calculation

After a small adjustment to the ESMR-5  $T_B$  for scan angle and diurnal variation (Adler and Rodgers, 1977), the rain rate for each scan point of each satellite pass confined to a circular area of 444 km radius centered at the tropical cyclone center of circulation, was computed using the adjusted empirical relationship. The center of circulation was based on the microwave image and concurrent THIR image and storm location from 1973, 1974 and 1975 Annual Typhoon Report. The center of circulation is usually well defined in the microwave data, particularly for more mature systems. For disturbances and depressions, a center of circulation is less discernible in the images and usually not documented in the Annual Typhoon Report. However, it can be estimated from the curvature of the rain bands as observed from ESMR-5. No horizontal variation of the temperature and moisture profiles and the rain-layer depth was considered even for mature storms when substantial horizontal gradients of these parameters are present near the center.

The latent heat release (LHR) over an area is given by

$$LHR = \rho \int_A R da, \quad (1)$$

where  $\rho$  is the density of the rain (assumed to be equal to  $1.0 \times 10^3 \text{ kg m}^{-3}$ ),  $L$  the latent heat of condensation ( $2.5 \times 10^6 \text{ J kg}^{-1}$ ),  $da$  the incremental area, and  $A$  the area of integration. The integration is performed over circular areas of radii 111, 222, 333 and 444 km from the center of circulation. As previously mentioned, the rainfall rate  $R$  was determined from the rainfall rate and ESMR-5  $T_B$  empirical relationship. In addition to storm LHR calculations, the radial

ORIGINAL PAGE IS  
OF POOR QUALITY

distributions of rainfall rate and the fraction of rainfall contributed by rain rates  $>5 \text{ mm h}^{-1}$  [hereafter called the precipitation intensity parameter (PIP)], are also examined in reference to tropical cyclone intensity.

Adler and Rodgers (1977) discussed sources and the possible magnitude of the errors affecting the ESMR-5 derived rainfall parameters. Because of the sensitivity of the absolute values of these rainfall parameters to possible errors due to the ESMR-5 IFOV, scan angle, ESMR-5  $T_p$  rainfall rate relationship, selection of rain depth and ESMR-5 calibration, the emphasis in this paper is on relative changes with time and on spatial variations in the same storm.

o Case Study data

There were 71 ESMR-5 observations of 21 western and eastern North Pacific Ocean tropical cyclones at different stages of development during 1973, 1974 and 1975. There are 49 observations of 18 western Pacific tropical cyclones and 22 observations of 3 eastern Pacific tropical cyclones. No attempt was made to include North Atlantic tropical cyclones due to the lack of ESMR-5 observations caused by a satellite interrogation problem over the Atlantic Ocean and the small number of tropical cyclones during the years ESMR-5 was operating. The sample of ESMR-5 observations of the western Pacific Ocean tropical cyclones in this study was restricted to an area located between the equator and  $25^{\circ}\text{N}$  and east of  $125^{\circ}\text{E}$ . This eliminated storms which had recurved or crossed the Philippine Islands. Over both the eastern and western Pacific Oceans, a restriction was made on the width of the ESMR-5 swath that was used in each observation. As previously mentioned, only storms that fell within  $40^{\circ}$  of nadir ( $\sim 2000 \text{ km}$  ground swath) were used. This allowed some storm observations to be lost between swaths. Since ESMR-5 was operational only part of the time between December 1972 and January 1975 and because of the narrow swath and imposed geographic restriction, only 71 ESMR-5 tropical cyclone observations were available for this study.

11. Results

o LHR

Fig. 1, which shows the relation between intensity [maximum winds ( $\text{m s}^{-1}$ )] and LHR for a circular area 444 km in radius, indicates a positive correlation. The cross marks depict tropical disturbances with their intensity arbitrarily plotted at  $10 \text{ m s}^{-1}$ . Circled crosses and dots depict small storms as reported in the Annual Typhoon Reports. All values are calculated based on the 5 km freezing level relationship. There is a large scatter in the diagrams, but there is still an obvious correlation between storm intensity and storm LHR. The linear correlation coefficient was 0.71 with an average error estimate in the maximum wind of  $10.1 \text{ m s}^{-1}$ . The F ratio test determined this relationship to be significant at the 1% level. Ambiguous results occur, however, when observing small storms. For

example, Typhoon Patsy (October 9, 1973), which was a small storm that had a maximum surface wind up to  $40 \text{ m s}^{-1}$  that corresponded with LHR of only  $3.0 \times 10^{14} \text{ W}$ .

It was shown from case studies (Rodgers and Adler, 1981) that the ESMR-6 observations could be used to monitor tropical cyclone intensification prior to the time when the tropical cyclone was first named (storm stage or greater with maximum winds  $>17 \text{ m s}^{-1}$ ) and sometimes prior to the aircraft reconnaissance flights. To illustrate this further, Fig. 2 shows the LHR value for each tropical cyclone observation relative to the time when the tropical cyclone was first named. The heavy line in the middle represents this reference time and the negative (positive) numbers represent the number of days prior to (after) the naming of the tropical cyclone. The dots represent tropical cyclone observations with maximum winds  $<32 \text{ m s}^{-1}$  and the triangles represent tropical cyclone observations with maximum winds greater or equal to  $32 \text{ m s}^{-1}$ . Circles around triangles and dots indicate small tropical cyclones. All tropical cyclones occurring prior to the time that the tropical cyclone was first named, of course, are less than storm stage. The solid line is a quadratic fit to the data given by

$$\text{LHR} = 1.8947 \pm 0.00086 h + 0.00018 h^2 \quad (2)$$

where LHR is latent heat release in  $10^{14} \text{ W}$  and h is hours beginning at day -5 and continuing consecutively to day +5. The correlation coefficient is 0.73 with an average error estimate in the LHR of  $2.08 \times 10^{14} \text{ W}$ .

The fitted curve in Fig. 2 suggests that the increase in the storm LHR begins one to two days prior to the time the storm is named. This indicates that the increase in LHR may precede tropical cyclone intensification. After the tropical cyclone becomes named, LHR is seen to continue to increase with time even though there are a few observations (some of which are ESMR-5 observations of small tropical cyclones) that indicate low LHR values. Therefore, it is suggested from this sample of western Pacific tropical cyclones that ESMR-5 derived LHR observations can be used to help detect tropical cyclone intensification 1-2 days prior to storm stage. This information could, therefore, supplement information obtained from current aircraft reconnaissance flights.

o PIP and Radial Distribution of Rainfall

Fig. 3 (same format as Fig. 1), which shows the relation between storm intensity and PIP value indicates a similar positive, but a poorer correlation than that in Fig. 1. The linear correlation coefficient was 0.52 with an average error estimate in the maximum wind of  $12.2 \text{ m s}^{-1}$ . The F ratio test determined this relationship also to be significant at the 1% level. For weak systems (whose strength is less than or equal to a depression) the PIP average is  $\sim 0.24$  even though there are four values  $>0.35$ . This indicates that the



rain in the weak and developing storm is primarily light (rain rates  $<5 \text{ mm h}^{-1}$ ). This does not rule out small, intense showers, but means that on the scale of the IFDV of ESMR-5 ( $>625 \text{ km}^2$ ) relatively light rain prevails. For tropical cyclones at stronger intensities, the PIP increases from an average of 0.33 at storm stage to an average of 0.39 at typhoon stage (this includes Super Typhoon Nora). Thus, as the storms intensify, more of the LHR is being contributed by rainfall rates  $>5 \text{ mm h}^{-1}$ . Typhoon Patsy (October 9, 1973), the "small" typhoon in Fig. 3 has a PIP value of only 0.16 along with a low value of storm LHR.

The variation of rainfall intensity with storm intensity is also shown in Fig. 4. This diagram shows the distribution of volume rain rate per unit rain rate (units in terms of area) as a function of rain rate for the composite tropical cyclone at four different stages of development. The numbers within the parentheses indicate the number of ESMR-5 observations. This parameter is computed for a circular area of 444 km distance from the center of circulation. The area under the curve is the volume rain rate in the storm, which is proportional to LHR. It is seen that as the composite tropical cyclone intensifies, the area under the curve grows, indicating rising LHR, and there is also a greater relative contribution to LHR from rain rates  $>5 \text{ mm h}^{-1}$ .

Fig. 5, which shows the radial distribution of rain rate for the composite tropical cyclone at different stages of development, illustrates the increase of rain rate with intensification (the numbers within the parentheses given the number of ESMR-5 observations). It is seen that as a tropical cyclone intensifies, the rain rate at all distances from the center of circulation increases. At a radial distance of  $\sim 80$ - $100$  km from the center of circulation, there is a maximum in rain rate for all stages. There is no indication from these curves that the maximum rain rate moves toward the center with increasing intensity. However, the contraction of the rain maximum toward the center is weakly observed in the mean fractional amount of LHR within 222 km. This parameter increases from 0.44 at depression stage to 0.51 at storm stage to finally 0.53 at typhoon stage. A decrease was noted as the mean tropical cyclone developed from disturbance (0.47) to depression (0.44), which may be due to the difficulty in locating the center of circulation at disturbance stage.

- b. Extratropical Cyclones
  - i. Data preparation and calculation
    - o Brightness temperature-rainfall rate relationship

In this study, the LHR was calculated using the same method as that used for the tropical cyclone study. However, rainfall rate was obtained from the ESMR-5  $T_b$  by using the radiative transfer model described by Wilhelm et al. (1977). Again, it must be emphasized that because of the sensitivity of the absolute values of the rainfall estimate to

possible errors, emphasis will be on relative changes. One of the largest source of errors in this study is that caused by the selection of the rain depth. Because of the variable freezing level within an extratropical system, the absolute value of rainfall estimates may be more questionable than in the tropical cyclone study. What is needed to resolve this problem is independent temperature profile data within the storm as possibly measured from a microwave sounder.

#### o Case Study

Observations at seven times were obtained from September 6-10, 1974. A freezing level height of 4 km was assumed based on coastal radiosondes and National Meteorological Center (NMC) analyses over the North Atlantic Ocean. The LHR is calculated over the area of rain in the storm's rain shield, excluding precipitation along the trailing cold front.

The extratropical cyclone case involved cyclogenesis just off the eastern coast of North America. Two of the observations show a portion of the rain areas touching the coast. Surface observations also indicate rain along the coast. Using the surface observations and the ESMR-5 data, the rainfall rate distribution over the land was approximated and included in the LHR calculation. These two calculations will be identified in the presentation of the results.

#### ii. Results

The storm began to develop on September 7, 1974, just off New Jersey. During the subsequent three days, it moved east-northeastward across the Atlantic Ocean intensifying to a central pressure of 973 mb, and then weakening. The calculated LHR magnitudes are shown in Fig. 6 along with the central low pressure of the storm as an indicator of storm intensity. In Fig. 6, the LHR values are those which result from the integration over the entire rain shield. The two occasions when a portion of the rain shield was over land, so that the rainfall rate there had to be approximated, are shown as circled data points in the diagrams.

The LHR calculation are for the area of steady rain in the storm's rain shield, generally located to the northeast, north and northwest of the storm center. Precipitation along the trailing cold front is not included. In general, the dividing point between cold front rain and rain shield precipitation is easily defined in this case. The one exception is the last observation, at 12 GMT September 10. At this point, the storm was very occluded and there were two main areas of rain. Including both areas in the calculation results in the point connected by the solid line in Fig. 6. If the computation is performed with just the northern-most area, the point connected by the dotted line results.

The first closed isobar (denoting cyclone formation) is found on the 18 GMT September 7 surface map. Intensification of the low followed shortly. Before this formation and intensification, the LHR shows an increase of

ORIGINAL PAGE IS  
OF POOR QUALITY

over 50%. Although two of the points upon which this observation is based are the ones which include the estimated land precipitation, the change is large enough and the land contribution small enough that the observation of the increase is still valid. This implies, at least in this case, that an increase in LHR precedes cyclogenesis. This is reasonable if there is adequate moisture available. The energy for development is dependent on vertical motions, and the release of condensation heating enhances the upward vertical motion and, therefore, should lead to intensification (Danard, 1964).

The maximum LHR took place on September 8, preceding the period of most rapid pressure decrease. The storm's lowest pressure was then recorded 24 hours later. Therefore, the decrease in LHR occurred before the decrease in storm intensity. Thus in this case, there appears to be a tendency for changes in LHR to precede the changes in storm intensity.

Fig. 7 shows the area of precipitation during the life cycle of the storm. This parameter also shows the initial increase and the later decrease. The maximum area is found to occur at 03 GMT September 9, although the observation immediately preceding is almost as large. This is in contrast to the LHR in Fig. 6, which had a sharp peak on September 8. The difference is in the mean rainfall rate.

The maximum average rainfall rate coincides with the maximum LHR in Fig. 6. For the integration over the entire rain shield, the maximum is  $2.4 \text{ mm hr}^{-1}$ . Over the limited area of maximum rainfall, it is  $4.1 \text{ mm hr}^{-1}$ . These are reasonable values and compare with those of Danard (1964).

It is interesting to note that cyclogenesis occurred with the precipitation area expanding, but the mean rainfall rate held constant. Then as the area continued to enlarge, the rainfall rate also went up, producing the maximum LHR. The decrease in LHR occurred with lowering values of both parameters.

### 3. ESMR-6 Study

Savage and Weinman (1975) and Savage et al. (1976) demonstrated theoretically that a 37.0 GHz (the frequency at which the Nimbus-6 ESMR sensor measures upwelling radiance) the scattering by hydrometeors is strong enough to provide a qualitative estimate of rain coverage over land. Furthermore, Weinman and Guetter (1977) demonstrated from a theoretical consideration that the upwelling radiation at 37.0 GHz emerging from rain clouds was essentially unpolarized and, therefore, was in contrast with the radiation emanating from wet surface background. According to the electromagnetic theory, if the emissivity of a surface is reduced by increasing its dielectric constant (as by adding moisture), then the large emissivity will be highly polarized when the surface is viewed obliquely.

Thus, the sum and substance of these theoretical investigations is that the

obliquely viewed 37 GHz radiation emitted by wet soil surfaces is polarized ( $T_v > T_h$ ), whereas radiation emanating from dry land or heavy rainfall areas is essentially unpolarized ( $T_v \approx T_h$ ). Moreover,  $T_b$ 's upwelling from dry land areas are distinguishably higher than those from heavy rainfall areas or wet land surfaces. Hence, according to these theoretical conclusions rainfall over land can be at least qualitatively delineated and, therefore, its coverage and movement can be monitored irrespective of the land background by employing 37 GHz measurements from the ESMR on board Nimbus-6. Quantitative measurement of rainfall over land, using a 37 GHz radiometer, however, appears less promising.

It is the purpose of this study to substantiate the above conclusions and to arrive at an algorithm for the detection of rain over land by statistically analyzing ESMR-6 data. This statistical analysis will be performed by first sampling three categories of ESMR-6  $T_b$ 's (representing rain over land, wet land surfaces without rain and dry land surfaces), then testing these populations for uniqueness and separability, and finally developing a classification algorithm to delineate rain over land.

#### a. The ESMR-6 System

The ESMR-6 system flown aboard Nimbus-6 (Wilheit, 1975) receives the thermal radiation upwelling from the earth's surface and atmosphere in a 250 MHz band centered at 37 GHz. The antenna beam scans electrically an arc of  $70^\circ$  in 71 steps ahead of the spacecraft along a conical surface with a constant earth incidence angle of  $40^\circ$  every 5.3 s. The nominal resolution is 20 km cross-track and 45 km down-track. The instrument measures both horizontal and vertical polarization components by using two separate radiometric channels. The data are calibrated using warm (instrument ambient) and cold (cosmic background) inputs to the radiometer.

The  $T_b$ , as observed from the satellite, is dependent upon the emission from the earth's surface modified by the intervening atmosphere. The emissivity, a function of the dielectric constant, is variable over land surfaces (depending on vegetation, soil type, soil moisture, etc.) and generally is large ( $\sim 0.9$ ). In rain situations, three constituents contribute significantly to the absorption: molecular oxygen, water vapor and liquid water droplets. Water droplets contribute more significantly to absorption and reemittance than the other constituents and are the only source of scattering at this frequency. Ice crystals are essentially transparent at this frequency.

#### b. Data Sampling

Simultaneous ground station and radar measurements of rain and ESMR-6  $T_b$  were needed in order to develop an algorithm which classified a given ESMR-6 IFOV as rain over land, dry land surface or wet land surface. Eight daytime synoptic-scale rainfall cases

over the southeastern United States were used where surface rainrate data taken from stations reporting hourly rainfall amounts and from the WSR-57 radar coincided with Nimbus-6 overpass to within 5 min. The surface temperature in each of these cases was not less than 50°C. Rain areas were sampled within areas delineated as rain by either the WSR-57 radar (rain rates  $>2.5 \text{ mm h}^{-1}$ ) and/or the stations reporting hourly rainfall amounts. The dates and time of the occurrence of these cases are given in Table 1. Wet land surfaces were sampled upwind and adjacent to the raincells observed on the WSR-57 radar, and dry land surfaces were sampled over areas where rain had not fallen within a 24 h period, previous to the Nimbus-6 pass.

### c. Statistical Analysis

Elementary statistics of the total sampled data (ESMR-6 measurements where surface thermodynamic temperatures were greater than 50°C) are presented in Table 2. The table gives for each category the sample size, the mean and standard deviation of the horizontally and vertically polarized  $T_B$ , and the correlation and the mean difference between horizontally and vertically polarized  $T_B$ s. These data are also shown as a scatter plot in Fig. 8. In this figure, the C represents the mean of the population and each frequency concentration ellipse encompasses 68% (one standard deviation) of the data within the population. The ellipses reveal the extent of scattering of data from each population, the correlation between the dual polarization  $T_B$ s ( $T_H$  and  $T_V$ ) within each eccentricity of the ellipse, and the extent of overlap among the populations. The three concurrent lines drawn in this figure are the Fisher (1938) linear discriminant lines, which separate two-by-two, the rain over land area ( $S_R$ ), the dry land surface ( $S_D$ ), and the wet land surface ( $S_W$ ) populations represented by the  $T_B$  pairs ( $T_H$ ,  $T_V$ ).

It can be seen from Fig. 8 and Table 2 that  $T_B$ s from rain areas over land are colder than those  $T_B$ s from dry land surface areas. Further, the difference between the mean horizontally and vertically polarized  $T_B$ s from rain areas over land (6.45 K) is much smaller than that for wet land surfaces (16.81 K). This is in accordance with theoretical findings that microwave radiation emerging from hydrometeors is essentially unpolarized (Weinman and Gjetter, 1977), whereas radiation emanating from wet land surfaces is polarized. It is also seen from Fig. 8 that the largest overlap occurs between the data obtained from rainfall areas and wet land surfaces. The reason for this is that sometimes in sampling rain over land, the total upwelling radiance received by the radiometer contains a direct surface contribution. This may occur when an IFOV of the ESMR-6 measurement is partially filled with moderate to heavy rain or when it is completely filled with light rain (background being wet land surface). Consequently, the  $T_B$ s for each category are somewhat similar, thus producing the overlap between rain over land and wet land surface classes.

Since the surface emission is given by  $eT_s$ , where  $e$  is the surface emissivity and  $T_s$  is the surface thermodynamic temperature, there is an influence of  $T_s$  on ESMR-6 measured dry land surface  $T_B$ . A decrease in  $T_s$  results in a decrease in  $T_B$  from dry ground and consequently, the  $T_B$  contrast between dry land surfaces and rain over land will also decrease.

The Chi-square test showed that the ESMR-6 data from each population were normally distributed and the F test showed that the populations were statistically distinguishable from one another (Rodgers et al., 1979). However, the F test showed that the difference between rainfall over land and wet land surface  $T_B$ s is smaller than those of the other two pairs. This indicates that it will be more difficult to distinguish an area of rain over land from wet land surfaces.

### b. Classification Algorithms

Since the populations were found to be statistically distinguishable and satisfied, the Gaussian frequency distribution, the Bayesian classification technique was considered with the purpose of developing an efficient and effective classification algorithm to detect and delineate active rainfall over land from dry and wet land surfaces.

The Bayesian classifier is a Gaussian parametric maximum likelihood quadratic classifier, which requires the knowledge of the a priori probabilities for the occurrence of each class (Duda and Hart, 1973; Fu et al., 1969). It minimizes the average loss due to misclassification while assuming that each misclassification is equally costly.

The Bayesian algorithms also has the capability to classify at a given confidence level.

This maximum likelihood decision rule selects one class from a set of predetermined classes to which a pixel represented by  $x = (T_H, T_V)$  most likely belongs. The associated confidence value measures the distance in probabilistic terms of  $x$  from the mean point of the selected class. The hypothesis that a pixel actually belongs to a selected class may be accepted or rejected based on this confidence value. If the confidence value is greater than a predetermined value, the hypothesis is accepted and the pixel is put in the selected class; otherwise, the hypothesis is rejected and the pixel is put in the unknown class. The problem, of course, is to assign the appropriate values for thresholding the confidence value parameter.

### e. Algorithm Evaluation

A case not previously used in sampling was tested to verify qualitatively the performance of the Bayesian classification algorithm. This case consisted of a synoptic-scale rain pattern over the southeastern United States (September 14, 1976), which was observed by the ESMR-6 sensor (surface thermodynamic temperature  $>15^\circ\text{C}$ ). Fig. 9 shows

the rainfall area delineated by the WSR-57 radars and hourly rainfall reporting stations. The approximate time of the radar PPI images was 1630 GMT (within 5 min of the Nimbus-6 pass). The reporting times of the hourly precipitation amounts were 1500, 1600 and 1700 GMT. The shaded area within the WSR-57 radar PPI range (232 km) is rainfall area with rain rates  $>2.5 \text{ mm h}^{-1}$ . The radars were located at Waycross and Macon, Georgia; Charleston, South Carolina; and Wilmington and Cape Hatteras, North Carolina. Surface station data (present weather, temperatures, cloud type and amount, precipitation amount in 3 hours, and wind velocity and direction) were taken at 1800 GMT. Hourly rainfall is also shown. (See model in Fig. 9).

The Bayesian (70% confidence) classification maps are seen in Fig. 10. Areas of clouds most likely producing rain are delineated by the Nimbus-6 THIR  $11.5 \mu\text{m}$  channel where equivalent blackbody temperatures  $T_{\text{BB}} < 270 \text{ K}$  (Shenk et al., 1976). Rain areas in the absence of rain producing clouds are considered misclassifications. Regions only covered by clusters of contiguous pixels classified into a single individual class are shown, since the probability of misclassifying clusters is much less than that of a single pixel.

It is seen by comparing the Bayesian classification map at 70% confidence level (Fig. 10) with the map delineating observed rain (Fig. 9) that they agree well. No attempt was made to verify wet land surfaces.

The main discrepancies found between the ESMR-6 observed rainfall and ground observed rainfall is seen over North Carolina and southwestern Georgia. The rainfall indicated by ESMR-6 over North Carolina may be suspended liquid water in the clouds and/or virga ahead of the rain area (the area of rain was moving northeastward toward North Carolina). The ESMR-6 delineated rain over southwestern Georgia, which was upstream from the rain area, may be due to wet land surfaces produced by the rain that fell a few hours prior to the Nimbus-6 pass.

The Bayesian classification algorithm was applied to another test case (1645 GMT August 27, 1976, surface thermodynamic temperatures were  $>15^\circ\text{C}$ ) over the same geographical area as the previous case in order to determine whether the surface characteristics (vegetation soil moisture and surface roughness) had influenced the classification performed in the previous case. During these periods, the area was under the influence of Bermuda high. Also, there was a squall line located in southwestern Virginia and extending southwestward into Tennessee. The regions in the previous case where the algorithm showed rainfall were classified as dry land surfaces. Hence, there were no influences of extraneous surface characteristics on the outcome of the previous case study.

However, contradicting results occurred when the Bayesian classification algorithm was applied to a nighttime Nimbus-6 pass over the same geographical area (0525 GMT,

September 13, 1976) where surface thermodynamic temperatures were  $>15^\circ\text{C}$  and there was no synoptic-scale rainfall. Almost all pixels were classified by the algorithm as rain over land. An examination of the ESMR-6 vertically polarized  $T_{\text{S}}$  showed that the temperatures were below  $0^\circ\text{C}$ . Since calibration of the nighttime data is better than that of daytime data (Wilheit, 1978), this anomaly may be attributed to the changes in the surface emissivity caused by the presence of dew on the vegetation. The 0600 GMT National Weather Service map indicated that the conditions were ideal for the formation of dew. A large anticyclone centered over Virginia produced clear skies, winds less than 5 kt and dew point temperature differences of less than  $3^\circ\text{C}$  over the majority of the reporting stations in the southeast United States. Therefore, the classification algorithm trained by data sampled from Nimbus-6 daytime passes can be employed only when dew is absent.

#### 4. Conclusions

Considering the limitations of the passive microwave sensors to observe rain, it has been demonstrated that it is possible to monitor synoptic scale rainfall over land and water and to quantize rainfall over water in order to monitor and predict the intensity changes of tropical and extratropical systems. However, with the advent of satellite flown multifrequency passive microwave sensor that had just been launched, such as the Nimbus-7 Scanning Multifrequency Microwave Radiometer (SMR) or that may be launched during the 1980's that have improved IFOV, such as the Large Antenna Multifrequency Microwave Radiometer (LMR) or possibly the Advanced Microwave Moisture Sounder (AMMS), these limitations may be greatly reduced.

#### 5. References

- Ailer, R. F. and E. B. Rodgers, 1974: Satellite-based case studies of latent heat release in a tropical and extratropical storm. NASA X-Document X-911-75-324. p. 12.
- \_\_\_\_\_ and E. B. Rodgers, 1977: Satellite observed latent heat release in a tropical cyclone. *Mon. Wea. Rev.*, 105, 956-963.
- Bell, G. J., and Tsui Kar-Sing, 1973: Some typhoon soundings and their comparison with soundings in hurricanes. *J. Appl. Meteor.*, 12, 74-93.
- Charney, J. G. and A. Eliassen, 1964: On the growth of the hurricane depression. *J. Atmos. Sci.*, 21, 68-75.
- Danard, H. B., 1964: On the influence of released latent heat on cyclone development. *J. Appl. Meteor.*, 3, 27-37.
- Duda, R. O., and P. E. Hart, 1973: Pattern classification and scene analysis. Wiley pp. 482.

ORIGINAL QUALITY  
OF FOUR QUALITY

- Frank, W. M., 1977: The structure and energetics of the tropical cyclone. Part 1: Storm structure. Mon. Wea. Rev., 105, 1119-1135.
- Fisher, R. A., 1938: The statistical utilization of multiple measurements. Ann. Eugenics., 8, 376-386.
- Fu, F. S., D. A. Langrebe and T. L. Phillips, 1969: Information processing of remotely sensed agricultural data. Proc. IEEE, 57, 631-653.
- Gray, W. M., E. Ruprecht and R. Phelps, 1975: Relative humidity in tropical weather systems. Mon. Wea. Rev., 103, 685-690.
- Griffith, G. C., W. L. Woodley, S. Browner, J. Teijeiro, M. Maier, D. W. Martin and D. N. Sikdar, 1978: Rain estimation from geosynchronous satellite imagery-visible and infrared studies. Mon. Wea. Rev., 106, 1153-1171.
- Lovejoy, S. and G. L. Austin, 1980: The estimation of rain from satellite borne microwave radiometers. Quart. J. Roy. Meteor. Soc., 106, 255-276.
- Negri, A. J. and R. F. Adler, 1980: Detection of heavy convective precipitation using radar satellite data. Preprint, 19th Conf. on Radar Meteorology, Miami, FL, AMS Boston, MA. 264-271.
- Rodgers, E. B., H. Siddalingaiah, A. T. C. Chang and T. Wilheit, 1979: A statistical technique for determining rainfall over land employing Nimbus-6 ESMR measurements. J. Appl. Meteor., 18, 978-991.
- \_\_\_\_\_ and R. F. Adler, 1981: Tropical cyclone rainfall characteristics as determined from satellite passive microwave radiometer. To appear in Mon. Wea. Rev. in March 1981.
- Savage, R. C. and J. A. Weinman, 1975: Preliminary calculations of the upwelling radiance from rain clouds at 37.0 and 19.35 GHz. Bull. Amer. Meteor. Soc., 56, 1272-1274.
- \_\_\_\_\_, P. J. Guetter and J. A. Weinman, 1976: The observation of rain clouds over land in Nimbus-6 electrically scanned microwave radiometer (ESMR-6) data. Preprints 7th Conf. Aerospace and Aeronautical Meteorology and Symp. on Remote Sensing from Satellite, Melbourne, Amer. Meteor. Soc., 131-136.
- Scofield, R. A. and V. J. Oliver, 1977: A scheme for estimating convective rainfall from satellite imagery. NOAA Tech. Memo. NESS 86, pp. 47.
- Shenk, W. E. R. J. Holub and R. A. Neff, 1976: A multispectral cloud type identification method developed for tropical ocean areas with Nimbus-3 MRIR measurements. Mon. Wea. Rev., 104, 284-291.
- Weinman, J. A. and P. J. Guetter, 1977: Determination of rainfall distribution from microwave radiation measured by the Nimbus-6 ESMR. J. Appl. Meteor., 16, 437-442.
- Wilheit, T. T., 1972: The electrically scanning microwave radiometer (ESMR) experiment. Nimbus-5 Users Guide, NASA Goddard Space Flight Center, 55-105.
- \_\_\_\_\_, 1975: The electrically scanning microwave radiometer (ESMR) experiment. Nimbus-6 Users Guide, NASA Goddard Space Flight Center, 87-108.
- \_\_\_\_\_, T. C. Chang, M. S. V. Rao, E. B. Rodgers and J. S. Theon, 1977: A satellite technique for quantitatively mapping rainfall rates over the oceans. J. Appl. Meteor., 16, 551-560.
- \_\_\_\_\_, 1978: The effect of wind on the microwave emission from the ocean's surface at 37 GHz. NASA Goddard Space Flight Center Tech. Memo. 79588, pp. 24. (To be published in J. Geophys. Res.)

TABLE 1 Dates of synoptic rain cases used to develop  
ESMR 6 classification algorithms

Case	Date	Time (GMT)
1	31 Jul 1975	1620
2	4 Aug 1975	1635
3	1 Oct 1975	1700
4	7 Nov 1975	1700
5	12 Nov 1975	1700
6	29 Dec 1975	1717
7	3 Jan 1976	1715
8	6 Jan 1976	1655

TABLE 2 Elementary statistics of sampled data  
(surface temperature  $\geq 5^{\circ}\text{C}$ )

Sample size (N)	Rain area 216		Dry ground 189		Wet soil 66	
	$T_{so}$	$T_{rw}$	$T_{so}$	$T_{rw}$	$T_{so}$	$T_{rw}$
Mean ( $\mu$ )	254.53	260.96	271.66	278.18	252.05	260.86
Mean brightness temperature difference	6.45		6.72		10.81	
Standard deviation ( $\sigma$ )	7.31		5.81		6.18	
Sample correlation coefficient between $T_{so}$ and $T_{rw}$ ( $r$ )	0.55		0.37		0.82	

WESTERN PACIFIC TROPICAL CYCLONES

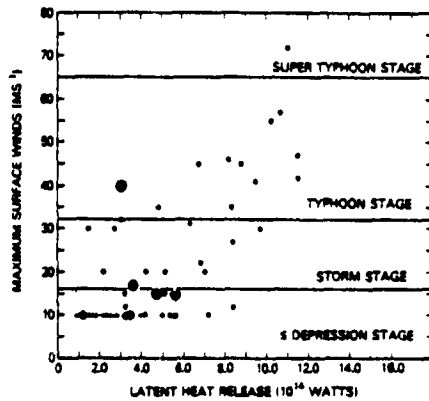


Fig. 1. Scatter diagram of storm intensity versus latent heat release (LHR) for western Pacific Ocean tropical cyclones. Crosses indicate tropical disturbances. Circled dots and crosses indicate small storms.

WESTERN PACIFIC TROPICAL CYCLONES

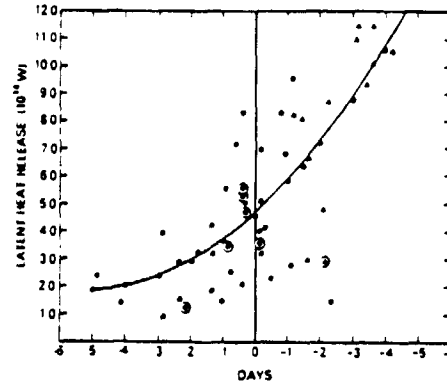


Fig. 2. Scatter diagram of western Pacific Ocean tropical cyclone latent heat release (LHR) versus time when the tropical cyclone reaches storm stage. The heavy line in the middle represents the time the tropical cyclone reached storm stage and the negative (positive) numbers represent the number of days prior to (after) the time that the tropical cyclone reached storm stage. Dots (triangles) represent storms with maximum wind  $< 32 \text{ m s}^{-1}$  ( $> 32 \text{ m s}^{-1}$ ). Circled triangles and dots indicate small storms. The solid line is quadratic fit to the data.

WESTERN PACIFIC TROPICAL CYCLONES

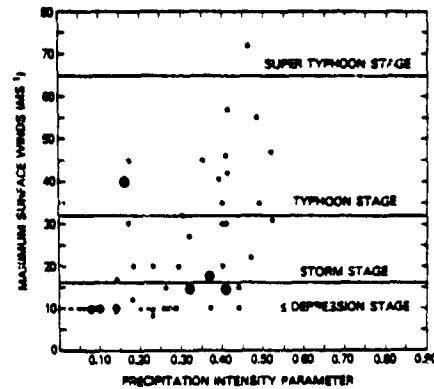


Fig. 3. Scatter diagram of storm intensity versus the precipitation parameter (PIP) for western Pacific Ocean tropical cyclones. Otherwise, the notation is the same as in Fig. 1.

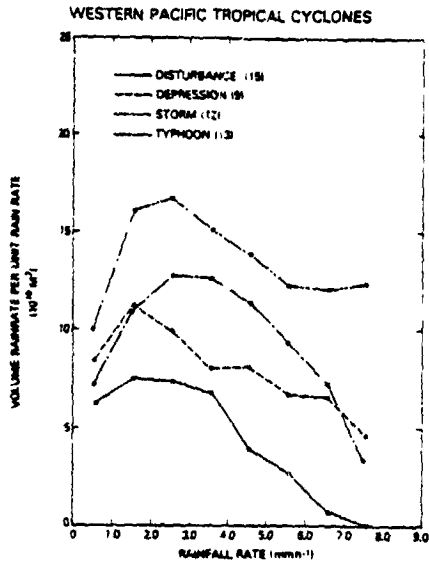


Fig. 4. Contribution of various rainfall rate magnitudes to total volume precipitation for western Pacific Ocean tropical cyclones at various stages of development.

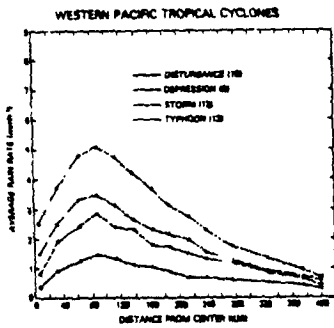


Fig. 5. Mean rainfall rate as a function of radial distance from the storm center for western Pacific Ocean tropical cyclones at various stages of development.

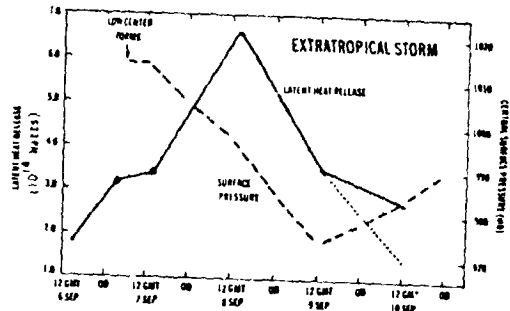


Fig. 6. Latent heat release (LHR) over the area of the rain shield of an extratropical cyclone (September 6-10, 1974). Central surface pressure is also plotted. Additional dashed line connects point at 12 GMT on September 10, representing one of two separate areas in rain shield.

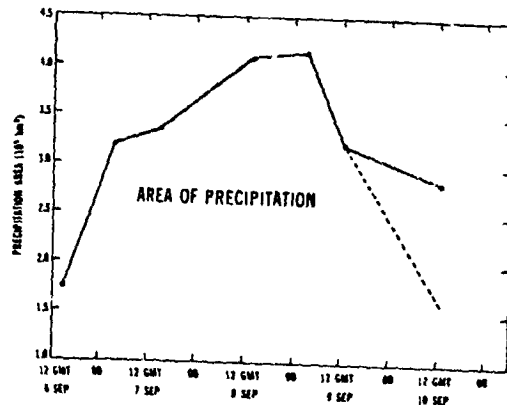


Fig. 7. Areas of precipitation in the rain shield of extratropical cyclone (September 6-10, 1979). Dashed line connects point, representing one of two separate areas in rain shield.

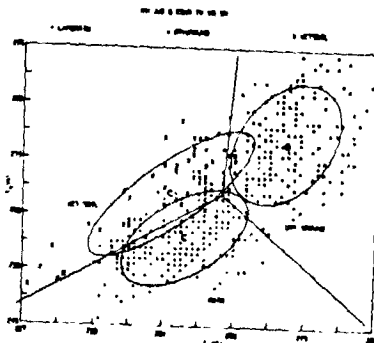


Fig. 8. Vertically polarized vs. horizontally polarized ESMR-6 T<sub>b</sub> for each sampled category (rain over land and wet and dry surfaces).

PRECEDING PAGE BLANK NOT FILMED

ORIGINAL PAGE IS  
OF POOR QUALITY

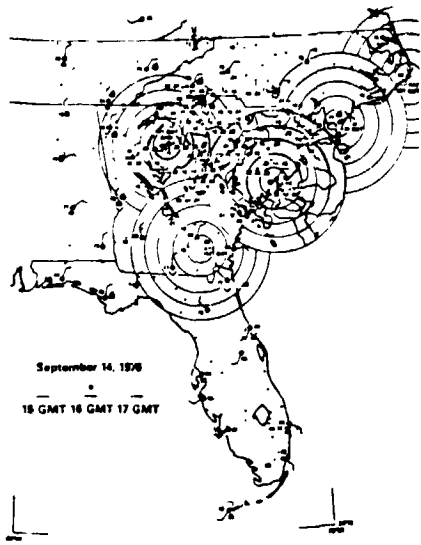


Fig. 9. Rainfall over the southeast United States as delineated by the WSR-57 radar and hourly rainfall reporting stations. Time of the data is approximately 630 GMT September 14, 1976.

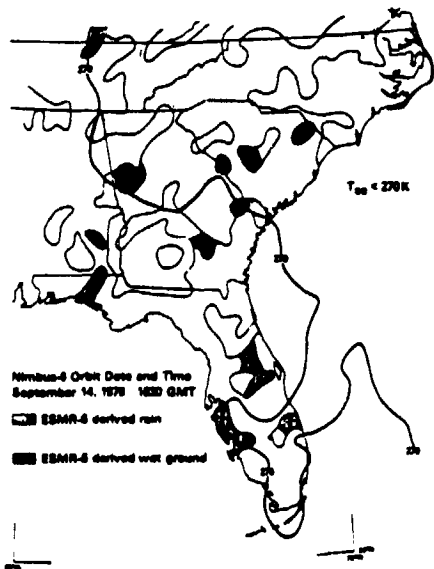


Fig. 10. ESMR-6 derived rainfall distribution using the Bayesian classifier with a confidence level of 70%. Time of Nimbus-6 pass was 1630 GMT September 14, 1976.



D31 EN83 25306

ORIGINAL PAGE IS  
OF POOR QUALITY

THE DMSP MICROWAVE IMAGER (SSMI)--UNFINISHED PLANS

Richard C. Savage  
11230 Kentucky Rd  
Papillon, NE 68133

1. INTRODUCTION

A microwave imaging sensor, the SSMI, is being built for flight on spacecraft of the Defense Meteorological Satellite Program (DMSP) in the mid 1980s. Although both Fleet Numerical Oceanography Center (FNOC) and AF Global Weather Central (AFGWC) have software to process data from the SSMI into products useful to their operations, no plans have been made to archive data or products for research programs, such as the Climate Observing System and the National Climate Program. This paper, for the NASA workshop on Precipitation Measurements from Space, is intended to summarize the existing major elements of the SSMI program as background for planning an archival program useful for climate research.

2. REQUIREMENTS

During 1978, scientists of the U.S. Navy and U.S. Air Force, working through USAF's Space Division, Los Angeles, specified performance requirements for an imaging microwave sensor (the SSMI), to fly on spacecraft of the Defense Meteorological Satellite Program (DMSP). The requirements were formulated with the intent of allowing offerors to propose the best system to meet operational agency needs for cloud and rainfall maps, sea ice charts, ocean wind charts, and land surface moisture. A software system to process satellite data bits into radiances (Sensor Data Records, SDRs) and environmental data records (EDRs) at Fleet Numerical Oceanographic Center (FNOC) and AF Global Weather Central (AFGWC) was also called for. The system was, necessarily, subject to some restrictions of weight, power, volume, data rate, and so forth imposed by the spacecraft interface and the ground software interface. A contract was signed with Hughes Aircraft Company in July 1979. Hughes had engaged a subcontractor for additional expertise in modelling the radiative signatures of the phenomena of interest, ERT Inc. The contract called for development of a refurbishable

prototype, operational software, documentation, and options for production of three flight units. In defining the hardware and software parameters of the SSMI system, Hughes and ERT modelled a large number of simulations of precipitation, wind-roughened ocean surfaces, ocean ice, and surface moisture variations, as well as combinations of these (rain over wind-roughened ocean, clouds over wet ground, etc). From this simulation data base came a better specification of the required signal-to-noise ratio, spatial resolution, choices of frequency and polarization, calibration accuracy, and so forth. Fortunately, the phenomenology of some of the environmental parameters (ocean wind speeds, ice cover, precipitation over ocean) was reasonably understood from the literature on previous experiments. The contractor was encouraged to use the results from NASA's Electrically Scanned Microwave Radiometers (ESMRs, NIMBUS 5 and 6), microwave sounders (NEMS, SCAMS), and other microwave instruments (e.g., SMRR) in defining the system and its software algorithms. Some parameters necessarily were based to a greater extent on theoretical modelling (e.g., precipitation). However, the process of specifying the desired result rather than the engineering details is believed, in retrospect, to have been a good one. The environmental parameters to be derived from the SSMI are tabulated in Table 1.

Because no one could guarantee in advance the complete accuracy of all the extraction algorithms, given the assumptions necessarily involved in the a priori modelling, the contractor and subcontractor agreed to provide software to verify the EDRs produced by the SSMI system, based on data sources routinely available in the FNOC and AFGWC data bases. Such data is, of course, overwhelmingly of a synoptic nature; the opportunity to verify the algorithms on the basis of data from research sources was not contemplated. In the absence of synoptic reports of many parameters, verification must depend on climatology. As a result of verification, the numerical values

ORIGINAL PAGE IS  
OF POOR QUALITY

9  
Y

TABLE 1. SSM/I ENVIRONMENTAL PARAMETERS

PARAMETER	ABSOLUTE ACCURACY	RANGE	RESOLUTION
Ocean Surface Wind Speed	$\pm 2$ m/s	3 - 25	25 km
-----			
Sea Ice			
Area Covered	$\pm 12\%$	0 - 100	25 km
Age	First year, multiyear	1, 2+	50 km
Edge Location	NA	NA	25 km
-----			
Precipitation Intensity			
Ocean	$\pm 5$ mm/hr	0 - 25	25 km
Land	$\pm 5$ mm/hr	0 - 25	12.5 km
-----			
Columnar Water Content			
Rain	$\pm 2$ kg/m <sup>2</sup>	0 - 6	25 km
Cloud	$\pm 0.1$ kg/m <sup>2</sup>	0 - 1	25 km
-----			
Surface Moisture	$\pm 3\%$	0 - 30	50 km
-----			

Note: cloud water content over land surfaces is "best effort" only.

in the algorithm equations may be updated, at the will of the operating agency (FNOC, AFGWC). Note that the contractor and subcontractor were not obligated to perform verification or update; they were, rather, asked to provide a tool to permit verification. The tool is unlikely to be used often by the operating agencies beyond the demands of operational necessity, since research is not their charter. The tool is, however, available for those of the research community who wish to use it. It is considered a very valuable part of the SSM/I system. A further discussion of the verification/update part of the system is given in section 4 of this paper, and in the paper of Dr. H. K. Burke, "Retrieval of Rain Utilizing Satellite Microwave Radiometry Techniques and Its Verification."

### 3. HARDWARE

All SSM/I hardware (and some software) is the result of a combination of tradeoffs. In the SSM/I, the following alternatives were considered (the first of the pair is the chosen alternative): radiometer type (total power/Dicke switched), resolution (radiometric/spatial), ground processing (simple, fast, linear/complex, non-linear), antenna-feed configuration (fixed/variable), calibration (external/internal), spacecraft mounting (deployment/fixed), spectral channels (as few as required/as many as possible), earth location algorithms (polynomial fit to a few mapped points/map all pixels), scan pattern (conical/planar).

Not all the chosen alternatives were, in isolation, the preferred ones. The most compelling spacecraft constraint was to use effectively a volume on the anti-earth side where a free space external calibration could be obtained. This requires a deployment into the scanning position post-launch, after the heat shields are jettisoned. It also requires input/output of power, signals, telemetry, and so forth through slip rings. These are elements of danger, though careful design can minimize the risk of failure. The deployment, however, permits a 24 by 26 inch (61 by 66 cm) antenna rotating in fixed alignment with its feed horn, with a hot and a cold (space look) calibration during each scan. The scan pattern is conical, with a local zenith angle of 53° (45° cone angle), as were the NIMBUS 6 ESMR and the SMMR. The choice of the conical scan for both constant footprint size (circular at 85 and 37 GHz, elliptical at 22 and 19 GHz) and preservation of polarization information in the signal was both the preferable and the chosen alternative. The conical scan does, however, limit the data swath width to 1400 km--approximately half the width required for contiguity between orbits at the equator. Accordingly, there will be gaps between orbits.

Extensive modelling by contractor and subcontractor, in response to the parameter accuracy requirements, led to the following choice of data channels: 19.35 GHz, vertical and horizontal polarization (V,H); 22.235 GHz (V only); 37.0 GHz (V,H); and 85.5 GHz (V,H).

ORIGINAL PAGE IS  
OF POOR QUALITY

The first five channels are, of course, based on the merit of commonality with previous satellite and aircraft instruments, as well as their own merits. The two 85.5 GHz channels will provide the first spaceborne observations in the spectrum beyond the 50-60 GHz O<sub>2</sub> absorption band. They are expected to provide both increased spatial resolution and the increased sensitivity to radiation scattering which permits quantitative estimates of precipitation over high emissivity surfaces. Though not quite at the minimum absorption frequency near 95 GHz, they are close enough for practical purposes. The combination of frequency (wavelength), antenna size, zenith angle, and signal integration time leads to the following set of effective fields-of-view (km): 69 x 44, 60 x 40, 36 x 29, and 16 x 14. Although better spatial resolution would have been possible, it was slightly degraded for the sake of better signal-to-noise performance.

A major constraint, affecting both hardware and software, was a requirement to process 100 minutes of satellite data (one orbit) in 100 seconds of central arithmetic unit (CAU) time on an AFGWC UNIVAC 1110 computer. This demanded simple, fast algorithms for both preprocessing and parameter extraction. Earth location of picture elements (pixels), for example, is based on fitting a LaGrange polynomial to four mapped pixel points. This is a part of the system in which those who can afford the resources required can make improvements in the data for research purposes. (The LaGrange polynomial method is still expected to provide location accuracy better than half a pixel.) Likewise, parameter extraction is by matrix multiplication, using only the channels required to meet accuracy specifications. The channel/algorithm summary is shown in Table 2.

The reader may observe from Table 2 that the 85 GHz channels are used only in the estimate of parameters over land. Accuracy specifications for parameters over ocean can be met by the use of the lower frequency channels. This greatly increases the speed of processing over ocean surfaces, since the 85 GHz pixels represent approximately 60% of the data. (One scan consists of 64 22 GHz pixels, 128 19 GHz pixels, 128 37 GHz pixels, and 256 85 GHz pixels. The next scan consists only of 256 85 GHz pixels. Thus 85 GHz data comprises 512 pixels out of 832 in each pair of scans.)

The SSM/I will fly with the normal DMSP configuration, that is, a sun-synchronous 833 km circular orbit with a local sun time near sunrise/sunset or near noon/midnight. The instrument complement will include a visible (0.4 - 1.1 μm) and thermal infrared (10.5 - 12.5 μm) imager, as well as a sounder. The infrared sounder (SSH) is similar to the VTPR, with the addition of channels in the 18-30 μm water vapor band. The microwave sounder (SSMT) has channels centered at 50.5, 53.2, 54.35, 54.9, 58.4, 58.825, and 59.4 GHz. Either the SSH or the SSMT may be flown with a given SSM/I, but not both.

4. SOFTWARE

The SSM/I software is organized into four major parts. For our purposes, in describing them, we may refer to them as SDP, EPE, VER, and UPD.

In the process of producing sensor data records from the raw bit stream, the SDP software does five things. The first is to unpack

TABLE 2. CHANNEL USE SUMMARY

Parameters	Channels	19		22		37		85	
		V	H	V	H	V	H	V	H
Ocean Surface Wind Speed			X	X	X	X			
Sea Ice Conditions									
Concentration			X		X	X			
Age						X			
Edge Location									
Edge Location									
Precipitation Intensity									
Ocean			X	X	X	X			
Land						X	X	X	X
Columnar Water Content									
Rain									
Ocean			X	X	X	X			
Land						X	X	X	X
Cloud									
Ocean			X	X	X	X			
Land		X	X		X			X	
Surface Moisture		X	X						

## GENERAL ANALYSIS OF POOR QUALITY

and decode the readout information (orbit number, time, spacecraft identifier, etc), ephemeris information, and the raw sensor data. The next is to calibrate the raw data, converting the voltage samples to brightness temperatures. The brightness temperatures are next earth located, then tagged with a surface type indicator. This surface type indicator is useful in determining the parameters to be produced, and in screening out the 85 GHz data not required over the oceans. Finally, the antenna pattern correction is applied, to remove the effect of energy outside the central pixel. The earth located brightness temperatures, corrected for antenna pattern and tagged with surface type, are called sensor data records (SDRs). A software option is available to retain the 85 GHz data in the total SDP processing. At AFGWC, the SDRs are contained in a temporary file, which ceases to exist when the environmental parameters are produced. At FNOC, it is planned to retain the SDRs (from all channels) in a mass storage file of several orbits. There are, however, no plans to archive such SDRs.

The EPE software has one major function, as well as two minor ones. The first is to calculate the environmental parameters (environmental data records, EDRs) to the required accuracy, by applying a D-matrix to the vector of SDRs. (A D-matrix is formed from the correlation matrix of parameters and brightness temperatures, multiplied by the inverse of the correlation matrix of brightness temperatures with each other.) Because the D-matrix technique is linear, separate matrices are required for the high and low ranges or some parameters, in order to meet accuracy specifications.

In addition to producing the EDRs, the EPE software saves EDRs and SDRs within specified areas for verification purposes. In addition, at the exercise of an option in the EPE module, estimates of radiative transmissivity at the four frequencies used may be produced. (The computation of optical depth and transmissivity is a natural product of the modeling for the environmental parameters, from which D-matrices for transmissivity may be produced.)

At FNOC, the earth-located EDRs are filed in mass storage according to their latitude-longitude coordinates. At AFGWC, EDRs are remapped into the AFGWC data grid, a cartesian grid superimposed on a polar stereographic projection of each hemisphere. Because the nominal resolution of the AFGWC grid is 40 km, some EDRs are lost in the AFGWC mapping.

The VER software module provides the ability to verify the EDRs produced by the SSM/I system. This verification is needed for two reasons, and, in the two different contexts, "verification" has two slightly different meanings.

In day to day operations with satellite data, it is necessary to detect changes in system performance, due to sensor degradation, to catastrophic changes in sensor response, to noise introduced by, for example, tape recorders or transmitters, and, not least, to software errors introduced by the ground processing facility. It may not be easy to determine whether the problem is in space or on the ground, or perhaps partially in both places. Nevertheless, recognition that a problem exists is the first, essential step. The VER module, designed to be executed every twelve hours, provides such diagnostic evidence of changes in the system.

In addition, it is desirable both to improve algorithm performance on the basis of empirical corrections, and to overcome, to the extent possible, sensor degradation. The VER module can also provide this capability. Let us hypothesize, for example, that ground truth allows clear demonstration that some algorithm has a bias - some parameter is consistently over-estimated. The VER module allows a quantitative modification of the algorithm to remove the bias. It may even be possible to make corrections for a slowly changing component in the SSM/I sensor - a slowly drifting frequency, for example, which would slowly alter the signal response to atmospheric or surface phenomena.

In an extreme application of the VER module, it is feasible to overcome the complete loss of a data channel. If, for example, one of the 85 GHz data channels ceased operation, it might be possible to substitute another channel, or to formulate a new D-matrix without the missing 85 GHz data, on empirical grounds. Likewise, it is conceptually possible to insert into the code a new D-matrix for some parameter not included in the specifications - snow depth, for example. Even without an a priori inversion matrix, one could start with a null matrix, or identity matrix, and accumulate enough statistics from the VER module (modified to accommodate the new parameter and its ground truth) to arrive at an empirical inversion matrix. Obviously, such an empirical inversion matrix is only as good as the ground truth that was used in its formation. In addition, it would be difficult to transfer the results from such a matrix to a sensor with slightly different frequencies. In fact, if the sensor upon which such an empirical matrix were based had drifted away from its original frequencies, the matrix might not be transferable to data from another sensor nominally the same.

The VER module saves statistics of ground truth and the corresponding EDRs, but not the actual EDRs and ground truth. It does, however, save the SDRs used in the EDR production.

ORIGINAL PAGE 13  
OF POOR QUALITY

Three parameters are verified against ground truth from the FNOC and AFGWC data bases: ice parameters, ocean surface winds, and surface moisture (actually verified as Antecedent Precipitation Index, API). The remaining parameters, rain intensity, cloud water content, and liquid water content in rain, are verified by comparison to climatology. For the parameters verified by comparison to climatology, a judgment must be made whether the actual conditions observed were representative of climatological values.

Research organizations with access to better sources of ground truth than synoptic data bases have obvious opportunities to make better use of the verification tools provided in the VER module.

As is apparent from the preceding description, the UPD module, used for update of the inversion matrices, is closely connected to the VER module, much as the EPE module is connected to the SDP software. UPD requires a conscious decision by the operating facility for its execution. Upon such decision, new matrices are formed, based on a weighted combination of the correlation matrices used in the previous D-matrix, and statistics generated from verification. The weights are set by the analyst; either weight may be a maximum of 2, or minimum of 0. Their sum must equal 2. Intermediate

values of the weights allow a melding of old and new data according to the user's wish.

The software provided under contract also includes a full orbit of simulated data, including representative operational data stream errors, such as data dropouts, time discontinuities, sync losses, and missing data. The simulated data is based on fifty simulated scenes (given in Table 3), and includes realistic exercise of the other parts of the software, as well as providing "hands-on" experience for users of the system.

5. UNFINISHED PLANS

The following section contains the opinions of the author. They are not official statements of any government agency.

Since the SSMI program began, events have occurred which will limit its usefulness if some new arrangements are not made. Among these events, the lack of definitive results from SMMR weakens the confidence we might otherwise have in the SSMI algorithms. In addition, the recent decision to defer the National Oceanic Satellite System (NOSS), with its Large Aperture Multifrequency Microwave Radiometer (LAMMR),

TABLE 3. SIMULATION SCENE DISTRIBUTION

OCEAN (22)

Non-rain (14)

Surface wind (14): 3.1 - 23.6 m/s

Cloud water (14): 0.0 - 0.86 kg/m<sup>2</sup>

Rain (8): 4.95 - 22.1 mm/hr

LAND (16)

Non-rain (6)

Surface moisture (6): 11 - 23 %

Cloud water content (6): 0.07 - 0.87 kg/m<sup>2</sup>

Rain (10): 3.3 - 15.1 mm/hr

Surface moisture (10): Indefinite - Saturated

Cloud water content (10): Indefinite - 1.05 kg/m<sup>2</sup>

Liquid water content (10): 0.4 - 3.54 kg/m<sup>2</sup>

ICE (12)

Non-rain (12)

Cloud water content : 0.0 - 0.31 kg/m<sup>2</sup>

Concentration

First year (3): 29 - 100 %

Multiyear (3): 80 - 100 %

Mixed (6)

Note: rain of sufficient intensity renders other parameters indefinite.

ORIGINAL PAGE 05  
OF POOR QUALITY

leaves the SSM/I as the only microwave imager planned for space flight in the 1980's. It would benefit both operational (tropical storm analysis and forecasting, ship routing, cloud analysis and forecasting, agricultural meteorology, water resources management, communications management) and research (desertification, cyclogenesis, storm moisture and heat budgets, earth radiation budgets, cryosphere monitoring) areas of environmental science to cooperate in using SSM/I data. Such cooperation should be relatively easy to arrange, since there are no major technical problems in doing so.

The major hindrance in making SSM/I data available for climate research programs is the lack of an archive facility. Such archival is not within the charter of the military meteorological agencies. There are, however, precedents for archival of DMSP data. Visible and Infrared imagery from the DMSP, in the form of film strips, is archived by NOAA at the Space Science and Engineering Center (SSEC). Likewise, precipitating electron data from the SSJ sensor, along with visible imagery of the polar aurorae, are archived at World Data Center A, Boulder. It seems appropriate, therefore, for NOAA to arrange for archival of SSM/I SDRs, EDRs, verification data, and the current D-matrices. The processing software (SDP, EPE, VER, UPD) should be made available to researchers from either the archival facility, or from NTIS. A set of documentation should be provided to NTIS for those who require technical details. Since both FMOC (with Control Data Corporation computers) and AFGWC (with UNIVAC hardware) versions of the software are available it seems desirable to archive both. An orbit of SSM/I data will produce about 1.3 million SDRs, and approximately the same number of EDRs. Thus, the SSM/I data and output parameters for a day could easily be archived on a single 9-track magnetic tape. Establishment of an archive facility would permit research on new applications of SSM/I data, verification on the basis of non-synoptic ground truth, and critical evaluation of the update of inversion matrices. The Department of Defense is already a participant in the National Climate Program. One of the military meteorological agencies (Naval Oceanography Command, Air Weather Service) should be chosen to act as DoD's agent in providing SSM/I data and products for archival.

The author notes that an SSM/I in the customary DMSP orbits will not observe local conditions during the afternoon. This limitation could be overcome by flying a modified SSM/I on an afternoon NOAA spacecraft. Since the DMSP SD2 and NOAA vehicles are very similar, the required modification need not be severe. This would provide operational benefits, as well as increased research and climate data. In addition, the proposal to launch a low altitude satellite into a near-equatorial orbit offers an opportunity to increase observation of

precipitation in the tropics, to the benefit of both operational and research programs.

ACKNOWLEDGEMENTS I wish to thank Mrs. H. Koga for her preparation of the manuscript.

#### 6. REFERENCES

The following short list of references is condensed to save space. All the authors on the list have multiple contributions in this field, but only a single reference for each is shown. My apologies to the many contributors who are not listed at all.

Burke, H.K., K.R. Hardy, et al, 1980: Detection of Rainfall Rates Over Ocean and Land Backgrounds Using Spaceborne Microwave Radiometers. International Conference on Communications, Seattle, WA, June 1980, pp 49.2.1 - 49.2.6.

Falcone, V.J., L.W. Abrev and E.P. Shettle, 1979: Atmospheric Attenuation of Millimeter and Submillimeter Waves: Models and Computer Code. AFGL-TR-79-0253, AF Systems Command, Hanscom AFB, MA 01731, 76 pp.

Hollinger, J.P., 1973: Microwave Properties of a Calm Sea. Naval Research Lab Report No. 7110-2, Washington D.C., 69 pp.

Paris, J.F., 1971: Transfer of Thermal Microwaves in the Atmosphere. Dept of Meteorology, Texas A&M University, College Station, TX 257 pp.

Savage, R.C., 1976: The Transfer of Thermal Microwaves Through Hydrometeors. Ph.D. Thesis, Dept of Meteorology, University of Wisconsin, Madison, Wisconsin 53706.

Sze, N.D., 1976: Variational Methods in Radiative Transfer Problems. J. Quant. Spectros. Radiat. Transfer, 16, 763.

Weinman, James A. and P. Guetter, 1977: Determination of Rainfall Distribution from Microwave Radiation Measured by the NIMBUS-6 ESMR. J. Appl. Meteor., 16, p 437.

Wilheit, T.T. et al, 1977: A satellite Technique for Quantitatively Mapping Rainfall Rates Over the Oceans. J. Appl. Meteor., 16, 551.

D38

N83 25307

ORIGINAL PAGE IS  
OF POOR QUALITY

3  
Y

REMOTE SENSING OF STORED PRECIPITATION, i.e., SOIL MOISTURE AND SNOW

T Schmugge

Hydrological Sciences Branch  
NASA/Goddard Space Flight Center  
Greenbelt, Maryland 20771

1. INTRODUCTION

After it has fallen, precipitation can be stored on the ground in the forms of snow or soil moisture. There have been major advances in the remote sensing of these quantities with microwave radiometers during the past several years. Microwave radiometers measure the thermal emission from the surface at microwave wavelengths. This emission depends on the temperature and emissivity of the surface medium. The emissivity of the land depends on its surface geometry or roughness, dielectric properties and surface cover. The moisture content of the soil has a strong effect on its dielectric constant and thus on its emissivity. Similarly, the presence of snow cover has a strong effect on the emissivity of the land at certain wavelengths.

For the purpose of this discussion the wavelength range from 0.3 cm to 50 cm will be considered the microwave portion of the spectrum. The particular advantages of microwave sensing are: (a) the all weather capability, especially true at the longer wavelengths ( $\lambda \geq 5$  cm), which is important for any periodic observations from space of these surface parameters; (b) greater penetration depth into the soil or snowpack than with optical or infrared sensors; and (c) the large changes in the dielectric properties of media such as soil and snow produced by changes in water content.

The basic theory relating microwave emissivity to these hydrologic parameters will be presented along with data from field and aircraft measurements to support the theory. Data from the ESMR on Nimbus-5 and the S-194 L-Band radiometer on Skylab has been compared with Antecedent Precipitation Indices (API) to show the sensitivity of spaceborne observations to soil moisture. Similarly, data from the ESMR and SMMR on the Nimbus spacecraft have been compared with surface measurements of snow depth with good results.

The intensity of the thermal emission from the surface at microwave wavelengths is essentially proportional to the product of the temperature and emissivity of the surface (Rayleigh-Jeans approximation). This product is commonly referred to as brightness temperature. All our results will be expressed as brightness temperatures ( $T_B$ ). The value of  $T_B$  observed by a radiometer at a height  $h$  above the ground is

$$T_B = \tau(rT_{sky} - (1 - r)T_{surf}) + T_{atm} \quad (1)$$

where  $r$  is the surface reflectivity and  $\tau$  the atmospheric transmission. The first term is the reflected sky brightness temperature which depends on wavelength and atmospheric conditions; the second term is the emission from the surface ( $1 - r = \epsilon$ , the emissivity); and the third term is the contribution from the atmosphere between the surface and the receiver.

2. SOIL MOISTURE

2.1 Dielectric Properties of Soils

The unique dielectric properties of water afford two possibilities for the remote sensing of the moisture content in the surface layer of the soil. The dielectric constant ( $\epsilon$ ) for water is an order of magnitude larger than that of dry soils at the longer microwave wavelengths, approximately 80 compared with 3 or 4 for dry soils. As a result the surface emissivity and reflectivity for soils are strong functions of their moisture content. The changes in emissivity can be observed by passive microwave approaches and the changes in reflectivity can be observed by active microwave approaches.

The dependence of the dielectric constant for a soil on its moisture content is shown in Figure 1 where the results of laboratory measurements at wavelengths of 21 and 1.55 cm are presented. The wavelength dependence is due to the difference in the dielectric properties of water at the two wavelengths and indicates that there is a greater dielectric difference at the longer wavelengths. At low levels there is a slow increase with soil moisture but above a certain level there is a sharp increase in the slope of the curve. This bilinear result is due to the behavior of the water in the soil. When water is first added to a soil it is tightly bound to the soil particles and in this state the water molecules are not free to become aligned and the dielectric properties of this water are similar to those of ice. As the layer of water around the soil particle becomes larger, the binding to the particle decreases and the water molecules behave as they do in the liquid, hence the greater slope at the higher soil moisture values. The transition depends on the soil texture, i.e., particle size distribution being lower for a sand and large for a clay. This effect has been demonstrated in laboratory measurements of the dielectric constant (Lundien, 1971; Newton, 1976; Wang and Schmugge, 1980).

The range of dielectric constant presented in Figure 1 produces a change in emissivity from greater than 0.9 for a dry soil to less than 0.6 for a wet soil, assuming an isotropic soil with a smooth surface. This change in emissivity for a soil has been observed by truck mounted radiometers in field experiments (Poe et al., 1971; Blinn et al., 1972; Newton, 1976, and Newton and Kouse, 1980), and by radiometers in aircraft (Schmugge et al., 1974 and 1976; Estes et al., 1977; Barton, 1973; Basharnov and Shutko, 1978, and Burke et al., 1979) and satellites (Eggleman and Lin, 1976; and McFarland, 1976). In no case were emissivities as low as 0.6 observed for real surfaces. It is believed that this is primarily due to the effects of surface roughness which generally has the effect of increasing the surface emissivity.

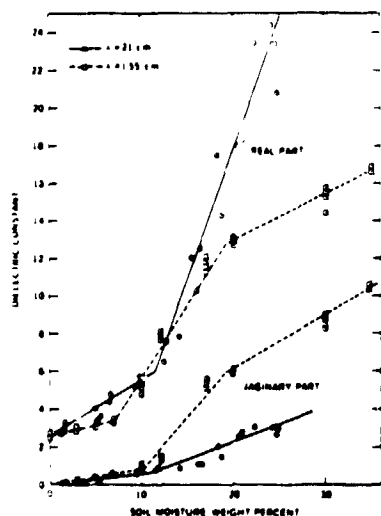


Figure 1. Real and imaginary parts of the dielectric constant for clay loam soils at wavelength of 21 cm (Lundien, 1971) and 1.55 cm (Wang et al., 1978).

As can be seen in Figure 1 there is a greater range of dielectric constant for soils at the 21 cm wavelength compared to the shorter wavelength. This fact combined with a larger soil moisture sampling depth and better ability to penetrate a vegetative canopy make the longer wavelength sensors better suited for soil moisture sensing.

## 2.2 Field Measurements

The results of field measurements by 1.4 and 5 GHz radiometers for wet and dry fields are presented in Figure 2. The two curves represent calculated values of the horizontal and vertical polarizations of the emitted radiation with a radiative transfer model (Wilheit, 1976) using the measured soil temperature and moisture profiles. Horizontal polarization is that

state in which the electric field of the wave is parallel to the emitting surface, while vertical polarization has an electric field component perpendicular to the surface. As incidence angle moves away from nadir the vertically polarized emissivity increases until it reaches 1.0 at what corresponds to the Brewster angle of physical optics. As a result, the difference in emissivity between wet and dry soils for vertical polarization decreases for off-nadir angles. For horizontal polarization the difference between wet and dry soils remains essentially constant with angle. Figure 2 presents results of field measurements conducted at the Beltsville Agricultural Research Center (BARC) verifying this behavior at wavelengths of 6 (C-Band) and 21 (L-Band) cm (Wang et al., 1980). These results were for a bare field with relatively smooth surface in a wet condition, Figure 2a, and in a dry condition, Figure 2b. There is about a 70K difference in  $T_b$  for the 14% difference in the soil moisture. Note the good agreement between the observations and calculations. The agreement was maintained for the range of profiles observed in the experiment (Wang et al., 1980).

A vegetative canopy acts as an absorbing layer which absorbs some of the upwelling radiation from the soil and also emits radiation at its own temperature. The magnitude of the effect depends on the amount of vegetation and the wavelength of observation. A thick canopy would approximate a Lambertian black body, i.e., it would have an emissivity close to one and show no angular or polarization effects. Basharinov and Shutko (1978) and Kir'diashev et al. (1980) have reported on observations made in the USSR over the 3 to 30 cm wavelength range for a variety of crops. Their results indicate that for small grains and grasses the sensitivity to soil moisture is 80 to 90% of that expected for bare ground at wavelengths greater than 10 cm. Broad leaf cultures, like mature corn or cotton, transmit only 20-30% of the radiation from the soil at wavelengths shorter than 10 cm and about 60% at the 30 cm wavelength. They observed 30 to 40% sensitivity for a forest at the 30 cm wavelength, although they did not mention the type or height of trees.

In Figure 3 results from the BARC experiments for grass covered fields are presented at the 6 (C-Band) and 21 (L-Band) cm wavelengths. Data for two grass heights are presented 30 cm in Figure 3a and 10 cm in Figure 3b. There is little or no change of  $T_b$  with angle observed at the 6 cm wavelength for

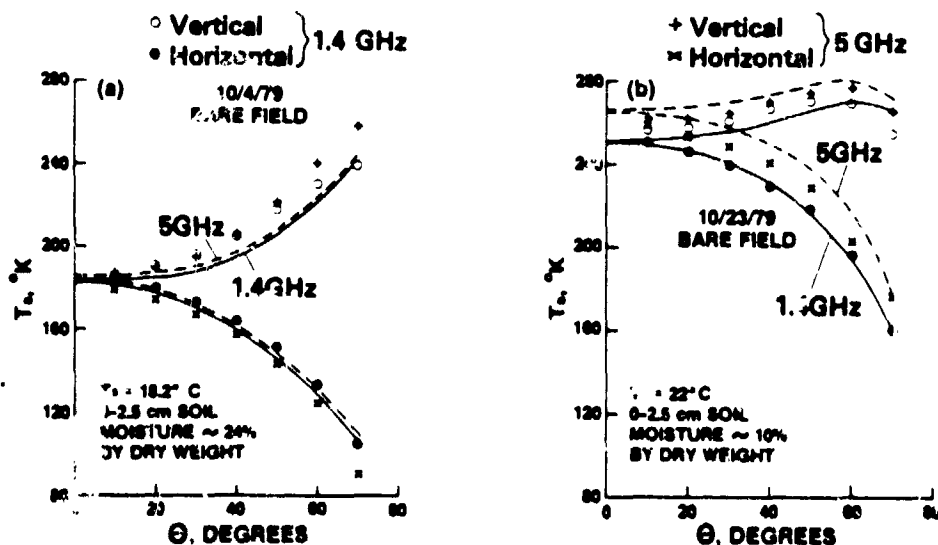


Figure 2. The measured brightness temperatures plotted against the incident angles for a bare field; (a) soil was wet; (b) soil was dry. Smooth curves (solid ones for 1.4 GHz and dashed ones for 5 GHz) are calculated results.  $T_s$  is soil temperature at top 2.5 cm layer. From Wang et al., 1980.



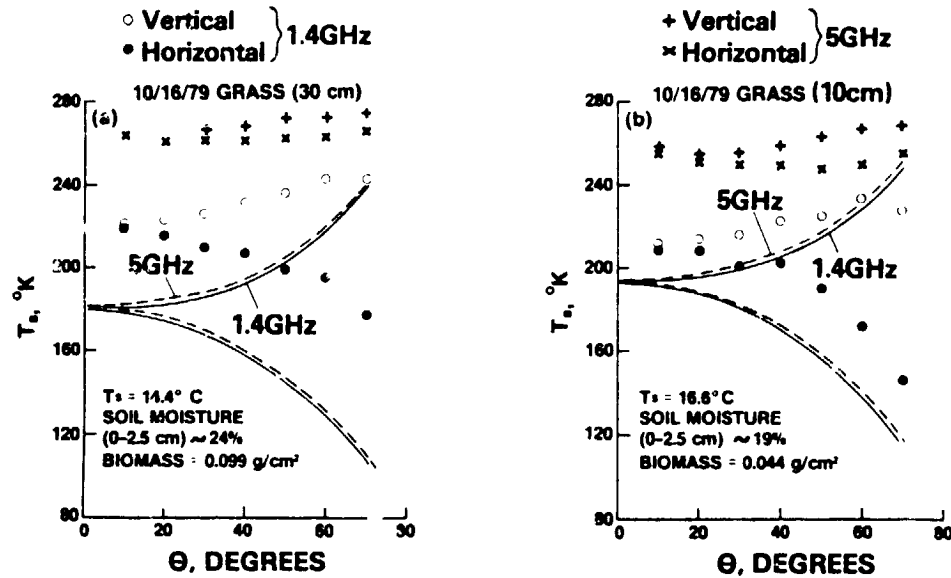


Figure 3. The measured brightness temperatures plotted against the incident angles for grasslands; (a) 30 cm tall grass; (b) 10 cm tall grass. The smooth curves (solid ones for 1.4 GHz and dashed ones for 5 GHz) are the calculated results assuming the fields were bare.  $T_s$  is soil temperature at top 2.5 cm layer. From Wang et al., 1980.

the 30 cm tall grass and  $T_b$  is about that which was observed for the dry field in Figure 2. Also, there is little difference between the values obtained at different polarizations, as would be expected for a thick canopy. The 21 cm results display angular and polarization effects similar to those seen in Figure 2 for the bare fields. However,  $T_b$  has increased: the 30 cm grass field has the same moisture content as the wettest of the two bare fields, but  $T_b = 220K$  compared to  $190K$  for the bare field. In comparison a dry field would be expected to have  $T_b = 270K$ . Thus, the dynamic range between wet and dry fields is reduced by the presence of vegetation from  $80K$  to about  $50K$ . Similarly, the polarization difference at  $\theta = 40^\circ$  is reduced from  $38K$  to  $21K$ . Both of these factors indicate that for a field with a dense 30 cm grass cover, sensitivity to soil moisture was reduced to about 60% of the bare soil case, which is a little less than the transmissivity reported by the Russians. The analyses of these data indicate that the attenuation can be expressed in terms of biomass or water content (Jackson et al., 1980). The quantification of vegetation in terms of wavelength and biomass parameters is a near term objective of our field research program.

### 2.3 Aircraft Results

Significant improvements in the understanding of the effects of individual scene parameters such as vegetation, surface roughness (Choudhury et al., 1979) and soil texture (Schmugge, 1980) on the relationship of brightness temperature to soil moisture have been achieved using ground-based measurements acquired during controlled experiments. However, demonstration of the potential of passive microwave sensors for estimating soil moisture on an operational basis must be performed with aircraft and spacecraft sensors that integrate large areas of natural, non-idealized terrain. A series of aircraft experiments performed over the last several years by a number of investigators have demonstrated the sensitivity of microwave radiometers to soil moisture in agricultural terrain. Skylab and Nimbus satellites have also provided significant results for very large areas of integration.

An example of aircraft data is presented in Figure 4. Here the results from 9 flights during 1976, 1977, and 1978 over a

Hand County South Dakota test site are compared with the regression results for data obtained over the Phoenix and Imperial Valley areas in 1973 and 1975. The agreement between these independent experiments is very good. In each case the correlation between soil moisture in the top 2.5 cm and observed  $T_b$  was  $\geq 0.85$ . These data were for a range of surface conditions including fallow fields, wheat, alfalfa, and pasture. The scatter in the aircraft data presented in Figure 4 arises from a number of sources, one of which is variability in surface characteristics, such as roughness and vegetative cover; another is the uncertainty of ground measurements. The standard deviation of the ground measurements is represented by the error bars in Figure 4. The number of samples ranged from 6 to 29 depending on the length of the fields. This difficulty of making accurate ground measurements has hampered the determination of the accuracy of remote sensing techniques.

### 2.4 Space Results

As noted in the Introduction, measurements of surface soil moisture can be used as a surrogate detector of recent precipitation, since for most land surfaces rainfall is the only mechanism for increasing surface soil moisture. This relationship has been demonstrated by microwave radiometers operating at the 1.55 cm and 21 cm wavelengths from spacecraft platforms. In spite of the obscuring effect of vegetation strong correlations have been obtained between satellite brightness temperatures observations at these two wavelengths and an Antecedent Precipitation Index (API) defined by

$$API_i = P_i^{0.9} + (API_{i-1} \times k_i)$$

where  $k_i$  is a time dependent recession factor  $< 1$  and  $P_i$  is the precipitation on the  $i^{th}$  day. The exponent 0.9 takes account of runoff. Analysis of ground data has a correlation of better than 0.8 between API and the soil moisture in the top 0.8 m of the soil (Blanchard et al., 1981a).

The 21 cm S-194 radiometer on Skylab had a one meter antenna producing a spatial resolution of approximately 110 km. Even with this coarse resolution data obtained with this radiometer over the central U.S. has shown a strong correlation

ORIGINAL PAGE IS  
OF POOR QUALITY

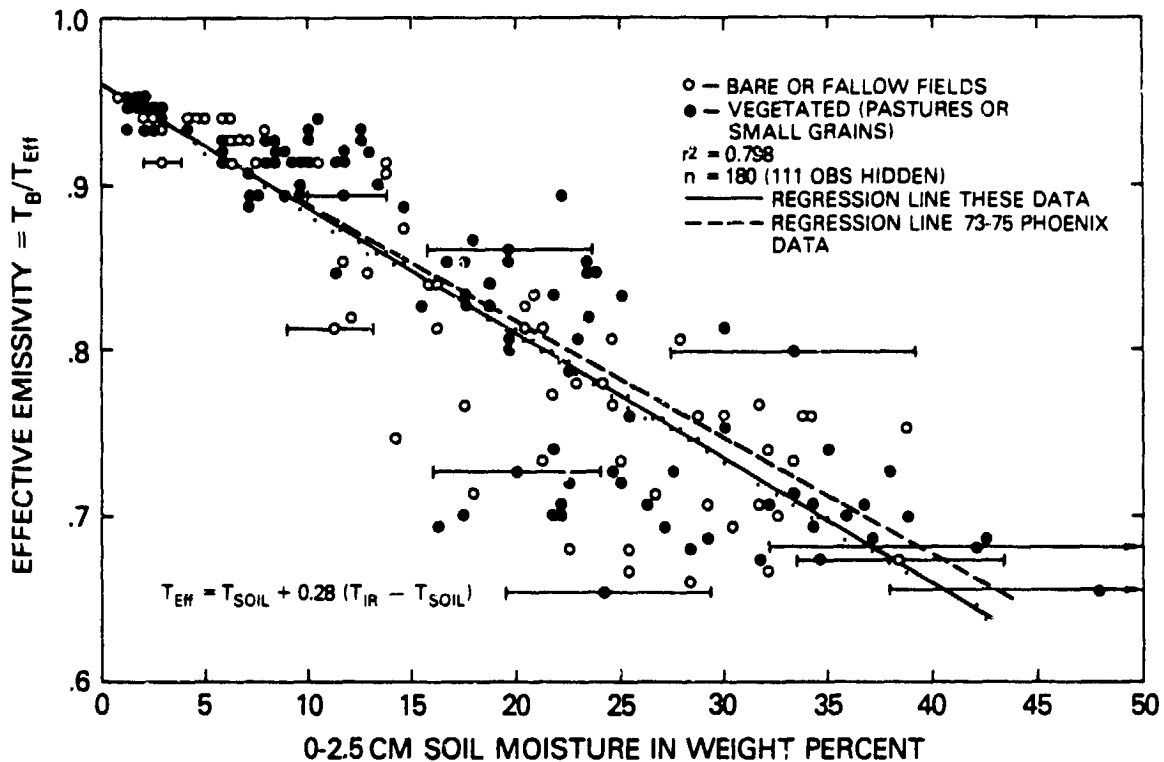


Figure 4. 21 cm microwave emissivities measured from an aircraft platform (alt. = 300m). Data from 9 flights during 1976-1978 over a test site in Hand County South Dakota.  $T_{IR}$  is the infrared surface temperature measured from the aircraft and  $T_{SOIL}$  is from ground measurements.

with API. For a pair of passes over the same track 5 days apart in June 1973, there was a 30-50K increase in  $T_B$  as the soil dried following heavy early June rains. An unpublished analysis by Wang and Schmugge of a set of 5 passes is presented in Figure 5. The  $T_B$  value for each nonoverlapping footprint is compared with the average of the API values calculated for the met stations within the footprint. A correlation analysis yielded an  $r^2 = 0.7$  for the 85 separate footprints. The error bars represent the standard deviation of the API values for each footprint and indicate that the spatial variability of the rainfall over the 110 km footprint of the radiometer is a major cause of the scatter  $\phi$  in the data. A radiometer with higher spatial resolution and more frequent coverage would produce a better correlation. Other analyses of the Skylab data in terms of soil moisture have been reported by Eagleman and Lin (1976) and McFarland (1976).

Analysis of two years of Nimbus-5 ESMR data for the southern great plains also has shown high correlations with API under suitable conditions (Blanchard et al., 1981b). Figure 6 is a comparison of ESMR emissivity with API for the states of Kansas, Oklahoma, and northern Texas using a 25 km grid. There is a clear correlation between the regions of low emissivity and high API. The emissivity was calculated by dividing the ESMR  $T_B$  by the maximum air temperature. The best correlations ( $r > 0.8$ ) were obtained for those areas in which a high percentage of the area was devoted to the production of winter wheat and during the early spring and fall. These areas which are relatively flat have limited vegetative cover during these periods. Areas with more rugged terrain or more vegetative cover show a poor correlation between  $T_B$  and API. These results indicate that spaceborne radiometers can respond to surface moisture changes and can be related quantitatively to the antecedent precipitation.

### 3. SNOWPACK PROPERTIES

The majority of the streamflow in most areas of the western United States is produced by the melting of the accumulated snowpack. In order to make efficient use of this snowmelt runoff, water resource agencies must be able to make early predictions of the total flow. In recent years satellite determinations of the snow covered area have been used to increase the accuracy of the early streamflow forecasts (Rango and Itten, 1976; Rango, 1975). An additional improvement could be made if it were possible to remotely sense the depth or water equivalent of the snow. At the present time this is not possible but preliminary studies with microwave systems indicate that the potential may be there for doing this.

In contrast to the case for soils the bulk dielectric properties of snow does not give an adequate prediction of the microwave response. For example, the dielectric constant of snow will be between that of air ( $\epsilon = 1.0$ ) and ice ( $\epsilon = 3.2$ ), the two components of snow, and can be estimated as a function of snow density using the standard dielectric mixing formulae. For a snow density of  $0.5 \text{ gm/cm}^3$  this yields a dielectric constant of 2. The resulting emissivity for smooth surface would be approximately 0.98 and a  $T_B$  very close to the physical temperature should be observed. Indeed this is approximately observed for long wavelengths ( $> 10 \text{ cm}$ ) and thick snowpacks, e.g., glaciers. For shorter wavelengths a more interesting phenomena is observed, volume scattering by the individual ice grains reduces  $T_B$  by scattering some of the radiation out of the sensor field of view. This has the effect of introducing some of the cold sky brightness temperature into the radiometer field of view, thus reducing the observed  $T_B$ . For the active microwave case volume scattering greatly increases the backscatter from the snow. This effect will become stronger as the wavelength in ice approaches the grain sizes in the snow, typically on the order of a mm.

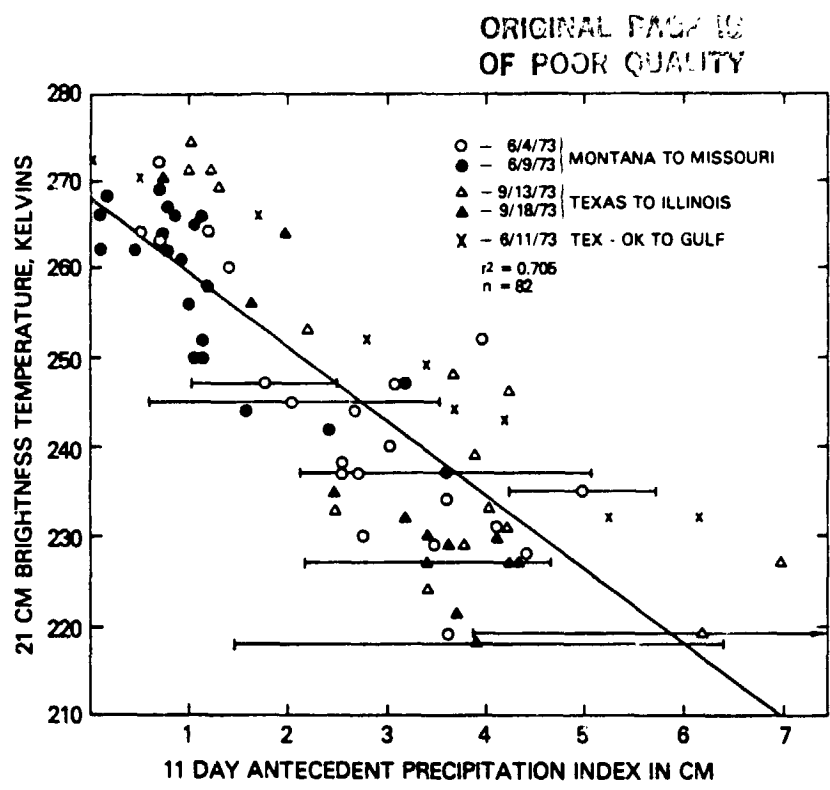


Figure 5. Comparison of 21 cm Skylab brightness temperatures over the U.S. Great Plains with API, which were averaged over the 110 km resolution element of the spacecraft sensor. The X's are from McFarland (1976).

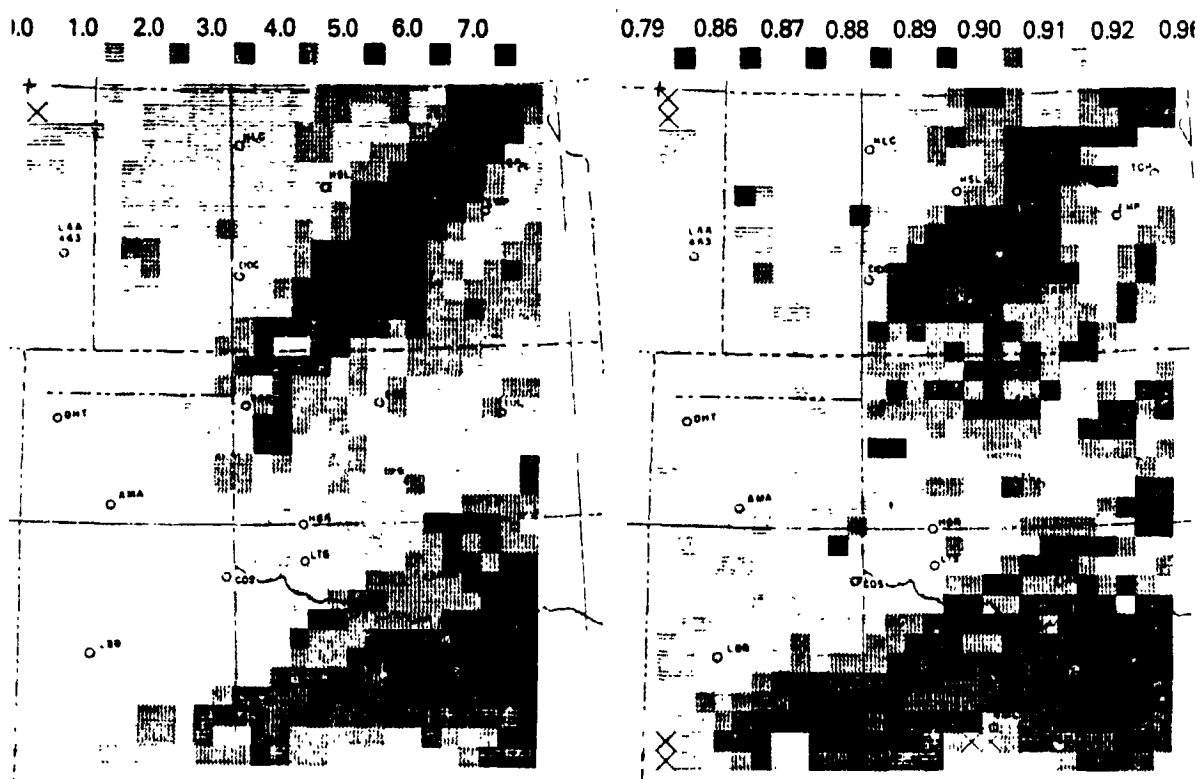


Figure 6. Comparison of Nimbus-5 ESMR emissivity over the southern Great Plains. Data from the Remote Sensing Center of Texas A&M University (Blanchard et al., 1981b).

## ORIGINAL PAGES OF POOR QUALITY

Experiments to date have indicated that the microwave response of snow is dependent on a number of parameters: depth, grain size, presence of liquid water, type and condition of the underlying media and the wavelength of the observation. Examples of these dependencies are presented in Figure 7 where results from radiometers operating in the wavelength range 0.8 to 21 cm are given. The radiometers were on the NASA Convair 990 aircraft which flew over snow targets in the western U.S. Three sites with different substrata were overflown. The first of these is Bear Lake, on the Utah-Idaho border, which had 15 cm of snow and 25 cm of ice over the water. The second site was a river valley south of Steamboat Springs, Colorado, which had 80 cm of snow over a wet soil. The third site was the South Cascade Glacier of the state of Washington which had 5 meters of snow over ice. This was at a point near the terminus or the end of the glacier.

In this figure  $T_B$  is plotted versus the wavelength of the radiometers. Note the large variation in brightness temperature observed by the longer wavelength radiometers, indicating their sensitivity to the media underlying the snow due to the transparency of snow at these wavelengths. The short wavelength radiometers, the 0.8- and 1.5-cm, displayed the least amount of variation and, in general, displayed a lower brightness temperature than the longer wavelength radiometers. This is due to the fact that they were responding primarily to the surface snow, which in general was dry with a density on the order of  $0.2 \text{ g/cm}^3$ . The lower brightness temperature for these wavelength radiometers is due to a volume scattering effect caused by the snow grains.

At Bear Lake, the 21-cm radiometer has the lowest brightness temperature, indicating that it is seeing the low brightness

temperature of water through the snow. As the wavelength decreases, the brightness temperature increases until the dry snow values for the 1.5- and 0.8-cm radiometers are reached. Similarly, at Steamboat Springs, the 21-cm radiometer has the lowest brightness temperature, indicating that it is able to see the wet soil through the snow.

At the glacier, the 21-cm and 11-cm radiometers had the highest brightness temperatures, and the values observed were in good agreement with those calculated using the known dielectric properties for ice and snow. As the wavelength decreases at the glacier, the brightness temperature also decreases, until the low brightness temperature values for the 0.8- and 1.5-cm radiometers are reached, which indicates that these low brightness temperatures are in disagreement with the values calculated using the bulk dielectric properties for snow and ice.

### 3.1 Snow Wetness

Another important snow property that has a large effect on the microwave response at the shorter wavelengths is the presence of liquid water in the snowpack. For dry snow volume scattering reduces the observed  $T_B$  by scattering some of the radiation out of the sensor field of view. When there is a film of liquid water on the ice grains the scattering is reduced, the medium becomes lossy and behaves radiometrically like a blackbody. In Figure 8 the diurnal variations of  $T_B$  are presented for a case in which there is some surface melting at mid-day. The snow temperature at 26 cm above ground (4 cm below snow surface) reached  $0^\circ\text{C}$  at 1030 hours and remained near  $0^\circ\text{C}$  until about 2200 hours by which time the air temperature had dropped down to about  $-4^\circ\text{C}$  causing the pack to cool again. The ground was in a frozen state throughout the diurnal cycle.

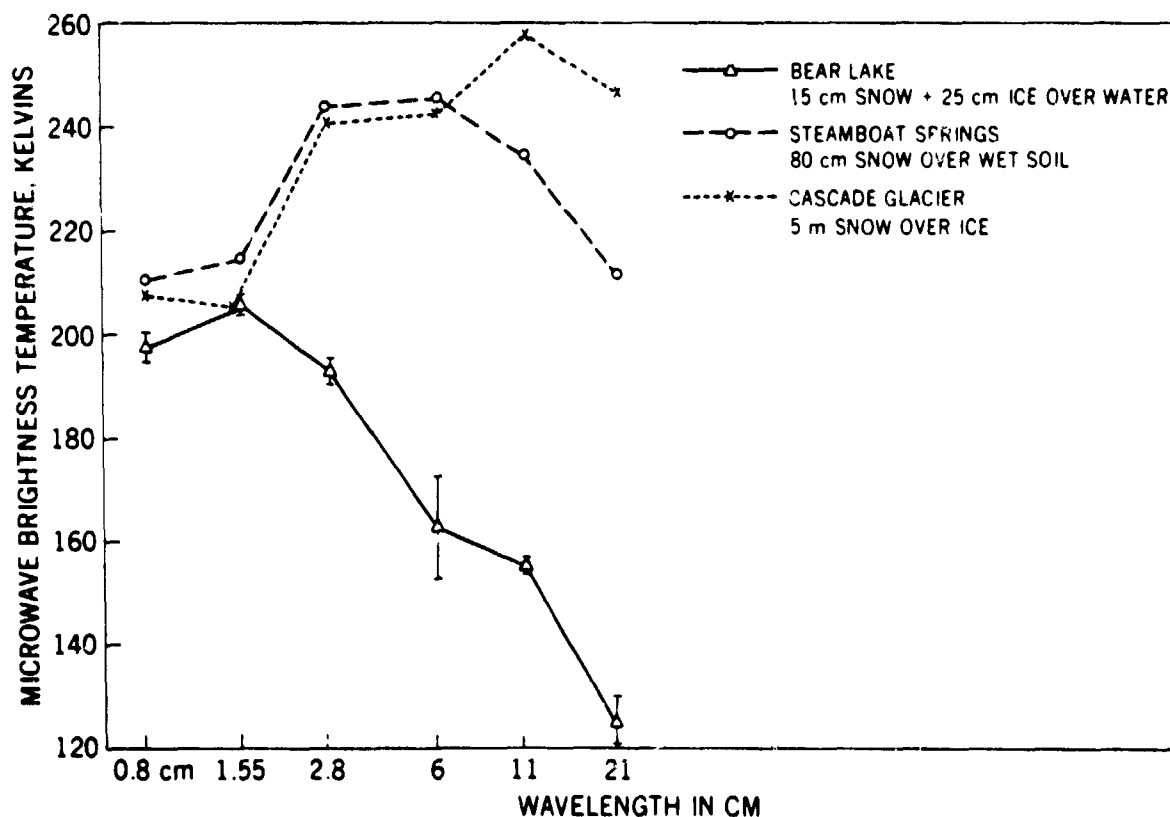


Figure 7. Variation of microwave brightness temperature for snow with radiometer wavelength (Schmugge, 1973).

Date: 2/17 - 2/18/77  
Polarization: H  
Angle of Incidence  
(Degrees): 55  
Snow Depth (cm): 30  
Water Equivalent (cm): 6.3

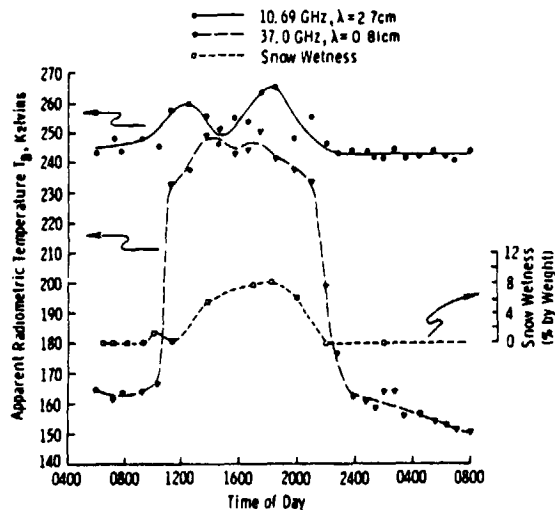


Figure 8. Diurnal variation of microwave brightness temperature measured from a tower at Steamboat Springs, Colorado. From Stiles & Ulaby, 1980.

The wetness, or percent free water by weight, lags the air temperature which went above  $0^{\circ}\text{C}$  at 900 hours, and continues to increase during periods of positive air temperatures. The wetness was measured by a calorimetric technique. The reason for the dip in free water at 1100 hours is unknown but does to some extent follow the air temperature drop. Very low values of  $T_B$  are observed for the dry snow of the 0.81 cm wavelength, with a large, 80K, rise in  $T_B$  when the snow becomes wet. The rise in  $T_B$  at the 2.7 cm wavelength is much less but  $T_B$  does come close to the physical temperature of the snow. From these results it is clear that microwave approaches can detect the presence of liquid water in the snow and thus the onset of melt in the pack, whether or not the amount of liquid water can be determined is a subject for further research. This large diurnal effect was also observed in field measurements made in Switzerland (Hofer and Matzler, 1980).

### 3.2 Snow Water Equivalent

The important question which remains is: can the microwave approaches yield a determination of the depth and/or water equivalent of the snow? Some studies have shown that this lowering of  $T_B$  at the shorter wavelengths for dry snow is a function of snow depth (Edgerton et al., 1971, Ulaby and Stiles, 1980). Figure 9 is a presentation of results from experiments conducted in Colorado by the University of Kansas which give an indication of this possibility. The microwave responses were observed for snowpacks which were artificially piled. The snow and air temperatures were below  $0^{\circ}\text{C}$  during these experiments, therefore the snow was dry. A  $T_B$  change of 50K was observed at the 2.8 cm wavelength for snowpack changes of 140 cm. At a shorter wavelength, 0.81 cm, there was a greater  $T_B$  change but the curve saturated for water equivalents greater than 30 cm. The difference between the two curves in Figure 9 points up the difficulty in applying these results, namely the dependence on snow density. There was a factor of two difference in the density between the two experiments. The first having been done with newly fallen snow while experiment three was done with twice as dense, older snow which presumably had larger grain

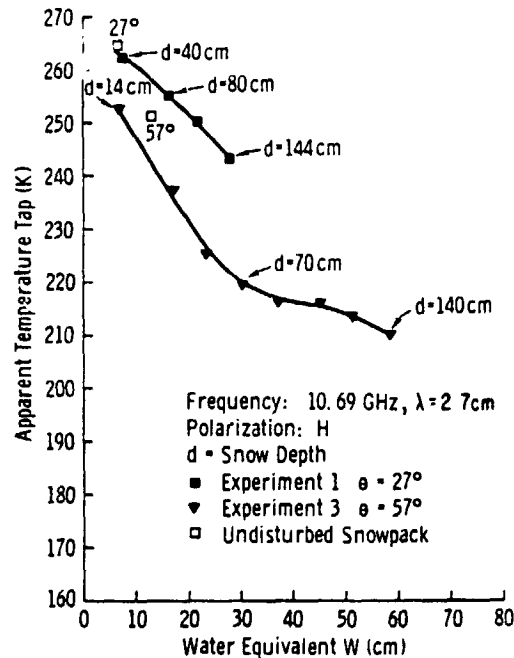


Figure 9. Variation microwave brightness temperature with snow water equivalent. From tower measurements at Steamboat Springs, Ulaby & Stiles, 1980.

sizes. Thus there is a sensitivity of the microwave responses to snow water equivalent, but this sensitivity will depend on the snow's history and the nature of the underlying medium.

The potential utility of microwave approaches is shown in Figure 10 where values of  $T_B$  observed by the Scanning Multichannel Microwave Radiometer (SMMR) operating at a wavelength of 0.81 cm on the Nimbus 7 spacecraft are compared with surface measurements of snow depth for Central Russia (Chang et al., 1981). Snow depth values from ground stations were used to draw isohyets of snow cover, which were then averaged over  $1^{\circ} \times 1^{\circ}$  grid cells for comparison with the similarly averaged SMMR  $T_B$ 's. An  $r^2$  of 0.75 was obtained from the correlation which is very encouraging. Similar results were obtained using the 1.55 cm and 0.81 cm data from the ESMR's on Nimbus 5 and 6 (Rango et al., 1979). In performing these analyses it is necessary that the air temperatures are below  $0^{\circ}\text{C}$  to insure that the snow is dry, and to know something of the history of the snowpack. These requirements are complications which hinder the application of these space data for snowpack observations.

These results are very encouraging for the possible use of microwave approaches to remotely monitor snowpack conditions for both total water content and the presence of liquid water. It is clear that the latter quantity can be observed with our current understanding while the former requires still further research to understand how the effects of the snowpack history on the water equivalent relationship can be taken into account.

### 4. CONCLUSIONS AND RECOMMENDATIONS

Results have been presented which show that microwave radiometric approaches are capable of monitoring the moisture content in the surface layer of the soil (5 cm thick), detecting the presence of liquid water in snow, and hold promise of being able to determine the water equivalent of snowpacks and

ORIGINAL PAGE IS  
OF POOR QUALITY

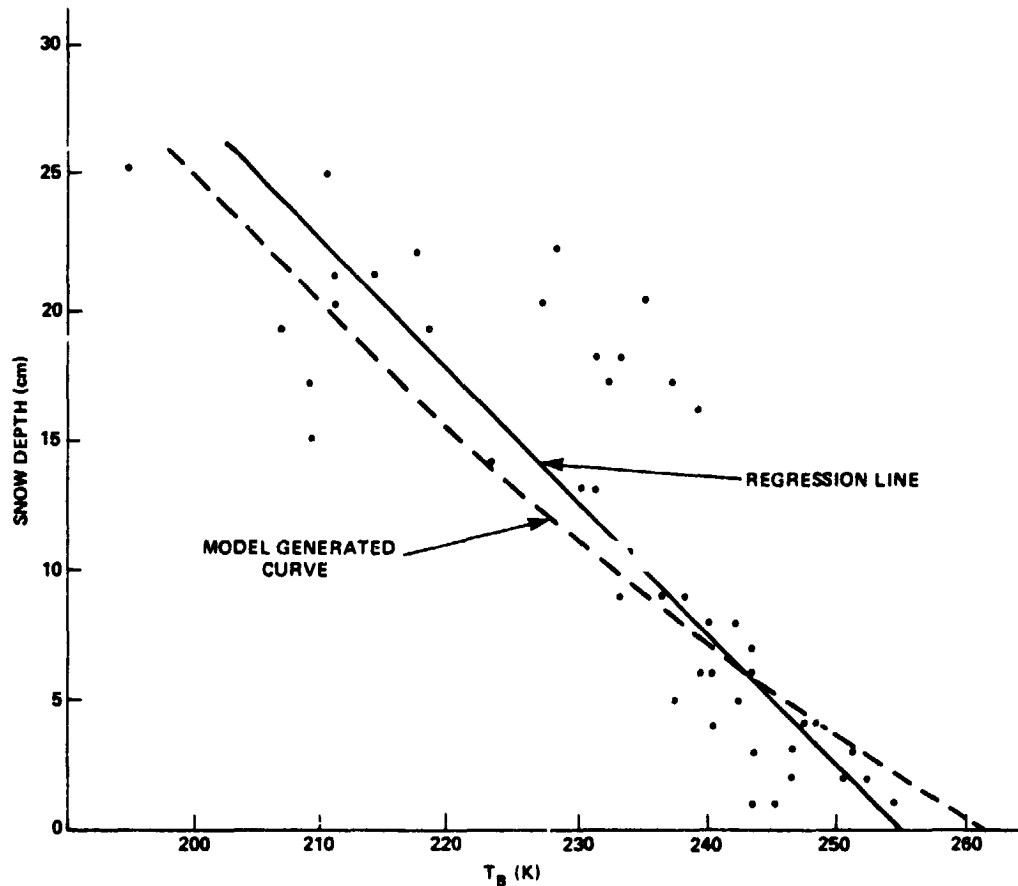


Figure 10. Nimbus-7 SMMR 37 GHz (0.8 cm) vertically polarized brightness temperatures versus snow depth measured in Central Russia. The dashed curve is from a model assuming snow grain sizes of 0.4 mm. From Chang et al., 1981.

delineating areas of rainfall over land. All these parameters are important for improved monitoring of precipitation.

Our understanding of the basic physics behind these applications has proceeded to the point where microwave sensors can be defined which would be specifically for hydrologic applications. These microwave sensors would complement the information currently available from existing visible and infrared sensors, specifically in such areas as soil moisture and snowpack monitoring.

At the present there are no plans to fly long wavelength radiometers for soil moisture purposes, and those currently in space, i.e., Nimbus-7 SMMR, have too short a wavelength to penetrate significant amounts of vegetation. However the SMMR data should be analyzed in a manner similar to that used for ESMR to determine its information content for critical wheat growing areas of the world. This may lead to the development of potential techniques which can be used with DOD SMI data when it becomes available. Studies of possible spaceborne long wavelength radiometers for soil moisture purposes should be initiated.

The short wavelength channels on the Nimbus-7 SMMR have been shown to be very effective for snowpack monitoring and the complete data set from this sensor should be analyzed when it becomes available. Systems with improved resolutions at these wavelengths should be pursued.

## 5. REFERENCES

- Barton, I. J., 1978: A Case Study Comparison of Microwave Radiometer Measurements over Bare and Vegetated Surfaces. *J. Geophys. Res.*, 83, 3513-3517.
- Blanchard, B. J., M. J. McFarland, T. J. Schmugge, and E. Rhoades. 1981a: Estimation of Soil Moisture with API Algorithms and Microwave Emission, To be published in *Water Resources Bulletin*.
- Blanchard, B. J., M. J. McFarland, S. Theis, and J. G. Richter, 1981b: Correlation of Spacecraft Passive Microwave System Data with Soil Moisture Indices (API) Final report RSC-3622-4, NASA contract NSG-5193, Remote Sensing Center, Texas A&M University, College Station, Texas 77843.
- Blinn, J. C., III, J. E. Conel, and J. G. Quade, 1972. Microwave Emission from Geological Materials: Observations of Interface Effects. *J. Geophys. Res.*, 77, 4366-4378.
- Burke, W. J., T. Schmugge, and J. F. Paris, 1979: Comparison of 2.8 and 21 cm Microwave Radiometer Observations over Soils with Emission Model Calculations. *J. Geophys. Res.*, 84, 287-294.

ORIGINAL PAGE IS  
OF POOR QUALITY

- Chang, A. T. C., J. L. Foster, D. K. Hall, A. Rango, and B. K. Hartline, 1981: Snow Water Equivalent Determination by Microwave Radiometry. NASA Technical Memorandum 82074, Goddard Space Flight Center, Greenbelt, MD 20771. Submitted for publication to Water Resources Research.
- Choudhury, B. J., T. J. Schmugge, R. W. Newton, and A. Chang, 1979: Effect of Surface Roughness on the Microwave Emission from Soils. *J. Geophys. Res.*, 84, 5699-5706.
- Eagleman, J. R., and W. C. Lin, 1976: Remote Sensing of Soil Moisture by a 21 cm Passive Radiometer. *J. Geophys. Res.* 81, 3660-3666.
- Edgerton, A. T., A. Stogryn, and G. Poe, 1971: Microwave Radiometric Investigations of Snowpacks, Aerojet General Corp., Final Report 1285R-4.
- Estes, J. E., M. R. Mel, J. O. Hooper, 1977: Measuring Soil Moisture with an Airborne Imaging Passive Microwave Radiometer. *Photogrammetric Engineering and Remote Sensing*, 43, 1273-1281.
- Hofer, R., and C. Matzler, 1980: Investigations on Snow Parameters by Radiometry in the 3 to 60 mm Wavelength Region. *J. Geophys. Res.* 85, 453-460.
- Jackson, T. J., T. J. Schmugge, and J. R. Wang, 1981: Effects of Vegetation on Passive Microwave Estimates of Soil Moisture. Proc. of IGARSS '81 Symposium, Washington, D.C., June 1981.
- Lundien, J. R., 1971: Terrain Analysis by Electromagnetic Means. Tech. Report No. 3-693. Report 5. U.S. Army Waterways Experiment Station, Vicksburg, Miss.
- McFarland, M. J., 1976: The Correlation of Skylab L-Band Brightness Temperatures with Antecedent Precipitation. Preprints Conf. on Hydrometeorology, Fort Worth, Texas, April 1976.
- McFarland, M. J., and B. J. Blanchard, 1977: Temporal Correlation of Antecedent Precipitation with Nimbus-5 ESMR Brightness Temperature. Preprints Second Conf. on Hydrometeorology, Toronto, Ont., Canada, October 1977.
- Newton, R. W., 1976: Microwave Sensing and its Application to Soil Moisture Detection. Technical Report RSC-81 of the Remote Sensing Center at Texas A&M University, College Station, Texas. Available from Univ. Microfilms order No. 77-20-398.
- Newton, R. W., and J. W. Rouse, 1980: Microwave Radiometer Measurements of Soil Moisture Content. *IEEE Trans. on Antennas and Propagation*, AP-28, 680-686.
- Njoku, E. G., and J. A. Kong, 1977: Theory for Passive Microwave Sensing of Near-Surface Soil Moisture. *J. Geophys. Res.*, 82, 3108-3118.
- Poe, G. A., A. Stogryn, and A. T. Edgerton, 1971: Determination of Soil Moisture Content Using Microwave Radiometry. Final Report No. 1684 FT-1, DDC Contract O-35239 Aerojet-General Corp., El Monte, California.
- Rango, A., (ed), 1975: Operational Applications of Satellite Snowcover Observations, National Aeronautics and Space Administration, NASA SP-391, Washington, D C , 430 pp.
- Rango, A., and K. I. Itten, 1976: Satellite Potentials in Snow-cover Monitoring and Runoff Prediction. *Nordic Hydrology*, 7, 209-230
- Rango, A., A. T. C. Chang, and J. L. Foster, 1979: The Utilization of Spaceborne Microwave Radiometers for Monitoring Snowpack Properties. *Nordic Hydrology*, 10, 25-40
- Schmugge, T., 1973: Microwave Signature of Snow. Proc. of the Annual Science and Technology Review GSFC, National Aeronautics and Space Administration, NASA SP-361, pp 193-195.
- Schmugge, T. J., P. Gloersen, T. Wilheit, and F. Geiger, 1974: Remote Sensing of Soil Moisture with Microwave Radiometers. *J. Geophys. Res.* 79, 317-323
- Schmugge, T. J., T. Wilheit, W. Webster, Jr., and P. Gloersen, 1976: Remote Sensing of Soil Moisture with Microwave Radiometers-II. NASA Technical Note TN D-8321. NTIS Order No. N76-32625.
- Schmugge, T. J., J. M. Meneely, A. Rango, and R. Neff, 1977: Satellite Microwave Observations of Soil Moisture Variations, *Water Resources Bull.*, 13, 265.
- Schmugge, T., 1978: Remote Sensing of Surface Soil Moisture, *J. of Appl. Meteor.*, 17, 1549-1557.
- Schmugge, T. J., 1980: Effect of Texture on Microwave Emission from Soils. *IEEE Trans. of Geoscience & Remote Sensing*, GE-18, 353-361.
- Stiles, W. H., and F. T. Ulaby, 1980: The Active and Passive Microwave Response to Snow Parameters, Part I: *J. Geophys. Res.* 85, 1037-1044.
- Ulaby, F. T., and W. H. Stiles, 1980: The Active and Passive Microwave Response to Snow Parameters, Part II: Water Equivalent of Dry Snow. *J. Geophys. Res.* 85, 1045-1049.
- Ulaby, F. T., A. K. Fung, and W. H. Stiles, 1978: Backscatter and Emission of Snow: Literature Review and Recommendations for Future Investigations, RSL Tech. Report 369-1, University of Kansas Center for Research, Lawrence, Kansas.
- Wang, J., T. Schmugge, and D. Williams, 1978: Dielectric Constants of Soils at Microwave Frequencies - II. NASA Tech Paper TP-1238.
- Wang, J. R., and T. J. Schmugge, 1980: An Empirical Model for the Complex Dielectric Permittivity of Soils as a Function of Water Content. *IEEE Trans. Geoscience & Remote Sensing*, GE-18, 288-295.
- Wang, J. R., J. C. Shiue, and J. E. McMurtrey, 1980: Microwave Remote Sensing of Soil Moisture Content over Bare and Vegetated Fields. *Geophys. Res. Lett.*, 7, 801-804.
- Wilheit, T. T., 1978: Radiative Transfer in a Plane Stratified Dielectric. *IEEE Trans. Geo. Electron.*, GE-16, 138-143

N83 25308

D39

ORIGINAL DOCUMENTS  
OF POOR QUALITYSPACEBORNE PRECIPITATION RADARJ. Eckerman and R. Meneghini  
NASA/Goddard Space Flight Center

Spaceborne precipitation radar design is shown to be tightly coupled to the application of the precipitation data. A methodology for selecting radar parameters is presented. Radar system performance results from simulations for several radar configurations are presented. In the studies thus far, more emphasis has been placed on rain rate retrieval algorithms and sources of errors than on selection or design of specific antenna and electronics components. Space applications requiring precipitation information are categorized as needing either rain rate or rainfall data. For the latter case, radar beam-averaged rain rates sampled several times daily will be adequate. Systems which provide rain rates on a global basis must retrieve the vertical distribution of precipitation. The accuracy of the retrieved rain intensities is a function of beam-filling, radar calibration, measurement strategy and sampling strategy (number of independent pulses per dwell time for storm snapshots and time between snapshots for rainfall). Measurement strategies include single frequency/unattenuated, single frequency/partially attenuated, single and multiple frequency/moderately attenuated, combined radar/radiometer, dual polarization and the surface reference technique. Methodologies are of two kinds: (1) assume empirical relations between radar reflectivity, attenuation coefficients and rain rate or (2) assume two parameter drop size distribution (DSD) and determine the DSD parameters from the radar-observables. Radar system design parameters (antenna, PRF, pulse duration, frequency, etc.) are directly determined from the meteorological requirements (storm types/dimensions, accuracies, minimum and maximum rain rates). Radar system performance has been studied using deterministic and statistical models. In general, multiple wavelengths are needed to provide reasonably accurate (25%) measurements over a sufficient range of rain intensities. Range cell beam filling causes significant uncertainty in rain rate retrieval for large beam widths (comparable to storm height). Precipitation retrieval for range cells close to the ground are ground clutter contaminated. Accurate vertical profiling is only feasible when the beamwidth is smaller ( $1/2$  to  $1/4$ ) than the storm height. In practice antenna dimensions for the narrow beamwidth case are much larger than for wide beamwidths and will probably be developed for the second generation systems. The more modest cost and complexity of the wide beamwidth radars are candidates for the initial effort.



ORIGINAL PAGE IS  
OF POOR QUALITY

The major tested space-based technique for mapping of precipitation is the microwave radiometer. The electronically-scanned microwave radiometer (ESMR) on Nimbus-5 has provided continuous global surveillance of the Earth since 1973. (1) At the 19 GHz ESMR frequency, beam-averaged rain rates are determined over oceans; over land the upwelling radiation from the surface masks the precipitation effects and does not permit a direct precipitation determination. Advanced spaceborne microwave radiometers with large antenna will not have the beam filling problem of ESMR-5 data. The radiometer determines the total attenuation by the precipitation in the main lobe. The specific attenuation is computed by ratioing the total attenuation to assumed climatological storm height. The rain rate is determined from an empirical linear relation between specific attenuation and rain rate. This relation is approximately independent of drop size at wavelengths of the order of 1 to 1.5 cm. The resultant precipitation rates are computed to be in error by about +50%. Extension of the radiometer technique to observations over land is under study now. However, it is not expected to result in a quantitative determination of precipitation intensity despite the fact that the Nimbus-6 ESMR and Nimbus-7 SMMR data have shown that under some conditions (wet soil) precipitation can be discerned. The measurements which cannot be made radiometrically but are feasible for radar are:

- Rain over land
- Vertical distribution of rain (profile)
- Determination of storm vertical structure
- Rain intensity measurements over 2 orders of magnitude

In many ways radar and radiometer can complement each other. The optimum precipitation sensor may be a combination of the two instruments. In the present paper we discuss the characteristics and performance of spaceborne precipitation radar systems.

Although precipitation is an important parameter in many of the space applications, there presently are no operational models which require precipitation data. Various space applications are listed in Table (1) below. (2)

Table (1)

	Rain Fall	Rain Rate
Global Weather	Storm location Severity	Global Circulation Models
Severe Storms	Latent heat, Amount of water	Floods, Tropical Cyclone paths
Climate	Latent heat Soil Moisture	
Agriculture	Soil Moisture	Crop Damage
Water Resources	Soil Moisture Amount of Water	Floods
Ocean Processes	Ship Routing	Oil Rig Safety

Beside each application are tabulated the uses or appropriate rain parameters under a heading of either rain fall or rain rates. It is important to make the distinction between these two quantities since rain rate data requires a radar which profiles the precipitation. Rain fall, the time integral of rain rate, can be obtained with beam-averaged observations and in some instances may not be as demanding as a rain rate measurement. An important part of precipitation determination by radar is the specification of the minimum and maximum rate for which accurate observations are to be made. This aspect of the problem is highly applications-oriented. Consider the statistical data in figure (1) on the percent of time various rain rates are exceeded for a maritime climate. This data leads to the percent of rainfall contributed at those rates as indicated in figure (1). Notice that less than 10% of the total rainfall is contributed by rain rates above 10 mm/hr. So that if we are primarily concerned with applications which need only rainfall, small error would be made by limiting the maximum rain rates to a relatively low value. Of course this type reasoning would have to be extended to other rain regions and the desired rainfall accuracy decided by the users before an upper limit was finally decided upon. Nevertheless, the philosophy of picking the primary applications and culling the requirements from them cannot be overstated. The precipitation radar system for a 10 mm/hr. maximum rain rate is considerably simpler and less expensive than one which must detect rains up to 200 mm/hr.

The output of precipitation radars is global storm snapshots which are very powerful meteorological tools. However, from polar low Earth orbit even with very wide swath, each place on Earth is visited at most 2 times daily. At lower orbital inclination, e.g.,  $50^\circ$ , this is increased to 3 or 4 times daily. With a single spacecraft, the utility of these infrequent snapshots is limited to such long-lived storm systems as hurricanes and other tropical cyclones. More frequent coverage requires either more low earth orbit satellites or use of geosynchronous orbit. At these large geosynchronous orbital distances, the antenna needed to resolve storm features is too large to be practical (500 m) within this century for real aperture radar.

### Introduction

The possibility of observing precipitation from a spaceborne radar has been feasible for many years.<sup>(3,4)</sup> Approaches have been advanced including scanning beam and pushbroom optics at frequencies from 10 to 35 GHz. However, until recently complete system simulations had not been performed so that estimations of radar performance were very restricted.

The design of a spaceborne radar is similar in many respects to a ground-based radar. The scanning beam of the ground radar generates a storm image by sweeping through the nearby storm at low elevation angle. Rain properties are inferred from the backscattered signal. From space the storm is illuminated at a large incidence angle ( $\sim 45^\circ$ ) in order to have a large swath width. The antenna must rotate fast enough so that consecutive beam arcs are contiguous. The satellite motion advances the scanning radar beam through the atmosphere building up a 3-D (RHI/PPI) image of the storm. The ways in which the spaceborne radar differs from a ground-based cousin are:

--The satellite-based radar is much further from the storm than the land-based radar. Consequently, the beamwidths (diffraction limited antennas) are larger (lower resolution)

--The space-based radar looks down on the storm.

a. In the case of stratiform rain, the radar penetrates both an ice layer and a melting layer before reaching the rain layer.

b. The space-based radar beam terminates at the Earth surface

--It is not possible to obtain storm drop size distributions with nearby disdrometers, etc.

The consequences of these key differences constrain the radar design significantly.

The lower resolution requires that the antennas be as large as possible and frequencies as high as possible in order to minimize the beam filling problem. The optimum resolution is of the order of the minimum storm

cell width (1 km). The minimum resolution is the average height of the rain layer ( $\sim 4$  km). The incidence of the beam on the ground has two negative aspects: (1) tight sidelobe control is necessary in order to minimize ground clutter, and (2) those main lobe range bins which contact the ground are not useful in observing the rain nearest the ground. On the plus side, however, the ground may provide a reference surface for determination of beam-averaged attenuation.

A consequence of not knowing the actual drop size distribution within the storm is that the precipitation retrieval method must either be independent of drop size or else two independent measurements of the rain must be made. If only a single measurement is made, then a drop size distribution must be assumed which results in errors in the retrieved rain rates. Several strategies are discussed in this paper.

#### The Relation of Application Requirements to Radar System

Precipitation radar system parameters are directly and tightly coupled to the applications requirements. Meteorological program priorities will provide the keys to the radar system designs. The importance of such lies in sensor economics; the more stringent the performance requirements, the greater the system cost. A systems trade off diagram, figure (2), illustrates these interrelations. For example, the resolution of the system is determined by the accuracy requirement through the beam filling and the types of storms to be emphasized, etc. The greater the required accuracy, the more resolution and the larger the antenna. The number of simultaneous radars and their frequencies is affected by the minimum and maximum rain rates.

Optimizing the radar for a special set of requirements does not obviate surveillance of other types of storms since performance of these radars degrades gracefully around the boundary limits. However, at extreme values of rain rate, only detection of upper range bins will be possible. This means that the storm cells will be mapped but quantitative information cannot be obtained. Similarly, for rain intensities below the lower bound, signal-to-clutter problems decrease the accuracy of the determination but again, detection is feasible below the optimized design values.

The mathematical formalism for computing the precipitation radar parameters is very straightforward and has been presented in several technical reports over the past few years and will not be repeated here. (3) The two major engineering decisions which must be made are the antenna configurations and the signal processing strategy. These are discussed in the next sections of this paper.

#### Radar Antenna Configurations

Mechanically scanned antennas dwell for a finite time at each resolution element. Contiguity requirements cause the dwell time to be reduced as the IFOV is decreased. Unambiguous precipitation radar PRF is constrained by the storm height. The number of pulses per resolution cell or independent samples then decreases with smaller IFOV. For the IFOV's of 4 km

ORIGINAL DOCUMENT  
OF POOR QUALITY

(melting layer height) approximately 13 pulses can be received. If additional independent samples are needed, several strategies are available. Additional radars can be added each with a separate feed. Using the same feed, frequency diversity methods will permit operating multiple radars through the same feed and receiver. Other approaches are the wise pulse method of Brook and Krehbiel or pulse compression technique. These last techniques decrease the signal-to-noise ratio while increasing the effective number of independent samples and reducing system sensitivity.

For IFOV of strong convective cell diameter (2 km D), a conventionally pulsed, single beam radar will receive only 4 pulses/IFOV. Twenty-five beams/radar are needed to integrate 100 pulses to achieve a 10% measurement accuracy. However, more than 12 beams displacement produces excessive distortion with an off-axis parabolic antenna.

An alternative geometry is the pushbroom or simultaneous fixed-beam approach. A phased array antenna is used in a multiple beam mode with a single beam/radar per IFOV. For very large swath width, this requires many more radars than the scanning multiple beam; however, the number of pulses available for integration/IFOV = 8,000. This results in a variance of approximately 1% in the retrieved signal making pushbroom the best configuration for achieving high accuracy with high resolution. At GSFC we have studied the pushbroom configuration and found it to be complex, but feasible.

The scanning multiple beam (whisk broom) system is currently under study. The off-axis parabolic antenna lends itself to multiple frequency, and combined radar/radiometer, as well as dual polarization operation. The basic antenna is simpler and less expensive than the pushbroom. For coarse resolution, the whiskbroom approach wins. Of course, beam filling problems will limit system accuracy.

#### Modelling of Spaceborne Radars

Some of the differences between ground-based and spaceborne radars have been mentioned above. For spaceborne applications, non-attenuating wavelength radars have several disadvantages. The restrictions of the size of spaceborne antennas make it difficult for an S-band radar to resolve the more intense regions of rain rate. As the resolution requirements are relaxed, the partially filled range cells lead to errors caused by spatial averaging and small signal-to-noise ratios. Apart from the errors caused by poor resolution, rain rate determination at S-band is hindered by lower sensitivity and errors in the calibration constant and Z-R law. Attenuating-wavelength radars provide better resolution for a fixed antenna size. However, if use is made of the standard rain rate algorithm for these wavelengths, the accuracy of the estimate is seriously degraded by errors in the calibration constant and in the k-R, Z-R relations. In fact, it is well known<sup>(6)</sup> that whenever the attenuation is significant, the errors in the standard rain rate estimate are usually much greater than that at non-attenuating wavelengths. There have been several proposed solutions to this problem, most of which have two common features: (1) the methods make use of two or more

independent measurements, at least one of which is directly related to the attenuation, and (2) the measured attenuation is used to obtain the DSD or the rain rate thus bypassing the need for using the calibration constant or the Z-R law. Some of the methods that conform to this description are the dual wavelength<sup>(7-9)</sup>, the radar-radiometer<sup>(10)</sup> and the surface reference/total attenuation<sup>(11-16)</sup> methods. It should be noted that even though the dual-polarization method<sup>(17,18)</sup> has been used primarily at S-band frequencies, it may be possible to generalize it to X- and K-band frequencies.

The discussion above implies that a fairly large number of methods (including the standard S-band method) need to be analyzed for their potential application to spaceborne radars. The survey of the techniques must be done in the context of a spaceborne geometry where effects such as partial beamfilling, ground clutter and the bright band can be properly assessed. It is also evident that the performance of the various methods depends on the radar design parameters such as the operating frequencies, beamwidth, range resolution, etc. Thus, the purpose of the model is to aid in selecting the best combination(s) of radar design-radar algorithm for a spaceborne radar. For the remainder of the paper we will discuss the development of such a model, present several examples from a simplified version of it and finally describe its application to one of the techniques mentioned above.

The model is composed of deterministic and statistical sections. In the former, the mean return power from the rain and the surface are calculated as functions of distance into the storm. For all cases we assume that the scanning antenna provides contiguous coverage over the swath. This requirement, in turn, places constraints on the resolution, scan rate and number of samples that are available in each range bin. The meteorological model can be constructed by using three-dimensional radar-derived reflectivities (obtained, for example, from the Spandar) or by employing storm models derived from this or comparable data. For most of the work done thus far at Goddard, simple meteorological models have been used. Once the number of potential methods and radar systems have been narrowed, however, the use of actual data or more realistic storm models are warranted. Among the more important meteorological parameters that influence spaceborne measurements are: the finite extent of the precipitation, variable rain rates, the presence of ice and the bright band. An account of the surface return is also necessary since it can be a major source of error, especially for rain rate determination just above the surface.

Among the radar system parameters to be investigated are: the antenna dimension and gain pattern, the operating frequencies, range resolution and alternative waveform strategies which include pulse compression<sup>(14)</sup>, the broad-band radar<sup>(15)</sup>, frequency agility and multi-beam techniques. The various waveform possibilities are of particular importance for high resolution radar since in these cases a single beam monochromatic radar does not provide a sufficient number of independent samples to accurately determine the mean return power.

C - S

Once the meteorological and radar parameters are set, the mean return power from the surface and the hydrometeors can be computed as a function of range. These profiles of return power do not in themselves tell us how well the rain rate can be estimated. They are useful, however, in that they show the effects of attenuation, clutter, partial beamfilling, etc. More importantly, the profiles provide the basic input data to the meteorological algorithms.

In figure 3 the range bins and a schematic of the return power are shown for a down-looking radar beam of width comparable to the storm height. The simple storm model used is a horizontal slab of uniform rain rate. In figures 4 and 5, the logarithm of the receiver noise,  $N$ , the rain rate,  $R$ , and the surface or clutter return,  $C$ , have been plotted at each range bin. The abscissa is the slant range measured from the storm top downward into the precipitation. In figure 4 we have chosen an antenna diameter-to-wavelength ratio,  $D/\lambda$ , equal to 300,  $\lambda = 0.86$  cm,  $R = 10$  mm/hr for a 5 km storm height, 700 km satellite altitude and 1000 w peak transmit power. Several features of the plot are worth noticing. In the first several range bins, the rain return power increases because of the progressively greater fractional volume filled with precipitation. After the peak rain return has been reached (corresponding approximately to the first fully filled bin) it begins decreasing with a slope proportional to the attenuation coefficient. This behavior continues until the range bin in the main lobe intercepts the surface; thereafter, the rain returns fall off more rapidly because of the smaller volume of rain contributing to the backscattered power. The surface clutter follows a somewhat reversed progression. This contribution arises from the backscattered power from the annulus formed by the intersection of concentric spheres with a flat earth. As the radar pulse propagates through the storm, the inner and outer diameter of the annulus expands until a portion of it intersects the main lobe. This intersection corresponds to the broad maximum of the ground return shown in the figure. From the figure it is evident that unless the clutter power can be separated from the rain return (by means of Doppler processing, for example), the rain rate can not be estimated at those range bins near the surface.

In figure 5,  $D/\lambda = 1000$  and all other parameters are unchanged from those in figure 4. It can be seen that the finer resolution reduces the number of range cells that are degraded by partial beamfilling or clutter. Furthermore, with resolutions of this order (1 km) the more intense rain rate cells can be detected. There are, however, system costs for the improved performance with antennas of this size such as the increased fabrication difficulty and cost as well as the need for a more complex system design to provide a sufficient number of independent samples.

The purpose of the deterministic model is to simulate the radar return power from a particular storm. To gauge the capability of the various techniques/algorithms to estimate the rain rate or other meteorological parameters, the sources of error must be accounted for. Some of the systematic errors include beamfilling effects and offsets in the radar calibration constant. Random errors include the variability in the return power as well as variability in the  $k$ - $R$ ,  $Z$ - $R$ ,  $k$ - $Z$  laws. These random errors depend on the number of independent samples (return power) as well as the deviations of the actual drop temperature, drop-size and velocity distribution from the assumed values

(k-R, Z-R, k-Z laws). The necessary data (with the sources of error included) is next inserted into one of the meteorological algorithms. By means of a Monte Carlo simulation, particular realizations of the estimate are computed. These realizations correspond to the values that the random variables assume in accordance with prescribed probability density functions. Continuing in this way over a sufficient number of such realizations, the sample mean and variance of the estimate are computed. Two examples of the simulation results are shown in figures 6 and 7. We have used the data from figure 4 to generate figure 6 and the data from figure 5 to generate figure 7. The algorithm employed is from the surface reference technique. Each plot gives the mean and standard deviation of the path-integrated rain rate,  $R_{AV}$ , (both normalized by the true rain rate) as well as the normalized mean and standard deviation of two estimates of range profiled rain rate,  $R_1$ ,  $R_2$ . Since  $R_{AV}$  is not a function of range, we obtain single values for the normalized mean and standard deviation. In the figures, this normalized mean is represented by a horizontal line. At the end of this line a vertical bar is plotted of magnitude equal to twice the normalized standard deviation of  $R_{AV}$ . The same conventions are used to display the normalized mean and standard deviation of  $R_1$ ,  $R_2$ ; in this case, however, we plot these values at each range bin. A comparison of the two figures shows that the accuracy of the rain rate estimates is improved by using a higher resolution radar.

#### Summary

The number of methods and the variety of radar parameters that must be studied as a first step toward building a spaceborne radar necessitates the development of a model. In this manner a systematic analysis can be carried through to determine the accuracies, dynamic range, and profiling capabilities of various radar designs and algorithms. In this paper we have discussed some of the features of spaceborne radars and described a possible model by which these features can be studied.



References

- (1) Wilheit, T., et al., "A Satellite Technique for Quantitatively Mapping Rainfall over the Oceans," J. Appl. Meteor., 16, pp. 551-560, 1977
- (2) Eckerman, J., E. A. Wolff, Saceborne Meteorological Radar Measurement Requirements Meeting, August 1975
- (3) Skolnik, M. I., "The Application of Satellite Radar for the Detection of Precipitation," NRL Memo Report 2896, NRL, October 1974
- (4) Eckerman, J., "Orbiting Meteorological Radar," IEEE/Intercon, April 1975
- (5) Eckerman, J., "Orbiting Meteorological Radar," IEEE/NTC, San Diego, Dec. 1974
- (6) Eckerman, J., "Orbiting Meteorological Radar," IEEE/NTC, New Orleans, Dec. 1975
- (7) J. N. Bucknam, R. P. Dooley, F. E. Nathanson, "A Shuttle Meteorological Radar Study," Technology Service Corporation Final Report, TSC-W3-38, March 19, 1975
- (8) W. Hitschfeld and J. Bordan, "Errors Inherent in the Radar Measurement of Rainfall at Attenuating Wavelengths," J. Meteor., Vol. 11, pp. 58-67, 1954
- (9) D. Atlas and C. W. Ulbrich, "The Physical Basis for Attenuation-Rainfall Relationships and the Measurement of Rainfall Parameters by Combined Attenuation and Radar Methods," J. Res. Atmos., Vol. 8, pp. 275-298, 1974
- (10) J. Golhirsh and I. Katz., "Estimation of Rain Drop Size Distribution Using Multiple Wavelength Radar Systems," Radio Science, Vol. 9, pp. 439-446, 1974
- (11) P. J. Eccles and E. A. Mueller, "X-Band Attenuation and Liquid Water Content Estimation by a Dual-Wavelength Radar," J. Appl. Meteor., Vol. 10, pp. 1252-1259, 1971
- (12) D. B. Hodge and G. L. Austin, "The Comparison Between Radar- and Radiometer-Derived Rain Attenuation for Earth-Space Links," Radio Science, Vol. 12, pp. 733-740, 1977
- (13) C. W. Ulbrich and D. Atlas, "The Use of Radar Reflectivity and Microwave Attenuation to Obtain Improved Measurements of Precipitation Parameters Preprints 16th Radar Meteor. Conf., Amer. Meteor. Soc., Boston, pp. 496-503, 1975

References (con't.)

- (14) R. T. H. Collis and M. G. H. Ligda, "A Radar Rainage," Proc. 9th Radar Conf., Amer. Meteor. Soc., Boston, pp. 391-395, 1961
- (15) R. T. H. Collis, "Radar Precipitation Measurements," Proc. 11th Radio Meteor. Conf., Amer. Meteor. Soc., Boston, pp. 142-145, 1964
- (16) T. W. Harrold, "The Attenuation of 8.6 mm Wavelength Radiation in Rain," Proc. Inst. Elect. Eng. (London), Vol. 114, pp. 201-203, 1967
- (17) D. Atlas and C. W. Ulbrich, "Path and Area-Integrated Rainfall Measurements by Microwave Attenuation in the 1-3 cm Band," Preprints 17th Radar Meteor. Conf., Amer. Meteor. Soc., Boston, pp. 406-413, 1968
- (18) J. Eckerman, R. Meneghini and D. Atlas, "Average Rainfall Determination from a Scanning Beam Spaceborne Radar," NASA TM 79664, Nov. 1978
- (19) T. A. Seliga and V. N. Bringi, "Potential Use of Radar Differential Reflectivity Measurements at Orthogonal Polarizations for Measuring Precipitation," J. Appl. Meteor., Vol. 15, pp. 69-76, 1976
- (20) S. M. Cherry, J. W. F. Goddard and M. P. M. Hall, "Examination of Rain Drop Sizes Using a Dual-Polarization Radar," Preprints 19th Radar Meteor. Conf., Amer. Meteor. Soc., Boston, pp. 526-531, 1980

ORIGINAL PAGE IS  
OF POOR QUALITY

# CLOCK-MINUTE AVERAGED RAINRATE (MARITIME CLIMATE)

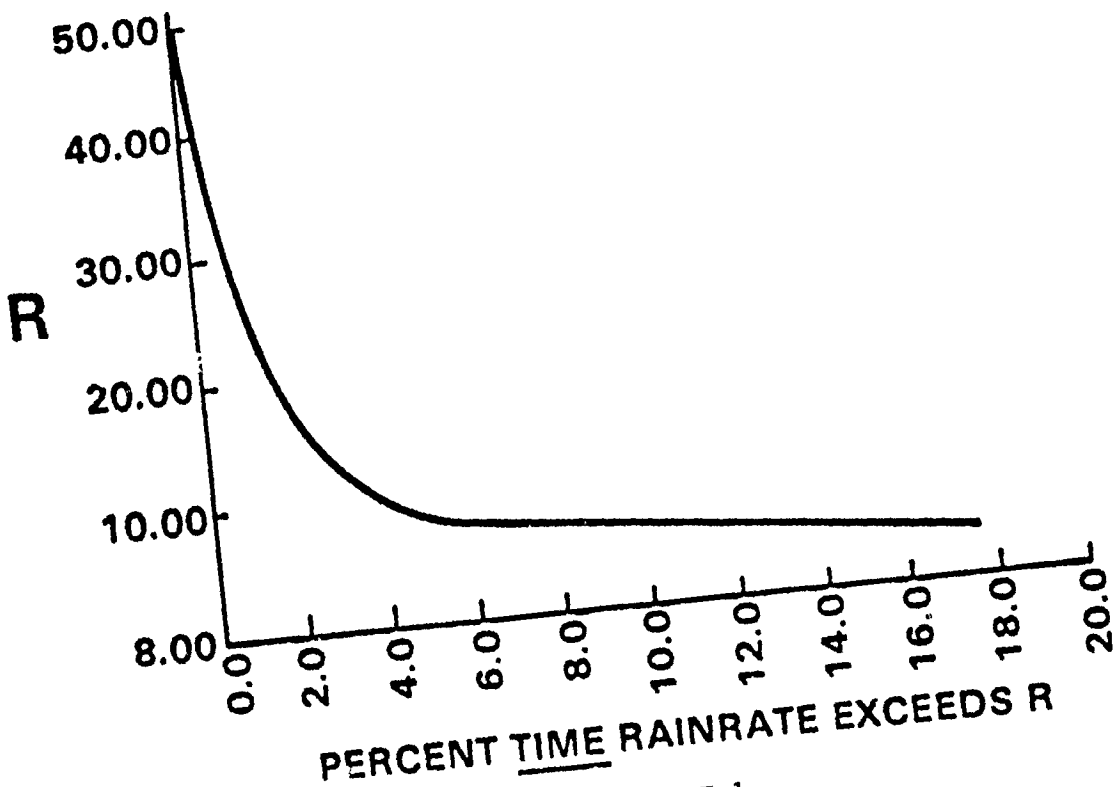
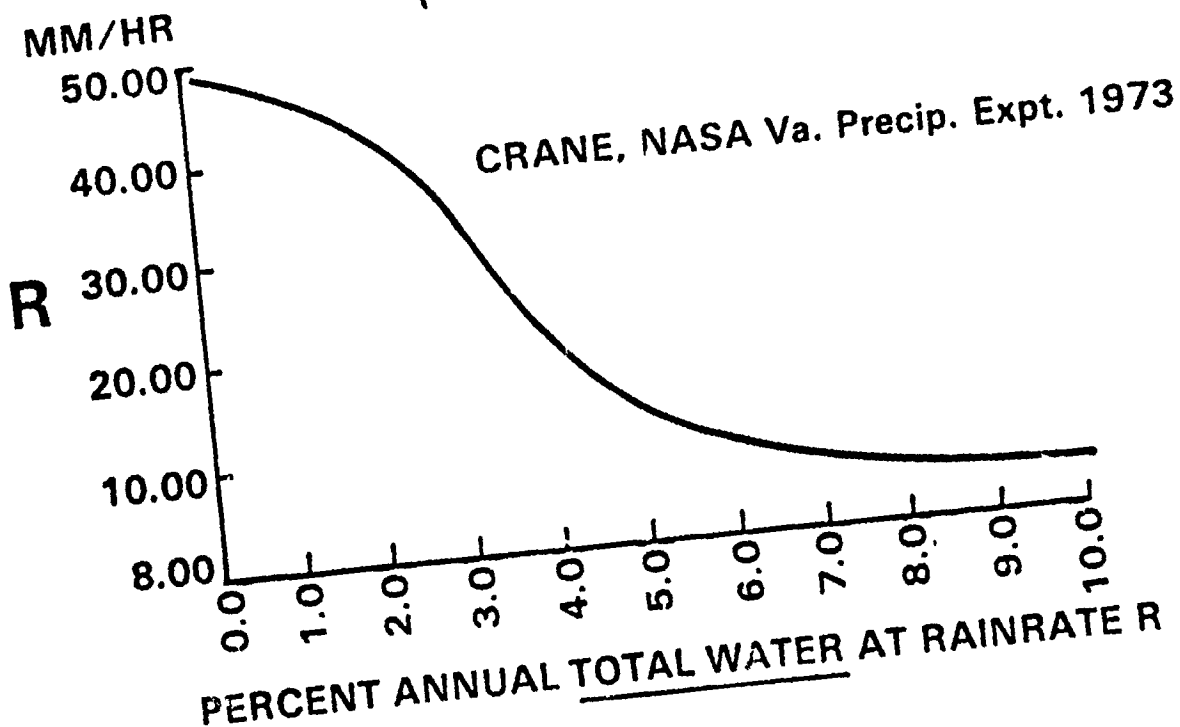


FIGURE 1

ORIGINAL PAGE IS  
OF POOR QUALITY

# COUPLING BETWEEN APPLICATIONS AND RADAR SYSTEM DESIGN PARAMETERS

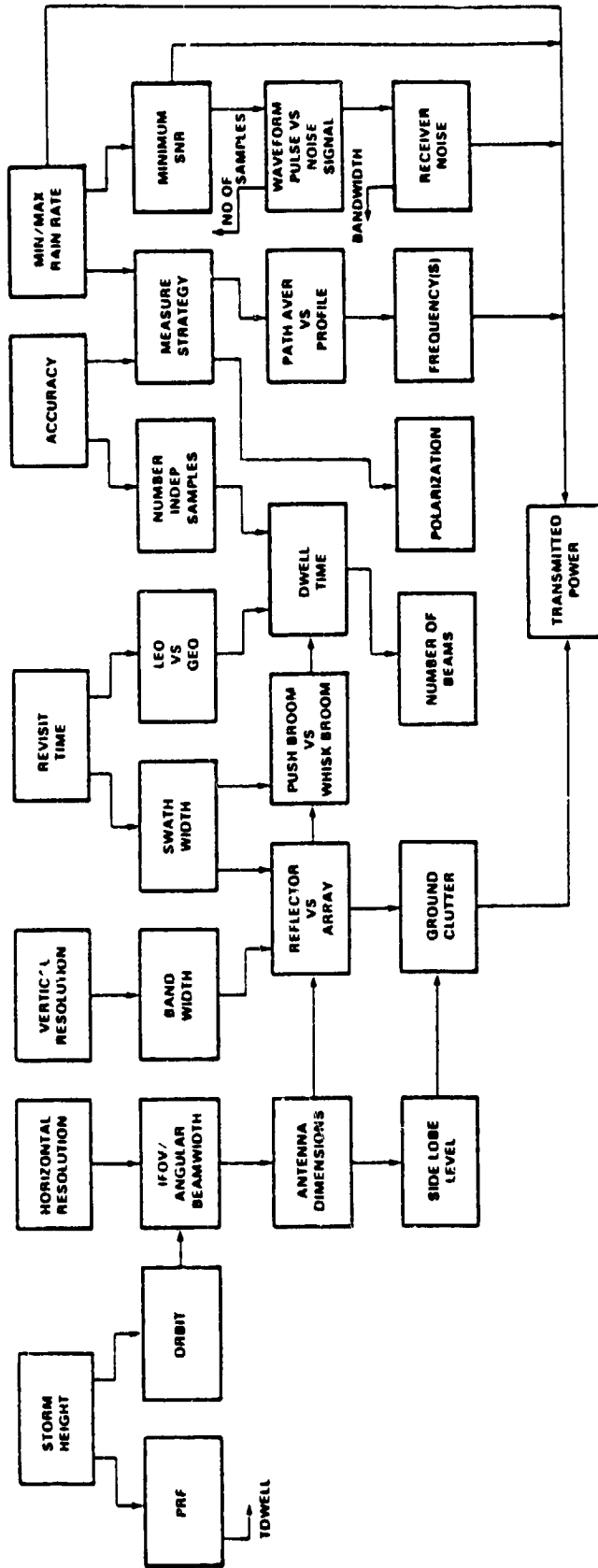


FIGURE 2

ORIGINAL PAGE 13  
OF POOR QUALITY

# SPACEBORNE RADAR GEOMETRY

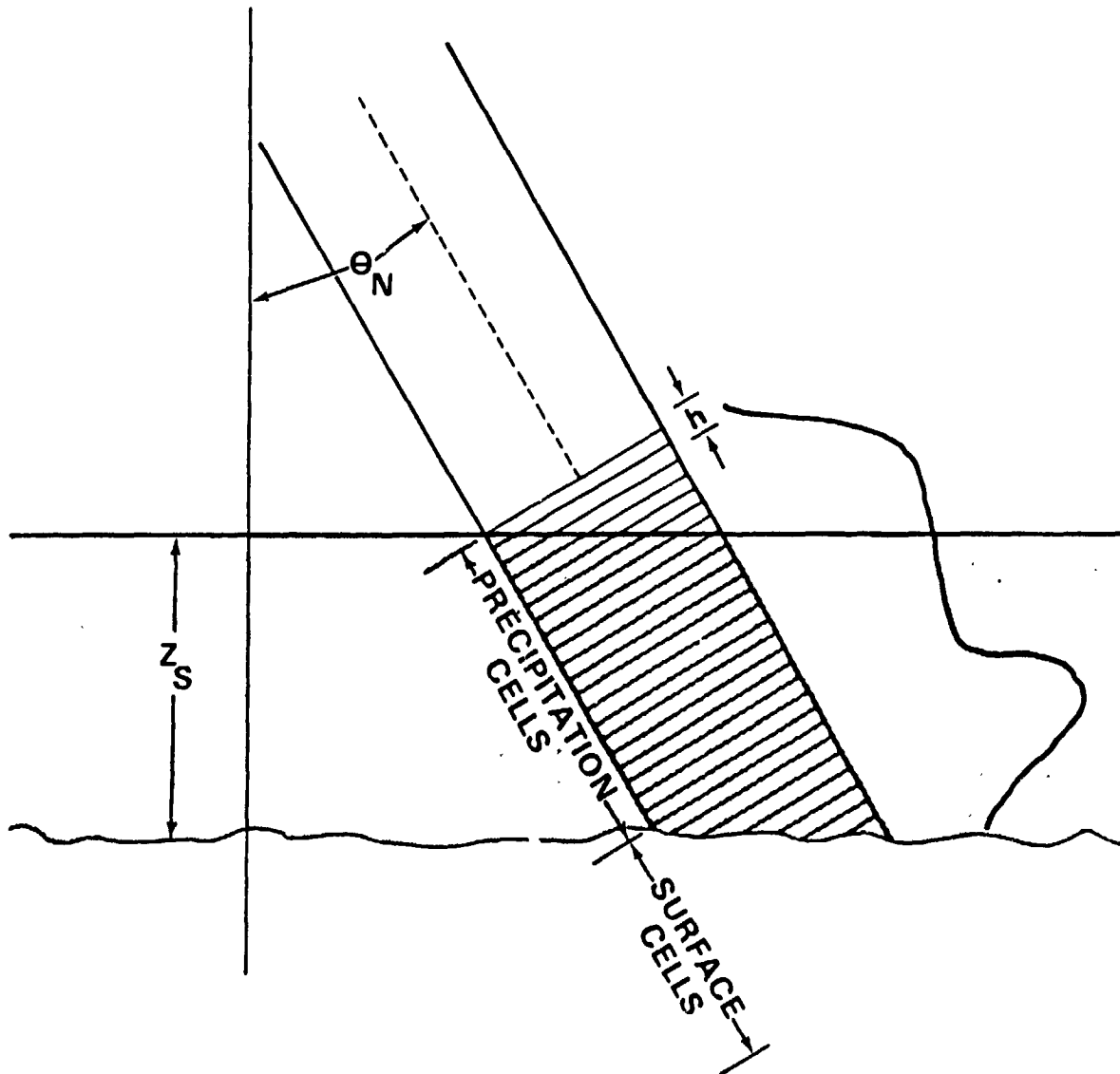


FIGURE 3

ORIGINAL PAGE IS  
OF POOR QUALITY

S  
Y

RADAR RETURN FROM RAIN R, NOISE N,  
AND GROUND CLUTTER C FOR A SPACE-  
BORNE PRECIPITATION RADAR USING THE  
DETERMINISTIC MODEL

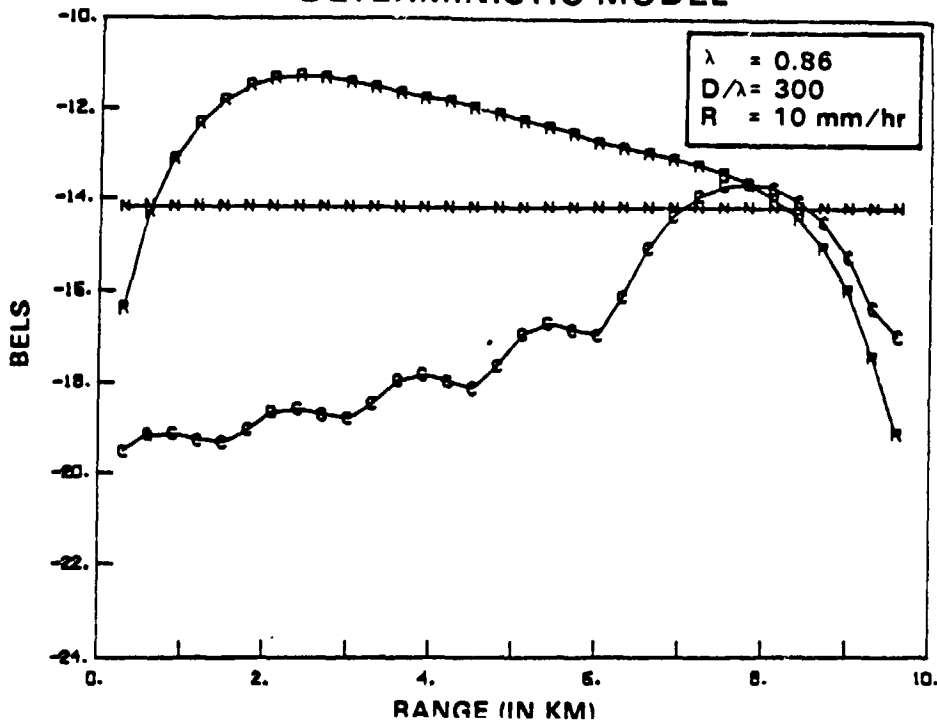


FIGURE 4

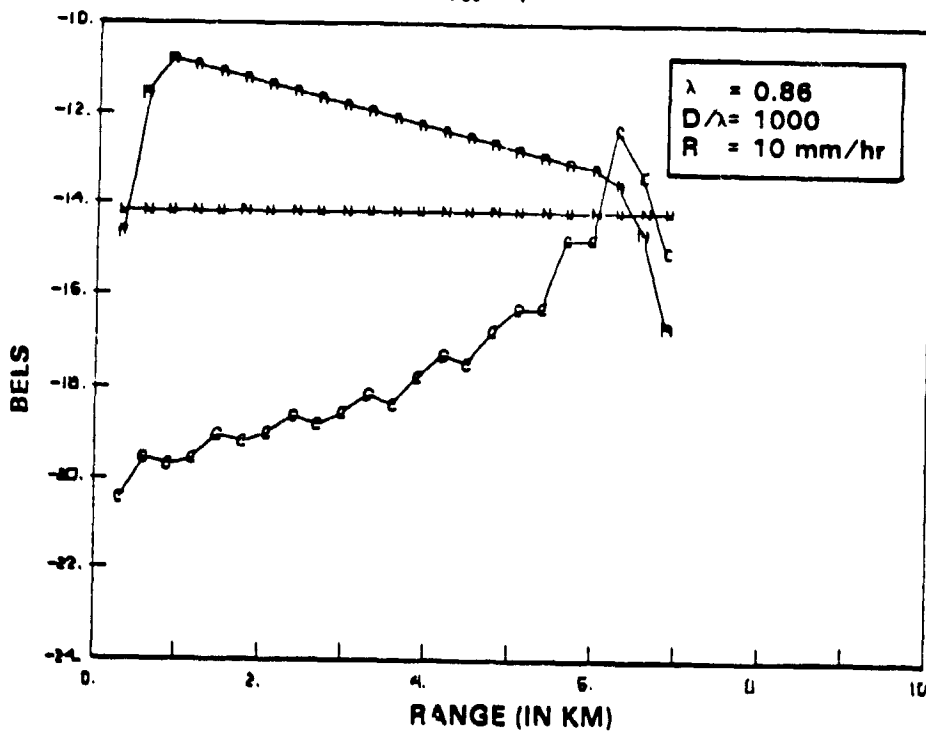


FIGURE 5

ORIGINAL PAGE IS  
OF POOR QUALITY

### SPACEBORNE PRECIPITATION RADAR PERFORMANCE SIMULATION USING THE STATISTICAL MODEL

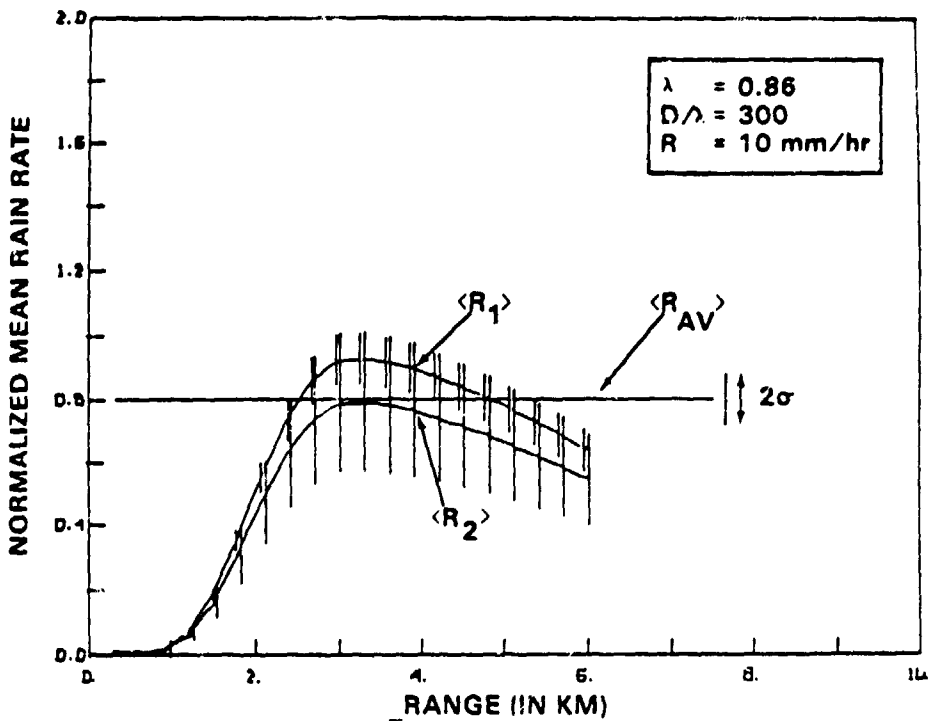


FIGURE 6

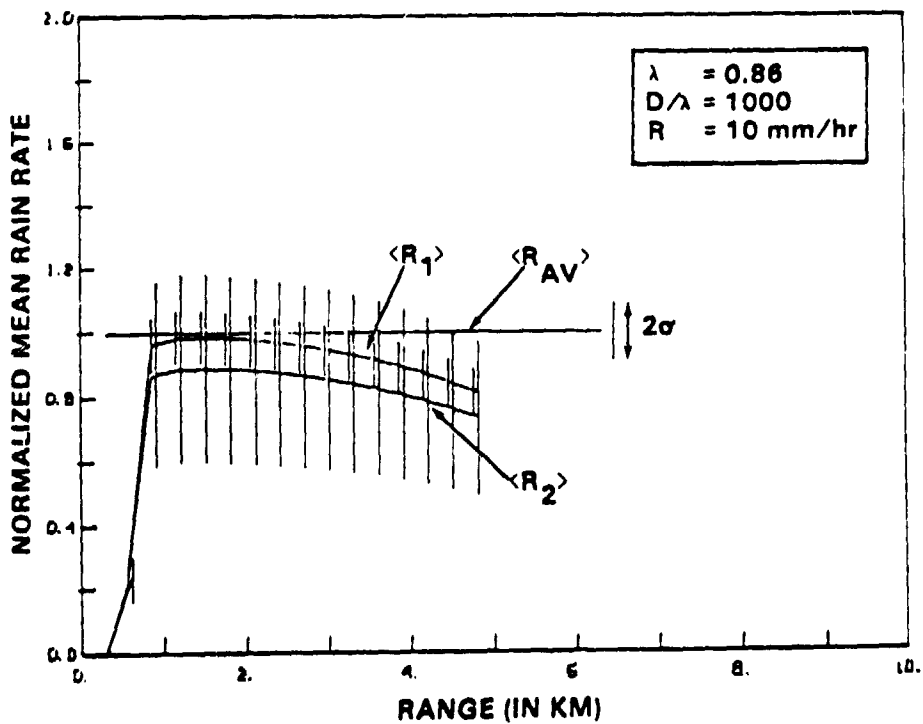


FIGURE 7

N83 25309

043

ORIGINAL COPY  
OF POOR QUALITY

SATELLITE BORNE DUAL MILLIMETRIC WAVE LENGTH RADAR

R. Lhermitre  
University of Miami  
Miami, Florida

1. Introduction.

Satellite borne instruments for atmospheric probing are presently restricted to passive radiometers operating in the infrared and microwave spectral regions and observing emission from earth surface, clouds and precipitation and the clear atmosphere for the channels set in the vicinity of strong gas absorption lines. These instruments do not provide ranging capability with the exception of indirect measurements of cloud top assuming black body radiation and thermodynamic equilibrium.

Direct ranging capabilities have to be obtained from an active system using some form of timing of a transmitter signal. Microwave radar and Lidar techniques provides such ranging capabilities but have been implemented only for sea state and wave height measurements. When applied to atmospheric probing by satellite, the microwave radar must rely on narrow antenna beams providing subsatellite foot prints comparable with that obtained by use of infrared radiometers. Since any instrument installed aboard a satellite is severely restricted in terms of antenna size and available power, this requirement is met only by a radar operating at a very short wavelength despite the increased attenuation of microwave radiation by hydrometeors at these frequencies. Fig. 1 shows the general behavior of atmospheric absorption as a function of radiation wavelength in the centimetric and millimetric wave spectral region, which also restricts the choice of wavelengths. Although the absorption increases gradually with decreasing wavelength, several acceptable windows at 35, 94, 140 and possibly 220 GHz are apparent.

This paper will explore the performances and characteristics of a satellite-borne radar operating in this millimeter wavelength region

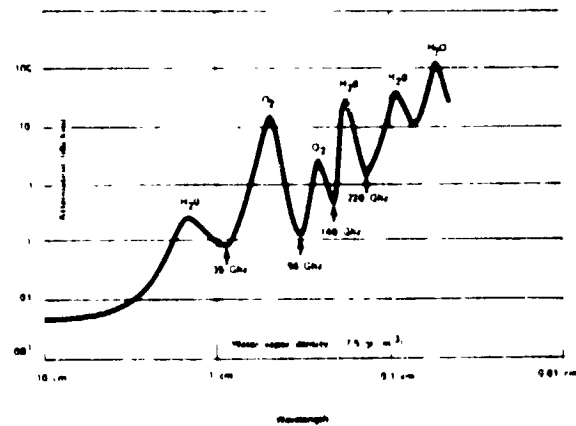


Fig. 1. Atmospheric attenuation at the earth surface in clear air.

of the spectrum with emphasis placed on the 35 and 94 GHz frequency bands for which basic hardware components and systems have been extensively developed. Although the installation and operation of a millimetric wavelength radar aboard a geostationary satellite is not completely unthinkable, we will concentrate on a satellite placed in a conventional sun synchronous polar orbit located at a mean altitude of approximately 600 to 1000 kms.

2. Attenuation at Millimeter Wavelengths.

In the Rayleigh region, i.e.  $D/\lambda < 0.1$  where  $D$  is the particle diameter and  $\lambda$  the radiation wavelength, the attenuation cross section of a spherical particle is given by

$$Q_t = Q_s = \frac{2}{3} \frac{D^3}{\lambda} \text{Im}(-k)$$

with the scattering attenuation term:



ORIGINAL PAGE IS  
OF POOR QUALITY

$$Q_c = \frac{2 \cdot 5 \cdot 6}{3 \cdot 4} |k|$$

negligible. The signal attenuation is proportional to the liquid water content and controlled by the imaginary part,  $IM(-k)$  of the index of refraction of the particle (essentially water or ice).  $IM(-k)$  increases roughly with  $1/\lambda$  in the centimetric wavelength region and then decreases slightly above  $\lambda = 1$  cm. Fig. 2 which shows the attenuation produced by a cloud of liquid droplets, illustrates this behavior and indicates a temperature effect which is considerably reduced at higher frequencies and essentially disappears at 170 or 180 GHz. Locations of the ka-band (35 GHz) and w-band (94 GHz) windows are also indicated.

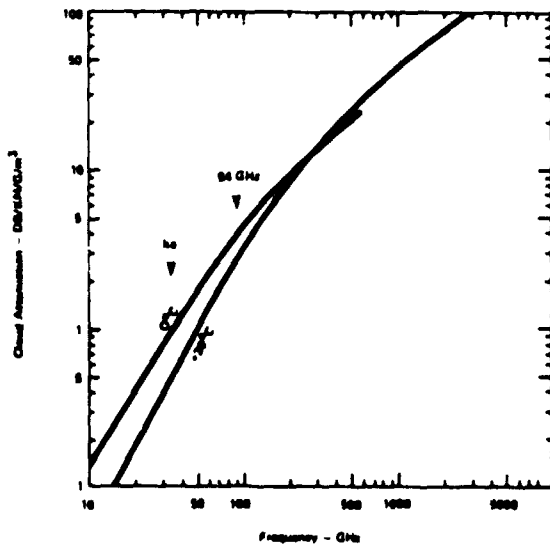


Fig. 2. Rayleigh attenuation by clouds. Note that the temperature effect disappears at approximately 200/300 GHz.

Raindrops are definitely outside of the Rayleigh region at millimetric wavelengths so that the calculation of attenuation must rely on some estimate of the distribution of liquid water as a function of particle size. Although drop size distributions may vary considerably with the precipitation nature and location, typical or conventional functions such as Marshall Palmer (1948) and Laws and Pearsons (1943),

etc. may be assumed. Many publications covering the subject can be found in the literature and Fig. 3 indicates typical results for the change of attenuation with radiation wavelength at the different precipitation intensities indicated, as derived from Setzer's (1970) computations which have been selected as matching experimental data quite well. One sees that the absorption coefficient increases steadily up to 100/150 GHz and then remain almost constant for higher frequencies. Note that attenuation in rain conditions still increases by a factor of 2 from 35 GHz to 94 GHz (from 4 to  $8 \text{ km}^{-1}$  to  $8 \text{ dB km}^{-1}$  for  $16 \text{ mm hr}^{-1}$  rain).

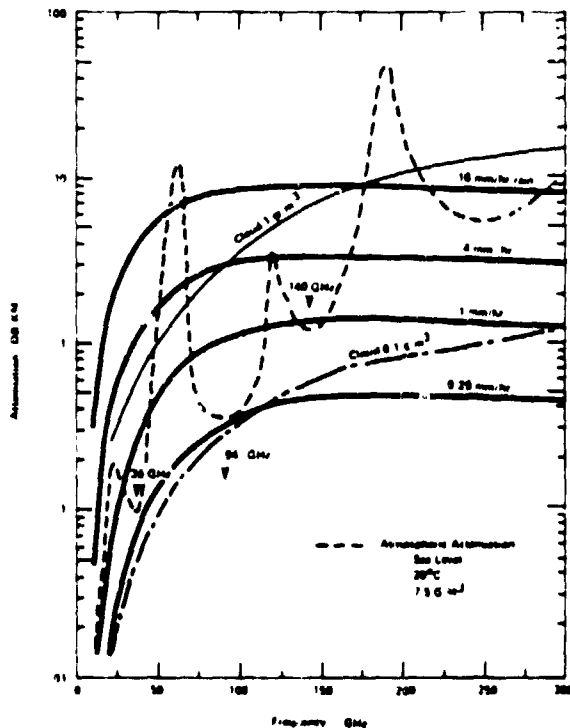


Fig. 3. Attenuation by atmospheric gases, clouds and precipitation at the rates indicated.

### 3. Back Scattering and Reflectivity.

In the Rayleigh region the backscattering cross section of a sphere is given by

$$\sigma = \frac{5 \cdot 6}{\lambda} |k|^2$$

and therefore increases drastically with shorter radar wavelength.  $|k|^2$  is derived from the

complex index of refraction of water whose real and imaginary parts vary appreciably from centimetric to millimetric waves. However,  $|k|^2$  does not change significantly (approximately 0.6 to 0.9) except for ice ( $|k|^2 \approx 0.2$ ). This is illustrated in Fig. 4 which shows the relationship between the backscattering cross section of a water droplet and its diameter at different wavelengths. One sees that the Rayleigh scattering domain virtually extends to 1 mm of diameter at w-band ( $\lambda = 0.33$  cm) and to 2 or 3 mm at  $k_a$  band. Therefore a substantial increase of reflectivity from  $\lambda = 0.33$  cm to  $\lambda = 0.85$  cm is only expected for particle diameter smaller than 1 mm; note that the  $k_a$  band is still superior to X band up to a 3 mm size.

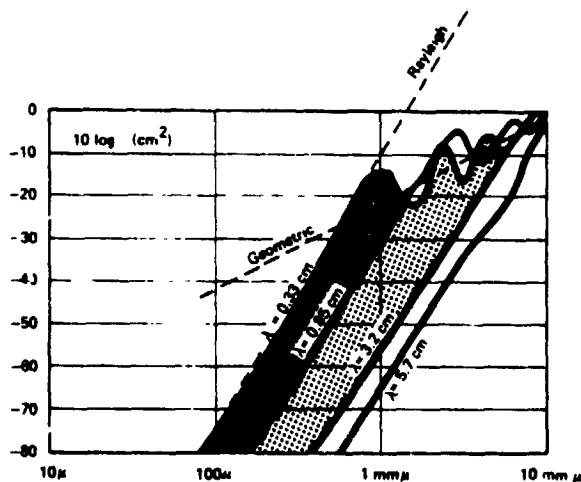


Fig. 4. Backscattering cross section of water spheres as a function of diameter for the radar wavelengths discussed in the text.

The evaluation of the radar reflectivity,  $\sigma = \int n(D) \sigma(D) dD$ , of a given cloud implies the specification of its droplet size distribution  $n(D)$ , which varies with the cloud type. To eliminate the need to specify  $n(D)$ , the  $\Delta\sigma$  reflectivity contribution due to a fraction  $M$  of the liquid water assigned to a given uniform particle size can be evaluated from:  $\Delta\sigma = N\sigma$ , where  $N$  is the ratio between  $M$  and the droplets individual mass.

We have:

$$\Delta\sigma = \frac{4\pi^3 D^3 |k|^2}{3\sigma_0 D} \Delta M$$

The results of this equation are shown in Fig. 5 for various LWC and for both 0.85 cm and 0.33 cm wavelengths. For instance, a cloud containing  $1 \text{ mgr m}^{-3}$  of liquid water divided into  $10 \mu$  size particles, has a reflectivity of  $7 \cdot 10^{-16} \text{ cm}^{-1}$  and  $3 \cdot 10^{-14} \text{ cm}^{-1}$  at ka-band and w-band respectively. These results should be interpreted in terms of actual droplet size distributions by assessing a "backscattering weighted" mean diameter.

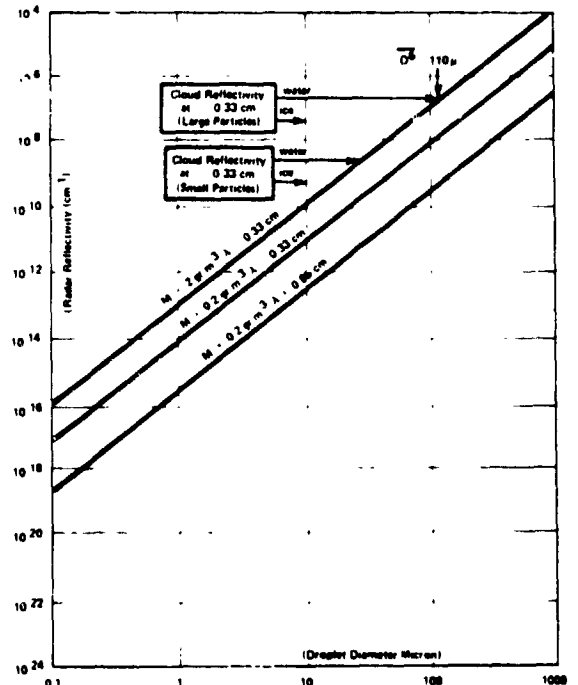


Fig. 5. Radar reflectivity of a cloud composed of droplets having identical size as a function of that size for given liquid water content. The cloud reflectivities calculated by Crane (1977) are also indicated.

#### 4. Detection Capabilities of Radar.

In order to assess the performance of a given radar for the observation of cloud and precipitation the above reflectivity estimates should be compared with sensitivity threshold of that radar. The sensitivity of several radars for distributed targets can be easily compared

by manipulating the radar equation in the following way. The power density  $\delta$  at range,  $R$ , is given by:

$$\delta = \frac{P_t G}{4\pi R^2}$$

where  $P_t$  is the transmitted power and  $G$  the antenna gain with respect to an isotropic radiator. The received power,  $P_r$ , is given by:

$$P_r = \frac{\delta \sigma A_e}{4\pi R^2}$$

where  $A_e$  is the effective area (including efficiency factor) of the receiving antenna. The antenna gain can be represented by  $G = 4\pi R^2/S$  where  $S$  is an effective beam cross section derived from the antenna radiation pattern and including antenna efficiency. The scattering volume,  $V$ , assuming a target filling the beam completely, is expressed by  $V = S \cdot h$  where  $h = \tau c/2$  ( $\tau$  pulse width) is its radial dimension. The effective radar cross section,  $\sigma$ , for the whole scattering volume,  $V$ , is given by  $\sigma = V \cdot \sigma$ . We therefore have:

$$P_r = \frac{P_t h A_e \sigma}{4\pi R^2}$$

If we impose the same constraints in terms of maximum available power, receiver noise figure and physical dimensions of the antenna for the three radars, the minimum reflectivity threshold is identical for the three radars regardless of wavelength, pulse length, etc. Such estimate of reflectivity sensitivity was made for a pulse radar installed aboard a satellite orbiting at an altitude of 800 kms. The radar parameters are the following: antenna diameter: 1.5 meters, pulse length: 300 meters, receiver bandwidth: 500 KHz, receiver noise figure: 8 db, and incoherent signal integration over 50 pulses. The results of these computations show that, in these conditions, a unity signal-to-noise ratio is obtained for a target reflectivity of  $3 \cdot 10^{-11} \text{cm}^{-1}$ . If we compare this evaluation with the estimates of reflectivity presented in Fig. 5, we see that such radar will be able to detect the top of practically all clouds including fair weather cumulus at the  $\lambda = .33 \text{ cm}$  wavelength. The longer  $\lambda = .85 \text{ cm}$  wavelength will detect only the cloud regions where particle's size reaches

100  $\mu$  and of course the precipitation regions.

Absorption will limit the possibility of detecting precipitation in the cloud low levels. We should remember, however, that the satellite is in an excellent position since it is observing storms from their top where absorption is reduced and this facilitates penetration of the storm. Therefore, the altitude levels where the intensity of backscattering adequately reflects the intensity of severity of the storm, are effectively reached. The use of two wavelengths proposed here should also offer means to assess the storm characteristics or intensity from both absorption and reflectivity viewpoints. Indeed, rather than attempting to accurately estimate radar reflectivity at selected altitudes.

by correcting for absorption, it would be more appropriate to design general algorithms accepting and processing the whole set of raw data input i.e. the vertical profiles of radar return. This procedure would be directed towards the interpretation of a set of data in terms of storm and cloud parameters useful at the synoptic scale such as intensity, severity, estimated rainfall output, etc. This requires that considerable effort be devoted to the design of representative models for convective or widespread storms and the processing algorithms.

This approach is not much different in principle from the use of the methods or algorithms applied to the inversion of atmospheric/earth radiation satellite measurements conventionally applied to microwave and infrared radiometer data. The radar technique, however, allows range discrimination, which is not the case for the radiative transfer equations as they blindly include all contributions along a line integral. Note that such emission data could also be obtained at the radar wavelengths by the intermittent use of the radar receiver as a radiometer.

Although the satellite is located at a great distance from the earth, the only region where backscattering is anticipated is limited to the range interval between the earth surface and the maximum altitude of clouds or storms. Therefore the unambiguous range requirement common to pulse radars is limited to that range interval only, which allows that a substantial repetition rate and pulse duty cycle be used.

ORIGINAL PAGE IS  
OF POOR QUALITY

The antenna beam must be narrow and capable of being scanned across the direction of the satellite flight in a manner analogous to some of the microwave sensors aboard the Nimbus satellites for instance. Two separate antennas for transmitting and receiving are recommended so that the receiver noise figure is easily optimized, the implementation of polarization techniques made simple and the use of the receiver section of the radar system as a sensitive radiometer made possible. If the antenna scanning angle is limited to  $\pm 15^\circ$  (approximately 500 kms swath) the range interval required by the maximum atmosphere "thickness" will be approximately 18 kms, allowing a pulse repetition period of 120  $\mu$ s.

The satellite is at an altitude of 750 to 1000 kms so that the radar signals reach the receiver approximately 5 ms after they have been transmitted. It is therefore proposed to keep the transmitting antenna pointed in a given direction for 5 or 10 ms during which 50 to 100 pulses will be transmitted. The transmitter antenna can then start to move to a different direction while the receiving antenna still remains in the same position until the last signal is received and then move to the next transmitter position. Such antenna scanning schemes may be associated with complex mechanical or electronic solutions difficult to implement aboard a satellite, but would optimize target dwell time. A radar beamwidth of approximately 0.15 to 0.2 degrees (for a practical antenna size of diameter 150 cm) is recommended. This beamwidth produces a 3 db footprint of 2 to 4 kms for a satellite orbit altitude of 800 kms, and the vehicle will move by one footprint in 0.3 to 0.75 s. If we assume that 10 ms are necessary to acquire one slant range profile, 100 separate beams covering a 500 kms swath can be obtained in one second, during which the satellite moves by approximately 6 kms. The radar bandwidth is reduced by signal integration which accepts all the signals for one beam and computes the mean signal intensity at 50 gates spaced by slightly over 300 meters for instance. The data rate will then be limited to approximately 5000 bytes  $s^{-1}$  per polarization and wavelength channel.

5. Conclusion.

Millimetric wavelengths provide an acceptable solution for the design of a satelliteborne active microwave equipment. The ranging capability of the system, the relatively low power consumption for adequate radar sensitivity and the enormous potential for the probing of clouds and storms on a large scale with, however, excellent resolution on both vertical and horizontal space, makes it a very attractive solution for future satellite instrument development. The radar sensitivity should be sufficient to allow detection of the melting band high reflectivity region in a widespread storm despite cloud and precipitation attenuation above the freezing level. This would offer a unique means for large scale mapping of the  $0^\circ\text{C}$  level altitude so that barotropic or baroclinic condition in warm front, occlusions and other large scale systems could be effectively probed by the satellite.

A considerable amount of effort has to be placed on methods for the interpretation of the data; however, the theory of absorption and scattering of microwave by hydrometeors has been known for years with excellent matching by field observations. The greatest uncertainties are certainly in the choice of adequate drop size distributions and in the assumption of ice particles' shape. Although algorithms for data interpretation can still be developed on the basis of cloud and precipitation modeling only, the operation, in known or assumed meteorological conditions, of a dual wavelength system such as proposed here aboard an airplane or the space shuttle, would provide some of the required empirical data. The sea surface reflectivity at the chosen wavelengths could also be assessed and related to sea state conditions so that data interpretation algorithms could include atmospheric absorption of the signal returned by the surface at the two wavelengths. This procedure can be carried on until atmospheric absorption is so overwhelming that no return from the sea surface is observed.

ORIGINAL COPY  
OF POOR COPY

6. References.

- Crane, R. and Burke, H. (1978): The Evaluation of Models for Atmospheric Attenuation and Backscatter Characteristic Estimation at 95 GHz. Environmental Research and Technology Report, p. 3606. Concord, Mass.
- Laws, J.O. and D.A. Parsons (1943): "The relation of raindrop-size to intensity", Amer. Geophys. Union Trans., 24, 452-460.
- Marshall, J.S. and W. McK. Palmer (1948): "The distribution of raindrops with size", J. Meteorol., 5, 165-166.
- Setzer, D.E., "Computed Transmission Through Rain at Microwave and Visible Frequencies," BSTJ, 49, p. 1873, 1970.

POTENTIAL OF DUAL-MEASUREMENT TECHNIQUES FOR ACCURATE  
DETERMINATION OF INSTANTANEOUS RAINFALL RATE FROM SPACE

Carlton W. Ulbrich

Department of Physics and Astronomy  
Clemson University, Clemson, SC 29631

## 1. INTRODUCTION

Attempts to remotely measure precipitation have, in the great majority of the cases, relied on the measurement of a single quantity which is then used to deduce the desired precipitation parameter through a theoretically or empirically derived relationship. Wilson and Brandes (1979) have reviewed the history of the use of radar to measure rainfall by such a method. Similar use of microwave radiometry in the 1.5 cm band is discussed by Wilheit, et al. (1977) and they suggest that the technique has potential for determining precipitation amounts over previously inaccessible ocean areas. These and other remote measurement methods are quite limited in the accuracy with which they can measure precipitation parameters and the reasons for these limitations are revealed through detailed examination of the method by which conventional radar is used for the remote measurement of precipitation. This method has, almost without exception, relied on empirically derived relationships between a radar measureable and the precipitation parameter of interest. Perhaps the best known of these techniques determines the rainfall rate  $R$  by use of an empirical relation between  $R$  and the one remote measureable obtainable from conventional radar, viz., the reflectivity factor  $Z$ . The type of empirical relation employed are usually of the form  $Z = aR^b$  where  $a$  and  $b$  are constants dependent on geographical location, type of rainfall (stratiform, convective, etc.), and other factors. The accuracy of the results obtained from this method has been reviewed by Atlas (1964) and Battan (1973). Wilson and Brandes (1979) conclude that considerable effort is required to produce radar measurements which are within a factor of two of the true rainfall 75% of the time. The agreement between radar-deduced rainfall amounts and those obtained by other means (e.g., raingauges) is good only when averaging is performed over long periods of time or large geographical areas. Individual measurements at a single time and place usually involve larger standard errors. In addition, even in those circumstances where the type of rainfall and geographical location are used to define the values for  $a$  and  $b$ , it is common to find very large deviations between radar-deduced and measured rainfall rates within the field of view of the radar.

The usual procedure for finding the empirical  $Z - R$  relations used in such methods is to calculate  $Z$  and  $R$  from experimentally observed raindrop size spectra and then fit the results

to an equation of the form  $Z = aR^b$ . This is illustrated in Fig.1 (at the end of the text) for a set of 180 raindrop spectra obtained with a Joss type raindrop spectrometer. Although the data display a systematic variation of  $Z$  with  $R$  there is considerable scatter about the regression line  $Z = 366R^{1.42}$ . In fact, a comparison of the rainfall rate as calculated from this  $Z-R$  relation to the actual rainfall rate, as shown in Fig.2, produces an average deviation (without regard for sign) of the calculated from the actual  $R$  of 32%. Even in this case where  $Z$  and  $R$  are known (i.e., can be calculated), the agreement between rainfall rates found from the  $Z-R$  relation and those calculated from the drop size spectra is, at best, fair. The implication is that, due to common variability in naturally occurring drop size spectra, the relationship between  $Z$  and  $R$  is not unique, can vary over short time scales and small geographical areas, and can therefore lead to large discrepancies between measured and radar-deduced rainfall rates.

The latter conclusion is supported by the work of Ulbrich and Atlas (1975, 1977) who demonstrate that the origins of these discrepancies lie in the form of the drop size distribution. Typical of the analytical forms used to approximate real drop size spectra are the exponential form of Marshall and Palmer (1948), the gamma distribution of Khrgian, Mazin and Cao (1952), the modified gaussian distribution of Best (1950), and the log-normal distribution of Levin (1954). The common feature of these analytical forms is that they require at least two parameters to completely specify the distribution. Generally, three parameters would be required, one parameter specifying the total number of drops per unit volume, a second determining the mean or median drop diameter, and a third indicating the spectral breadth of the distribution. However, it is usually found that the first two of these parameters are adequate to accurately depict the general behavior of the distribution. In such a case, then, all quantities defined in terms of the size distribution are dependent on two parameters, each of which is observed in nature to be independent and highly variable with respect to geographical location, rainfall type, and time, i.e., from moment to moment within a given rainfall type. Since a specific relationship between these two size distribution parameters does not in general exist, their fluctuations from moment to moment will be independent and variations in one precipitation parameter will not be uniquely related to the variations in any other parameter.

## ORIGINAL FORM OF OF POOR QUALITY

To put these ideas in quantitative language suppose, as an example, that the size distribution is exponential, i.e., let  $N(D)$  be the number concentration of drops per unit size interval and have the form

$$N(D) = N_0 e^{-3.67D/D_0} \quad (\text{m}^{-3} \text{cm}^{-1}) \quad (1)$$

where  $D(\text{cm})$  is the raindrop diameter and  $N_0$  ( $\text{m}^{-3} \text{cm}^{-1}$ ) and  $D_0(\text{cm})$  are parameters of the distribution. With this form for  $N(D)$ ,  $D_0$  is the median volume diameter and  $N_0 D_0 / 3.67$  is the total number of drops per unit volume, if all raindrop diameters are possible. The rainfall rate  $R(\text{mm h}^{-1})$  is defined in terms of the size distribution by

$$R = 0.6\pi \int_0^\infty N(D)v(D)D^3 dD \quad (2)$$

where  $v(D)$  ( $\text{ms}^{-1}$ ) is the fallspeed in still air of a raindrop of diameter  $D$ . If it is assumed, following Atlas and Ulbrich (1977), that

$$v(D) = 17.67 D^{0.67} \quad (3)$$

then, using Eq. (1) for  $N(D)$ ,  $R$  becomes

$$R = 1.136 N_0 D_0^{4.67} \quad (4)$$

the reflectivity factor  $Z(\text{mm}^6 \text{m}^{-3})$  is given by

$$Z = 10^6 \int_0^\infty N(D)D^6 dD = 8.03 \times 10^4 N_0 D_0^7 \quad (5)$$

It is immediately obvious from inspection of Eqs. (4) and (5) that  $R$  and  $Z$  are dependent on both  $N_0$  and  $D_0$ , and hence will be dependent on variations in both of these independently fluctuating distribution parameters. Hence, measurement of  $Z$  will not serve to determine  $R$  unless a specific restriction is placed on either  $N_0$  or  $D_0$  or unless a relationship between the two is assumed to exist. For example, if Eq. (4) is solved for  $D_0$  and the result substituted in Eq. (5) then one obtains

$$Z = 6.635 \times 10^4 N_0^{-0.5} R^{1.50} \quad (6)$$

It is clear from this result that although the moment-to-moment variations in  $D_0$  have no influence on the dependence of  $Z$  on  $R$  through Eq. (6), the variations in  $N_0$  do have an influence and will produce fluctuations in  $Z$  even when  $R$  remains constant. To proceed further with this type of analysis it is necessary to introduce an assumption regarding the dependence of  $N_0$  on  $R$ . For example, if it is assumed that  $N_0$  has a constant value independent of  $R$  and equal to the Marshall and Palmer (1948) value  $N_0 = 8 \times 10^4 \text{m}^{-3} \text{cm}^{-1}$ , then Eq. (6) becomes

$$Z = 235R^{1.50} \quad (7)$$

which is representative of the Z-R relations found from empirical analyses, e.g., that found in the above empirical analysis as well as those found by Marshall and Palmer (1948) for stratiform rain, by Joss, et al. (1970) for widespread rain, and by Sivaramakrishnan (1961) for thunderstorm rain. But it is evident from the example given here that deviations from Eq. (7) will be commonplace in nature because  $N_0$  is frequently observed to deviate from a constant value and these deviations are the source of the errors in rainfall rates found from empirical Z-R relations.

Another precipitation parameter of interest is the liquid water content  $W(\text{gm}^{-3})$  which, when Eq. (1) is assumed for the size distribution  $N(D)$ , is given by

$$W = \frac{\pi}{6} \int_0^\infty N(D)D^3 dD = 1.73 \times 10^{-2} N_0 D_0^4 \quad (8)$$

If  $D_0$  is eliminated between Eqs. (5) and (8) one obtains

$$Z = 9.73 \times 10^7 N_0^{-0.75} W^{1.75} \quad (9)$$

Substituting the Marshall-Palmer value  $N_0 = 8 \times 10^4 \text{m}^{-3} \text{cm}^{-1}$  yields

$$Z = 2.05 \times 10^4 W^{1.75} \quad (10)$$

which is similar to that found empirically by Marshall and Palmer (1948), and by Sivaramakrishnan (1961). As in the case of the Z-R relation Eq. (7), the coefficient in Eq. (10) is dependent on the choice for  $N_0$  and hence will be sensitive to fluctuations in this parameter from moment to moment and between rainfall types and geographical areas. Consequently the accuracy with which a Z-W relation like Eq. (10) can determine liquid water contents will be no better than that with which a Z-R relation can measure rainfall rates. In other words, the scatter in the experimental data about an empirical Z-W relation will be similar to that displayed by the data about an empirical Z-R relation. In fact, Ulbrich and Atlas (1975) have shown that all of the empirical relations which can be established between pairs of precipitation parameters involve scatter in the experimental data which is directly related and of approximately the same relative magnitude. For example, the percentage deviation of an experimental data point from an empirically derived Z-R relation will be of about the same magnitude and have the same sense as the deviations of this data point from all other empirical relations between pairs of quantities (e.g.,  $D_0$  -  $R$ ,  $Z$  -  $W$ ,  $N_0$  -  $R$ , etc.). The important implication of this result is that the accuracy with which an empirical relation employing a single radar measurable can measure a precipitation parameter is inherently limited because it fails to account for the natural variability of both of the size distribution parameters.

## 2. DUAL-MEASUREMENT METHODS

It is apparent from the above discussion that there exists a need for new techniques which will improve the accuracy of remote measurement of precipitation parameters. It is proposed here that this improvement in accuracy could be realized through the use of dual-measurement methods, i.e., techniques which involve measurement of two quantities. To demonstrate why such an approach is necessary suppose, as an example, that a dual-wavelength radar system is employed which consists of one wavelength for which the Rayleigh approximation is valid ( $\lambda \sim 10 \text{cm}$ ) and another more strongly attenuated wavelength ( $\lambda \sim 1-2 \text{cm}$ ). The longer wavelength serves to determine the reflectivity factor  $Z$  within a range gate and comparison of the power return at the two wavelengths in adjacent range gates determines the attenuation  $A$ , which is defined by

$$A = 0.4343 \int_0^L Q_t(D)N(D)dD \quad (11)$$

ORIGINAL FORMATS  
OF POOR QUALITY

where  $Q_t(D)$  ( $\text{cm}^2$ ) is the total attenuation cross section due to scattering and absorption. Atlas and Ulbrich (1974) have shown that for most radar wavelengths  $Q_t(D)$  can be represented by the form

$$Q_t(D) = CD^n \quad (12)$$

when the constant  $C$  and exponent  $n$  are dependent on wavelength and temperature. In this case, then, using Eq. (1) for the size distribution,  $A$  becomes

$$A = \frac{0.4343 \Gamma(n+1)}{(3.67)^{n+1}} N_0 D_0^{n+1} \quad (13)$$

where  $\Gamma(x)$  is the complete gamma function. The measured values of  $Z$  and  $A$  can then be used in Eqs. (5) and (13) to find unique solutions for  $N_0$  and  $D_0$  which describe the exponential approximation to the size distribution of the drops in the radar pulse volume. That is, if Eqs. (5) and (13) are solved simultaneously for  $N_0$  and  $D_0$  in terms of  $Z$  and  $A$ , one finds

$$D_0 = a_D Z^{5/5} A^{-5} \quad (14)$$

and

$$N_0 = a_N Z^{1-7/5} A^{-1/5} \quad (15)$$

where  $a_D$  and  $a_N$  are constants and the exponent  $s = (6 - n)^{-1}$

The important feature of this approach is that these solutions for  $N_0$  and  $D_0$  are determined directly and uniquely from measurements of  $Z$  and  $A$ . The method does not involve assumptions about the dependence of either  $N_0$  or  $D_0$  on rainfall rate, nor does it require the introduction of empirical relationships between any two precipitation parameters. Furthermore, since the liquid water content  $W$  [Eq. (8)] and the rainfall rate  $R$  [Eq. (4)] are each dependent on  $N_0$  and  $D_0$  only, then they too are determined directly from measurements of  $Z$  and  $A$ . That is, if Eqs. (14) and (15) are substituted into Eqs. (4) and (8) one obtains

$$W = a_W A^{5s} Z^{(3-n)s} \quad (16)$$

and

$$R = a_R A^{2.33s} Z^{(3.67-n)s} \quad (17)$$

where  $a_W$  and  $a_R$  are constants dependent on  $C$  and  $n$ . These solutions have been found using a power law approximation for the fallspeed law [Eq. (3)] and a similar approximation for the total attenuation cross section [Eq. (12)]. But these simple approximations have been used here only for the purposes of illustration and they are not a necessary part of the method. More accurate values of the rainfall rate and microwave attenuation can be found by numerically integrating Eq. (2) using the measured raindrop fallspeeds of Gunn and Kinzer (1949) and Eq. (11) using the calculated Mie total attenuation cross sections of Marler (1973). The results of such calculations have been displayed by Ulbrich and Atlas (1978) on a rain parameter diagram. Although they find that the relationships between  $N_0$ ,  $D_0$ ,  $Z$ ,  $A$ ,  $W$  and  $R$  are not as simple as those given above,

they lead to the same conclusion, viz., that dual-measurement systems possess the potential for significantly improving the accuracy of remote measurement of precipitation parameters. In addition, it is also shown by Ulbrich and Atlas (1978) that it is not necessary to assume that the size distribution is exponential; any size distribution can be used for which two of the moments can be calculated or are known a priori. This method has been applied to the raindrop spectra described previously and the comparison of the rainfall rate calculated from  $Z$  and  $A$  with the actual rainfall rate is shown in Fig. 3. It is obvious that there is significant improvement with the average deviation of the calculated  $R$  from the actual  $R$  being only 5%.

The above method of measuring  $Z$  and  $A$  by a matched pair of radar beams was originally suggested by Eccles and Atlas (1973) as a means of detecting hail. It is only one example of a variety of experimental methods by which rainfall rate and other quantities can be measured. Others have been alluded to by Atlas and Ulbrich (1974) and by Goldhirsch and Katz (1974). The latter authors suggest a measurement method which employs a matched pair of radar beams of different wavelengths with both subject to attenuation. Then, provided there are no severe reflectivity gradients in the storm under observation, the parameters  $N_0$  and  $D_0$  can be found from the differential attenuation of the two beams. The advantage of this method is that the solutions for  $N_0$  and  $D_0$  in terms of the attenuations at the two wavelengths are independent of the radar calibration constants so that knowledge of these constants is not required.

Another dual-measurement method suggested by Ulbrich and Atlas (1977) employs a combination of a radar to measure the reflectivity factor  $Z$  and lidar to determine the optical extinction  $\Sigma$  ( $\text{km}^{-1}$ ) which is defined by

$$\Sigma = \frac{\pi}{20} \int_0^\infty N(D) D^2 dD \quad (18)$$

When Eq. (1) is used for  $N(D)$  then Eq. (18) takes the form

$$\Sigma = 6.36 \times 10^{-5} N_0 D_0^3 \quad (19)$$

In this case the solutions for the size distribution parameters are especially simple in that they do not involve wavelength and/or temperature dependent quantities, as is the case with the microwave attenuation. These solutions are shown by Ulbrich and Atlas (1977) to be of the form

$$D_0 = 0.0168 Z^{1/4} \Sigma^{-1/4} \quad (20)$$

and

$$N_0 = 3.33 \times 10^7 Z^{-3/4} \Sigma^{7/4} \quad (21)$$

which can then be substituted in Eqs. (4) and (8) to yield solutions for  $R$  and  $W$ , respectively. Using measured raindrop size spectra, Ulbrich and Atlas (1977) show that this method produces estimates for  $R$  and  $W$  which are in excellent agreement with the experimental data and also produces an exponential distribution given by  $N_0$  and  $D_0$  which closely approximates the actual size spectrum. In a few cases, the actual size spectrum



## ORIGINAL P. OF POOR QUALITY

deviates appreciably from exponentiality, but even in these cases the method produces values for R and W which are in very good agreement with experiment.

Another dual-measurement method which has been proposed by Seliga and Bringi (1976) determines the reflectivity factor at orthogonal polarizations in rainfall. It is well known that as raindrop size increases the drop becomes increasingly distorted from spherical shape and that drops of this type become more numerous as the rainfall rate increases. Furthermore, observations indicate that these drops fall with a preferred orientation. The combination of oblateness and preferred orientation when integrated over a drop size distribution result in a differential scattering of horizontally and vertically polarized electromagnetic waves. Seliga and Bringi (1976) have deduced the dependence of  $Z_{DR}$ , the differential reflectivity at orthogonal polarizations, on  $D_0$  and show that it increases monotonically as  $D_0$  increases. They also demonstrate [Seliga and Bringi (1978)] how the method can be used to measure rainfall rates and find close agreement between radar-measured and raingauge-measured rainfall rates [Seliga et al. (1980)].

### 3. CONCLUSION

It is clear then from the above discussion that all of these dual-measurement methods show high promise for measuring precipitation parameters with greater accuracy than that which has been possible in the past. However, a truly adequate test of these methods has yet to be performed in the field. A system typical of that which could perform such a test would consist of a network of ground-based multi-wavelength, dual-polarization radars, microwave links, optical links (transmissometers or lidars), raingauges, and disdrometers. Operation of such a network over a period of at least one year would provide an abundance of data to determine whether these promising techniques are indeed capable of measuring precipitation parameters with the professed accuracy. The results of such an experiment would also permit a quantitative, detailed assessment of the requirements for satellite-based precipitation measurement systems. In addition, continued operation of the system would provide a ground-truth standard with which satellite measurements could be compared.

### 4. REFERENCES

- Atlas, D., 1964: Advances in Radar Meteorology, Adv. Geophysics, 10, pp. 317-478.
- Atlas, D. and C.W. Ulbrich, 1974: The physical basis for rainfall-attenuation relationships and the measurement of rainfall parameters by combined attenuation and radar methods. J. Rech. Atmos., 8, pp. 275-298.
- Battan, L.J., 1973: Radar Observation of the Atmosphere, University of Chicago Press, Chicago, IL
- Best, A.C. 1950: Empirical formulae for the terminal velocity of water drops falling through the atmosphere. Q.J. Roy. Meteor. Soc. 76, pp. 302-311.
- Eccles, P.J. and D. Atlas, 1973: A dual wavelength radar hail detector. J. Appl. Meteor., 12, pp. 847-854.
- Goldhirsch, J. and I. Katz, 1974: Estimation of raindrop size distributions using multiple wavelength radar systems. Radio Sci., 9, pp. 439-446.
- Gunn, R. and G.D. Kinzer, 1949: The terminal velocity of fall for water droplets in stagnant air. J. Meteorol., 6, pp. 243-248.
- Joss, J.K. Schram, J.C. Thams, and A. Waldvogel, 1970: On the quantitative determination of precipitation by radar. Wissenschaftliche Mitteilung Nr. 63. Zurich: Eidgenossische Kommission zum studium der Hagelbildung und der Hagelabwehr.
- Khrgian, A.K.A., I.P. Mazin and V. Cao, 1952: Distribution of drops according to size in clouds (in Russian). Tr. Tsent. Aerol. Observ., 7, p. 56.
- Levin, L.M., 1954: Size distribution function for cloud droplets and rain drops (in Russian). Dok Akad. Nauk. S. S. S. R., 94, pp. 1045-1053.
- Marker, W., 1973: Attenuation cross sections of water spheres for selected temperatures and radar wavelengths. Laboratory for Atmospheric Probing, University of Chicago. (Unpublished manuscript).
- Marshall, J.A. and W.M.K. Palmer, 1948: The distribution of raindrops with size. J. Meteorol., 5, pp. 165-166.
- Seliga, T.A. and V.N. Bringi, 1976: Potential use of radar reflectivity measurements at orthogonal polarizations for measuring precipitation. J. Appl. Meteor., 15, pp. 69-76.
- Seliga, T.A., V.N. Bringi and H.H. Al-Khatib, 1980: Differential reflectivity measurements of rainfall rate: raingauge comparisons. Preprints 19th Radar Meteor. Conf., pp. 440-447. American Meteorological Society, Boston, Mass.
- Sivaramakrishnan, M.V., 1961: Studies of raindrop size characteristics in different types of tropical rain using a simple raindrop recorder. Indian J. Meteor. Geophys., 12, pp. 189-217.
- Ulbrich, C.W. and D. Atlas, 1975: The use of radar reflectivity and microwave attenuation to obtain improved measurements of precipitation parameters. Preprints 16th Radar Meteor. Conf., pp. 496-503, American Meteorological Society, Boston, Mass.
- Ulbrich, C.W. and D. Atlas, 1977: A method for measuring precipitation parameters using radar reflectivity and optical extinction. Ann. des Telecomm. 32, pp. 415-421.
- Ulbrich, C.W. and D. Atlas, 1978: The Rain Parameter Diagram: Methods and Applications. J. Geophys. Res., 83, pp. 1319-1325.

ORIGINAL PAGES  
OF POOR QUALITY

Wilheit, T.T., A.T.C. Chang, M.S.V. Rao,  
E.B. Rodgers and J.S. Theon, 1977: A satellite  
technique for quantitative mapping rainfall  
rates over oceans *J. Appl. Meteor.*, 16, 551-560.

Wilson, J.W. and E.A. Brandes, 1979: Radar  
measurement of rainfall- A summary.  
*Bull. Amer. Meteor. Soc.*, 60, pp. 1048-1058.

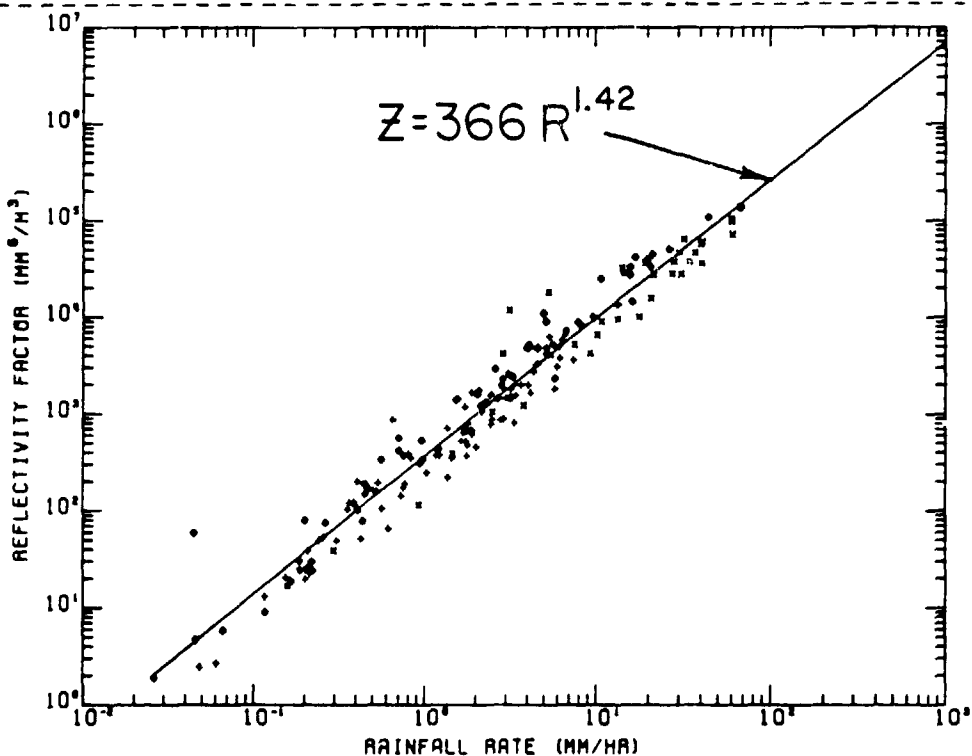


Fig. 1: Reflectivity factor  $Z$  vs rainfall rate  $R$  as calculated for 180 raindrop spectra obtained with a Joss type disdrometer. The straight line is the empirically determined  $Z$ - $R$  relation for these data found by least squares.

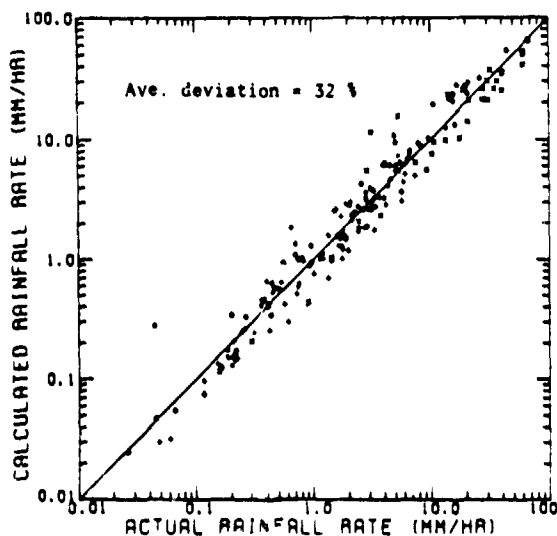


Fig. 2: Comparison of the rainfall rates found from the empirical  $Z$ - $R$  relation with the actual rainfall rates for the spectra described in Fig. 1

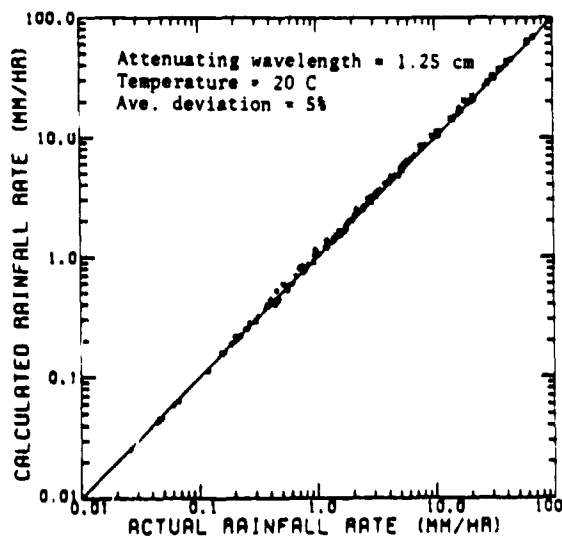


Fig. 3: Comparison of the rainfall rates found from  $Z$  and  $A$  with the actual rainfall rates for the spectra described in Fig. 1.

D42 N83 25311

ORIGINAL PAGE IS  
OF POOR QUALITY

RAIN RATE MEASUREMENT CAPABILITIES USING A SEASAT TYPE RADAR ALTIMETER

Julius Goldhirsh

The Johns Hopkins University/Applied Physics Laboratory  
Laurel, Maryland 20810

Edward J. Walsh

NASA/Wallops Flight Center  
Wallops Island, Virginia 23337

ABSTRACT

The incorporation in the 13.5 GHz Seasat type radar altimeter of a mode to measure rain rate is investigated. Specifically, an algorithm is developed relating the echo power at the various range bins to the rain rate, taking into consideration Mie scattering and path attenuation. The dependence of the algorithm on rain drop size distribution, and non-uniform rain structure are examined and associated uncertainties defined.

A technique for obtaining drop size distribution through the measurements of power at the top of the raincell and power difference through the cell is also investigated together with an associated error analysis.

A description of the minor hardware modifications to the basic Seasat design is given for implementing the rain measurements.

1. INTRODUCTION

An optimally designed radar located on board a satellite for making rain measurements near the ground should ideally have the following features: (1) Be capable of establishing rain rate profiles as a function of height above the ground, (2) Establish the rain rate along track and also cross track over a significant swath width, (3) Have a spatial resolution significantly smaller than the scale dimensions of typical rain cells and, (4) Be capable of obtaining world-wide samples over a short time span (e.g., 90 minutes).

The technique described here may be considered as "piggyback" to an already existing radar system since its implementation requires only minor modifications. The system in mind is the Seasat type radar altimeter operating at f=13.5 GHz [MacArthur, 1978] and flown aboard the Seasat Satellite. Although not optimally designed for possessing all of the above features, such a modified system would however enable a "first step look" at the rain rate profiles along track at relatively little additional cost. The experimental technique described here is an extension of the rain detection mode accepted for inclusion in the NOSS altimeter [Walsh, 1981].

2. FORMULATION OF THE 13.5 GHz RAIN ECHO POWER AT THE ALTIMETER INPUT

The radar echo power received from a pulse volume filled with a uniform rain rate, R, may be expressed by the modified Probert-Jones [1962] radar equation [Goldhirsh, 1979] given by

$$P_r = \frac{c}{1024\pi^2 \ln 2} P_t \tau \lambda^2 G^2 \theta_1 \phi_1 L_t L_r \frac{\eta}{r^2} \quad (2.1)$$

$$\times f(B_0) 10^{-0.2 \int_0^r (k_g + k_p + k_c) dr} \quad (\text{watts})$$

where

- c velocity of light ( $3 \times 10^8$  m/s),
- $P_t$  transmitted power (watts),
- $\tau$  pulsewidth (sec),
- $\lambda$  wavelength (m),
- G antenna gain,
- $\theta_1, \phi_1$  beamwidths along principal planes (rad),
- $L_t$  transmitted loss factor ( $< 1.0$ ) (losses from transmitted power measurement point to gain measurement point),
- $L_r$  receiver loss factor ( $< 1.0$ ) (losses from transmitter power measurement point to gain measurement point),
- $\eta$  Mie rain reflectivity ( $m^{-1}$ ),
- r range (m),
- $k_g, k_p, k_c$  attenuation coefficients due to atmospheric gas, precipitation, and clouds, respectively (dB/km),
- $B_0$  bandwidth of the receiver, Hz.

The factor  $f(B_0)$  represents the additional loss factor due to the radar receiver frequency response and has been calculated by Doviak and Zrnic [1979] for a Gaussian shape receiver response and rectangular transmitted pulse resulting in,

$$f(B_0) \approx -2.3 \text{ dB} \quad (2.2)$$

assuming a "matched filter" case.

## ORIGINAL PAPER OF POOR QUALITY

### 2.1 Rain Reflectivity Versus Rain Rate Relationship

The Mie reflectivity is theoretically given by,

$$\eta = \int_{D_{\min}}^{D_{\max}} \sigma(\lambda, D) N(D) dD \quad (\text{m}^{-1}) \quad (2.3)$$

where  $\sigma(\lambda, D)$  is the scattering cross-section ( $\text{m}^2$ ) of a spherical drop of diameter,  $D$ , at the wavelength,  $\lambda$ , and  $N(D)dD$  is the rain drop size distribution defined as the number of drops between diameters  $D$  and  $D+dD$  per unit volume where  $D_{\max}$  and  $D_{\min}$  are the maximum and minimum drop sizes in the pulse volume.

The rain rate,  $R$ , [mm/hr], may be theoretically expressed by,

$$R = \frac{\pi}{6} \int_{D_{\min}}^{D_{\max}} D^3 V(D) N(D) dD \quad (2.4)$$

where  $V(D)$  is the terminal velocity of a raindrop of diameter,  $D$  (e.g., cm/sec). As a nominal drop size distribution, we assume a Marshall-Palmer form [1948] (hereafter referred to as M-P) namely,

$$N(D) = N_0 \exp(-AD) \quad (2.5)$$

where  $N_0$  is fixed and given by,

$$N_0 = .08 \text{ cm}^{-4} \quad (2.6)$$

the reflectivity,  $\eta$ , and rain rate,  $R$ , as given by (2.3) and (2.4), respectively, were numerically computed and are plotted in Figure 1 against one another. The Mie scattering cross sections in (2.3) were obtained by frequency interpolating the results of Stephens [1961] at  $T=18^\circ\text{C}$  for 13.5 GHz. The integrands in (2.3) and (2.4) were approximately integrated over the drop diameter interval .03 to 0.5 cm ( $D_{\min}$  and  $D_{\max}$ ) which generally represents the range of drop diameters found in rain.

We note from Fig. 1 that the  $\eta$  versus  $R$  relationship may be expressed with good approximation by the relationship

$$\eta = AR^B \quad (\text{mm/hr}) \quad (2.7)$$

where

$$A = 3.143 \times 10^{-7} \quad (\lambda=2.22 \text{ cm})$$

$$B = 1.536 \quad (2.8)$$

where  $\eta$  is expressed in  $\text{m}^{-1}$ . The fitted curve given by (2.7) is in proximity of the computed curve  $\eta(\text{Mie})$  to within an rms deviation in rain rate better than 0.3 mm/hr over the rain rate interval 1 to 50 mm/hr.

Also plotted in Fig. 1 is the case assuming Rayleigh scattering alone which presumes

$$\frac{\pi D}{\lambda} \ll 1 \quad (2.9)$$

Under the assumption of (2.9),

$$\eta \approx \frac{\pi^5}{\lambda^4} |K_0|^2 \int_{D_{\min}}^{D_{\max}} D^6 N(D) dD \quad (2.10)$$

where  $|K_0|^2$  is dependent on the complex refractive index of the rain drops [Gunn and East, 1954; Ray, 1972] and is given by  $|K_0|^2 \approx 0.9$  in the frequency range 6 to 35 GHz and temperatures of  $0^\circ$  to  $20^\circ\text{C}$ . In comparing  $\eta(\text{Mie})$  with  $\eta(\text{Rayleigh})$  we note rain rate errors of 20, 43, and 55% at 10, 30, and 100 mm/hr respectively.

### 2.2 Attenuation Versus Rain Rate

The attenuation coefficient due to precipitation,  $k_p$ , is theoretically given by,

$$k_p = \int_{D_{\min}}^{D_{\max}} C_{\text{ext}}(\lambda, D) N(D) dD \quad [\text{dB/km}] \quad (2.11)$$

where  $C_{\text{ext}}(\lambda, D)$  is the extinction factor [ $(\text{dB/km})\text{cm}^3$ ] at the wavelength  $\lambda$  and drop diameter,  $D$ . Hereafter, the subscript  $p$  will be deleted for convenience. Assuming the Marshall-Palmer form (2.5) and (2.6), the integrand in (2.11) was numerically integrated over the diameter interval .03 to 0.5 cm resulting in the  $k$ - $R$  relationship depicted in Fig. 2. The extinction factors were obtained by frequency interpolating the tabulations of Medhurst [1965] ( $T=20^\circ\text{C}$ ). We note from Fig. 2 that the  $k$ - $R$  relationship may similarly be expressed with good approximation by the empirical relationship,

$$k = aR^b \quad \text{dB/km} \quad (2.12)$$

where

$$a = 2.038 \times 10^{-2}$$

$$b = 1.203 \quad (2.13)$$

which shows an rms deviation smaller than .2 mm/hr over the rain rate interval of 1 to 50 mm/hr (when compared to the calculated M-P curve).

### 2.3 Uncertainty of Attenuation Coefficient and Reflectivity With Variations in Drop Size Distributions

In order to establish a measure of uncertainty due to variations

ORIGINAL PAGE IS  
OF POOR QUALITY

9  
Y

of drop size spectra, an experimental data base of drop size distribution measurements at Wallops Island, Virginia was examined [Goldhirsh, 1980]. These measurements were made with an electro-mechanical disdrometer [Rowland, 1976] and cover 10 rain days; 5 during the summer of 1977 and 5 during the fall-winter of 1978-79. A cumulative number of approximately 1200 drop size distributions encompassing 17 hours of rain measurements were analyzed. The best fit results are tabulated in the first row of Table 1 for  $f=13.5$  GHz. The corresponding M-P parameters are given in the second row for comparison.

We note rms deviation in rain rates of approximately 50% and 22% for the  $\eta$ -R and  $k$ -R relationship, respectively, due to deviations of the individual measured distribution relative to the best fit case. Since the measurements were made over significant time durations of the storms, different parts of the precipitation structures were sampled. The best fit results are thus also representative of a spatial sampling of the distributions in rain.

In Figure 3 are plotted the disdrometer best fit  $\eta$ -R relationship (solid curve) plotted against the M-P curve (dot-dash). We note the two curves are in very close agreement giving percentage differences in rain rates of 10, 3, and 1% at 10, 30, and 100 mm/hr. Also plotted are the  $\pm$  rms percentage error bounds (dashed curves) relative to the disdrometer derived regression relationship.

In Figure 4 are plotted the corresponding curves for the  $k$ -R case. Again we note the measured best fit curve (solid line) to be nearly coincident with the M-P case (dot-dashed curve). Percentage differences of approximately 9, 5, and 2% are observed at

10, 30, and 100 mm/hr when comparing the M-P case relative to the measured regression line.

Because of the proximity of the measured  $\eta$ -R and  $k$ -R regression relationships with the M-P counterparts, we will consider the M-P cases to be the nominal ones and associate the measured uncertainties in rain rates given in the first row of Table 1 to the M-P case.

2.4 Influence of Cloud and Atmospheric Gaseous Constituents at 13.5 GHz

For a nadir pointing radar at 13.5 GHz the attenuation due to liquid cloud and atmospheric water vapor and oxygen may be ignored as they amount to a small fraction of a dB.

For liquid cloud at  $T=0^\circ\text{C}$  [Gunn and East, 1954],

$$k_c/M=0.1 \text{ [dB/km/gm/m}^3\text{]} \quad f=13.5 \text{ GHz} \quad (2.14)$$

where  $M$  = the cloud liquid water content [ $\text{gm/m}^3$ ]. We thus note, for example, that a 3 km thickness cloud with a nominally high liquid water content of  $0.5 \text{ gm/m}^3$  will amount to only 0.3 dB attenuation (two way).

Similarly the two way nadir attenuation due to all gaseous constituents is,

$$\int k_g \, dl < 0.2 \text{ dB; } f=13.5 \text{ GHz} \quad (2.15)$$

and nominally less than 0.1 dB [Crane, 1971].

3. RAIN ECHO POWER LEVELS AT A SEASAT TYPE ALTIMETER

Table 1 Measured and M-P best fit empirical parameters and associated rms deviations in rain rate

	Reflectivity vs Rain Rate				Attenuation Coeff. vs Rain Rate			
	$\eta = aR^b \quad (\text{m}^{-1})$				$k = aR^b \quad (\frac{\text{dB}}{\text{km}})$			
	A	B	Rain Rate rms deviation		a	b	Rain Rate rms deviation	
		(%)	mm/hr			(%)	mm/hr	
Meas.	$2.174 \times 10^{-7}$	1.620	48.9	6.9	$2.428 \times 10^{-2}$	1.170	22.1	2.5
M-P	$3.143 \times 10^{-7}$	1.536	<1.0	0.3	$2.038 \times 10^{-2}$	1.203	<1.0	0.2

ORIGINAL PAGES  
OF POOR QUALITY

3.1 Power Levels Assuming a M-P  
Drop Size Distribution

We shall incorporate the general formulations reviewed in the previous section with the radar parameters for the Seasat type altimeter assuming the family of drop size distributions for rain corresponds to those of M-P. Substituting the forms (2.7) and (2.12) into (2.1), the radar equation may alternately be expressed by,

$$P_r \text{ (dBm)} = A_1 + B_1 \log_{10} R + C_1 \Delta h R^b \quad (3.1)$$

where  $A_1$ ,  $B_1$ ,  $C_1$ , represent fixed radar parameters and  $\Delta h$  (km) is the one way path interval through rain. Although  $r$ , is variable, its range of variation is significantly small ( $< 10$  km) and hence the contribution to the echo power may be assumed with good approximation to be constant (to less than 0.1 dB variation).

The Seasat parameters are given by,

$$\begin{aligned} P_t &= 2 \text{ kw} \\ \tau &= 3.2 \text{ } \mu\text{sec} \\ r &= 800 \text{ km} \\ \theta_1, \phi_1 &= 1.6^\circ \text{ (} 2.792 \times 10^{-2} \text{ rad)} \quad (3.2) \\ G &\Rightarrow 40.6 \text{ dB (} 1.148 \times 10^4 \text{)} \\ L_t &\Rightarrow -0.9 \text{ dB} \\ L_r &\Rightarrow -1.2 \text{ dB} \end{aligned}$$

Substituting the parameters of (3.2) into (2.1) and converting to the form (3.1) we obtain,

$$\begin{aligned} A_1 &= -116.1 \\ B_1 &= 15.4 \\ C_1 &= -4.076 \times 10^{-2} \\ b &= 1.203 \end{aligned} \quad (3.3)$$

A nominal value of the noise level for the satellite altimeter is,

$$N = k T B_o F \Rightarrow -115 \text{ dBm} \quad (3.4)$$

where

$$\begin{aligned} k &= 1.38 \times 10^{-23} \text{ Jcules/}^\circ\text{K (Boltzmann's} \\ &\quad \text{constant)} \\ T &= 310^\circ\text{K} \\ F &\Rightarrow 5 \text{ dB (noise figure)} \quad (3.5) \\ B_o &= \frac{1}{\tau} = 3.125 \times 10^5 \text{ Hz (bandwidth)} \end{aligned}$$

The noise figure shown represents a 5 dB improvement to the 10 dB noise figure for the Seasat case.

In Figure 5 are plotted a family of curves representing the echo power at the altimeter as a function of rain rate corresponding to different height intervals,  $\Delta h$ , relative to the top of the raincell,  $\Delta h = 0$ , where negligible

attenuation is assumed to occur. The rain rate is also assumed uniform both over the height interval and within the main lobe. Also plotted is the -115 dBm unity signal to noise ratio level.

We note the curves for  $\Delta h \neq 0$  peak and ultimately fall below noise for increasing rain rates. The peaking is due to the interplay between two opposing tendencies; namely an increasing rain rate results in an increased backscatter power (the positive 2nd term in (3.1)) and a simultaneous increase of path attenuation (the negative 3rd term in (3.1)). At the higher rain rates, the attenuation term dominates. We note a maximum rain rate measurement of 55 mm/hr at 5 km and 280 mm/hr at 1 km into the rain.

3.2 Uncertainty in Rain Rates from  
Power and Power Difference  
Measurements Due to Variations  
in the Drop Size Distributions

We here incorporate the uncertainties in rain rates in (2.7) and (2.12) due to variations of drop size distribution as elaborated upon in Section 2.3 (summarized in Table 1). We alternately express (3.1) by

$$\begin{aligned} P_r \text{ (dBm)} &= A_1 + B_1 \log_{10} \left[ R_o (1 \pm \delta_1) \right] \\ &\quad + C_1 \Delta h R_o^b (1 \pm \delta_2)^b \end{aligned} \quad (3.6)$$

where  $R_o$  is the nominal rain rate assumed to follow the M-P family of distributions, and  $\delta_1$  and  $\delta_2$  are the rain rate uncertainties for the reflectivity and attenuation coefficient empirical relations, respectively. These are (from Table 1),

$$\begin{cases} \delta_1 = .49 \\ \delta_2 = .22 \end{cases} \quad (3.7)$$

In Figure 6 are plotted the nominal power levels as well as the upper and lower uncertainty bounds as a function of rain rate for both the storm top ( $\Delta h=0$ ) and  $\Delta h=5$  km into the rain. The power level bounds were determined by injecting the parameters (3.3) and (3.7) into (3.6) and selecting the extreme values relative to the nominal case (i.e.,  $\delta_1=\delta_2=0$ ) for each rain rate.

It may be deduced from Fig. 6 that a power measurement alone at  $\Delta h=5$  km results in both significantly larger uncertainties and ambiguities due to the multivalued nature of the rain rates. A more meaningful measurement at the larger rain rates is a power difference measurement (i.e., attenuation). Referring to (3.6), the power difference between  $\Delta h=0$  and  $\Delta h$  is given by,

$$\Delta P \text{ (dB)} = C_1 \Delta h R_o^b (1 \pm \delta_2)^b \quad (3.8)$$

ORIGINAL PAGE IS  
OF POOR QUALITY

We thus note that the uncertainties associated with the reflectivity vanishes and only those associated with the power difference remains (i.e.,  $(1 + \delta_2)^b$ ). In Figure 7 is plotted the nominal power difference (3.8) and the corresponding uncertainty bounds at  $\Delta h=5$  km. The associated error bounds in rain rate are within  $\pm 22\%$  of the nominal for any given power difference measurement.

We conclude from the results depicted in Figures 6 and 7 and the above discussion that it may be far more accurate to ascertain rain rate from the power difference (attenuation) than a power level measurement assuming the condition of beam filling and uniform rain rate over the range interval,  $\Delta h$ .

4. ECHO POWER FOR NON-UNIFORM BEAM FILLING

In this Section we examine the capability of ascertaining the rain rate characteristics for the case in which the altimeter main beam is not uniformly filled by the rain along the horizontal extent.

4.1 Power Levels and Differences as a Function of the Rain Features

We assume a rain rate variation along the ground to be Gaussian in shape [Hodge, 1977] and given by,

$$R = R_0 \exp \left[ -\left(\frac{\rho}{\rho_0}\right)^2 \right] \quad (4.1)$$

where  $R_0$  is the peak rain rate aligned with the main beam altimeter axis,  $\rho$  is the polar distance parallel to the earth (orthogonal to the main beam axis) and  $\rho_0$  is that distance corresponding to the  $\exp(-1)$  falloff of rain rate (i.e.,  $.37 R_0$ ).

It may be demonstrated [Goldhirsh and Walsh, 1981] that the altimeter power is given by,

$$P_r = P_{r0} F(g, \Delta h, R_0) \quad (4.2)$$

where  $P_{r0}$  is the power (2.1) for the uniform rain case at  $\Delta h=0$ , and  $F$  is a factor  $<1$  dependent on the extent of the rain inhomogeneity within the beam as it affects the reflectivity and the attenuation. It is given by,

$$F(g, \Delta h, R_0) = \left( \frac{32 \ln 2}{\pi} \right) \int_0^1 \int_0^1 \exp \left[ -8 \ln 2 (x^2 + y^2) \right] \exp \left[ -4gb (x^2 + y^2) \right] \exp \left\{ -4606aR_0^b \Delta h \exp \left[ -4gb(x^2 + y^2) \right] \right\} dx dy \quad (4.3)$$

The factor  $g$  is a parameter introduced to characterize changes in  $\rho_0$  and is defined by

$$\rho_0 = \frac{r\theta_1}{2\sqrt{g}} \quad (4.4)$$

Hence  $g=1$  corresponds to  $\rho_0$  representing half the beam resolution interval at the ground. All the other parameters in (4.3) have been previously defined.

Equation (4.3) has been numerically integrated for different values of  $R_0$  and  $\rho_0$  resulting in Figs. 8 and 9. In Fig. 8 the apparent rain rate  $R_a$  at the top of the raincell ( $\Delta h=0$ ; no attenuation) is plotted as a function of the peak rain rate,  $R_0$ , for a family of values of  $\rho_0$ . The apparent rain rate is obtained by computing the power from (4.2) and relating this power to the  $\Delta h=0$  curve in Fig. 5 (or by employment of (3.1)). It effectively represents the presumed rain rate obtained by assuming uniform beam filling with the reduced power level. We note that the apparent rain rate is critically dependent on the Gaussian parameters,  $\rho_0$  and  $R_0$ . The  $\rho_0 = \infty$  case corresponds to the uniform beam filling case.

In Fig. 9, we have plotted the dB power differences between the top of the rain and 5 km into the rain as a function of the peak rain rate,  $R_0$  for a family of values of  $\rho_0$ . For any given peak rain rate,  $R_0$ , the power difference is dependent on  $\rho_0$  for values down to  $\rho_0 = 2.5$  km ( $g < 20$ ) for the given range of rain rates. At smaller values of  $\rho_0$  (larger  $g$ ), the attenuation takes place over the region where the gain pattern function is relatively uniform (near the nadir axis) and the power difference is found to asymptotically approach a fixed level for each value of  $R_0$ .

4.2 A Technique to Ascertain Scale Dimension,  $\rho_0$ , and Peak Rain Rate,  $R_0$

It is demonstrated that a measurement of the power at top of the rain and a power difference measurement through the rain enables the determination of,  $\rho_0$  and  $R_0$ . It is tacitly assumed that the drop size distribution is that of M-P and the peak of the Gaussian rain cell coincides with the main beam axis of the altimeter.

In Fig. 10 are constructed constant apparent rain rate isopleths (dashed lines) of  $\rho_0$  vs  $R_0$  where each isopleth corresponds to a fixed level of  $R_a$  in Fig. 8. Also plotted are constant power difference isopleths (solid lines) of  $\rho_0$  vs  $R_0$  taken from constant power level differences in Fig. 9. The intersections of these isopleths, in general, uniquely define the values of  $\rho_0$  and  $R_0$ . At power differences of 20

ORIGINAL PAGE IS  
OF POOR QUALITY

dB and greater, ambiguities in these values may however arise due to the multivalued nature of these curves at these very high power difference levels. As an example, we note that a power difference of 10 dB and an apparent rain rate of 20 mm/hr results approximately in  $\rho_0 = 7$  km and  $R_0 = 50$  mm/hr.

In the event the Gaussian rain cell is not coincident with the main beam axis, or the rain cell has more arbitrary scale features as will usually be the case, the technique outlined here may continue to be used to find "equivalent" values of  $R_0$  and  $\rho_0$ . That is, a measurement of power at  $\Delta h=0$  and power difference will give rise to an equivalent centrally located Gaussian giving the same power levels as the real rain structure.

4.3 Power Parameters as a Function of Rain Cell Axis Displacement from Main Beam Axis

In the previous section we examined the very special case in which the main beam altimeter axis coincides with the peak rain axis,  $R_0$ , associated with the Gaussian rain structure given by (4.1). Here we consider the case for which the rain rate axis is displaced. That is,

$$R = R_0 \exp \left[ - \left( \frac{\rho-d}{\rho_0} \right)^2 \right] \quad (4.4)$$

Specifically, we shall examine the power signature at the altimeter as the main beam moves through the Gaussian structure along a principal rain rate axis. For such a geometry, (4.3) becomes,

$$\begin{aligned} \Gamma(g, \Delta h, R_0, D) = & \left( \frac{16 \ln 2}{\pi} \right) \int_0^1 \int_{(x)}^{-1} \exp \left\{ -8 \ln 2 \right. \\ & \left. [x^2 + y^2] \right\} x \exp \left\{ -4gB [x^2 + (y-D)^2] \right\} \\ & \times \exp \left\{ -4606aR_0^b \Delta h \exp \left[ -4gb(x^2 + (y-D)^2) \right] \right\} \\ & dx dy \end{aligned} \quad (4.5)$$

where D is given by,

$$D = \left( \frac{\theta}{\theta_1} \right) = \left( \frac{r\theta}{r\theta_1} \right) = \frac{d}{d_1} \quad (4.6)$$

with  $\theta_1$  being the altimeter beamwidth, and  $\theta$  the angular displacement of the altimeter beam axis to the peak rain rate axis. Also,  $d_1$  and  $d$  are the respective distances along the ground.

As an example, we have plotted in Figs. 11-13 the following as a function of the beam axis displacement  $d$ : (1) the power from the raincell top  $P(\Delta h=0)$ ;

(2) the power differences between the echos from the raincell top and the pulse volume 5 km into the rain,  $\Delta P(\Delta h=5)$ ; Fig. 12, and (3) the apparent rain rate,  $R_a(\Delta h=0)$ , from the rain cell top; Fig. 13. The curves were generated through the numerical evaluation of (4.5) for variable  $D, \rho_0$ , and a peak rain rate,  $R_0 = 30$  mm/hr. For example, when  $\rho_0$  is small ( $\rho_0 < 2.5$  km), the power difference is noted to be constant (Fig. 12) as the main beam sweeps through the Gaussian rain cell. As  $\rho_0$  increases,  $\Delta P$  undergoes larger variations with  $d$ . In addition,  $P(\Delta h=0)$  (Fig. 11) undergoes larger variations with slope changes for smaller values of  $\rho_0$ .

The peak apparent rain rate,  $R_a$ , and power difference,  $\Delta P$ , may be better identified from the signatures of Fig. 13 and Fig. 12. Hence the values of  $R_0$  and  $\rho_0$  should then be capable of being ascertained using the method described in Section 4.2.

5. DETERMINATION OF DROP SIZE DISTRIBUTION USING A TWO MEASUREMENT METHOD

A technique will be described in this section for ascertaining the average drop size distribution in the pulse volume through a measurement of rain echo power and power difference over an interval,  $\Delta h$ .

5.1 Elaboration of the Method

The technique employs a power measurement at the top of rain cell ( $\Delta h=0$ ) from which the reflectivity,  $\eta$ , may be deduced. This may be expressed from (2.1) by,

$$\eta = C_0 P_r(\Delta h=0) \quad (5.1)$$

where  $C_0$  is the inverse of the product of parameters multiplying  $\eta$  in (2.1) (i.e., a constant).

As previously mentioned,  $\eta$  is theoretically given by (2.3). Similarly the attenuation coefficient may be determined from (2.1) and is observed to be given by

$$k = \frac{1}{2\Delta h} 10 \log_{10} \left\{ \frac{P_r(\Delta h=0)}{P_r(\Delta h)} \right\} \left[ \frac{dB}{km} \right] \quad (5.2)$$

and theoretically it is given by (2.11).

We now assume the drop size distribution may be expressed by the two parameter exponential,

$$N(D) = N_0 \exp(-AD) \quad (5.3)$$



## ORIGINAL PAPER OF POOR QUALITY

where both  $\Lambda$  and  $N_0$  are unknown. It will be demonstrated that a measurement of  $k$  and  $\eta$  as given by (5.2) and (5.1) uniquely defines  $N_0$  and  $\Lambda$  and hence the drop size distribution. Once (5.3) is obtained, the rain rate as given by (2.4) is uniquely determined.

Substituting (5.3) into (2.3), (2.11) and (2.4), we obtain the normalized parameters,

$$\frac{\eta}{N_0} = \int_{D_{\min}}^{D_{\max}} \sigma(\lambda, D) \exp(-\Lambda D) dD \quad (5.4)$$

$$\frac{k}{N_0} = \int_{D_{\min}}^{D_{\max}} C_{\text{ext}}(\lambda, D) \exp(-\Lambda D) dD \quad (5.5)$$

$$\frac{R}{N_0} = \frac{\pi}{6} \int_{D_{\min}}^{D_{\max}} D^3 V(D) \exp(-\Lambda D) dD \quad (5.6)$$

Taking the ratio of (5.4) and (5.5),

$$\frac{k}{\eta} = \frac{\int_{D_{\min}}^{D_{\max}} C_{\text{ext}}(\lambda, D) \exp(-\Lambda D) dD}{\int_{D_{\min}}^{D_{\max}} \sigma(\lambda, D) \exp(-\Lambda D) dD} \quad (5.7)$$

As previously mentioned in Section 2,  $C_{\text{ext}}$  and  $\sigma$  have been tabulated at 13.5 GHz as a function of drop diameter. The right hand sides of (5.4) through (5.7) may thus be numerically computed as a function of  $\Lambda$ . The resultant expressions as a function of  $\Lambda$  are plotted in Figs. 14 and 15. As a basis for comparison, in Fig. 14 is also plotted the M-P rain rate as a function of  $\Lambda$  (i.e., (5.6) with  $N_0 = .08 \text{ cm}^{-4}$ ). In Fig. 16 is given, for easy reference, the echo power at  $\Delta h=0$  as a function of the Mie reflectivity. It is apparent that a measurement of  $k$  and  $\eta$  and the subsequent ratio  $k/\eta$  results via Fig. 14 in a unique determination of  $\Lambda$ . Substituting the value of  $\Lambda$  in (5.4) or (5.5) (Fig. 15), we determine  $N_0$ . Once  $N_0$  and  $\Lambda$  are evaluated, we may calculate the rain rate,  $R$  given by (5.6) or the liquid water content given by,

$$M = \frac{\rho \pi}{6} \int_{D_{\min}}^{D_{\max}} D^3 N(D) dD \left[ \frac{\text{gm}}{\text{m}^3} \right] \quad (5.8)$$

The technique described here is identical in general concept to the two frequency method examined by Atlas and Ulbrich [1974], Goldhirsh and Katz [1974] and Goldhirsh [1975]. The difference here is that we employ a single frequency (instead of two) and examine the Mie reflectivities instead of the Rayleigh values. Furthermore, we have

tacitly assumed that an unattenuated measurement at  $\Delta h=0$  is possible, the rain rate is uniform over  $\Delta h$ , and uniformly fills the beam.

In Section 7 an error analysis associated with the above technique is given.

### 6. RAIN MEASUREMENT IMPLEMENTATION FOR A SEASAT TYPE ALTIMETER

The Seasat radar altimeter achieved its 3.125 ns range resolution by transmitting a chirped pulse of 3.2  $\mu\text{s}$  duration in which the frequency was linearly swept over a 320 MHz bandwidth around a center frequency of 13.5 GHz. In normal surface tracking operations, the Seasat Altimeter tracked continuously utilizing 1000 per second chirped pulses and produced smoothed range and surface waveform data every 100 ms. The Seasat tracker was updated every 50 ms and we will assume any future altimeter would not allow this disparity and would output data every 50 ms. The proposed rain mode would allocate one 50 ms interval per second for measurement of rain backscatter using unmodulated CW pulses. No range data would be obtained during the CW transmissions and the tracker would coast, but that would result in a negligible degradation of the range and significant wave height (SWH) data (data over a 350 m ground track would be lost every 7 km). On a 1 second average, the noise in the range and SWH measurements would increase by approximately 2.5 percent. This is considered to be an acceptable penalty.

The normal Altimeter acquisition mode [MacArthur, 1978], used CW pulses to find the maximum signal and determine its range. The rain measurement mode would require the incorporation of a 10 bit A/D converter in the CW circuitry. That would permit CW received power measurements at a series of altitudes above the tracking surface.

The normal chirped range tracking mode samples 60 range gates spaced at approximately 0.5 m and centered on mean sea level. The same telemetry stream in the CW mode would allow the sampling of a 30 km interval above the sea surface with observations every 500 m (the approximate range extent of the uncompressed pulse) to determine the complete profile of the rain structure (Figure 17). The mode would measure radar system noise when the range was well above the rain, determine the location of the bright band near the melting layer, and then measure the rain backscattered power which diminishes in range as the attenuation through the rain increases.

#### 6.1 Altimeter Timing for Rain Detection

ORIGINAL PAGE IS  
OF POOR QUALITY

Figure 18 indicates the arrangement of the transmitted and received pulses in the proposed configuration. For the first 19/20 of each second, the altimeter would function in its normal manner transmitting chirp pulses. Then, during the last 1/20 of each second, the transmitter would switch to the CW mode and transmit 50 pulses. The decision to transmit in the chirp or CW mode must be made just before transmission and it cannot be changed for reception. As is shown in Figure 18, the last five pulses transmitted in the chirp mode will be lost because they will be still in transit when the mode switch is made. Similarly, the last five pulses transmitted in the CW mode will be lost when the transmitter switches back to chirp.

7. ERROR ANALYSIS FOR DETERMINATION OF DROP SIZE DISTRIBUTION

In view of Rayleigh fading and other system uncertainties, we here consider an error analysis for the method of determining drop size distribution described in Section 5.

For purposes of the simulation we will assume that the bright band occurs just above 5 km from the sea surface producing negligible absorption. We also assume we have 10 samples spaced at 500 m intervals over the 5 km extent of the rain structure.

For soundings by a short pulse radar, the backscatter return may be modeled as a Rayleigh process in which the received pulse power is an exponentially distributed random variable with a standard deviation equal to the mean. The predetection filter of the acquisition circuitry would be narrowed to match it to the pulse 320 KHz bandwidth and reduce the noise power. That means that the signal plus noise would also be an exponentially distributed random variable.

Averages would be made of the return power at each range for the 45 pulses available in the 50 ms rain measurement interval. Those averages would then be normally distributed random variables whose standard deviation would  $(45)^{-1/2}$  times the mean value. A simulation was developed using a least-squares fitted straight line to 10 values of rain backscattered power in dB spaced from 5 km to .5 km from the sea surface at 500 m intervals. The attenuation coefficient,  $k$ , was obtained from the slope of the line and the value of the line at 5 km was used for the backscattered power to determine  $\eta$ .

The standard deviation of the  $k$  estimate for a hundred trials was found to be 0.07 dB/km, independent of the magnitude of the slope, for values of  $k$  between 0 and 3 dB/km. Similarly, the standard deviation on  $\eta$  was 0.36 dB.

As an example in testing the method of Section 5, Figure 19 indicates the errors in the rain rate estimate which would result from those random errors if the drop size distribution had been the M-P ( $N_0 = 0.08$ ). The procedure used was to start with a value of rain rate and use the  $R/N_0$  curve from Figure 15 to determine  $\Lambda$ . Then the nominal values of  $k$  and  $\eta$  for  $\Lambda$  were also determined from Figure 15. These are the values which would result if there were no random or calibration errors. The desired random errors were added to the nominal  $k$  and  $\eta$  values to obtain the "measured" values and their ratio was taken so the "measured" value of  $\Lambda$  could be determined from Figure 14. Then the measured value of  $N_0$  can be computed from either the  $\eta/N_0$  or  $k/N_0$  curve in Figure 15. Finally, the measured value of rain rate can be determined from the value of  $N_0$  and the  $R/N_0$  curve of Figure 15.

Values of  $N_0$  of 0.8 and 0.008 were also used but the errors did not vary significantly for a particular rain rate. Figure 19 indicates that the total random error on rain rate using this procedure would generally be less than 5 mm/hr for rain rates above 5 mm/hr.

Future satellite altimeters will probably employ a PRF higher than 1000 pulses/second. For high sea states, a PRF as high as 4500 would still furnish independent samples for reducing tracking noise. For that PRF, 220 CW pulses would be available in 1/20 second and the standard deviations on  $k$  and  $\eta$  would be 0.03 dB/km and 0.16 dB respectively. Figure 20 shows the resulting errors for  $\pm 0.03$  dB/km errors in  $k$ . The errors corresponding to the random errors in  $\eta$  are not shown but they are reduced from the values in Figure 19 by the same percentages as the errors in  $k$ . The total random error would generally be below 3 mm/hr for rain rates above 3 mm/hr. Also shown in Figure 20 is the effect of  $\pm 1$  dB bias errors in system calibration. They would result in estimates being biased off by about 15% of the rain rate. The system should be able to be calibrated to at least this accuracy.

8. REFERENCES

- Atlas, D. and C.W. Ulbrich [1974], "The Physical Basis for Attenuation Rainfall Relationships and the Measurement of Rainfall Parameters by Combined Attenuation and Radar Methods", Journal De Recherches Atmospheriques Colloque De L'IUCRM, Vol. VIII, Janvier-Juin, pp. 275-298.
- Crane, R. K. [1971], "Propagation Phenomena Affecting Satellite Communication Systems Operating in the Centimeter and Millimeter Wavelength Bands", Proceedings of IEEE, Vol. 59, No. 2, February, pp. 173-188.

ORIGINAL LISTING  
OF POOR QUALITY

- Doviak, R.J. and D. Zrníc [1979], "Receiver Bandwidth Effect on Reflectivity and Doppler Velocity Estimates", *J. Appl. Meteor.*, Vol. 18, No. 1, January, pp. 70-76.
- Goldhirsh, J and E. J. Walsh [1981], "Precipitation Measurements from Space Using a Modified Seasat Type Radar Altimeter", APL Technical Report SLR81U-022, May.
- Goldhirsh, J. [1980], "Comparison of Radar Derived Slant Path Rain Attenuations with the COMSTAR Beacon Fades at 28.56 GHz for Summer and Winter Periods", *IEEE Trans. Antennas and Propagation*, Vol. AP-28, No. 4, July, pp. 577-580.
- Goldhirsh, J. [1979], "A Review on the Application of the Non-Attenuating Frequency Radars for Estimating Rain Attenuation and Space Diversity Performance", *IEEE Trans. on Geoscience Electronics*, GE-17, No. 4, October, pp. 218-239.
- Goldhirsh, J. [1975], "Improved Error Analysis in Estimation of Raindrop Spectra, Rain Rate, and Liquid Water Content Using Multiple Wavelength Radars", *IEEE Trans. on Antennas and Propagation*, September, pp. 718-720.
- Goldhirsh, J. and I. Katz, [1974], "Estimation of Raindrop Size Distribution Using Multiple Wavelength Radar Systems", *Radio Science*, Vol. 9, No. 4, April, pp. 439-446.
- Gunn, K.L.S. and T.W.R. East [1954], "The Microwave Properties of Precipitation Particles", *Quart. J. Roy. Meteor. Soc.*, Vol. 80, pp. 522-545.
- Hodge, D.B. [1977], "Frequency Scaling of Rain Attenuation", *IEEE Trans. on Antennas and Propagation*, Vol. AP-25, pp. 446-447.
- MacArthur, J.L. [1978], "Seasat-A Radar Altimeter Design Description", JHU/Applied Physics Laboratory contractor report SDO-5232, November.
- Marshall, J.S. and W. McK. Palmer [1948], "The Distribution of Raindrops with Size", *J. Meteor.*, Vol. 5, pp. 165-166.
- Medhurst, R.G. [1965], "Rainfall Attenuation of Centimeter Waves: Comparison of Theory and Measurement", *IEEE Trans. on Antennas and Propagation*, Vol. AP-13, pp. 550-554.
- Probert-Jones, J.R. [1962], "The Radar Equation in Meteorology", *Quart. J. Roy. Meteor. Soc.*, Vol. 88, pp. 485-495.
- Ray, P.S. [1972], "Broadband Complex Reflective Indices of Ice and Water", *Appl. Opt.*, Vol. II, pp. 1836-1844.
- Rowland, J.R. [1976], "Comparison of Two Different Raindrop Disdrometers", *Proc. 17th Conf. on Radar Meteor.*, October 26-29, Seattle, WA., pp. 398-405.
- Stephens, J.J. [1961], "Radar Cross-Sections for Water and Ice Spheres", *J. Meteor.*, Vol. 18, pp. 348-359.
- Walsh, F.J. [1981], "Altimeter Rain Detection (Appendix E)", Performance Specification for the Altimeter (ALT) Instrument for the National Oceanic Satellite System (NOSS), NASA GSFC, Document No. 485-1203-003, Revision A, February.

9. ACKNOWLEDGEMENT

The work was performed for the NASA Wallops Flight Center under contract (NASA HDPF S50748A; Radar Prediction of Rain Attenuation for Earth-Satellite Paths).

ORIGINAL QUALITY  
OF POOR QUALITY

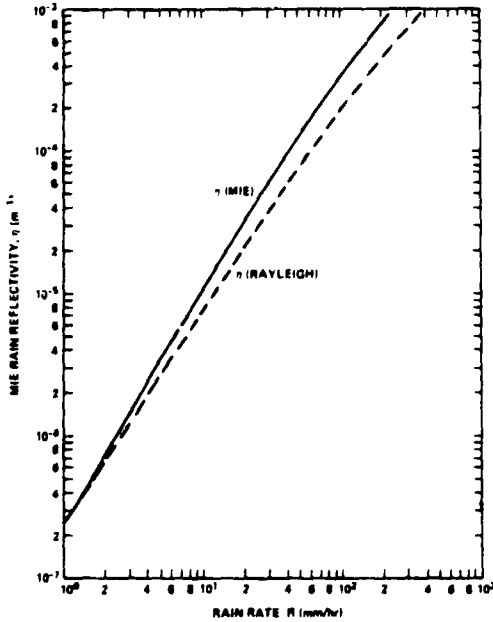


Figure 1. Mie and Rayleigh reflectivities versus rain rate (M-P distribution).

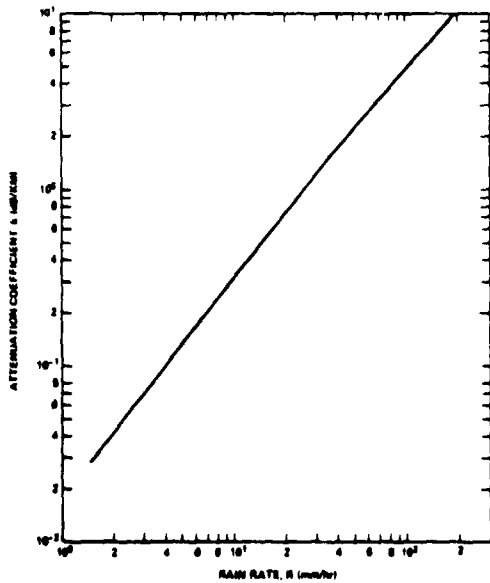


Figure 2. Attenuation coefficient versus rain rate (M-P distribution).

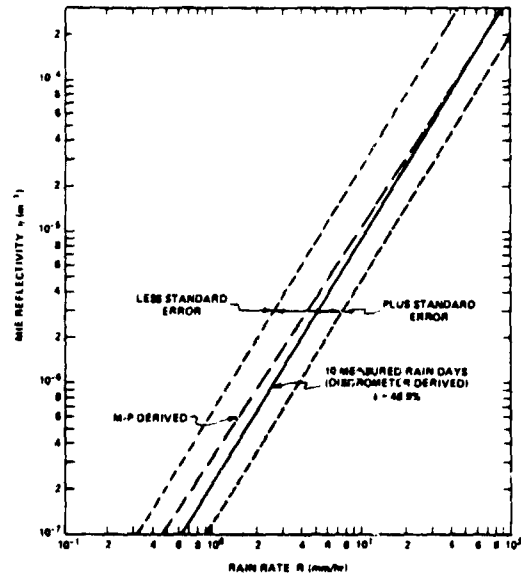


Figure 3. Reflectivity versus rain rate derived from disdrometer measurements. Comparison with M-P case is given.

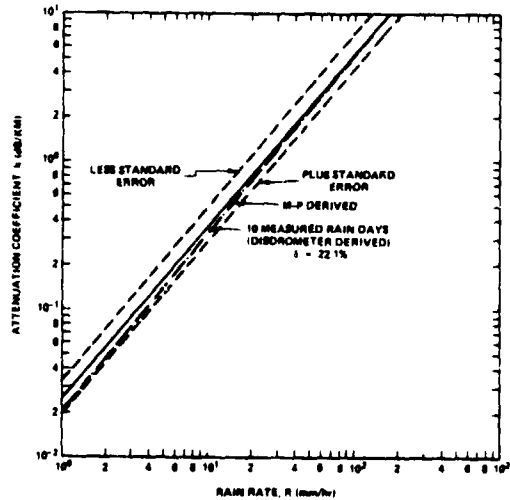


Figure 4. Attenuation versus rain rate derived from disdrometer measurements. Comparison with M-P case is given.

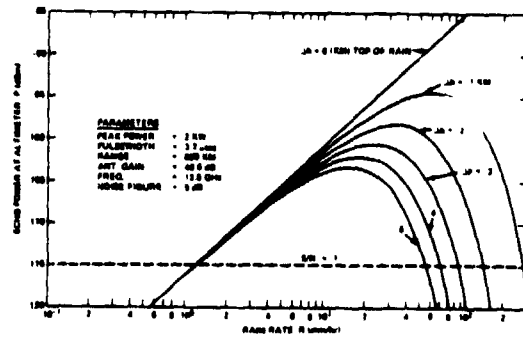


Figure 5. Echo power returned to the altimeter from various distances below the top of the rain versus rain rate.

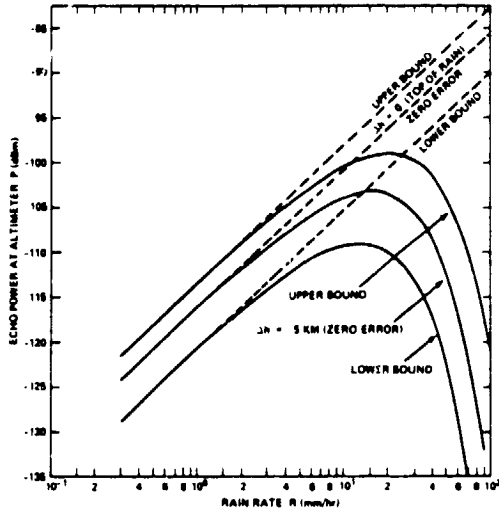


Figure 6. Nominal values and uncertainty bounds on power returned to the altimeter from the top of the rain and 5 km into rain versus rain rate.

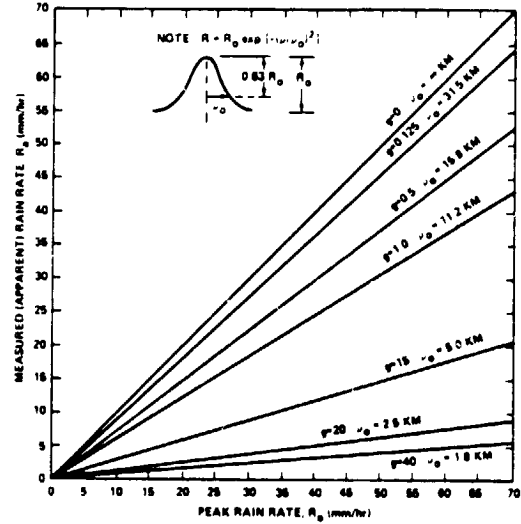


Figure 8. Apparent rain rate versus peak rain rate for Gaussian distributed rain cells of various widths.

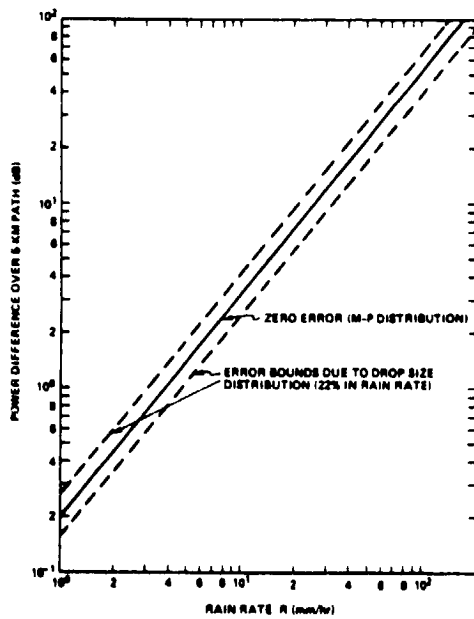


Figure 7. Nominal power difference and uncertainty bounds for 5 km path versus rain rate.

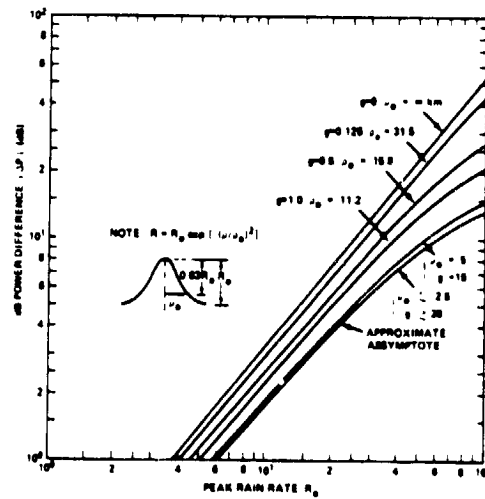


Figure 9. Power difference between top and 5 km into Gaussian distributed rain cells of various widths versus peak rain rate.

ORIGINAL QUALITY  
OF POOR QUALITY

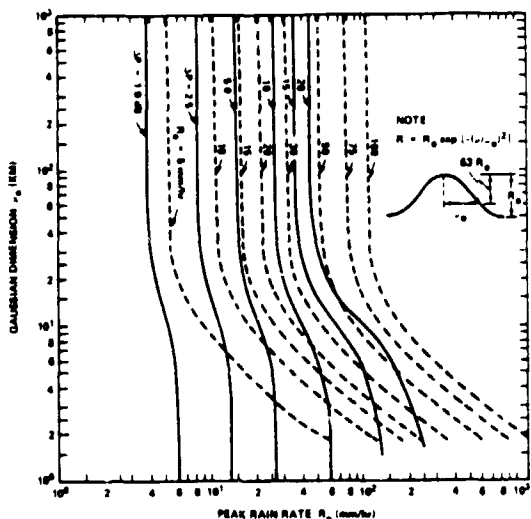


Figure 10. Constant apparent rain rate (dashed lines) and power differences (solid lines) isopleths versus peak rain rate.

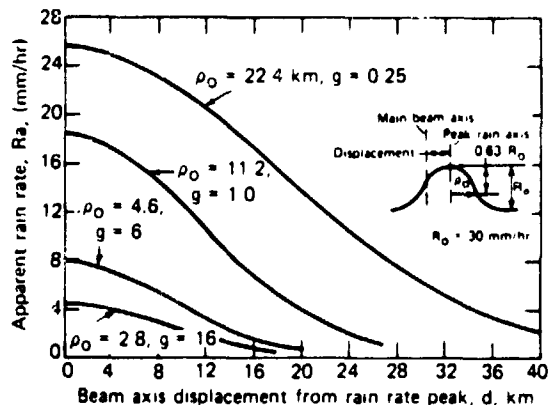


Figure 13. Apparent rain rate at rain top versus displacement of rain rate peak from antenna boresight.

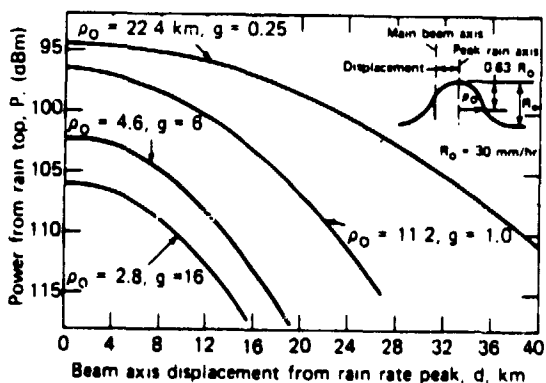


Figure 11. Power returned from the top of the raincell versus displacement of rain rate peak from antenna boresight.

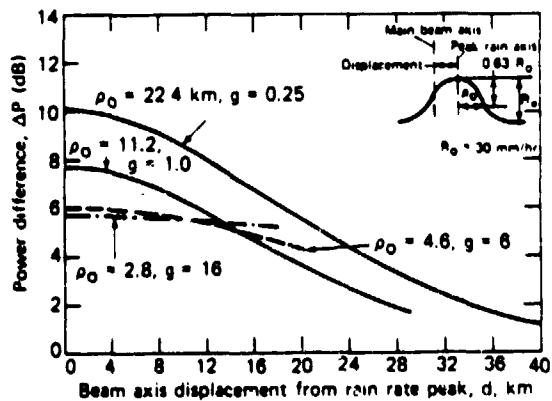


Figure 12. Power difference over 5 km vertical extent of rain cell versus displacement of rain rate peak from antenna boresight.

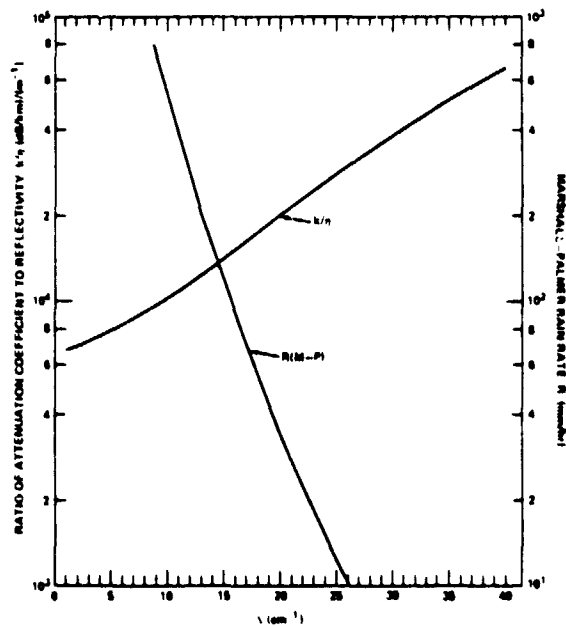


Figure 14. Ratio of measured attenuation coefficient to reflectivity as a function of  $\lambda$  at 13.5 GHz. M-P rain rate shown for reference.

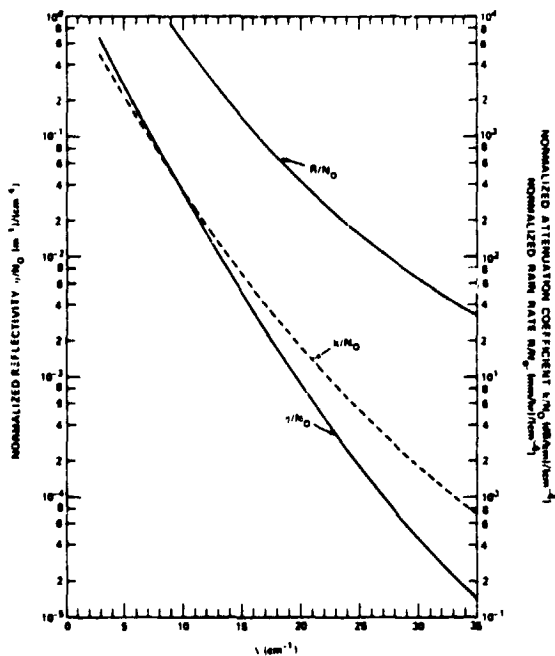


Figure 15. Normalized rain rate, attenuation coefficient, and Mie reflectivity versus  $\lambda$  at 13.5 GHz.

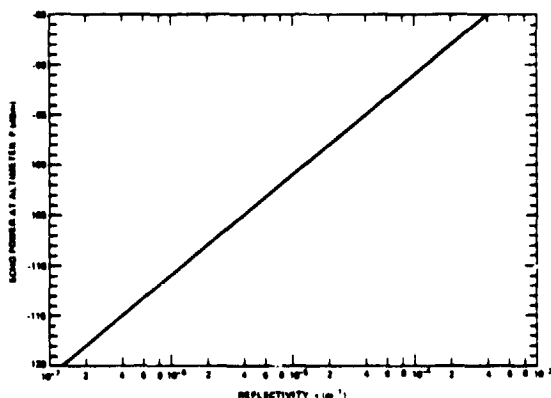


Figure 16. Echo power from rain top as a function of Mie reflectivity.

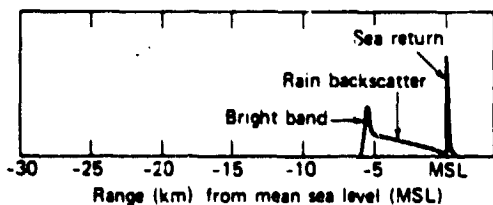


Figure 17. Illustrative example depicting variation of power returned to altimeter versus range.

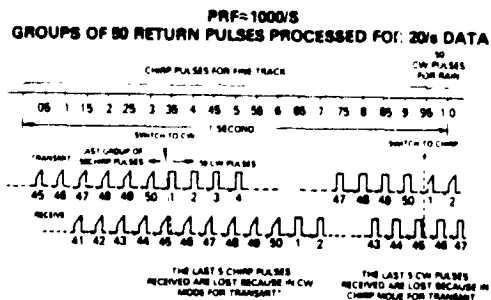


Figure 18. Arrangement of the transmitted and received pulses for the rain measurement mode.

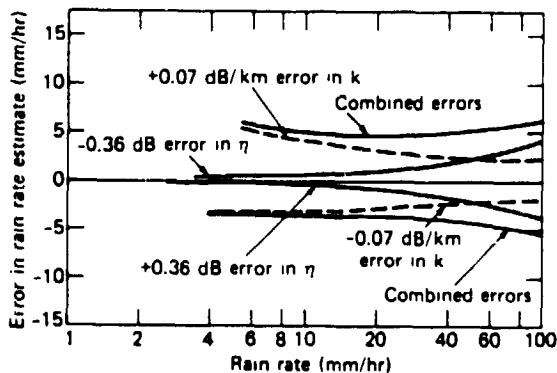


Figure 19. Rain rate errors for  $+1 \sigma$  random errors for a 45-pulse average.

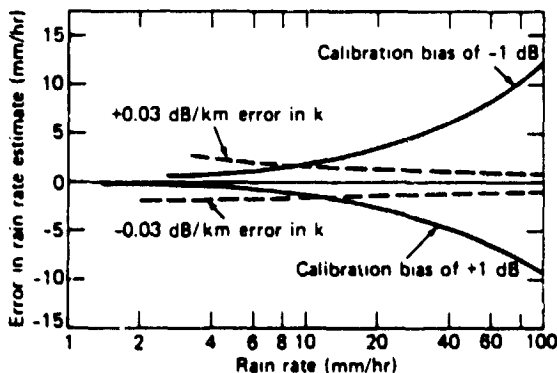


Figure 20. Rain rate errors for a 220-pulse average resulting from  $+1 \sigma$  random errors in  $k$  and  $\pm 1$  dB calibration biases in power.

D43

N83 25312

ORIGINAL SOURCE IS  
OF POOR QUALITY

9  
Y

USE OF COMBINED RADAR AND RADIOMETER SYSTEMS  
IN SPACE FOR PRECIPITATION MEASUREMENT -- SOME IDEAS

Richard K. Moore  
Remote Sensing Laboratory  
University of Kansas Center for Research, Inc.  
Lawrence, Kansas

ABSTRACT

Combined use of a radar and radiometer in space for measurement of precipitation offers some interesting possibilities. The most obvious application of the radiometer is to measure the attenuation experienced by the radar signal. To do this one must make certain assumptions about the distribution of the hydrometeors and temperature in the atmosphere. The biggest problem with both radiometer and radar in measurement of precipitation is discrimination against the background emission and scattering. Over the ocean this discrimination is much easier than over the land. The use of closely-spaced frequencies permits taking advantage of the more rapid variation of the atmospheric effects with frequency than the variation of the surface effects.

The various parameters of atmosphere, surface and system that may be used for such measurements are outlined here and five systems are postulated using unmodulated scatterometers and radars with reasonably good range resolution along with radiometers. The radiometers are always helpful, even if the radars are capable of measuring precipitation by themselves, because the radiometers permit estimating the attenuation experienced by the radar signal and thus improving the estimate of precipitation.



ORIGINAL DOCUMENT  
OF POOR QUALITY

USE OF COMBINED RADAR AND RADIOMETER SYSTEMS  
IN SPACE FOR PRECIPITATION MEASUREMENT -- SOME IDEAS

R.K. Moore  
Remote Sensing Laboratory - University of Kansas Center for Research, Inc.  
Lawrence, Kansas

INTRODUCTION

Radars on aircraft and the ground are routinely used for precipitation measurement, and multifrequency microwave radiometers in space have been used for precipitation measurements. Radiometers and scatterometers have been used together in space for determining attenuation in the atmosphere and wind speed over the ocean, but not for precipitation measurement. Thus, this paper represents not a description of results but rather a proposed framework for considering joint use of active and passive microwave instruments for precipitation measurements from space.

Three fundamental premises underlie this discussion:

- (1) We want to measure rainfall over land and sea on a global scale.
- (2) Low-orbit satellites will necessarily only provide samples of the rainfall but cannot provide continuous measurement.
- (3) Stationary orbit satellites should be used for part of the system if feasible, because they can provide nearly continuous data.

With regard to premise number 1, although the desire is to measure rainfall over both land and sea, a system that would work on either land or sea alone would be a major improvement, particularly one that would work over the sea. With regard to premise number 2, even though we may provide a wide swath of coverage from a low-orbit satellite, the orbital constraints necessarily restrict its measurements to relatively infrequent

ORIGINAL PAGE IS  
OF POOR QUALITY

samples of the precipitation. Therefore it is of more climatological than forecasting interest. Stationary-orbit satellites would be most desirable, but the antennas required to achieve the needed resolution from such systems are so large that the systems are not specifically considered in the proposals advanced here. However, one can conceive of such systems using radar alone if the combination of beamwidth, range resolution, and speed resolution can be properly used together.

Before proceeding, let us consider the measurements made by the two instruments and the significant atmospheric and surface parameters that are measured. The atmospheric parameters are related to rainfall and the surface parameters govern the background that must be discriminated

The power received by the radar  $P_r$  is given by

$$\overline{P_r}(t) = \overline{P_{ratm}}(t) + \overline{P_{rsur}}(t) \quad (1)$$

where the subscripts are obvious. The overbars indicate that average powers must be used because fading of the signal due to random phase addition of components from different parts of the volume or surface have no meaning and must be averaged out. The average power received from the atmosphere is given by

$$\overline{P_{ratm}}(t) = \int \frac{P_t \lambda^2 G^2 \sigma_v dV}{(4\pi)^3 r^4} \tau(h, \theta) \quad (2)$$

where  $P_t$  is the transmitted power,  $\lambda$  is the wavelength,  $G$  is the antenna gain in the direction of  $dV$ ,  $\sigma_v$  is the scattering cross-section per unit volume, and  $r$  is the range between the radar and  $dV$ ,  $\tau(h, \theta)$  is the atmospheric transmissivity from height  $h$  to the top of the atmosphere  $h_0$  at an angle with the vertical of  $\theta$  and is given by

Significant  
atmospheric &  
surface  
parameters:

$\sigma_v, \tau(h, \theta)$

ORIGINAL PAGE IS  
OF POOR QUALITY

Significant  
parameters:

$\alpha(h)$

$$\tau(h, \theta) = \exp \left[ -\sec \theta \int_h^{h_0} \alpha(z) dz \right] \quad (3)$$

where  $\alpha(h)$  is the attenuation coefficient of the atmosphere at height  $h$ .

The power received from the surface is given by

$\sigma^0; \tau(0, \theta)$

$$\overline{P_{\text{sur}}}(t) = \int \frac{P_t \lambda^2 G^2 \sigma^0 dA}{(4\pi)^3 r^4} \tau(0, \theta) \quad (4)$$

where the only new quantity is the differential scattering coefficient or scattering cross-section per unit area  $\sigma^0$ . These equations may be normalized to indicate the effect of pulse shape and beamwidth giving

$$\overline{P_{\text{ratm}}}(t) = \frac{P_{t0} \lambda^2 G_m^2}{(4\pi)^3} \int \frac{p_r(t-2r/c) g^2(\frac{1}{r}) \sigma_v(\frac{1}{r}) dV}{r^4} \tau(h, \theta) \quad (2a)$$

$$\overline{P_{\text{sur}}}(t) = \frac{P_{t0} \lambda^2 G_m^2}{(4\pi)^3} \int \frac{p_r(t-2r/c) g^2(\frac{1}{r}) \sigma^0(\frac{1}{r}) dV}{r^4} \tau(0, \theta) \quad (4a)$$

Here  $P_{t0}$  is the peak transmitter power,  $p_r(t)$  is the pulse shape,  $g$  is the antenna pattern with a maximum value of 1,  $\underline{l}_r$  is a unit vector in the direction from the radar to  $dV$ . Thus the radar must take advantage of the pulse shape and the antenna gain (as well as, perhaps, the Doppler frequency) to discriminate between the desired signal for a rainfall measurement  $\sigma_v$  and the undesired background  $\sigma^0$ .

The radiometer measures antenna temperature  $T_a$  which is given in general terms by

$\epsilon(\theta, T_s); \tau(0, \theta)$

$$T_a = \epsilon(\theta, T_s) T_s \tau(0, \theta) + T_{sc}(\theta) \tau(0, \theta) + T_{up}(\theta) \quad (5)$$

Significant parameters: Here  $\epsilon$  is the emissivity of the surface in the direction  $\theta$  relative to vertical,  $T_s$  is the physical temperature of the surface,  $T_{sc}$  is the effective temperature of the surface due to scattered radiation from above, and  $T_{up}$  is the direct radiation from the atmosphere to the radiometer on the satellite.  $T_{sc}$  is given by

$$T_{sc}(\theta) = \frac{1}{4\pi} \int [T_{dn}(\underline{s}) \gamma_{ii}(\theta, \underline{s}) + T_{dn}(\underline{s}) \gamma_{ij}(\theta, \underline{s})] d\Omega_s \quad (6)$$

$\gamma_{ii}; \gamma_{ij}$

where the subscripts  $i, j$  refer to two polarizations.  $T_{dn}(\underline{s})$  is the downward radiation from the atmosphere in a direction indicated by  $\underline{s}$ .  $\gamma_{ij}(\theta, \underline{s})$  is the scattering coefficient relative to projected area for scattering in the direction  $\theta$  of radiation incident in the direction  $\underline{s}$ , and  $d\Omega_s$  is the differential solid angle in the direction of  $\underline{s}$ . In (6) we must define  $T_{dn}$ , the downward radiation. It is given by

$T_{atm}(h)$

$\alpha(h); T_{sky}$

$$T_{dn}(\theta_s) = \sec \theta_s \int_0^{h_a} T_{atm}(z) \alpha(z) \exp[-\sec \theta_s \int_0^z \alpha(h) dh] dz + T_{sky}(\underline{s}) \quad (7)$$

where all quantities except  $T_{sky}$  have been defined.  $T_{sky}$  is the effective microwave temperature of the sky in the direction  $\underline{s}$ . The last term in (5) is the upwelling radiation temperature which is given by

$T_{atm}(h); \alpha(h)$   
 $\tau(h, \theta)$

$$T_{up}(\theta) = \sec \theta \int_0^{h_a} T_{atm}(z) \alpha(z) \tau(z, \theta) dz \quad (8)$$

One can see from the above discussion that the relevant parameters for atmospheric measurement are more complicated to extract from the radiometer measurement than from the radar measurement; but use of multiple angles, polarizations and frequencies should make it possible to extract these. Indeed, various algorithms have been designed to do just this.

ORIGINAL  
OF FOUR QUANTITIES

The situation is more complicated even than indicated because the transmissivity  $\tau$  and its related quantity the loss  $L(h, \theta)$  may be broken down into pieces associated with the different kinds of attenuations in the atmosphere. That is,

$$L(h, \theta) = 1 - \tau(h, \theta) = L_r + L_i + L_c + L_g \quad (9)$$

where  $L_r$  is the loss due to rain,  $L_i$  is the loss due to ice particles,  $L_c$  is the loss due to cloud, and  $L_g$  is the loss due to molecular absorption in atmospheric gasses. The problem of separating these is important, both for the radiometer and the radar, where  $\sigma_v$  also contains terms due to rain, ice and cloud that need to be separated if one is to establish the rainfall rate.

PHENOMENA TO EXPLOIT OR OVERCOME

Table 1 is an extensive, but not necessarily complete, list of the atmosphere and background parameters that either can be used or must be overcome to measure rainfall with either the active (radar) system or the passive (radiometer) system, or the two together. Atmospheric parameters are listed first, some of which are associated with rain and therefore desirable, and some of which are associated with ice and cloud and therefore undesirable. Background parameters associated with the surface are listed next.

The usual method for measuring precipitation by radar is to measure the volume scattering cross-section  $\sigma_v$  and relate it to the parameter  $Z$  by some empirical relationship of the form

$$R = k_R Z^{a_r} \quad (10)$$

## ORIGINAL MANUSCRIPT OF POOR QUALITY

These empirical relationships have, of course, been derived on the assumption of various drop-size distributions and on the basis of measurements.

One can also relate the rain rate to the loss in the rain by an empirical relation

$$R = f_R(L_R) \quad (11)$$

The steps required to obtain such a relationship are much more complex than those associated with (10) because of the complexities indicated in (5) through (8). Furthermore a model of the variation of mass per unit volume of liquid water, of drop size, and of temperature must be obtained for the atmosphere as a function of height before one can obtain a relation like that of (11). Note that while (10) may be used only with radar, (11) may be used with both radar and radiometer for rain rate determination if suitable models are available.

One way to distinguish between the rain backscatter and the ground is by the frequency variation of the rain backscatter, which is given by

$$\sigma_{vr} = S_r(\lambda)/\lambda^4 \quad (12)$$

The function  $S_r(\lambda)$  is a constant for wavelength longer than some critical value:

$$S_r(\lambda) = \text{constant} \quad \lambda > \lambda_c \quad (13)$$

where the critical value is associated with the distinction between the Mie and Rayleigh scattering regions for the drop sizes encountered in the rain.

ORIGINAL DRAFT IS  
OF POOR QUALITY

Excess temperature  $T_{ex}$  is defined as the difference between the temperature observed by the radiometer and the temperature that would be observed if the atmosphere did not attenuate and emit. Thus,  $T_{ex}$  is the contribution to the radiometer measured temperature due to the atmosphere. It may be empirically related to the loss in the atmosphere:

$$L_r = W(T_{ex}) \quad (14)$$

and through that loss to the rain rate by use of (11).

If the Doppler frequency shift can be measured for the rain, it can give information about the wind shear and terminal velocity of the raindrops. In fact, if one could measure the individual Doppler speeds of the falling raindrops in the absence of wind one could determine the drop size distribution! The Doppler frequency is, of course, given by

$$f_D = \frac{2u}{\lambda} \quad (15)$$

Information must also be available about the volume scatter and attenuation by ice particles in cloud and some means must be devised for separating these effects out if either volume scatter or attenuation or a combination is to be used for determining rain rate.

All of the background parameters must be considered as possible ways to discriminate against the surface background scatter or emission. The subject of variations of the scattering coefficient  $\sigma^0$  and the emissivity  $\epsilon$  is beyond the scope of this paper, but it is significant to note in connection with some of the proposed systems that neither varies rapidly with frequency, but both vary significantly with ocean wind speed.

BASIC MEASUREMENT PROBLEMS

There are two basic measurement problems associated with use of combined radar/radiometer systems for a rain rate determination, as illustrated in Table 2. The most important physical problem is that of distinguishing the rain effect from the backgrounds such as surface, cloud, and the bright band effect associated with water-covered ice particles. Research problems, however, exist to determine many of the relationships associated with Table 1 that are at present poorly defined.

INSTRUMENTS TO CONSIDER

Because a radar can be modulated in various ways and the modulation used to set range resolution; and because a radar, if it uses coherent detection, can measure Doppler frequencies, several kinds of radar systems need to be considered. Only a single radiometer system exists (although with many variations). The active systems include those listed in Table 3.

With the different systems of Table 3 or with the radiometer, many parameters may be varied. Somewhat more parameters are available for variation with the radar than with the radiometer because of its modulation and speed-measurement capability. Table 4 lists some of these parameters. Each of the parameter variations possible has implications for the capability of the systems to determine rain rate over a wide area. The last item on the list, the phase between polarizations, is listed with a question mark. Some researchers have indicated that measuring the relative phase of backscatter in different polarizations can give significant information whereas others feel that such measurements do not give any useful information. Thus this is a questionable parameter for measurement but could be important.



### POSTULATED OCEAN SYSTEMS

This section deals with a few sample systems involving both radar and radiometer postulated for use over the ocean. The reason for separating these from the possible land and sea systems indicated in the next section is that the background from the ocean, both for the radar and the radiometer, is considerably weaker than it is over land, and more is known about its variations. Thus, systems that would work over the ocean might not work over land because of difficulty in discriminating against the background. Three possible systems are postulated here. Others could, of course, be conceived, but these are illustrative.

Table 5 lists possible ocean system 1, using a radiometer-scatterometer system at a single frequency in X- or Ku-band. The scatterometer is designed to look in two directions, 90° apart, at each element on the surface because the average scattering coefficient for two such orthogonal looks is related to wind speed but only slightly related to wind direction. Thus one may use the scatterometer for determining wind speed which can then be used for correcting the radiometer measurement.

The principle of operation is outlined in detail in the table. Note that the excess temperature used to determine the estimate of loss is based on the difference between the antenna temperature  $T_a$  and the brightness temperature of the surface  $T_B$  which itself includes both the emission and scattering effects on the surface. Since the brightness temperature of the surface is proportional to wind speed, one must start off with an assumed wind speed for this to come up with a first estimate of the loss. Fortunately the attenuation effects in the atmosphere cause much larger variations in antenna temperature than the variations due to wind speed so that  $\hat{L}$  is

ORIGINAL PAGE IS  
OF POOR QUALITY

a reasonable estimate even with an assumed wind speed. Unfortunately,  $T_B$  is also strongly dependent upon surface temperature, and one must obtain the surface temperature from some other measurement or at least from climatological data.

The scatterometer measures the power returned, which is corrected by using  $\hat{L}$  to obtain an estimate of the mean scattering coefficient for the two directions. The wind speed may then be estimated from this measurement and this improved estimate of wind speed used to improve the assumed brightness temperature of the surface so that the  $\hat{T}_{ex}$  is a better value than the first estimate. This better value may then be used to estimate the loss with more precision and the liquid water content estimated from the loss. In turn, the rain rate may be estimated from the liquid water content. Thus this system is one that uses the radiometer to determine the rain rate but corrects the radiometer estimate of  $T_{ex}$  by use of the scatterometer.

Table 6 lists another possible ocean system using a dual-frequency scatterometer and a three-frequency radiometer. One would not need as many radiometer frequencies as indicated, but they are all desirable because each band is relevant to a different range of rain rate. The dual-frequency scatterometer uses the C-band portion to estimate the wind speed because the C-band signal is affected only to a very limited extent by attenuation in the atmosphere. However, the estimate can be improved by use of the X-band radiometer to estimate the loss at C-band. The wind speed determined from the C-band scatterometer can then be used to estimate both  $\sigma^0$  and  $T_B$  at the other frequencies used by the scatterometer and radiometer. One then proceeds to estimate the loss at both the scatterometer frequency and radiometer frequency by use of the excess temperature measured. The received

power for the higher-frequency scatterometer is then corrected by using this loss estimate, and an excess estimated  $\sigma^0$  is determined by the difference between the corrected value for the measured  $\sigma^0$  and that predicted by use of the C-band data. This excess is then assumed to be not truly due to  $\sigma^0$  but rather due to  $\sigma_v$ . With a suitable atmospheric model one can then estimate Z from  $\sigma_{ex}^0$  and from that estimate the rain rate. One can also estimate the rain rate from the losses at the various frequencies determined by the radiometer so that two independent estimates of rain rate, based on somewhat different uses of the atmospheric model, are obtained. The estimates may then be compared and the best estimate established. Further study is needed to determine how best to perform this last step.

Table 7 lists a third possible ocean system involving a radar having modulation to determine the location of the rain, but only modest resolution, and a step-frequency radiometer that can use the frequency variation of the antenna temperature to distinguish the contribution due to the atmosphere from the contribution from the surface that varies slowly with frequency (see paper by Harrington in this workshop).

In this case the radar determines the height of the precipitation, with an accuracy of 1 or 2 km, and the  $\sigma_v$  at that height. By knowing the height of the precipitation one can improve the model used to estimate the losses. The step-frequency radiometer is then used to estimate the loss. The value of Z at the height of the radar measurement is determined from  $\sigma_v$  and the rain rate is estimated both from the loss determined by the radiometer and from the value of Z at the heights where discrimination against the ground is assured by range resolution. These estimates are then compared and the best estimate established.

Note that a system like this might work over the land but it is much more certain to work over the sea because of the better discrimination against background by the radiometer. The radar part would work over the land by itself.

#### POSTULATED LAND - SEA SYSTEMS

Because of the stronger backscatter and emission from the land and because their variation is greater and not readily tied to a parameter such as wind speed, a land - sea system has more difficulty discriminating against the background than does a system that operates over the ocean alone. Two possible land-sea systems are postulated here.

Table 8 lists the possible land - sea system number 1. The instrument involves a fine-height-resolution radar operating at X- or Ku-band. Its capability for resolving rain would be in the range of 200 to 1200 m. A step-frequency radiometer is used along with this to help correct the radar and provide an independent estimate of the attenuation and consequently the rain rate.

The radar is the primary instrument in this system. It is used to measure an estimate of return power  $\hat{P}_r$  as a function of height. The step-frequency radiometer is then used to determine an estimate of attenuation  $\hat{L}$ . A single-frequency radiometer would not be satisfactory for this purpose over land because of the large brightness temperature of the land itself. However, a radiometer stepping across a narrow band can take advantage of the fact that the brightness temperature of the surface is less likely to vary rapidly with frequency than the contribution to the antenna temperature from the atmosphere. Thus it is the magnitude of the variation of  $T_a$  across the frequency band that is used to estimate  $\hat{L}$ .  $\hat{L}$  is used to correct  $\hat{P}_r$  so that a better estimate of  $\hat{\sigma}_v$  may be obtained. This is then converted into

an estimate of  $\hat{Z}$  as a function of height.

The rain rate  $R$  is then estimated from the profile of  $\hat{Z}$ . The rain rate may also be estimated from  $\hat{L}$ , but this estimate is likely to be poorer than that obtained from the radar measurement. The estimates are then compared and a best estimate established.

Table 9 illustrates possible land - sea system number 2. This system uses the step-frequency technique both with an unmodulated scatterometer and a radiometer. The systems can operate in X- or Ku-band, or perhaps both. The choice of frequencies for this system as for others is based on picking a frequency that is sensitive to the rain parameters and at the same time is low enough so that one can see from the satellite well into the rain, rather than having the signal highly attenuated in the upper part of the raining region.

In this system the loss is estimated by the step-frequency radiometer and used to correct the received power for the scatterometer. This corrected received power is used to determine an excess  $\sigma^0$ , which can be related to the backscatter from the precipitation by using it to estimate a value for  $\hat{Z}$ . The rain rate then may be estimated from  $\hat{Z}$ . The rain rate may also be estimated independently from  $\hat{L}$  and the two compared. The reason that the step-frequency scatterometer can be used for determining  $\hat{\sigma}_{ex}$  is the same as the reason the radiometer can be used for such a purpose. That is, the variation of scattering coefficient over the land or sea is relatively slow with frequency compared with the variation of scattering from rain.

Since one of the difficulties with such systems is distinguishing the amount of backscatter and attenuation associated with the "bright band region" so that it may be removed from the rain estimate, one might be able to use a cross-polarized receiver for the scatterometer and allow the cross-polarization

ratio to aid in estimating the bright-band contribution. The cross-polarized signal is very low compared with the like-polarized signal when the return is from nearly spherical small droplets; whereas in the bright band where the particles are not so uniformly shaped and are much larger, the cross-polarized signal is also much larger. If this is done, the estimate of the bright-band contribution to  $\hat{\sigma}_V$  is removed from  $\hat{\sigma}_V$  before estimating  $\hat{Z}$ .

### CONCLUSIONS

The combined use of a radar and a radiometer for measurement of precipitation offers some interesting possibilities. The most obvious application of the radiometer is to measure the attenuation experienced by the radar. If a multifrequency radiometer is used, one may be able to estimate a profile of the attenuation, although none of the systems proposed here call for this except ocean system 2. Otherwise, one must always assume a model for the vertical distribution of rainfall and other attenuating hydrometeors.

If it is possible to get the fine altitude resolution of land-sea system 1, this system probably has the most promise because it does allow measuring a profile of  $Z$  and therefore learning more about the nature of the rainstorm than would be learned with any of the systems that only determine an average over the entire height of the storm.

Before any of these systems could be implemented, one needs to conduct many more detailed studies of the performance of the systems with various model atmospheres. These detailed studies will also provide information on the relationships associated with Table 1 for which more research is needed. Many of these relationships are not very well defined at present, so a good deal of research is needed to provide accurate enough estimates

of the relationship so that the postulated systems could work.

More complex systems could also be postulated, involving large numbers of frequencies for both the radar and the radiometer, and also involving Doppler frequency measurements for the radar. These systems have not been discussed here because of time limitations. One should first investigate the simple systems before looking into the more complicated ones, anyway!

TABLE 1  
PHENOMENA TO EXPLOIT OR OVERCOME

<u>NAME OF PHENOMENON</u>	<u>SYMBOLIC FORM</u>	<u>ACTIVE</u>	<u>PASSIVE</u>
ATMOSPHERIC PARAMETERS			
RAIN RATE VS RAIN-VOLUME SCATTERING	$R$ VS $Z_R$	X	
RAIN RATE VS RAIN ATTENUATION	$R$ VS $L_R$	X	X
RAIN VOLUME SCATTER VS FREQUENCY	$\sigma_{VR}$ VS $F$	X	
RAIN ATTENUATION VS FREQUENCY	$L_R$ VS $F$	X	X
RAIN ATTENUATION VS ANGLE OF INCIDENCE	$L_R$ VS $\theta$	X	X
RAIN ATTENUATION VS EXCESS TEMPERATURE	$L_R$ VS $T_{EX}$		X
DOPPLER FREQUENCY SHIFT	$F_D$	X	
VOLUME SCATTER FROM ICE PARTICLES	$\sigma_{VI}$ VS $F$	X	
VOLUME SCATTER FROM CLOUD	$\sigma_{VC}$ VS $F, P$	X	
ATTENUATION BY ICE PARTICLES	$L_I$ VS $F, \theta$	X	X
ATTENUATION BY CLOUD	$L_C$ VS $F, \theta$	X	X



TABLE 1 (CONTINUED)  
PHENOMENA TO EXPLOIT OR OVERCOME

<u>NAME OF PHENOMENON</u>	<u>SYMBOLIC FORM</u>	<u>ACTIVE</u>	<u>PASSIVE</u>
BACKGROUND PARAMETERS			
SCATTERING COEFFICIENT VS FREQUENCY	$\sigma^0$ VS F	X	
SCATTERING COEFFICIENT VS ANGLE OF INCIDENCE	$\sigma^0$ VS $\theta$	X	
SCATTERING COEFFICIENT VS AZIMUTH ANGLE	$\sigma^0$ VS $\phi$	X	
SCATTERING COEFFICIENT VS POLARIZATION	$\sigma^0$ VS P	X	
SCATTERING COEFFICIENT VS OCEAN WIND SPEED	$\sigma^0$ VS U	X	
EMISSIVITY VS FREQUENCY	$\epsilon$ VS F		X
EMISSIVITY VS ANGLE OF INCIDENCE	$\epsilon$ VS $\theta$		X
EMISSIVITY VS SURFACE TEMPERATURE	$\epsilon$ VS $T_s$		X
EMISSIVITY VS OCEAN WIND SPEED	$\epsilon$ VS U		X
EMISSIVITY VS POLARIZATION	$\epsilon$ VS P		X

TABLE 2  
BASIC MEASUREMENT PROBLEMS

DISTINGUISHING RAIN EFFECT FROM BACKGROUNDS:

SURFACE EFFECTS

CLOUD EFFECTS

BRIGHT-BAND EFFECTS

DETERMINATION OF POORLY-DEFINED RELATIONS IN TABLE 1

TABLE 3  
ACTIVE SYSTEMS -- BASIC TYPES

- UNMODULATED SCATTEROMETER WITH NONCOHERENT DETECTION
- RANGING SCATTEROMETER WITH NONCOHERENT DETECTOR
- UNMODULATED DOPPLER SCATTEROMETER (COHERENT DETECTOR)
- RANGE-DOPPLER SCATTEROMETER (MODULATED WITH COHERENT  
DETECTOR)

TABLE 4  
ACTIVE AND PASSIVE SYSTEMS:  
PARAMETERS TO VARY OR DUPLICATE

	<u>ACTIVE</u>	<u>PASSIVE</u>
FREQUENCY	X	X
POLARIZATION	X	X
ANGLE OF INCIDENCE	X	X
AZIMUTH ANGLE	X	X
ANGULAR RESOLUTION	X	X
RANGE RESOLUTION	X	
SPEED RESOLUTION	X	
BISTATIC ANGLE	X	
INTEGRATION TIME	X	X
BANDWIDTH	X	X
SCAN PATTERN	X	X
PHASE BETWEEN POLARIZATIONS (?)	X	

TABLE 5  
POSSIBLE OCEAN SYSTEM 1

INSTRUMENT: RADOMETER - SCATTEROMETER (2 ORTHOGONAL LOOKS)

FREQUENCY: X- OR KU-BAND

PRINCIPLE:

RAD GETS  $\hat{L}$  FOR ASSUMED U FROM  $\hat{T}_{EX} = T_A - \hat{T}_B(u)$

SCAT MEASURES  $\hat{P}_R$  FOR 2 LOOKS

$\hat{\sigma}^c$  CORRECTED TO  $\hat{\sigma}^c$  BY USING L

$\hat{U}$  ESTIMATED FROM  $\hat{\sigma}^c$

$T_B(\hat{U})$  USED TO GET  $\hat{T}_{EX}$

$\hat{T}_{EX}$  USED TO ESTIMATE  $\hat{L}$

LIQUID WATER ESTIMATED FROM  $\hat{L}$

R ESTIMATED FROM LIQUID WATER

(REQUIRES MODEL OF HEIGHT OF PRECIPITATION LAYER)

TABLE 6  
POSSIBLE OCEAN SYSTEM 2

INSTRUMENT: DUAL-FREQUENCY SCATTEROMETER (C-BAND AND X- OR KU-BAND) + 3-FREQUENCY RADIOMETER (X-BAND, KU-BAND, KA-BAND)

PRINCIPLE:

X-BAND RAD ESTIMATES  $L$  AT C-BAND

CORRECTED C-BAND  $\hat{\sigma}^c$  USED TO ESTIMATE  $\hat{U}$

$\hat{U}$  USED TO ESTIMATE

1) X- OR KU-BAND  $\sigma^c$

2) X-, KU-, KA-BAND  $\hat{T}_B$

$T_A$  AND  $\hat{T}_B$  USED TO ESTIMATE  $\hat{T}_{EX}$  AT X-, KU-, KA-BANDS

$\hat{T}_{EX}$  USED TO ESTIMATE  $\hat{L}$  AT X/KU-BAND SCAT FREQUENCY

$\hat{P}_R$  FOR X/KU-BAND SCAT CORRECTED BY  $\hat{L}$

$\hat{\sigma}_{EX}^e = \sigma^c_{CORRECTED} - \sigma^c_{PREDICTED}$  FOR X/KU-BAND SCAT

$\hat{Z}$  ESTIMATED FROM  $\hat{\sigma}_{EX}^e$

$R$  ESTIMATED FROM  $\hat{Z}$

$R$  ESTIMATED FROM  $\hat{L}(X)$ ,  $\hat{L}(KU)$ , AND/OR  $\hat{L}(KA)$

$R$  ESTIMATES COMPARED AND BEST ESTIMATE ESTABLISHED

TABLE 7  
POSSIBLE OCEAN SYSTEM 3

INSTRUMENT: MODEST HEIGHT-RESOLUTION RADAR (X- OR KU-BAND)  
+ STEP-FREQUENCY RADIOMETER (X- OR KU-BAND)

PRINCIPLE:

RADAR DETERMINES HEIGHT OF PRECIPITATION  
(ACCURACY 1-2 KM) AND  $\sigma_v$  AT THAT HEIGHT

STEP-FREQUENCY RADIOMETER USED TO ESTIMATE  $\hat{L}$

$\hat{Z}$  ESTIMATED FROM  $\sigma_v$

R ESTIMATED FROM  $\hat{L}$

R ESTIMATED FROM  $\hat{Z}$  AT HEIGHTS WHERE  $\sigma^c$  DOES NOT CONTRIBUTE

R ESTIMATES COMPARED AND BEST ESTIMATE ESTABLISHED

NOTE: THIS SYSTEM MIGHT WORK OVER LAND, BUT IT IS MORE  
CERTAIN OVER SEA.

TABLE 8  
POSSIBLE LAND-SEA SYSTEM 1

INSTRUMENT: FINE HEIGHT RESOLUTION RADAR (X OR KU-BAND)  
(RESOLUTION IN HEIGHT 200-1200 M)  
+ STEP-FREQUENCY RADIOMETER (X OR KU-BAND)

PRINCIPLE:

RADAR MEASURES  $\hat{P}_R$  VS H

RADIOMETER DETERMINES  $\hat{L}$

$\hat{P}_R$  CORRECTED BY  $\hat{L}$  TO DETERMINE  $\hat{\sigma}_V$

$\hat{Z}$  ESTIMATED FROM  $\hat{\sigma}_V$

R ESTIMATED FROM  $\hat{Z}$  PROFILE

R ESTIMATED FROM  $\hat{L}$

R ESTIMATES COMPARED AND BEST ESTIMATE ESTABLISHED

TABLE 9  
POSSIBLE LAND-SEA SYSTEM 2

INSTRUMENT: STEP-FREQUENCY UNMODULATED SCATTEROMETER + STEP-FREQUENCY RADIOMETER

FREQUENCY: X OR KU-BAND

PRINCIPLE:

$\hat{L}$  ESTIMATED BY RADIOMETER

$\hat{P}_R$  FOR SCAT CORRECTED BY  $\hat{L}$

$\hat{\sigma}_{EX}^c$  DETERMINED FOR SCAT USING  $\hat{P}_R$  (CORRECTED)

$\hat{Z}$  ESTIMATED FROM  $\hat{\sigma}_{EX}^c$

R ESTIMATED FROM  $\hat{Z}$

R ESTIMATED FROM  $\hat{L}$

R ESTIMATES COMPARED AND BEST ESTIMATE ESTABLISHED

POSSIBLE VARIATION:

USE CROSS-POLARIZATION RATIO TO DETERMINE "BRIGHT-BAND" CONTRIBUTION TO  $\hat{\sigma}_{EX}^c$ .

SUBTRACT THIS BEFORE ESTIMATING  $\hat{Z}$



D44  
N83 25313

ORIGINAL PAGE IS  
OF POOR QUALITY

USE OF THE OPTIMAL POLARIZATION CONCEPT IN ELECTROMAGNETIC  
IMAGING OF HYDROMETEOR DISTRIBUTIONS

Wolfgang-M. Boerner

Communications Laboratory, Information Engineering Department  
University of Illinois at Chicago Circle  
SEU 1104, P.O. Box 4348, Chicago IL 60680

ABSTRACT

This paper presents a brief revisit of some fundamental physical concepts of optimal polarization characteristics of a transmission path or scatterer ensemble of hydrometeors. It will be shown that based upon this optimal polarization concept we are certain to expect further definite advances in remote atmospheric sensing. Here our main objective is to clearly identify the basic properties of Kennaugh's optimal polarization theory.

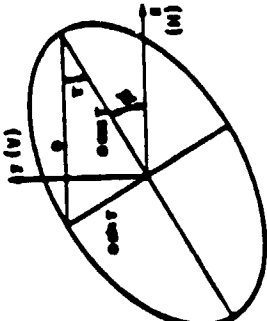
1. Introduction

In recent years radar meteorology has undergone a dramatic phase of change using doppler weather radars and a national network of such advanced remote sensing systems is imminent [1]. The doppler radars have several advantages above the currently used incoherent radars, which are invaluable in locating storms, determining their sizes, and heights. Coherent doppler radars provide additional information and the mean velocity vector and its dispersion as well as improved sensitivity in more precise forecasting of storms and particularly tornadoes. Although the coherent doppler radars will provide another absolutely required remote sensing feature, they do not present a cure-all of the ultimately most complete atmospheric radar remote sensing system. In fact, all recent partial advancements made with experimental dual polarization radar systems [2, 3, 4, 5] indicate that an integrated doppler radar system, with adaptive dual polarization facility will represent the ultimate remote sensing system in radar meteorology of clear air turbulence and/or hydrometeors. Thus, we are now in the design and development phase of a more complete polarization doppler radar system which most likely will replace or at least complement doppler and incoherent weather radars in the next five to ten years.

Thus, it is the objective to introduce basic polarization descriptors useful for the complete description of interfaces between various regions of different hydrometeor states within a cloud, storm or tornado, as well as for the imaging of these entities.

2. Polarization Descriptors

In this brief introduction to optimal polarization descriptors, we will schematically introduce basic definitions (Table 1), describing the polarization ellipse in time and frequency domain (Fig. 1) and its relationship with the Poincaré sphere.

Table 1: Polarization Descriptors	
Parameter	Definition
<p>a. Radar Cross Section</p> <p>i) no polarization corrections</p> <p>ii) with polarization corrections</p>	$\sigma = \lim_{R \rightarrow \infty} 4\pi R^2 \frac{ E ^2}{ E_0 ^2} = \lim_{R \rightarrow \infty} 4\pi R^2 \frac{ M ^2}{ N ^2} \quad (1)$ $\sigma = \lim_{R \rightarrow \infty} 4\pi R^2 \frac{ h^r \cdot \hat{e} ^2}{ h^i ^2} \quad (2)$
<p>b. The Polarization Vector</p> <p>i) time domain</p> <p>ii) frequency domain</p> <p>iii) geometric parameter</p> <p>iv) Polarization ratio</p>	$h(t) = a_M \cos \omega t \hat{h}_M + a_Y \cos (\omega t + \delta) \hat{h}_Y$ <p>where <math>\delta = \phi_Y - \phi_M</math></p> $h(t) = a_M e^{j\omega t} \hat{h}_M + a_Y e^{j(\omega t + \delta)} \hat{h}_Y$ $\underline{h} = a_M \hat{h}_M + a_Y e^{j\delta} \hat{h}_Y$ $\underline{h} = a \begin{pmatrix} \cos \delta \cos \phi \sin i \\ \sin \delta \cos \phi \sin i \\ 0 \end{pmatrix} e^{j\omega t}$ $\underline{h} = a_M e^{j\delta} M(\hat{h}_M + \hat{h}_Y), \text{ where } \rho = \frac{a_Y}{a_M} e^{j\delta} \quad (6)$
<p>c. The Polarization Ellipse</p>	 <p>Fig. 1</p> $\left(\frac{h_M}{a_M}\right)^2 + \left(\frac{h_Y}{a_Y}\right)^2 - 2\left(\frac{h_M}{a_M}\right)\left(\frac{h_Y}{a_Y}\right) \cos \delta = \sin^2 \delta \quad (7)$ <p>Linear: <math>\delta = 0</math>, horizontal (<math>a_Y = 0</math>), vertical (<math>a_M = 0</math>), linear 45° (<math>a_M = a_Y</math>)          Left circular (LC): <math>\delta = 90^\circ, a_M = a_Y</math>          Right circular (RC): <math>\delta = -90^\circ, a_M = a_Y</math>          Left elliptic: <math>\sin \delta &gt; 0</math>          Right elliptic: <math>\sin \delta &lt; 0</math></p>
<p>d. The Stokes Vectors</p>	$\underline{S} = \begin{pmatrix} S_0 \\ S_1 \\ S_2 \\ S_3 \end{pmatrix} = \begin{pmatrix}  h_M ^2 +  h_Y ^2 \\  h_M ^2 -  h_Y ^2 \\ 2\text{Re}(h_M h_Y^*) \\ -2\text{Im}(h_M h_Y^*) \end{pmatrix} = \begin{pmatrix} a_M^2 + a_Y^2 \\ a_M^2 \cos 2\cos 2\phi \\ 2a_M a_Y \cos \delta \\ 2a_M a_Y \sin \delta \end{pmatrix} = \begin{pmatrix} a^2 \\ a^2 \cos 2\cos 2\phi \\ a^2 \cos 2\sin 2\phi \\ a^2 \sin 2\phi \end{pmatrix} \quad (8)$ <p>where</p> $S_0^2 = S_1^2 + S_2^2 + S_3^2 = I^2 = Q^2 + U^2 + V^2$ $M: \underline{g} = \begin{pmatrix} 1 \\ 0 \\ 0 \end{pmatrix} \cdot \underline{v} \quad \underline{g} = \begin{pmatrix} 1 \\ 0 \\ 0 \end{pmatrix} \cdot \text{LC: } \underline{g} = \begin{pmatrix} 0 \\ 0 \\ 1 \end{pmatrix} \cdot \text{RC: } \underline{g} = \begin{pmatrix} 0 \\ 1 \\ 0 \end{pmatrix}$
<p>e. The Polarization Ratio</p>	<p>Modified Stokes Vector <math>\underline{S}_M = (I(1 + \rho), I(1 - \rho), U, V)</math></p> $\rho = \frac{V}{h_M} = \left(\frac{a_Y}{a_M}\right) e^{j\delta} \quad (9)$ <p>Linear: <math>\text{Im}(\rho) = 0, M: \rho = 0, V: \rho = \pm 1</math>          Circular: <math> \rho  = 1, \text{LC: } \rho = j, \text{RC: } \rho = -j</math>          Elliptic: left elliptic: <math>\text{Im}(\rho) &gt; 0</math>, right elliptic: <math>\text{Im}(\rho) &lt; 0</math></p>
<p>f. The Poincaré Sphere</p>	<p>i) Cartesian coordinates = (<math>\theta_1, \theta_2, \theta_3</math>)          ii) Spherical = (<math>\theta, \phi, \chi</math>)          iii) In terms of Polarization ratio</p> $\underline{u} = \frac{1 -  \rho ^2}{1 +  \rho ^2} \hat{e}_1 + \frac{2\text{Re}(\rho)}{1 +  \rho ^2} \hat{e}_2 + \frac{2\text{Im}(\rho)}{1 +  \rho ^2} \hat{e}_3 \quad (10)$

### 3. Scattering Matrices: $[S]$ , $[M]$ , $[P]$

There exist three matrices of specific value to the description of hydro-meteor ensembles in the coherent and the incoherent cases which are defined here and the interactions are derived.

#### 3.1 The Scattering Matrix $[S]$

The  $2 \times 2$  complex scattering matrix  $[S]$  is relating the polarization vector of the scattered field  $\underline{h}^s$  to the corresponding one of the incident field  $\underline{h}^i$  through the relation:

$$\underline{h}^s = [S] \underline{h}^i \quad (11)$$

Different representations for  $[S]$  with absolute and relative phase in the bistatic and monostatic cases are summarized as follows: in the bistatic case, the scattering matrix with absolute phase is defined by:

$$[S]_{SMA} = \begin{pmatrix} S_{AA} & S_{AB} \\ S_{BA} & S_{BB} \end{pmatrix} = \begin{pmatrix} |S_{AA}| e^{j\phi_{AA}} & |S_{AB}| e^{j\phi_{AB}} \\ |S_{BA}| e^{j\phi_{BA}} & |S_{BB}| e^{j\phi_{BB}} \end{pmatrix} \quad (12)$$

$$= \begin{pmatrix} |S_{AA}| e^{j(\phi_{AA} - \phi_{AB})} & |S_{AB}| \\ |S_{BA}| e^{j(\phi_{BA} - \phi_{AB})} & |S_{BB}| e^{j(\phi_{BB} - \phi_{AB})} \end{pmatrix} e^{j\phi_{AB}}$$

$$= e^{j\phi_{AB}} [S]_{SMR} \quad (13)$$

where  $\phi_{AB}$  is the absolute phase,  $[S]_{SMR}$  is the target scattering matrix with relative phase and it can be written in the bistatic case as:

$$[S]_{SMR} = \begin{pmatrix} |S_{AA}| e^{j(\phi_{AA} - \phi_{AB})} & |S_{AB}| \\ |S_{BA}| e^{j(\phi_{BA} - \phi_{AB})} & |S_{BB}| e^{j(\phi_{BB} - \phi_{AB})} \end{pmatrix} \quad (14)$$

Eqs. (12), (14) satisfy the reciprocity condition  $S_{AB} = S_{BA}$  ( $|S_{AB}| = |S_{BA}|$ ,  $\phi_{AB} = \phi_{BA}$ ) in the monostatic case. In this paper, we are considering the monostatic case only.

#### 3.2 The Mueller Matrices

The Mueller (Stokes reflection) matrix  $[M]$ , the modified Mueller matrix  $[M']$  are presented in this section. The reconstruction of these matrices from the scattering matrix elements is given in Table 2.

The  $4 \times 4$  real Mueller matrix  $[M]$  relates the scattered Stokes vector  $\underline{q}^s$  to the corresponding incident vector  $\underline{q}^i$  with the following relationship:

$$\underline{q}^s = [M] \underline{q}^i \quad (15)$$

where the Stokes vector is defined in Table 1. A similar relationship relating the modified scattered and incident Stokes vectors is given by:

$$\underline{q}_m^s = [M_m] \underline{q}_m^i \quad (16)$$

The relationship between [M] and [M<sub>m</sub>] is given by [6]:

$$[M_m] = [R][M][R^{-1}] \quad (17)$$

and

$$[M] = [R^{-1}][M_m][R] \quad (18)$$

where the constant matrix  $[R] = \begin{pmatrix} \frac{1}{2} & \frac{1}{2} & 0 & 0 \\ \frac{1}{2} & -\frac{1}{2} & 0 & 0 \\ 0 & 0 & 1 & 0 \\ 0 & 0 & 0 & 1 \end{pmatrix}$

The Mueller matrices are 4 x 4 real and asymmetric. The symmetric Mueller matrix [M] can be deduced as follows:

The received power [7], [8 #9] is

$$P_r = \frac{1}{2} [g_0^s g_0^r + g_1^s g_1^r + g_2^s g_2^r - g_3^s g_3^r] = [Q] \underline{q}^s \cdot \underline{q}^r, \quad (19)$$

where  $\underline{q}^s$ ,  $\underline{q}^r$  are the scattered wave and receiving antenna Stokes vectors respectively and [Q] is a constant matrix and is given by:

$$[Q] = \frac{1}{2} \begin{pmatrix} 1 & 0 & 0 & 0 \\ 0 & 1 & 0 & 0 \\ 0 & 0 & 1 & 0 \\ 0 & 0 & 0 & -1 \end{pmatrix}$$

substituting (16) into (19), then

$$P_r = [Q][M] \underline{q}^i \cdot \underline{q}^r = [M_s] \underline{q}^i \cdot \underline{q}^r \quad (20)$$

where  $[M_s] = [Q][M]$  is a symmetric Mueller matrix.

### 3.3 Graves Power Scattering Matrix [P] and its Associated [P<sub>H</sub>] and [P<sub>V</sub>]

The total backscattered power from a target is given by [9]

$$P_b = \underline{h}^{s*} \cdot \underline{h}^s = (\underline{h}^{s*})^T \underline{h}^s \quad (21)$$

where  $\underline{h}^s$  is the backscattered polarization vector. Substituting (11) into (21):

$$P_b = (\underline{h}^i)^T [S^T]^* [S] \underline{h}^i = (\underline{h}^i)^T [P] \underline{h}^i \quad (22)$$

where the matrix [P] is known as Graves power scattering matrix and it is given by:

$$[P] = [S^T]^* [S] = \begin{pmatrix} a & c \\ c^* & b \end{pmatrix} \quad (23)$$

where a, b are real and c is complex. The reconstruction of the elements of [P] in terms of the elements of the scattering matrix [S] is given in Table 2 [10].

The matrix [P] can be decomposed into two measurable matrices [P<sub>H</sub>] and [P<sub>V</sub>] where [P] = [P<sub>H</sub>] + [P<sub>V</sub>] (24)

The elements of [P<sub>H</sub>] and [P<sub>V</sub>] in terms of the elements of [S] are also shown in Table 2 [10].

Table 2: Reconstruction of [M], [M<sub>m</sub>], [P], [P<sub>H</sub>], [P<sub>V</sub>] and Optimal Polarization from [S]

[M] [6]	[M <sub>m</sub> ] [6]
$m_{11} = \frac{1}{2}( S_{AA} ^2 + 2 S_{AB} ^2 +  S_{BB} ^2)$	$M_{11} =  S_{AA} ^2$
$m_{12} = m_{21} = \frac{1}{2}( S_{AA} ^2 -  S_{BB} ^2)$	$M_{12} =  S_{AB} ^2 - M_{21}$
$m_{13} = m_{31} = \text{Re}(S_{AA}S_{AB}^* + S_{AB}S_{BB}^*)$	$M_{13} = \text{Re}(S_{AA}S_{AB}^*) = \frac{1}{2}M_{31}$
$m_{14} = -m_{41} = \text{Im}(S_{AA}S_{AB}^* + S_{AB}S_{BB}^*)$	$M_{14} = \text{Im}(S_{AA}S_{AB}^*) = -\frac{1}{2}M_{41}$
$m_{22} = \frac{1}{2}( S_{AA} ^2 - 2 S_{AB} ^2 +  S_{BB} ^2)$	$M_{22} =  S_{BB} ^2$
$m_{23} = m_{32} = \text{Re}(S_{AA}S_{AB}^* - S_{AB}S_{BB}^*)$	$M_{23} = \text{Re}(S_{AB}S_{BB}^*) = \frac{1}{2}M_{32}$
$m_{24} = -m_{42} = \text{Im}(S_{AA}S_{AB}^* - S_{AB}S_{BB}^*)$	$M_{24} = \text{Im}(S_{AB}S_{BB}^*) = -\frac{1}{2}M_{42}$
$m_{33} = \text{Re}(S_{AA}S_{BB}^*) +  S_{AB} ^2$	$M_{33} = \text{Re}(S_{AA}S_{BB}^*) +  S_{AB} ^2$
$m_{34} = -m_{43} = \text{Im}(S_{AA}S_{BB}^*)$	$M_{34} = \text{Im}(S_{AA}S_{BB}^*) = -M_{43}$
$m_{44} = m_{33} + m_{22} - m_{11}$	$M_{44} = M_{33} - 2M_{12}$
[P] = [P <sub>H</sub> ] + [P <sub>V</sub> ] [10]	CO-POL & X-POL Nulls [6,11]
$[P] = \begin{pmatrix} a & c \\ c^* & b \end{pmatrix}, \quad \begin{aligned} a &=  S_{HH} ^2 +  S_{HV} ^2 \\ b &=  S_{HV} ^2 +  S_{VV} ^2 \\ c &= S_{HH}^*S_{HV} + S_{HV}^*S_{VV} \end{aligned}$	<p>COLATITUDE: <math>\theta = \cos^{-1} \left\{ \frac{ u ^2 - 1}{ u ^2 + 1} \right\}</math></p> <p>LONGITUDE: <math>\phi = -\tan^{-1} \left\{ \frac{\text{Im}(u)}{\text{Re}(u)} \right\}</math></p> <p>where: <math>u = \frac{1 - j\alpha}{1 + j\alpha}</math></p> <p>and <math>\alpha = \frac{-B \pm \sqrt{B^2 - 4AC}}{2A}</math></p> <p><u>CO-POL Nulls</u></p> <p>A = S<sub>BB</sub></p> <p>B = 2S<sub>AB</sub>, C = S<sub>AA</sub></p> <p><u>X-POL Nulls</u></p> <p>A = S<sub>BB</sub>S<sub>AB}^* + S<sub>AA}^*S<sub>AB} = -C^*</sub></sub></sub></p> <p>B =  S<sub>AA} ^2 -  S<sub>BB} ^2</sub></sub></p>
$[P_H] = \begin{pmatrix} a_H & c_H \\ c_H^* & b_H \end{pmatrix}, \quad \begin{aligned} a_H &=  S_{HH} ^2 \\ b_H &=  S_{HV} ^2 \\ c_H &= S_{HH}^*S_{HV} \end{aligned}$	
$[P_V] = \begin{pmatrix} a_V & c_V \\ c_V^* & b_V \end{pmatrix}, \quad \begin{aligned} a_V &=  S_{HV} ^2 \\ b_V &=  S_{VV} ^2 \\ c_V &= S_{HV}^*S_{VV} \end{aligned}$	

#### 4. The Concept of Optimal Polarization Pairs

It was first shown by Kennaugh (1952) that there exist two pairs of optimal polarizations which can be useful in describing target properties at one aspect and at one frequency. The concept is based on invariance of polarization state transformation under consideration of reciprocity as we will introduce next.

##### 4.1 Polarization State Transformation

In the following we shall limit ourselves exclusively to the monostatic case ( $\theta = \theta_i, \phi_s = \phi_i$ ) and we may define the "normalized monostatic scattering matrix  $S$  with relative phase" in terms of two arbitrary elliptical but orthogonal polarization base vectors  $\hat{h}_A$  and  $\hat{h}_B$  so that with  $\underline{h} = \hat{h}_A \hat{h}_A + \hat{h}_B \hat{h}_B$

$$\underline{h}^S = [S] \underline{h}^S, [S] = \begin{bmatrix} S_{AA} & |S_{AB}| \\ |S_{AB}| & S_{BB} \end{bmatrix} \quad \begin{aligned} S_{AB} &= S_{BA} \\ \phi_{AB} &= \phi_{BA} = 0 \end{aligned} \quad (25)$$

Thus, assuming reciprocity of the propagation path ( $S_{AB} = S_{BA}$ ) and conservation of energy, we require five real or seven positive real quantities to determine  $[S]$  completely [8 #1, #4]. However, we note that in case  $S_{AB} \neq S_{BA}$  i.e., reciprocity of the propagation paths is violated, the definition of (25) cannot be used [12] as may be encountered for a propagation path within a highly ionized cloud containing various dense liquid and solid ice states of hydrometeors [13].

Assuming reciprocity holds, there exists an infinite number of general pairs of orthogonal elliptical polarization base vectors  $\hat{h}_A, \hat{h}_B$  and an infinite number of possible invariant transformations [8 #12]. Numerically, the transformation properties of  $S(A,B)$  assuming no polarization losses from any one orthogonal polarization pair  $\underline{h} = \hat{h}_A \hat{h}_A + \hat{h}_B \hat{h}_B$  to another orthogonal pair  $\underline{h}' = \hat{h}'_A \hat{h}'_A + \hat{h}'_B \hat{h}'_B$  can be expressed in terms of a single complex transformation parameter  $\rho$  and its complex conjugate  $\rho^*$  so that

$$[S'(A', B')] = [T]^T [S(A, B)] [T]$$

and for the normalized representation of the unitary transformation matrix  $[T]$  becomes

$$[T] = (1 + \rho\rho^*)^{-1/2} \begin{bmatrix} 1 & -\rho^* \\ \rho & 1 \end{bmatrix}, \quad (26)$$

where the transformed elements then are given for the general bistatic case by

$$\begin{aligned}
 S'_{A'A'} &= (1 + \rho\rho^*)^{-1} [S_{AA} + \rho^2 S_{BB} + \rho(S_{AB} + S_{BA})] \\
 S'_{A'B'} &= (1 + \rho\rho^*)^{-1} [-\rho^* S_{AA} + \rho S_{BB} + S_{AB} - \rho\rho^* S_{BA}] \\
 S'_{B'A'} &= (1 + \rho\rho^*)^{-1} [-\rho^* S_{AA} + \rho S_{BB} + S_{BA} - \rho\rho^* S_{AB}] \\
 S'_{B'B'} &= (1 + \rho\rho^*)^{-1} [\rho^2 S_{AA} + S_{BB} - \rho^* (S_{AB} + S_{BA})],
 \end{aligned}
 \tag{27}$$

satisfying the transformation invariants

$$\det \{ [S(A, B)] \} = \det \{ [S'(A', B')] \} = \text{invariant},
 \tag{28}$$

and

$$\begin{aligned}
 \text{Span} \{ [S(A, B)] \} &= |S_{AA}|^2 + |S_{AB}|^2 + |S_{BA}|^2 + |S_{BB}|^2 = p \\
 = \text{Span} \{ [S'(A', B')] \} &= |S'_{A'A'}|^2 + |S'_{A'B'}|^2 + |S'_{B'A'}|^2 + |S'_{B'B'}|^2 \\
 &= \text{invariant}
 \end{aligned}
 \tag{29}$$

we note that if  $S_{AB} = S_{BA}$ , then  $S'_{A'B'} = S'_{B'A'}$  for all  $\rho$ ; i.e. if reciprocity is satisfied for any one pair of orthogonal polarizations it is satisfied for all such pairs. Furthermore, we must emphasize the important property that for any one given aspect and for one frequency, the transformation is polarization invariant, i.e. the transformation occurs on one and the same polarization sphere of radius  $p = \text{span} \{ [S(A, B)] \}$ . Thus, if  $[S(A, B)]$  is known and reciprocity as well as conservation of energy is satisfied,  $[S'(A', B')]$  for any other orthogonal pair  $h(A', B')$  can be obtained as is known for example for the transformation from linear to circular polarization base vectors in Long [14]. In case of polarization losses properties of the coherency matrix need to be used [15], and the transformation will not occur on the same polarization sphere [6].

#### 4.2 Calculation of the Optimal Polarizations

It was shown by Kennaugh [8] that there exist two pairs of optimal polarizations, the Co-polarization Null Pair for which  $S'_{A'A'}$  and  $S'_{B'B'}$  in (27) vanish and the Cross-polarization Null Pair for which  $S'_{A'B'}$  and  $S'_{B'A'}$  vanish. In Table 2, the optimal polarization (CO-POL and X-POL) nulls are given in terms of  $[S]$  elements and are represented on the Poincaré sphere.

Table 3: Reconstruction of  $[S]_{SMR}$  from  $[M]$ ,  $[M_m]$ ,  $[P_H]$ ,  $[P_V]$  and Optimal Polarizations

elements of $[S]_{SMR}$	from $[M]$	from $[M_m]$	from $[P_A]$ and $[P_V]$ ( $A=H, B=V$ )
$ S_{AA} $	$\sqrt{\frac{1}{3}(m_{11} + 2m_{12} + m_{22})}$	$\sqrt{M_{11}}$	$\sqrt{a_A}$
$ S_{AB}  =  S_{BA} $	$\sqrt{\frac{1}{3}(m_{11} - m_{22})}$	$\sqrt{M_{12}}$	$\sqrt{b_A} = \sqrt{b_B}$
$ S_{BB} $	$\sqrt{\frac{1}{3}(m_{11} - 2m_{12} - m_{22})}$	$\sqrt{M_{22}}$	$\sqrt{b_B}$
$AA \leftrightarrow AB$	$\tan^{-1} \left\{ \frac{m_{14} + m_{24}}{m_{13} + m_{23}} \right\}$	$\tan^{-1} \{ M_{14}/M_{13} \}$	$\tan^{-1} \left\{ \frac{\text{Im } C_A}{\text{Re } C_A} \right\}$
$BB \leftrightarrow AB$	$\tan^{-1} \left\{ \frac{m_{41} - m_{42}}{m_{31} - m_{32}} \right\}$	$\tan^{-1} \{ M_{42}/M_{32} \}$	$\tan^{-1} \left\{ \frac{\text{Im } C_B}{\text{Re } C_B} \right\}$

from optimal polarizations [6]

$$[S(A, \theta)] = \kappa \begin{pmatrix} x & z \\ x & y \end{pmatrix}$$

CO-POL nulls are known:

$$\kappa = \sqrt{\frac{\rho}{2}} (|a_1^{CO} + a_2^{CO}|^2 + 2|a_1^{CO} a_2^{CO}|^2 + 2)^{-1/2}$$

$$x = -2a_1^{CO} a_2^{CO} \exp(-j\phi_E), \quad \phi_E = \text{phase}(a_1^{CO} + a_2^{CO})$$

$$y = -2 \exp(-j\phi_E)$$

$$z = |a_1^{CO} + a_2^{CO}|$$

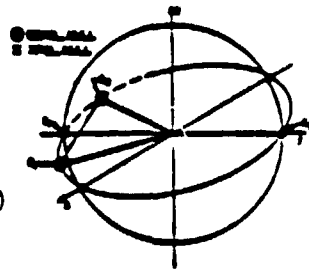


Fig. 3: Polarization Fork

One CO-POL and one X-POL are known:

$$\kappa = \sqrt{\rho/8}, \quad \theta = 2 \left\{ (a^{X})^* (a^{CO})^2 + |a^X|^2 + |a^{CO}|^2 \left[ |a^{CO} - a^{CO}| |a^X|^2 - 2|a^X|^2 \right] \right. \\ \left. - 2a^{CO} (a^X)^* - |a^X|^2 + 1 \right\}$$

$$x = a^{CO} [a^{CO} - a^{CO} |a^X|^2 - 2a^X] \exp(-j\phi_E), \quad \phi_E = \text{phase}((a^X)^* (a^{CO})^2 + |a^X|^2)$$

$$y = -[2a^{CO} (a^X)^* - |a^X|^2 + 1] \exp(-j\phi_E)$$

$$z = |(a^X)^* (a^{CO})^2 - a^X|$$

It should be noted that the CO-POL and X-POL nulls lie on one major circle on the Poincaré polarization sphere and that their locations define the polarization fork (Fig. 3). The X-POL nulls are anti-podal on this sphere and the line joining them bisects the angle between the CO-POL nulls as shown in Fig. 3. We note here that this unique description of a scatterer under monostatic conditions given for one frequency and aspect is of paramount importance to target description at one aspect and one frequency and its properties have been overlooked in the past.

#### 4.4 Reconstruction of $[S]_{SMR}$

The reconstruction of  $[S]_{SMR}$  from  $[M]$ ,  $[M]$ ,  $[P]$ ,  $[P_H]$  and  $[P_V]$  or optimal polarizations is shown in Table 3. This means Tables 2 and 3 give a complete interrelationship between these scattering matrices as well as the optimal polarizations. From a measurement point of view, this is very important because it suffices to measure one of the matrices or the optimal polarization to calculate the other matrices. The reconstruction of  $[S]_{SMR}$  from the optimal polarizations is of great importance to target polarization synthesis. In these Tables, A and B are any two orthogonal bases e.g. horizontal and vertical. We note here that in the incoherent or quasi-coherent case, clustering properties of the CO-POL nulls need to be taken into consideration as is discussed in Section 6.

#### 4.5 Measurements of $[S]$ , $[P]$ and $[M]$

The measurements of the scattering matrices  $[S]$ ,  $[P]$ , and  $[M]$  are intricate, and various methods exist which have been summarized recently in Boerner, et al., 1981, [17]. Of particular interest here is the measurement of  $[S]$  and in particular the retrieval of both amplitude and phase of all of the relevant elements of  $[S]_{SMR}$ , i.e.  $|S_{AA}|$ ,  $|S_{BB}|$ ,  $|S_{AB}| = |S_{BA}|$ ,  $\phi_{AA}$ ,  $\phi_{BB}$  assuming that  $\phi_{AB} = \phi_{BA} = 0$ . Since this brief introduction does not allow a complete treatment, we refer to the above report and point out only that it is absolutely necessary to measure the relative phase between the two co-polarized components in addition to the relative phase between the co-/cross-polarized components as well as the amplitudes of  $|S_{AA}|$ ,  $|S_{BB}|$ ,  $|S_{AB}|$ , which requires isolation of at least 25 to 30 dB between co- and cross-polarized channels.



ORIGINAL FIGURE IS  
OF POOR QUALITY

5.0 Optimal Polarizations for Different Target Shapes and Clutter

The CO-POL and X-POL nulls are calculated here for different target shapes. Table 4 shows the calculated nulls for simple shapes, e.g. ideally conducting flat plate or sphere, metallic trough, right and left metallic screws. The optimal polarizations are also calculated for linear targets e.g. horizontal, vertical, 45° with horizontal as shown in Fig. 4.

Table 5 and 5 show the optimal polarization for sea clutter and snow pack, respectively.

Table 4: CO-POL and X-POL null for simple target shapes

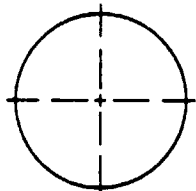
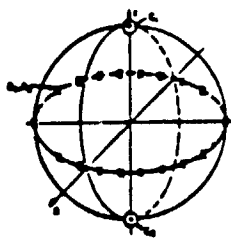
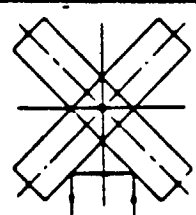
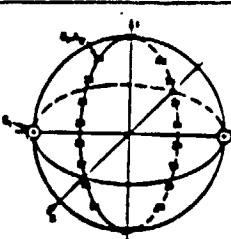
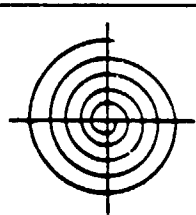
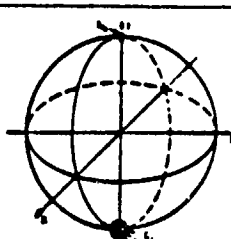
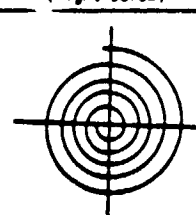
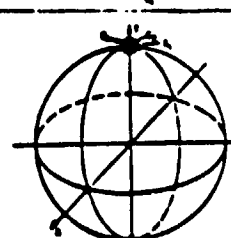
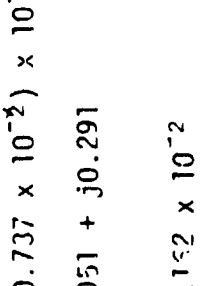
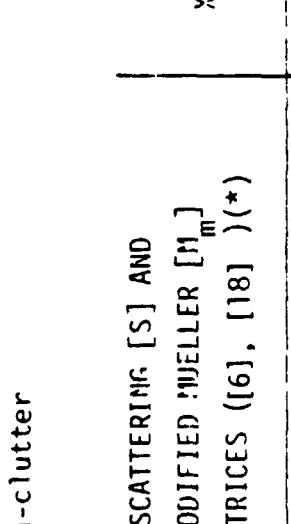
TARGET	SCATTERING [S] AND MODIFIED MUELLER [M <sub>m</sub> ] MATRICES	CO-POL (C) AND X-POL (X) NULLS ON POINCARÉ SPHERE
 <p>a. Ideally conducting flat plate or sphere</p>	$[S] = \begin{pmatrix} 1 & 0 \\ 0 & 1 \end{pmatrix}$ $[M_m] = \begin{pmatrix} 1 & 0 & 0 & 0 \\ 0 & 1 & 0 & 0 \\ 0 & 0 & 1 & 0 \\ 0 & 0 & 0 & 1 \end{pmatrix}$	
 <p>b. Metallic trough</p>	$[S] = \begin{pmatrix} 1 & 0 \\ 0 & -1 \end{pmatrix}$ $[M_m] = \begin{pmatrix} 1 & 0 & 0 & 0 \\ 0 & 1 & 0 & 0 \\ 0 & 0 & -1 & 2 \\ 0 & 0 & 0 & -1 \end{pmatrix}$	
 <p>c. Metallic helix (right screw)</p>	$[S] = \begin{pmatrix} 1 & -j \\ -j & -1 \end{pmatrix}$ $[M_m] = \begin{pmatrix} 1 & 1 & 0 & 1 \\ 1 & 1 & 0 & 1 \\ 0 & 0 & 0 & 0 \\ -2 & 2 & 0 & -2 \end{pmatrix}$	
 <p>d. Metallic helix (left screw)</p>	$[S] = \begin{pmatrix} 1 & j \\ j & -1 \end{pmatrix}$ $[M_m] = \begin{pmatrix} 1 & 1 & 0 & -1 \\ 1 & 1 & 0 & -1 \\ 0 & 0 & 0 & 0 \\ 2 & 2 & 0 & -2 \end{pmatrix}$	

Table 5: CO-POL and X-POL null data for sea-clutter

TARGET SEA CLUTTER ([6], [18])	SCATTERING [S] AND MODIFIED MUELLER [M <sub>m</sub> ] MATRICES ([6], [18]) (*)	CO-POL ( $\theta^C, \phi^C$ ) AND X-POL ( $\theta^X, \phi^X$ ) NULLS [6]
 <p>dielectric const. of sea water 70 - j70</p> <p>wind velocity 10 m/s</p> <p>tilt angle 4°</p> <p>depression angle 10°</p> <p>aspect angle 80°</p>	$S_{hh} = (0.347 + j0.206) \times 10^{-1}$ $S_{hv} = (0.686 + j0.737 \times 10^{-2}) \times 10^{-1}$ $S_{vv} = 0.951 + j0.291$ $M_{11} = 0.152 \times 10^{-2}$ $M_{12} = 0.471 \times 10^{-2}$ $M_{13} = 0.239 \times 10^{-2}$ $M_{14} = 0.138 \times 10^{-2}$ $M_{22} = 0.989$ $M_{23} = 0.555 \times 10^{-1}$ $M_{24} = -0.193 \times 10^{-1}$ $M_{33} = 0.36 \times 10^{-1}$ $M_{34} = 0.946 \times 10^{-2}$	 $\theta_1^C = 109.4^\circ, \phi_1^C = -4.1^\circ$ $\theta_2^C = 66.5^\circ, \phi_2^C = -11.7^\circ$ $\theta_1^X = 92.05, \phi_1^X = 172.1^\circ$ $\theta_2^X = 87.95, \phi_2^X = -7.9^\circ$

(\*)  $S_{vh} = S_{hv}, M_{21} = M_{12}, M_{31} = 2M_{13}, M_{41} = -2M_{14}, M_{32} = 2M_{23}, M_{42} = -2M_{24}, M_{43} = -M_{34}, M_{44} = M_{33} - 2M_{12}$

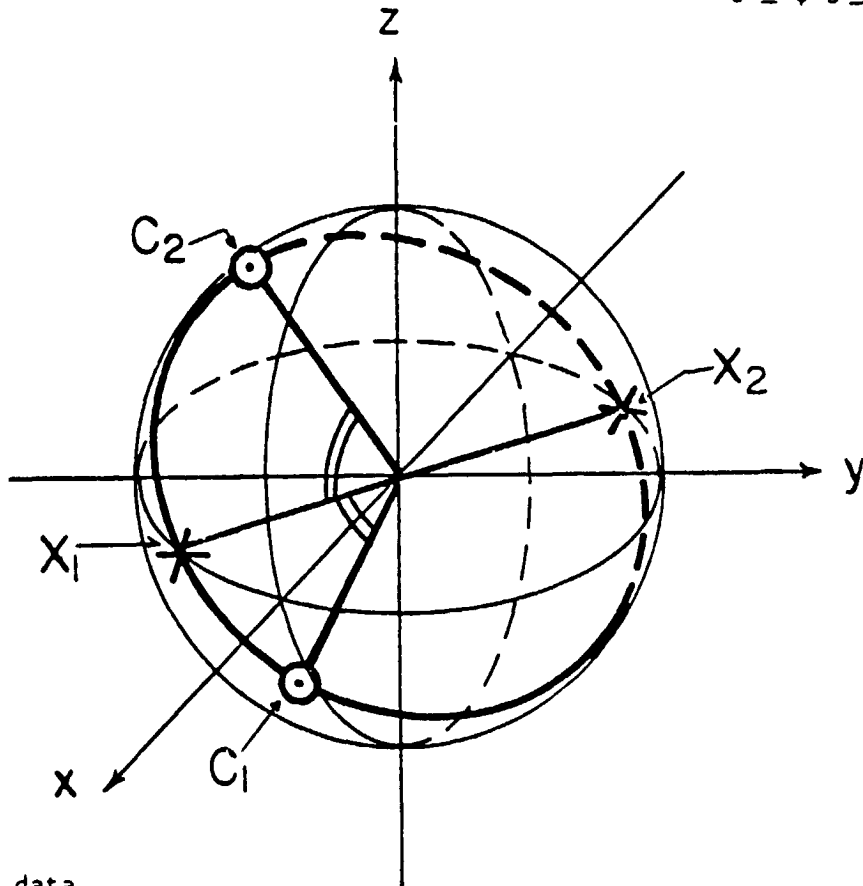
Table 6: OPTIMAL POLARIZATION OF SNOW-PACK CLUTTER

(Using data made available from Report Number RSL 34-3, by Stiles and Ulaby 10/79)

Measured data

Steamboat Spring, Colorado:  
Date: February 21, 1977  
Time: 07:05  
Aspect Angle: 10°  
Frequency: 3.6Ghz

$\sigma_{hh} = -11.70$  dbs  
 $\sigma_{hv} = -20.90$  dbs  
 $\sigma_{vv} = -10.70$  db  
randomly generated relative phases  
 $0 \leq \phi's \leq 360^\circ$



Calculated data

$\phi_{hh} - \phi_{hv} = 32.60^\circ$   
 $\phi_{vv} - \phi_{hv} = 28.98^\circ$

Scattering Matrix

$$[S] = \begin{bmatrix} 0.219 + jo.14 & 0.0902 \\ 0.0902 & 0.255 + jo.141 \end{bmatrix}$$

CO-POL Nulls

CO-POL 1:  $\theta_1^C = 160.7^\circ, \phi_1^C = -46.61^\circ$   
CO-POL 2:  $\theta_2^C = 19.04^\circ, \phi_2^C = -110.72^\circ$

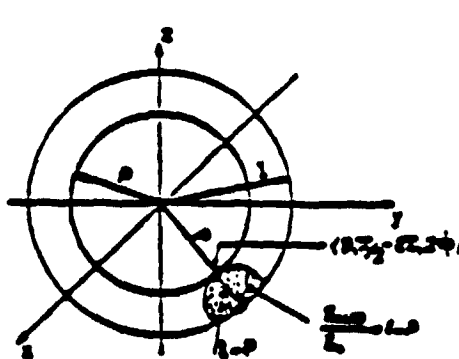
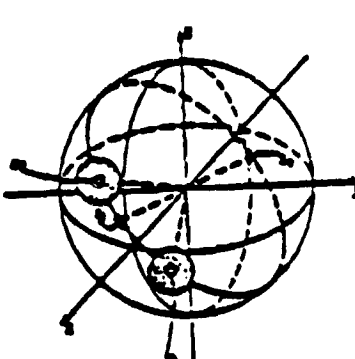
X-POL Nulls

X-POL 1:  $\theta_1^X = 90.15^\circ, \phi_1^X = 101.57^\circ$   
X-POL 2:  $\theta_2^X = 89.85^\circ, \phi_2^X = -78.43^\circ$

6. Optimal Polarization for the Quasi-Coherent Case

In the quasi-coherent time varying case the coherent concept introduced before cannot be used and we need to decompose the Stokes vector into a coherent and a non-coherent component as is summarized in Table 7.

Table 7: Analysis of Coherent-to-noncoherent Time Varying Clutter Statistics

Parameter	Description
Average Stokes Vector	$\underline{g} = g(\langle \underline{E}(t) \rangle) = \begin{pmatrix} g_0 \\ g_1 \\ g_2 \\ g_3 \end{pmatrix} = \begin{pmatrix} \langle  E_x ^2 \rangle + \langle  E_y ^2 \rangle \\ \langle  E_x ^2 \rangle - \langle  E_y ^2 \rangle \\ 2 \operatorname{Re} \langle E_x E_y^* \rangle \\ -2 \operatorname{Im} \langle E_x E_y^* \rangle \end{pmatrix}$
Coherency Matrix	$[J] = \begin{pmatrix} \langle E_x E_x^* \rangle & \langle E_x E_y^* \rangle \\ \langle E_y E_x^* \rangle & \langle E_y E_y^* \rangle \end{pmatrix} = \begin{pmatrix} J_{xx} & J_{xy} \\ J_{yx} & J_{yy} \end{pmatrix}$
Relation between $\underline{g}$ and $[J]$	$J_{xx} = \frac{1}{2}(g_0 + g_1), J_{xy} = J_{yx} = \frac{1}{2}(g_2 - jg_3), J_{yy} = \frac{1}{2}(g_0 - g_1)$
Polarization Decomposition pp=partially polarized cp=completely polarized up=unpolarized	$\begin{pmatrix} g_0 \\ g_1 \\ g_2 \\ g_3 \end{pmatrix}_{pp} = \begin{pmatrix} g_0 \\ g_1 \\ g_2 \\ g_3 \end{pmatrix}_{cp} + \begin{pmatrix} g_0 - g_0 \\ 0 \\ 0 \\ 0 \end{pmatrix}_{up}, g_0 \geq g_0^2 = g_1^2 + g_2^2 + g_3^2$
Degree of Polarization	$P = \frac{g_0}{g_0} \sqrt{1 - \frac{4 \det([J])}{(J_{xx} + J_{yy})^2}}$ $0 \leq P \leq 1, P = 0$ for up wave, $P = 1$ for cp wave
Degree of Coherence	$ u_{xy}  = \sqrt{\frac{J_{xy} J_{yx}}{J_{xx} J_{yy}}} \leq P \leq 1$
Geometric representation of partially polarized wave and example for sea clutter	$\begin{pmatrix} g_0 \\ g_1 \\ g_2 \\ g_3 \end{pmatrix}_{pp} = \begin{pmatrix} 1 - P \\ 0 \\ 0 \\ 0 \end{pmatrix} g_0 + \begin{pmatrix} P \cos 2\alpha \cos 2\tau \\ P \cos 2\alpha \sin 2\tau \\ P \sin 2\alpha \end{pmatrix} g_0$
	
Geometric Representation for pp wave	Sea clutter example

ORIGINAL PAGE IS  
OF POOR QUALITY

As can be observed from Table 7, the completely polarized part of the partially polarized wave can be represented by one point on the polarization sphere with radius equal to the degree of polarization  $P$  and spherical co-ordinates  $(P, \pi/2 - 2\tau, 2\phi)$ . The unpolarized part can be represented anywhere inside a sphere with radius  $(1 - P)$  representing the intensity of the unpolarized part. The center of this sphere is the intersection point of the extended line from the center of the Polarization sphere and the point representing the completely polarized wave with unit sphere. Thus, we observe that instead of one isolated point representing the co-polarization nulls, we obtain circular cluster regions about the location of the "averaged coherent" CO-POL null locations whose radius is equal to about  $(1 - P)$  and represents a measure of incoherency. The particular property of the optimal polarization concept applied to the incoherent clutter case will be of paramount importance to the description and imaging of hydrometeor distributions. Due to the lack of coherent radar systems with complete polarization diversity, we are not able to provide any examples at this time, and refer to the examples provided for the cases of sea-clutter and snowpacked terrain clutter provided in Tables 7, 6.

### 7. Application to the Classification and Imaging of Hydrometeor Distributions

We have introduced the basic background to show how optimal polarization properties of a scatterer in isolation and/or distribution are of paramount importance for the complete description of radar targets, clutter or voluminous distributions of particulate scatterers. We have also shown that it is essential that the relative phase between the two co-polarized channels be measured which indeed is a difficult request. However, it can be shown that the relative phase term  $\phi_{\text{CO-POL}} = \phi_{\text{AA}} - \phi_{\text{BB}}$  contains optimum information on geometrical as well as material properties of a scatterer in specular direction as well as on the electromagnetic properties of the boundary separating ensembles of different species of scatterers. It is particularly this property which will become essential in the application of the optimal polarization concept to hydrometeor classification and imaging.

### 8. Conclusions and Recommendations

We conclude here that the optimal polarization concept is an important tool for radar classification and imaging of targets in isolation as well as in ensemble distribution. We have provided computational examples for the CO-POL and X-POL nulls for some simple as well as for some distributed scatterers. We require more measurement input data on amplitude as well as phase measurements of the elements of the relative phase scattering matrix  $[S]_{\text{SMR}}$  for stationary and moving distributions of scatterers such as terrain, sea as well as hydrometeor distributions so that the optimal polarization concept can be further advanced.

Specifically, we recommend that one dual polarization radar system for complete measurement of  $[S]_{\text{SMR}}$  be made available to the research community for the analyses of the optimal polarization concept as applied to various kind of clutter as well as hydrometeor distributions. Based on such an investigation, we then will be able to recommend which simplified incomplete dual polarization radar system can be used on a space platform satisfying cost-benefit considerations.

### Acknowledgements

We wish to acknowledge the many discussions with Drs. J. Metcalf, T. Seliga,

ORIGINAL DRAFT IS  
OF POOR QUALITY

V. Bringi, R. Doviak, M. Hall, B. Barge, R. Humphries, A. Hendry, G. Mc Cormick, J. Goldhirsch, D. Atlas, F. Nathanson, E. M. Kennaugh- W. Keydel, . Scrrott, H. Schuster, D. T. Gjessing and R. J. Huynen on the subject matter, which were most helpful. I also wish to thank my research collaborators, Dr. M. B. El-Arini, Mr. C-Y. Chan, Dr. S. K. Chaudhuri, and Mr. B-Y. Foo for assistance in preparing the manuscript. The partial support for related research by research officers Dr. H. W. Mullaney, Mr. J. Willis, Dr. J. Mink and Dr. S. Brodsky is highly appreciated and their continual encouragement to extend my research base is highly appreciated. I thank Ms. Pamela VanderLaan Brouwer for typing the manuscript.

References

- [1] R.J. Doviak, "Doppler Weather Radar for Forecasting and Warning", presented at the International Geoscience and Remote Sensing Symposium, Washington, DC, June 8-10, 1981, Proceedings, pp. 152-157.
- [2] D. Atlas, "The Promise of Remote Sensing in the Atmospheric Sciences", presented at the International Geoscience and Remote Sensing Symposium, Washington, DC, June 8-10, 1981, Proceedings, pp. 142-151.
- [3] J.I. Metcalf and J.S. Echard, "Coherent polarizations-diversity radar techniques in meteorology,": J. Atmosph. Sci. Vol. 35, pp. 2010-2019, 1978.
- [4] A.B. Schneider and P.D.L. Williams, "Circular polarization in radars: An assesment of rain clutter reduction and likely loss of target performance", Radio Electron. Eng., vol 47, pp. 11-29, 1976.
- [5] M.P.N. Hall, S.M. Cherry, J.W.F. Goddard, and G.R. Kennedy, "Rain drop size and raindrop rate measured by dual-polarization radar", Nature vol. 285, pp. 195-198, May 22, 1980.
- [6] W-M. Boerner, M.B. El-Arini, C-Y. Chan, S. S. Saatchi, W-S. Ip, P.M. Matoris and B-Y. Foo, "Polarization Utilization in Radar Target Re-construction", Technical (Interim) report, # CL-EMID-NANRAR-81-01, Electromagnetic Imaging Divison, Communications Laboratory, UICC, P.O. Box 4348, Chicago, IL 60680.
- [7] J. R. Huynen, "Phenomonological Theory of Radar Targets", Ph.D. Dissertation, Drukkerij Bronder-Offset N.V. Rotterdam, The Netherlands, 1970.
- [8] E. M. Kennaugh, "Effects of the Type of Polarizatons on Echo Characteristics" Reports #389-1 to 389-24, The Ohio State University Research Foundation, Columbus, OH (1949-1954).
- [9] C.D. Graves, "Radar Polarization Power Scattering Matrix", Proc. IRE vol. 44, pp. 248-252, Feb., 1956.
- [10] C-Y. Chan, "Studies on the Power Scattering Matrix of Radar Targets", M.Sc. Thesis, Department of Information Engineering, UICC, Chicago, IL, May 1981.

ORIGINAL PAGE  
OF POOR QUALITY

- [11] L.A. Morgan and S. Weisbrod, "Radar Target Discrimination Based on Polarization Effects", NAVAIR Review, March 1979.
- [12] D.B. Kanareykin, N.F. Pavlov, and U.A. Potekhin, The Polarization of Radar Signals, Moscow: Sovyetskoye Radio, English translation of Chs. 10-12: Radar Polarization Effects, New York, Macmillan.
- [13] H.G. Heske, Ed., Atmospheric Effects on Radar Target Identification and Imaging, Proc. NATO ASI Golar, Dordrecht, Holland: D. Reidel, 1976.
- [14] M. W. Long, Refectivity of Land and Sea, Lexington, MA: Lexington Books, DC. Heath, 1975.
- [15] H.D. Kraus, Radio Astronomy, McGraw Hill Book Co., New York, 1966.
- [16] G.A. Deschamps, "Geometrical representation of the polarization of a plane electromagnetic wave," Proc. IRE, vol. 39, pp. 543-548, 1951 (see also: "A hyperbolic protractor for microwave impedance measurements and other purposes," Federal Telecommunications Labs., ITT, Nutley, NJ 1953.)
- [17] W-M. Boerner, M. B. El-Arini, C-Y. Chan, S. S. Saatchi, and B-Y. Foo, "Polarization Utilization in Radar Classification and Imaging", NAVAIR Review, May 1981.
- [18] J.C. Daley, "Radar Target Discrimination", NAVAIR Review, March 1979.
- [19] W. H. Stiles and F. T. Ulaby, "Microwave Remote Sensing of Snowpacks and Data Set Appendices", Remote Sensing Laboratory RSL Technical Report #340-3 (NASA Contractor Report # 3263), The University of Kansas, Lawrence, Kansas 66945.

ORIGINAL PAGE IS  
OF POOR QUALITY

245  
N83 25314

#### BISTATIC RADAR METEOROLOGICAL SATELLITE

Fred E. Nathanson  
Technology Service Corporation  
8555 16th Street  
Silver Spring, Md. 20910

In studies of the best methods for obtaining complete U.S. radar meteorological coverage or coverage of a particular region such as the Caribbean or portions of the Atlantic Ocean, the use of orbiting active meteorological radar facility at a nominal altitude of 700 kilometers has been investigated.\* While this is adequate to monitor meteorological events such as hurricanes, typhoons, or specific storm fronts, it is limited as a general meteorological tool by the fact that a single satellite only monitors a given area perhaps twice a day. Coverage for those events would be desired about five or ten times as frequently.

The technique discussed here is that a radar transmitter with a moderate size antenna be placed in a geosynchronous orbit with either a  $0^\circ$  or a low inclination orbit. The reflected signals from the precipitation are then received either on a single beam from a satellite having a beamwidth of about  $6^\circ$  or preferably with a beam that scans the U.S. in a "raster" pattern with about  $0.9^\circ$  beamwidth. While it would seem that a bistatic system with the transmitter at synchronous altitude and the receivers near the surface would not be a very efficient way of designing a radar system, it is somewhat surprising that the required power and antenna sizes are not that great.

Two factors make the meteorological application somewhat more attractive than the bistatic detection of point targets. First, the bistatic reflections of radar signals from precipitation are to a large extent omnidirectional, and while raindrops are spheroids rather than spheres, the relationship of the reflectivity of the rain to rainfall rate can be easily derived. The second reason is that the rain echo signal level is independent of range from a receive only radar, and if the bistatic system works at all, it will work at long ranges. That is, the signals impinging at a passive receiver resulting from illumination from a geosynchronous satellite, will yield more or less constant reflective power at reasonable ranges from a ground station. While the power intensity at a ground receiver falls off inversely as the square of the range from the reflectors, the beam volume increases directly as the square of the range. Obviously the angular resolution degrades with increasing range.

---

\* Bucknam, J.N., R. P. Dooley and F. E. Nathanson. "A Shuttle Meteorological Radar Study" Final Report to NASA GSFC under Contract NAS5-20058 March 1975.



ORIGINAL PAGE IS  
OF POOR QUALITY

The reason that the power and aperture sizes are not that great is related to the volume search mission of a meteorological radar. Since at any point on the earth's surface it is desired to scan a preselected area (or volume), there is not a significant difference whether that area is scanned with a short intense beam for a short period of time or the received power is integrated over a long period of time. Basically, the criterion for an area search is the energy incident on that area in the desired period. It is more efficient to have the satellite illuminate an area of the U.S. 400 to 700 kilometers in diameter at one time rather than flood the entire U.S. with a lower power density. Since this only requires a 10 to 15 foot aperture at a wavelength of 5 centimeters (C Band), there is no severe demand on satellite state of the art. Power levels required to detect light rains on the ground are approximately 250 watts of average radiated power from the satellite which also is well within the envelope of what has been accomplished. The next sections show some brief calculations to illustrate this. Due to the geometry involved, it is only necessary to scan the satellite beam by plus or minus  $3^\circ$  in one plane and plus or minus  $1\frac{1}{2}^\circ$  in the other plane. This scanning can either be accomplished mechanically, since it is rather slow, or electronically using multiple feeds, or by frequency scanning techniques.

ORIGINAL PAGE IS  
OF POOR QUALITY

SAMPLE CALCULATIONS-BISTATIC METEOROLOGICAL SATELLITE

The Power Density on the Earth's surface to cover the entire U.S. (~3600 Km diameter) is:

$$P_{den} = \frac{P_t G_T}{4\pi R_1^2} = \frac{\hat{P}_t}{\theta_t \phi_t R_1^2} \quad (1)$$

where  $\hat{P}_t$  is the transmit power, the transmit beamwidths are  $\theta_t$  and  $\phi_t$ , and  $R_1$  is the distance from the satellite; If as in Figure 1,

$$\theta_t \doteq \frac{3600 \text{ km}}{36000 \text{ km}} \doteq 0.10 \text{ radians}$$

where 36.000 km is approximately geosynchronous altitude.

$$G_t \approx \frac{4\pi}{\theta_t \phi_t} \approx 31 \text{ dB}$$

Let  $\hat{P}_T = 60 \text{ kw}$  radiated

$\tau = 5.5 \mu\text{sec}$  pulse duration

$\bar{P}_t = 250 \text{ w}$

$T = 1.3 \text{ msec}$  interpulse period

$$\begin{aligned} P_{den} &= \frac{0.6 \times 10^5}{10^{-2} \times 1.3 \times 10^{+15}} \\ &= .45 \times 10^{-3} \text{ watts/M}^2 \approx -83 \text{ dB watts/M}^2 \end{aligned}$$

The power reflected toward the receiver, neglecting polarization losses, is:

$$\begin{aligned} P_{refl} &= P_{den} \sigma = P_{den} (\text{Vol}) (\Sigma\sigma) \\ &= P_{den} R_2 \theta_R R_2 \phi_R \Delta R \Sigma\sigma \end{aligned}$$

The ground geometry is illustrated in Figure 2 where  $\theta_R$ ,  $\phi_R$  are the receive beamwidths and  $\Sigma\sigma$  is the reflectivity per unit volume,  $R_2$  is the range from precipitation toward the receiver and  $\Delta R$  is the range resolution. If the receive aperture has an effective area  $A_e$ ,

ORIGINAL PAGE 13  
OF POOR QUALITY

### SYNCHRONOUS SATELLITE

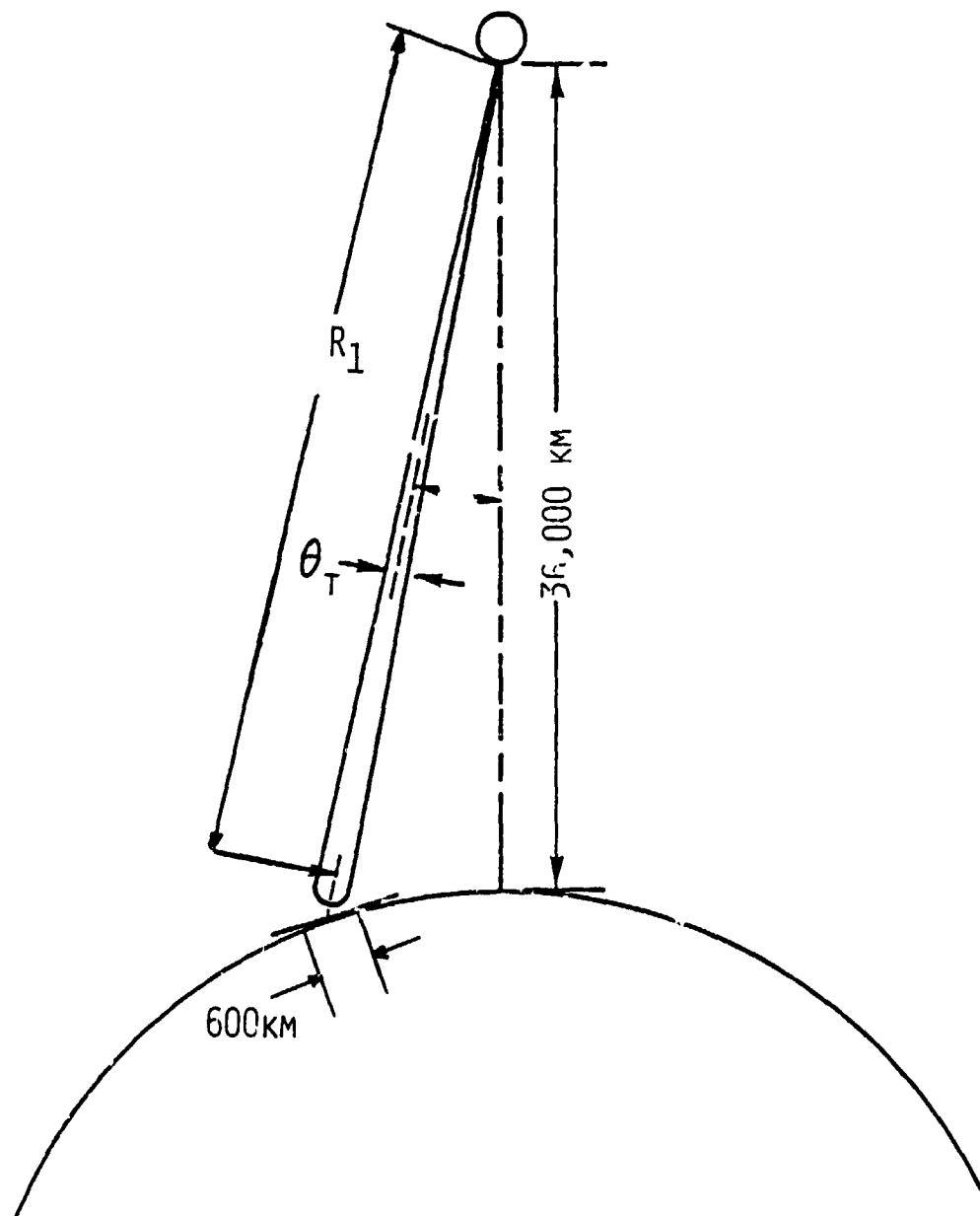


FIGURE 1 - GEOMETRY OF A DOWNWARD-LOOKING RADAR AT SYNCHRONOUS ALTITUDE

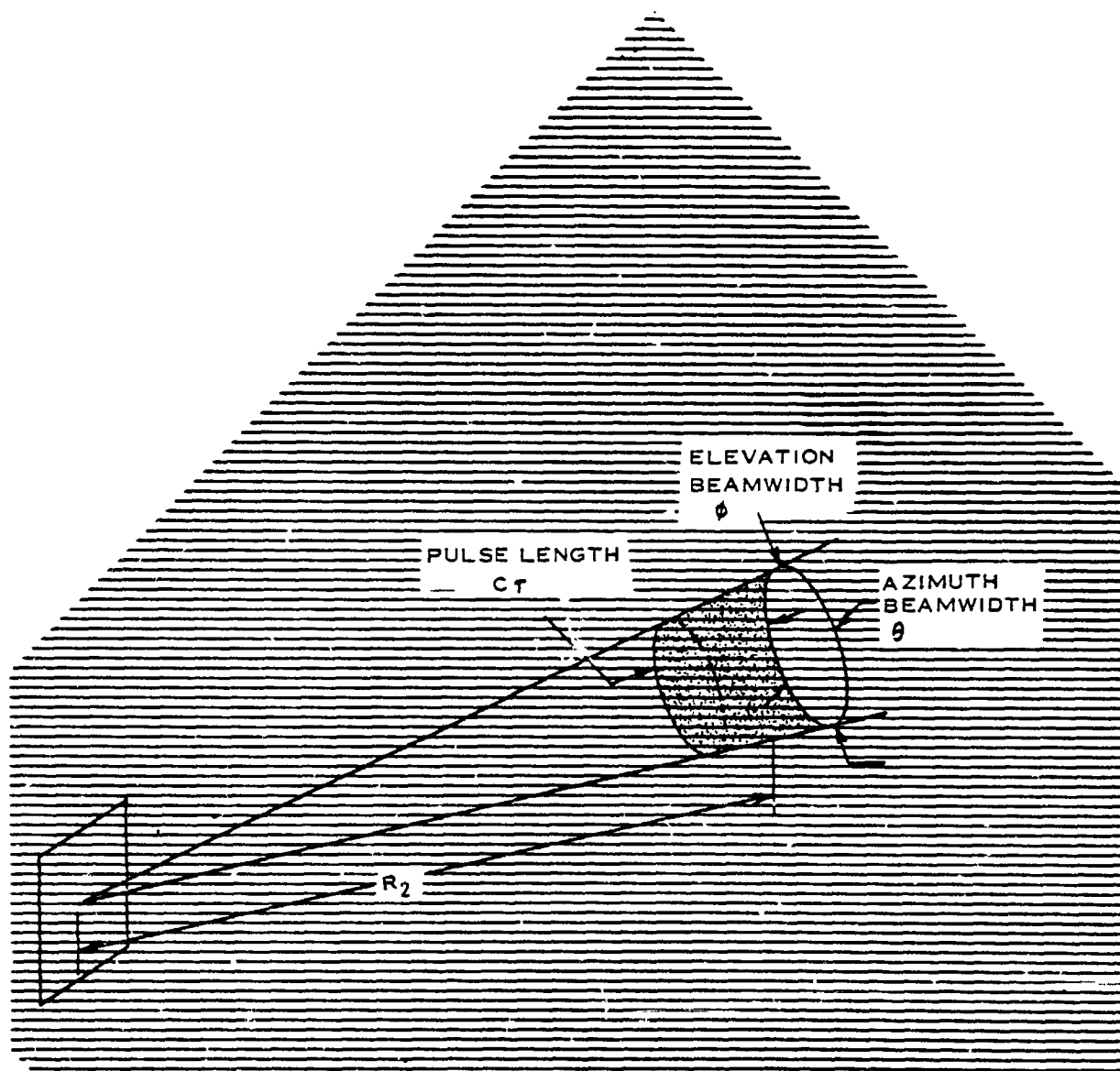


FIGURE 2 - SURFACE RECEIVER GEOMETRY FOR BISTATIC METEOROLOGICAL RADAR

ORIGINAL PAGE IS  
OF POOR QUALITY

$$P_r = \frac{P_{\text{refl}} A_e}{4\pi R_2^2} = \frac{P_{\text{den}} R_2 \theta_R R_2 \phi_R \Delta R \Sigma \sigma A_e}{4\pi R_2^2} \quad (2)$$

$$P_r = \frac{P_{\text{den}} \theta_R \phi_R \Delta R \Sigma \sigma A_e}{4\pi}$$

Note that  $P_r$  is independent of  $R_2$ . Also,

$$A_e = \frac{\lambda^2}{\theta_R \phi_R}$$

then

$$P_r = \frac{P_{\text{den}} \lambda^2 \Delta R \Sigma \sigma}{4\pi} \quad (3)$$

At  $\lambda = 5.0 \text{ cm} = \text{C Band}$   
 $\Sigma \sigma = -79 \text{ dB at } r = 1 \text{ mm/hr}$   
 $= -70.0 \quad r = 4 \text{ mm/hr}$   
 If  $\Delta R = 1.6 \text{ km}$

In decibel notation from (3)

$$P_r = -83 - 13 - 13 + 32 - 79 - 11 \text{ dBw}$$

$$= -167 \text{ dBw per pulse for full U.S. Coverage at all times}$$

$$= -137 \text{ dBm per pulse}$$

The receiver sensitivity can be expressed by  $kT_g B$  where  $B$  is noise bandwidth. For a receiver system noise temperature\* of  $300^\circ$ , an 80 KHz bandwidth,

$$kT_g B = -204 \text{ dB} + 49 \text{ dB} + 30 \text{ dBm/dBw} = -125 \text{ dBm.}$$

The signal-to-noise ratio per pulse would be  $-12 \text{ db}$ .

Since this power is not adequate, consider sequential U.S. coverage as illustrated in Figure 3. Then  $\theta_t \phi_t$  can be reduced by 17 dB,  $P_{\text{den}} = -66 \text{ dBw/M}^2$  and  $P_r = -120 \text{ dBm per pulse}$ .

$$\begin{aligned} P_r / N_{\text{rec}} &= S/N = 5 \text{ dB at } 1\text{mm/hr rainfall rate} \\ &= 14 \text{ dB at } 4\text{mm/hr} \\ &= 23 \text{ dB at } 16\text{mm/hr} \end{aligned}$$

For 8 pulses Integrated, a S/N or 5 dB per pulse is adequate. For 16 pulses integrated about 3 dB is adequate.

\* Self contained parametric amplifiers are currently available with noise temperatures of  $75^\circ\text{k}$  at 3.0 GHz and  $120^\circ$  at 10 GHz.

ORIGINAL PAGE IS  
OF POOR QUALITY

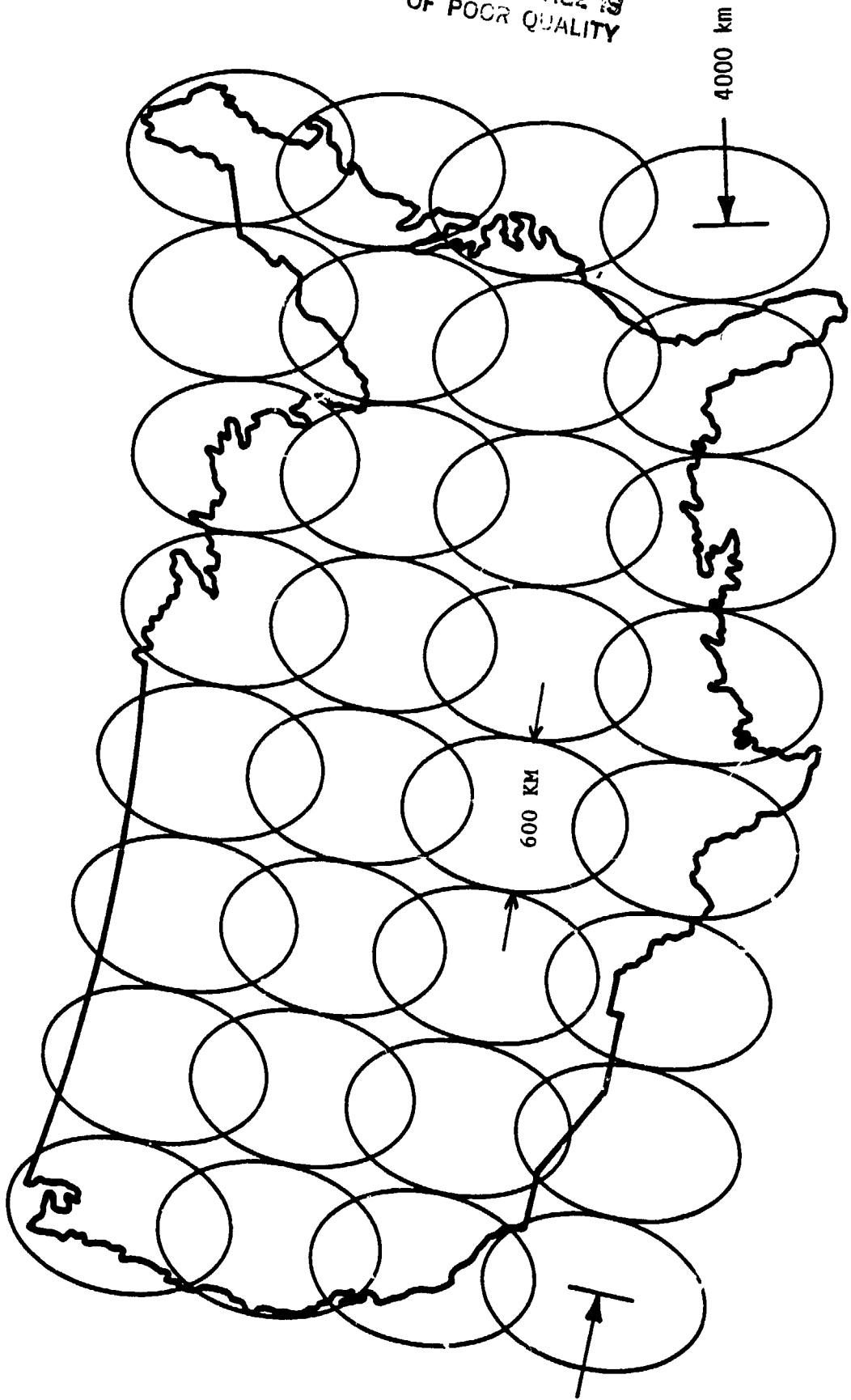


FIGURE 3 FOOTPRINT OF RASTER SCAN ILLUMINATION

ORIGINAL PAGE IS  
OF POOR QUALITY

Note that the S/N is independent of the receive aperture size since the beam volume increases as the receive aperture decreases. Thus the receiver aperture size is solely dependent on the desired resolution. Larger apertures would help sensitivity in the sense that more spatial averaging could be performed before the final product is delivered. Using a range resolution of 1.6 km, an angular resolution of 3 km at  $R_2 = 200$  km would seem to be adequate and would be better than the current WSSR-57. Then,  $\theta_R \phi$  and  $\phi_R = 3/200 = .015$  radians ( $\sim 0.9^\circ$ ) and the required dish size is 3.2 meters (11'). In practice, 3 meters high by 4 meters wide would be more than adequate.

TIMING

The timing of the received signals will provide a limitation. To illustrate this, assume that coverage of the U.S. at 90 minute intervals is desired. With the coverage illustrated, this allows about 2.8 minutes per "foot print." If we choose the  $0.9^\circ$  receive beamwidth, there are 400 beams on the horizon of the receiver, and the time allowed for each azimuth at beam position is 420 milliseconds. If the interpulse period is 1.3 milliseconds there are about 320 pulse per azimuth position. If we assume that 10 elevation beams are desired there are about 32 pulses per beamwidth for a single channel receive system. This is somewhat marginal for accurate averaging of the reflected signals. A spiral scan could be used for the 2.8 minute period. Two adjacent range cells could also be averaged. A better design would be to have multiple simultaneous receive beams to take advantage of the footprint being fully illuminated for 2.8 minutes. Since the illuminated area is well known at any given time, the antenna scan can be planned to look "into" the footprint as it arrives and look at the opposite direction as it leaves.

Carrier Frequency Selection

A carrier frequency of 6 GHz (C Band) was selected for the sample calculation. From equation (2), the product  $\theta_R \phi_R A_e$  will vary inversely as the square of carrier frequency if either resolution or aperture area are held constant. Conversely  $\Sigma \sigma$  increases as the fourth power of frequency. Thus,  $P_r$  increases as the square of frequency if attenuation in precipitation is neglected. Attenuation in precipitation can usually be neglected at S band (3GHz). At C band, the coefficient is of the order of .01 db/km/mm/hr. With the bistatic geometry, the signal from the satellite only passes through a small part of the atmosphere. The attenuation is primarily "one-way" through the receive path and thus is much less than the normal two-way radar attenuation. With a 100 km path of light rain, the attenuation would be about 1.0 db at C band and about 3.0 db at X band (10 GHz). With a typical 25 km diameter 4 mm/hr rain the attenuation would be about the same. A small amount of attenuation in the transmit path must be added, as would the increases in clear atmosphere losses ( $\sim 1$  db) going from C to X band. Receiver sensitivity would also degrade by 1 db. With widespread rain the reflectivity increases faster with rainfall rate than does attenuation. Intervening storms would be the problem.

Since the receive system is simpler, a dual frequency system could be implemented. This could consist of 6 GHz for measurements of greater than 1 mm/hr and perhaps 13.9 for measurements at 0.25 to 4.0 mm/hr. The state of the precipitation could be determined at closer ranges.

Since the X band reflectivity is about 9 db higher than at C band there remains some (3-4 db) benefit to the X band system. In addition, the satellite antenna aperture area would be less than 1/2 that of the C band set. For a 500 km footprint, the diameter of the satellite antenna would be 70-90 wavelengths. This 11-15 ft. at C band or 7-9 ft. at X band. The weight saving may be significant.

#### Doppler

The system can have a doppler capability by making the transmitter and the receiver coherent. The ground receiver is in the "footprint," and would have an auxiliary horn to receive the transmitted pulses. The output of the horn is used both as a time reference and to phase lock the receiver. Since the orbit will be known, corrections can be made. To achieve doppler accuracy and resolution comparable to NEXRAD requirements would require larger higher resolution systems.

#### Horizon

At long range, multipath would be less of a problem, but land clutter might be more of a problem since the sidelobe reduction would be "one-way" rather than "two-way." A low sidelobe ground system antenna would be important. MTI could also be utilized.

#### Other Variations

If a frequency such as X band is utilized, the attenuation of the direct signal to the ground radar is a measure of the liquid water content directly above the ground site. Calibration would be practical since there are at least 32 ground stations receiving the signal on any raster and some of them would be in non-precipitating regions. To extend this, a series of reflectors 2m x 2m can be placed in a circle on small towers at about a 45° angle to the vertical. If located 10 km from the receiver sites, the reflections from these would be about 20 db above the receiver noise in the absence of rain.

Airborne receive systems could be built for special studies. For example, the transmitted beams could be diverted to the Caribbean Sea for observations of new hurricanes. Sea backscatter could also be observed to infer wind patterns.

#### Conclusions

The ideas presented here are preliminary, but show that it is practical to design a Satellite Radar Meteorology Network to cover a large area such as the U.S. A single synchronous satellite that merely transmits pulses from a coherent source is all that is needed. Its scan angle is small. The ground receivers would be relatively simple having no transmitter or highly stable oscillators. There is no radiation problem on the ground. Ground receivers can be placed wherever desired and added at low cost. No Sensitivity Time Control (STC) would be needed. The required dynamic range would be over 20 db less than active radar saving 4-5 bits in A/D conversion. The single beam radar without doppler would cost about \$140K plus another \$100K for a basic doppler capability. Data processing, distribution, displays, etc. would require additional cost.



The system is simpler in the sense that many high data rate, high resolution goals of projected ground based doppler radars have been compromised. The calculations shown are for a 90 minute data rate rather than the 2.5 - 5.0 minute systems proposed for tornado detection. The system output could be combined with the use of ground doppler radars placed at key locations.

Key areas to be addressed include the correction for attenuation in severe storms, and how to keep heavy land clutter from degrading performance.

The relatively low data rate and simplicity of the system lends itself to unattended receivers connected by telephone lines to central processors.

N83 25315 D46

9  
Y

ORIGINAL PAGE IS  
OF POOR QUALITY

ADAPTIVELY POINTING SPACEBORNE RADAR FOR  
PRECIPITATION MEASUREMENTS

by

David Atlas  
Goddard Laboratory for Atmospheric Sciences  
NASA/Goddard Space Flight Center

1. INTRODUCTION

The implication of precipitation as one of the key factors in the climate system has greatly heightened the interest in measuring it globally, and thus from space. While visible and infrared techniques have been developed to obtain proxy measurements of rainfall, the consensus view is that such methods are not generally applicable to all precipitation types and climatic regimes (NASA, 1981). On the other hand, it is generally conceded that the presently known limitations of passive microwave radiometry can probably be overcome by the use of higher resolution over the oceans, but that the outlook for useful measurements over land is hopeless (NASA, 1981). This leaves spaceborne microwave radar as the only likely general solution to the problem.

A variety of approaches to the radar measurement of precipitation from space have been proposed (NASA, 1975; Eckerman, 1975; Eckerman et al., 1978). Basically, these all depend on one of three concepts or combinations thereof: (1) measurements of rain reflectivity, Z, and estimating rain rate, R, from a general Z-R relation; (2) measurement of the attenuation rate, k, within the rain itself and relating it to rain through an appropriate k-R relation; and (3) measuring the path integrated attenuation through the rain by the loss in echo intensity from a surface reference echo, the expected loss-free echo being estimated from similar adjacent terrain or ocean outside the raining area or, over land, using backscatter cross-sections measured previously. It is not our purpose here to discuss the relative merits of these various methods. Rather we propose an auxiliary concept of adaptive pointing which would greatly aid any candidate radar method.

2. THE PROBLEM

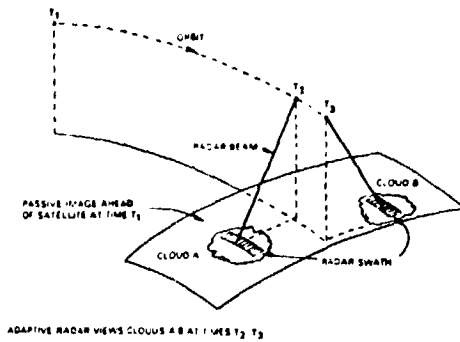
One of the critical problems faced by any radar, and especially by a spaceborne system, is the conflict between speed of scan or swath width, resolution, and dwell time per resolution element. We require the narrowest possible beams to assure filling of the instantaneous field of view (IFOV) for accurate measurement of both the peak and average rain rates and for the discrimination of precipitation echoes from surface clutter. The widest possible swath width is required to assure total coverage of the globe. Together, small IFOV and large swath width from an orbiting satellite imply very large scan speeds, but rapid scan is inconsistent with obtaining a sufficient number of independent pulses per IFOV to assure adequate signal to noise ratio and a good estimate of echo power.

Is there some way to resolve these conflicting requirements? For one thing, it is hardly necessary to spend costly radar energy and time scanning a wide swath when only a small fraction of the area is likely to be occupied by precipitation. Obviously, we need not look at cloudless regions at all and should spend as much time as required in precipitating areas.

3. CONCEPTUAL SOLUTION

The prior discussion suggests an adaptively pointing space radar system such as that depicted conceptually in Fig. 1.

At time  $T_1$  a passive IR imager scans a swath ahead of the spacecraft; an appropriate algorithm indicates which clouds are probably producing precipitation. These locations are then used by the on-board antenna controller to program the antenna



ADAPTIVE RADAR VIEWS CLOUDS A & B AT TIMES  $T_2$ ,  $T_3$

Fig. 1. Schematic of adaptively pointing spaceborne precipitation radar; see text for details.

scan so that the radar samples clouds A and B at times  $T_2$  and  $T_3$ , respectively. In Fig. 1 we visualize fixed phased array antennas on either side of the spacecraft with control of only the beam elevation angle and rely upon the spacecraft motion to perform the scanning parallel to the track. However, two dimensional electronic scanning is desirable for some purposes. Of course, fixed antennas offer considerable advantages, particularly if they are as large as we anticipate.

In any case, we propose that the radar measurement scenario proceed roughly as follows: (1) scan suspect cloud region rapidly to better define actual storm boundary and probable peak than is possible with passive schemes; this requires less dwell time than do reflectivity measurements; (2) reposition beam to measure peak reflectivity and an array of selected points around the peak accurately; the number of measurements required to obtain a sufficiently accurate area integral needs to be determined, but is not likely to exceed 10 or 20 depending upon the storm complexity. With a gaussian model storm, 95% of the rainfall is included within the area encompassed by the echo power contour only 13 db down from the peak; thus, one need not measure outside of these bounds provided the true peak can be isolated; (3) the larger the storm, the more uniform is the rainfall so that the sampling density for synoptic scale storms may be greatly reduced and relatively simple sampling patterns may be used. In

short, the adaptively pointing radar is used effectively as an optimum movable rain gage network.

In this mode we visualize the radar as a means of calibrating the precipitation intensity and refining the storm area estimates made by either IR or, during the day, by combined visible and IR techniques. An assessment of such techniques for precipitation measurements from space has recently been presented (NASA, 1981). It is generally believed that IR methods provide reasonable estimates of precipitating areas, although this author finds that they tend to overestimate the rainfall areas of convective storms. This is probably advantageous since it provides an outer bound within which the radar search for precipitation may be confined. In the case of stratiform precipitation, much less is known about the relation of IR temperature thresholds to actual precipitation.

It should be obvious that a radar carried aboard a low earth orbiter (LEO) can make only two measurements a day. Thus we shall have to rely on 24 hour per day IR cloud surveillance from geosynchronous satellites to provide proxy measurements with which we expect to account for diurnal variations of precipitation.

Clearly, we have presented only the outlines of a concept. Much study needs to be done before the feasibility of this approach can be properly assessed. Nevertheless, the method warrants consideration since it appears to overcome one of the major obstacles which has impeded development of a spaceborne radar since it was first studied by Dennis (1963).

#### 4. REFERENCES

- Dennis, A. S., 1963: Rainfall determinations by meteorological satellite radar. Stanford Research Institute, Project No. 4080.
- Eckerman, J., 1975: Meteorological radar facility for the space shuttle. IEEE/National Telecommunications Conf., New Orleans, Louisiana, Dec.
- NASA, 1975: Active microwave workshop report. NASA Report SP-376, pp. 270-367.
- NASA, 1981: Precipitation measurements from space. NASA/Goddard Space Flight Center (in press).

N83 25316

347

ORIGINAL PAGE IS  
OF POOR QUALITY

THE OUTLOOK FOR PRECIPITATION MEASUREMENTS FROM SPACE

David Atlas, Jerome Eckerman, Robert Meneghini

NASA/Goddard Space Flight Center  
Goddard Laboratory for Atmospheric Sciences

and

Richard K. Moore

University of Kansas  
Lawrence, Kansas

1. INTRODUCTION

The interest in measuring precipitation globally, and thus from space, has been intensified by recent international research activities aimed at understanding and predicting climate. The importance of precipitation in maintaining the mean global temperature structure and general circulation may be seen from the three principal sources of energy flux to and from the atmosphere over the globe: (1) IR losses to space at a rate of  $5.1 \times 10^{16}$  watts; (2) latent heating by precipitation of  $4.4 \times 10^{16}$  watts; and (3) heating by turbulent diffusion at about  $0.7 \times 10^{16}$  watts (Newell et al., 1974). As the key heat source, anomalies in precipitation, which are undoubtedly triggered by other anomalous boundary conditions (e.g., sea surface temperature, soil moisture) are strongly implicated in the chain of events responsible for climate variability. And of course precipitation is one of the key parameters which characterizes climate and must be predicted. We may cite an extensive list of other requirements for observations of precipitation, but the above should suffice for present purposes. We hasten to add that not all the needs may be met by spaceborne observations. Here we concentrate on those required to serve in climate monitoring and research and global weather prediction.

In spite of the extreme importance of precipitation, our knowledge of either the synoptic or climatological distributions of precipitation over more than 90% of the globe is abysmal. The question we address in this paper is the outlook for providing precipitation measurements of useful accuracy and/or precision from space.

2. THE PRESENT SITUATION

Our present capabilities and future directions were recently reviewed in a workshop on "Precipitation Measurements from Space" (NASA/GSFC, 1981), hereafter referred to as P.W. At this writing, the report of the workshop is not yet available; thus, the following statements must be considered as preliminary, although we have attempted to reflect the consensus views faithfully.

2.1 Visible and IR Techniques

Visible and IR techniques of estimating rainfall work surprisingly well especially for large areas and durations for convective rainfall in the subtropics. For monthly precipitation, simple counts of highly reflective clouds provide remarkably good estimates. Even for 6 hour average rainfall, the fractional cloud cover at various IR thresholds and visible brightness appears to delineate the area of rain well, so that the use of known climatological rain rates provides volumetric amounts. More complex schemes involve both the area and its time derivative, again with some IR threshold. The P.W. working group found both advantages and disadvantages to the methods noted above and others not mentioned here, but concluded that no single visible and/or IR approach can perform adequately for climatic purposes in all regions.

Lovejoy and Austin (1979) argue persuasively that the skill of both visible and IR methods lies almost entirely in their ability to represent the rainfall area. Based on radar data, they find a correlation coefficient of about 0.9 between hourly rain areas and rain amounts in both Montreal and the GATE experiment, while area-rain rate correlations are negligible (see also Lovejoy, 1981). (We must be careful in distinguishing between a good "correlation" of radar rain areas and rain amounts and the ability of the satellite imagery to faithfully depict the rain areas.) This is reasonable because there is no direct physical link between either the visible or IR brightness and rainfall. (The exceptions are time derivatives of the latter, which reflect updraft velocities, or its minimum value, which is a measure of its maximum height.)

The above findings already suggest that VIS/IR techniques be exploited for their relatively good rain area depiction capabilities but that we use other methods such as microwave radiometry or radar to estimate the rain rates. Such a combination is also indicated if either of the latter instruments are to be flown on low orbitors, allowing only twice per day samples of rain rate. In that event, corrections for diurnal variability would have to be made through the use of the 24 hr sequence of cloud imagery from GOES.

## ORIGINAL COPY OF POOR QUALITY

### 2.2 Microwave Radiometry

The P.W. working group on microwave radiometry concluded that: (1) passive measurements in the 10-40 GHz region represent a viable technique for measuring rain over the ocean, but (2) rain over land represents a much more difficult problem due to the highly variable background. The group also highlighted the following problems: (1) A negative bias (i.e., rainfall underestimate) and large variance due to the non-uniform distribution of rainfall or incomplete filling of the relatively large instantaneous fields of view (i.e., FFOV of 20 x 44 km at nadir on the Nimbus 6 Electrically Scanning Microwave Radiometer); (2) variability of the effective rain layer height, defined as the path integrated attenuation divided by the surface attenuation coefficient. This variability decreases with increasing area and is believed to be related climatologically to the freezing level, so it appears to remain a potentially serious problem only in intense convective storms; (3) significant and variable amounts of cloud liquid water content which introduce errors in retrieved rain rates and places a lower bound on the rate which can be detected. A significant factor omitted from the above is the presence of a mixture of hydrometeors of large drops, graupel, and hail in the more intense convective storms which will surely confound the relatively simple retrieval algorithms. Of course, unless it can be assumed that the rain begins at the freezing level, one gets only a measure of the effective integral with height and not of the rain intensity itself.

Of the above problems, it now appears that the unfilled FFOV dominates the errors in the ESMR data. However, a simulation by Lovejoy (1981) using an 8 x 8 km FFOV such as that anticipated for the LAMMR (Large Aperture Multichannel Microwave Spectrometer) has shown that the bias becomes negligible and random errors would be greatly reduced; i.e.,  $\pm 20\%$  RMS for 12 hr accumulations; these would be reduced further for extended period climatological averages. We therefore conclude that microwave radiometry has an important role to play in space precipitation measurements over the oceans. Indeed, its failure over land is the key reason to consider spaceborne radar.

### 3. SPACEBORNE RADAR

The essential questions are: (1) can spaceborne radar provide sufficiently accurate observations of rain over both land and ocean? (2) can it replace or supplement the VIS/IR methods which are acknowledged to estimate rain area better than rate? and (3) how can we optimize a hybrid system which exploits the best features of the various methods? There is little doubt that radar could provide precision global distributions of rain rate given no constraints on the number of spacecraft, antenna size, and power. But what is achievable within realistic technological and monetary bounds? In what follows we outline several promising approaches. We note that some of these were previously proposed in the report of the Active Microwave Workshop (NASA, 1975). But let us first highlight some

of the key obstacles which have hampered progress to date. These are briefly reviewed below.

### 3.1 Key Obstacles

One of the major problems encountered in previous proposed designs is the antenna size required to achieve beam filling and reduce the effects of surface clutter both in the main and side lobes. Both problems can be largely overcome by a sufficiently large antenna. To keep the antenna dimensions within bounds, we have frequently resorted to shorter wavelengths than we prefer to use in ground-based systems. This then results in large rainfall attenuation and potentially excessive errors in attempting to correct for the losses (Mitschfeld and Bordan, 1954). Proposed solutions have been either (1) to use two wavelengths, one attenuating and the other not, or two attenuating wavelengths as a means of controlling the errors. On the other hand, one can exploit the attenuation as a measure of path integrated rainfall (Atlas and Ulbrich, 1977; Eckerman et al., 1978). A hybrid system with microwave radiometry also appears valuable as a means of estimating total attenuation over the oceans.

A problem which is interwoven with antenna and beam size and which is intrinsic to all radar methods is the signal averaging time needed to obtain a reliable estimate of the echo power. This implies either a high pulse repetition frequency (PRF) or a very slow scan. The latter in turn reduces the attainable swath width. The trade-off between high resolution, scan time, and swath width is a related concern. Pulse to pulse frequency agility (Marshall and Mitschfeld, 1953) or a wide band "noise" pulse (Krehbiel and Brook, 1979) have been suggested solutions.

With all these problems in mind, Eckerman (1975) and Nathanson et al., (1975) proposed a very sophisticated radar with a multiplicity of receiving beams, thus achieving high resolution (1 km FFOV), low clutter, adequate signal dwell time, and a wide swath all simultaneously. The key problems with the latter were high cost and power consumption; these factors are constraints on any space system. In what follows we have therefore backed off from such a sophisticated system and consider a variety of less complex options. Another related consideration is to design the system as an add-on to a planned radar, thus accomplishing two purposes at little added cost.

### 3.2 Radar Options

#### 3.2.1 Modified Altimeter

The simplest and least costly approach is to incorporate a rain measurement mode in the 13.5 GHz (2.2 cm) SEASAT type radar altimeter (Goldhirsh and Walsh, 1981). The retrieval algorithms for recovering rain rate and an effective drop size distribution are discussed in the latter reference. In one form, one essentially measures echo power near the top of the rain where attenuation is negligible and assumes constant rain rate down to the surface. This is shown by the  $\ln \rho = 0$  curve in

Fig. 1. Assuming constant rain rate with height, the decrease of signal level with depth is also a measure of rain rate. Under the same assumption, the authors show that the ratio of attenuation coefficient,  $k$ , to reflectivity,  $n$ , provides a unique measure of the slope or median volume diameter of the Marshall-Palmer drop size distribution; when this is used with the absolute value of either  $k$  or  $n$ , one also gets the intercept of the distribution. Of course, the assumption of constant rain rate with height facilitates the retrieval, but it is also a key weakpoint of the method. The authors also treat corrections for non-uniform beam filling. RMS rain rate errors over the range 10 to 100 mm/hr are about  $\pm 5$  and  $\pm 2$  mm/hr for an average of 45 and 220 pulses, respectively. Calibration uncertainties of  $\pm 1$  dB also result in bias errors of 13 to 20% between 10 and 100 mm/hr.

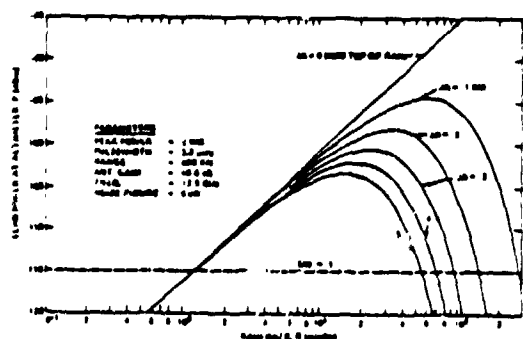


Figure 1. Echo power returned to the altimeter from various distances below the top of the rain versus rain rate (after Goldhirsh and Walsh, 1981).

The SEASAT type altimeter would be modified by allocating 5% of the altimeter pulses to the rain mode; i.e., 50 pulses each of 3.2  $\mu$ sec or 500 m vertical resolution. (Note: the normal pulses are "chirped" with 3.125 nsec or 0.47 m range resolution). Use of the SEASAT radar parameters also results in a minimum detectable rain rate of about 1 mm/hr from 800 km orbit. This is a marginal value for many purposes; a threshold rate of  $\sim 0.1$  mm/hr would be more useful.

Of course, the most serious limitation of the altimeter is its restriction to nadir measurements. Thus, it would have to be used in conjunction with a wide-swath IR or microwave radiometer. In either case, the radiometers would provide estimates of the rain areas while the radar would provide nadir rain rate calibration along the satellite track. The joint use of the altimeter with the microwave radiometer is preferable over the oceans because the radar provides an independent estimate of the total attenuation. Of course, a high resolution microwave radiometer also provides rain rate estimates off nadir so that in such a configuration the radar should be considered as supporting the radiometer rather than vice versa.

### 3.2.2 Short-Wavelength Scanning Radar

This system differs only slightly from the nadir radar altimeter in that it would scan cross-track to provide a wide swath measurement. A short wavelength (say 0.85 cm) would be used to attain the narrowest possible beams with a reasonable size antenna. A diameter to wavelength ( $D/\lambda$ ) ratio of 400, or an antenna of 3.4 m would provide 2 km resolution from an 800 km orbit. Of course, we assume large enough power and PRF to get reliable measurements down to just below the melting level. Since attenuation is likely to reduce the signal below noise in moderate to heavy rain, one must assume constancy of rain rate with height below the 0°C level as in the first method. Rain rate would be recovered from the reflectivity-rain rate relation adjusted to 0.85 cm and also from the attenuation rate. Over the ocean, retrievals would be greatly aided by a microwave radiometer. This would be especially useful in convective storms where either radiometer or radar alone is likely to be confounded by a variety of hydrometeors above the 0°C level.

It should be noted that an approach which combines dual wavelength radar and dual wavelength radiometry in the 3 cm and 0.86 cm bands, is being pursued in Japan (Inomata et al., 1981). The method has been implemented in an aircraft with promising preliminary results.

### 3.2.3 Surface Target Attenuation Radar (STAR)

This method, previously called "the surface reference technique," uses the scattering properties of the surface as a calibration point for meteorological attenuation measurements. The method depends upon both the fact that the path-averaged rainfall rate can be determined by means of a direct measurement of the attenuation (Atlas and Ulbrich, 1977) and the assumption that the fixed calibration target in the ground-based attenuation method can be replaced by the backscattering coefficient of the surface (Eckerman et al., 1978; Meneghini et al., 1981). Two variations of STAR can be distinguished: the surface comparison and the frequency agility methods. Both systems can utilize either fixed or scanning, real or Doppler azimuth sharpened beams. These systems operate at incidence angles of the order of 40° in order to achieve a sufficiently wide swath.

#### 3.2.3.1 Surface Comparison Method

To explain the method we first note that in the presence of rain the backscattered power from a range bin which intercepts the surface is proportional to the product of the backscattering coefficient of the surface  $\sigma_b$  (i.e., the scattering cross-section per unit area) and the attenuation factor,  $A$ , the two way fractional loss through the rain. If a second return power measurement is made either in the rain-free area adjacent to the storm cell or by a prior measurement at the actual target in the absence of rain, the power will be proportional to some new scattering coefficient,  $\sigma_b'$  say where the difference between  $\sigma_b$  and  $\sigma_b'$  will depend on the temporal

or spatial inhomogeneities of the surface. A ratio of the two measurements approximately equals  $\sigma_0^0/\sigma_0^0$ . The Skylab S-193 (Moore, 1974) and the University of Kansas (Ulaby, 1980) data have shown, however, that for a 10 km IFOV at K-band and incidence angles greater than  $30^\circ$ , the ratio  $\sigma_0^0/\sigma_0^0$  exhibits fairly small spatial fluctuations. Thus, the ratio of return power measurements provides an estimate  $\sigma_0^0$  from which the path-averaged rain rate is found by means of a k-R law and a measurement of the path length through the rain. The principal problems with this method are: (1) sensitivity of  $\sigma_0^0$  to soil moisture and (2) lack of knowledge of the footprint size needed to achieve stability in  $\sigma_0^0$ .

The technique can be generalized to obtain the profiled rain rate. This is accomplished by starting with the equation for rain rate from an attenuating radar (Nitschfeld and Bordan, 1954) and using the attenuation, as determined above, to bound the total error of the estimate. An analysis of the method has brought out some of its major advantages and drawbacks. Moreover, for narrow beamwidths, the accuracy of the profiled rain rate is comparable to that of the path-averaged rain rate. For example, with a radar located on a low earth orbiter pointing at a  $30^\circ$  incidence angle with respect to nadir and with  $\lambda = 0.86$  cm,  $P_t = 1$  kw, a storm height of 5 km and a standard deviation ( $s$ ) in  $\sigma_0^0$ , of 1 db, the rain rate can be estimated within about 20% of the true value for rain rates from 2 to 12 mm/hr. For  $s_0 = 2$  db the range extends from about 4 to 12 mm/hr. At longer wavelengths the range is shifted upward; e.g., if  $\lambda = 1.87$  cm and  $s = 1$  db then  $R_{min} = 8$  mm/hr and  $R_{max} = 55$  mm/hr.

To explicitly show the system performance, the mean return powers from the rain (R) and the surface (C) are plotted in Fig. 2 as a function of distance into the storm. Here, 0 km corresponds to the storm top and the region between 6 km and 9.5 km to the intersection of the range bin of the main beam with the surface. The gradual build up of the rain return (0 to 2 km) and the rapid decrease (7 to 9.5 km) represent regions where the range bins are only partially filled with rain. The decrease in the rain return power between 2.5 and 7 km is proportional to the total attenuation. Where the rms fluctuation of  $\sigma_0^0/\sigma_0^0$  is comparable to this total attenuation, then the method will be unreliable; this is the major source of error at low rain rates. At high rain rates, the return power at the surface will be smaller than the noise, so that attenuation cannot be estimated reliably. Accordingly, a single wavelength STAR would yield a limited dynamic range. Thus STAR requires two wavelengths to cover a wide enough range. Also, at very low rain rates where attenuation cannot be measured accurately, one must rely upon use of the ordinary reflectivity-rain rate relations.

It is worth noting that the STAR method has been analyzed primarily for rain over land. Over ocean it is expected to be less accurate because of the dependence of  $\sigma_0^0$  on wind speed for angles other than  $10^\circ$ . For measurements over ocean, a radar-radiometer sensor appears promising. In this mode the total

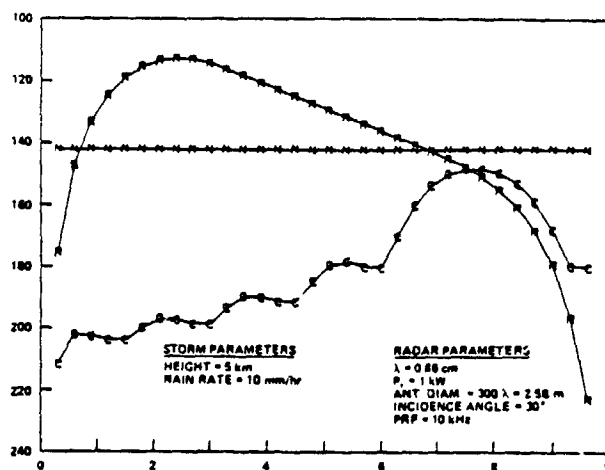


Figure 2. Radar return from rain R, noise N, and ground clutter C for the STAR radar (after Meneghini et al., 1981).

attenuation would be obtained from the radiometry while the radar would provide a measure of the storm height and the range profiled reflectivities. From these data the path-averaged and profiled rain rates could be obtained readily. In principle, a radar scatterometer which measures  $\sigma_0^0$  to estimate near surface windspeed over the ocean could also be used to obtain  $\sigma_0^0$  for use with STAR. Indeed one can use STAR itself as a scatterometer, but this approach has not been studied.

### 3.2.3.2 Frequency Agility Rain Radar (FARR)

This variant of the surface reference technique exploits the weak frequency dependence of ground radar reflectivity  $\sigma_0^0$  (0.25 dB/GHz at horizontal polarization). Two approaches should be considered, pulsed and CW.

With the pulsed FARR the radar ranges on the ground range bin. As with the ground comparison method, the received power from the surface range bin in the presence of rain is proportional to the product of the reflectivity, the attenuation and the radar constant. When volume scattering from the rain is negligible compared with surface scattering, the method is simplified. The ratio of received power from two simultaneous observations with slightly separated frequencies is proportional only to the product of the ratio of the radar constants and the attenuation factors at the two frequencies. The calibration constant ratio can be considered as known since it can be measured often during non-raining intervals. Thus, the measured power ratio is proportional only to the logarithm of the differential attenuation, which is proportional to the rain rate. The advantages of this approach are the simple algorithm, independence from variability of the drop size distribution, and the fact that the required storm height is also obtained by the measurement. The disadvantage (compared with CW) is the high peak power. With the CW FARR approach, the

radar signal contains contributions from both the attenuated ground return and the attenuated volume scatter of the rain within the beam. The markedly different frequency dependence of the ground reflectivity, precipitation attenuation and precipitation scatter offers the potential for separation of these factors. Rain rate can be determined from either the attenuation or volume reflectivity coefficients. Three measurements are required since there are three unknowns. The advantage of the CW approach is the lower peak power than with the pulse radar. However, the rain retrieval algorithm is complex, and the drop size dependence of the volume reflectivity may introduce significant uncertainty into the measurement. Further study is required to determine the feasibility of these concepts and to assess their relative merit.

The main advantage of the frequency agility method over the comparison method is its applicability to ocean and land scenes. It is feasible to use both methods over land to cross-check the validity of the assumptions and models.

### 3.2.4 Adaptive Pointing Beam

Many microwave antenna configurations can be used to image precipitation in storms, each having advantages and disadvantages depending on the required range of rain rate, resolution, swath width and accuracy. The systems proposed include: mechanical, conically scanned, single beam (Skolnik, 1974) and a pushbroom, fixed simultaneous multibeam phased array (Nathanson, et al., 1975). Contiguous coverage is obtained from these systems; however, it is necessary for the transmitter to be functioning continuously. Since precipitation normally covers limited areas, scanning time is being wasted while average power and data rates are higher than needed, and dwell time is too small to attain accurate samples. A solution to this problem is an Adaptive Pointing Beam which functions only over precipitating clouds (Atlas, 1981).

The key to such an adaptive approach is either an infrared or microwave radiometer which scans the horizon ahead of the spacecraft and identifies those cloud systems which are probably precipitating. It is only necessary for the look-ahead radiometer to sense the presence of rain and control the subsequent beam position to sample the rain areas in some optimal fashion.

The radar receiver and transmitter antennas are preferably phased arrays which electrically scan cross-track through nadir. There is a complete system for each side of the track. Several strategies are feasible including: a single pencil transmit and receive beam; multiple fixed receive beams; or multiple stepped pencil receive beams and scanned broad transmit beams. Scanning rates and beam multiplicity must be selected during tradeoff studies. However, the possibilities extend from a detailed high resolution snapshot of the storm to characterization of features such as boundaries and peaks.

The adaptively pointing concept is applicable to any of the measurement algorithms

since it solves problems common to all. Of course, the major concern with this approach is that of adequate sampling. Can we find a passive detection scheme which adequately identifies all significant precipitation regions, and can we then devise a set of radar sampling scenarios which insures sufficiently accurate estimates of the total precipitation?

Initial thinking about the antenna suggested that we use a real aperture in the vertical direction and synthetic (SAR) in the along track direction. In order to attain a sufficiently narrow vertical beamwidth, a diameter/wavelength ( $D/\lambda$ ) ratio of about 300 is desirable, giving a nadir beamwidth from 600 km orbit of 2 km with a 6 meter high antenna at  $\lambda = 2$  cm. With a real aperture, the antenna would thus be a 6 x 6 m array with face oriented normal to the track. For certain scan-track patterns, the horizontal dimension of the array can be reduced and the resolution improved by the use of Doppler beam-sharpening techniques. For Doppler beam-sharpening to be effective, the bandwidth used to achieve resolution should be about 5 times the bandwidth due to random motions of the hydrometeors; this places a limitation on the minimum pixel dimension that is much more stringent than that due to the radar motion itself. However, in directions within, say,  $60^\circ$  of the side, resolutions of 2 to 3 km due to Doppler beam-sharpening can be achieved, depending on spacecraft height, provided a spectral width for the random motions of 2 m  $\text{sec}^{-1}$  is assumed reasonable. Mean velocities of the hydrometeors will provide mean Doppler shifts that will appear as horizontal displacements of their apparent position. Use of this technique, however, would allow scanning a wide area of the ground with a fixed conical antenna beam from an antenna, say, 25 cm (horizontal) by 6 m (vertical).

## 4. DISCUSSION

It is clear that the solution to the measurement of precipitation with a spaceborne radar is not yet certain. However, the new concepts presented here provide considerable promise and deserve to be studied more carefully both theoretically and in aircraft trials.

We have not discussed the use of long wavelength ( $\lambda > 5$  cm) scanning systems which are essentially free of attenuation because they would require excessively large antennas to achieve narrow beam widths and IFOV's (i.e., 2-3 km at nadir). On the other hand, larger beam widths introduce virtually insuperable problems with surface clutter and unfilled IFOV's. Even with narrow beams, however, the retrieval algorithm rests on the existence of a well defined Z-R relation; aside from the large scatter about such relations, we know that they vary markedly with precipitation type and thus with climatic region.

Neither have we dealt with dual wavelength methods such as proposed by Eccles and Atlas (1973) or Goldhirsh and Katz (1974) because: (1) the non-attenuating wavelengths are subject to the same criticisms discussed above, and (2) at the attenuating wavelengths, it is difficult to achieve the kind of accuracies required in short range intervals, especially at the lower rainfall rates which contribute most



to the global rainfall. Furthermore, we have excluded 1 km FFOV sophisticated multibeam systems (Eckerman, 1973; NASA, 1975) largely on the basis of anticipated costs.

Despite the sampling deficiencies of the modified SEASAT-type altimeter and some concern about the basic algorithm, its simplicity and economy speak highly for it. Moreover, the probability of an ocean radar altimeter mission in the next 5 years seems high.

The hybrid approach which combines the surface reference technique (STAR), the frequency agility system (FARR), the short wavelength reflectivity schemes, and the adaptive pointing approach, all supplemented by microwave radiometry over the oceans appear attractive for an initial system. Of course, forward looking IR imagery is implicit in adaptive pointing. Adaptive pointing of the STAR would enhance its accuracy considerably through signal averaging. Over the oceans, microwave radiometry would provide an independent estimate of total attenuation, also improving accuracy. Where excessive rain rates cause loss of surface targets the STAR automatically becomes the short wavelength system in which rainfall is estimated through both reflectivity and the attenuation rate just below the bright band assuming uniformity from there down. Finally, the short wavelengths and sensitivities involved in all of the above provide for detecting and estimating rates of snowfall, also an important climatological requirement which has not been adequately addressed before.

We again note that sampling considerations are critical with any orbiting precipitation system. If the orbiter is sun synchronous, the diurnal variability will have to be accounted for through proxy measurements of clouds from a synchronous satellite. However, for climatological purposes we can choose an inclined orbit such that the local observing time varies over the month to provide a reasonably accurate monthly mean. Much more needs to be done on sampling and orbital considerations.

## 5. CONCLUSIONS

This paper does not pretend to define the ultimate solution to the problem of precipitation measurements from space. However, we have identified several new promising avenues of attack which go a long way toward overcoming the most serious obstacles which have impeded progress in the past. The role of precipitation in climate, and its accurate specification for use in regional and global weather prediction impel us to move forward with a serious effort to further assess and develop some of the more hopeful approaches described here and elsewhere (NASA, 1975).

## 6. ACKNOWLEDGEMENT

We are indebted to Mrs. Sharon Anderson for typing and editing.

## 7. REFERENCES

- Atlas, D., and C. W. Ulbrich, 1977: Path and area integrated rainfall measurement by microwave attenuation in the 1-3 cm band. *J. Appl. Meteor.*, **16**, 1322-1331.
- Atlas, D., 1981: Adaptively pointing spaceborne radar for precipitation measurements. Workshop on Precipitation Measurements from Space. NASA/Goddard Space Flight Center (in press).
- Eccles, P. J., and D. Atlas, 1973: A dual-wavelength radar hail detector. *J. Appl. Meteor.*, **12**, 847-854.
- Eckerman, J., 1975: Meteorological radar facility for the space shuttle. IEEE/National Telecommunications Conf., New Orleans, Louisiana.
- Eckerman, J., R. Meneghini, and D. Atlas, 1978: Average rainfall determination from a scanning beam spaceborne meteorological radar, NASA TM 79664.
- Goldhirsh, J., and I. Katz, 1974: Estimation of raindrop size distribution using multiple wavelength radar systems. *Radio Science*, **9**, 439-446.
- Goldhirsh, J., and E. J. Walsh, 1981: Precipitation measurements from space using a modified Seasat type radar altimeter. Johns Hopkins Univ., Applied Physics Lab., No. SIR81U-022, 77 pp.
- Hitschfeld W., and J. Bordan, 1954: Errors inherent in the radar measurement of rainfall at attenuating wavelengths. *J. Meteor.*, **11**, 58-67.
- Inomata, M., K. Okamoto, T. Ajima, H. Masuko, S. Yohikada, and M. Gugono, 1981: Remote sensing of rainfall rates using airborne microwave rain-scatterometer/radiometer. Proc. 15th Internat. Sym. on Remote Sensing of Environment.
- Krehbiel, P. R., and M. Brook, 1979: A broadband noise technique for fast-scanning radar observations of cloud and clutter targets. IEEE Trans. Geoscience Electronics, GE-17, 196-204.
- Lovejoy, S. M., and G. L., Austin, 1979: The delineation of rain areas from visible and IR satellite data for GATE and mid-latitudes. *Atmosphere-Ocean*, **17**, 77-92.
- Lovejoy, S. M., 1981: The remote sensing of rain. Dissertation submitted to Department of Physics, McGill University, Montreal, April 1981.
- Marshall, J. S., and W. Hitschfeld, 1953: Interpretation of the fluctuating echo from randomly distributed scatters, Part 1, *Can. J. Phys.*, **31**, 962-994.
- Meneghini, R., J. Eckerman, and D. Atlas, 1981: Determination of rain rate from a spaceborne radar using measurements of total attenuation. NASA TM 82153.
- Moore, R. K., 1974: Design data for radars based on 13.9 GHz Skylab  $\sigma^0$  measurements. Univ. of Kansas, Center for Research. NASA Contract NAS 9-13331.
- NASA, 1975: Active Microwave workshop report. NASA Report SP-376, 270-367.
- NASA, 1981: Precipitation measurements from space. NASA/Goddard Space Flight Center (in press).
- Nathanson, F. E., J. N. Bucknow, and R. P. Dooley, 1975: A shuttle meteorological study. Final report, Technology Service Corp. TSC-W3-38.
- Skolnik, M. I., 1974: The application of satellite radar for the detection of precipitation. NRL Memo. Report 2896.
- Ulaby, F. T., 1980: Vegetation clutter model. IEEE Antennas and Propag., AP-28, 538-545.